International Atomic Energy Agency

INDC(NDS)-129/GJ

INDC INTERNATIONAL NUCLEAR DATA COMMITTEE

Proceedings of the IAEA Consultants Meeting on Uranium and Plutonium Isotope Resonance Parameters

with the cooperation of the
OECD Nuclear Energy Agency Nuclear Data Committee (NEANDC)

28 September - 2 October, 1981
Vienna, Austria

Edited
by
Dermott E. Cullen
Nuclear Data Section
IAEA

IAEA NUCLEAR DATA SECTION, WAGRAMERSTRASSE 5, A-1400 VIENNA

INDC(NDS)-129/GJ

Proceedings
of
the IAEA Consultants Meeting on
Uranium and Plutonium Isotope Resonance Parameters

with the cooperation of the
OECD Nuclear Energy Agency Nuclear Data Committee (NEANDC)

28 September - 2 October, 1981
Vienna, Austria

Edited
by
Dermott E. Cullen
Nuclear Data Section
IAEA

Table of Contents

I. Programme
of
Consultants Meeting on
Uranium and Plutonium Isotope Resonance Parameters
with the cooperation of the
OECD Nuclear Energy Agency Nuclear Data Committee (NEANDC)

28 September - 2 October, 1981
Vienna, Austria

Organization

This Consultants Meeting was sponsored by the IAEA Nuclear Data Section under the auspices of the IAEA International Nuclear Data Committee (INDC), with the cooperation of the OECD Nuclear Energy Agency Nuclear Data Committee (NEANDC). It was held at IAEA Headquarters in Vienna from 28 September - 2 October 1981. The Scientific Secretary of the meeting was Mr. D.E. Cullen from the IAEA Nuclear Data Section. He was assisted by Mr. C. Nordberg from the OECD NEA Data Bank for making contacts for participation from NEA member countries.

Scope

This meeting considered resolved and unresolved resonance parameters for the major isotopes of uranium and plutonium, namely: ^{235}U, ^{238}U, ^{239}Pu, ^{240}Pu, ^{241}Pu and ^{242}Pu.

Objective

The meeting first reviewed the accuracy requirements of resonance parameters for reactor applications for the above mentioned isotopes with an emphasis on nuclear safety coefficients. Next, the meeting focussed on the current status of resonance parameters with regard to these accuracy requirements and identified outstanding problem areas. Then, there was an intercomparison of currently used major evaluated resonance parameter sets, with the aim of reconciling discrepancies and assigning realistic error estimates. Finally, the meeting addressed the problem of future work that should be performed to eliminate the remaining discrepancies.

Organizing Committee

The international organizing committee for this meeting consisted of the follwing ten members:

H. Derrien,	CEN Cadarache, France
G. de Saussure,	ORNL, USA
D.E. Cullen	IAEA, Nuclear Data Section
F. Froehner	KFZ Karlsruhe, Fed. Rep. of Germany
Y. Gur	Soreq Nuclear Research Centre, Yavne, Israel
S. Igarasi	JAERI, Japan
C. Nordborg	OECD/NEA Data Bank, Saclay, France
V. Konshin	Institute of Heat & Mass Transfer, Minsk, USSR
E. Menapace	CNEN Contro di Calcolo, Bologna, Italy
M. Sowerby	AERE Harwell, UK

Format

The first two days of the meeting were devoted to presentations of review papers on the requirements, current status and intercomparison of resonance parameters. The remaining three days were devoted to working groups on:

(1) Requirements for nuclear applications
(2) Fissile isotopes
(3) Fertile isotopes.

Location

The meeting was held at the IAEA headquarters located in the Vienna International Center (VIC).

Organization of sessions

Session chairmen organized individual sessions. The various sessions include

Meeting Chairmen: G. de Saussure/F. Froehner

Mon. a.m. J. Rowlands
"Accuracy requirements of uranium and plutonium isotope resonance parameters for reactor applications"

This session was devoted to paper presentations detailing the accuracy requirements of resonance parameters for actual applications: nuclear safety (e.g. Doppler coefficients), fuel cycle, etc. in order to provide background material to Working Group 1 to arrive at a realistic estimate of requirements.

Mon. p.m. H. Derrien
"Current status and outstanding problem areas associated with fissile uranium and plutonium isotope resonance parameters".

Tues. a.m. G. DeSaussure/F. Froehner
"Current status and outstanding problem areas associated with fertile uranium and plutonium isotope resonance parameters".

These two sessions were devoted to presentations of recent experimental work and of the current status of the evaluated resonance parameter sets currently used in major evaluated data libraries and individual evaluators' estimates of outstanding problem areas and uncertainties.

Tues. p.m. V. Pronyaev/O. Schwerer
"Intercomparison of current uranium and plutonium isotope resonance parameters".

This session was devoted to a comparison of the resonance parameter sets, presented in the two preceding sessions with emphasis on quantifying the impact of differences in resonance parameters for specific applications and attempting to reconcile differences.

Wed. a.m. J. Rowlands
"Working group on accuracy requirements of uranium and plutonium resonance parameters for reactor applications".

This working group synthesized the various contributions presented at the Monday morning session on accuracy requirements, with the objective of recommending a consistent set of accuracy requirements for resolved and unresolved resonance parameters for all of the isotopes covered by this meeting.

Wed. p.m. - Fri. a.m.

H. Derrien	F. Froehner/G. deSaussure
Working group on <u>fissile</u> isotopes.	Working group on <u>fertile</u> isotopes.

These two working groups met in parallel with the objective of reconciling discrepancies between existing evaluated resonance parameter sets and of recommending future work that should be performed in order to eliminate remaining discrepancies.

Fri. p.m. G. DeSaussure/F. Froehner
Discussion and approval of working group reports
Summary of meeting conclusions and recommendations.

Because of the last minute cancellation of several papers that were to be delivered, several papers were moved from one section to another to balance the length of sections. Therefore in several instances papers on fertile isotopes were presented during the session on fissile isotopes. This did not create any problems since the full meeting participated in both fertile and fissile sessions.

PROGRAMME

Mon. a.m. 9:00 Opening Remarks
G. deSaussure, ORNL

Mon. a.m. J. Rowlands
<u>"Accuracy Requirements of Uranium and Plutonium Isotope Resonance Parameters for Reactor Applications"</u>

9:20 a.m. Some Views on Cross Section Requirements for Uranium and Plutonium Isotopes in the Resolved and Unresolved Resonance Region.
J. Rowlands, Winfrith.

10:30 a.m. Resonance Parameter Data Uncertainty Effects on Integral Parameters of Fast Reactors.
M. Salvatores, CEN Cadarache.

11:10 a.m. Effective Integral and Reactivity Effects of ^{238}U and ^{240}Pu Resonance Parameter Uncertainties.
H. Tellier, Saclay.

11:50 a.m. ^{238}U Resonance Self-Indication Capture Measurements.
R.C. Block, RPI.

Mon. p.m. H. Derrien
"Current Status and Outstanding Problem Areas Associated with Fissile Uranium and Plutonium Isotope Resonance Parameters".

2:00 p.m. Problems and Progress regarding Resonance Parametrization of ^{235}U and ^{239}Pu for ENDF/B.
M.S. Moore, LANL.

2:40 p.m. Review of ^{241}Pu Resonance Parameters.
H. Derrien, CEN Cadarache.

3:20 p.m. Level Density Estimation with Account of Unresolved Multiplets Applied to Uranium and Plutonium Resonance Data.
F. Froehner, KFZ Karlsruhe.

4:00 p.m. Resonance Parameters of ^{238}U below 4.2 keV.
H. Weigmann, BCMN.

Tues. a.m. G. DeSaussure/F. Froehner
"Current Status and Outstanding Problem Areas associated with Fertile Uranium and Plutonium Isotope Resonance Parameters"

9:00 a.m. The Neutron Capture Cross Section of ^{238}U from 0.01 to 10 eV.
M.C. Moxon and J.E. Jolly, Harwell.

9:40 a.m. ^{238}U Unresolved Resonance Parameters.
M. Sowerby and N.J. Bee, Harwell.

11:00 Parity Assignment of the Pronounced Structure in the Radiative Capture of Neutrons by ^{238}U below 100 keV.
M.S. Moore, LANL.

11:40 Review of ^{240}Pu and ^{242}Pu Resolved Resonance Parameters.
H. Weigmann, BCMN.

Tues. p.m. V. Pronyaev/O. Schwerer
"Intercomparison of Current Uranium and Plutonium Isotope Resonance Parameters".

2:00 Review of ^{240}Pu and ^{242}Pu Unresolved Resonance Region.
K. Wisshak, KFK.

2:30 p.m. Temperature Dependent Transmission: Comparison of Measurements to Calculations.
N. Bee, AERE Harwell.

3:00 p.m. Comparison of Uranium and Plutonium Group Averaged Cross Sections and Staircase Plots.
D.E. Cullen, IAEA.

3:30 p.m. Comparison of the ENDF/B and SOKRATOR evaluations of ^{235}U, ^{239}Pu, ^{240}Pu and ^{241}Pu at Low Neutron Energies.
G. deSaussure, ORNL.

4:00 p.m. Comparison of Strength Functions and Average Level Spacing for U and Pu Isotopes.
V. Pronyaev, IAEA.

4:30 p.m. Intercomparison of Methods Used to Determine Average Parameters from Sets of Resonance Parameters.
N. Tubbs, C. Nordborg, NEA.

II. Working Group Reports

1. Accuracy Requirements
   J.L. Rowlands, Winfrith

2. Fissile Isotopes
   H. Derrien, Cadarache

3. Fertile Isotopes
   F. Froehner, Karlsruhe

Working Group on Accuracy Requirements of Uranium and Plutonium Resonance Parameters for Reactor Applications

by
J.L. Rowlands, Winfrith

Introduction

There are requirements for files of evaluated resolved and unresolved resonance region data (and associated uncertainty estimates) for all the uranium and plutonium isotopes. For some of the isotopes, resonance shielding effects and temperature dependent effects are small (in reactor applications) and the required information on resonance structure is not stringent (except for the few lowest energy resonances). For these isotopes a resonance parameter analysis serves to apply the constraints of nuclear theory in the evaluation of the measured data and makes possible a simultaneous evaluation of all the partial and total cross-section meausrements. The discussion on accuracy requirements concentrated on the principal isotopes, for which resonance shielding and Doppler effects are particularly important.

The following topics were discussed:

1. Ways of specifying accuracy requirements.

2. Requirements for the principal isotopes.
   - 2.1. Thermal region cross-section shapes
   - 2.2. Lowest energy resonances (for thermal reactor applications)
   - 2.3. Fast reactor requirements

3. The representation of resonance region data in files of evaluated nuclear data.

4. Specification of uncertainties in evaluated data.

5. Measurements suitable for testing evaluations.

6. Crystalline binding effects.

1. Specification of accuracy requirements

Specification of accuracy requirements for resonance parameters is complicated by the covariance relationships between the different parameters of each resonance and between the parameters of different resonances. These covariance relations have not in the past been predicted in advance of measurements being made and analyses being completed, although it should be possible to give some guidance on the probable form of the covariance relationships. Measurers and evaluators are asked to formulate such guidance. Calculated values of reactor parameters are sensitive to particular groupings of resonance parameters (such as those determining capture areas or shielding effects), and reactor physicists should be encouraged to specify what the required resonance characteristics are.

Because of the covariance relations in the uncertainties in measured and evaluated resonance parameters and the effect that these could have on the uncertainties in calculated reactor properties alternative ways of specifying the requirements were discussed. A recommended alternative way is to specify the accuracies required in the following average properties for an energy range:

(i) The average infinitely dilute cross sections for reaction r in isotope I,

$$\sigma_{\infty r}^{I} = \int \sigma_{r}^{I}(E)\ \phi\ (E)\ dE \Big/ \int \phi\ (E)\ dE$$

(ii) The average shielding factor for a specified dilution, σ_o and temp, T

$$\bar{f}\ (T,\sigma_o) = \int \frac{\sigma_r^I(E)}{\sigma_t^I(E)+\sigma_o}\ \phi\ (E)\ dE \Big/ \sigma_{\infty r}^{I} \cdot \int \frac{\phi\ (E)\ dE}{\sigma_t^I(E)+\sigma_o}$$

(iii) The Doppler change in the average shielding factor

$$(\partial \bar{f}(T,\ \sigma_o)\ /\ \partial\ T)_{oT}$$

The weighting spectra, $\phi(E)$, would take a simple form through the resonance region in these specifications

$\phi\ (E) = 1/E$ for thermal reactor requirements and low energy resonances.

$\phi\ (E) = 1$ for fast reactors.

The energy range for fast reactors might, for example be a decade in energy and the values of σ_o = 30 b for ^{238}U and 300 b for ^{239}Pu. (Alternatively, the fully shielded values, σ_o = 0 might be chosen).

It was emphasized that these are not the nuclear data requirements, but only a possible way of specifying the accuracy requirements. To evaluate the resonance shielding uncertainties in a partial cross section (fission, capture or scattering) it is necessary to have data for both the partial cross section and a consistent total cross section. Consequently, it might not be a form of specification convenient for capture or fission cross-section measurers to use, but only for use by evaluators (and measurers of total cross sections). However, it is thought that the selection of total cross section parameters, used to evaluate a capture or fission cross section measurement resonance shielding accuracy, will not be critical, provided that it is consistent with the capture or fission cross section measurement (i.e. resonance energies the same).

2. Accuracy requirements

2.1 The thermal energy region

Dr. Lemmel described the current status of thermal region data. There is now consistency between the 2200 m/sec and thermal Maxwellian values for ^{239}Pu but a 2% discrepancy for ^{235}U fission. This could possibly be due to an error in the shape of the fission cross section at thermal energies or to an error in the assumed shape of the thermal spectrum. Dr. Leonard has carried out a resonance parameter analysis of the ^{235}U thermal data and has obtained a fit consistent with the currently adopted cross section shapes. His resonance parameter analysis for ^{239}Pu requires further work to resolve some problems.

In the UK, thermal reactor physicists have adjusted the shape of the ^{235}U thermal eta curve to improve predictions of moderator temperature coefficients. However, French reactor physicists resolve the temperature coefficient problem by adjusting the shape of the ^{238}U capture cross section at thermal energies. They also increase the ^{235}U thermal eta value uniformly (relative to the 1975 IAEA evaluation) to reproduce integral measurements of lattice reactivity.

Work is required to resolve the discrepancies for ^{235}U and ^{238}U cross sections at thermal energies, consistently with a resonance parameter analysis of measured data. A resonance parameter analysis for ^{239}Pu should be completed to give confidence in the consistency of the data.

2.2 Low energy resonance data for thermal reactors

Dr. Tellier specified the requirements for the three lowest energy s-wave resonances in ^{238}U and for the 1 eV resonance in Pu.

^{238}U: Γ_γ = 1 MeV: Γ_n = 2 %, 3 %, and 5 %

for the first, second and third resonances.

Dr. Tellier said that he considered this requirement to be met noting that there is now consistency between thermal reactor lattice measurements of ^{238}U capture and calculated values in the resonance region.

For the 1 eV ^{240}Pu resonance the requirements are $\Gamma_\gamma \pm 1$ meV, $\Gamma_n \pm 3$ %. Dr. Tellier pointed out that although it appears that this requirement is met in current evaluations there are indications in French studies of a discrepancy in isotopic composition predictions for irradiated fuel. For fissile isotopes the resonance shielding and Doppler effects are much smaller and it is considered that the existing data meet the requirements (the accuracy requirements for the parameters being about $\pm$ 20 %). However, there are more stringent requirements for the infinite dilute cross sections and eta values in the resolved resonance range ($\sim$3%) up to 100 eV.

2.3 Fast reactor requirements

Dr. Salvatores had made sensitivity studies for fast reactor K_{eff} values, Doppler effects, sodium voiding effects and control rod worths. He explained that the resonance parameter accuracy requirements are strongly dependent on the energy correlation assumed. To give a rough guide he proposed an accuracy requirement of $\pm$ 5 % in the systematic, or average uncertainty in all averaged resonance parameters, Γ_γ, S_o, S_1, and D for ^{238}U and ^{239}Pu (Γ_f also).

Rowlands also made estimates of the cross section requirements based on broad judgements of the reactor property requirements. For the energy range 100 eV to 100 keV the following requirements were proposed:

	σ_∞	$\bar{f}$	$(\partial\bar{f}/\partial T)$
^{239}Pu fission	3 %	0.5 %	20 %
capture	10 %	2 %	20 %
^{238}U capture	3 %	1 %	5 %
^{240}Pu capture	10 %	5 %	30 %

The requirements for ^{235}U are similar to those for ^{239}Pu but have a lower priority.

The values of f and $\partial f/\partial T$ are to be calculated for values of σ_o of 30 b for ^{238}U, 300 b for ^{239}Pu and 1,000 b for ^{240}Pu. A temperature of T = 300 K is suggested.

3. Representation of resonance region data

The reactor physics codes used in some countries require the provision of resonance parameters, with individual values being given in the resolved resonance range and point values of average resonance parameters and distributions in the unresolved range. It was agreed that the resonance formalism used should be such that any background cross section to be added is smooth. Some evaluations use energy point tabulations both in the resolved resonance range and in the unresolved region up to about 25 keV, with a single ladder of resonances in the unresolved region. The data can be provided either as the resonance parameters or as the energy point tabulation. The ladder in the unresolved region should give the best possible fit to all the relevant data, including approximately resolved data (large resonance) broad resolution and thick sample transmission and self-indication measurements. Above 25 keV statistical resonance parameters are required up to about 300 keV.

It is required that the resolved resonance ranges should be extended to as high an energy as possible, particularly for ^{238}U and ^{239}Pu.

4. Uncertainty information

The provision of uncertainty information was considered to be possibly the highest priority requirement. This should take the form of covariance data on the individual parameters of the few lowest energy resonances (for example 3 in ^{238}U, 1 in ^{240}Pu) and uncertainties in the parameters averaged over broad energy ranges, e.g. in $\Sigma\Gamma_n$ over a range (or in the values of σ_∞, $\bar{f}$ and $\partial \bar{f}/\partial T$) at higher energies.

It might be necessary to develop computer formats to represent the uncertainty data. However, documented data could suffice for the present.

5. Data for testing resonance region cross sections

It was considered important that the thick sample transmission and self indication measurements should be compiled in a form convenient for testing resonance region data and that evaluators should test their evaluations using them.

6. Crystalline binding effects

Several recent studies have indicated significant crystalline binding effects on the Doppler broadening of resonances, in uranium compounds. There is a need for the different results to be resolved. Some studies indicate an effective Debye temperature of about 250°K for UO_2 and other studies a Debye temperature of about 600°K. Experiments performed at Dresden show a more complicated (two component oscillator) dependence and an asymmetrical effect on the resonance shape.

Working Group on Fissile Isotopes

by
H. Derrien, Cadarache

General recommendations

1. - The use of non-smooth background should be avoided for the cross-sections in the resonance region. The multilevel formalism should be used if a single level formalism cannot reproduce experimentally measured data without a non-smooth background.

2. - The shape analysis should be performed simultaneously on transmission, fission and capture experimental data, bearing in mind that the best values for Γ_n, Γ_f and Γ_γ should come respectively from transmission data, transmission and fission data, transmission and capture data.

3. - The shape analysis method could be applied to total cross sections derived from transmission measurements of different sample thicknesses only if the experimental resolution is good enough, i.e. resolution width much smaller than the Doppler width. Experimentalists should give as much information as possible to describe how the total cross sections have been obtained from the different sample thicknesses transmission measurements.

4. - It is recommended to experimentalists that they send their transmission data to the data centres. These data should be stored in the EXFOR format and all relevant information (original report, detailed information on error evaluations, background, normalization, etc...) should be kept in the data centres and should be available upon request to the evaluators.

5. - New measurements should be made; some important total cross-section data are more than 15 years old. With present day intense pulsed neutron sources background problems are greatly reduced and much higher accuracy is possible.

6. - Even the presently available fission cross-section data, and in particular, the best multilevel resonance parameter sets are not used in some of the most recent evaluations. It is urgent that this backlog be eliminated and evaluations be brought up-to-date as soon as possible.

Specific Recommendations for Individual Isotopes

235U

1. In the thermal region there is still a 2 % discrepancy between the measured Maxwellian average fission cross section and that evaluated from the recommmended 2200 m/s value and the Westcott g-factor representing the shape. There is a need for new fission measurements down to below room thermal (down to at least 10 meV) to remove this discrepancy.

2. In the resonance region, most of the evaluations do not use the spin-separated fission cross sections of Moore et al. New evaluations are needed and new total cross-section measurements would be most useful (see general recommendation no. 5).

239Pu

1. Continuation of Leonard's least square adjustment of the cross sections below 1 eV is considered to be of importance.

2. Multilevel resonance parameter sets that are available since many years are not incorporated in most files. Such incorporation is recommended. New total cross-section measurements in the resonance region are also recommended (see general recommendation no. 5).

3. The most stringent accuracy requirement on self-shielding factors is 0.5 % for ^{239}Pu fission (review paper by Rowlands). It is recommended that calculations be done in order to assess the accuracy requirement on resonance parameters which follows from the above request.

4. It should further be assessed whether the inclusion of intermediate structure in the 1^+ fission channel in the unresolved region influences the self-shielding factor to more than the above 0.5%.

5. The evaluation of ^{239}Pu in the unresolved region is unsatisfactory.

241Pu

1. Same as ^{239}Pu first recommendation.

2. General recommendations concerning this nucleus are found in the review paper by H. Derrien.

Working Group on Fertile Isotopes
Conclusions and Recommendations for Fertile Nuclei

by
F. Froehner, Karlsruhe

1. The thermal region

238U

The good agreement between the various newer evaluations seems to indicate that an accuracy of about 3% is achieved for the neutron widths and about 0.8 meV for the radiation widths of the first four resonances of ^{238}U. This would satisfy the needs for thermal reactor calculations. A number of problems persists, however. The participants agreed on the following recommendations.

(1) Crystal effects in Doppler broadening of low-energy resonances can lead to errors in Γ_γ of several percent if not properly taken into account. Average radiation widths deduced mainly from the first few resonances could therefore differ from the true average. This question should be investigated.

(2) The shape of σ_γ below 6 eV should be remeasured to see whether a suspected p-wave level is present there or not. The use of a Ge(Li) detector with a thick sample could alleviate the high-purity requirements imposed by the low cross section. In this context it should be noted that the moderator temperature coefficient discrepancy still seems to require modifications to the ^{238}U (n,γ) cross section shape.

2. The resolved resonance region

Generally valid recommendations for the resolved resonance region concern a universally adopted energy scale and resonance analysis techniques:

(3) The energy scale recommended by James, Symposium on Neutron Standards and Applications, NBS SP493 (1977) 493. (reproduced in the INDC(NEANDC Standards File, INDC-36/LN) should be used in all evaluations, in particular for ^{238}U.

(4) Backgrounds, normalization constants and other experimental characteristics should be adjusted in resonance fits simultaneously with the resonance parameters. Total (transmission) and partial cross section data (capture yields etc.) should be fitted simultaneously.

238U

(5) A covariance matrix should be established for the first three resonances (plus the bound level). More general covariance information from resonance fits would be useful and resonance analysts are urged to supply such information to the data centres.

(6) It is recommended to extend the resolved-resonance region to 10 keV. At least the stronger s-wave levels should be analyzed for Γ_n. This would put calculations of self-shielding and Doppler effect on a firm basis as about 90% of it are due to energies below 10 keV.

(7) Since no direct measurement of any p-wave radiation width is available for ^{238}U a fresh attempt should be made to determine Γ_γ for one or more suitable p-wave levels, with cooled samples.

240Pu

(8) No measurements are requested before those of Liou and Chrien and of Weston et. al. have been assessed.

(9) Covariance information on the parameters of the first resonance (plus possibly a bound level) is to be included in evaluated files.

(10) An extension of the resolved-resonance region to 10 keV is desirable but has lower priority than for ^{238}U.

242Pu

(11) The same recommendation concerning covariance information for the first resonance (plus possibly a bound level) as for ^{240}Pu applies also to ^{242}Pu.

(12) Conflicting evidence as to the presence or absence of p-wave levels among presently known ^{242}Pu resonances should be clarified.

3. The unresolved resonance region

238U

The capture cross section for infinite dilution is estimated to be known with an accuracy of 3-5% below 50 keV and 5% above. The fast-reactor requirements (3% or better) are therefore not quite met and further experimental effort would be very useful provided a significant improvement in accuracy could be achieved. In contrast to infinite-dilution cross sections the accuracy of self-shielding factors calculated from average resonance parameters is quite difficult to assess without suitable benchmark data.

(13) An accurate set of benchmark data for the testing of self-shielding calculations should be established with high priority. It should comprise broad-group, thick sample transmission data (e.g. ORNL data), capture self-indication data (e.g. RPI, Van'kov et al.) and temperature-dependent thick sample transmission data (e.g. Haste + Sowerby, Brugger). The benchmark data must be extensively documented and be available at the data centres.

240Pu

(14) There seems to be no stringent needs for new measurements from a reactor physics viewpoint.

242Pu

(15) Although not needed directly for reactor calculations the insufficiently known total cross section below 200 keV should be remeasured with about 3-4% accuracy. This would define the strength functions for =0 and 1 which are needed for level-statistical and optical-model calculations of capture and inelastic scattering.

(16) Above about 100 eV error files should contain broad-group information on the variances of, and covariances between, the average resonance parameters (S_ℓ, D_J, $\Gamma_{\gamma\ell}$, $\Gamma_{f\ell}$ ...).

Because of the fact that essentially the same total cross sections can be obtained with quite different pairs of S_0 and R' the covariances are essential.

A very general final recommendation was agreed upon:

(17) Evaluators should make full use of rection theory and nuclear models. Theoretical methods should be adequately documented. At the same time it should be kept in mind that theory can never be a substitute for good data.

III. List of Working Papers

The working papers used at this meeting may be divided into three general categories: invited (I), contributed (C), background (B). Besides the invited and contributed papers a selection of recently published material on the subject of uranium and/or plutonium isotopes was also used as background reference material. As each paper was received it was assigned a paper number. In this section a list of the titles and authors of all three types of papers is enclosed. In the following sections of these proceedings the full text of invited and contributed papers are enclosed. The text of background papers is not enclosed in these proceedings, since all of this material has already been published in the literature. In the following list papers are identified as: invited (I), contributed (C), or background (B).

Working Papers for IAEA Consultants Meeting on U/Pu Resonance Parameters

C (1) 24 – Differences in the Doppler Broadening of Neutron Resonances in Crystals and Gas studied at the 6.7 eV Resonance of ^{238}U.
A. Meister, D. Pabst+, L.B. Pikelner+, W. Pilz+, D. Seeliger, K. Seidel, R. Tschammer+ - Dresden, DDR + Dubna, USSR.

C (2) 269 – Estimate of Average Level Spacing and S-Wave Neutron Strength Functions for ^{241}Pu Resonance Data.
C. Bonifazzi and e. Menapace, Bologna.

C (3) 271 – Doppler Measurements of ^{238}U.
R.M. Brugger and H. Aminfar, University of Missouri, Columbia.

I (4) 83 – Review of ^{241}Pu Resonance Parameters.
H. Derrien, Cadarache.

C (5) 282 – Evaluation of Resonance Parameters of ^{238}U, ^{240}Pu and ^{242}Pu.
T. Nakagowa, JAERI, A. Zukeran, Hitschi, M. Kawai, NAIGL.

C (6) 309 – Evaluation of Resonance Parameters of ^{233}U, ^{235}U, ^{239}Pu and ^{241}Pu.
Y. Kikuchi, JAERI, A. Asami, NLHEP, T. Yoshida, NAIGL.

B (7) – Resonance Shielding in Thermal Reactor Lattices.
W. Rothenstein, Technion, Haifa.

B (8) – Self-shielding Fission Rates for Uranium-235.
J.B. Czirr, Livermore.

I (9) 74 – Problems and Progress Regarding Resonance Parameterization of ^{235}U and ^{239}Pu for ENDF/B.
M.S. Moore, G. deSaussure and J. Richard Smith.

B (24) Representation of the Neutron Cross Sections of Several Fertile and Fissile Nuclei in the Resonance Regions.
- G. deSaussure and R.B. Perez.

B (25) A Study of the Temperature Dependence of the Neutron Transmission of Uranium Dioxide.
- T.J. Haste and M.G. Sowerby.

B (26) The Measurement of the Total and Scattering Cross Sections of ^{235}U for Neutrons with Energies 2 and 24.5 keV.
- V.P. Vertebnii, N.L. Guidak, A.V. Grebnev et al.

B (27) The Measurement of the ^{233}U and ^{235}U Fission Cross Section for Neutrons with Energy 24.5 keV.
- A.V. Mursin, A.F. Rudyk, V.A. Libman.

B (28) The Total cross Section and the Resonance Self-Shielding of Capture Cross Section Measurements for ^{238}U in Neutron Energy Region 5-80 keV.
- V.N. Kononov, E.D. Poletaev.

B (29) Total-Neutron Cross Sections of Heavy Nuclei.
- W.P. Poenitz, J.F. Whalen and A.B. Smith.

B (30) Neutron Cross Section Measurement at ORELA.
- J.W.T. Dabbs.

B (31) ^{235}U (n,f) Cross Section Measurements and Normalization Problems.
- C. Wagemans, G. Coddens, A.J. Deruytter.

B (32) Fragmentation of Single-Particle States and Neutron Strength Functions in Deformed Nuclei.
- L.A. Malov, V.G. Soloviev.

B (33) Chemical Binding Effects on Resonance Line Shape and Neutron Capture Rates.
- H.St. John, R.A. Karam.

B (34) Neutron Nucleus Optical Potential for Actinide Region.
- D.G. Madland, P.G. Young.

B (35) Measurement of the Doppler Effect of ^{238}U as a Metal and as an Oxide.
- R.M. Brugger, F.Y. Tsang.

I (36) 218 Comparison of the ENDF/B-V and SOKRATOR Evaluations of ^{235}U, ^{239}Pu, ^{240}Pu and ^{241}Pu at Low Neutron Energies.
- G. deSaussure and R.Q. Wright.

C (37) 330 Reich-Moore Formalism as Applied for Searching Resonance Parameters From Experimental Data.
- V.F. Zharkov.

I (52) 103 Level Density Estimation with Account of Unrecognized Multiplets Applied to Uranium and Plutonium Resonance Data.
F.H. Froehner.

I (53) 249 N.E.A. Nuclear Data Committee Intercomparison of Methods Used to Determine Average Resonance Parameters.
Coordinated by P. Ribon.

I (54) 165 Review of the ^{240}Pu and ^{242}Pu Unresolved Resonance Region.
K. Wisshak, F. Kaeppeler.

C (55) 438 Neutron Cross Sections and Doppler Effect of the 1.056 eV Resonance in ^{240}Pu.
H.I. Lion and R.E. Chrien.

IV. Invited Papers

In the following section the full text of the invited papers, presented at the meeting, are enclosed in the order in which they were presented at the meeting (see: I. Programme).

Some views on cross section requirements for uranium and plutonium isotopes in the resolved and unresolved resonance regions

John L ROWLANDS

United Kingdom Atomic Energy Authority
Winfrith, Dorchester, Dorset

1 Introduction

It is necessary to take account of the detailed resonance structure of the cross sections of a substance in reactor calculations when this structure produces a corresponding fine structure in the neutron flux or when the resonance structure of a second substance produces a flux fine structure which overlaps with the resonance structure of the first substance. The first effect is called resonance self-shielding and the second is called the internuclide resonance interference or overlap effect or the mutual shielding effect.

Reactor neutronics calculations involve the calculation of the neutron flux, $\phi(E)$, and relative reaction rates. The reaction rate, R_r^I, for reaction r, isotope I, is a flux integral of the cross section, $\sigma_r^I(E)$, : $R_r = \int \sigma_r^I(E)\ \phi(E)\ dE$. The flux is a function of the cross sections of all the isotopes in the reactor and of the geometry, or heterogeneity. This functional form depends on the relationship between the widths and spacings of resonances and the energy loss in scattering. For resonances which are narrow or wide compared with this energy loss simplifying approximations can be made.

The degree of detailed information required about the resonance structure for an isotope in a particular energy range depends on the possible strength of resonance shielding effects and on the simplifying approximations which can be made in the dependence of the neutron flux on the resonance structure. When certain approximations, such as the narrow resonance approximation , are valid it is sufficient to know the probability distribution of cross-section values or, alternatively , measures of the probability distributions such as cross section shielding factors as a function of the concentration of a diluent material or of sample thickness. The dependence of these on nuclide temperature is also required. For some applications, when the variation of temperature across a fuel element must be taken into account, the probability distributions must be formulated to represent the inter-relationship of cross section values at different temperatures. However, for many applications this temperature correlation information is not required.

Resonance parameters are not required explicitly for reactor calculations, although some processing systems used to generate group averaged cross sections do require them. Energy point representations of resonance cross sections in both the resolved and unresolved energy ranges can be used as the basis for reactor physics calculations (with a single representative ladder of resonances in the unresolved range). When a uniform energy grid is used in order to simplify the neutron flux calculation (as in the GENEX-SRD system of Brissenden and Durston (1)) of the order of 10^5 energy points are needed to represent the cross sections of the principal actinide isotopes up to about 25 keV. These representations form the basis for the derivation of simpler representations used in more routine reactor calculations. The GENEX tabulations were used directly to derive the fine group plus resonance sub-group (or probability table) data of the fine group libraries, FGL4 (2) and FGL5 (3). The 150,000 point values of the GENEX tabulation are reduced to about 5,000 fine group plus resonance sub-group values. SDR neutron flux calculations in simple cell geometries were used with the GENEX point cross section data to validate the fine group library. SDR flux calculations and GENEX cross section data were also used to derive the resonance shielding factors and sub-group data used in the WIMS cross section library (4).

However, resonance parameter analyses play a most important part in the generation of the energy point representations both in the resolved and unresolved energy ranges. A resonance parameter analysis supplements the measured data in the resolved energy range by applying nuclear theory constraints when correcting for the effects of resolution broadening and other measurement errors. It also makes possible the simultaneous evaluation of different partial and total cross section measurements for a nuclide (such as capture plus transmission measurements). Clearly, the resonance formula used must be capable of accurately representing the resonance structure and be consistent with nuclear theory. In the unresolved resonance region a ladder of resonances must be constructed

which is consistent with the broad resolution infinite dilution cross section measurements, with thick sample transmission and self-indication measurements and also with the average resonance characteristics (and their statistical distributions) determined for the resolved resonance region. It is sufficient to generate a single ladder in the unresolved resonance region for use in reactor flux calculations. However, to evaluate uncertainties, a range of ladders which satisfy the constraints (and take into account the uncertainties in the constraints) can be used. Alternatively, a simpler method of estimating uncertainties from the ranges of resonance parameters which would satisfy the constraints in each energy interval could be used. An example of the generation of resonance ladders to meet the constraints of broad resolution capture and fission cross section measurements is the work of Ishiguro et al(5). The constraints provided by broad resolution infinite dilution cross section measurements, temperature dependent thick sample transmission measurements (6) and self-indication measurements (7) are also available for U238 for future evaluations in the unresolved resonance region. The statistical basis for the construction of a resonance ladder in the unresolved resonance region is complicated by the forced sampling to fit the braod resolution measurements and could well be a subject requiring more detailed study.

The adjustment of cross sections to take account of integral measurements has a more satisfactory physical basis when the adjustments are made to resonance parameters, either to parameters of individual resonances or to average resonance parameters. This has been described, for example, by Gandini and Salvatores (8), (9). In the adjustment of U238 capture at thermal energies to improve agreement between calculated and measured moderator temperature coefficients (10), parameters of negative energy resonances were changed and the cross section curves calculated.

Doppler broadened crosssections can be calculated either directly from the resonance parameters or by broadening an energy point tabulation at a reference temperature (usually either $0^{o}K$ or $300^{o}K$) to a higher temperature. The latter approach is adopted, for example, in the MLBW-TEMPO code (11), the SIGAR-DOPCUB code (12) and the SIGMA1 code (13). The TEMPO and SIGMA1 codes assume linear interpolation whereas the DOPCUB code uses a cubic spline fit to the energy points. In broadening from an intermediate temperature to a higher temperature the gas model is assumed (14).

The effective Debye temperatures characterising the thermal motion of uranium and plutonium nuclei in the crystal lattices of metal and oxide are still not generally agreed. Broad resolution integral Doppler experiments give high values for oxides. Golinelli et al (15) concluded that using a Debye temperature of $620^{o}K$ for UO_2 improves the interpretation of thermal reactor lattice Doppler experiments made in MINERVE. Brugger and co-workers (16) have also deduced values of about $600^{o}K$ for uranium oxide Doppler effect measurements made at KeV energies. Earlier studies by Butland (17) and Willis et al (18), based on neutron scattering measurements, had derived much lower equivalent Debye temperatures. Butland derived values of $250^{o}K$ for U and $749^{o}K$ for O in UO_2 at a thermodynamic temperature of $293.6^{o}K$. The equivalent Debye temperatures depend on the thermodynamic temperature but are calculated to have negligible effect on the effective temperature for the uranium nuclei at temperatures above about $500^{o}K$. The Debye temperature calculated for the UO_2 lattice as a whole is $630^{o}K$ at a thermodynamic temperature of $293.6^{o}K$. Debye temperatures have also been deduced from an analysis of the dependence of the shapes of uranium resonances on the sample temperature and the uranium compound (19).
The analysis of the temperature dependent thick sample transmission measurements of Haste and Sowerby (6) was consistent with the low value derived by Butland. There is,therefore, a discrepancy between the values derived from recent measurements of integral capture Doppler effects and other measurements.

Uncertainty information on cross sections in resonance regions is needed to enable the broad energy group infinite dilution cross sections, resonance shielding factors and Doppler effect changes to be calculated, and hence the reactor spectrum averaged values to be derived.

2 Approximations in the representation of resonances

An accurate representation of the energy positions of resonances is required when the mutual shielding effects between substances could depend on the relative positions of the resonances in the two substances. This is of importance at lower energies, below about 300 eV, to treat the mutual resonance shielding between different uranium and plutonium isotopes. (Calculations made by Haggblom (20) show that a statistical treatment of the interaction effect between U238 and Pu239 resonances below 240 eV can be in error by a few percent). At higher energies

a statistical treatment is probably adequate to treat the mutual shielding effect between uranium and plutonium isotopes. However, there are important resonances at higher energies for which a statistical treatment would be unsatisfactory. One possible example is the 1.15 KeV resonance in iron which makes a major contribution to capture in fast reactor structural materials. The relative position of this resonance and U238 resonances could be important. In our data files there are large U238 resonances at 1.140 and 1.167 KeV.

The relative positions of the different resonances in a substance can be of significance if the spacing correlates with the fluctuations in the collision density (the source of scattered neutrons) caused by the resonances. When there are many resonances in an interval from E to 2E a statistical treatment of the spacing is satisfactory. A sub-group or probability table approach is acceptable for the representation of a number of resonances in an energy region when the collision density can be treated as constant through each resonance and the same in each resonance, (the maximum energy loss for scattering by U235 being 0.017E). This approximation can be used more generally to represent the variation of cross sections in an energy interval which is small compared with the maximum energy loss in scattering by uranium and plutonium isotopes. This is the approach adopted in the fine group libraries, FGL4 and FGL5, the fine group being sufficiently narrow compared with 0.017E for the within fine group cross sections to be regrouped into sub-group data (with up to 50 sub-groups per fine group in FGL5). It is necessary to take into account the temperature correlation in the sub-group data in order to treat a range of temperatures in a fuel element, although, for most applications, this temperature correlation is not required. In order to generate this probability table or sub-group data it is necessary to have energy point tabulations at a range of temperatures. Although probability table data can be derived from shielding factor measurements made for a range of material thicknesses it is better to derive an energy point representation first (via a resonance parameter analysis) because this can be Doppler broadened and the temperature correlations can be calculated.

Shielding factor representations of resonance structure, $f(T, \sigma_o)$ (in terms of temperature T and background cross section , σ_o) have a wide range of applications, but these are limited in the geometrical heterogeneity which they can treat by the available equivalence relationships and can only treat mutual shielding effects via average cross sections. Probability table data can be used in calculations for quite general geometries, as in the Monte Carlo code VIM (21).

It is considered preferable, therefore, to derive resonance parameter ladders and, from these, energy point tabulations, up to about 25 KeV, for the principal uranium and plutonium isotopes. Sub-group data can be derived from such energy point tabulations for use in more general geometry calculations and validated against the detailed representation in simple geometry reaction rate calculations.

3 Energy ranges for which resonance data are required

In the UK fast reactor cross section sets, resonance shielding is treated up to 300 KeV. This range was chosen to cover hard spectrum systems (such as metal fuelled and gas cooled fast reactors) and thick samples in which shielding effects are stronger than in normal compositions. For a typical sodium cooled fast reactor composition resonance shielding effects are calculated to be less than 1% at 300°K above the following energies:

U238 capture	75 Kev
Pu239 capture	15 KeV
Pu239 fission	3 KeV
Pu240 capture	3 KeV

The contributions to the individual reaction Doppler effects are calculated to be less than 1% and 5% respectively, above the following energies:

	1%	5%
U238 capture	50KeV	25Kev
Pu239 capture	15KeV	3KeV
Pu239 fission	200KeV	40KeV
Pu240 capture	20KeV	3KeV

The Pu239 and Pu240 Doppler effects are smaller than the U238 effect and so the significant energy range is below the 5% level for the plutonium isotopes.

In U238 85% of the fast reactor Doppler effect is calculated to come from energies below 5 KeV and so it is most important for the resolved resonance region data to be accurate. The Doppler effect is sensitive to the division of the total capture between s-wave and p-wave resonances (22) the main contribution coming from the s-wave resonances.

The Pu239 Doppler effect is a balance between the fission and capture terms, the net capture effect being about 70% of the fission effect. There is a difference between the energy dependences of the two components, as is shown in Table 1. Below 750 eV, (the energy range which contributes 75% of the capture component and 50% of the fission component) the two components are approximately equal. The net Pu239 Doppler effect is only about 5% of the U238 effect.

The Pu240 contribution to the fast reactor Doppler effect depends on the plutonium isotopic composition and is typically about 1% of the U238 Doppler effect.

4 Resonance shielding in fissile nuclides in thermal reactors

The resonance shielding factors in the three lowest energy s-wave resonances of U238 have values of about 0.06 in a PWR spectrum. The average resonance shielding factor in U235, however, is about 0.90 in the capture cross section and 0.96 in the fission cross section, the shielding being greatest in the energy range 5 - 25 eV where the shielding factor averages about 0.8 for the capture cross section and 0.9 for the fission cross section.

The shielding in Pu239 in a uranium fuelled thermal reactor depends on the fuel burnup and can be similar in magnitude to the shielding in U235. The mutual resonance shielding effects between U238 resonances and fission and capture in the fissile isotopes are typically about 20%.

For the fissile isotopes most capture and fission reactions occur in the thermal energy region, with about 10% in the resonance region. The resonance self-shielding and mutual shielding effects are of significance but an accuracy of about 10% in the prediction of these is probably adequate. The resonance parameters, must, of course, reproduce the average cross sections and eta values accurately in the resonance region.

5 Conclusions

The form in which data are required for reactor calculations in the resolved resonance regions and the more important energy ranges of the unresolved regions, (typically up to about 25 KeV) is either a single energy point tabulation or a single set of resonance parameters from which such a tabulation can be generated. In the unresolved resonance region this single set of parameters should be chosen to fit broad resolution infinite dilution partial and total cross section measurements and thick sample measurements. The energy point tabulation can be chosen to have a compact form (such as cubic spline) which is then expanded for reactor calculations. At higher energies, where resonance shielding and Doppler effects are small and many resonances contribute to the cross section in an energy range E to 2E, statistical resonance data are required.

For the estimation of cross section and shielding factor uncertainties simpler representations, in terms of uncertainties in average resonance parameters and their distributions, would be satisfactory.

Mutual shielding effects between the resonances of different substances, (such as U238 and Fe) could lead to a requirement for more accurate data on the relative energies of resonances.

The direct derivation of shielding factors, sub-group , or probability table data from thick sample measurements produces data which is useful for a wide range of reactor calculations, but cannot treat all effects, such as the effect of the temperature distributions within a fuel element. A resonance representation is preferable.

There are discrepancies between equivalent Debye temperatures deduced from different measurements and this discrepancy is significant in the interpretation of some Doppler effect measurement.

TABLE 1

Fast Reactor Doppler Effects and Resonance Shielding Factors

Relative Doppler effect per atom

Group	Lower Energy (KeV)	U238 capture	Pu239 capture	Pu239 fission	Pu240 capture
	302				
A	111	3	-	9	-
B	40.9	15	-	17	1
C	15.0	38	2	11	3
D	5.53	66	8	18	6
E	2.04	69	11	19	8
F	0.748	369	76	175	107
G	0.275	212	181	212	98
H	0.101	58	97	81	58
I	0.037	2	12	5	3

Resonance shielding factors at $300^{o}K$

Group	Lower Energy (KeV)	U238 capture	Pu239 capture	Pu239 fission	Pu240 capture
	111				
B	40.9	.99	-	-	-
C	15.0	.97	.990	.998	.99
D	5.53	.91	.987	.995	.99
E	2.04	.80	.985	.991	.98
F	0.748	.47	.952	.953	.97
G	0.275	.33	.820	.840	.87

REFERENCES

1 R J Brissenden and C Durston
Paper 20. Symposium on Fast and Epithermal Neutron Spectra in Reactors, Harwell (December, 1963). Also UKAEA Report AEEW-R622 (August, 1968).

2 J L Rowlands and J D Macdougall
Described in: Paper 1.16 International Conference on the Physics of Fast Reactor Operation and Design, London (June, 1969). Also report AEEW-M843.
For a disucssion on the sub-group, probability table or histogram method see:
M N Nikolaev. Bulletin of the Information Centre on Nuclear Data No. 3 Part II, (1966).
L B Levitt. N S & E 49, 450 (1972)
D E Cullen. N S & E 55, 387 (1974)
J D Macdougall. International Symposium on Physics of Fast Reactors Vol. III p.1172 Tokyo (October, 1973).

3 J L Rowlands et al
International Symposium on Physics of Fast Reactors Vol. III p.1133 Tokyo (October, 1973)

4 J R Askew, F J Fayers and P B Kemshell
Jour. Brit. Nuclear En. Soc. Vol. 5 p. 564 (1966)

5 Y Ishiguro et al
N S & E 40, 25 (1970)

6 T J Haste and M G Sowerby
UKAEA Report AERE-R8961 (January, 1978)

7 T Y Byoun, R C Block and T Semler.
Kiamesha Lake Meeting. CONF-720901, p.1115 (September, 1972)

8 A Gandini, M Petilli and M Salvatores
International Symposium on Physics of Fast Reactors. Vol. II, p.612, Tokyo (October, 1973).

9 M Salvatores
Paper to the Topical Meeting of the NEANDC.
Aix-en-Provence, (April, 1981).

10 J Bouchard.
Private communication. Thesis by Erradi to be published.

11 K Gregson, M F James and D S Norton
UKAEA report AEEW-M517 (1965)

12 M F James and J Story
To be published

13 D E Cullen
UCRL-50400. Vol. 17 Part B Rev. 2
(October, 1979).

14 M F James
UKAEA Report AEEW-M790
Winfrith Nuclear Data Group Notes on Topics in Nuclear Data
Evaluation, by M F James and J S Story (1968).

15 Golinelli et al
Proc. Conf. Advances in Reactor Physics and Shielding.
p.243 Sun Valley (September, 1980)
N. El Idrissi and H Tellier. SERMA/SPM No. 1442 "T"

16 F Y Tsang and R M Brugger. N S & E 72, 52 (1979)

17 A T D Butland. Annals of N S & E, 1 p.575 (1974)

18 B T M Willis. Proc . Roy. Soc. A 274 p.134 (1963)

19 Jackson and J E Lynn. Phys. Rev. 127 p.461 (1962)

20 E M Gelbard and R E Prael. ANL-75-2, p.201 (1975)

21 H Haggblom. Nukleonik 12, p189 (1969)

22 J L Rowlands. Proc. Conf. Nuclear Data Evaluation Methods and
Procedures p.23 Brookhaven (September, 1980)

"Resonance Parameter Data Uncertainty Effects
on Integral Characteristics of Fast Reactors"

M. SALVATORES[*], *G. PALMIOTTI*[*], *H. DERRIEN*[*],
E. FORT[*], *G. OLIVA*[**].

[*] *CEA - Cadarache - France*

[**] *CNEN - Casaccia - Italy*

ABSTRACT

Sensitivity studies are presented of integral parameters of interest for fast reactors to uncertainties of resonance parameters of U-238, Pu-239, Pu-240 and Pu-241. Consequences due to some uncertainty correlation hypothesis are also considered.

1 - INTRODUCTION

Resonance data for actinides play a major role in the calculations of fast neutron reactor neutronics characteristics. All major parameters, from critical mass to safety parameters, like the Doppler reactivity effect, are dependent on actinide nuclear data in the resonance region.

The reactor physicist is faced by a twofold problem, namely to correctly process the basic nuclear parameters in order to produce multigroup cross sections, and to assess the effects of the uncertainties that affect these basic data.

The first problem has been treated in detail in the years '70, and one should quote in particular the fundamental work in this field by R. HWANG at Argonne /1,2,3/ that lead to algorithms to process the resonance data. Even if it is not quite completely closed and uncertainties are still present in the basic data processing in the resonance regions, this problem will not be treated here.

In what follow we will try to indicate a methodology to assess the resulting uncertainties on integral parameters of interest for fast reactors and in particular the safety related parameters, due to uncertainties on the resonance parameters of U-238, Pu-239, Pu-240 and Pu-241.

First, sensitivity tables will be generated for separate variation of individual resonance parameters in selected energy regions. The sensitivity coefficients are relevant to the main integral and safety related parameters of a typical large power fast reactor, i.e. Keff, control rod worth, Doppler and sodium void reactivity coefficients, breeding gain, and are calculated according to the standard methods of generalized perturbation theory.

Both infinite dilution and self-shielding effects will be considered separately.

Finally, several hypothesis of correlation of data uncertainties will be used, to indicate, if possible, realistic estimates of integral parameters uncertainties. This is by far the most delicate point in the uncertainty analysis, and the present work is intended only to point out the main areas where more work is needed.

For what concerns the consistency between integral and differential data, the ideas of the consistent method of basic data adjustement are recalled, and an experimental program to be performed on the critical facility ERMINE indicated, which will be mainly devoted to the low energy data validation ($E \leqslant 50$ KeV).

In fact, resonance data can be considered to be mainly related to the energy range below 50 KeV and in this energy region the number of significant clean integral experiments, which have been widely used

in the past in many leading programs of Fast Reactors to validate or to adjust basic data, have been fairly scarce.

2 - SENSITIVITY ANALYSIS

2.1 - Basic Hypothesis

The standard techniques of the generalized perturbation methods /4/ were used to calculate sensitivity coefficients defined, for each isotope, as :

$$S_{iKj} = \frac{\partial R_i}{R_i} \Big/ \frac{\partial p_{Kj}}{p_{Kj}} \qquad (1)$$

Where R_i is the following set of integral parameters, calculated in diffusion theory in one-dimension, for a large 1200 MWe fast power reactor of the homogeneous type (see table I) :

- Keff
- control rod worth of a two absorber ring system of partially inserted rods, for a total antireactivity of :

$$\varrho = -1.31 \ \% \ \Delta K/K$$

- core Doppler reactivity coefficient (ΔT = 1500 K)
- internal core sodium void scattering component
- total breeding ratio.

The reference values of the R_i parameters calculated with the CARNAVAL IV formulaire are shown in table II. The P_{Kj} represent parameters of type K in energy range ΔE_j and they are indicated in table III.

The hypothesis in the calculation of the sensitivity coefficients S_{iK} was that of complete independence of each type of resonance parameter for each isotope. The correlations that actually can occur among parameters will be introduced at the moment of the use of the sensitivity coefficients, and their folding with data uncertainties (see paragraph 4).

For what concerns energy correlations, the following hypothesis were used.
First, for sake of simplicity, and to reduce the amount of computational work, the energy range of interest (i.e. approximately from 100 keV to 100 eV) was subdivided according to a standard multigroup cross-section scheme, based on half - lethargy widths (see table IV). In each energy range (corresponding to a group, in a multigroup scheme), all the parameters of each resolved resonance (or energy point where average parameters are defined, in the unresolved resonance region) which falls in that energy range, were varied simultaneously. In this way, each S_{iKj} actually represents the variation of the integral parameter R_i due to the variation of all the parameters of type K in the energy range j, all of the same percentage amount.

The different energy ranges were not correlated at this stage. Correlations in energy will be introduced successively.

The advantage of this type of definition of the sensitivity coefficients is that physical correlation of different type, related to different evaluation techniques or to different conservation hypothesis, can be introduced using always the same basic set of sensitivity coefficients S_{iKj}.

Finally, it should be noted that, in the case of partial width variation $\delta\Gamma_x$, the total resonance width was varied accordingly :

$$\frac{\delta\Gamma}{\Gamma} = \frac{\delta\Gamma_x}{\Gamma_x} \frac{\Gamma_x}{\Gamma} \qquad (2)$$

2.2 - Self-shielding effects

The expression of S_{iKj} can be given more explicitely if one adopts the Bondarenko formalism of self-shielding factors :

$$S_{iKj} = \frac{\partial R_i}{\partial \sigma_j} \frac{d\sigma_j}{dp_{Kj}} \frac{p_{Kj}}{R_i} = \qquad (3)$$

$$\left(\frac{\partial R_i}{\partial \sigma_{\infty j}} \frac{d\sigma_{\infty j}}{dp_{Kj}} f_j + \frac{\partial R_i}{\partial f_j} \frac{df_j}{dp_{Kj}} \sigma_{\infty j} \right) \frac{p_{Kj}}{R_i} = S^{\infty}_{iKj} + S^{f}_{iKj}$$

The two terms in equation (3) correspond to the effects of the variation of the resonance parameters p_{Kj} on the infinite dilution cross section $\sigma_{\infty j}$ and on the self-shielding factor f_j, according to the prescription that :

$$\sigma_j = \sigma_{\infty j} f_j \qquad (4)$$

Even if in general the self-shielding effects are thought to be smaller than the infinite dilution cross-section effects in particular for the Pu isotopes, for which the f values are usually close to one, the self-shielding effects can play a significant role in the resolved resonance region for U-238, for which the f values can be fairly far from the asymptotic values in the standard fast reactor fuel composition (see table V).

In summary the following procedure was adopted :

1 - Calculate by means of standard GPT methods in one dimension (code system HOPES developed at CADARACHE /6/), the sensitivity of the integral parameters R_i to multigroup data σ_j.

2 - Calculate by means of standard cross section processing codes, compatible with the Bondarenko format, the sensitivity of the multigroup $\sigma_{\infty j}$ and f_j values to the variation of the resonance parameters p_{Kj}. The base data file used for the calculation of this step was ENDF/B-IV and the resonance parameter variation for the different energy intervals, according to what was said in paragraph 2.1, was chosen to be ± 20%. Linearity tests were carried out to verify the validity of this procedure.

3 - Folding of the sensitivity coefficients generated in step 1 and 2 to produce the sensitivity coefficients of tables VI - XI.

It should be again stressed that, in view of the hypothesis of the Γ variation due to Γ_x variation (see equation 2), in the case of Pu-239 and Pu-241 σ_f and σ_c variations were both involved as a consequence of Γ_γ (or Γ_f) variations.

This is obviously the case of $<D>$ variations.

Conservation and correlation laws will be introduced in a later stage, as already mentioned.

2.3 - Comparison with previous sensitivity calculations

Previous sensitivity studies on resonance parameters effects can be found in References 7, 8, 9, 10, 11.

In particular, the relevance of the self-shielding factors was indicated in Ref. 8 with simplified calculation for isolated resonances. In Ref. 7 an example was worked out to show the relevance of p-wave parameter effects on U-238 cross sections. By the way, it is interesting to note that in that work the conservation laws were directly taken into account in the definition of the sensitivity coefficients.

The present work however gives data in a format directly exploitable to assess the consequences of parameters uncertainties on integral reactor parameters, together with the impact of different uncertainty correlation rules.

3 - NUMERICAL RESULTS

3.1 - Infinite dilution cross section variation effects

In table VI - XI the calculated sensitivity coefficients are shown for the effects due to σ_∞ (S^{∞}_{iKj} coefficients of expression 3).

The most important effects are obviously found for Pu-239 and U-238 data. Minor effects, shown only for Keff and control rod antireactivity, are found in the case of Pu-240 and Pu-241 (Tables X-XI) For what concerns the different integral parameters, the sensitivity coefficients are shown group-wise (energy group structure in Table IV), for the energy groups which cover the energy range 40 KeV - 200 eV.

K_{eff} effects are clearly shown both in the case of U-238 and of Pu-239 resonance parameters. In this last case, the hypothesis of combined variation of Γ_γ (or Γ_f) and Γ, leads to sensitivities to Γ_γ on Γ_f variations which are comparable in the energy region < 1 KeV, where Γ_n becomes negligible , due to the compensating effects on $\nu\sigma_f$ and σ_a. The $g\Gamma_n$ and $<D>$ effects are shown separately, even if the most reasonable way to look to these effects should be in the light of a constant (and fairly well known) strenght function value S_o.

Relatively small effects are found on the Doppler reactivity coefficient. It is to be noted that, in the case of the U-238 resonance parameters, the sensitivity coefficients shown in the table take into account both the effect on the cross section variation due to the temperature and the flux variation effects. In fact, if we define the Doppler coefficient in a simplified way as :

$$\varrho_D = \int_{\Sigma_j} \left(\sigma^{T_1}_{U\text{-}8} - \sigma^{T_2}_{U\text{-}8} \right)_j \phi_j \, \phi_j^+ \, dV \qquad (5)$$

$$= \int_{\Sigma_j} \Delta\sigma_j^T \, \phi_j \, \phi_j^+ \, dV$$

one can write formally :

$$d\varrho_D = \int \left(\sum_j d(\Delta\sigma^T)_j \, \phi_j \, \phi_j^+ + \sum_j \Delta\sigma_j^T \, (d\phi_j + d\phi_j^+) \right) dV \qquad (6)$$

where $d(\Delta\sigma^T)$, $d\phi$ and $d\phi^+$ are the variation induced by the resonance parameter variations.

In the case of Pu-239, only $(d\phi + d\phi^+)$ effects are present.

In the case of the sodium void scattering component, the integral parameter taken into account is, in a simplified form :

$$\varrho_{Na} = \int_{\text{core 1}} \Sigma_{jK} \, N_{Na} \, \sigma^{Na}_{j \to K} \, \phi_j \, (\phi_K^+ - \phi_j^+) \, dV \qquad (7)$$

For this parameter only $d\phi$ and $d\phi^+$ effects are present, and, due to the peculiar form of the adjoint function ϕ^+ at low energies, these effects are fairly large both in the case of U-238 and of Pu-239.

Small effects, but not negligeable in view of the high precision requirements, are found in the case of the control rod system antireactivity. For this parameter the accuracy requirements of few percent, are such that even 1÷2% uncertainty due to low energy data, can be significant.

For all the integral parameters studied, it is valid the commentary previously made on Γ_f and Γ_γ variation effects in the case of Pu-239.

Moreover, it should be noted the compensating effects of the variation of $<D>$ and Γ_γ in the case of the unresolved resonance region for U-238, due to the large values of $g\Gamma_n$ in that energy range ($g\Gamma_n \approx 10$ times Γ_γ).

3.2 - Self - shielding variation effects

As it was previously described (see paragraph 2.2), self-shielding factor variation effects have been considered in the case of the variation of U-238 resonance parameters in the resolved resonance region. The main results are shown in table XII. The effects are smaller than the effects on the infinite dilution cross-section and non negligible only in few cases.

For what concerns the unresolved resonance region in principle one can say that apparently self-shielding effect can play a minor role. However two recent results indicate that much care should be exerced in dealing with these effects.

First, a recent self-shielding measurement in the USSR (Ref. 12) have indicated that the experimental self-shielding factor for U-238 capture, can be different from the calculated value by approximately 5 ÷ 10% in the energy region between 100 KeV and 20 KeV for a potential σ_p cross section corresponding approximately to the range 1 - 10 barns.

Second, calculations performed at ORNL /Ref. 7/ have shown that a large self-shielding variation effect can be obtained at approximately 20 KeV if the average p-wave neutron width is changed, with a corresponding change in the average s-wave neutron width, to keep constant the infinite dilution cross section.

Actually, this is directly consequence of the fact that at these energies the self-shielding is mainly due to the narrow p-wave resonances, which contribute for approximately 30% ($< \sigma_R >_{l=0} \; / \; < \sigma_R >_{l=1} \; \tilde{\approx} \; 2.8$) to the resonant cross-section if one takes as p-wave and s-wave strenght function the following values :

$$S_o \tilde{\approx} \; 1.17 \times 10^{-4}$$

$$S_1 \tilde{\approx} \; 1.93 \times 10^{-4}$$

Calculations similar to those of ref. 7 have been performed for U-238. $< \Gamma_n >_{l=1}$ has been changed by + 5% , and $< \Gamma_n >_{l=0}$ has been changed to keep constant the infinite dilution cross-section. The following results have been obtained at 300°K :

Energy Group \ σ_p (barn)	1	10	50	100
10	.02	- 0.01	- 0.06	- 0.08
11	0.32	- 0.11	- 0.27	- 0.38
12	0.95	0.29	- 0.11	- 0.27
13	1.61	0.90	0.19	0.0
14	2.09	1.41	0.76	0.45
15	1.61	1.08	0.64	0.42

(Percentage values of self-shielding factor variation).

Of course, a similar calculation can be performed with a different combination of S and p wave $< \Gamma_n >$ values. As an example, the variation of $< \Gamma_n >_{l=1}$ of + 20% , (with the corresponding $< \Gamma_n >_{l=0}$ variation to keep σ_∞ constant), gives a variation of 4,14 % in the self-shielding factor of the 15 th group (energy range 5.53-3.36 KeV) at σ_p = 10 b.

Finally the same calculations for T = 1800°K, show the following effects on the Doppler related self-shielding variation for U-238 :

$$\left[\left(f'(1800K) - f'(300K)\right) - \left(f(1800K) - f(300K)\right)\right] / \left(f(1800K) - f(300K)\right)$$

where f'represent the self-shielding factors obtained with a variation of $< \Gamma_n >_{l=1}$ of + 5 %, as explained above :

Energy Group \ σ_p (barn)	1	10	50	100
10	- 1.3	- 5.71	- 8.17	- 9.24
11	- 6.64	- 2.84	- 10.26	- 10.54
12	- 11.36	- 9.08	- 10.0	- 12.87
19	- 7.54	- 9.38	- 8.2	- 10.27
14	- 3.07	- 4.10	- 7.07	- 6.43
15	- 0.49	- 1.17	- 2.4	- 2.67

(percentage values of the Doppler related self-shielding variation)

If these hypothesis are made (i.e. p wave and s wave parameter changes without affecting σ_∞) , $\delta\sigma/\sigma$ is equal to $\delta f/f$ and a new type of TABLE XII, related to high energies, where p-wave effects are important, can be written :

Energy Group	Na void	Doppler	Keff	Control Rod Antireactivity
10	.0	- 0.14	.0	.0
11	.0	- 0.36	.01	.0
12	- .01	- 0.70	.0	.0
13	+ .06	- 0.75	- .01	- .02
14	+ .07	- 0.26	- .02	- .03
15	- .10	- 0.16	- 0.1	- .02

(percentage values, relative to $< \Gamma_n >_{l=1}$ variation of + 5%)

Except for Doppler, these values are fairly small, but, as wehave seen,they are dependent on the hypothesis made an parameter variation.

Finally, the entire validity of the EDNF/B technique to represent resonance effects in this energy region, should be tested against more extended resolved resonance type representation.

3.3 - Effects on breeding

In table XIII the effects of the resonance parameter variations are shown in the case of the total breeding ratio.

The general trends already observed are again found here, and in general significant effects are found, mainly related to direct changes in the capture cross-section of U-238 and absorption cross-section of Pu-239. The data shown are relevant to the infinite dilution cross-section variations.

4 - CORRELATION HYPOTHESIS

The indicative results of the previous paragraphs are strongly dependent on the correlations that are assumed on the uncertainties on the separate resonance parameters. We recall that no explicit correlation was taken into account, nor among different resonance parameter neither in energy.

However, correlations play a central role in assessing realistic estimates of integral parameters, but are a difficult task to be properly established.

In fact they depend on the evaluation techniques used to establish the basic data files, on the experimental data type used, and on the model chosen to represent the different corss-sections.

Since the data of the previous paragraph were based on the simplest hypothesis, mainly the zero-correlation hypothesis (which is by no means the most realistic), we will try in what follows to examine the consequences of other correlation hypothesis.

Case A - For each resonance parameter type p_K a complete energy correlation hypothesis is introduced, which covers both the resolved and the unresolved resonance ranges.

Case B - In the unresolved resonance region the $< D >$ and $< \Gamma_n^o >$ values are completely correlated in order to keep constant, within an uncertainty limit, the S_o strength function.

Case C - A correlation was introduced among the Γ_γ and Γ_f values of Pu-239 in order to avoid extreme changes in the σ_c / σ_f ratio. Since the variation of both parameters produces a nearly constant $\delta\nu\sigma_f - \delta\sigma_a$ value (and of opposite sign), a correlation hypothesis was used, with the introduction of fictitious correlation coefficients (1, 0.8, 0.5 and 0.3).

Case D - A total width conservation law is considered by means of the correlation between Γ_n and Γ_γ (or Γ_f).

This last type of correlation was introduced both in the case of U-238 and of Pu-239. Several fictitious correlation coefficients (1, 0.8, 0.5 and 0.3) were introduced to simulate different ratios between the two parameters.

Obviously, more hypothesis should be compared on the basis of the particular stategy followed in each evaluation. The data presented here, can however indicate major trends.

The numerical results are shown in table XIV and XV. The uncertainty on Keff and on the sodium void coefficient are the most significant and are strongly dependent on the correlation hypothesis adopted.

Several correlation hypothesis lead to uncertainties on Keff from ± 0.2% to ± 0.5% ΔK/K and to uncertainties on the sodium void scattering component up to 10%. Effects on the Doppler coefficient are, on the contrary, fairly small, due to compensating effects in the $\Delta\sigma_T^{U-238}$. It should be mentioned that other effects related to resonance parameters uncertainties could be introduced at very high temperatures /13/ or in the unresolved resonance region, according to what was previously discussed. Finally, it should be recalled that no multilevel effects were treated in the present work, and that the conclusion of previous work in this field /14,15/, indicated small effects due to the multilevel formalism.

For what concerns the control rod system worth, the small effects obtained can became not negligible, in view of the high accuracy required for this integral parameter.

5 - INTEGRAL EXPERIMENTS AND DATA ADJUSTEMENTS

The results presented in the previous sections are related to a large fast power reactor. The sensitivity, when they are significant, are related to the low energy range (generally < 10 KeV).

The data used in many leading fast reactor programs for neutronics calculations, have been adjusted using the so-called clean integral experiments /16-17-18/.

However, many of these experiments have shown a limited sensitivity to the low energy data. This means that low energy data (i.e. mainly in the resonance region) have been seldom adjusted, and that some integral parameter in fast power reactors can be affected directly by resonance parameter uncertainties in a significant way.

Moreover, future design of large fast power reactors can put even stronger emphasis on the low energy spectrum.

The situation is represented in fig.1, where the product $\phi_j \phi_j^+$ is plotted as a function of the energy group :

a) in the case of the power reactor considered as a reference in this work,

b) in the case of the large core used as Benchmark for comparison and proposed by NEACRP /19/ and

c) in the case of a typical fast reactor critical assembly.

With the aim to gain informations on this energy region data, ad-hoc tailored spectra will be obtained in an experimental program on the critical facility ERMINE at CADARACHE, to enhance the low energy neutron contribution. This will be mainly obtained with the introduction of graphite in $K_\infty \approx 1$ media with PuO_2/UO_2 fuel.

A larger sensitivity will be obtained to Pu-239 and U-238 data at energies lower than 10 KeV.

The analysis of these experiments could be done using sensitivity and uncertainty analysis of the type outlined in the preceding paragraphs in such a way that adjustments could be envisaged on the most signifiant resonance parameters, according to the principle of the so-called consistent method of basic parameter adjustment /5/.

6 - CONCLUSIONS

In the present paper an attempt has been made to indicate the main consequences on integral, mainly safety related, parameters of fast reactors due to the uncertainties on the resonance parameters of the major actinides (U-238, Pu-239, Pu-240 and Pu-241).

As expected, these consequences are strongly dependent on the assumed uncertainty level on individual parameters and their correlations. The 20% uncertainty value, assumed in the present work, can be considered as an upper limit at the present state of the art in this field for most parameters. Moreover, the uncertainties of different parameters are certainly correlated and the good knowledge of total cross-sections (and of total resonance widths), must also be taken into account.

However, numerical results have indicated that, for many significant resonance parameters like U-238 $g\Gamma_n$ in the resonance region and Γ_γ and Γ_f of Pu-239 in the unresolved resonance region, uncertainties in the range $\pm$ 5 - 10% are necessary to mesure a good use of standard integral experiments to produce both adjusted data or bias factors for the design calculation of large power reactors.

In fact, higher uncertainties will produce in a reference design system uncertainties on Keff, Sodium void effects, control rod system worth etc... which could not be easily related to the standard integral experiment results due to the different sensitivities to low energy data in critical experiments and in large power reactor configurations.

In this context, uncertainties on Pu-240 and Pu-241 play a more limited role. A further source of uncertainty, which was only touched upon in this paper, could be a substantial uncertainty in the calculation of self-shielding factors in the unresolved resonance region (case of U-238 in particular) due to both not yet entirely explained p-wave data effects, and cross-section representation in this energy range. This type of uncertainty seems to be pointed out by recent experimental results obtained in the USSR.

Finally, some low energy data dependent integral parameter, not mentionned in the present report, like structural material activation, can also be strongly influenced by the quality of the major actinide data in energy region below 10 KeV and should enhance the need for higher accuracy data.

The first step towards meeting these requirements should be however an appropriate assessment of resonance parameter uncertainties and their correlation within the current evaluated data files, and with the performance of ad-hoc integral experiments, enhancing the low energy neutron importance, which should be coupled to sensitivity and consistency analysis based on a consistent method of resonance parameter ajustment.

7 - REFERENCES

1 - R.N. HWANG
Nucl. Sci. Eng. 36, 67 (1969)

2 - R.N. HWANG
Nucl. Sci. Eng. 36, 82 (1969)

3 - R.N. HWANG
In ANL-7710, pag. 387 (1970) and in ANL-7910, pag. 475 (1971)

4 - See, among many references, A. GANDINI
J. Nucl. Energy 21,755 (1967)

5 - A. GANDINI , M. SALVATORES
"Nuclear Data and Integral Measurements Correlation for Fast Reactors. Part 3 : The consistent Method"
CNEN -RT/FI (74)3 (1974)

6 - G. PALMIOTTI
Private communication

7 - J.L. MUNOZ COBOS, G. de SAUSSURE, R.B. PEREZ
Trans. Am. Nucl. Soc. 38, 666 (1981)

8 - E. GREENSPAN et al.
In ORNL - RSIC - 42 (1979)

9 - S. GANESAN
Nucl. Sci. Eng. 74, 49 (1980)

10 - G.U. ANTSIPOV et al.
INDC (CCP) 143/GJ, IAEA Translation Vienna (1980)

11 - F.G. PEREY
"Estimated Uncertainties in Nuclear Data. An approach"
Proc. Conf. Nucl. Cross Sections and Tech.
NBS - SP 425 (1978)

12 - V.N. KONONOV et al.
In INDC (CCP) - 169G (Kiev Conference 1980)

13 - A.T.D. BUTLAND et al.
"An assessment of methods of Calculating Doppler effects in Pu-fuelled fast reactors".IAEA SM-244/32 (1980)

14 - R.N. HWANG
"Theoretical Considerations Pertinent to the Treatment of Unresolved Resonances" in BNL 50387 (ENDF - 187) (1973)

15 - C.L. COWAN "Resonance Treatment in Reactor Applications"
ibidem

16 - J.L. ROWLANDS et al.
"The production and performance of the adjusted cross-sections set FGL5" Proc. Int. Symp. on Physics of Fast Reactors, Tokyo (1973) Paper A30

17 - H. KUROI et al.
"Arts and Effectiveness of Data Adjustment"
Trans. Am. Nucl. Soc. 27, 877 (1977)

18 - J.P. CHAUDAT et al.
"Data Adjustments for Fast Reactor Design",
Trans. Am. Nucl. Soc. 27, 877 (1977).

19 - L. LESAGE et al ANL-80-78 (1980).

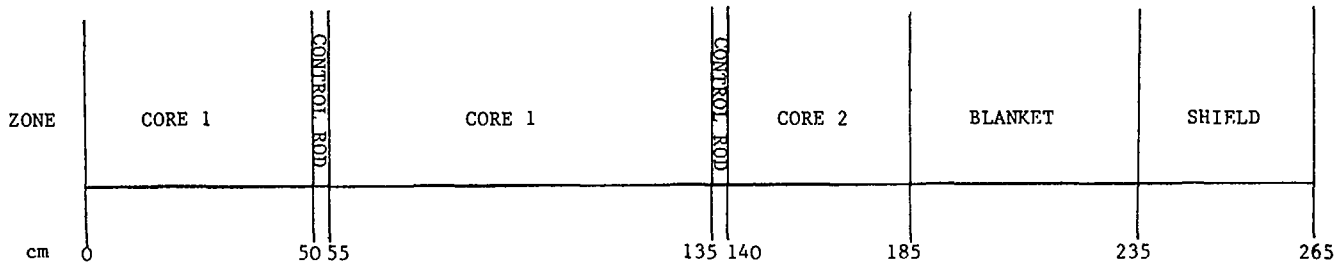

ENRICHMENT ($Pu\ O_2/UO_2$)	14%	14%	17%

TABLE 1 - 1200 MWe FAST REACTOR GEOMETRY SPECIFICATIONS
(1D CYLINDRICAL GEOMETRY, $B^2_{AX} = 5.4 \times 10^{-4}$)

TABLE II - SENSITIVITY COEFFICIENTS WERE CALCULATED FOR THE FOLLOWING R INTEGRAL PARAMETERS

1 - Keff (= 1.0087)

2 - Core Doppler reactivity (ΔT = 1500 °K ϱ = -1.92% $\Delta K/K$)

3 - Internal core sodium coefficient
(Scattering component ϱ = 1.25% $\Delta K/K$)

4 - Control rod system worth (insertion equivalent to ϱ = -1.31% Δ K/K)

5 - Total breeding ratio (=.96).

TABLE III RESONANCE PARAMETERS CONSIDERED

U-238 : s-wave $g\Gamma_n$, Γ_γ both in the resolved (100 eV - 4 KeV) and unresolved resonance range (4-45 KeV) and $< D >$ in the unresolved range.

Pu-239 : s -wave, J=0 and J=1 $g\Gamma_n$, Γ_γ and Γ_f both in the resolved (100 - 300 eV) and in the unresolved range (300 eV - 25 KeV) and $< D >$ in the unresolved range.

Pu-240 : s-wave $g\Gamma_n$ and Γ_γ in the resolved (100 eV - 3.9 KeV) and unresolved range (3.9 KeV - 40 KeV), and $< D >$ in the unresolved range.

Pu-241 : s-wave $g\Gamma_n$, Γ_γ, Γ_γ and $< D >$ in the unresolved resonance region (100 eV - 52.4 KeV).

TABLE IV

ENERGY STRUCTURE

Group	Upper Energy
10	67.4.KeV
11	40.9
12	24.8
13	15.0
14	9.12
15	5.53
16	3.36
17	2.04
18	1.23
19	.748
20	.454
21	.275 (to .101 KeV)

TABLE V

U-238 CAPTURE SELF-SHIELDING FACTORS FOR POTENTIAL SCATTERING σ_p = 50b

Group	f
16	.719
17	.570
18	.465
19	.367
20	.322
21	.120

TABLE VI

U-238 Sensitivity Coefficients of Integral parameter R to variation of 20% of Resonance parameter p (percentage values). Effects due to σ_∞ variation.

Energy group	Na void			Doppler		
	$g\Gamma_n$	Γ_γ	$<D>$	$g\Gamma_n$	Γ_γ	$<D>$
10	-.02	.0	.01	.01	-.02	.01
11	-.02	- .01	.03	.0	-.15	.13
12	.04	.57	- .53	.0	-.36	.31
13	.17	1.17	-1.17	-.05	-.51	.53
14	.15	.70	- .74	-.10	-.60	.61
15	-.34	-1.58	1.04	-.16	-.79	.53
16	.09	.25	-	-.12	-.35	-
17	1.45	4.05	-	-.47	-.13	-
18	1.76	3.88	-	-.64	-1.40	-
19	1.65	2.09	-	-.54	-.87	-
20	.77	.83	-	.34	-.37	-
21	.50	1.12	-	-.29	-.55	-

TABLE VII

U-238 Sensitivity coefficient of integral parameter R to variation of 20% of resonance parameter p (percentage values). Effects due to σ_∞ variation.

Energy group	K_{eff}			Control Rod antireactivity		
	$g\Gamma_n$	Γ_γ	$<D>$	Γ_γ	$g\Gamma_n$	$<D>$
10	.0	-.02	.02	-.01	.0	.01
11	-.01	-.10	.10	-.10	-.01	.09
12	-.01	-.17	.17	-.22	-.01	.21
13	-.03	-.18	.19	-.31	-.04	.31
14	-.03	-.15	.17	-.30	-.07	.32
15	-.03	-.16	.11	-.29	-.09	.20
16	-.02	-.06	-	-.11	-.04	-
17	-.06	-.15	-	-.58	-.16	-
18	-.06	-.13	-	-.63	-.27	-
19	-.04	-.06	-	- .43	-.25	-
20	-.02	-.02	-	-.20	-.19	-
21	-.01	-.02	-	-.33	-.14	-

TABLE VIII

Pu-239 Sensitivity Coefficients of Integral Parameter R to variation of 20% of resonance parameter p (percentage values). Effects due to σ_∞ variation.

Energy group	Na void				Doppler			
	$g\Gamma_n$	Γ_f	Γ_γ	$<D>$	$g\Gamma_n$	Γ_f	Γ_γ	$<D>$
12	.32	.02	.18	-.46	-.52	-.17	-.05	.65
13	-.35	-.38	.48	.20	-.51	-.10	-.11	.64
14	.12	-.10	.23	- .23	-.45	-.06	-.13	.56
15	2.12	.10	-.83	-1.98	-.46	-.02	-.18	.58
16	.0	-.09	.14	-.05	-.28	.0	-.13	.36
17	-5.27	-2.90	2.92	4.44	-.49	.28	-.57	.69
18	-6.03	-3.48	3.32	5.26	.16	.63	-.82	.04
19	-4.78	-2.58	2.57	4.04	.50	.66	-.83	-.26
20	-2.29	-1.75	1.79	1.25	.34	.56	-.63	-.12
21	-1.83	-1.66	1.62	-	.42	.66	-.68	-

TABLE IX

Pu-239 Sensitivity Coefficients of Integral Parameter R to variation of 20% of resonance parameter p (percentage values). Effects due to σ_∞ variation.

Energy group	K_{eff}				Control Rod Antireactivity			
	$g\Gamma_n$	Γ_f	Γ_γ	$<D>$	$g\Gamma_n$	Γ_f	Γ_γ	$<D>$
12	.25	.16	-.11	-.26	-.16	-.02	-.07	.22
13	.23	.13	-.10	-.22	-.11	.02	-.10	.17
14	.17	.09	-.08	-.15	-.06	.04	-.10	.11
15	.14	.08	-.07	-.12	-.04	.05	-.10	.08
16	.07	.04	-.04	-.06	-.01	.03	-.06	.03
17	.23	.12	-.12	-.19	.22	.26	-.34	-.11
18	.20	.11	-.11	-.18	.49	.43	-.47	-.38
19	.14	.07	-.07	-.12	.50	.41	-.47	-.36
20	.06	.05	-.05	-.03	.29	.36	-.39	-.13
21	.04	.04	-.04	-	.35	.44	-.45	-

TABLE X

Pu-240 Sensitivity Coefficients of Integral parameter R to variation of 20% of Resonance parameter p (percentage values). Effects due to σ_∞ variation.

Energy Group	Na void		Doppler		K_{eff}	Control Rod worth
	$g\Gamma_n$	Γ_γ	$g\Gamma_n$	Γ_γ	Γ_γ	Γ_γ
12	.01	.04	.0	-.02	-.01	-.02
13	.02	.07	-.01	-.03	-.01	-.02
14	.01	.04	-.01	-.03	-.01	-.02
15	-.02	-.08	-.01	-.04	-.01	-.02
16	.01	.02	-.01	-.02	.0	-.01
17	.16	.44	-.06	-.14	-.02	-.06
18	.24	.60	-.10	-.21	-.02	-.10
19	.25	.22	-.11	-.09	-.01	-.05
20	.24	.28	-.11	-.13	-.01	-.07
21	.35	.27	-.18	-.13	-.01	-.08

TABLE XI

Pu-241 Sensitivity Coefficients of Integral Parameter R to variation of 20% of Resonance parameter p (percentage values). Effects due to σ_∞ variation

Energy Group	Na void				K_{eff}	
	$g\Gamma_n$	Γ_f	Γ_γ	< D >	$g\Gamma_n$	< D >
10	.02	.01	.0	-.02	.01	-.01
11	.05	.02	-.01	-.06	.02	-.02
12	.01	.0	.01	-.02	.02	-.02
13	-.05	-.03	.02	.05	.02	-.02
14	.0	-.01	.01	.0	.02	-.02
15	.20	.08	-.05	-.20	.01	-.01
16	-.01	-.01	.01	.01	.01	-.01
17	-.52	-.19	.15	.49	.02	-.02
18	-.48	-.17	.15	.44	.02	-.01
19	-.35	-.13	.11	.31	.01	-.01
20	-.24	-.09	.08	.22	.01	-.01
21	-.18	-.06	.06	.16	.0	.0

TABLE XII

U-238 Sensitivity Coefficients of Integral Parameter R to variation of 20% of Resonance Parameter p (percentage values). Effects due to self-shielding factor variation.

Energy Group	Na void		Doppler		K_{eff}		Control Rod antireactivity	
	$g\Gamma_n$	Γ_γ	$g\Gamma_n$	Γ_γ	$g\Gamma_n$	Γ_γ	$g\Gamma_n$	Γ_γ
16	-.03	-.04	.03	.06	.01	.01	.01	.02
17	-.33	-.91	.11	.03	.01	.03	.04	.13
18	-.47	-.88	.17	.32	.02	.03	.07	.14
19	-.80	-.37	.26	.15	.02	.01	.12	.08
20	-.35	-.17	-.15	.08	.01	.0	.09	.04
21	-.27	-.07	.15	.03	.01	.0	.07	.02

TABLE XIII

U-238 and Pu-239 Sensitivity Coefficients of Total Breeding Ratio to variation of 20% of Resonance Parameter p (percentage values).

Energy group	U-238			Pu-239			
	$g\Gamma_n$	Γ_γ	$<D>$	$g\Gamma_n$	Γ_f	Γ_γ	$<D>$
10	.01	.08	-.08	.0	.0	.0	.0
11	.07	.45	-.45	-.01	.0	.0	.01
12	.13	.75	-.76	-.54	-.12	-.16	.72
13	.16	.76	-.80	-.54	-.09	-.14	.67
14	.15	.64	-.69	-.44	-.06	-.11	.54
15	.16	.65	-.44	-.41	-.05	-.10	.49
16	.08	.22	-	-.22	-.03	-.06	.26
17	.22	.59	-	-.70	-.05	-.12	.76
18	.21	.45	-	-.63	-.05	-.08	.66
19	.13	.21	-	-.46	-.03	-.06	.48
20	.07	.08	-	-.25	-.01	-.02	.17
21	.05	.10	-	-.20	-.01	-.02	-

Table XIV

U-238 Resonance Parameter Uncertainty.
Effects (Standard Deviations in % due to ± 10% uncertainty in each parameter).

Correlation Hypothesis		K_{eff}	Na void	Doppler	Control Rod worth
No energy correlation :	$g\Gamma_n$	± 0.05	± 1.50	± 0.54	± 0.60
	Γ_γ	.21	3.26	1.09	.24
	$<D>$	.17	.90	.51	.27
Complete energy correlation	$g\Gamma_n$	± 0.16	± 3.10	± 1.01	± 1.75
	Γ_γ	.61	6.53	3.08	.63
	$<D>$	.38	6.8	1.06	.54
Correlation between $g\Gamma_n$ and $<D>$		± 0.14	± 2.56	± 0.16	± 1.30
Correlation between Γ_n and Γ_γ with correlation coefficient W =	1.	± 0.45	± 3.43	± 2.06	± 1.14
	0.8	.33	2.13	2.45	1.25
	0.5	.24	.17	.54	1.44
	0.3	.02	1.14	.08	1.56

Table XV

Pu-239 Resonance Parameter Uncertainty.
Effects (Standard deviations in % due to ± 10% uncertainty in each parameter).

Correlation Hypothesis		K_{eff}	Na void	Doppler	Control Rod worth
No energy correlation :	$g\Gamma_n$	± 0.27	± 5.00	± 0.68	± 0.44
	Γ_f	.15	2.88	.65	.43
	Γ_γ	.14	2.78	.81	.48
	$<D>$	.25	4.17	.73	.32
Complete energy correlation	$g\Gamma_n$	± 0.77	± 9.00	± 0.64	± 0.74
	Γ_f	.44	6.41	1.22	1.01
	Γ_γ	.39	6.20	2.06	1.27
	$<D>$	.66	6.22	1.55	.19
Correlation between $g\Gamma_n$ and $<D>$		± 0.23	± 4.00	± 0.61	± 0.59
Correlation between Γ_n and Γ_f with correlation coefficient W = (complete correlation in energy)	1.	± 0.32	± 2.59	± 1.90	± 0.27
	0.8	.41	3.87	1.62	.07
	0.5	.54	5.79	1.25	.23
	0.3	.63	7.07	1.01	.43
Correlation between Γ_n and Γ_f with correlation coefficient W = (complete correlation in energy)	1.	± .05	± .20	± 0.85	± 0.28
	0.8	.13	1.44	.43	.0
	0.5	.25	3.30	.19	.37
	0.3	.33	4.55	.60	.63

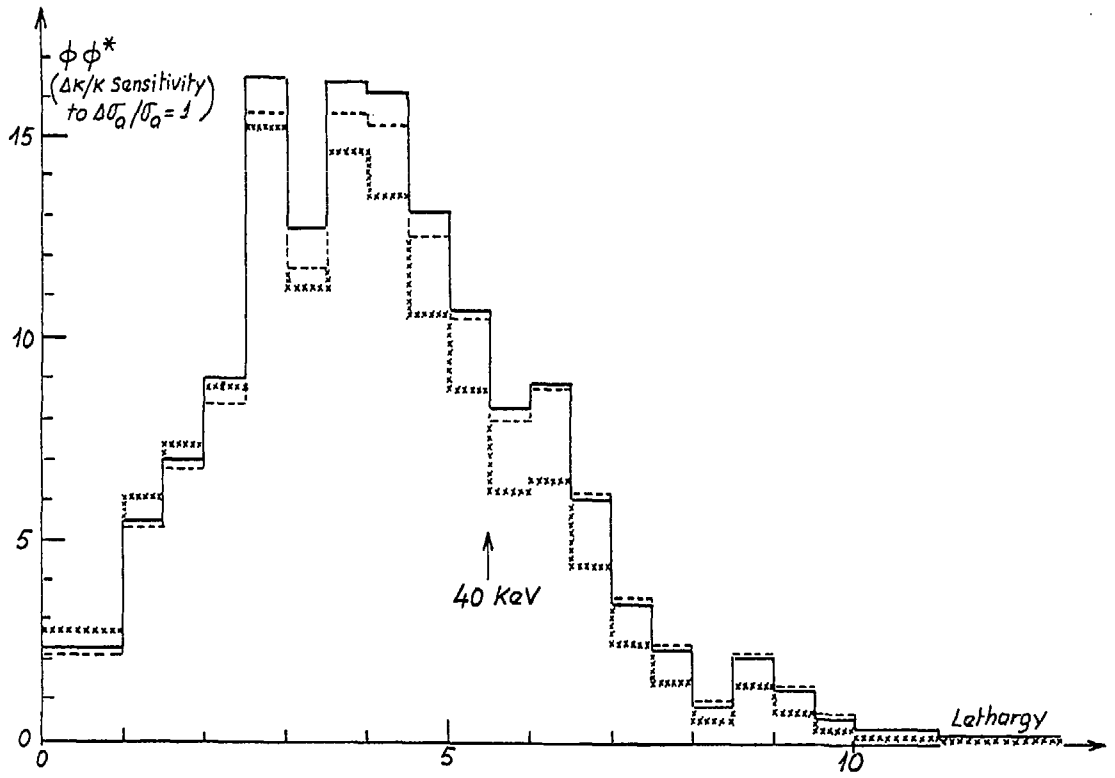

Fig. 1

Effective Integral and Reactivity Effects of 238 U and 240 Pu Resonance Parameter Uncertainties

Henry TELLIER
Service d'Etudes des Réacteurs et de Mathématiques Appliquées
Centre d'Etudes Nucléaires de SACLAY
91191 GIF SUR YVETTE Cedex (FRANCE)

ABSTRACT

The resonance parameters of Uranium 238 and Plutonium 240 are known with an uncertainty which induces an inaccuracy in the calculation of the effective multiplication factor of light water lattices. This effect was computed by using the different available files which take into account the successive improvements of the resonance parameter measurements. For Uranium 238, although the reactivity shift between UKNDL 68 and the new evaluations is about 270×10^{-5}, the recent values seem to be satisfactory for the reactor physicist. It is not the same thing for Plutonium 240. For this nuclide the resonance parameters are not known with a good enough accuracy and their values must be improved, specially for the 1.056 eV resonance.

I. INTRODUCTION

To perform reactor core calculations, the physicists use nowadays very accurate cell computation codes. These new generation codes solve the Boltzman transport equation without mathematical approximations as far as simple geometries are concerned. For example, we use in France the Apollo Code which solves the integral form of the transport equation by the first collision probability method in the multigroup approximation and for one or two dimension geometries [1]. For this reason the neutron cross section adjustment process which were used in the first generation calculation codes is no more justified. If we don't have a good cell calculation, it is because we don't use accurate neutron data. Of course the neutron cross section knowledge was improved this last years. Nevertheless it remains some uncertainties. And these uncertainties lead to an inaccuracy in the computation results. This inaccuracy can have sometimes important consequences. For instance, the inaccuracy of the criticality factor of a power nuclear reactor at the beginning of the core life induces consequences relating to the fuel cycle length. This fact has financial involvements. Thus it seems interesting to study the reactivity effects of the neutron data uncertainties. In the resonance region, the most important heavy nuclides are Uranium 238 and Plutonium 240 in the case of thermal neutron reactors. In the following sections, we shall study, one after the other, the effect of the Uranium 238 and Plutonium 240 resonance parameter uncertainties. Then we shall try to define the accuracy of the neutron data requests.

II. URANIUM 238

The actual thermal neutron power reactors are mainly pressurized water reactors which use slightly enriched uranium. The fuel elements of these reactors contain about 97 % of Uranium 238. Thus this isotope is very important for the neutron balance because it has a very important absorption rate, about 20 % of the total absorption rate of the cell. The largest part of this absorption occurs in the resonance region. But only the first resonances, below 200 eV, have an important weight in the case of thermal neutron reactors, as it is shown in table I. Therefore it is necessary to know their parameters with a very good accuracy. During a long time this accuracy was not good enough for reactor physics purposes. But more and more accurate measurements of these resonance parameters have been carried out for the last ten years. The new results are slightly different from the previous ones. This change of the resonance parameter values appeared in the different evaluated data files which were succesively recommended and available. As an example we give in table II the resonance parameters which are recommended in some recent files such as ENDF/B3 and B4, the French file now

used in Saclay [2] and the Oak Ridge evaluation [3]. We can see in this table the variations of the partial widths and essentially of the capture width. The value which is now recommended is generaly lower than the value previously used.

It is obvious that a variation of the resonance parameters leads to a change of the effective resonance integral and of the effective multiplication factor. This last change can be computed by cell calculation using the self shielded cross section which are obtained with the different sets of data. The self shielded cross section are computed by solving the slowing down equation. In Saclay this is done in the multigroup approximation by the Autosecol Code [4]. The self shielded cross sections are calculated for several values of the fuel temperature and background cross section. Table III gives the values of the effective capture resonance integral obtained with the following files : UKNDL 68, ENDF/B4 and the Saclay file. For each of these parameter sets, the natural cross section is computed with the Breit and Wigner single level formalism. The Doppler broadening is obtained with the Ψ and Φ functions. Although we know that it is necessary to use a multilevel formalism for uranium 238 cross section calculation [2], we have used the single level formalism to reduce the computation time. This process is not a disadvantage because in this study we only need comparisons between several data sets and not comparisons between a computed value and an experimental one. For the effective resonance integral computation, the energy range corresponds to the resolved and unresolved resonance region, that is from 2.76 eV up to 37 keV.

With the self shielded cross sections, which correspond to the various evaluated data files, we calculated the reactivity effect of the change of library in the case of a typical PWR cell. (The main characteristics of this cell are given in table IV). For this comparison we chose as reactivity level reference the result obtained with UKNDL 68 without adjustment. The results of the comparison are given in table V, for two different fuel temperatures. The first one corresponds to critical experiments at room temperature, the second one to operating temperature in a power reactor. The reactivity change is about 300×10^{-5} at 700 °C. This uncertainty exceeds the experimental error bars which are about 200×10^{-5} for light water lattices. This is significant. More over such an uncertainty could have financial consequences on the fuel cycle cost. As a matter of fact an uncertainty of 300×10^{-5} on the effective multiplication factor at the beginning of core life leads to an uncertainty of 300 MWd/t on the fuel burn up at the end of the core life, that is to say about 8 days of full power running. This is not negligible. Therefore we must calculate the reactivity with a good accuracy and we cannot indifferently use any file. The choice must be carrefully checked with integral experiments.

By using several recommended data sets we computed the integral effect of the change of each resonance. The total effect can be minimized because one parameter of one resonance can move in one direction and another parameter of another resonance in another direction. So, if it is necessary to know this total effect, it is also interesting to know the sensibility of one particular resonance. Thus, with the same method we calculated the reactivity effect of the change of one parameter for one resonance. This computation was successively performed for a 5 % change of Γ_n and Γ_γ of the three first levels. For Γ_γ this change corresponds about to 1 meV which is close to the error bar of the new measurements. For Γ_n, this variation is generally lower than the experimental uncertainties. The results are given in table VI. They show that an improvement of the Γ_n measurement would be welcome, in particular for the 20.9 eV resonance.

III. PLUTONIUM 240

The case of plutonium 240 is slightly different from the case of uranium 238. The plutonium 240 is also a nuclide which has a strong resonance structure but almost the whole absorption rate occurs in the 1.056 eV resonance. In a light water reactor, the 1.056 eV absorption rate is equal to 89 % of the total resonance absorption rate. In addition this resonance is at low energy and is generally considered, in the reactor computation codes, as being in the thermal range. In this energy range the

multigroup libraries have a fine energy mesh. Thus, it is possible to compute the flux and the reaction rate without using the self shielding technique. A resonance parameter change only introduces a modification of its contribution to the multigroup cross section. The study is easier than for uranium 238. As a matter of fact it is only necessary to make the modification of the multigroup cross section which corresponds to the change of the resonance parameter values. The table VII displays the different values of the partial width which are recommended in the recent evaluation files : the French evaluation [5] which is included in UKNDL 73 and the versions B4 and B5 of ENDF. It seems that the resonance parameters are not as accurate as for uranium 238. But fortunately the neutron weight of plutonium 240 is not of prime importance in a PWR because its concentration is very low. A significant amount of plutonium 240 only appears for end of life burn up. It is in the case of plutonium recycle that the plutonium 240 weight can become important. Thus we computed the reactivity effect of resonance parameter change in the case of a plutonium loaded fuel, the one of the Chooz reactor. The cell characteristics are given in table VIII. In this cell, the reactivity effects of the different files are the following ones. With regard to UKNDL 73 the use of ENDF/B4 increases the reactivity by 25×10^{-5}, the use of ENDF/B5 decreases the reactivity by 130×10^{-5}. These changes are small because it exists a balancing between the variations of Γ_n and Γ_γ in the different files. Therefore we computed the effect of the modification of only one of the two parameters. An increase of 2 % of the neutron width leads to a decrease of 110×10^{-5} for the effective multiplication factor. An increase of 2 % of the capture width gives a decrease of 105×10^{-5} for the effective multiplication factor.

As the physicist wants to perform his reactor calculation with an uncertainty lower than the 200×10^{-5} experimental error bars, we can conclude from the above calculation that we must know the resonance parameters with an accuracy better than 3 %. It is not yet the case and new differential measurements would be very useful to improve the knowledge of the 1.056 eV resonance of plutonium 240. If we do not use the plutonium recycle the required accuracy can be lower than 3%. For the calculation of the irradiated fuel isotopic composition the required accuracy is the same as for plutonium recycle.

IV. CONCLUSION

From the above sensitivity studies, we can infer two conclusions. First, it is necessary to know the resonance parameters of uranium 238, and specially the radiative width, with an uncertainty lower than the difference between ENDF/B4 and the new recommended values. An accuracy of 1 meV on Γ_γ is required for the reactor physicist purposes. It seems to be the case with the new experimental results. Moreover we obtain with these evaluations a very good interpretation of integral experiments, so the absolute values of the parameters are satisfactory. We can consider that it does not remain a discrepancy for the uranium 238 resonances as a whole.

Secondly, we have not a so satisfactory situation for plutonium 240. In this case we also need an accuracy of 1 meV for the 1.056 eV resonance radiation width, for plutonium recycle and isotopic composition calculations. It is not yet the case because the uncertainty is about 3 meV. For the neutron width we require an uncertainty of 3 %. This is better than the 6 % which are now obtained. A comparison between isotopic composition of irradiated fuel calculations and measurements indicates that the radiative width of the 1.056 eV resonance is about 2 meV too large, new differential measurements are necessary to improve the knowledge of plutonium 240.

REFERENCES

[1] A. KAVENOKY
"Mathematical Models and Computationnal Techniques for Analysis of Nuclear System"
ANN ARBOR - CONF 730414, I, 95 (1973)

[2] H. TELLIER and M. GRANDOTTO
"Advances in Reactor Physics"
GATLINBURG, CONF 780401, 17 (1978)

[3] G. de SAUSSURE & al.
US Report ORNL/TM 6152 (1978)

[4] M. GRANDOTTO
French Report CEA-N-1961 (1977)

[5] J.P. L'HERITEAU and P. RIBON
French Report CEA-N-1273 (1970)

Table I

Absorption Rate in the First Resonances
of Uranium 238 Relatively to the Total Resonance Absorption

Resonance eV	6.67	20.9	36.7	66	80.7	102.6 116.4 189.6
Absorption %	27.7	15.2	11.9	5.2	2.8	6.7

Table II

Evaluated Resonance Parameters of Uranium 238 (in meV)

Energy eV		UKNDL 68 (1968)	ENDF/B3 (1972)	ENDF/B4 (1974)	SACLAY (1978)	ORNL (1978)
6.67	Γ_n	1.52	1.50	1.50	1.48	1.51
	Γ_γ	26.0	25.6	25.6	23.0	23.5
20.9	Γ_n	8.7	8.8	8.8	9.7	10.1
	Γ_γ	26.5	26.8	26.8	23.0	23.1
36.7	Γ_n	31.0	31.1	31.1	33.0	33.9
	Γ_γ	27.7	26.0	26.0	23.0	22.9
66.0	Γ_n	23.8	25.3	25.3	25.0	24.6
	Γ_γ	24.5	23.5	23.5	23.0	23.7
80.7	Γ_n	2.0	2.0	2.0	1.9	1.9
	Γ_γ	21.2	23.5	23.5	24.0	24.2
102.6	Γ_n	65.1	69.5	71.0	70.0	71.6
	Γ_γ	25.1	26.1	26.0	24.0	24.4
116.4	Γ_n	24.7	27.2	28.3	26.0	27.5
	Γ_γ	22.4	24.3	23.5	22.5	22.7
189.6	Γ_n	146	169	169	169	167
	Γ_γ	22.9	24.7	24.7	23.5	23.0

Table III

Computed Values of Uranium 238 Effective Capture Resonance Integral Between 2.76 eV and 37 keV

Data File / Background Cross Section (barn)	θ = 20 °C			θ = 700 °C		
	UKNDL 68	ENDF/B4	SACLAY	UKNDL 68	ENDF/B4	SACLAY
20	13.7	13.6	13.1	14.9	14.8	14.4
50	19.9	20.0	19.3	22.0	22.3	21.6
100	27.0	27.2	26.3	30.7	31.0	30.0
250	41.4	41.6	40.1	48.9	49.1	47.7
500	57.9	57.9	55.9	70.1	70.4	68.3
1000	81.0	80.9	78.1	99.3	99.5	96.7
10000	--	197.5	192.7	--	220.4	216.2
∞	275.8	275.9	272.0	275.8	275.9	272.0

Table IV

Typical Parameters of a Light Water Cell

Isotopic Composition	$\frac{U235}{U238}$ = 0.03239
Pin Radius	0.4127 cm
Zircalloy can Radius	0.4744 cm
Cell Radius	0.7135 cm

Table V

Reactivity Effects of the Different Uranium 238 Evaluated Data Files

Δk_{eff} 10^{-5}	k_{eff}(ENDF/B4)-k_{eff}(UK68)	k_{eff}(SACLAY)-k_{eff}(UK68)
θ = 20 °C	- 153	+ 371
θ = 700 °C	- 305	+ 272

Table VI

Reactivity Effect in Unit 10^{-5} of a 5 % Change of Γ_n or Γ_γ

Energy (eV)	6.67	20.9	36.7
Γ_n	116	59	46
Γ_γ	111	60	57

Table VII

Resonance Parameter of the 1.056 eV Resonance of Plutonium 240

	UKNDL 73	ENDF/B4	ENDF/B5
Γ_n meV	2.30±0.15	2.44	2.28
Γ_γ meV	32.2 ± 2.0	29.9	33.3

Table VIII

Typical Parameters of a Plutonium Recycle Cell

Isotopic Composition	$\frac{U235}{U238} = 0.00724$	$\frac{Pu239}{U238} = 0.03837$
	$\frac{Pu240}{U238} = 0.01052$	$\frac{Pu241}{U238} = 0.00551$
Pin Radius	0.4435 cm	
Stainless Stell can Radius	0.4890 cm	
Cell Radius	0.7352 cm	

^{238}U RESONANCE SELF-INDICATION CAPTURE MEASUREMENTS≠

Robert C. Block, Donald R. Harris, Si Hwan Kim* and Katsuhei Kobayashi**

Gaerttner Linac Laboratory
Department of Nuclear Engineering
Rensselaer Polytechnic Institute

ABSTRACT

Neutron self-indication measurements simulating ^{238}U capture in reactors have been carried out over the energy range from 3 eV to 3 keV using shielding samples at 77°K, 293°K, and 873°K. The data have been reduced to open and self-shielded capture yields provided on magnetic tape as benchmark data for comparison with nuclear design calculations. The important energy range below 100 eV has been analyzed in detail both to obtain improved resonance parameters for the levels at 6.67, 20.9, 36.8, 66.1 and 80.7 eV and to examine the accuracy with which cross sections are calculated from resonance formalisms. The improved resonance parameters, when used with an accurate but practical multi-level formalism, reduce by about one-half the long-standing discrepancy between calculated and measured ^{238}U resonance capture integrals.

≠ Electric Power Research Institute Research Project 511-1, NP-996

* Babcock and Wilcox Company, P.O. Box 1260 Lynchburg, Virginia 24505

** Visiting Research Associate from Kyoto University Research Reactor Institute, Kumatori, Japan

Submitted for publication in Nuclear Science and Engineering

I. Introduction

One of the outstanding discrepancies in power reactor design has been the overprediction of the ^{238}U resonance capture integral in heavily-self-shielded rods and lattices. This discrepancy, of many years standing, was summarized by McCrossen and Hardy (1) who concluded that calculations based on ENDF/B-IV evaluated data (2) predicted a resonance capture integral approximately 0.6 barn larger than that measured in water-moderated lattices and isolated samples. While this value for the discrepancy is somewhat less than estimates made a dozen years ago (3), the associated uncertainty in ^{238}U capture rate has considerable impact on reactor analysis, particularly in the absence of fuel recycle (4).

Of the numerous experimental and calculational aspects of the discrepancy, attention has been focused on the possibility that it might be caused by errors in the ^{238}U+n resonance parameters and by inaccuracies in the resonance formulae used in calculating cross sections from these parameters (5). Self-shielded absorption in the important low-energy neutron resonances saturates near the resonance peaks where the integrand of the resonance integral is insensitive to the ^{238}U cross sections. Only where saturation diminishes in the resonance wings at energies corresponding to practical width (6) does the resonance integral become markedly sensitive to the ^{238}U cross sections. An extensive series of self-indication measurements has been carried out at RPI (7,8,9) to determine resonance parameters and shapes in terms of an observable, the self-indication capture yield, which resembles the integrand of the resonance integral in the resonance wings.

The self-indication experiments consisted of time-of-flight measurements of neutron capture in a thin ^{238}U sample which was shielded by another sample of the same material. The first-collision self-indication yield, expressed later as Eq. (3), contains a factor $\exp[-N_1\sigma_t(E)]$ representing the penetration of the beam flux through the shielding sample whose thickness is N_1 atoms per barn; here $\sigma_t(E)$ represents the ^{238}U total cross section at neutron energy E. The neutron beam flux is essentially zero near the resonance center and is reduced by one-half at energies $E^{SI}_{J^\pi}$ such that $N_1\sigma_t(E^{SI}_{J^\pi})$ equals $\ell n\ 2$. In order to show the relationship of the self-indication measurement to resonance integrals it is useful to consider the wide-resonance (WR) approximation which is often appropriate for the important low-energy ^{238}U resonances (6). The integrand of the WR resonance integral is $\sigma_c(E)\phi_F(E)$, where $\sigma_c(E)$ represents the ^{238}U capture cross section at energy E, and $\phi_F(E)$ is an appropriately normalized effective flux in a sample or in the fuel region of a reactor lattice. Self-shielding reduces the effective flux by one-half at the practical width energies determined by setting $\sigma_c(E^{WR}_{J^\pi})$ equal to $(\Sigma_{sF}+\Sigma_e)/N_{28}$, where Σ_{sF}/N_{28} is the scattering cross section of other nuclides in the sample or fuel region per ^{238}U nucleus. In a rational approximation Σ_e is $(1-C)/D_F$, where C is the Dankoff factor and D_F is the mean chord of the sample or fuel region. We note that in this approximation the integrand of the resonance integral is $(\Sigma_{sF}+\Sigma_e)/N_{28}E_r$ at the resonance energy E_r, quite independent of the ^{238}U cross section. Thus as was noted earlier the ^{238}U cross sections near the centers of strong resonances are not very important. At the centers of strong resonances the self-indication yield blanks out, providing no cross section information (where none is needed), but providing as we shall see, uniquely useful background information for analysis of the measurements. In the resonance wings, however, the self-indication yield resembles the integrand of the resonance integral when the shielding sample thickness is chosen so that the parameters $E^{SI}_{J^\pi}$ approximate $E^{WR}_{J^\pi}$.

This requirement is met, for UO_2 fuel rods similar to those used in light water reactor lattices, when the thickness of our ^{238}U metal shielding sample is approximately 1/8", so this is selected as the central shielding sample thickness for our experiments. Shielding samples both thicker and thinner by factors of two and four also were used, as was the open configuration with zero shielding sample thickness. Thus shielding sample temperatures 77°K, 293°K, and 873°K, were employed; the first was selected to eliminate much of the Doppler broadening, the second was selected to correspond to the important room temperature measurements of resonance integrals in isolated samples and critical facility fuel elements, and the third was selected to correspond to an average temperature of a hot fuel pin in a power reactor.

II. EXPERIMENTAL METHOD

The measurements were carried out at the Gaerttner Linear Accelerator Laboratory of Rensselaer Polytechnic Institute. The accelerator, capture tank, and other apparatus have been described in detail (7,10,11) and the description given here is limited to special features of these measurements.

Nuetron Source

The experimental arrangement is shown in Fig. 1. A pulsed beam of approximately 70-MeV electrons from the linear accelerator struck a water-cooled tantalum target producing a pulse of gamma rays and photoneutrons. The fast neutrons were moderated by a CH_2 disk 18 cm in diameter by 2.54-cm thick which was placed next to the tantalum target. This target geometry was selected to obtain a large neutron intensity; the intensity of this arrangement is approximately twice that obtained with the usual 135° "bounce" target geometry (11,12). In this geometry the water-cooled tantalum target was not completely shielded from the collimation system, and some moderated neutrons arose from the water.

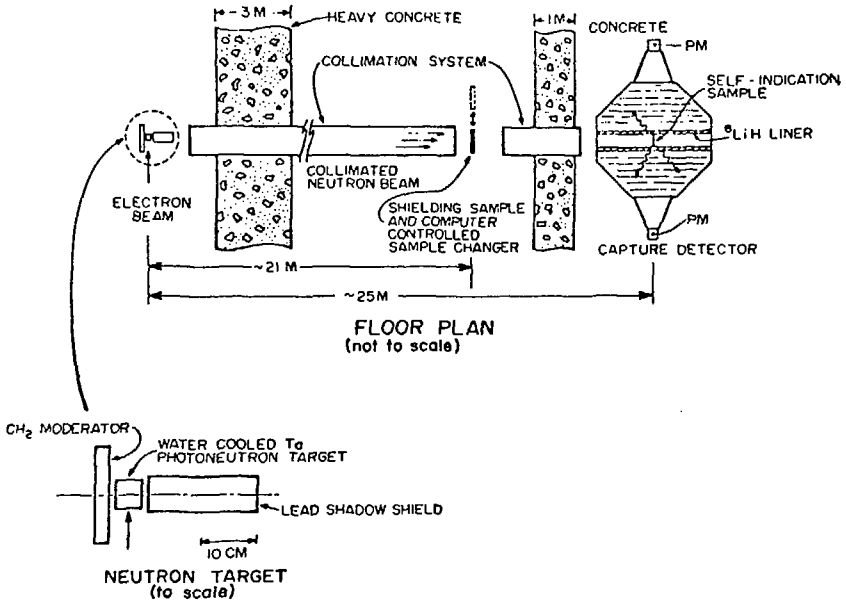

Figure 1

Experimental arrangement.

Moderated neutrons moving down the evacuated flight tubes passed through a shielding sample at about 21 m from target and struck the capture sample. The neutron beam was collimated to a diameter of approximately 5 cm at the shielding sample position and approximately 6 cm at the capture detector position. A 0.32-cm-thick lead sheet was placed in the beam to suppress the intense flash of photons emanating from the target. In addition cadmium or B_4C filters were placed in the beam to remove thermal neutrons and to suppress the overlapping of neutrons from successive neutron pulses.

Detectors and Electronics

The 1.25-cm-diameter liquid scintillator capture detector (10-12) was used in these measurements. It consists of about 1100 liters of a xylene-based liquid scintillator solution which is loaded with boron to suppress background caused by neutron capture in hydrogen. The detector bias was set to accept gamma ray energies between 3 MeV and 15 MeV. The capture sample was placed in the center of the capture detector at a distance of 25.65 m from the reference plane of the neutron source which is located midway between the CH_2 moderator and the target water coolant. A long annular shield of 5-cm-thick ^{6}LiH was placed around the capture sample to prevent low energy neutrons scattered by the sample from reaching the solution and to prevent low-energy neutrons moderated in the solution from returning to the sample.

The neutron flux spectrum was measured by a $^{10}B_4C$-NaI detector (11,12) located at 28.28 m from the source reference plane. This detector consists of a 1.27-cm-thick slab of 91.7 w/o $^{10}B_4C$ in the beam. Gammas from $^{10}B(n,\alpha\ 478\text{-keV}\ \gamma)$ reactions in the slab were detected by two 5-cm-thick by 50.8-cm-diameter NaI detectors located outside of the neutron beam. Neutron intensity was monitored by a ^{10}B-plastic scintillator detector located in a separate flight tube about 8 m from the neutron source.

Pulses from the capture detector and from the neutron flux detector were timed by a 32-MHz clock interfaced to a PDP-7 computer. The computer cycled samples in and out of the beam, started timing gates, allocated pulses to time channels with up to four regions of time compression, and stored data from the neutron intensity monitor. The timing gates were set to emphasize the neutron energy range from 3.5 eV to 2.5 keV.

Samples

The thickness and enrichments of the shielding and capture samples are listed in Table 1. The shielding samples used in these experiments were depleted uranium metal sheets of nominal thicknesses (in inches) 1/2", 1/4", 1/8", 1/16", and 1/32". The selection of the shielding sample thicknesses has already been described. The capture sample thickness was selected as a compromise to obtain high counting rate and low multiple scattering correction. The thermal expansivity for uranium metal sheet depends on direction and on the mode of fabrication; thus the actual thicknesses of the shielding samples shown at 77°K and 873°K in Table 1 were determined from the measurements of Byoun (12) with similar samples. He measured the transmission of off-resonance neutrons as functions of sample temperature and deduced the thermal expansivity. An analysis carried out at the RPI Nuclear Engineering Department Mass Spectrometry Laboratory showed that the ^{235}U content of the shielding samples is 0.26±.03 atom percent (13).

An eight-position sample changer cycled the five 7.6-cm by 7.6-cm shielding samples and an Open position into the neutron beam for the room temperature measurements. A two-position sample changer cycled the 1/2", 1/8", or 1/32" sample into and out of the neutron beam in a cryostat for the low temperature measurements, and another two-position sample changer cycled similar samples into and out of the neutron beam in an oven for the high-temperature measurements. The cryostat (12) consisted of two glass dewars surrounding an isothermal aluminum cavity that was maintained at 77°K by a pool of liquid nitrogen. The shielding sample moved up and down inside the cavity to cycle in and out of the neutron beam. For the high temperature measurements the shielding sample was mounted in an electrically heated vacuum oven (12). The temperature of the

Table 1. Shielding and Capture Uranium Samples

Shielding Samples

Nominal Thickness (in.)	Actual Thickness (10^{-3} atom/barn)		
	77°K	293°K	873°K
1/32"	3.77 ± 0.01	3.713 ± 0.004	3.64 ± 0.02
1/16"	7.40 ± 0.01	7.373 ± 0.008	-
1/8"	15.44 ± 0.02	14.66 ± 0.02	14.93 ± 0.10
1/4"	-	29.43 ± 0.03	-
1/2"	60.65 ± 0.09	61.42 ± 0.06	58.66 ± 0.40

^{235}U Content: (0.26 ± 0.03)%

Capture Samples

	2.320 ± 0.004	2.320 ± 0.004	2.475 ± 0.004
^{235}U Content	<4 ppm	<4 ppm	<10 ppm

midpoint of the oven was held at 873±5°K. At the end of each measurement there was no evidence of distortion or change in oxidation of the uranium sheets.

The capture sample used for the room-temperature and low-temperature measurements consisted of highly enriched ^{238}U which was kindly loaned by the Oak Ridge National Laboratory. For the high-temperature measurement another capture sample of highly enriched ^{238}U was prepared from the USDOE Materials Research Collection of stable isotopes.

Data Acquisition

Two classes of measurements were carried out, one designed for investigation of the ^{238}U resonances below 36.8 eV and another for investigation of higher energies up to about 2.5 keV. For the low-energy measurement the 0.16-cm- thick cadmium overlap filter was placed in the neutron beam, and the linear accelerator was operated to produce 70-MeV electron pulses of 170-ns duration at a repetition rate of 300 Hz; the average power on target was 6 kw. For the high energy measurement the boron-carbide overlap filter was used, and the accelerator was operated with the same electron energy and pulse width but with a repetition rate of 500 Hz.

The self-indication data were obtained by cycling the shielding samples in and out of the neutron beam. A cycle time of 15 to 30 minutes was used and data were typically collected in a run that extended over a 4 to 8 hour period in order to average out the effects of neutron source intensity fluctuations. A comparison, at the end of each run, of the recorded neutron monitor counts and the cycle times for each sample position showed that intensity fluctuations averaged to less than 1%. Several runs were made for the same conditions and agreement between runs was within statistics. The neutron flux was measured

with the $^{10}B_4C$-NaI detector by cycling an Open, a 1/32" and a 1/16" uranium sample into the beam. The two uranium samples provided the background in the vicinity of the blanked-out resonances.

Self-Indication Capture Yield

The self-indication capture yield is defined here as the number of neutrons penetrating the shielding sample and being captured in the capture sample per neutron in the incident beam directed toward the capture sample. Because of multiple scattering, resolution broadening, and other effects, the defined quantity differs somewhat from the measured. It is useful to introduce the measured self-indication capture yield for channel i,

$$Y_i = \frac{C_i - B_i}{(\eta k)\,\phi_i} \qquad (1)$$

where C_i is the dead-time-corrected count in time channel i, B_i is the background count in channel i, ϕ_i is the relative neutron fluence in channel i averaged over the surface of the capture sample, η is the capture detector efficiency, and k is defined so that $k\phi_i$ is the actual integrated neutron fluence. The product (ηk) is determined from experiment. The detector electronics deadtime was about 1 μs, and deadtime corrections were less than a few percent for all the self-indication data.

The determination of background, particularly time-dependent background, is a significant feature of resonance measurements. In this experiment, The background below 50 eV was determined from the counting rate observed between the resonances, where the capture counting rate was very small compared to background, and from the counting rate in the blanked-out regions at resonance centers when the shielding samples were in the beam. The observation of these three background points per resonance, at the blanked-out center and in the distant wings of each resonance, makes the self-indication technique uniquely useful in characterizing time-dependent background. For the Open sample data there were no blanked-out regions, so the background at resonance was obtained by extrapolating the shielded-sample backgrounds to a shielding sample of zero thickness. The Open sample background at the 6.67, 20.9 and 36.8 eV resonances was determined to be 1.3±0.5 percent of the counting rate at resonance. For the energy region above 50 eV, there was no blanked-out region at the resonance centers, so the background was obtained from the counting rate between resonances. In this energy region, the background at resonance was assumed to have the same relative variation with shielding sample thickness as was observed for the 20.9- and 36.8-eV resonances. The channel-by-channel background was determined in all cases by linear interpolation in time-of-flight between the measured or inferred values in the wings and at the resonance center; this is referred to as the triangular background model.

The relative neutron fluence ϕ_i was obtained from the $^{10}B_4C$-NaI measurement. The relative detector efficiency was calculated from ENDF/B-IV cross sections for boron and carbon, taking into account neutron and gamma-ray multiple scattering in the $^{10}B_4C$ slab. Below the 100 eV the $^{10}B_4C$ slab absorbs nearly all of the incident neutrons so that the detector efficiency is effectively constant.

The normalization constant ηk was obtained from the saturated capture in the Open sample at the center of the 6.67-eV resonance. The Cd-filtered data associated with the 293°K shielding samples were used for the normalization, and all other data sets were normalized to this saturated capture. The 6.67-eV capture yield was determined from a multilevel first collision calculation

using ENDF/B-IV resonance parameters, and from a single-level Monte Carlo multiple scattering calculation. The calculated saturated yield was 0.935, of which only about 4% was the result of multiple scattering. The resonance parameters determined from the present measurements lead to a calculated saturated yield of 0.983, within the estimated error of the assumed value. For the 77°K data the neutron flux was normalized in the vicinity of each resonance and for each shielding sample by integrating over the relative Open yield measured during cycling of the shielding samples and by setting this integral equal to the corresponding integral obtained with the 293°K Cd-filter data. For the 873°K Cd filter data Monte Carlo calculations were carried out with ENDF/B-IV data to correct for the slight difference in the capture sample thicknesses used in the 293°K Cd-filter data and the 873°K data; then a normalization similar to that used for the 77°K data was applied. The neutron fluxes for the B_4C-filter data at 293°K were normalized to the 293°K Cd-filter flux value. The relative yield for the Open sample position was integrated over the 36.8-eV resonance for the B_4C-filter data, and this integral was set equal to the 36.8-eV integrated capture yield obtained with the Cd filter. Finally, the 77°K and 873°K B_4C data were normalized to the 293°K B_4C data.

III. Experimental Results

Measured Capture Yields

Complete time-of-flight data were obtained for a number of combinations of six shielding sample thicknesses, B_4C or Cd neutron-beam filters, and shielding sample temperatures of 77°K, 293°K, or 873°K. The experimental data, reduced to measured self-indication capture yields according to Eq. (1), are shown in Figs. 2 to 4 for times-of-flight near the important 6.67-eV, 20.9-eV and 36.8-eV s-wave resonances. Errors in these data were combined from statistical counting errors for the capture, flux detector, and background data, from errors in calculating the saturated Open capture yield at the 6.67-eV resonance as well as the energy variation of the $^{10}B_4C$-NaI (relative) fluence detector, and from uncertainties in estimating the time-dependent component of the background. The data shown in these figures are of various accuracies. The Open data, for which the counting rates were highest, had counting rates at the peaks of the three lowest-energy resonances that were more than 50 times the rates obtained between resonances. The counting statistical uncertainties near these peaks generally were lower than 1% per channel. On the other hand, for the 1/2" shielding sample the signal-to-background ratio on the high-energy side of the resonances was as small as 1:5 near the peak of the self-indication capture yield and correspondingly the statistical counting uncertainties were much worse. The 293°K data had the best statistical accuracy because these data were obtained over a longer period of time and because it was possible to use a larger neutron intensity resulting from a collimation system of larger area.

At resonance the data are characterized by saturated interaction in the Open sample position for the three lowest-energy levels. The shielding samples remove neutrons near the resonance energies, and there are progressively wider blanked-out regions as the shielding sample thickness and temperature increase. For the three low-energy resonances the blanked-out region separates the high-energy (left) and low-energy (right) peaks in the self-indication capture yield. For the 6.67-eV resonance in Fig. 2 the height of the right peak is generally larger than that of the left peak, and this becomes more pronounced as the thickness of the shielding sample increases. Only for the 873°K data with the 1/32" shielding sample is the left peak higher. For the 20.9- and

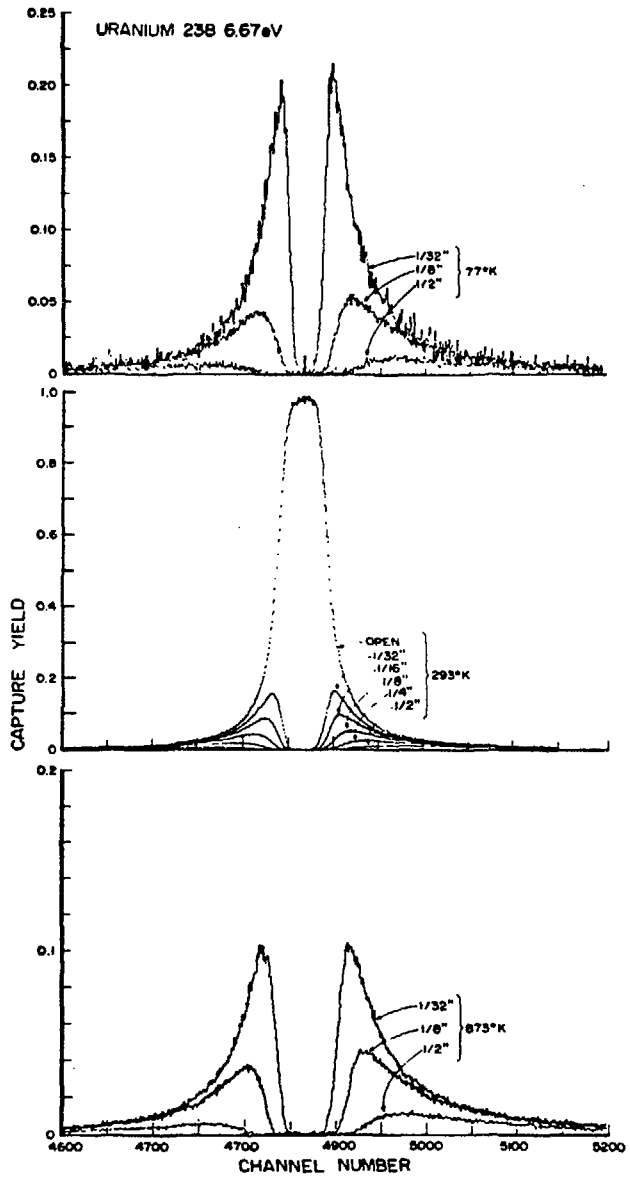

Figure 2. Capture yield vs. time-of-flight channel number near the 6.67-eV resonance. The nominal sample thickness and temperatures refer to the shielding sample.

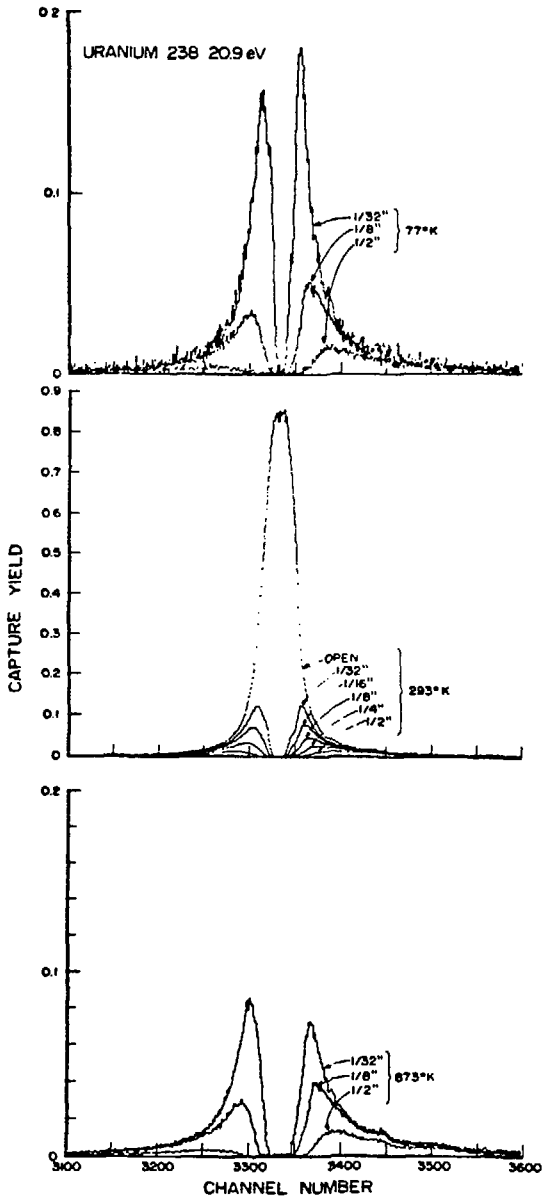

Figure 3. Capture Yield Vs. Time-of-Flight Channel Number Near the 20.9-eV Resonance. The Nominal Sample Thicknesses and Temperatures Refer to the Shielding Sample.

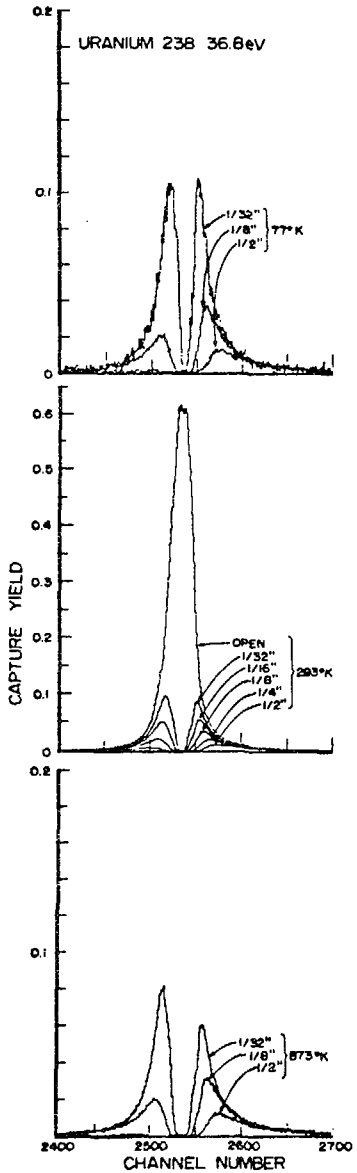

Figure 4. Capture Yield Vs. Time-of-Flight Channel Number Near the 36.8-eV Resonance. The Nominal Sample Thicknesses and Temperatures Refer to the Shielding Sample.

36.8-eV resonances in Figs. 3 and 4 the left peak is higher than the right peak for the 873°K, 1/32" shielding sample; for the 36.8-eV resonance this is so even for the 273°K, 1/32" data. This pattern is a result of the combined effect of Doppler broadening and the fact that the neutron width changes from about 5% of the total width at 6.67 eV to about 25% at 20.9 eV and 55% at 36.8 eV. Figures 2 through 4 indicate that the left-right asymmetry increases more rapidly with increasing sample thickness for resonances with larger neutron widths and hence larger resonance-potential scattering interference.

Summed Capture Yields

The primary purpose of this experiment was to clarify the resonance capture integral of ^{238}U in heavily-self-shielded configurations. Area analyses are useful for this purpose and were carried out for all levels below 100 eV. Selected shape analyses were made as well.

The self-indication capture yield summed over all channels near a resonance is related to neutron capture under similar conditions of self-shielding in a reactor lattice, as was noted in the Introduction. Thus in the present analysis the Summed Capture Yields (SCY)

$$SCY = \sum_{i=a}^{i=b} Y_i \qquad (2)$$

summed over time-of-flight channels a through b near a resonance were determined from the measurements for comparison with theoretical predictions. The sum of self-indication capture yields over the whole resonance is appropriate for Open sample data. For the self-shielded samples, however, the blanked-out region at the center of the resonance provides a well-defined left area and right area. This is useful not only in determining background, but in addition

the effects of multiple scattering are highly asymmetric and are appreciable only on the left (high energy) side of the resonance. Erroneous multiple scattering corrections would be expected to reveal themselves when the left and right SCY sums are analyzed separately. In addition, the increasing left-right asymmetry with thicker shielding samples makes the statistical accuracy of the areas under the left peaks considerably poorer than the accuracy of the right areas. Thus it is useful to sum the self-indication capture yields separately over the left and right peak regions when there is a well-defined division between the two peaks. This occurs for all shielding samples, except for the Open, for the three lowest-energy resonances. However, for all the Open sample positions and for the 1/32" and 1/16" shielding samples for the 66.1- and 80.7-eV resonances it was not possible to separate the left and right areas, so the sum was taken over the full resonance.

The same channel limits were used for all the SCYs for a given resonance. The data for the 1/8" shielding sample at 293°K were selected as being representative, and the channel summation limits were selected so that approximately 90% of the area under the 1/8" shielding sample yield curve was included. The channel numbers of these summation limits (these are required for testing nuclear engineering calculations against the measurements), the corresponding neutron energies, and the channel widths are listed in Table 2. The subscripts L and R represent respectively the left and right channel boundaries of the summation, and the subscript o denotes the center of each resonance. The experimental SCY areas are listed in Table 3 for the channel limits of Table 2. Here the left area L was summed from channels i_L through i_o and the right area R was summed from channels (i_o+1) through i_R. The experimental uncertainty for each area is given in percent and is shown in parentheses next to the area. It represents one standard deviation and is the uncertainty derived only from the counting statistics and from the estimated systematic error in the background. Systematic uncertainties such as those in relative neutron flux and in the product of efficiency times flux normalization are not included as they are common to all the SCY data and thus are not independent.

The uncertainties listed in Table 3 were determined by combining the channel-by-channel uncertainties noted earlier; they range from as little as 0.8% for the 1/32", 293°K sample data to as large as several tens of percent for the left areas of the 1/2" shielding samples. The larger uncertainties resulted from low signal-to-background ratio in the capture counts on the high energy side of heavily self-shielded capture samples, where the effect of constructive interference resulted in a very low neutron transmission. The 3 to 4% uncertainties shown for the Open data (summed over the whole resonance) are considerably larger than the uncertainties for the 1/32", 1/16" and 1/8" cases for the 293°K data even though the Open data had considerably more counts under the integral. However, the Open data did not have a blanked-out region near E_o for use in determining the time-dependent background, so as was noted earlier it was necessary to determine the Open background by extrapolation of shielded-sample data, thus leading to the relatively large uncertainties.

Table 2. Channel and Energy Limits of Integration for Summed Capture Yields

Channel Number			Neutron Energy			Channel Width
i_L	i_o	i_R	E_L(eV)	E_o(eV)	E_R(eV)	τ(μs)
4677	4868	5105	7.656	6.670	5.690	0.250
3200	3332	3495	22.71	20.90	18.94	0.125
2444	2533	2639	39.64	36.79	33.78	0.125
1878	1912	1954	68.62	66.09	63.15	0.125
1726	1739	1754	81.94	80.66	79.21	0.125

Table 3. Experimental Summed Self-Indication Capture Yields (SCY). Percent Uncertainties are Shown in Parentheses.

				Nominal Thickness of Shielding Sample				
E_0(eV)	Temp.	Open	Region	1/32"	1/16"	1/8"	1/4"	1/2"
	77°K		L	9.17(3.3)		3.52(3.6)		.665(21.)
			R	11.46(3.2)		5.27(3.0)		
6.67	293°K	70.99(3.0)	L	8.04(0.8)	5.54(1.0)	3.34(1.5)	1.67(2.7)	.595(5.9)
			R	9.78(0.8)	7.28(1.0)	4.92(1.3)	2.97(2.1)	1.40 (4.0)
	873°K		L	6.20(1.0)		3.00(2.4)		.589(10.)
			R	7.66(1.3)		4.54(2.0)		1.49 (5.6)
	77°K		L	5.43(3.1)		1.80(2.7)		.272(18.)
			R	5.96(3.6)		2.89(2.4)		1.12 (5.9)
20.9	293°K	38.35(4.3)	L	4.55(0.8)	3.07(1.0)	1.73(3.1)	.799(2.7)	.247(7.3)
			R	4.71(1.0)	3.68(1.0)	2.65(1.2)	1.81 (1.5)	1.03 (2.3)
	873°K		L	3.50(1.0)		1.59(2.8)		.288(12.)
			R	3.49(1.3)		2.42(1.7)		1.04 (3.4)
	77°K		L	2.82(3.5)		.743(3.7)		.065(37.)
			R	2.75(4.3)		1.37 (2.5)		.632(5.0)
36.8	293°K	20.57(3.6)	L	2.58(0.9)	1.51(1.2)	.784(1.8)	.294(4.1)	.067(15.)
			R	2.36(1.2)	1.81(1.2)	1.35 (1.3)	.931(1.6)	.578(21.)
	873°K		L	2.23(1.0)		.766(2.3)		.047(30.)
			R	1.88(1.5)		1.27 (1.7)		.595(3.0)
	77°K		L+R		1.415(4.0)			
66.1	293°K	6.554(2.2)	L+R	1.426(2.2)	1.038(3.0)	.753(3.7)	.461(5.4)	.252(8.7)
	873°K		L+R	.987(3.6)		.556(6.3)		
	77°K		L+R		.675(2.8)			
80.7	293°K	1.742(2.3)	L+R	.959(1.2)	.575(1.9)	.293(4.9)	.136(6.0)	.062(11.)
	873°K		L+R	1.140(1.2)		.293(4.0)		

IV. ANALYSIS

The self-indication measurements were analyzed by means of a model that included an accurate but practical multilevel cross section calculation, Doppler broadening calculations using an effective temperature, Monte Carlo calculations of multiple scattering in the capture sample, calculations of capture gamma ray attenuation in the capture sample, and resolution broadening based on shape analysis as well as on properties of the target and moderator.

The first-collision capture yield Y_i^1 for neutrons in the time-of-flight channel i is

$$Y_i^1 = e^{-N_1\sigma_t(E_i,T_1)}\left[1-e^{-N_2\sigma_t(E_i,T_2)}\right]\frac{\sigma_c(E_i,T_2)}{\sigma_t(E_i,T_2)} . \qquad (3)$$

Here, as was noted in the Introduction, $\sigma_t(E_i,T_1)$ is the total cross section of ^{238}U at the neutron energy E_i corresponding to time-of-flight channel i and at the temperature T_1 of the shielding sample, while N_1 is the thickness of the shielding sample in atoms per barn. Similarly $\sigma_t(E_i,T_2)$ and $\sigma_c(E_i,T_2)$ represent the total and capture cross sections at neutron energy E_i but at the temperature T_2 of the capture sample, and N_2 is the thickness of the capture sample. The components of Y_i and the successively applied corrections are discussed in turn.

Doppler Broadened Cross Sections

The resonance parameters determined from these measurements are to be used by engineering groups for nuclear calculations which must be sufficiently rapid as well as sufficiently accurate. The Wigner-Eisenbud (WE) formalish (14) sets the standard of accuracy; but it requires matrix inversion, its Doppler broadening requires kernel integration, and it is parameterized by numerous Largely unknown partial channel widths. At the other extreme, sums of single level (SSL) formulae, which are rapidly calculated and are Doppler broadened by the ψ and X functions (6), are widely used in nuclear engineering but are significantly in error for ^{238}U. (5,15) Here we use a cross section representation which has been shown to be rapid and accurate. (7,16) At each neutron energy (E) a dominant resonance R is selected for each interfering sequence of levels in ^{238}U+n having the same spin J and parity Π. The scattering cross section at neutron energy E for temperature T then is calculated as,

$$\sigma_{nn}(E,T) = \sum_{\ell}\sum_{J\Pi}\frac{\Pi}{k_n^2}g_J\left[S_1^2 + S_2^2 + \frac{\Gamma_{Rn}(\Gamma_R-S_1\Gamma_R)}{\Gamma_R^2/r}\psi(\theta,x) + \frac{\Gamma_{Rn}S_2}{\Gamma_R/2}X(\theta,x)\right] \qquad (4)$$

and the capture cross section is,

$$\sigma_{n\gamma}(E,T) = \sum_{\ell}\sum_{J\Pi}\frac{\Pi}{k_n^2}g_J\left[\frac{\Gamma_{Rn}\Gamma_{R\gamma}}{\Gamma_R^2/4}\psi(\theta,x) + \sum_{r\neq R}\frac{\Gamma_{rn}\Gamma_{r\gamma}}{(E_r-E)^2+\Gamma_r^2/4}\right]. \qquad (5)$$

Here E_r, $\Gamma_r(E)$, $\Gamma_{rn}(E)$, and $\Gamma_{r\gamma}$ represent the laboratory system energy, total width, neutron width, and capture width for level r, while $k_n(E)$ is the neutron wave number, and g_J is the statistical weight. (6,7) Several hundred s-wave (ℓ=0) and p-wave (ℓ=1) levels were used in the summations for ^{238}U+n. Positive energy level data outside the energy range of analysis were taken from the ENDF/B file. The functions $S_1(E)$ and $S_2(E)$ represent non-Doppler-broadened but interfering contributions from explicit levels other than the dominant level,

$$S_1 = 2\sin^2\phi_\ell - \sum_{r\neq R}\frac{\Gamma_{rn}\Gamma_r/2}{(E_r-E)^2+\Gamma_r^2/4} , \qquad (6)$$

$$S_2 = 2\sin\phi_\ell\cos\phi_\ell + \sum_{r\neq R}\frac{\Gamma_{rn}(E-E_r)}{(E_r-E)^2+\Gamma_r^2/4} . \qquad (7)$$

64 The energy dependences of the functions ϕ_ℓ and the level parameters were taken from Ref. 14. Contributions from very distant levels are included in the effective scattering lengths used to calculate ϕ_n (14,17).

The function $S_2(E)$ is odd in $E-E_r$, and the scattering cross section is erroneously calculated at low energies unless appropriate negative energy levels are present to balance the positive energy contributions (7). Negative energy levels, not present in the ENDF/B-IV files, were supplied by a picket fence of levels at $E_1-\bar{D}$, $E_1-2\bar{D}$, etc, where for p-waves E_1 is the energy of the first positive energy level, and $\bar{D}$ is the average level spacing. For s-waves E_1 is the energy of the first negative level which was chosen to maintain $\sigma_{n\gamma}$ (0.0253 eV) at 2.70 b. The average capture width and reduced neutron widths $\Gamma_{rn}/|E_r|^{\ell+1/2}$ used for the negative energy levels are listed in Table 4. The ENDF/B file includes 192 positive energy s-wave levels and 210 p-wave levels, so balancing (around E) numbers of negative energy levels were supplied in each case. Numerical experimentation has shown that for convergence to 1 part in 2000 only about 30 or fewer levels on each side are actually required; in this case the computer time for cross section calculation decreased by about a factor of five. The radiative width $\Gamma_{r\gamma}$ employed in these expressions is the sum over the partial widths for all radiative channels. This approximation has been shown to lead to cross sections which are at least in the envelope of cross sections calculated from WE for reasonable alternative sets of partial widths (7,16).

Doppler broadening was carried out using the $\psi(\theta,x)$ and $\chi(\theta,x)$ functions (6), where

$$\theta = \Gamma_r(E)\sqrt{\frac{M/m}{4kT_e E}} \quad , \tag{8}$$

$$X = 2(E-E_r)/\Gamma_r(E) \quad . \tag{9}$$

Table 4. Parameters of Negative-Energy Levels

	s-wave	p-wave
Energy of First Negative-Energy Level	-11.0 eV	-1.51 eV
Negative-Energy Level Spacing	17.0 eV	11.73 eV
Radiation Width	0.023 eV	0.0235 eV
Nuetron Strength Function	1.1×10^{-4}	1.03×10^{-4}

Multiple Scattering

Multiple scattering of neutrons in the capture sample produced a significant correction on the left-hand, low time-of-flight, high-energy side of a resonance. A neutron with energy slightly higher than the resonance energy can have its energy reduced after scattering to an energy near resonance where there is a high probability of capture and subsequent detection of the resulting gamma ray. For opposite reasons there is little multiple scattering correction on the low-energy side of the resonance.

The Monte Carlo code of Sullivan et al. (20) was used to determine multiple scattering corrections. These were large at energies larger than resonant, e.g., up to (63±2)% at 21.2 eV just above the 20.9-ev resonance. Below the resonances the multiple scattering corrections were very small, eg, at 20.6 ev the correction was (1±0.5)% (7). The multiple scattering correction is channel-dependent and even after running large numbers of neutron histories there remained appreciable sampling uncertainties as well as uncertainties in interpolating to find the correction for a particular channel from the more broadly-binned Monte Carlo results. These uncertainties were estimated to be appreciably larger than those arising from the use of single-level cross section treatment in the Monte Carlo code (20). In later sections the calculated and measured SCY areas are analyzed separately for the high- and low-energy values

of the summed capture yields. No discrepancies were found within experimental uncertainties, which were relatively large for the high-energy areas. The shape analyses to be discussed later indicated deficiencies in the detailed, channel-by-channel multiple scattering but because these did not affect the final reported results they were ignored.

Gamma Ray Attenuation in the Capture Sample

The combination of low binding energy and high multiplicity leads to a relatively soft $^{238}U+n$ capture gamma-ray spectrum. As a result a significant number of the capture gamma-rays are absorbed in the capture sample, and the gamma-ray escape probability depends on the location of the neutron captures in the sample. This leads to a change in the detection efficiency of the capture tank as the capture process changes from surface capture near the peak of a resonance to volume capture in the resonance wings.

An auxiliary measurement was carried out with a thin ^{238}U foil (about 1/3 as thick as the capture sample) and lead foils which together approximated the total gamma-ray absorption of the capture sample. Capture measurements were carried out with the thin ^{238}U foil on the front surface of a uranium-lead sandwich, with the ^{238}U foil in the middle of the sandwich, and with the ^{238}U foil approximately two thirds of the way through the assembly. The variation in the relative capture gamma detection efficiency with depth in the capture sample was approximated by a one-parameter expression symmetric around the sample center,

$$\eta_g(Z) = 1-C\ \frac{Z}{N_2}\left(1 - \frac{Z}{N_2}\right) . \qquad (12)$$

Here Z is the depth (atoms/barn) in the sample along the direction of the neutron beam, N_2 is the thickness of the sample, and C is a parameter fitted to the auxiliary measurements, C was found to be 0.205. Thus the detection efficiency, relative to that on the surface of the capture sample, varies from unity on the surface to 0.949 in the center. It was assumed that the spatial distribution of the capture gamma ray source in the capture sample is that of the first collision neutron capture events. Thus, the relative efficiency $\bar{\eta}_g(E)$ for incident neutron energy E, averaged over the thickness of the sample, was computed as

$$\bar{\eta}_g(E) = \frac{\int_0^{N_2} e^{-\sigma_{nt}(E,T_2)Z}\,\sigma_c(E,T_2)[1-C\,(Z/N_2)(1-Z/N_2)]dZ}{\int_0^{N_2} e^{-\sigma_{nt}(E,T_2)Z}\,\sigma_c(E,T_2)dZ} \qquad (13)$$

The relative efficiency $\bar{\eta}_g(E)$ was found to vary from unity at 6.67 eV, where capture is nearly all at the front surface of the sample, to 0.966 for the volume capture in the resonance wings.

Resolution Broadening

The final calculated yield for channel j was determined from the resolution broadened expression,

$$Y_g = \sum_{i=j-m}^{j+m} R_{ji}\, Y_i^1\, [1 + (\tfrac{M}{F})_i \bar{\eta}_{gi} . \qquad (14)$$

Here Y_i^1 is the first collision capture yield calculated from Eq. (3), $(M/F)_i$ is the multiple scattering correction (multiple scattering component relative to the forced first collision component), and $\bar{\eta}_g$ is the gamma-ray escape correction from Eq. (13) evaluated at the midpoint energy of the channel. The resolution function R_{ji} was computed as the sum of two Gaussian distributions. The separation, widths, and magnitudes of the Gaussians were

determined from the physical separation and dimensions of the CH_2 and target coolant moderators used in the experiment (7). Shape analyses of the higher energy resonances were used to make small modifications in the Gaussian parameters (7,9).

V. Results and Discussion

Comparison with ENDF/B-IV

Experimental capture yields near the 6.67-eV resonance are compared with ENDF/B-IV calculations in Fig. 5 for shielding samples at 293°K. Here ENDF/B-IV parameters were used with the multilevel formulae noted earlier. The calculated capture yields for the thinner samples are generally higher than are the experimental values, expecially in the vicinity of the left- and right-peaks and on the outer extremities of both peaks. Only on the rapidly-varying inner sides of the peaks are the calculated and measured values in better agreement, but here minor effects such as inexact resonance energies and resolution broadening can complicate the comparison of calculations and measurements. Similar results were found for other resonances and for other sample temperatures (7). Single-level calculations were shown to be similarly discrepant with the measured values (7). The discrepancy between the ENDF/B-IV calculations and the measurements was observed to be in the same direction and of comparable magnitude to that indicated by the resonance integral measurements noted earlier. This suggested that at least part of the problem might lie in the values of the ENDF/B-IV resonance parameters and that these experiments could lead to a set of resonance parameters more appropriate for self-shielded capture applications.

Area Analysis

Summed Capture Yields (SCY) were calculated for each left-, right-, or total area for which a measured SCY is listed in Table 3. The channel limits noted in Table 2 were employed, and the calculations were carried out as described in Section IV. A reference set of SCY values were calculated based on multilevel cross sections using ENDF/B-IV resonance parameters, and for each resonance two other sets of SCY values were calculated using neutron widths

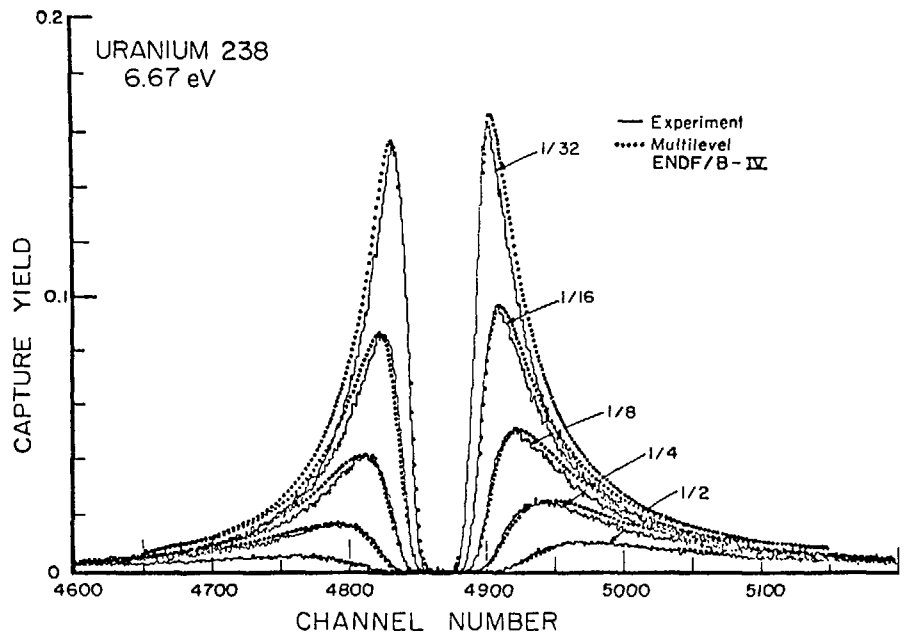

Figure 5.

Comparison Near the 6.67-eV Resonance of the Experimental Capture Yield Data and a Multilevel Calculation Using ENDF/B-IV Data. The Experimental Curves are Labeled with the Nominal Thickness (in Inches) of the Shielding Sample at 293°K.

less 10% or using radiation widths less 10%. The three calculated values of SCY for each case provided sensitivity coefficient $(\Gamma_n/SCY)\Delta SCY/\Delta\Gamma_n$ and $(\Gamma_\gamma/SCY)\Delta SCY/\Delta\Gamma_\gamma$ for that case; e.g., for the left-area at the 6.67-eV level and for the 1/8" sample at 293°K, these sensitivity coefficients were + 0.18 and +0.39, respectively. A complex pattern of sensitivity coefficients resulted, with most being positive but becoming less positive and even negative for thicker shielding samples.

These sensitivity coefficients were used in least squares fits to determine improved resonance parameters for the s-wave levels below 100 eV. The fits were highly overdetermined. Only two parameters, Γ_n and Γ_x, were fitted for each level, and considering left- and right- areas and various thicknesses and temperatures of the shielding samples, the numbers of SCY values fitted for the 6.67-eV, 20.90-eV, 36.80-eV, 66.15-eV, and 80.74-eV levels were 23, 23, 23, 9 and 9, respectively. The fitted resonance parameters and their uncertainties are listed in Table 5. The overall goodness of fit was examined by the chi-squared test; the probabilities that chi-squared for the 6.67-eV, 20.9-eV, 36.8-eV, 66.15-eV and 80.74-eV levels can exceed the values obtained for the fits of Table 5 were 30%, 3%, 6%, 65%, and 85%, respectively. Substantial parts of the somewhat large chi-squared values for the 20.9-eV and 36.8-eV levels arose from the 873°K data for the 1/8"-thick samples. If these cases are eliminated the fitted resonance parameters do not change within their uncertainties, but the associated probabilities become 60%, 68%, 30%, 63%, and 83%, respectively. It is possible that the sample changer was slightly out of alignment for the 1/8" sample in the oven. These goodness-of-fit results suggest both that the uncertainty determinations are reasonable and that measurements and calculations are in accord for the area analyses.

Shape Analysis

Calculated self-indication capture yields are compared with measured channel-by-channel values in Figs. 6, 7 and 9 for the 6.67 eV, 20.9 eV, and 36.8 eV levels. These calculations utilized the RPI resonance parameters listed in Table 5 together with the analysis methods described in Section IV. The calculated and measured shapes are evidently in good agreement for the 6.67-eV level on both sides and for the other two-levels on the right-hand (negligible multiple scattering) side. For these cases least squares fits of calculated shapes to the observed shapes yielded values of Γ_n and Γ_γ which were within one standard error of the results from area analyses (9). Hence the RPI resonance parameters of Table 5, which are basically those inferred from the area analysis, are confirmed by the shape analysis.

The calculated self-indication yields exceed the observed values near the left-hand peaks for the 20.9-eV and 36.8-eV levels and fall below them at other energies so that the left-hand SCY areas are not greatly affected. The discrepancies are within the uncertainties of the relatively large multiple scattering corrections, so shape analyses of Γ_n and Γ_γ were not carried out for these cases.

Comparison with Other Results

The least-squares-fitted resonance parameters from this experiment are compared in Table 5 with the evaluated parameters from ENDF/B-IV (2) and ENDF/B-V (21) and with the experimental parameters from JAERI (22), Geel (23,24), Brookhaven (25), Oak Ridge (26), Harwell (27) and Columbia University (28). With the exception of the neutron widths of the 20.9- and 36.8-eV resonances, the RPI results are in good agreement with the bulk of the other experimental results. However, the RPI neutron widths for the 20.9- and 36.5-eV resonances

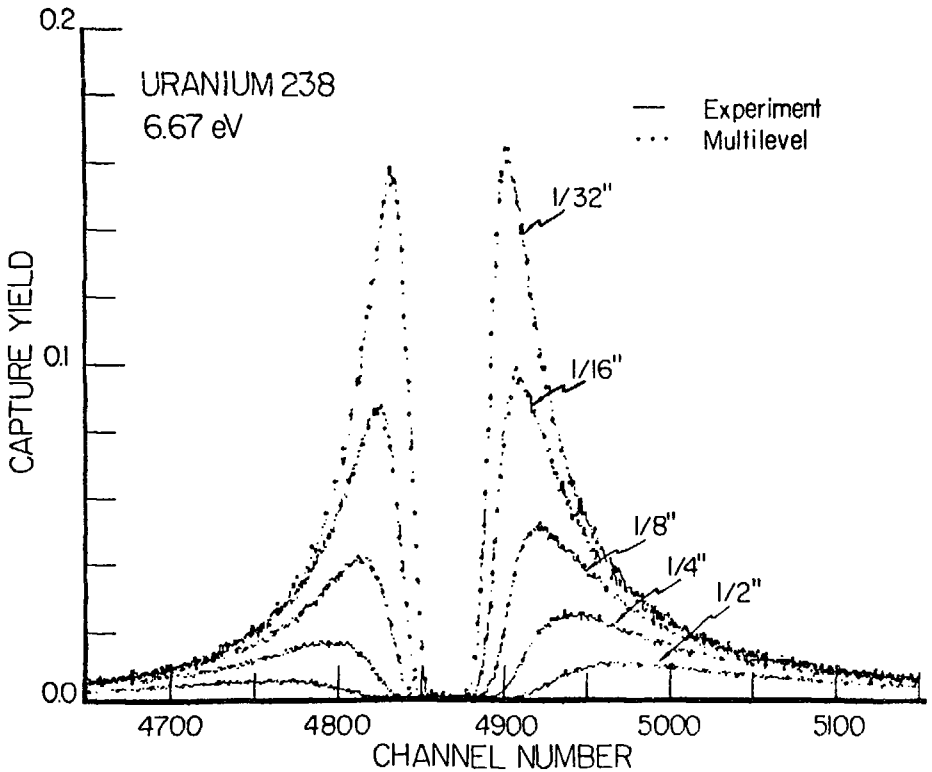

Figure 6

Comparison of experimental and calculated capture yields for the 6.67-eV resonance.

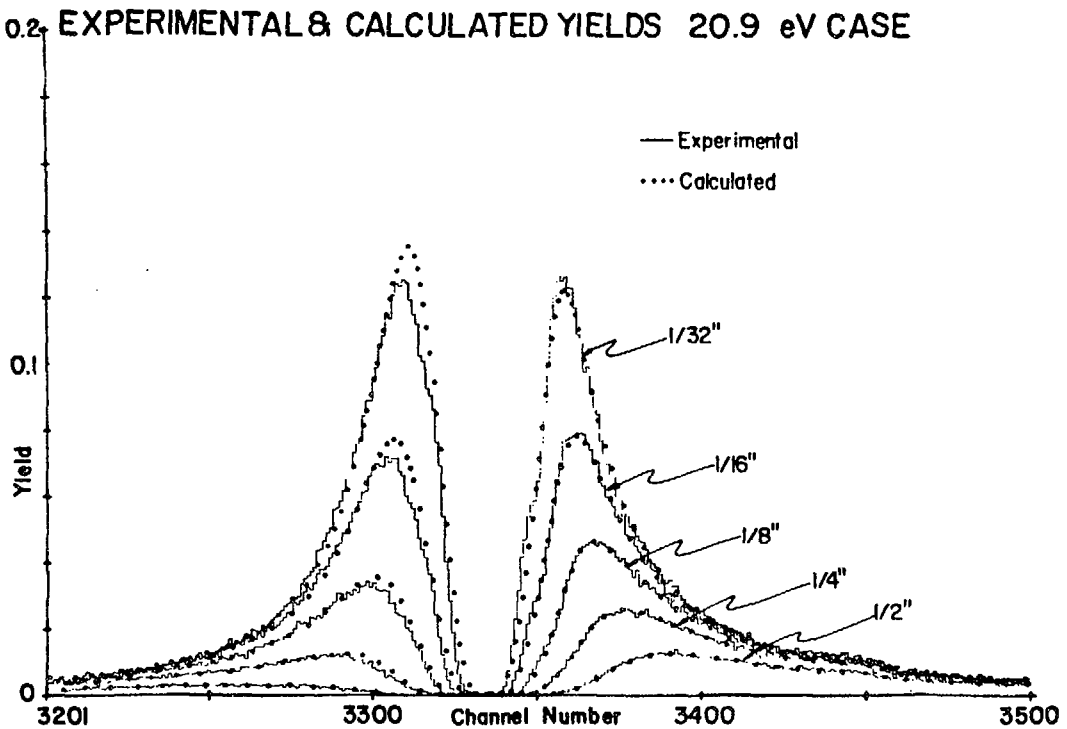

Figure 7

Comparison of experimental and calculated capture yields for the 20.9-eV resonance.

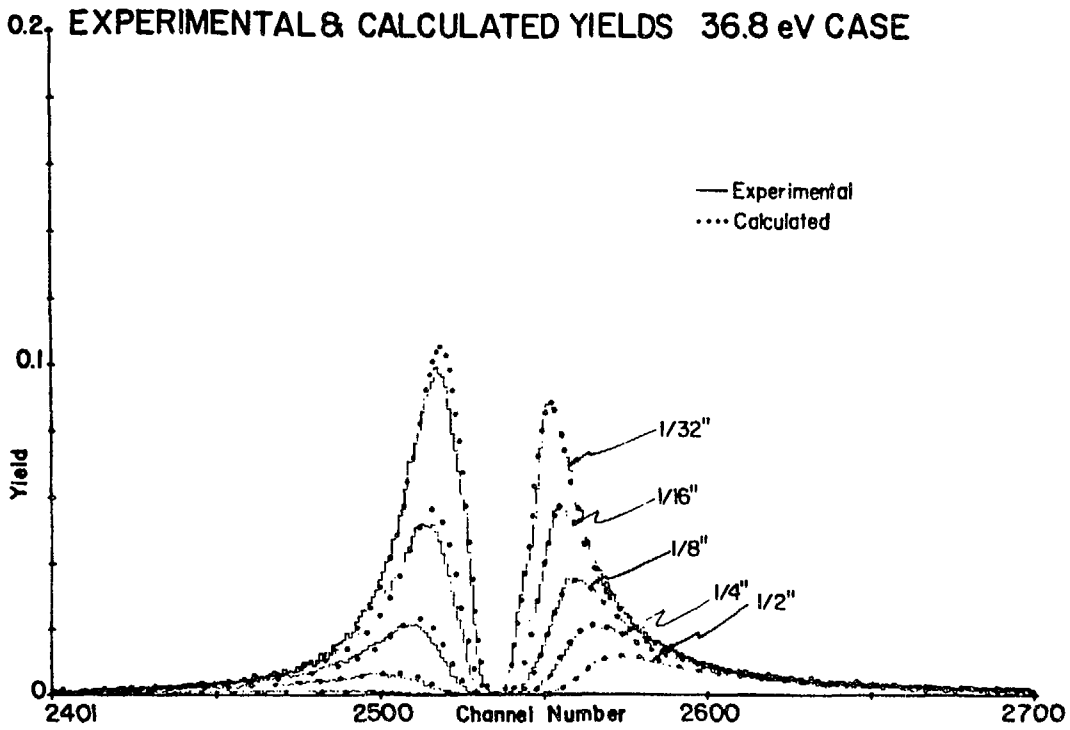

Figure 8

Comparison of experimental and calculated capture yields for the 36.8-eV resonance.

are about 8% lower than the average neutron widths determined from the other measurements. This represents a difference of the order of 4 to 5 standard deviations. The neutron widths for these two resonances are relatively large, and it is possible that the 8% discrepancy results from intrinsic differences between the self-indication measurement and the bulk of the other, predominantly transmission, measurements. The self-indication parameters are more strongly influenced by the thinner samples (up to about 1/8" thick) placed in the beam, while the transmission parameters are strongly influenced by thicker transmission samples. Thus self-indication measurements for resonances with large neutron widths are less dependent upon interference effects and therefore are less dependent on the selection of the potential scattering radius R' and on the parameters of nearby strong resonances. The weighted-average radiation width for all five resonances is 23.56 $\pm$ 0.11 meV from the RPI measurements and is 23.27 $\pm$ 0.14 meV from all the other measurements, where the individual radiation widths were weighted by the inverse squares of the quoted experimental errors.

Uncertainty in Capture Cross Section Between Resonances

These measurements have determined the neutron and radiation widths of the five lowest-energy s-wave resonances in ^{238}U, and from these values and the parameters of neighboring resonances, the neutron scattering and capture cross sections can be determined from Eqs. (4) and (5). However, the approximations used to derive the sums-of-single-level (SSL) capture cross section expression, Eq. (5), require that the effects of interference among the partial radiation channels average out to zero. This assumption cannot be completely accurate and to test it we have compared Wigner-Eisenbud and SSL calculations (16). The partial width parameters Γ_{rc} for resonance r and channel c were stochastically selected from normal distributions (29) with means zero and with equal variances or with variances proportional to El radiative transition probabilities from the neutron binding energy to available levels in $^{239}U^*$.

Table 5. ^{238}U+n Resonance Parameters

Reference	E_0 = 6.67 eV		E_0 = 20.90 eV		E_0 = 36.80 eV		E_0 = 66.1 eV		E_0 = 80.7 eV	
	Γ_n(meV)	Γ_γ(meV)	Γ_n(meV)	Γ_γ(meV)	Γ_n(meV)	Γ_γ(meV)	Γ_n(meV)	Γ_γ(meV)	Γ_n(meV)	Γ_γ(meV)
RPI	1.51±0.05	22.36±0.66	9.39±0.16	23.76±0.31	31.47±0.13	23.55±0.13	27.54±1.84	23.34±0.56	1.92±0.05	25.60±0.94
ENDF/B-IV (2)	1.50	25.6	8.8	26.8	31.1	26.1	25.3	23.5	2.0	23.5
ENDF/B-V (21)	1.50	22.53	10.12	23.07	33.91	22.92	24.61	23.69	1.907	24.17
Nakajima (22)			10.09±0.68		33.85±0.73		25.42±0.81		2.24±0.18	
Staveloz et al. (23)		24.2±0.8								
Poortmans et al. (24)	1.50±0.01	24.2±0.6	10.20±0.10	23.2±0.6	34.1±0.5	22.9±0.3	23.9±0.8	24.0±0.4	1.81±0.08	
Liou and Chrien (25)	1.50±0.03	21.8±1.0	9.86±0.5	23.5±1.5	33.3±1.2	23.6±2.0	25.6±1.8	22.2±2.0	2.16±0.18	23.7±2.5
Olsen et al. (26)	1.48±0.032	23.0±0.8	10.16±0.21	22.8±0.8	33.76±0.7	22.9±0.8	24.37±0.53	23.2±0.8	1.823±0.046	24.3±1.3
Haste and Moxon (27)	1.507±0.008	23.54±0.53	10.17±0.10	22.44±0.43	34.41±0.41	24.03±0.87	25.64±0.66	23.46±0.50	1.794±0.058	
Rahn et al. (28)	1.52±0.05		8.5±0.8	22.0±3.0	38.0±2.0	23.0±2.0	26.0±2.0	21.0±2.0	1.71±0.18	

Figure 9 illustrates typical results for SSL calculations compared with five sets of Wigner-Eisenbud calculations assuming 40 equally probable radiation channels. In the cross section valleys between resonances the Wigner-Eisenbud values form an envelope about 0.1 barn wide, and this includes the SSL result. When 800 radiation channels are used the envelope is only about 0.02 barn wide and again includes the SSL result. Wasson et al. (30) have measured partial capture cross sections for ^{238}U+n for relatively strong gamma rays, but their partial radiation widths only add up to 4% to 8% of the total radiative strengths for the five low-energy levels. When we include their values for $\Gamma_{rc}^{1/2}$ the envelopes of the results are largely unchanged.

An effective number of radiation channels can be inferred from the fluctuations in radiation widths from level to level. If the channels are taken to be of equal partial widths then $\Gamma_{r\gamma}$, the sum of $(\Gamma_{rc}^{1/2})^2$ over the effective radiative channels c, is distributed as chi-squared. The measured RPI values for radiation width have little fluctuation from level to level, and from these data the inferred number of effective radiation channels was found to be~800. Poortmans et al. (24) similarly inferred from their measurements a large value, 1250, for the effective number of radiation channels.

Combining these results it is concluded that the practice of calculating the capture cross section between resonances from measurements made essentially at the resonance, and without direct measurements of the off-resonant cross sections, may not be adequate for highly self-shielded applications. An uncertainty of 0.1 barn, if present over several lethargy units, could give rise to an appreciable uncertainty in the self-shielded resonance integral.

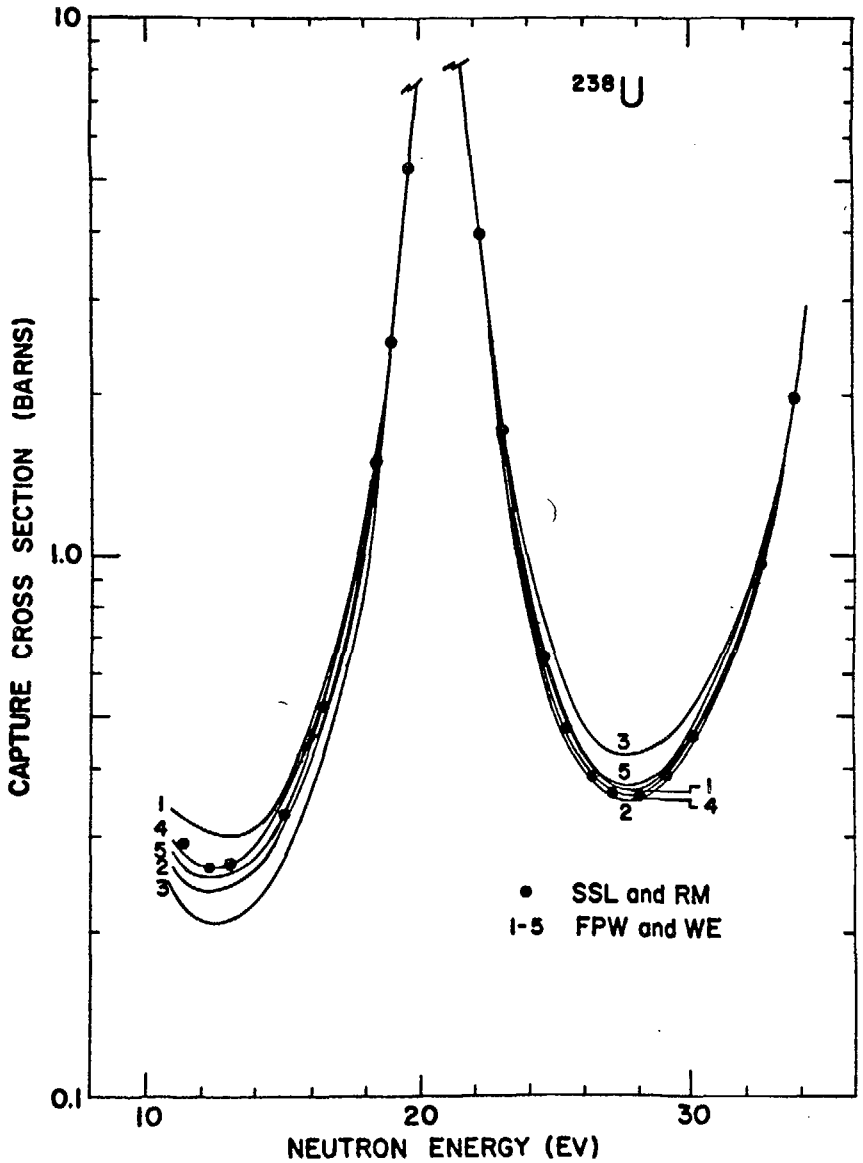

Figure 9. Capture cross sections from Sums-of-Single-Level (SSL) and Wigner-Eisenbud expressions. Case 1-5 are for five distinct sets of stochastically-selected partial widths for 40 radiation channels.

The relatively large numbers of effective radiation channels inferred from our measurements and those of Poortmans et al. (24), together with asymmetries observed in the interference effects (for example those displayed in Fig. 9), suggest but do not demonstrate that the uncertainty is marginal. It seems doubtful that capture spectrum measurements will resolve the issue because of the relatively small fraction of the radiation width resolved by Wasson et al. (31). Probably low-background direct measurements are required.

Engineering Implications

The RPI set of ^{238}U multilevel resonance parameters consists of (i) the neutron and radiation widths listed in Table 5 for the five lowest-energy s-wave resonances, (ii) a picket fence set of negative-energy levels which have constant radiation width and for which the first level has zero reduced neutron width, the second level has 58.8% of the average reduced neutron width, and all other levels have the average reduced neutron width, and (iii) ENDF/B parameters for all remaining s- and p-wave resonances. This set of parameters fits the self-indication data obtained in this experiment and reproduces the thermal capture cross section of 2.70 b.

For LWR systems a major concern is the prediction of the heavily-self-shielded ^{238}U capture resonance integral. Resonance integrals were calculated with these parameters over the energy range from 5-eV to 101.3 eV for an infinitely dilute system, a TRX-1 isolated metal rod, a TRX-1 lattice (1), a typical PWR isolated rod, and a typical PWR lattice. The PWR calculations was made at middle of exposure. The results are listed in Table 6 where ΔI, the change in the resonance integral between the RPI parameter set and the base ENDF/B-IV parameter set, is presented for the five systems. The TRX-1 and PWR calculations were carried out with the multi-region slowing-down program

Table 6. Comparison of Resonance Integrals Calculated with RPI and ENDF/B-IV Parameters.

E_o	Energy Range	ΔI^*_∞	ΔI^*_{eff}			
			TRX-1 Isolated Rod	TRX-1 Lattice	PWR Isolated Rod	PWR Lattice
(eV)	(eV)	(b)	(b)	(b)	(b)	(b)
6.67	5.0-14.0	-0.230	-0.207	-0.185	-0.326	-0.267
20.9	14.0-28.8	+0.996	-0.047	-0.042	-0.072	-0.059
36.8	28.8-51.5	-2.106	-0.062	-0.055	-0.108	-0.085
66.15	51.5-73.5	+0.424	+0.018	+0.017	+ .016	+0.016
80.74	73.5-101.3	-0.036	+0.001	+0.001	- .003	-0.001
	5.0-101.3	-0.952	-0.297	-0.264	-0.493	-0.396

*$\Delta I \equiv$ I(RPI parameters) - I(ENDF/B-IV parameters)

FASTR (7). Dancoff factors were obtained from Monte Carlo calculations. The net change in the infinitely dilute resonance integral, ΔI_∞, between ENDF/B-IV and RPI parameters is only -0.95 b. This is small compared to the 275 b infinitely dilute resonance integral (3), and we thus conclude that the RPI parameters do not effectively change the infinitely dilute integral. However, for the heavily-self-shielded resonance integrals listed in columns 4 to 7 of Table 6 the net change ΔI_{eff} of -0.264 to -0.396 b represents a significant reduction in the resonance integral. The TRX 1 isolated-rod measured resonance integral is 15.7 b, and the ENDF/B-IV calculated resonance integral is 0.7 b higher than the measured value. The RPI parameters reduce this difference by 0.297 b, which is in the right direction but only about half of the magnitude to bring the calculations into agreement with the isolated rod measurements. For the TRX-1 lattice, the resonance integral is lowered by approximately the same fractional amount as for the TRX-1 isolated rod. For the typical middle-of-cycle PWR isolated rod and lattice the resonance integral is lowered by 0.493band 0.396 b respectively, which is slightly larger than the changes in the corresponding TRX-1 integrals. Uncertainties in the measured RPI resonance parameters lead to about $\pm$.06 b uncertainties in the resonance integral reductions for the TRX and PWR rods. In summary, the RPI set of ^{238}U multi-level resonance parameters reduces by about one-half the discrepancy between calculated and measured resonance integrals.

References

1. F.J. McCrosson and J. Hardy, Jr., Seminar on ^{238}U Resonance Capture, March 18-20, 1975, BNL-NCS-50541, p 13.
2. Evaluated Nuclear Data File/B, Version IV, National Nuclear Data Center, Brookhaven National Laboratory, 1975.
3. J.R. Askew, "Some Problems in the Calculation of Resonance Capture in Lattices," Reactor Physics in the Resonance and Thermal Regions, Vol. II, Eds. A.J. Goodjohn and G.C. Pomraning, the MIT Press, Cambridge, 1966, p 395.
4. M. Becker, D.R. Harris, B. Quan, and J.M. Ryskamp, "The Relationship Between Basic Nuclear Data and LWR Fuel Cycle Parameters," Proc. Conf. Nuclear Data for Thermal Reactor Applications, Brookhaven National Lab., May 22-24, 1978, Electric Power Research Institute, 1979.
5. W. Rothenstein, "Discrepancies in Thermal Reactor Lattice Analysis", Reference 1, p 2.
6. L. Dresner, Resonance Absorption in Nuclear Reactors, Pergamon Press, N.Y. 1960.
7. R.C. Block, D.R. Harris, K. Kobayashi and S.H. Kim, "^{238}U Resonance Self-Indication Capture Measurements and Analysis," Electric Power Research Institute Report NP-996, 1979.
8. R.C. Block, D.R. Harris, S.H. Kim, and K. Kobayashi, Trans. Am. Nuc. Soc., 27, 868 (1977).

9. D.R. Harris, R.C. Block, and S.H. Kim, Trans Am. Nuc. Soc., (1979).

10. R.W. Hockenbury, Z.M. Bartolome, J.R. Tatarczuk, W.R. Moyer and R.C. Block, Phys. Rev. 178, 1746 (1969).

11. Z.M. Bartolome, R.W. Hockenbury, W.R. Moyer, J.R. Tatarczuk and R.C. Block, Nucl. Sci. Eng., 37, 137 (1969)

12. T.Y. Byoun, Ph.D. Thesis, "Experimental Investigation of the Resonance Self-shielding and Doppler Effect in Uranium and Tantalum," Rensselaer Polytechnic Institute, 1973.

13. M. Koslin (private communication).

14. E.P. Wigner and L. Eisenbud, Phys. Rev., 72, 29 (1947).

15. G. deSaussure, D.K. Olsen and R.B. Perez, Nucl. Sci. Eng., 61, 496 (1976).

16. S.H. Kim, D.R. Harris, and R.C. Block, Proc. of Int. Conf. on Neutron Physics and Nuclear Data for Reactors, Harwell, pg.730, Sept. 1978.

17. J.E. Lynn, The Theory of Neutron Resonance Reactions, Clarendon Press, Oxford, 1968.

18. W.E. Lamb, Phys. Rev. 55, 190, (1939).

19. H.E. Jackson and J.E. Lynn, Phys. Rev. 127, 461 (1962).

20. J.G. Sullivan, G.G. Warner, R.C. Block and R.W. Hockenbury, RPI Report 328-155 (1969).

21. Evaluated Nuclear Data File/B, Version V, National Nuclear Data Center, Brookhaven National Laboratory, 1979.

22. Y. Nakajima, "Neutron Resonance Parameters of ^{238}U", J. Nucl. En. 7, 25 (1980).

23. P. Staveloz, F. Portmans, L. Mewissen, and E. Cornelis, Nuc. Sci. Eng. 66, 349 (1978).

24. F. Poortmans, E. Cornelis, L. Mewissen, G. Rohr, R. Shelley, T. van der Veen, G. Vanpraet, H. Weigmann, Proc. of IVth Soviet Conference on Neutron Physics, Kiev, 1977.

25. H.I. Liou and R.E. Chrien, Nuc. Sci. Eng., 62, 463 (1977).

26. D.K. Olsen, G. deSaussure, R.B. Perez, E.G. Silver, F.C. Difilippo, R.W. Ingle and H. Weaver, Nuc. Sci. Eng., 62, 479 (1979).

27. T.J. Haste and M.C. Moxon, Proc. Int. Conf. on Neutron Physics and Nuclear Data for Reactors, Harwell, Sept. 1978, IAEA (1979), p 337.

28. F. Rahn, H.S. Camarda, G. Hacken, W.W. Havens, Jr., H.I. Liou, J. Rainwater, M. Stagolitz, and S. Wynchank, Phys. Rev. C 6, 1854 (1972).

29. C.E. Porter and R.G. Thomas, Phys. Rev. 104, 483 (1956).

30. O.A. Wasson, R.E. Chrien, G.G. Slaughter and J.A. Harvey, Phys. Rev. C 4, 900 (1971).

PROBLEMS AND PROGRESS REGARDING RESONANCE PARAMETERIZATION OF ^{235}U AND ^{239}Pu FOR ENDF/B

M.S. Moore
University of California, Los Alamos National Laboratory,
P.O. Box 1663, Los Alamos, NM 87544

G. de Saussure
Oak Ridge National Laboratory,
P.O. Box X, Oak Ridge, TN 37830

and

J. Richard Smith
EG&G, Idaho, Inc.,
P.O. Box 1625, Idaho Falls, Idaho 83401

Abstract

The procedures used to obtain the resolved and unresolved resonance parameterization of ^{235}U and ^{239}Pu contained in the U.S. Evaluated Nuclear Data File ENDF/B-V are reviewed. For ^{235}U, recommendations are made to improve the representation by including information on resonance spins and fission-channel vector orientations, and some preliminary results are presented. We review evidence that it is the fission channels rather than the spins of the resonances that lead to differences in fission mass distributions, the number of neutrons emitted per fission, and fission kinetic energies. The improved parameterization may thus have physics content that will prove of interest in future applications.

I. Status of ENDF/B

In the early years of the development of the U.S. Evaluated Nuclear Data File, ENDF/B, the reduced R-matrix representation of resolved-resonance cross sections of fissile nuclei was an approved alternative description. It was never used, however, because it led to difficulties in processing the data, in particular in the treatment of Doppler broadening. The recommended procedurewas to use a single-level formulation to calculate symmetric resonance poles, and to correct for possible asymmetries in the cross-section shapes about the poles by adding a pointwise contribution from a tabulated file (File 3). Doppler broadening of the symmetric poles could be easily carried out using Voigt profiles, and it was expected that the File-3 contribution would be small enough that the Doppler broadening could be neglected.

This procedure worked reasonably well. For ^{235}U, Smith and Young[1] provided a resonance evaluation below 82 eV that was approved for inclusion in ENDF/B-III. There was only fragmentary information available at that time on the resonance spins, but for ^{235}U, with a spin of 7/2, this deficiency was not thought to be of primary importance, and the Smith-Young evaluation was found to give a reasonably consistent description of the total and partial cross sections.

For ^{239}Pu, Simpson and Simpson[2] carried out a preliminary evaluation to 300 eV for ENDF/B-III, finding that it was impossible to achieve an internally consistent description of the measured total and partial cross sections. Derrien[3] attributed this difficulty to the fact that the Simpson-Simpson evaluation also did not contain resonance-spin information. The Simpson-Simpson evaluation was then revised by Smith, Kinsey, and Garber,[4] who found that the internal inconsistencies were not removed by an improved spin treatment, and concluded that the problem is one of consistency among total cross section measurements using different sample thicknesses. The total cross section data file had been constructed as weighted averages of total cross sections deduced from transmission measurements on several samples of different thicknesses. This weighting procedure does not appear to treat properly the problems associated with uncertainties in the knowledge of the number of atoms in the samples. When such a mixed set of total cross section data is included in a multiple fit with both fission and capture data, the inconsistencies in the total cross section data are revealed. In reality it is improper to use such a total cross section file directly in a multi-cross section fit. A better procedure would be to fit the transmission data from all of the individual sample thicknesses, along with the partial cross sections. However, the transmission data are usually not available in the necessary detail.

The fit by Smith et al. was not a complete reanalysis of the data, but a revision of the Simpson and Simpson parameters with spins assigned to the resonances. In general the total widths were retained, with adjustments made to the fission and capture widths to yield the ratios of capture to fission indicated by Gwin's ORELA data[5]. Since these data had not yet been completely reduced, fission and capture normalizations were based on data from the single run selected by Gwin as being best for this purpose. While this evaluation was not documented, and there are some areas where the fit is rather unsatisfactory, it was approved for inclusion in ENDF/B-IV and continued in ENDF/B-V, the current version.

Perhaps the most stringent testing of the resonance region evaluations of ^{235}U and ^{239}Pu was done by Koenig and Carter,[6] and by Cullen and Plechaty,[7] who used the ENDF/B-III evaluations to calculate resonance-self-shielded fission measurements of Bramblett and Czirr.[8,9] The results of these data-testing calculations were somewhat surprising: The ^{239}Pu resonance evaluation of ENDF/B-III was found to give rather good agreement with the Czirr-Bramblett measurements on ^{239}Pu, while the ^{235}U evaluation seemed to overpredict the measured self-shielded fission rates on ^{235}U by 20-30%. This descrepancy for ^{235}U was a source of concern for many years. In their review paper at the Harwell conference in 1978, Keyworth and Moore[10] carried out an assessment for various evaluations of resonance parameters for ^{235}U and concluded that there is no adjustment of parameters consistent with the body of microscopic data that could give agreement with the Bramblett-Czirr measurement. They recommended as a first step that this measurement be repeated and verified. This was done by Czirr,[11] who found that the earlier measurements were not corrected properly for background, and that the discrepancy was largely removed if one compared calculations based on the existing evaluations with the results of his remeasurement.

No attempt was made to improve the ^{235}U resonance parameter set for ENDF/B-IV. For ENDF/B-V, it was first proposed to use the evaluation of Reynolds[12] for ^{235}U. The Reynolds evaluation is an R-matrix analysis below 60 eV and does contain the preliminary resonance spin assignments of Keyworth et al.[13] However, two obstacles to the incorporation of the Reynolds parameters presented themselves. The first was a consequence of the exclusive utilization of the fission and capture data of Perez et al.[14] in the fitting procedure. As is the case with many measurements in which boron filters are used to suppress backgrounds, the Perez data become progressively low in the region of the cutoff of the boron filter. Unfortunately the cutoff region almost exactly corresponds to the energy span of the Reynolds evaluation. In the intermediate normalization region 7.8-11 eV the fission integral of the Perez data is 8% lower than the best value based on the comparison of all of the known measurements. The second problem with the Reynolds parameter set was a reluctance on the part of the Cross Sections Evaluation Working Group (CSEWG) to decrease the span of the resolved resonance region from 82 to 60 eV. An effort was made to utilize Adler-Adler parameters, converted from the Reich-Moore parameters through the program POLLA, from 1-82 eV. Below 60 eV the Reynolds parameters would be used. From 60 to 82 eV the parameters would be taken from the multilevel fit by Smith[1], which was tailored to yield very closely the same description of cross sections as the single-level representation of Smith and Young. However, the mixed set of Adler-Adler parameters was found to generate rather severe interference anomalies, and the approach was finally abandoned.

The current version of the U.S. Evaluated Nuclear Data File, ENDF/B-V, contains the Smith-Young[1] parameter set for ^{235}U and the Smith, Kinsey, and Garber[4] set for ^{239}Pu. Neither of these is completely satisfactory, as noted above, for the following reasons: 1) The ^{235}U parameter set does not contain spin information, and the single-level description plus smooth background lends itself to accurate Doppler broadening only if kernel broadening is performed on the complete cross sections obtained by adding the smooth files to the resonance calculations. 2) The ^{239}Pu set represents an uncompleted analysis, as the effort was terminated by the time considerations, not by the adequacy of the fit. There are several regions involving overlapping resonances in which the fit is poor. These regions should be cleaned up, and the fit extended to approximately 700 eV, incorporating the fission and capture data of Gwin et al.[15]

The restriction to a single-level or Kapur-Peierls description of the resonance cross sections of fissile nuclei in future versions of ENDF/B appears unlikely to be removed. Fröhner[15] recently noted that an important simplification would result if one were to use Turing's method for analytical Doppler broadening of the Reich-Moore or reduced R-matrix parameterization. This method was studied some years ago by Bhat and Lee-Whiting[16]; its adoption would effectively obviate the necessity for the simpler descriptions. We feel that this approach is desirable, in that it also seems to offer the possibility of including in the evaluation physical information, such as the detailed energy dependence of ν, that is presently included only in a limited pointwise representation. But there appears to be considerable reluctance in the user community to implement the code changes required for a multiple-channel R-matrix evaluation for ^{235}U as a part of ENDF/B. The question is to be decided at the October 21-22 meeting of CSEWG.

For (^{235}U + n) in the unresolved resonance region (82 eV to 25 keV), a complete re-evaluation was carried out for ENDF/B-V by Bhat and Moore.[17] In order to provide a consistent energy scale, fission data of Keyworth et al.,[18] Perez et al., [14] and Gwin et al.[19] were shifted to match the energy scale of Lemley et al.[20] by maximizing the correlation coefficients between the data sets, and then averages were taken to obtain the absorption and fission cross sections from the Perez et al., Gwin et al., and Lemley et al. sets. After correcting for p-wave fission, the spin-dependence of the unresolved-resonance s-wave fission cross section was obtained by normalizing the spin-separated fission cross sections of Keyworth et al.[18] to the average fission cross section of Perez, Gwin, and Lemley et al. Finally, with the unresolved resonance code UR of Pennington,[21] a set of spin-dependent s-wave average resonance parameters was obtained by simultaneously fitting the absorption and spin-dependent fission cross sections. The intermediate structure in (^{235}U + n) is thus described below 25 keV in this evaluation as an s-wave phenomenon; the evaluation was accepted for inclusion in ENDF/B-V.

The ENDF/B-V representation of the unresolved resonance region for ^{239}Pu (300 eV to 25 keV) is considered to be inadequate. The situation was reviewed by Weston[22] at a recent evaluation conference at Brookhaven National Laboratory. The fission cross sections are thought to be too high, the energy scale is thought to be incorrect, and the capture-to-fission ratio has the wrong shape. Weston attributes the problem to an inadequate treatment of inelastic scattering, recommending a re-evaluation that takes into account recent measurements by Haouat et al.[23]

At a meeting at Brookhaven National Laboratory on May 14-15, 1981, the U.S. Cross Sections Evaluation Working Group (CSEWG) reviewed progress in data testing of ENDF/B-V and set tentative goals for the future. According to the summary of the meeting made by the chairman (S. Pearlstein), plans for ENDF/B-VI (the next version) are as follows:

> The milestone tasks for ENDF/B-VI include fixing of formats, completion of standards, definition of objectives, upgrading of codes, completion of evaluations, and data testing. Because the results of data testing ENDF/B-V are not yet complete and interpreted the goals for ENDF/B-VI cannot be detailed. Therefore, the Executive Committee agreed that only the following tasks could be scheduled at this time:
>
> | | |
> |---|---|
> | Formats fixed | Spring 1982 |
> | Standards complete | Spring 1983 |
> | ENDF/B-VI goals detailed | Fall 1982-Spring 1983 |

At the same meeting, the CSEWG subcommittee on General Purpose Evaluations considered minimum goals for ENDF/B-VI heavy nuclide evaluations. L. Weston and L. Stewart provided a list of such goals to form the basis for the discussion; this list contained the following items in the resolved and unresolved resonance regions for ^{235}U and ^{239}Pu:

92 U-235	0 - 1 eV	Compare thermal shape with prediction using resolved parameters. New measurements are needed (Weston).
	1 - 100 eV	Multilevel representation must replace the Version V (really III) single-level Breit-Wigner. This requires a reanalysis using recent experimental data. Check for reasonable x/s for normalization integral between 7.8 and 11 eV (de Saussure).
	Unresolved	Check end points and for possible improvements. for possible for possible improvements.
94 Pu-239	0 - 1 eV	Compare thermal shape with that calculated from resonance parameters. New measurements needed (Weston).
	300 eV - 200 keV	Cross sections are inconsistant. New evaluation needed. Representation of inelastic levels is poor. See B-III data (Weston).

II. Fission Channels and Scission-Point Variables

The fission process is often pictured as occurring in multiple stages. For low-energy neutron-induced fission, the first stage is the formation of a compound nucleus, where the excitation energy afforded by the binding energy of the incident neutron is shared among the nucleons. Connected with this stage are resonance properties such as neutrons widths, spins, and resonance spacings. The second stage (perhaps given in detail by several sequential stages) is the crossing of a double- or triple-humped barrier. At the tops of these barriers the nucleus is relatively cold, the excitation energy being largely taken up by the potential energy of the mass surface. Only a few modes of motion are allowed, and the average fission width is determined by the sums of partial widths in the few channels or saddle-point states that may exist. The angular distributions of the fragments are assumed to be related to the channel structure at the outer barrier. The next stage is the transition from the outer saddle point to scission, beyond which the nuclear interaction between the nascent fragments vanishes, by definition. It follows that at scission the primary fission-fragment mass and charge distributions have been established. The time required for and the nature of the saddle-to-scission transition remains an open question, but there is evidence that the mass, charge, and kinetic-energy distributions do depend on the fission-channel configuration at the outer barrier. After scission, as the fragments separate under the influence of long-range coulomb forces, they reorient themselves from the possibly highly deformed scission-point configuration and emit most of the prompt neutrons and prompt fission-gamma radiation.

There is a small but significant variation of all these scission-point variables with neutron energy in the resonance region for neutron-induced fission of both ^{235}U and ^{239}Pu. For ^{239}Pu, the observed variations in both the mass distributions and in ν are found to be spin dependent.[24,25] Frehaut and Shackleton[25] found that the variation in ν is anticorrelated with the prompt fission-gamma yield and depends on the size of the fission width; they suggested that the variation in ν is dominated by competition of the (n,f) and (n,γf) processes. For ^{235}U, the variations in the mass distributions[26] and ν[27,28] are smaller than for ^{239}Pu, and do not appear to depend on the resonance spin, but on the fission channel properties. While it is well known[29] that the mass-distribution variation in (^{235}U + n) is strongly correlated with the fission channel properties, evidence that the variation in ν is similarly correlated has not appeared in the literature and deserves to be reviewed. Pattenden and Postma[30] provided the definitive measurement of the fission channel structure of (^{235}U + n). Following the preliminary work of Dabbs et al.,[31,32] they measured the anisotropy of fission fragments emitted by an aligned sample of ^{235}U irradiated by neutrons at the Harwell linear accelerator. The fragment anistropy is described in terms of A_2, the coefficient of the second Legendre term in the angular distribution expansion, and depends strongly on the K-value of the channel, For ^{235}U, with spin $7/2^-$, the Pattenden-Postma data suggest that neutron-induced fission takes place for 3- resonances in three open channels with K = 0,1,2, and for 4- resonances in two open channels with K = 1,2. Pattenden and Postma measured anisotropies and reported A_2 values for 61 resonances in (^{235}U + n); these values are strongly correlated[29] with variations in the mass distribution of (^{235}U + n) fission measured by Cowan et al.[26]

The variation of ν for (^{235}U + n) was measured by Howe et al.[27] and by Reed et al.[28]. Howe et al. compared their results, by calculating correlation coefficients, with the resonance spins determined by Keyworth et al.,[18] and with the Pattenden-Postma fission-channel angular anisotropies, and concluded that no significant correlation exists. Reed et al.[28] used a different technique, similar to that developed by Weinstein et al.[33] If we calculate the correlation coefficient of the ν measurements of Howe et al.

and of Reed et al., we conclude that the variation is significant and that the two experimental data sets are measures of the same quantity. In other words, we can assume that an average of the Howe et al. and Reed et al. data is likely to be a more nearly accurate representation of the energy dependence of ν than either individual set. The energy dependence of this average, the A values of Pattenden and Postma, the mass distribution variations of Cowan et al,[26] and the effective J values of Keyworth et al. are shown in Table I. The correlation of ν with resonance spin is not significant, but the correlation of ν with the mass distribution measure R is significant at the 0.5% level (i.e., there is a probability of only 0.5% that the sampling of values of ν and R are randomly distributed). The correlation of R and the fission-changed measure A_2 is significant at the 10^{-5} level. We conclude that it is the fission channel properties that lead to the measured variation in ν.

Studies by Auchampaugh[34] have shown that reduced R-matrix fitting of fission cross sections, when there are more than a single open fission-channel, is completely non-unique, in that there are many solutions with different relative fission-vector orientations that give equivalently good fits to the data. In a two-fission-channel description, the number of such solutions was estimated by Adler and Adler[35] as (N-1)(N-2)/2 + 1, where N is the number of levels. However, if the angular distributions of Pattenden and Postma are used as a constraint in such a two-fission-channel description, the fits can be unique.

We expect that a significant improvement in the resonance parameters of (^{235}U + n) can be made. The deficiencies noted in the previous section should be corrected. If carried out under the constraint of a two-fission-channel reduced R-matrix representation, the parameterization should reflect the fission-vector orientations that describe the Pattenden-Postma angular distributions. We feel that such an approach could also describe, at least to first order, the energy dependence of certain scission point variables such as ν and the fragment mass and kinetic energy distributions.

A preliminary analysis of this type has been attempted; the results are given in Table II and shown in Figs. 1-5. We fitted only the spin-separated fission cross sections of Keyworth et al,[10] using as initial-guess parameters the recommended values of Moore et al.,[36] in which the initial-guess fission-vector orientations were chosen to reflect the Pattenden-Postma fission-fragment anisotropies.

A comparison of the preliminary set of Table II with other evaluations shows that most of the narrow resonances listed have fission widths that are too high and neutron widths that are correspondingly too low (such that the resonance fission areas are preserved). This is undoubtedly a consequence of using a slightly incorrect resolution or Doppler width in the fitting. This kind of deficiency can easily be corrected by including total and/or capture cross section data in the fitting.

There are three other modifications that should be made to the set in Table II: 1) In the vicinity of the strong resonance in ^{139}La at 72 eV, Keyworth's data do not describe the actual fission cross section, and one should use a different data set. 2) The fission-width vector orientations are not always given correctly. For example, as shown in Fig. 6, in the region around the 8.8 eV resonance, a clockwise rotation of the vectors by 30° would more nearly represent the Pattenden-Postma results. Between 15 and 20 eV, the vector orientations are given adequately for three of the four strong 4- resonances, but we were unable to achieve a fit that would describe the 15.6 eV resonance as being mostly in the K=1 channel. 3) No fitting was done over the 0.3 eV resonance. Here the Pattenden-Postma data suggest that the fission widths are about equally divided between K=0 or 1 and K=2, with constructive interference above the 0.3 eV resonance in the K=2 channel. While the preliminary parameters of Table I should not be considered definitive, they are expected to prove useful as starting parameters for a more nearly complete analysis.

REFERENCES

1. J.R. Smith and R.C. Young, ANCR-1044 (1971); and J.R. Smith, USAEC report ANCR-1129, p. 10 (1973).
2. O.D. Simpson and F.B. Simpson, ANCR-1045 (1971).
3. H. Derrien, CEA-N 1638, EANDC (E) 158 (L) (1973).
4. J.R. Smith, R.R. Kinsey, and D.E. Garber, unpublished (1974).
5. R. Gwin, L.W. Weston, G. de Saussure, R.W. Ingle, J.H. Todd, F.E. Gillespie, R.W. Hockenbury, and R.C. Block, Nuc. Sci Eng. 45, 25 (1971).
6. D.R. Koenig and L.L. Carter, Trans. Am. Nuc. Soc. 17, 490 (1973).
7. D.E. Cullen and E.F. Plechaty, Trans, Am. Nuc. Soc. 17, 490 (1973).
8. R.L. Bramblett and J.B. Czirr, Nuc. Sci. Eng. 35, 350 (1969).
9. J.B. Czirr and R.L. Bramblett, Nuc. Sci. Eng. 28, 62 (1967).
10. G.A. Keyworth and M.S. Moore, in "Neutron Physics and Nuclear Data," OECD, Paris, p. 241 (1978).
11. J.B. Czirr, Nuc. Sci. Eng. 70, 307 (1979).
12. J.T. Reynolds, KAPL-M-7396 (1975); and private communication (1974).
13. G.A. Keyworth, C.E. Olsen, F.T. Seibel, J.W.T. Dabbs, and N.W. Hill, Phys. Rev. Letters 31, 1077 (1973).
14. R.B. Perez, G. de Saussure, E.G. Silver, R.W. Ingle, and H. Weaver, Nucl. Sci. Eng. 52, 46 (1973) and USAEC report ORNL-TM-3696 (1972).
15. F. Frohner, in "Nuclear Data Evaluation Methods and Procedures," BNL-NCS-51363, p. 375 (1980).

16. M.R. Bhat and G.E. Lee-Whiting, Nuc. Inst. Meth 47, 277 (1967).

17. M.R. Bhat and M.S. Moore, unpublished (1977), see summary description in ENDF-201, compiled by R. Kinsey (1979).

18. G.A. Keyworth, C.E. Olsen, J.D. Moses, J.W.T. Dabbs, and N.W. Hill, in Nuclear Cross Sectionsand Technology, (R.A. Schrack and C.D. Bowman, eds.), NBS Spec. Pub. 425(1975), Vol. II, p. 576.

19. R. Gwin, E.G. Silver, R.W. Ingle, and H. Weaver, Nuc. Sci. Eng. 59, 79 (1976).

20. J.R. Lemley, G.A. Keyworth, and B.C. Diven, Nuc. Sci. Eng. 43, 281 (1971).

21. E. Pennington, unpublished (1973).

22. L. Weston, in "Nuclear Data Evaluation Methods and Procedures," BNL-NCS-51363, (1980) and private communication (1981).

23. G. Haouat, Ch. Lagrange, J. Lachkar, J. Jary, Y. Patin, and J. Sigaud, in "Nuclear Cross Sections for Technology," Knoxville, NBS Spec. Pub. 594, 672 (1980).

24. G.A. Cowan, B.P. Bayhurst, R.J. Prestwood, J.S. Gilmore, and G.W. Knobeloch, Phys. Rev. 144, 979 (1966).

25. J. Frehaut and D. Shackleton, in "Physics and Chemistry of Fission III, Rochester" IAEA, Vienna, p. 201 (1973).

26. G.A. Cowan, B.P. Bayhurst, R.J. Prestwood, J.S. Gilmore and G.W. Knobeloch, Phys. Rev. C2, 615 (1970).

27. R.E. Howe, T.W. Phillips, and C.D. Bowman, Phys. Rev. C13, 195 (1975).

28. R.L. Reed, Doctoral dissertation, Rensselaer Polytechnic Institute, unpublished (1969), see also R.L. Reed, R.W. Hockenbury, and R.C. Block, RPI Linear Accelerator Report COO-3058-29 (1968).

29. M.S. Moore, in "Statistical Properties of Nuclei," J.B. Garg, ed., Plenum Press, New York, p. 55 (1972).

30. N.J. Pattenden and H. Postma, Nuc. Phys. A167, 225 (1971).

31. J.W.T Dabbs, F.J. Walter, and G.W. Parker, in "Physics and Chemistry of Fission I, Salzburg," IAEA, Vienna, Vol. I, p. 39 (1965).

32. J.W.T. Dabbs, C. Eggerman, B. Cauvin, A. Michaudon, and S. Sanche, in "Physics and Chemistry of Fission II, Vienna," IAEA, Vienna, P. 521 (1969).

33. S. Weinstein, R.L. Reed, and R.C. Block, ibid., p. 477 (1969).

34. G.F. Auchampaugh, Nuc. Phys. A175, 65 (1971).

35. D.B. Adler and F.T. Adler, Phys. Rev. C6, 985 (1972).

36. M.S. Moore, J.D. Moses, G.A. Keyworth, J.W.T. Dabbs, and N.W. Hill, Phys. Rev. C 18, 1328 (1978).

Table I.

The energy dependence from resonance to resonance of $\bar{\nu}$ (ref. 27, 28), the fragment angular anisotropy measure A_2 (ref. 30), the mass distribution measure R(ref. 26), and the effective spin (ref. 36).

Energy (eV)	Relative $\bar{\nu}$	$-A_2$	R	Jeff	Energy (eV)	Relative $\bar{\nu}$	$-A_2$	R	Jeff
0.29	1.0025	1.35	-	3.20	24.25	0.9962	1.50	1.100	3.00
1.14	1.0022	1.63	-	3.76	24.50	0.9968	-	-	3.04
2.03	0.9929	1.87	-	3.44	25.2-25.6	0.9995	0.97	1.032	3.00
2.84	0.992	-	-	3.6	26.49	1.0008	1.55	0.619	3.37
3.14	1.0053	1.60	-	3.33	27.82	1.0020	1.70	0.554	3.92
3.61	1.0055	1.96	-	3.83	28.36	1.0050	1.25	1.250	3.01
4.84	0.9869	1.74	-	3.53	29.65	1.0017	1.71	0.943	3.74
6.21	1.0045	0.96	-	3.22	30.6-30.9	0.9962	2.04	0.441	3.78
6.39	0.9983	1.70	-	3.65	32.07	0.9984	1.88	0.708	3.71
7.08	0.9994	2.29	-	3.83	33.53	0.9967	2.11	0.401	3.95
8.78	0.9992	1.78	-	3.87	34.4-34.8	1.0024	1.42	0.934	3.46
9.28	0.9985	1.81	-	3.74	35.20	1.0013	0.99	1.027	3.29
10.18	0.9914	1.89	-	3.83	36.5	-	0.93	1.344	3.26
11.66	0.9918	1.84	-	3.74	38.36	-	1.01	1.038	3.75
12.39	0.9941	1.17	-	3.10	39.41	0.9985	1.71	1.008	4.00
12.85	1.0026	1.91	-	3.81	41.3-42.7	0.9987	1.16	-	3.42
14.0-14.5	0.9955	1.20	-	3.10	43.4-45.8	0.9972	1.53	0.784	3.50
15.40	0.9930	2.11	-	3.86	46.8-47.0	1.0015	1.81	0.620	3.88
16.08	0.9894	1.87	-	3.91	48.0-49.4	1.0003	1.54	0.807	3.41
16.68	0.9944	2.27	-	3.99	50.5-52.2	0.9984	1.04	0.906	3.31
18.05	0.9958	1.64	-	3.34	55.1-56.5	0.9996	1.93	-	3.77
19.30	0.9941	1.82	0.402	3.83	57.8-58.7	0.9930	1.74	0.649	3.44
21.07	0.9976	1.93	0.517	3.47	59.8-61.2	0.9918	2.28	0.652	3.40
22.94	0.9962	2.15	0.374	3.93	63.6-64.3	0.9950	-	-	3.72
23.4-23.6	0.9982	2.16	0.404	3.19	65.8-67.3	1.0126	-	1.119	3.56

Correlation coefficients and significance levels (2-sided distribution):

$\rho(\bar{\nu},A_2)$ = +0.342 with 54 degrees of freedom. Significance level = 0.01.

$\rho(\bar{\nu},R)$ = 0.553 with 23 degrees of freedom. Significance level = 0.005.

$\rho(\bar{\nu}, Jeff)$ = -0.089 with 46 degrees of freedom.

$\rho(A_2,R)$ = +0.817 with 22 degrees of freedom. Significance level $\sim 10^{-5}$.

$\rho(A_2,Jeff)$ = -0.641 with 44 degrees of freedom. Significance level $\sim 10^{-5}$.

$\rho(R,Jeff)$ = -0.500 with 23 degrees of freedom. Significance level = 0.01.

Table II. Reduced R-matrix parameters that give the solid curves in Figs. 1-5. For all resonances, the radiation width was taken as 35 meV. The signs on the quantities Γ_{f1} and Γ_{f2} (and occasionally Γ_n) are the signs to be associated with the products $\sqrt{\Gamma_a \Gamma_b}$ in a three-reaction-channel reduced R-matrix description.

E_o(eV)	Γ_n(meV)	Γ_{f1}(meV)	Γ_{f2}(meV)	J	E_o(eV)	Γ_n(meV)	Γ_{f1}(meV)	Γ_{f2}(meV)	J
-2.000	1.0245	273.3	-407.9	4	25.493	1.2138	-218.7	443.6	3
-0.250	0.0727	-150.0	4.1	3	26.310	0.1886	-102.6	260.6	3
0.285	0.0036	-51.2	-35.2	3	26.475	0.2925	12.8	-127.6	4
1.129	0.0141	16.8	91.2	4	27.229	0.0288	0.8	-59.4	3
2.022	0.0042	-20.2	10.2	3	27.774	0.5503	-83.0	-20.0	4
2.781	0.0012	50.7	-60.4	4	28.384	0.2368	-4.8	-215.2	3
3.089	0.0268	158.1	58.3	3	28.679	0.0594	124.9	8.4	4
3.517	0.0064	-243.2	-196.7	3	28.900	0.0153	-48.9	-31.7	3
3.613	0.0419	-40.6	2.3	4	29.625	0.1064	-39.5	-21.4	4
4.845	0.0389	2.0	-4.4	4	30.596	0.2130	41.9	-102.0	3
5.481	0.0204	-8.9	-453.1	4	30.839	0.3091	-1.4	54.9	4
6.186	0.0730	42.2	150.4	3	32.032	1.0126	-84.0	11.4	4
6.379	0.1686	15.6	0.3	4	32.056	0.4625	-54.3	1.0	3
7.082	0.1054	-23.2	13.6	4	32.441	0.0112	-132.2	-1515.0	4
7.162	0.0025	-209.4	-163.6	3	33.498	1.1136	51.2	2.8	4
7.617	0.0037	1.0	-324.8	4	34.337	1.2298	-2.2	-70.0	4
8.772	0.9052	8.4	-85.7	4	34.678	1.1069	-445.9	-15.0	3
8.922	0.1151	-277.0	163.3	3	34.893	0.3665	44.1	0.1	3
9.274	0.1063	68.3	5.1	4	35.077	3.0976	0.1	-340.7	3
9.721	0.1057	339.3	150.0	3	35.165	1.6098	31.3	6.7	4
10.150	0.0604	-41.6	-67.9	4	36.310	0.0997	-329.7	1761.5	4
10.589	0.0143	380.9	1.3	4	38.294	0.1696	424.6	1103.8	3
10.852	0.0029	-589.4	-183.3	3	38.328	0.3402	-129.7	-219.7	4
11.667	0.3331	-0.1	6.9	4	39.386	1.8950	-29.9	47.9	4
12.384	1.3082	-3.3	21.8	3	39.870	0.3927	182.8	35.8	3
12.430	0.0856	-242.1	23.3	4	40.494	0.3531	-36.3	-168.5	4
12.873	0.0657	120.4	-6.7	4	41.071	0.3370	-169.3	377.9	4
13.243	0.0334	-42.6	-67.7	4	41.363	0.5259	-33.7	-337.6	3
13.925	0.6503	44.2	506.8	3	41.887	0.6707	-7.0	18.4	3
14.552	0.2613	-2.6	-1.8	3	42.204	0.3171	41.0	-115.9	4
14.996	0.0018	284.6	-40.3	3	42.429	0.0709	3.1	6.6	3
15.395	0.1923	-26.7	32.5	4	42.696	0.1220	-80.6	111.2	4
16.073	0.3812	10.5	-5.0	4	43.357	0.3410	-54.7	16.6	3
16.642	0.2368	108.6	3.0	4	43.932	0.3772	-11.9	-195.3	4
18.022	0.2621	58.4	-46.3	3	44.547	0.4741	-115.5	10.4	4
18.024	0.1108	40.8	159.3	4	44.786	1.4068	373.0	393.4	3
19.001	0.2114	-1.2	-0.0	4	45.746	0.1614	120.4	1.4	4
19.278	2.3476	-29.0	32.4	4	46.785	0.9109	1.5	-163.7	4
19.365	0.3779	-399.4	-1.1	3	46.968	0.4790	-47.8	-19.1	4
20.152	0.0868	-135.7	-62.8	4	47.937	0.5843	-29.4	105.7	4
20.604	0.1534	53.1	-44.2	4	48.104	0.1431	-162.9	-1026.1	3
21.053	1.0610	-25.8	-8.9	4	48.301	0.7860	310.1	40.4	3
21.963	0.0637	136.6	743.3	3	48.409	0.3139	-376.5	-628.3	4
22.292	0.0201	0.1	375.6	4	48.760	0.8000	-0.5	-59.9	3
22.923	0.3576	21.3	-48.8	4	49.402	0.2948	-34.7	22.9	4
23.386	1.6417	2.5	0.2	4	49.746	-.0001	433.9	93.6	4
23.589	0.9350	239.9	-2.5	3	50.137	0.1276	21.2	29.8	3
24.204	0.2521	13.0	-66.8	3	50.439	0.8914	-67.0	0.3	3
24.818	0.0640	155.4	283.9	4	51.068	0.9247	6.3	346.8	3
25.188	0.0272	203.6	20.9	4	51.233	2.1042	-2.8	132.3	4

Table II. (Con't.)

E_o(eV)	Γ_n(meV)	Γ_{f1}(meV)	Γ_{f2}(meV)	J
51.647	0.5992	310.8	-4.0	4
52.159	1.7991	2.0	284.0	3
52.338	0.4869	-86.2	-188.4	4
53.452	0.5530	-0.0	-149.3	3
53.983	0.3697	66.1	461.9	4
54.893	0.8452	-15.0	118.3	3
55.059	2.5593	0.0	-17.7	4
55.765	2.0690	-296.5	21.4	4
55.954	0.6982	411.4	-2.9	3
56.471	2.8492	33.6	-53.5	4
56.525	0.9277	-238.5	-221.9	3
57.736	0.5564	-54.0	88.0	3
57.779	0.4875	-99.1	161.7	4
58.028	1.1869	40.7	4.2	3
58.617	1.1589	-4.1	-155.2	4
59.736	0.3212	426.7	-34.6	4
60.144	0.9692	61.1	168.1	3
60.791	0.5230	-4.8	205.3	4
61.096	0.7861	-11.7	0.3	3
61.412	0.2511	4.5	-314.1	4
61.775	0.1602	-10.4	-534.6	3
62.418	0.0774	47.4	139.6	4
62.866	0.0301	-317.6	484.4	3
63.562	0.8192	438.0	110.5	3
63.923	0.4481	-526.8	64.6	4
64.253	1.4745	-0.0	-3.7	4
64.801	0.1178	-6.5	1.7	4
65.458	0.1630	-473.5	733.6	4
65.708	1.8572	-0.0	3.3	3
65.957	0.2886	-568.2	237.5	4
66.366	1.9925	-0.4	4.0	4
66.689	0.0986	796.7	125.6	3
67.155	0.3138	0.2	-1.7	4
67.578	-.0003	10.8	-147.9	4
68.011	-.0088	-397.3	270.6	4
68.345	0.0838	40.7	-0.9	3
69.259	0.3999	-173.2	37.4	4
70.223	3.3069	1.7	-9.1	4
70.436	3.8378	-3.9	8.4	3
70.452	1.7285	140.1	1391.1	4
70.696	2.0749	60.3	105.4	3
71.464	0.3209	-226.3	30.5	4
72.437	0.8670	181.3	178.2	4
72.820	0.1836	328.2	58.0	3
74.440	1.5305	-147.8	41.2	3
74.540	0.8395	-170.4	47.5	4
74.995	0.3880	-17.5	15.3	4
75.465	1.6398	291.3	14.2	3
76.751	0.2667	1127.1	87.0	3
77.461	0.6603	194.4	26.9	4
77.991	0.8954	192.7	10.0	3
78.143	0.3436	-27.5	0.1	4
78.396	0.2093	1.9	0.0	3
79.591	0.3861	-8.7	-158.8	4
79.758	1.3304	0.8	-1.6	3
80.287	0.7375	-0.0	-140.4	3
80.962	0.2473	369.1	643.1	4
81.392	0.7790	-58.9	-75.5	3
82.367	0.7778	-0.6	-5.0	3
82.656	0.4001	-87.7	4.9	4
83.545	0.9595	-13.1	-0.9	3
84.001	2.6240	261.8	-198.4	4
84.345	1.8315	-224.6	-115.0	3
84.873	1.2939	-0.1	7.5	4
85.208	0.6674	-12.3	14.9	3
85.643	0.5783	-377.1	-52.3	4
86.905	0.5951	-2.4	6.3	3
87.064	0.1324	12.2	-553.9	4
87.785	0.3524	-159.5	279.4	3
88.165	0.3441	-1379.9	4.9	4
88.719	3.3162	-0.0	598.7	3
88.889	1.4827	-10.5	-4.6	4
89.740	0.5641	8.2	-5.4	3
90.148	0.8760	48.3	145.9	4
90.434	3.7716	-3.5	-0.8	4
91.167	3.4279	-2.0	448.9	3
92.037	0.7001	-138.7	-98.7	4
92.525	1.4740	0.1	35.8	4
92.700	-.0949	83.9	63.4	3
93.164	0.4520	157.0	310.5	3
93.974	3.3471	0.6	-3.4	4
94.454	0.2881	19.5	287.7	4
94.766	0.4761	21.0	48.4	3
95.133	0.3912	40.2	-22.2	4
95.500	0.6719	-21.8	26.7	4
95.805	0.5996	33.6	210.2	3
96.051	0.2709	24.6	57.5	4
96.331	0.9868	15.5	400.1	3
97.606	0.3130	-43.4	33.8	4
98.019	2.3619	-68.0	82.5	3
99.446	0.4954	-25.6	0.1	3
100.560	1.8084	134.8	-89.6	4

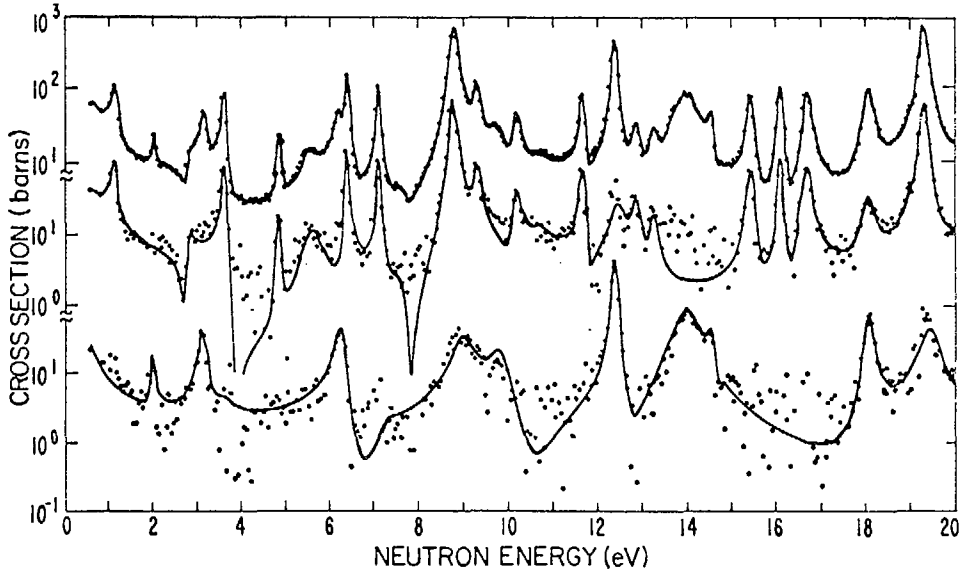

Fig. 1. The fission cross section of ^{235}U below 20 eV. The lowest curve shows the spin 3 cross section, calculated from the reduced R-matrix parameters of table II; the middle curve is the spin 4 cross section; and the top curve is the sum of the other two. Data points above 1 eV are the measurements of Keyworth et al.

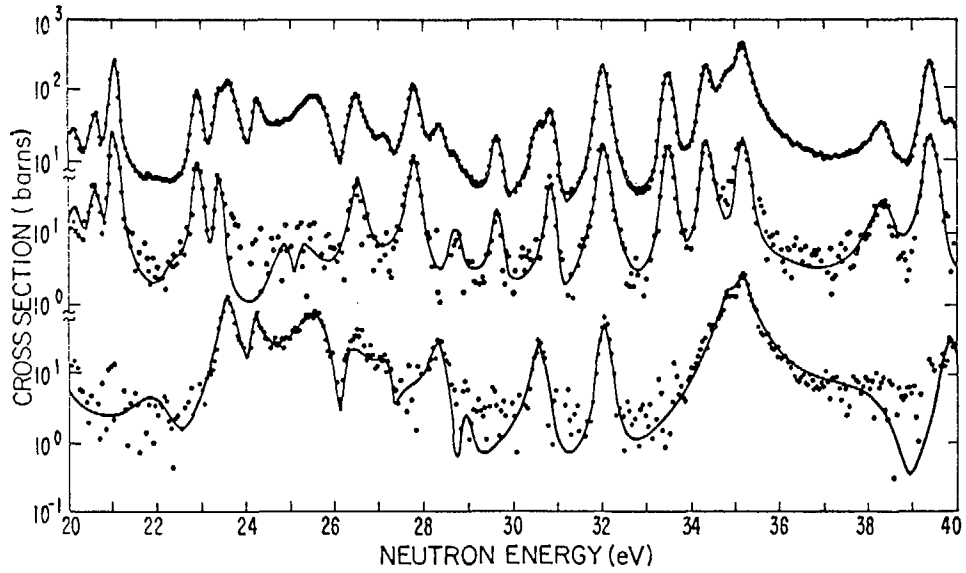

Fig. 2. The fission cross section of ^{235}U from 20 to 40 eV, as in Fig. 1.

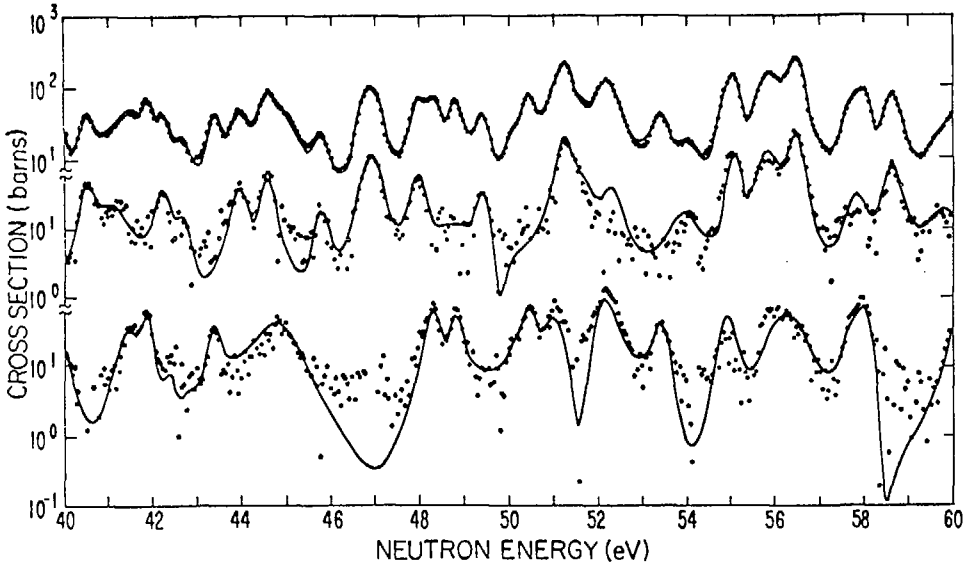

Fig. 3. The fission cross section of ^{235}U from 40 to 60 eV, as in Fig. 1.

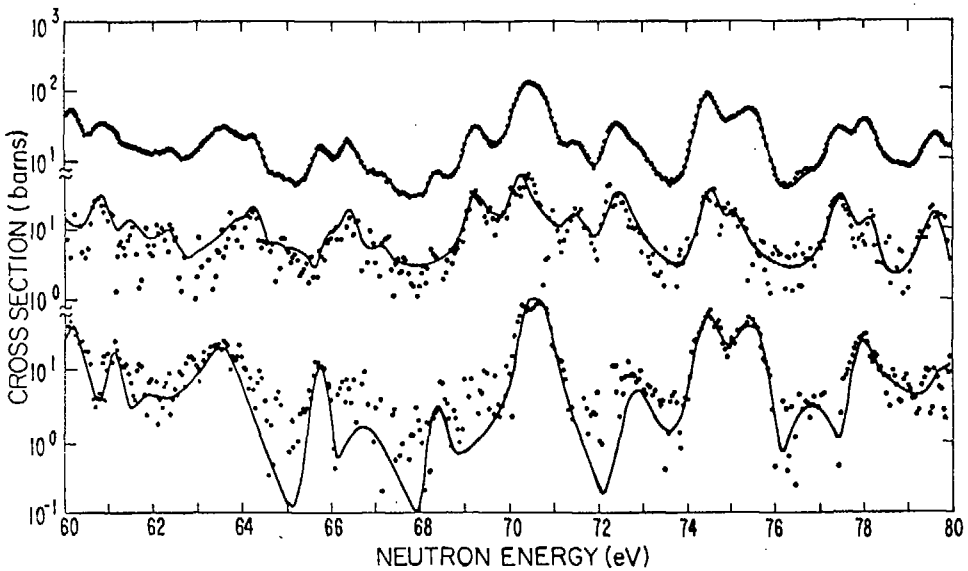

Fig. 4. The fission cross section of ^{235}U from 60 to 80 eV, as in Fig. 1.

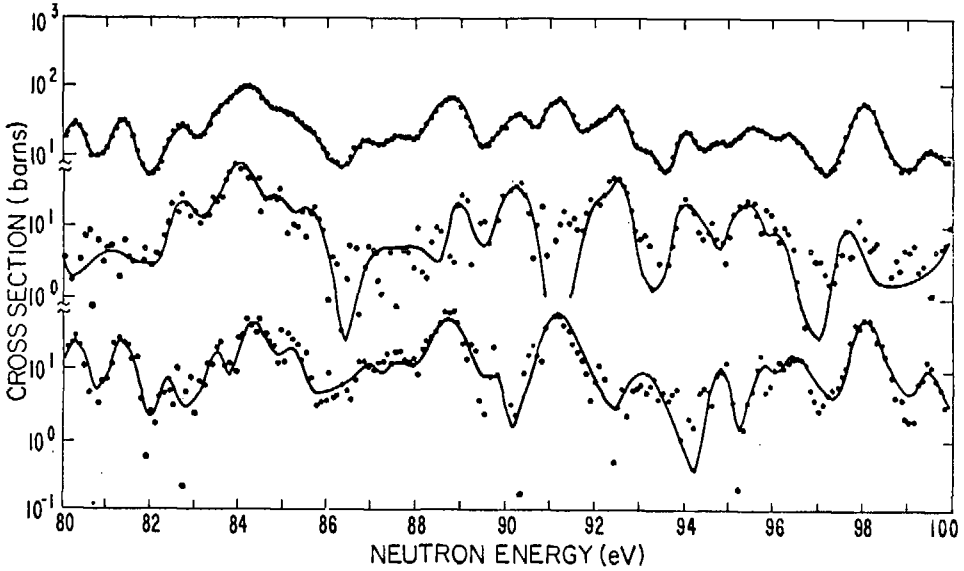

Fig. 5. The fission cross section of ^{235}U from 80 to 100 eV, as in Fig. 1.

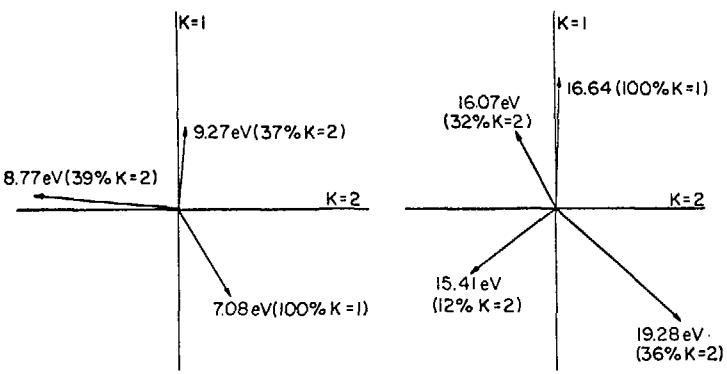

^{235}U FISSION VECTOR ORIENTATIONS

Fig. 6.

Fission-width vector orientations for 4- resonances in ^{235}U near 8 and 19 eV, from Table II.

These two energy regions are not strongly interdependent, so that a 30° clockwise rotation of all the vectors in Fig. 6A can be done without affecting the vector orientation in 6b appreciably.

REVIEW OF 241 Pu RESONANCE PARAMETERS

H. DERRIEN

SECTION DE PHYSIQUE DES NEUTRONS RAPIDES

CENTRE D'ETUDES NUCLEAIRES DE CADARACHE

FRANCE

ABSTRACT

The status of 241 Pu resonance parameters is reviewed. The most important recent results are compared in some energy ranges, both from single level and multilevel point of view. It appears that an accurate set of resonance parameters is not still obtained for a general description of the cross-sections in the resonance region. Some recommendations are given for further experiments or evaluations.

INTRODUCTION

At the Harwell conference on Neutron Physics and Nuclear Data, G.A. KEYWORTH and M.S. MOORE (21) presented an extensive review of the status of the major actinide isotope resonance parameters. They pointed out that resonance cross-section measurements made for several isotopes on the same experimental arrangement, with the same resolution, using the same standards and analysed by the same technique should be of much greater value than measurements performed at different times in different laboratories, using different experimental techniques or analysis methods. It is also worthwile to mention that a complete set of accurate resonance parameters should be obtained from total, fission, scattering and capture measurements performed in the same laboratory and simultaneously analysed. That is an ideal case which is never accomplished , since the capture or the scattering cross-sections are often very difficult to be measured with a reasonable accuracy. In most cases the completeness of a resonance parameter set is achieved by using theoretical assumptions such as the non variation of the capture width from resonance to resonance. However, it is sometime possible to approach the ideal conditions of measurement. One can quote as example the ^{239}Pu total, fission and scattering cross-section measurements performed at Saclay.

The purpose of this paper is to review the status of ^{241}Pu resonance parameters and the problems encountered in the analysis of the experimental data. One should be tempted to believe that the conditions of measurements realized for ^{241}Pu are not too bad, since 1) a simultaneous measurement of the fission and the capture cross-sections have been performed at Oak-Ridge[17] ; 2) total and fission cross-sections have been measured at Geel [10],[11] and simultaneously analysed. Unfortunatly, it seems that there are some other reasons for which a consistent set of resonance parameters cannot be established at the present stage of the analysis. Particularly, the complexity of the resonance structure (see Fig.1.4), cannot be accuratly analysed without the use of a multilevel-multichannel formulation of the cross-sections.

One is faced with the important problem of the apparent non unicity of the R-matrix parameters and of the personal feeling of the evaluators.

The review is divided in the following parts :

- review and status of the experimental data,
- comparison of the most recent results,
- average parameters for the unresolved region,
- outstanding problems and recommendations.

The first set of ^{241}Pu resonance parameters is due to O.D. SIMPSON et al.[1] who analysed the total cross-section measured in the energy range 0.02ev - 2 kev[2] (MTR fast chopper, 1961). They used the Reich-Moore multilevel formalism[22] and obtained all the parameters for 8 resonances up to 10.2 ev neutron energy by assuming a constant value of 40 mev for the capture width. The main feature of this analysis was the separation of the resonances in two non interfering families caracterised by different average fission widths and assumed to pertain to two different fission channels. The next set of parameters was obtained by M.S. MOORE et al.[3] from the analysis of their measured fission cross-sections in the energy range 2ev-100ev (RPI linac, 1964). All the parameters were also given for 21 resonances up to 35 ev, assuming a constant $\Gamma\gamma$ value of 40 mev. The previous results of SIMPSON et al[1] were confirmed and an attempt of interpretation was proposed : the large fission widths could be due to a fully open 2^+ fission channel belonging to the K=0 fondamental rotational band, and the small fission widths to one or several 3^+ fission channels open to a small extent. At the same time, D.S. CRAIG et al[4] measured the total cross-section in the energy range 0.025 ev -1 kev (Chalk River fast chopper, 1964) and obtained the single level parameters(energy, total widths and fission widths) for 14 resonances in the energy range 12.8 ev - 31 ev.
The fission cross-section was also measured by G.D. JAMES[5] from 0.01 ev to 3 kev (Harwell linac, 1964) and analysed with the VOGT formalism[23] in 6 resonances between 12.84 ev and 16.70 ev. Another measurement in this early period is the total cross-section measurement by N.J. PATTENDEN et al.[6] (Harwell linac, 1963) who obtained the energies and the neutron widths for 32 resonances from a single level analysis in the energy range 12ev to 50 ev.

All these measurements were performed with a relatively poor experimental resolution. The importance of these old data consists in the fact that very few recent data exist in the thermal region, in particular in the 0.26 ev resonance region for which no total cross-section measurement has been performed since the measurement of CRAIG et al.

Better resolution and more detailed fission data were obtained from the PETREL nuclear explosion[7]. A Reich-Moore multilevel analysis of these fission cross-sections was performed by O.D. SIMPSON et al.[8] in the energy range 20 ev - 60 ev. A complete set of parameters was obtained for 56 resonances by assuming a constant value of 40 mev for $\Gamma\gamma$ as in the previous analysis (1), (3). The statistical accuracy of the nuclear explosion data is particularly excellent and the shape of the cross-section is very well defined, consequently the deformations or the dissymetries due to small resonances or interference effects are better seen on these data than on those obtained from classical time-of-flight experiments. However, SIMPSON et al. used 30% of unobserved small resonances to improve the fit to their data, in addition to 10 observed non interfering small resonances. As in the previous analyses, two groups of resonances were found, tentatively identified as belonging to the spin states 2^+ and 3^+ of the coumpound nucleus.

The only scattering cross-section measurement is due to G.D. SAUTER et al.[9] (Livermore linac, 1968). The spin assignment was made for 20 resonances in the energy range 4 ev - 30 ev from a simultaneous Reich-Moore fit to the scattering data and to the WATANABE et al[3] fission cross-sections.
The two groups of resonances resulting from this spin assignment were in agreement with those obtained by MOORE et al.[3] except for the resonances between 12.8 ev and 17.8 ev where the results were opposite. The average fission widths were found to be $\langle\Gamma f\rangle_{2^+}$ = 510 mev and $\langle\Gamma f\rangle_{3^+}$ = 190 mev, corresponding to an effective number of fission channels equal respectively to 0.77 and 0.55. These numbers were interpreted as evidence of one fission channel at least half open in each spin state. No consideration was made concerning a possible missing of small resonances.

In the last ten years several high resolution measurements have been performed on the linacs of Saclay, Geel and Oak-Ridge, with a nominal resolution equal or better than 1 ns/m. Such quality of resolution allows the resonance to be analysed up to about 150 ev. The fission and the total cross-sections have been measured at Geel[10],[11] and analysed up to 100 ev with the single level Breit-Wigner formalism. The simultaneous fit to the total and fission cross-sections provided with a complete set of single level parameters for 78 resonances between 12 ev and 100 ev. The authors proposed an average level spacing of (1.00±0.10) ev not corrected for a possible missing of small resonances. They obtained an average capture width of (47.5 ± 7.0) mev from 9 measured values considered as enough accurate and an average fission width of (253 ± 42) mev from all the resonances analysed.

Only the fission cross-section was measured by BLONS et al[12] at Saclay. A preliminary least-square shape analysis of the data, along with the transmission measured at Geel[10], was performed using the single level Breit-Wigner formalism[13]. Neutron widths, fission widths and capture widths were given for 117 resonances in the energy range 4.28 ev to 160 ev which is the largest energy range analysed. These parameters were then used as starting point in a Reich-Moore multilevel analysis simultaneously on the Saclay fission and on the Geel total cross-sections[14]. The results of this least square shape analysis - the programm and the code are described in reference(15) - are shown on fig. 1-4.

The difference between this analysis and the multilevel analyses of reference (2), (3), (8) is that two fission channels were used in each interfering group, each fission width being split in two parts Γ_{f1} and Γ_{f2}. The assumptions concerning the fission channels were the following : 1) in the group of wide resonances, most of the contribution to the fission is due to the 2^+ channel of the K=0 rotational band of the fondamental, fully open; this contribution is Γ_{f1} ; other 2^+ fission channels may exist in the K=0 and K=2 vibrationnal bands at about 1 Mev above ; they contribute in Γ_{f2} which is relatively small. 2) The group of narrow resonances is considered to be 3^+ resonances ; the 3^+ channels exist in the quadrupole and octopole vibrational bands, but none of them is fully open. Here, the splitting between Γ_{f1} and Γ_{f2} has no physical meaning ; it is only used to improve the fit to the experimental data by minimizing the interference effects in the narrow and nearly symmetrical resonances. The average fission widths of 595 mev and 87 mev were obtained for the two groups of resonance, which are somewhat different from the values of 500 mev and 180 mev obtained by SIMPSON at al[8]. No attempt was made to obtain the capture widths in the least square fitting, the shape of the cross-sections being not enough sensitive to the variations of Γ_γ around a reasonable average value. A constant value of 40 mev was then used in agreement with the value of 41.2 mev obtained from the single level analysis in the low energy range.

The most recent set of resonance parameters is due to WESTON et al[16] from a Adler multilevel[24] analysis of a simultaneous measurement of the fission and capture cross-sections[17] in the energy range 0.01 ev to 100 ev. This analysis was considered as the most efficient method for an accurate representation of the experimental data. However, the results of WESTON et al. can be directly compared to the results of the other single level analyses, for the contribution of the Adler dissymetrical part of the resonances was taken equal to zero, apart the energy ranges thermal to 10 ev and 25 ev to 32 ev in the fission cross-sections. Then, for most of the resonances, the energy, the total width, the fission area and the capture area can be easily obtained and could be used for the determination of Γ_f and Γ_γ. That will be done in the next section for sake of comparison in some energy ranges.

This brief review of the experimental data available for the evaluation of the ^{241}Pu resonance parameters shows a wide range of method used in deriving these parameters from the experimental cross-sections. As a matter of fact the value of $\langle\Gamma_f\rangle/\langle D\rangle$ is close to 0.5 and

the probability of strong interferences in the fission channels and of resonance overlappings is very high. The interferences and resonance overlappings are a source of ambiguities in the interpretation of the shape of the cross-sections, since the dissymetries could be interpreted as hidden resonances or interference effects. That is probably the main reason of the apparent inconsistency which exists among the most important sets of data and which will be shown in the next section.

COMPARISON BETWEEN DIFFERENT SETS OF DATA

This comparison will be restricted to the PETREL [8], Geel [10],[11] Saclay [13],[14] and Oak-Ridge [16],[17] data, both from single level and multilevel point of view. The purpose of this review being not to propose an evaluation of ^{241}Pu resonance parameters, we will only compare the results in some selected energy ranges.

The single level data

The published single level parameters have been converted to $2g\Gamma n$, $\sigma_0\Gamma f$ and Γ which are directly comparable ; the other parameters such as Γf and $\Gamma\gamma$, are derived from these measured values with an accuracy correlated to the accuracies achieved on $2g\Gamma n$, $\sigma_0\Gamma f$ and Γ. A particular case is the conversion of the WESTON et al. Adler parameters ; that is done by the following relations :

$$\Gamma = 2\,\nu$$
$$\sigma_0\Gamma f = 2\,Gf/\sqrt{E}$$
$$\sigma_0\Gamma\gamma = 2\,Gc/\sqrt{E}$$

Table I shows the results obtained by BLONS et al., KOLAR et al. and WESTON et al. in the energy range 17.4 ev to 25 ev. Two series of parameters (A and B) were proposed by KOLAR et al. in this energy range. The parameters for the small resonances at 19.50 ev and 21.35 ev are not given in BLONS et al data. On the average the $2g\Gamma n$ values from KOLAR (A) and KOLAR (B) are 16% and 23% larger than those from BLONS, which is very surprising since the same transmission data were analysed . The total widths are very different for most of them. The fission area $\sigma_0\Gamma f$ represent quite well the average fission cross-sections (Table VI) in this energy range.

The results in the energy range 46 ev to 55 ev are compared in Table II. Only 4 resonances are given by BLONS et al. against 6 resonances by WESTON et al. and 7 by KOLAR et al., which correspond to different ways of analysing the cross-sections in the vicinity of the broad resonance at 48 ev. On the average the $2g\Gamma n$ values from KOLAR are still larger (10%) than those from BLONS. The sum of the fission area in KOLAR data are much smaller than the others and does not correspond to the average fission cross-section in this energy range (Table VI).

These two examples show the diversity of the results of the single level analyses. Then, a consistent set of fission widths and capture widths could hardly be obtained. However, the capture widths are given for all the resonances in KOLAR data and for 46 resonances in BLONS data. They are very different and fluctuate strongly from resonance to resonance. The fluctuations are obviously due to the fact that the capture widths were obtained by difference between the total widths and the other partial widths, the difference being in most cases of the same order of magnitude than the accuracy achieved on the total or the fission widths. The average value proposed by KOLAR et al. is (47.5 ± 7.0) mev against 43.6 mev obtained by averaging all the individual values of BLONS et al. More precise values could be obtained by using also the capture area from WESTON et al. analysis. In table III, several ways of obtaining the capture widths are shown for some well isolated resonances for which the accuracy could be expected to be reasonably good. As a matter of fact, the fluctuations from resonance to resonance remain very strong within each set of data, and the results obtained for the same resonance from different ways are discrepant. Even for these well isolated resonances the capture width is not known with better than 30% of accuracy.

The multilevel data

We shall only compare the results from SIMPSON et al.[8] and from BLONS et al.[14] in two typical energy range. These analyses are of same nature, using both the Reich-Moore formalism. Table IV shows the results in the energy range 25ev - 37ev where SIMPSON et al. used 16 resonances and BLONS et al. only 12 resonances. The difference corresponds to 4 unobserved weak resonances used by SIMPSON et al. to improve the fit to the experimental data. The choice of the interfering groups is the same, except for the large resonance at 26.32 ev. The values of the neutron widths are quite similar. However, the values from BLONS et al. should be more accurate, for they were obtained from a simultaneous analysis of the total and fission cross-sections. More important are the differences which are seen on the total fission widths. That is mainly due to the different assumptions used by the authors : one fission channel and addition of unobserved weak resonances by SIMPSON et al ; use of two fission channels by BLONS et al.

Another example of results is shown in Table V in the energy range 46 ev - 56 ev ; 10 resonances are found in SIMPSON et al. data and only 5 resonances in BLONS et al. data. The 3 important resonances interfere in the same way, but the spin attribution should be inverted . The large $2g\Gamma_n$ values are different by 30%, but the total fission widths are quite similar.

One can consider that both analyses give an excellent fit to the corresponding experimental data, but the resonance parameters are different. There is an apparent non unicity of the set of resonance parameters. As a matter of fact, it depends mainly on the kind of data analysed, on the way the analysis is performed and on the assumptions made when starting the analysis. BLONS et al. work is an example of how far it is possible to go in the interpretation of ^{241}Pu cross-sections in the resonance region; but it is probably not the only interpretation possible.

THE AVERAGE RESONANCE PARAMETERS

Average level spacing, strength functions and average partial widths are needed to calculate the cross-sections in the unresolved resonance region and at higher energy from statistical model. Table VII collects all the average data available in the publication reviewed in the previous sections. The data from references (1) - (6) are only given for information ; they have not to be taken into account since more accurate values are given in references (8) - (14). The average level spacing depends on the estimation of the number of resonances missed in the experimental data. Such estimation has been made by SIMPSON et al[8] and by BLONS et al[14] and yields similar results. The So strength function should be obtained with good accuracy from the analysis of Geel total cross-sections. However the value proposed by KOLAR et al[10] is 25% larger than the one obtained in the single level or multilivel analysis of BLONS et al[13][14]. As a matter of fact, if one calculates the strength function by the relation :

$$S^0 = \sum_{E_1}^{E_2} 2g\Gamma_n^0 / 2 \, (E_2 - E_1)$$

one find 1.158×10^{-4} from BLONS et al. multilevel parameters in the energy range 4ev - 104 ev and 1.153×10^{-4} from KOLAR et al. single level parameters in the energy range 12 ev - 100 ev.

From the selected resonances shown on Table III, one obtains an average capture width of about 41 mev by combinating BLONS analysis and WESTON analysis, and of about 44 mev by combinating KOLAR analysis and WESTON analysis. These values are significantly higher than those of (35.9 ± 1.0) mev and (35.6 ± 1.0) mev obtained by MOORE[25] from a systematics for the 2^+ and 3^+ spin states. As for the properties of the fission channels, the results depend strongly on the way the analysis has been performed ; one can only say that there is an overall agreement on the existence of one 2^+ fully open fission channel.

Figs. 5-7 show the neutron width distributions from SIMPSON et al[8], KOLAR et al[11] and BLONS et al[14]. In SIMPSON data there is apparently an excess of small values ; this excess could be a part of the 30% non observed resonances used to improve the fit in the multilevel shape analysis ; this distribution can be hardly described by a Porter-Thomas law . In KOLAR data the absence of small Γ_n values is obvious, as the absence of very large values. Maximum likelihood or missing level estimator methods should not work when applied to these distributions. The data from BLONS are more regular and can be reasonably well described by a Porter-Thomas law by assuming that about 20% of small resonances are missed ; maximum likelihood and missing level estimator methods give respectively 0.97 ev and 0.92 ev for the average level spacing. On the other hand, BLONS et al.[14] have shown by using a Monte-Carlo technique that 9% of doublets - unresolved resonances with comparable neutron width values - coul also exist in the experimental data in addition to the 20% of hidden very small resonances. Then the average level spacing should be 0.8ε ev or 0.84 ev.

OUTSTANDING PROBLEMS AND RECOMMENDATIONS

It appears from this review that an accurate set of resonance parameters which could be used for a general description of the 241Pu total, fission and capture cross-sections is not still obtained. However the parameters which are available from different authors have mostly been obtained by shape or least square shape analysis and give a good representation of the particular cross-sections from which they were derived. Several high resolution fission cross-section measurements are available[7],[11],[12],[17],[18]; they are in rather good agreement, as it is shown on Table VI , and the parameters describing one of these cross-sections could also describe reasonably well the others. Only one total cross-section[10] and one capture cross-section[17] measurement have been performed with good resolution on a wide energy range. But it is not obvious that the parameters obtained in reference (8), (11), (14) or (15) should described the measured capture cross-section with enough accuracy.

An improvement of the situation should be obtained by performing a simultaneous shape analysis on the total, the capture and one or several fission cross-sections. This analysis could be achieved easily by using the Adler formalism and should be a complement of WESTON et al. work[16]. However, in the purpose of obtaining the average R-matrix parameters for the calculations in the unresolved region, more informations should be obtained from the Reich-Moore formalism ; the analysis should not be too difficult, nor too much time consuming by using BLONS et al[14] parameters as starting point. Then the Reich-Moore parameters could be translated to the more easy to handle Adler parameters by the code POLLA of DE SAUSSURE et al[19]. Part of this work was already done by WESTON et al[20]. for ENDF/B - V starting from all the existing sets of REICH-MOORE parameters.

A particular problem is the cross-sections in the resonance at 0.26ev.

Evaluating the data in the thermal region WESTON et al.[20] found a discrepancy of 14% in the capture cross-section over the 0.26 ev resonance when compared to ENDF/B-IV evaluation (fig.8). The latter was based on SIMPSON et al.[2] total cross section and on WATANABE et al.[3] fission cross-section, which mean that the capture cross-section was calculated by difference. Now, if one compares the WESTON et al. absorption cross section to the total cross-section of SIMPSON et al. one finds that the absorption cross section is 4.5% larger than the total cross section on the peak of the resonance, 7.5% at 0.15 ev and equivalent around 0.33 ev, as it is shown on fig.9. One should note that the scattering cross-section is about 0.6% of the total at the resonance peak ; then, the absorption should be almost equal to the total. The discrepancy cannot be resolved without a remeasurement of the total cross-section. For the moment, one should trust the more direct capture measurement of WESTON et al., bearing in mind that integral experiments suggest a larger capture in the thermal range of energy[20]

The recommendations concerning the measurements or the evaluations of ^{241}Pu resonance parameters can be summarized as follows.

1) A Reich-Moore multilevel analysis performed simultaneously on the total and capture cross-sections and one or several fission cross-sections should give an accurate set of parameters for a general description of the cross-sections in the resonance region. More accurate average parameters could also be obtained from this set of R-matrix parameters.

2) This set of R-matrix parameter could then be translated to Adler parameters by using the code POLLA[19].

3) It is not clear from WESTON et al. report[20] if the above two recommendations are fulfilled or not by the evaluation for ENDF/B-V. Therefore, these recommendations depend on the availability of ENDF/B-V.

4) A total cross-section measurement should be performed in the thermal region including the resonance at 0.26 ev.

5) Polarization measurements should be most useful to obtain the spin separated cross-sections. Such measurements have shown to be most efficient in improving the status of 235 U resonance parameters[26] and should give the same improvement in the case of ^{241}Pu.

The author is indebted to L.W.WESTON in providing him with material used in Oak-Ridge ^{241}Pu evaluation.

REFERENCES

1/ - O.D. SIMPSON AND M.S. MOORE,
Physical Review 123, 559 (1961)

2/ - O.D. SIMPSON and R.P. SCHUMAN,
Nucl. Scien. Eng.11 ,111 (1961)

3/ - M.S. MOORE, O.D. SIMPSON and T. WATANABE,
Physical Review 135, 945 (1964)
T. WANATABE and O.D. SIMPSON, IDO-16995 (1964)

4/ - D.S. CRAIG and C.H. WESTCOTT,
Canadian Journal of Physics 42, 2384 (1964)

5/ - G.D. JAMES
Nuclear Physics 65, 353 (1965)

6/ - N.J. PATTENDEN and S. BARDSLEY
AERE - PR/NP6 10 (1964)

7/ - B.C. DIVEN,
Neutron Experiments with Underground Nuclear explosions, Proceedings of the International conference on the Study of Nuclear Structure with Neutrons, Antwerp, July 19-23, 1965

8/ - O.D. SIMPSON, R.G. FLUHARTY, M.S. MOORE, N.H. MARSHALL, B.C. DIVEN and A. HEMMENDINGER, Washington 1966, vol. 2 page 910.

9/ - G.D. SAUTER and C.D. BOWMAN,
Physical Review 174, 1413 (1968)

10/- W. KOLAR and G. CARRARO,
Neutron cross-sections and Thechnology, Knoxville 1971, vol 2 p. 707

11/- W. KOLAR,J.P. THEOBALD and J.A. WARTENA;
Neutron cross-sections and Technology, Knoxville 1971, vol.2 p.823

12/- J. BLONS, G. DEBRIL, J. FERMANDJAN, A. MICHAUDON,
Nuclear data for reactors, Helsinki (1970), vol I, page 469

13/- J.BLONS, H. DERRIEN, A. MICHAUDON,
Neutron cross-sections and Technology, Knoxville (1971) vol. 2,
page 836

14/- J. BLONS and H. DERRIEN,
Journal de Physique 37, 659 (1976)

15/- H. DERRIEN, J. BLONS, A. MICHAUDON,
Nuclear data for Reactors, Helsinki (1970), vol 1
page 481

16/- L.W. WESTON and J.H. TODD
Nucl. Sci. Eng 68, 125 (1978)

17/- L.W. WESTON and J.H. TODD,
Nucl. Sci. Eng. 65, 454 (1978)

18/- C. WAGEMANS and A.J. DERUYTER,
Nuclear cross-sections and technology, Washington (1975), Vol 2
page 603.

19/- G. DE SAUSSURE and R.B. PEREZ
ORNL - TM - 2599 (1969)

20/- L.W. WESTON and R.Q. WRIGHT, Nuclear Cross-Section for
Technology, Knoxville (1979)

21/- G.A. KEYWORTH and M.S. MOORE,
Neutron Physics and Nuclear Data, Harwell sept. 1978,
page 241

22/- C.W. REICH and M.S. MOORE,
Phys. Rev. 111, 929 (1958)

23/- E. VOGT,
Phys. Rev. 112, 203 (1958)

24/- D.B. ADLER and F.T. ADLER,
ANL-6492 (1963)

25/- M.S. MOORE,
Neutron Physics and Nuclear data,Harwell (1978), page 313

26/- G.A. KEYWORTH, C.E.OLSEN, J.D. MOSES, J.W.T. DABBS and N.W. HILL,
Nuclear Cross-Sections and Technology, Washington (1975),
Vol II, p. 576.

ENERGIES (EV)				NEUTRON WIDTHS (MEV)			TOTAL WIDTHS(MEV)				FISSION AREA (B.EV)			
BLONS	WESTON	KOLAR		BLONS	KOLAR		BLONS	WESTON	KOLAR		BLONS	WESTON	KOLAR	
		A	B		A	B			A	B			A	B
17.83	17.87	17.81	17.81	2.98	3.17	3.46	57	56	56	67	73.7	76.2	74.4	75.9
18.22	18.26	18.22	18.21	0.19	0.26	0.21	64	24	173	108	4.5	4.4	8.7	6.1
	19.46	19.50			0.12			900	900			6.6		
20.71	20.76	20.69	20.68	0.36	0.47	0.48	105	180	109	102	15.4	20.3	16.0	16.3
	21.35	21.35			0.12			800	800			5.6		
21.93	21.98	21.91	21.92	0.16	0.20	0.19		80	82	68	3.2	2.1	2.7	2.7
23.02	23.05	22.99	22.97	1.17	1.25	1.10	368	214	380	320	57.8	43.2	54.6	49.4
23.71	23.71	23.66	23.64	0.38	0.57	0.55	286	416	394	380	16.9	26.0	24.8	24.7
24.07	24.11	24.07	24.03	1.31	1.66	1.32	118	120	114	126	45.5	45.1	39.5	41.8
24.61	24.62	24.70	24.31	0.20	0.51	0.51	600	376	1420	1130	9.0	7.5	20.1	18.9
										SUM OF $\sigma o\ \Gamma_f$:	226.0	237.0	240.8	235.8
										SUM OF $\frac{\pi}{2}\ \sigma o\ \Gamma_f$:	355.0	372.0		370.0
										EXPERIMENTAL FISSION INTEGRAL :	(1) 351.0	(1) 385.5		(1) 378.5

(1) FROM WESTON PRIVATE COMMUNICATION (SEE ALSO TABLE 6)

TABLE 1
SINGLE LEVEL ANALYSES IN THE 17.4 EV TO 25.0 EV ENERGY RANGE

ENERGIES			N. WIDTHS (MEV)		TOTAL WIDTHS (MEV)			FISSION AREA (B.EV)		
BLONS	WESTON	KOLAR	BLONS	KOLAR	BLONS	WESTON	KOLAR	BLONS	WESTON	KOLAR
46.570	46.696	46.520	1.71	1.705	295	278	280	41.3	40.0	23.6
		47.300		0.908			100			13.5
48.110	47.970	48.020	6.20	4.019	500	114	345	144.0	11.4	64.3
	48.269	48.450		2.116		540	940		147.1	31.7
50.350	50.452	50.210	0.80	0.850	518	592	435	20.0	22.8	12.8
		52.000		N.GIV.			200			
52.240	52.348	52.600	0.10	N.GIV.	160	422	200	1.7	1.9	
	53.483					990			1.5	
						SUM OF $\sigma o\ \Gamma_f$:		207.0	224.7	145.9
						SUM OF $\frac{\pi}{2}\ \sigma o\ \Gamma_f$:		325.2	353.0	229.2
						EXPERIMENTAL FISSION INTEGRAL :		(1) 319.8	(1) 345.2	(1) 294.4

(1) FROM WESTON PRIVATE COMMUNICATION (SEE ALSO TABLE 6)

TABLE 2
SINGLE LEVEL ANALYSES IN THE 44.0 EV TO 54.0 EV ENERGY RANGE

RESONANCE ENERGIE (EV)	1	2	3	4		5		6	
				A	B	A	B	A	B
4.28	41.5	36.7							
6.95	32.3	34.8							
8.63	27.6	30.0							
13.45	49.3	43.8		37.5		39.3		35.2	
14.78	48.1	38.4		40.6		34.7	35.1	39.9	43.0
17.87	32.7	31.6	35	40.7	44.6	40.7	44.6	34.7	43.3
20.76	45.4		33	47.3	43.4			49.1	46.0
21.98				45.5	39.8	44.4	46.8	63.0	51.3
24.11	45.5	45.9	41	42.9	45.3	45.2	43.2	47.0	51.2
26.45	50.6	46.0	38	50.6	49.1	44.6	47.1	64.9	50.3
31.09	42.8	55.3	54	49.0		55.0		57.9	53.7

1 - FROM BLONS PARAMETERS AND WESTON CAPTURE AREA
2 - FROM WESTON PARAMETERS AND BLONS TOTAL AREA
3 - DIFFERENCE BETWEEN TOTAL AND PARTIAL WIDTHS FROM BLONS SINGLE LEVEL ANALYSIS
4 - FROM KOLAR PARAMETERS AND WESTON CAPTURE AREA
5 - FROM WESTON PARAMETERS AND KOLAR TOTAL AREA
6 - DIFFERENCE BETWEEN TOTAL AND PARTIAL WIDTHS FROM KOLAR SINGLE LEVEL ANALYSIS

TABLE 3
CAPTURE WIDTHS FOR SOME ISOLATED LEVELS

ENERGIES (EV)		NEUTRON WIDTHS (MEV)		FISSION WIDTHS (MEV)			
SIMPSON (1)	BLONS (1)	SIMPSON	BLONS	SIMPSON	BLONS (2)		
25.64 B		0.005		- 50			
26.32 A	26.38 B	5.335	4.538	270	264	257	- 7
27.27 A	27.50 A	0.005	0.030	750	22	0	22
27.34 B	27.72 B	0.042	0.542	300	900	- 900	0
28.68 B	28.72 B	5.676	3.942	750	595	543	52
29.59 B	29.60 B	0.479	0.460	- 50	201	- 123	- 78
30.05 A	30.10	0.000	0.035	- 20	32		
30.91 A	30.97 A	2.613	2.553	220	212	0	-212
32.38 A		0.017		50			
33.27 A	33.30 A	0.214	0.176	-150	110	60	50
33.37 B		0.058		50			
33.65 A	33.74 A	0.366	0.327	-100	62	0	62
34.15 A		0.117		300			
34.72 B	34.97 B	2.003	2.167	-900	1292	-1169	123
	34.98 A		0.403		16	10	6
36.00 B	36.19 A	0.204	0.070	500	36	5	31
36.65 B		0.000		900			

(1) A AND B INDICATE THE INTERFERING GROUPS
(2) TOTAL , FIRST CHANNEL AND SECOND CHANNEL FISSION WIDTHS

TABLE 4
REICH-MOORE MULTILEVEL ANALYSIS IN THE 25 EV TO 37 EV ENERGY RANGE

ENERGIES (EV)		NEUTRON WIDTHS (MEV)		FISSION WIDTHS (MEV)			
SIMPSON (1)	BLONS (1)	SIMPSON	BLONS	SIMPSON	BLONS (2)		
46.38 B	46.51 A	2.111	1.605	-280	245	0	-245
47.05 B	47.10	0.137	0.120	300	227		
47.95 A	48.04 B	7.271	5.782	480	433	-291	142
50.14 B	50.31 A	0.637	0.697	300	441	6	435
50.90 B		0.036		-300			
51.90 B	52.13	0.036	0.100	50	32		
52.60 B		0.007		-200			
53.40 A		0.000		300			
54.15 A		0.022		500			
55.40 B		0.019		300			

(1) A AND B INDICATE THE INTERFERING GROUPS
(2) TOTAL , FIRST CHANNEL AND SECOND CHANNEL FISSION WIDTHS

TABLE 5
REICH-MOORE MULTILEVEL ANALYSIS IN THE 44 EV TO 54 EV ENERGY RANGE

E1 — E2 (EV)	ENDF/B5	WAGEMANS REF (18)	WESTON REF (16)	BLONS REF (13)		KOLAR MIGNECO REF (10)	SIMPSON REF (8)
0.02 - 0.03	10.20	10.36	10.15				
0.03 — 0.10	49.2	49.7	49.6				
0.10 — 0.50	270.1	272.6	275.7				
0.50 — 3.00	70.7		76.7				
3.00 — 4.90	348.8	361.1	367.6	347.8		358.1	
4.90 — 8.00	892.4	871.6	884.7	882.2		897.9	
8.00 — 9.00	239.3	239.9	241.6	235.7		236.7	
9.00 — 12.0	310.8	311.4	319.8	303.8		320.0	
12.0 — 14.0	260.9	290.0	283.4	273.9		286.4	
14.0 — 17.4	863.0	942.0	948.4	926.6		901.5	
17.4 — 20.0	122.8	136.3	145.2	133.7		139.9	
20.0 — 25.0	240.4	234.5	240.3	217.3	242.4	238.6	204.6
25.0 — 27.2	292.9	285.9	285.1	270.0	271.9	273.2	245.0
27.2 — 30.0	339.9	324.2	335.2	313.3	314.4	316.7	278.5
30.0 — 36.1	326.8	335.3	344.2	320.7	318.5	320.9	264.7
36.1 — 44.0	271.0	272.7	284.4	253.1	254.7	243.7	207.8
44.0 — 54.0	335.1		345.2	319.8	313.0	299.4	294.4
54.0 — 64.7	400.8		446.6	418.1	406.6	434.7	412.8
64.7 — 74.5	303.5		338.2	315.8	301.9	326.2	303.8
74.5 — 84.0	440.1		571.4	514.1	513.2	556.7	578.4
84.0 — 93.0	361.2		403.1	378.1	358.6	392.3	404.3
93.0 —100	203.4		227.2	231.3	205.5	241.1	253.1

TABLE 6
FISSION CROSS SECTIONS INTEGRALS IN THE RESONANCE REGION
(FROM L.W. WESTON , PRIVATE COMMUNICATION)

REFERENCE	LEVEL SPACING (EV)	STRENGTH FUNCTION X 10^4	AVERAGE FISSION WIDTHS (EV)	AVERAGE CAPTURE WIDTHS (MEV	DATA AND ENERGY RANGE
(1)			GROUP (A) : 0.847 GROUP (B) : 0.074	40 (ASSUMED)	TOTAL 0 - 12 EV
(2)	1.3	1.0			TOTAL 0 - 20 EV
(4)	1.3	1.9			TOTAL 12 - 31 EV
(5)	1.3 + _ 0.2	1.4 + _ 0.6		40 (ASSUMED)	FISSION 0 - 20 EV
(6)	1.13 + _ 0.21	1.3 + _ 0.3			TOTAL 13 - 50 EV
(8)	0.76		GROUP (A) : 0.500 GROUP (B) : 0.180	40 (ASSUMED)	FISSION 20 - 60 EV
(9)			2 + : 0.510 3 + : 0.190	42	SCATTERING FISSION 4 - 30 EV
(10),(11)	1.00 + _ 0.10	1.24 + _ 0.35	ALL SPIN STATES : 0.253 + 0.042	47.5 + _ 7.0 (FROM SELECTED VALUES)	TOTAL FISSION 12 - 100 EV
(13)		0.99 + _ 0.14	ALL SPIN STATES : 0.300	41.2 (FROM SELECTED VALUES)	TOTAL FISSION 1 _ 160 EV
(14)	0.83	1.08 + _ 0.17	TOTAL 2 + : 0.595 FOND. 2 + : 0.356 TOTAL 3 + : 0.087	40 (ASSUMED)	TOTAL FISSION 1 - 104 EV

TABLE 7
AVERAGE RESONANCE PARAMETERS

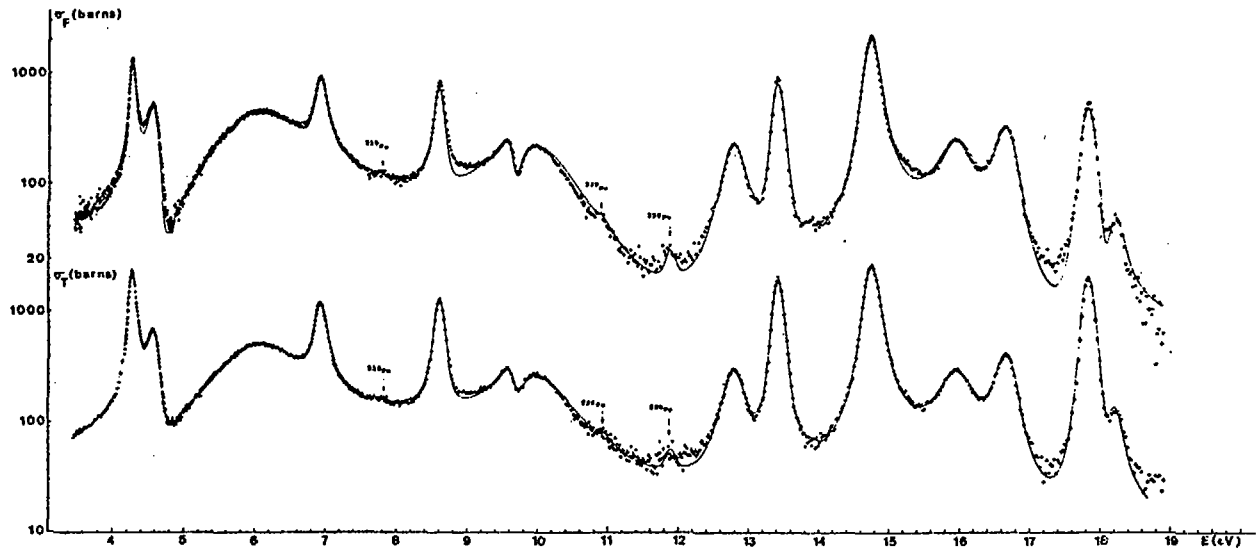
σF (barns)
1000
100
20
σf (barns)
1000
100
10
4
5
6
7
8
9
10
11
12
13
14
15
16
17
18
19
E(eV)

FIG. 1.

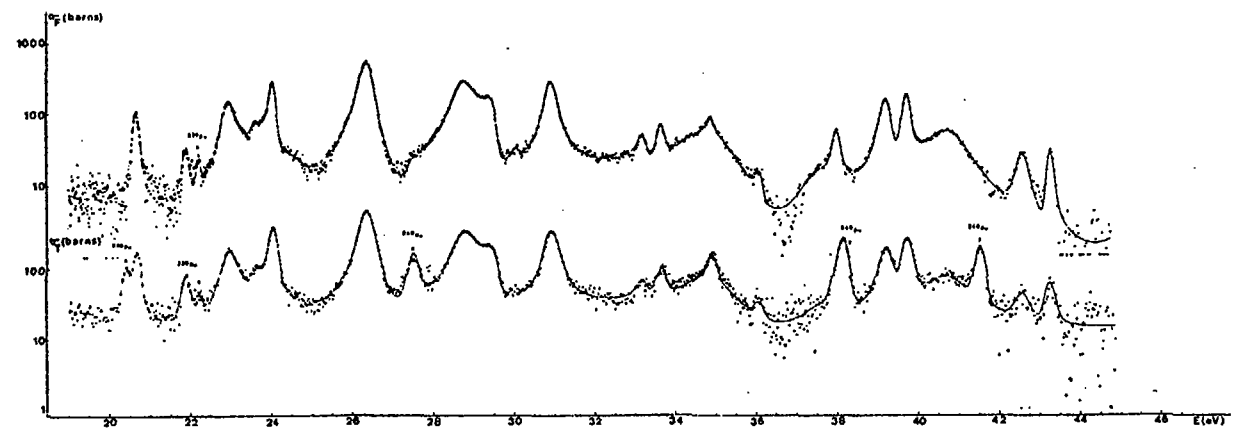
σF (barns)
1000
100
10
σf (barns)
100
10
1
20
22
24
26
28
30
32
34
36
38
40
42
44
46
E(eV)

FIG. 2.

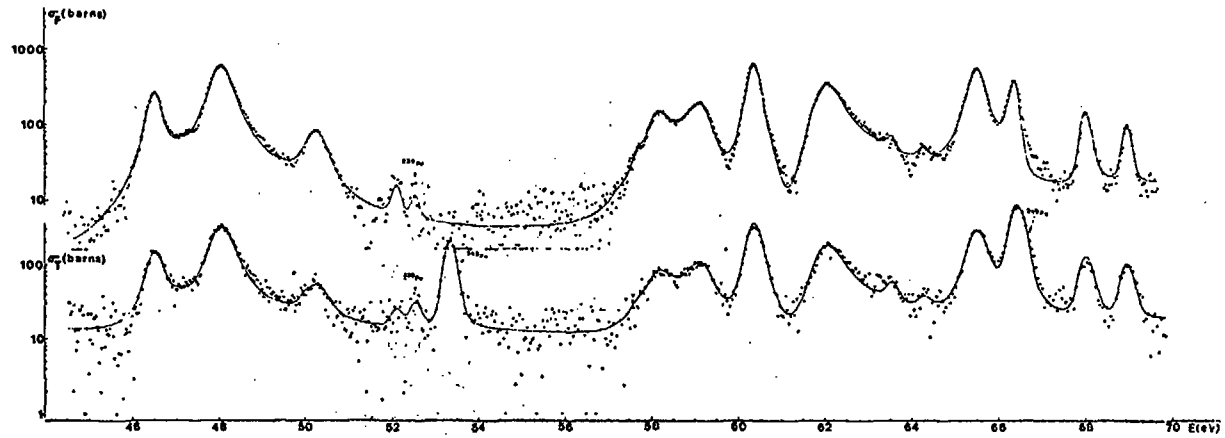

FIG. 3.

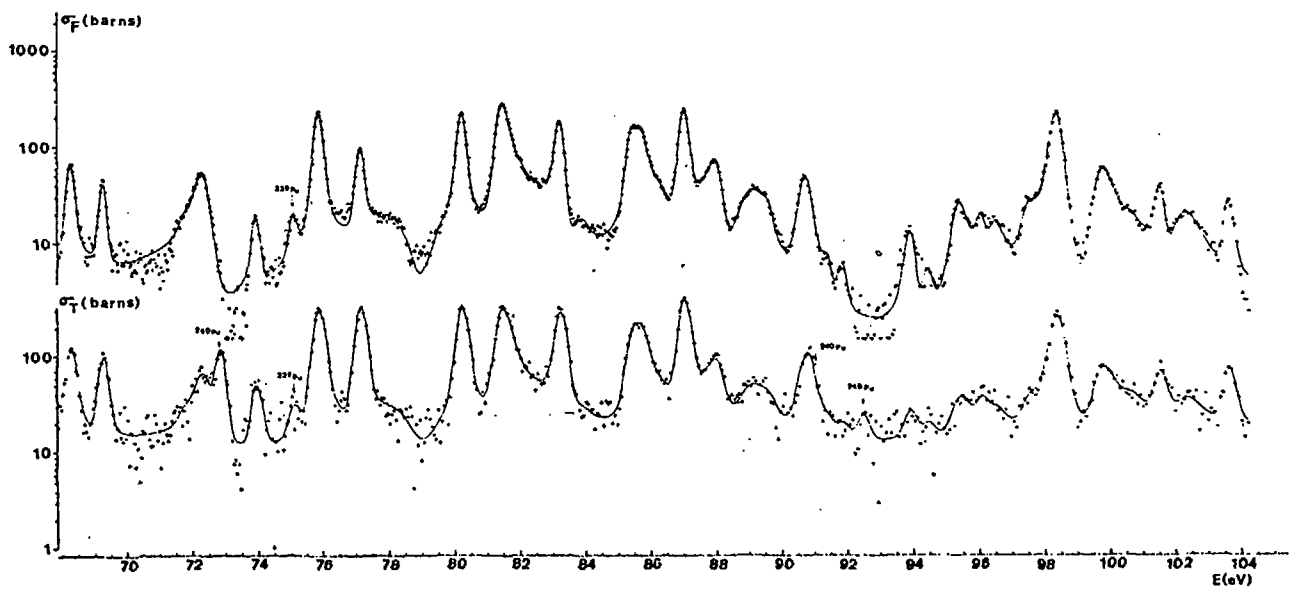

FIG. 4.

Fig. 1, 2, 3, 4 : Total cross-sections from KOLAR et al. ; fission cross-sections from BLONS et al. The curves represent the Reich Moore multi-level fit of BLONS and DERRIEN

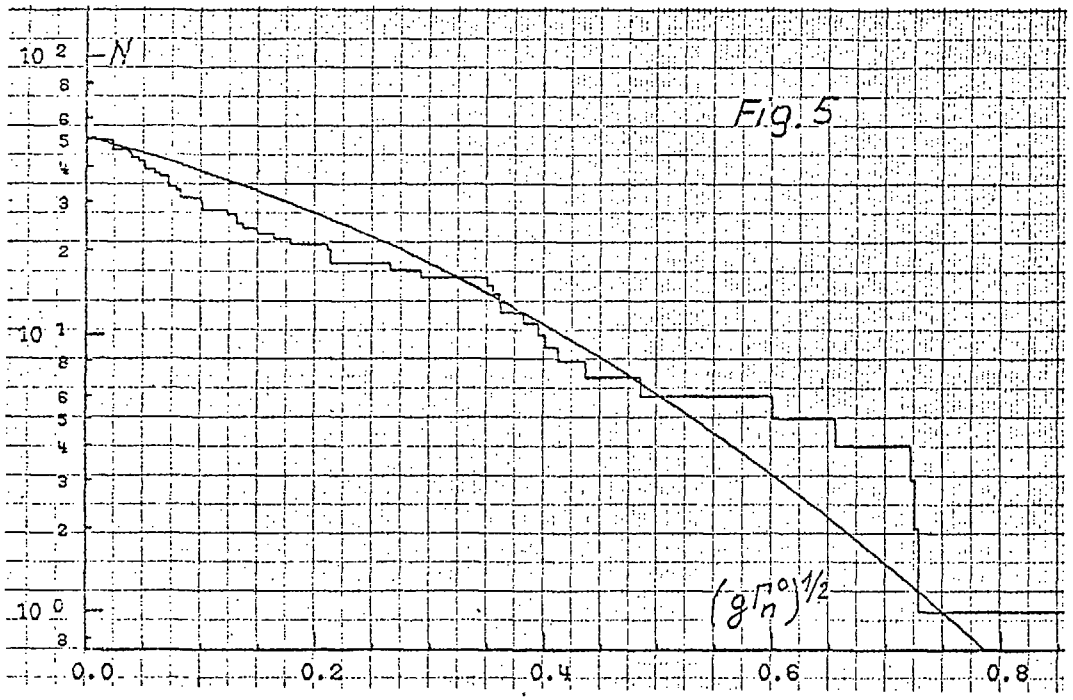
N
10^2
10^1
10^0
0.0
0.2
0.4
0.6
0.8
$(g\Gamma_n^\circ)^{1/2}$

Fig. 5

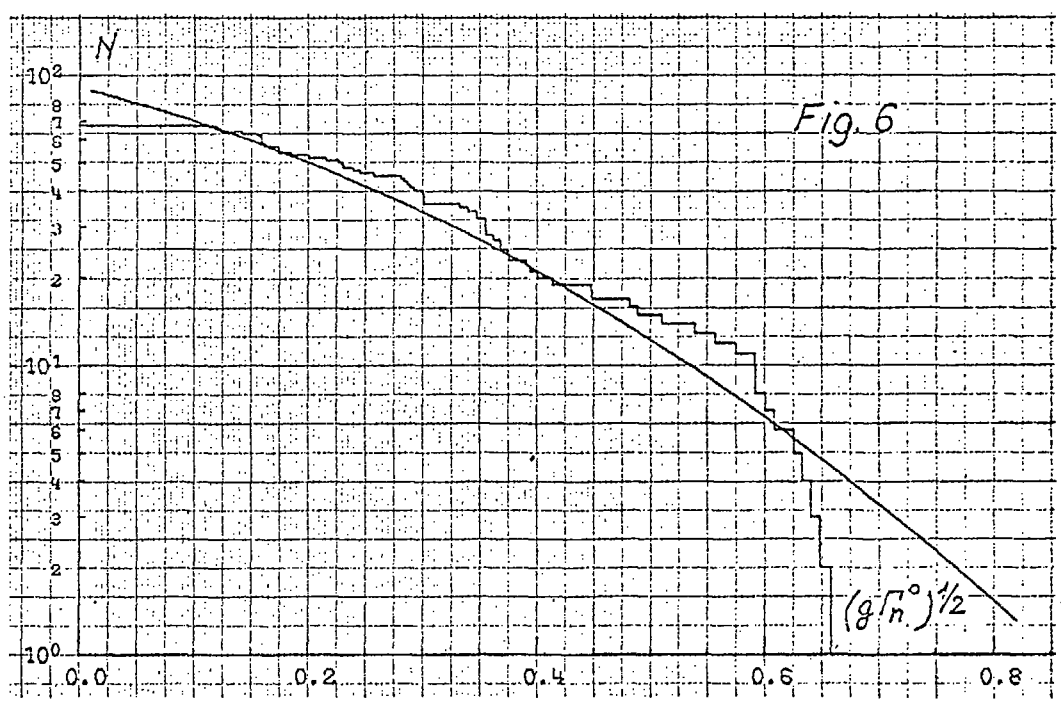
N
10^2
10^1
10^0
0.0
0.2
0.4
0.6
0.8
$(g\Gamma_n^\circ)^{1/2}$

Fig. 6

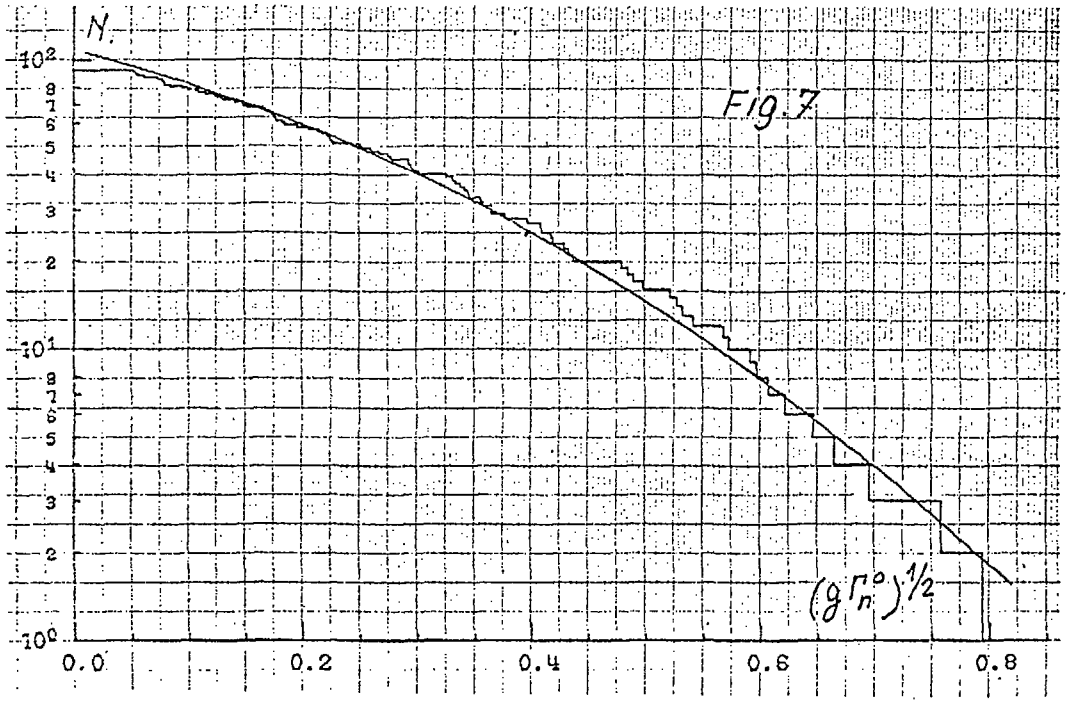

Integral distribution of the fission widths from SIMPSON et al. (Fig. 5), KOLAR et al. (Fig. 6) and BLONS et al (Fig. 7). The curves are examples of Porter Thomas distributions.

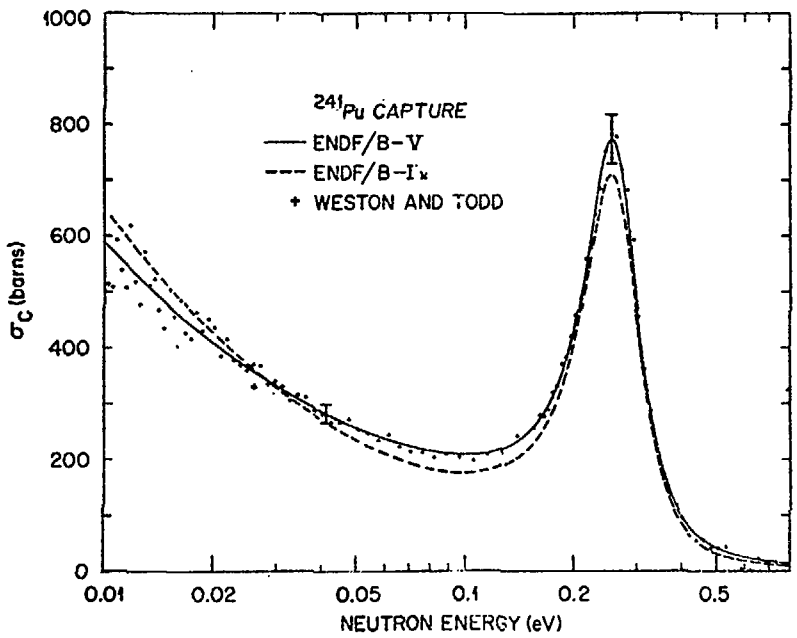

Fig. 8 : From WESTON et al.[20]

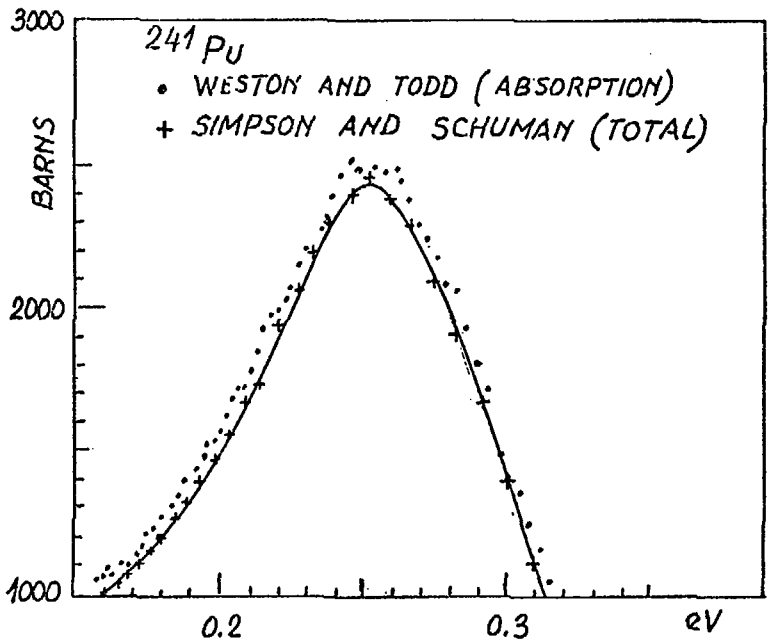

Fig. 9

Level Density Estimation with Account of Unrecognised Multiplets Applied to Uranium and Plutonium Resonance Data

F.H. Fröhner

Kernforschungszentrum Karlsruhe
Institut für Neutronenphysik und Reaktortechnik
Postfach 3640, D-7500 Karlsruhe

Abstract - The maximum-likelihood method for estimation of level densities and strength functions from resonance parameters is extended so that not only levels missing because of a finite detectability threshold are accounted for but also those lost in unresolved and unrecognised multiplet peaks. The resulting prescription was checked against a recently issued benchmark problem and applied to the estimation of level densities and strength functions for ^{235}U, ^{238}U, ^{239}Pu, ^{240}Pu, ^{241}Pu and ^{242}Pu and, as an additional check, for ^{241}Am where Monte Carlo calculations of multiplet losses are available.

1. Introduction

For statistical-model calculations of average capture und fission cross sections and of the associated self-shielding factors one needs average widths and, in particular, level densities. The latter are most directly obtained in the resolved resonance region by counting the observed resonances and correcting for missing levels. Due to the preponderance of small neutron widths in the Porter-Thomas distribution /9/ the correction is always quite important. In the past its estimation has often been based on the distribution of observed resonance energies (ladder statistics), but even if derived from the most refined level spacing theories (e.g. the Dyson-Mehta Δ_3 statistic derived from orthogonal-ensemble theory /2/) the ladder methods were found inferior /3, 4/ to methods based on the distribution of observed neutron widths. A number of techniques is available to exploit the differences between the observed and predicted neutron width distributions: (i) straightforward least-squares fit to a Porter-Thomas distribution to the upper, presumably unperturbed part of the observed width distribution /5/, (ii) the Keyworth-Moore missing-level estimator /3/ which is in essence the ratio of the second moment to the squared first moment of the distribution of reduced width amplitudes, (iii) maximum-likelihood estimation of $\langle \Gamma_n^0 \rangle$ from the observed width distribution above some given energy-dependent threshold /4, 6, 7, 8/ or with a diffuse threshold automatically inferred from the observed level energies and widths /9/. The methods based on the observed neutron width distribution usually give quite good results when tried on Monte Carlo generated resonance parameter sets, with reduced widths sampled from the Porter-Thomas distribution, level energies from the Wigner distribution or orthogonal-ensemble theory, and levels with a reduced neutron width below some cutoff discarded as missing. It came, therefore, as an unpleasant surprise when in a recent benchmark exercise /10/ all methods systematically overestimated the level spacing by several (4-8) percent in cases which must be considered as quite favorable, viz. large, almost pure s-wave samples resembling those met in practice in the actinide region. As shown below the reason seems to be that none of the width-distribution-based estimators so far can account for unrecognised multiplets. The present paper describes the modifications necessary to take unrecognised multiplets into account. The newly derived prescription is applied to resonance parameter data on ^{235}U, ^{238}U, ^{239}Pu, ^{240}Pu, ^{241}Pu, ^{242}Pu and ^{241}Am.

2. Evidence for bias caused by unrecognised multiplets

The test material for the level density benchmark /10/ mentioned above differed from the test material with which codes for level density estimation and missing-level estimators are usually checked. Although

Contribution to the IAEA Consultants Meeting on Uranium and Plutonium Resonance Parameters, Vienna, 28 September - 2 October 1981

neutron widths and level energies were also generated from the Porter-Thomas distribution and from orthogonal-ensemble statistics these "true" resonance parameters were not provided directly. Instead, total cross sections were calculated from them which were subsequently resolution-broadened and subjected to simulated counting statistics. The "experimental" data thus produced were shape-analysed and the extracted resonance parameters were distributed. This test material is expected to be more realistic than Monte Carlo sampled resonance ladders since it simulates the effect of finite counting statistics more directly than a sharp cutoff does. Furthermore it contains resonance parameters extracted from peaks mistakenly analysed as singlets when in fact they were unresolved doublets or triplets, an effect that is totally absent in Monte Carlo sampled resonance ladders. That this resolution effect must be significant can be seen in Table I which shows the characteristics of that part of the test material which did not contain much p-wave admixture, together with results obtained with the maximum-likelihood program STARA /9/. The strength functions estimated were all right but the number of missing levels and thus the level density were always underestimated. It was recognised that adding the true numbers of levels lost in multiplets, which was known from listings distributed after the benchmark exercise, one gets almost exactly the correct numbers and thus the correct level spacings in all three cases. It was concluded that at least a large part of the bias in the STARA results was due to unrecognised multiplets that had been analysed as singlets.

Table I – Characteristics of NEANDC benchmark data and STARA results. Numbers in parantheses give STARA results modified by adding the true numbers of levels lost in multiplets to STARA estimates of missing levels

Benchmark Case	S_0 (10^{-4})	D_0 (eV)	missing levels	lost in multiplets	all levels	origin
5A	2.22	1.85	4	16	173	true
	2.23±.30	2.02±.08	26±2	0	158±2	STARA
		(1.84)	(42)	(16)	(174)	
5B	2.47	1.43	50	22	224	true
	2.52±.34	1.56±.05	30±1	0	204±1	STARA
		(1.42)	(52)	(22)	(226)	
5C	1.79	1.82	40	13	170	true
	1.81±.25	1.90±.09	32±3	0	162±3	STARA
		(1.77)	(45)	(13)	(175)	

3. Distortion of the Porter-Thomas distribution by unresolved multiplets

Instead of treating the effect of unresolved multiplets in all generality we restrict the present discussion to isotopically pure s-wave samples of neutron widths. For target spin I = 0 we have then a single resonance sequence with level spin J = 1/2, for I > 0 two superposed sequences with $J_+ = I + 1/2$ and $J_- = I - 1/2$. For each sequence we consider the reduced neutron widths as obeying the Porter-Thomas distribution. For I > 0 the same distribution governs the ensemble of the quantities

$$G = g\Gamma_n^0 \tag{1}$$

(for all levels regardless of spin, g being the spin factor) to the extent that the strength function can be taken as independent of J and the level density as proportional to 2J+1. Since g = 1 for I = 0 we can write the reduced-width distribution for both I = 0 and I > 0 in the form

$$p(G)dG = \frac{e^{-x}}{\sqrt{\pi x}}\,dx\,, \qquad 0 < x \equiv \frac{G}{2G^0} < \infty\,, \tag{2}$$

$G^0 \equiv \langle g\Gamma_n^0 \rangle$ denoting the true average. We now admit the possibility that two or more closely spaced levels are mistaken for a single peak. Let us assume that this happens whenever spacings are smaller than some limiting value D_c which, of course, must be of the order of the instrumental resolution. The fraction of spacings smaller than D_c is equal to

$$q = \int_0^{D_c} p(D)dD, \tag{3}$$

where p(D)dD is the probability for a given spacing to lie in dD at D. Neglecting correlations between adjacent, second next etc. spacings one finds for the probabilities that a given level belongs to a singlet, doublet, triplet ... peak

$$p_1 = (1-q)^2,$$
$$p_2 = (1-q)2q(1-q),$$
$$p_3 = (1-q)3q^2(1-q) \quad \text{etc.} \tag{4}$$

If ρ is the true level density the densities of singlet, doublet, triplet ... peaks are

$$\rho\, p_1 = \rho(1-q)^2,$$
$$\rho\, p_2/2 = \rho(1-q)^2 q,$$
$$\rho\, p_3/3 = \rho(1-q)^2 q^2 \quad \text{etc.} \tag{5}$$

The sum of these is the overall peak density (as opposed to level density)

$$\rho \sum_{\nu=1}^{\infty} \frac{p_\nu}{\nu} = \rho(1-q). \tag{6}$$

Next we assume that the apparent width extracted from an unresolved multiplet is the sum of the true component widths, $G = \sum_{\mu=1}^{\nu} (g\Gamma_n^0)_\mu$. This is the usual situation, especially with thin-sample data, and is also in good agreement with the benchmark test material /10/. One realises that under this assumption the apparent widths of doublets, triplets etc. are distributed according to χ^2-distributions with $\nu = 2, 3, \ldots$ degrees of freedom and average widths $2G^0$, $3G^0$ etc. We may therefore write the overall distribution of peak widths as

$$p(G)dG = (1-q) \sum_{\nu=1}^{\infty} \Gamma\left(\frac{\nu}{2}\right)^{-1} e^{-x} x^{\nu/2-1} q^{\nu-1} dx, \quad 0 < x \equiv \frac{G}{2G^0} < \infty, \tag{7}$$

The series can be summed. The even terms yield an exponential. The odd terms, upon differentiation, yield a linear differential equation which is readily solved. The result is the distorted Porter-Thomas distribution

$$p(G)dG = (1-q)(1+v)\frac{e^{-x}}{\sqrt{\pi x}}\,dx \tag{8}$$

with

$$v = \sqrt{\pi} z\, e^{z^2}(1 + \operatorname{erf} z), \quad z \equiv q\sqrt{x}. \tag{9}$$

The distortion v reduces the relative frequency of small widths and increases that of large widths as compared to the undistorted Porter-Thomas distribution, eq. (2). For a detectability threshold G_c smaller than the cross-over point the number of missing levels is therefore smaller, the sample average $\bar{G}$ larger than for the undistorted distribution. The detectable fraction of peaks is

$$\int_{G_c}^{\infty} p(G)dG = \frac{1}{1+q}\left(\operatorname{erfc}\sqrt{x_c} + v_c \frac{e^{-x_c}}{\sqrt{\pi x_c}}\right). \tag{10}$$

4. The fraction of levels lost in unresolved multiplets

We shall assume that the minimal observable level separation D_c is known at least approximately, for instance from the observed distribution of spacings. For the calculation of q we simply take the Wigner distribution,

$$p(D)dD = 2ye^{-y^2}dy, \quad 0 < y \equiv \frac{\sqrt{\pi}}{2} D\rho < \infty, \tag{11}$$

which is a very good approximation to the more rigorous orthogonal-ensemble distribution /12/. This distribution is valid for a single level sequence. For two superposed sequences with level densities $\rho_+ = g_+\rho$, $\rho_- = g_-\rho$ one has

$$p(D)dD = 2\left\{y\left(g_-^3 e^{-y^2 g_-^2} \operatorname{erfc} yg_+ + g_+^3 e^{-y^2 g_+^2} \operatorname{erfc} yg_-\right) + \frac{2}{\sqrt{\pi}} g_- g_+ e^{-y^2(g_-^2 + g_+^2)}\right\}dy \tag{12}$$

(see ref. /13/), where g_+ and g_- are just the spin factors if we assume 2J+1 proprtionality of ρ. Integrating eq. (12) one gets

$$q = 1 - g_- e^{-y^2 g_-^2} \operatorname{erfc} yg_+ - g_+ e^{-y^2 g_+^2} \operatorname{erfc} yg_-, \quad y = \frac{\sqrt{\pi}}{2} D_c\rho. \tag{13}$$

It may be noted that eqs. (12) and (13) are valid for both $I = 0$ and $I > 0$ since $g_- = 1 - g_+ \to 0$ for $I \to 0$. Fig. 1 shows q as a function of y for the limiting cases $I = 0$ with $\rho_- = 0$, $\rho_+ = \rho$, and $I = \infty$, with $\rho_- = \rho_+ = \rho$. If the resolution is good, $D_c\rho \ll 1$, the fraction of levels lost in unresolved multiplets is smaller for a spinless target nucleus than for one with spin thanks

to the unmitigated level repulsion for I = 0 and to the finite probability for zero level spacing for I > 0. For $D_c\rho \gtrsim 0$, however, there is not much difference, and for still worse resolution things are reversed.

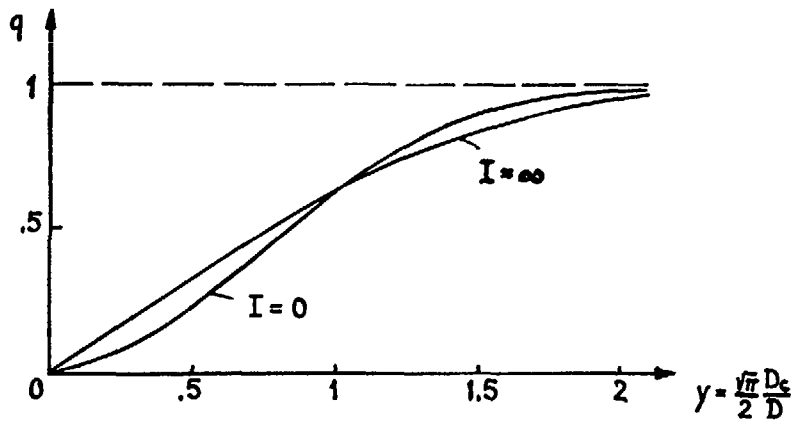

Fig. 1

5. Level density estimation based on the width distribution

As indicated above the best methods for level spacing estimation from experimental neutron resonance data seem to be those which, in essence, infer the true average width from the upper, unperturbed portion of the observed width distribution and the number of missing levels from the lower, perturbed portion. The case of negligible perturbation may serve to illustrate the general statistical approach. In this case one has to infer G^0 and its uncertainty from a sample G_1, G_2, ... G_N consisting of members of the unperturbed Porter-Thomas distribution, eq. (2). This is accomplished in a straightforward manner by application of Bayes' theorem. The joint probability that in a random sample of size N, drawn from a Porter-Thomas distribution with given average G^0, the sample values lie in the intervals dG_1 at G_1, dG_2 at G_2, ... dG_N at G_N can be written down as

$$L(G_1,\ldots G_N|G^0)dG_1\ldots dG_N = \prod_{i=1}^{N} p(G_i)dG_i \ . \qquad (14)$$

The inverse probability that the ensemble average G^0 lies in the interval dG^0 at G^0, given the sample G_1, ... G_N, is obtained according to Bayes' theorem (cf. e.g. ref. /13/) by multiplication of the likelihood function L by the a-priori probability $p_0(G^0)dG^0$ for G^0 in dG^0,

$$p(G^0|G_1,\ldots G_N)dG^0 \propto L(G_1,\ldots G_N|G^0)p(G^0)dG^0, \quad 0 < G^0 < \infty \ . \qquad (15)$$

Now G^0 acts as a scale factor in our problem. Jaynes /14/, using invariance arguments, showed that for such scale parameters the appropriate prior probability is $dG^0/G^0 = d \ln G^0$, thus proving a conjecture due to Jeffreys /13/. Properly normalising we get therefore

$$p(G^0)dG^0 = \frac{L \, d \ln G^0}{\int L \, d \ln G^0} \ . \qquad (16)$$

The Jeffreys-Jaynes prior ensures that we get the same most probable Porter-Thomas distribution regardless whether we maximise this probability with respect to G^0 or, equally possible for a scale parameter, with respect to $1/G^0$: This is the case if we regard $\ln G^0$ as the basic parameter and maximise with respect to it,

$$\frac{d\,L}{d \ln G^0} = \frac{dL}{dG^0} G^0 = -\frac{dL}{d(1/G^0)} \frac{1}{G^0} = 0 \ . \qquad (17)$$

In any case we have to maximise the likelihood function. Thus the maximum-likelihood solution coincides with the rigorous Bayesian solution in the case of scale parameter estimation. Inserting the Porter-Thomas distribution in L one gets the well known results /15/

$$G^0 = \frac{1}{N}\sum_{i=1}^{N} G_i \equiv \overline{G} \ , \qquad (18)$$

$$p(G^0)dG^0 \equiv \Gamma(\tfrac{N}{2})^{-1} e^{-y} y^{N/2-1} dy \ , \quad 0 < y \equiv \frac{NG}{2G^0} < \infty \ . \qquad (19)$$

Confidence limits are readily calculated from this χ^2-distribution.

Let us now proceed to the more realistic case where the sample contains only widths exceeding an unknown cutoff G_c. The Porter-Thomas distribution is now truncated,

$$p(G)dG = \frac{1}{\mathrm{erfc}\sqrt{x_c}} \frac{e^{-x}}{\sqrt{\pi x}} dx , \quad x_c \equiv \frac{G_c}{2G^0} < x < \infty , \tag{20}$$

and the likelihood function becomes maximal for any positive G^0 if G_c is taken as large as possible. Now the upper limit for G_c is the smallest member of the sample, G_1 say. Inserting $G_c = G_1$ in (15) one gets an expression for G^0 alone which can be maximised with respect to G^0. The resulting maximum-likelihood estimator is biased, however, since on average G_1 will be somewhat larger than G_c. In order to remove the bias we consider the quantities

$$u_i \equiv \mathrm{erfc}\sqrt{x_i} \quad \text{and} \quad u_c = \mathrm{erfc}\sqrt{x_c} , \tag{21}$$

with which we write

$$p(G_i)dG_i = -\frac{du_i}{u_c} , \qquad 0 < u_i \le u_c . \tag{22}$$

The quantities u_i are seen to be uniformly distributed between zero and u_c. Suppose for the moment that G^0 is known. We get then $u_c = u_1$ as a biased estimate. The distribution of u_1 can be written down immediately as the joint probability that u_1 is found in du_1 and that the other N-1 members of the sample are larger than G_1:

$$p(u_1)du_1 = N \left(\frac{u_1}{u_c}\right)^{N-1} \frac{du_1}{u_c} , \quad 0 < u_1 \le u_c . \tag{23}$$

The expectation value of u_1 is then $\bar{u}_1 = u_c N/(N+1)$ which implies that

$$\mathrm{erfc}\sqrt{x_c} = \frac{N+1}{N} \mathrm{erfc}\sqrt{x_1} \tag{24}$$

is an unbiased estimator for u_c. If on the other hand G_c is given the likelihood becomes maximal for

$$G^0 = \bar{G}\left(1 + \frac{2}{\sqrt{\pi}} \frac{e^{-x_c}\sqrt{x_c}}{\mathrm{erfc}\sqrt{x_c}}\right)^{-1} . \tag{25}$$

The term in parantheses is obviously a correction for missing levels. If both G_c and G^0 are unknown we must find them as the common solution of eqs. (24) and (25). This can be achieved by iteration, starting with $G_c = G_1$, $G^0 = \bar{G}$.

The next complication we must consider is an energy dependence of the threshold. In practice it was found to be quite adequate if the apparent level density is taken as linearly decreasing with energy. This corresponds to a quadratic behavior of the cumulative number of observed peaks. Examples are given in ref. /9/. Under this assumption the observed peak density is related to the true level density ρ by

$$\rho_o = \rho \,\mathrm{erfc}\sqrt{x_c} = \bar{\rho}_o \left(1 - \kappa \frac{E-\bar{E}}{I/2}\right) , \tag{26}$$

where $\bar{E}$ is the center and I the length of the energy interval from which the sample is taken. The constant κ determining the slope can be obtained by fitting a parabola to the observed cumulative level number stairstep curve. We shall consider it as known. The joint probability to find a peak in the interval dE and its width in the interval dG at G is now

$$p_o dE dG = \frac{\rho_o dE}{\int \rho_o dE} \frac{pdG}{\int pdG}$$

$$= \frac{\rho_o dE}{\bar{\rho}_o I} \frac{1}{\mathrm{erfc}\sqrt{x_c}} \frac{e^{-x}}{\sqrt{\pi x}} dx = -\frac{dE}{I} \frac{du}{\bar{u}_c} ,$$

$$\bar{E} - I/2 < E < \bar{E} + I/2 , \quad 0 < u \le \bar{u}_c\left(1 - \kappa \frac{E-\bar{E}}{I/2}\right) = \frac{\rho_o}{\rho} . \tag{27}$$

This shows that the two-dimensional distribution of sample members in the (E,u) plane is uniform up to a straight line (see Fig. 2). As before one can maximise L with respect to the threshold by lowering $\bar{u}_c$ as much as possible while keeping κ constant. The lowest possible value is reached when the straight line hits the outermost sample point,

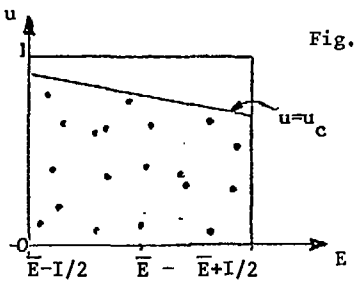

Fig. 2

(E_1,u_1) say. Then

$$u_1 = \bar{u}_c \left(1-\kappa \frac{E-\bar{E}}{I/2}\right) . \tag{28}$$

Solving for $\bar{u}_c$ one gets the maximum-likelihood estimator which is biased again. One can determine the bias as before by establishing the distribution of the estimator and calculating its expectation value. The distribution of the estimator is given by eq. (23) and the bias factor by N/(N+1), as before. The generalisation of eq. (24) for a linear dependence of ρ_o on E is thus

$$\operatorname{erfc} \bar{x}_c = \frac{N+1}{N} \frac{\operatorname{erfc} \sqrt{x_1}}{1-\kappa \frac{E_1-\bar{E}}{I/2}} , \tag{29}$$

and the equation analogous to (25) is

$$G^0 = \bar{G} \left(1 + \frac{2}{\sqrt{\pi}} \frac{e^{-\bar{x}_c} \sqrt{\bar{x}_c}}{\operatorname{erfc} \sqrt{\bar{x}_c}} \right)^{-1} , \tag{30}$$

with $\bar{x}_c = G_c(\bar{E})/(2G^0)$. The last pair of equations can again be solved by iteration, starting from $G^0 = \bar{G}$. This method works well if the threshold is really sharp. In practice the threshold is normally diffuse, however. Then it is better to use the following approach. Integrating out the peak energy in eq. (27) one gets the marginal distribution of widths,

$$p_o dG = \frac{s}{\bar{u}_c} \frac{e^{-x}}{\sqrt{\pi x}} dx = -s \frac{du}{\bar{u}_c} \tag{31}$$

where s is the trapezoidal step function (see Fig. 3)

$$s = \begin{cases} 1 & \text{if} \quad u \le (1-\kappa)\bar{u}_c , \\ \frac{1}{2}\left(1 - \frac{u-\bar{u}_c}{\kappa \bar{u}_c}\right) & \text{if} \quad (1-\kappa)\bar{u}_c < u < (1+\kappa)\bar{u}_c , \\ 0 & \text{if} \quad (1+\kappa)\bar{u}_c < u . \end{cases} \tag{32}$$

Maximisation of the likelihood function corresponding to this width distribution with respect to G^0 and $\bar{u}_c$ yields the two equations

$$G^0 = \bar{G} \left(1 + \frac{1}{N} \sum_i{}' \frac{-2x_i \, \partial u_i/\partial x_i}{(1+\kappa)u_c - u_i} \right)^{-1} , \tag{33}$$

$$0 = 1 + \frac{1}{N} \sum_i{}' \frac{u_i}{(1+\kappa)\bar{u}_c - u_i} , \tag{34}$$

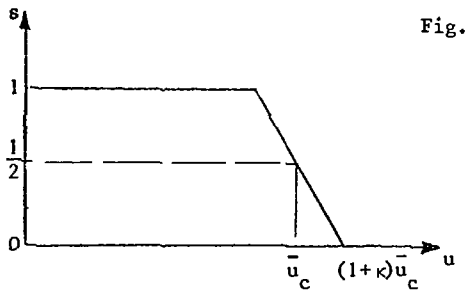

Fig. 3

where the primes indicate that the sums contain only terms from the fringe where s is not constant. Eq. (33) is obviously a recipe for the correction of $\bar{G}$ for missing levels. Eq. (34) is the likelihood equation obtained for the distribution sdu of u values, if the parameter $\bar{u}_c$ is to be estimated from the sample $u_1, \ldots u_N$. These equations, given previously in slightly different notation /9, 16/, are the basis of the statistical resonance analysis code STARA mentioned above, where they are solved for G^0 and $\bar{u}_c$ with the Newton-Raphson method. If the threshold does not depend on energy eqs. (24) and (25) are used instead.

We are now prepared to deal with the last complication, viz. unresolved multiplets. Again we consider the energy dependence of ρ_o as linear, with κ known from a fit to the level number stairstep curve. The fraction q of levels lost in multiplets is also assumed as known. The observable peak density is now

$$\rho_o = \rho \, (1-q) \int_{G_c}^{\infty} p dG \tag{35}$$

so that

$$p_o dE dG = \frac{\rho}{\rho_o} \frac{dE}{I} (1-q) \, p \, dG = -\frac{dE}{I} \frac{du}{\bar{u}_c} ,$$

$$0 < u \equiv \frac{1-q}{1+q} \left(\operatorname{erfc} \sqrt{x} + v \frac{e^{-x}}{\sqrt{\pi x}} \right) < \frac{\bar{\rho}_o}{\rho} \left(1-\kappa \frac{E-\bar{E}}{I/2}\right) , \tag{36}$$

(compare eq. (8)). The marginal distribution of G-values is obtained as before as

$$p_o dG = - s \frac{du}{\bar{u}_c} , \qquad (37)$$

where s is the trapezoidal step function of fig. 3. The generalisation of the likelihood equations (33), (34) is

$$G^0 = \bar{G} \left[1 - \frac{2}{N} \sum_i \left(\frac{G^0}{s_i} \frac{\partial s_i}{\partial G^0} + \frac{G^0}{1+v_i} \frac{\partial v_i}{\partial G^0} \right) \right]^{-1} \qquad (38)$$

$$0 = 1 - \frac{1}{N} \sum_i \frac{\bar{u}_c}{s_i} \frac{\partial s_i}{\partial \bar{u}_c} . \qquad (39)$$

These equations are used in a recent modified version of the STARA code, with a rounded step function

$$s_i = \frac{1}{2} \left(1 - \tanh \frac{u_i - \bar{u}_c}{\kappa \bar{u}_c} \right) \qquad (40)$$

which is more convenient mathematically than the trapezoidal step function with its discontinuities. The function (40) approximates the trapezoidal step function near the middle of the fringe region ($u_i \approx \bar{u}_c$) quite closely. It also leads to very similar estimation results. It can be considered as arising from a somewhat fuzzy threshold that rises linearly with energy. Since a perfectly sharp threshold is somewhat artificial anyway it can be expected that eq. (40) gives a more realistic description of the true situation. The fraction q of levels lost in unresolved multiplets is assumed to be a constant fraction of the total fraction of missing levels at each energy,

$$q = \bar{q} \frac{\rho - \rho_o}{\rho - \bar{\rho}_o} . \qquad (41)$$

Its energy average $\bar{q}$ is estimated from the smallest spacings in the sample by means of eq. (13) with the level density taken as that estimated for q = 0. This modified version of STARA was checked against the benchmark problem.

The improved results are listed in Table II.

Table II – Comparison between benchmark values and STARA results obtained with due account of levels lost in multiplet peaks

Benchmark Case	S_0 (10^{-4})	D_0 (eV)	origin
5A	2.22	1.849	true
	2.20±.30	1.81± .19	STARA-81
5B	2.47	1.428	true
	2.49±.30	1.44±.05	STARA-81
5C	1.79	1.824	true
	1.78±.22	1.86±.09	STARA-81

As a further check we calculated the level density and the strength function from the resonance parameters of ref. /17/. The authors had attempted to estimate the number of missing levels with a Monte Carlo method similar to that used in the benchmark exercise. Their result for the region 0-150 eV, D_0 = (0.55±.05) eV, S_0 = (0.94±.09) 10^{-4} is in good agreement with the STARA-81 result, D_0 = (0.52±.04) eV, S_0 = (0.92±.09) 10^{-4}.

6. Reanalysis of actinide resonance parameters

The new version of the STARA code was employed to reanalyse resonance parameter sets for the main actinides. Results from the old and the new code version are listed in Table III.

Table III - Results of statistical resonance analysis without and with account of levels lost in unresolved multiplets

Target Nucleus	Energies (eV)	Sample Size	S_0 (10^{-4})	D_0 (eV)	Multiplets Considered?	Resonance Parameter Source
^{235}U	0-100	196	.97±.12	.44±.01	no	Moore+ 78 /18/
			.96±.12	.43±.01	yes	
^{238}U	0-4000	188	1.16±.13	20.4±.2	no	Keyworth+ 78 /19/
			1.15±.12	20.3±.2	yes	
^{239}Pu	0-660	257	1.26±.12	2.28±.05	no	Derrien 74 /20/
			1.27±.12	2.20±.05	yes	
^{240}Pu	0-3000	172	1.03±.10	13.1±.5	no	KEDAK-3 77 /21/
			1.02±.10	12.4±.7	yes	
^{241}Pu	0-161	123	1.20±.18	.90±.04	no	KEDAK-3 77 /21/
			1.23±.13	.73±.08	yes	
^{242}Pu	0-500	37	.82±.26	12.6±.6	no	KEDAK-3 77 /21/
			.83±.27	13.3±.4	yes	

The differences in D_0 are quite small (1-2%) for the well studied nuclides ^{235}U and ^{238}U, about 5% for the Pu isotopes with the exception of ^{241}Pu where a 20% reduction of the average level spacing is found, indicating a lower quality of the resonance data with a significant number of unresolved multiplets.

7. Conclusions

Level density estimation methods based on the neutron width distribution were reviewed with special emphasis on the treatment of detectability thresholds and their energy dependence. The influence of unresolved and unrecognised multiplets was treated analytically. The new formulation was utilised in a reanalysis of resonance parameter sets for the main actinides. The differences relative to the conventional estimation without regard to the multiplet losses were found to be quite small for ^{235}U and ^{238}U whereas for the plutonium isotopes effects ranging from 4%(^{239}Pu) to 23% (^{241}Pu) were calculated. These should be taken into consideration in applications of level spacings such as Hauser-Feshbach calculations of compound reactions, especially neutron capture.

Acknowledgements

The author wants to express his appreciation to P. Ribon who initiated the level density benchmark exercise and to F. Perey who introduced him to the modern theory of prior probabilities.

References

1. C.E. Porter, and R.G. Thomas, Phys. Rev. 104, (1959) 483

2. F.J. Dyson and M.L. Mehta, J. Math. Phys. 4, (1963) 701

3. M. S. Moore, J.D. Moses, G.A. Keyworth, J.W.T. Dabbs, and N.W. Hill. Phys. Rev. C18, (1978) 1328

4. E. Fort, H. Derrien and D. Lafond. Proc. Spec. Meeting on Neutron Cross Sections of Fission Product Nuclei, Bologna (1979). RIT/FIS-LDN(80) 1, p.121

5. H. Weigmann, Neutron Physics and Nuclear Data, Harwell (1978), p.969

6. T. Fuketa and J.A. Harvey, Nucl. Inst. Math. 33, (1965) 107

7. C. Coceva and M. Stefanon, Nucl. Phys. A 315 (1979) 1,
M. Stefanon, Proc. Spec. Meeting on Neutron Cross Sections of Fission Product Nuclei, Bologna (1979), RIT/FIS-LDN(80) 1, p.161

8. G. Rohr, L. Maisano and R. Shelley, Proc. Spec. Meeting on Neutron Cross Sections of Fission Product Nuclei, Bologna (1979), RIT/FIS-LDN(80) 1, p.197

9. F.H. Fröhner, Proc. Spec. Meeting on Neutron Cross Sections of Fission Product Nuclei, Bologna (1979), RIT/FIS-LDN (80)1, p.145

10. P. Ribon, Report NEANDC&E)213-AL, 1st part (1980);
P. Ribon and P. Johnston, Report NEADNC(E)213-AL , 2nd part (1981), with associated lists of "true" resonance parameters

11. E.P. Wigner, Conf. on Neutron Time-of Flight, Gatlinburg (1956), Report ORNL-2309 (1957) p.59 .

12. J.E. Lynn, The Theory of Neutron Resonance Reactions, Oxford (1968), p. 194

13. E.T. Jaynes, Trans. Systems Sci. and Cybern. 4 (1968) 227

14. H. Jeffreys, Theory of Probability, Oxford (1939)

15. D.D. Slavinskas and T.J. Kennett, Nucl. Phys. 85 (1966) 641

16. F.H. Fröhner, Nuclear Theory for Applications, Trieste (1980), p. 59
also issued as report KfK-2669 (1978)

17. H. Derrien and B. Lucas, Nuclear Cross Sections and Technology, NBS Special Publication 425, Washington (1975), vol. II, p. 637

18. M.S. Moore, J.D. Moses, G.A. Keyworth, J.W.T. Dabbs and N.W. Hill Phys. Rev. C18 (1978) 1328

19. G.A. Keyworth and M.S. Moore, Neutron Physics and Nuclear Data, Harwell (1978) p. 241

20. H. Derrien, Specialists Meeting on "Resonance Parameters of Fertile Nuclei and 239 Pu", NEANDC (E) 163 U, Saclay (1974)

21. B. Goel and F. Weller, Report KfK 2386/III (1977)

Resonance Parameters of ^{238}U below 4.2 keV *

F. Poortmans, L. Mewissen
S.C.K./C.E.N., B 2400 Mol, Belgium

G. Rohr, R. Shelley, T. van der Veen, H. Weigmann
CEC, JRC, CBNM Geel, Belgium

E. Cornelis, G. Vanpraet
R.U.C.A., University of Antwerp, Belgium

1. Introduction

Neutron cross section and resonance parameters for ^{238}U are of extreme importance for nuclear reactor design. For that reason, many differential cross section experiments have been performed in the past at several laboratories [1-21]. In most of these experiments, the resonance parameters were deduced from capture and transmission measurements or in a few cases from elastic scattering or self-indication ratio measurements. Only a few experiments cover the energy range up to 4 keV [9,14,17,19,21]. Also subtreshold fission in ^{238}U below 4 keV has been investigated [22-27].

In this paper we describe the final results from an analysis of a large amount of data from capture, scattering and transmission experiments performed at the CBNM Linac.
The present results have already been used in a recent evaluation of ^{238}U resonance parameters by de Saussure et al. [28].

The experiments were largely stimulated by two meetings on Resonance Parameters of ^{238}U respectively at Saclay [29] and at Brookhaven [30]. Partial results from our work have been communicated at Conferences on Nuclear Data [31-32] and the results for the important 6.6 eV resonance have been published [33]. However a complete description of the experiments and a complete list of resonance parameters have never been published.

* work supported by the International Atomic Energy Agency

We would also like to draw the attention to the reader that the present experimental conditions at the CBNM linac are no longer the same as described in this paper. In fact since the time we completed the ^{238}U experiments the linac was upgraded, a new neutron-producing target was installed and the data-acquisition system was changed.

2. Experimental details

The experiments have been performed using the 65 MeV linear electron accelerator as a pulsed neutron source. A pulsed beam of fast neutrons was produced by (γ,n) reaction and fission in a mercury cooled uranium target placed in the electron beam. The fast neutrons were slowed down in a polyethylene moderator surrounding the uranium target. The total diameter of the neutron target, central uranium part plus surrounding moderator, was 19 cm. The moderator thickness was 4 cm. Three lead rings, each 4.5 cm high and 5 cm thick were placed around the neutron target to shield the experiment from the strong gamma flash produced in the central uranium part of the target.

The collimated neutron beam passed through an evacuated 50 cm diameter aluminium tube. The flight paths used for the present experiments made an angle of 9° with the normal on the moderator surface. The most important experimental parameters for the three measurements are listed in Table 1. A more detailed discussion on the experiments follows below.

2.1. Transmission experiments

The transmission detector system consisted of four ^{3}He gaseous scintillators, LND type 800. The anode signals were amplified and mixed and the bias level was set using a Canberra extrapolated zero strobe, model 1426. The time resolution (F.W.H.M.) due to the detector and associated electronics was 5 nsec.

The time-of-flight was measured using a multistop time-coder, type Laben 8270, with a channel width multiplication unit. The minimum channel width was 10 nsec. The time-of-flight spectra could be subdivided into a maximum of four zones, each with a channel width multiplication factor ranging from 1 to 128.

The data were stored in a 4096 channel memory which was interfaced with a IBM 370/135 computer.

The automatic sample changer with cryostat was located at 30 meter. The ^{238}U samples (99.8% ^{238}U) were circular metallic discs with a diameter of 10 cm. They were cooled at liquid nitrogen temperature.

Because of the limited memory capacity, the measurements had to be subdivided into eight runs. Each experiment had a permanent black resonance filter in the beam to normalize the background. Separate background-law measurements were performed for each sample thickness. The black resonance filters used were W (18.8 eV), Mo (44.7 eV), Co (132 eV), Mn (337 eV) and Na (2850 eV).

All these background measurements showed the following results :

1. The background law did not change during the time of the experiments.
2. The absolute value of the background was of course dependent on the filter combination in the beam but the background law was not.
3. The background law was the same as for the sample out measurement when the three thinnest samples were in the beam but was slightly different for the two thickest samples.

The background changes very slowly above 300 eV (4.8% at 340 eV and 4.2% at 2.85 keV) but starts to increase at lower energy due to the ^{10}B overlap filter : 200 eV (5.3%), 100 eV (5.9%), 50 eV (7.1%) and 20 eV (9.3%). For this reason we used four black resonance filters between 15 eV and 350 eV, so that a sufficiently accurate determination of the background was possible by a simple linear interpolation between the black resonance positions. We estimate the total error on the background to be of the order of 10%. The transmission experiments with the thick ^{238}U sample offers us a check on the background and, indeed, in five ^{238}U resonances the neutron beam was completely absorbed over several time-of-flight channels.

The dead-time was 1 μsec and was due to the channel width multiplication unit. However the count rate stored in memory was only of the order of 1 count per burst so that the total dead-time correction was always less than 1%.

2.2. Elastic scattering cross section experiments

The scattering detector system consisted of six ^{3}He gaseous scintillators mounted around an evacuated cylindrical tube with sample holder. The angle between the scattered and the incoming neutron beam was 140 deg. The electronics associated to the scattering detector system was the same as used for the transmission experiments.

Scattering experiments on thin samples are only possible if the detectors are shielded against room background. The drawback of such a shielding is that a small fraction of the scattered neutrons are detected after being reflected by the shielding wall. We have tried to make the shielding so that the fraction of backscattered neutrons was reduced as much as possible. The best result was obtained by using a 5 cm thick inner shielding of B_4C powder, canned in thin aluminium, surrounded by a 10-cm-thick shielding composed of a mixture of paraffin and borax. However, we still noticed a small tailing on the low-energy side of the resonance, and we estimated this contribution to be 3%.

The scattering cross section was measured relative to lead for which $\sigma_n = 11.28 \pm 0.06$ b [34].

The background was determined using the black resonance technique, using the same black resonance filters as in the transmission experiments. The background could be subdivided into two components a sample-independent and sample dependent component. The first could be measured without a sample in the scattering chamber and was due to room background and scattering of the beam by the windows of the evacuated central tube of the scattering chamber. This part of the background was roughly equivalent to the count yield one should obtain if 0.3% of the incoming beam should be scattered by a sample. The sample-dependent background was due to neutrons scattered by the sample and detected much later after having made several collisions in the shielding material surrounding the detectors. This component was about 6% of the scattering signal.

In the experiment with the lead reference sample, which scatters 7% of the incoming beam, the total background was 8% at 1 keV and increases slowly to 12% at 10 eV.

2.3. Capture cross section measurements

The capture cross sections were measured using two cylindrical hexafluorid liquid scintillators (C_6F_6 detectors of Type NE 226), each with a diameter of 4 inches and a length of 3 inches.

The weighting method has been used to achieve a detector response proportional to the total energy released in the capture process. The weighting factors were calculated by means of a computer program developed at Oak Ridge. The time and pulse height information of the detected γ-rays have been recorded in two parameters, 13 time-of-flight and 7 amplitude bits, stored event by event on magnetic tape.

The weighting procedure for the time-of-flight spectra has been performed off-line using eight amplitude windows and these spectra have been subdivided into 4 zones with channel widths ranging from 10 - 640 nsec.

In total five different ^{238}U samples have been used and in order to reduce the background caused by the natural activity of the old ^{238}U samples, different biases in the pulse height amplitude have been chosen to a γ-ray energy of 0.300 and 1.2 MeV respectively for the two thin and the 3 thick samples (Table 1).

Absolute calibration of the capture yield with the thin ^{238}U samples was obtained by the "black resonance technique" using 5 resonances in Ag at 16, 30, 51, 55 and 71 eV. An Ag sample of $2.93 \cdot 10^{-3}$ at/barn has been used.

The neutron flux was measured under the same experimental conditions as the capture measurement with the capture sample replaced by a $^{10}B_4C$-slab.

3. Analysis of the data

3.1. Transmission experiments

For the analysis of the transmission experiments we have applied two different procedures : a resonance area analysis using a single-level Atta-Harvey code [36] and a shape fitting analysis using the multi-level Breit-Wigner code due to de Saussure , Olsen and Perez [37].

The advantage of an area analysis is that the results are much less dependent on the knowledge of the resolution functions. On the other hand it has been proven [37] that for the case of ^{238}U, a multi-level Breit-Wigner formalism results in a much better description of the total cross section shape than a single-level approximation,especially in the regions between resonances and in the resonance-potential interference minima.

The time-of-flight resolution function was assumed to be a gaussion function with the following value for the width (F.W.H.M.)

$$W = (AE^2 + BE^3)^{1/2}$$

In this expression the neutron energy E and the width W are expressed in eV and the constants A and B have the following values :

$A = 1.52 \cdot 10^{-6}$

$B = 0.62 \cdot 10^{-11}$ (for a channel width of 20 nsec.).

The first term is the dominant one and is determined mainly by the equivalent moderator thickness. By fitting narrow resonances in the keV range, we have obtained for the equivalent moderator thickness (F.W.H.M.) a value of 3.56 ± 0.36 cm.
This value is approximately 10% larger than obtained from Monte-Carlo calculations [38].

We have noticed a good agreement between the neutron widths obtained from a single level area analysis and from a multi-level Breit-Wigner shape analysis when certain precautions were taken for the area analysis. In fact the sample had to be sufficiently "thin" which means a minimum transmission at resonance energy not smaller than 30%. This allowed us to determine the area over a narrow energy interval around E_0 so that the influence of neighbouring resonances or uncertainties on the transmission base-line fits were minimized.

An area analysis over a narrow energy interval required of course a good knowledge of the resonance energy E_0 . We therefore first deduced E_0 from a shape analysis and used that value as an input parameter in the area analysis .

3.2. Capture experiments

The capture data have been analyzed using a modified TACASI [39] area analysis program which includes corrections for Doppler and resolution effects. The influence of multiple scattering on the capture area is taken into account by a Monte Carlo routine.

3.3. Elastic scattering experiments

The scattering data were also analysed using a single-level Breit-Wigner area analysis program. After subtraction of the background, the data were corrected for multiple scattering and absorption of the scattered neutrons using a Monte Carlo computer code. By normalization to the lead scattering results, the data were converted to scattering cross sections versus time-of-flight channel. An area analysis of the corrected data yielded Γ_n as a function of Γ_γ.

This method of analysis was explained in more detail in ref. 33 where it was applied on the 6.67 eV resonance of ^{238}U.

4. Resonance Parameters

The resonance parameters obtained from the analysis of our data are listed in Table 2.
The values for the resonance energies are taken form the capture experiments.

The large amount of data from the transmission, scattering and capture experiments each performed with several sample thicknesses, allowed us to look for possible systematic errors in the data and to a certain extent also in the methods of analysis. This procedure has yielded the following conclusions :

1. The comparison of the results from the capture data measured with various sample thicknesses were consistent within the statistical error. This means that there is no systematic error due to the correction for multiple scattering in the sample. The same conclusion was valid for the scattering experiments.
2. For small resonances ($\Gamma_n \ll \Gamma_\gamma$), the neutron width can be obtained from the area analysis of the capture data. There is no systematic difference between the results for Γ_n obtained from the capture data and from the transmission data.
3. For resonances with $\Gamma_n \approx \Gamma_\gamma$, the results from the area analysis of the three experiments, capture, scattering and transmission are consistent. Two examples namely for the 36.8 eV and for the 66 eV resonances are shown on fig. 1.

The results shown in Table 2 were obtained in the following way :

1. The small neutron widths ($\Gamma_n \leq 6$ meV) were all the results of an area analysis of the capture data. Because of the potential scattering contribution in the total cross section, the transmission experiments can not yield the same accuracy for these weak resonances.
2. The larger neutron widths were obtained from the analysis of the transmission data. Below 1 keV, the transmission was measured through five different sample thicknesses. So for nearly each resonance there was what one can call "a suitable sample thickness" (min $\cong$ 0.5) and the results for Γ_n in table 2 are from an area analysis of the data taken with the optimum sample thickness.

   Above 1 keV, two transmission runs were performed, respectively with a sample thickness of 1.009 10^{-2} at./b. and 3.481 10^{-2} at./b. We have performed a single level area analysis on the thin sample data and a multi-level Breit-Wigner shape analysis on the thick sample data. On average there was no systematic difference in the results for Γ_n although in certain individual cases the disagreement was as high as 25%. Finally we decided to take the results from the single level area analysis except for some difficult cases, as for example in case of partly overlapping resonances where an area analysis was difficult to apply.
   Above 2 keV the analysis became very difficult due to the time-of-flight resolution which becomes more than an order of magnitude larger than the average total width.
3. The capture widths could of course be determined only for relatively large resonances ($\Gamma_n \geq \Gamma_\gamma$) by combining the results of the area analysis of the partial cross section measurements and the neutron widths from the transmission experiments. The reason why the number of resonances, for which the capture width was determined, decreases with increasing energy is explained as follows. Our time-of-flight resolution width (F.W.H.M.) was 1.3 eV at 1 keV and 5.5 eV at 4 keV. This is comparable with the average spacing between resonances (s- and p-wave). For that reason, more and more p-wave resonances start to overlap with broad s-wave resonances in the experiment.

Below 1 keV, the distribution of the capture width is very narrow, the dispersion being only 0.67 meV. However with increasing energy, there are more and more larger values for Γ_γ. We consider this as an indication for overlap of resonances and indeed, by looking carefully to the shape of these resonances with large Γ_γ values, in most of these case this effect was apparent. For that reason, we did not take into consideration those Γ_γ values which were larger than the average by more than three times the dispersion.

5. Average properties of resonance parameters

5.1. Average capture width

For reasons explained above, we have deduced the average capture width from the results below 1 keV. This has yielded the following result :

$$\Gamma_\gamma = 23.60 \text{ meV} \pm 0.11 \text{ (meV)} \pm 0.50 \text{ meV (syst. error)}.$$

The distribution of the Γ_γ values around the mean value is very narrow, the dispersion being only 0.67 ± 0.11 meV.

5.2. Mean level spacing for s-wave resonances

This parameter was deduced by fitting the reduced neutron width distribution to a Porter-Thomas distribution above a bias value $\Gamma_n^o = 0.25$ meV. Fig. 2 shows the integral distribution of the reduced neutron widths after subtraction of the p-wave resonances. To do this, we have taken the ℓ-assignments by Corvi et al.[18] below 1.5 keV and by Rahn et al.[17] above 1.5 keV.
If we take $S_0 = 1.15\ 10^{-4}$ for the energy range 0 - 4260 eV, we obtain 196 s-wave resonances, giving :

$$D_0 = (21.7 \pm 0.9) \text{ eV}$$

5.3. s-wave strength function

$$S_0 = (1.0 \pm 0.21)\ 10^{-4} \qquad 0 - 1000 \text{ eV}$$
$$S_0 = (1.15 \pm 0.12)\ 10^{-4} \qquad 0 - 4260 \text{ eV}$$

Fig. 3 shows the sum of reduced neutron widths versus neutron energy. Between 1.9 keV and 2.9 keV about 50% of the strength is due to only 6 resonances.

References

1. J.S. Levin and D.J. Hughes
Phys. Rev. 101, 1328 (1955)

2. J.A. Harvey, D.J. Hughes, R.S. Carter, V.E. Pilcher
Phys. Rev. 99, 10 (1955)

3. J.E. Lynn and N.J. Pattenden
Proc. Geneva Conf. 1955, Vol.4, paper 423, page 210

4. R.G. Fluharty, F.B. Simpson and O.D. Simpson
Phys. Rev. 103, 1778 (1956)

5. L.M. Bollinger, R.E. Cote, D.A. Dahlberg and G.E. Thomas
Phys. Rev. 105, 661 (1957)

6. J.L. Rosen, J.S. Desjardin, J. Rainwater and W.W. Havens
Phys. Rev. 118, 687 (1960)

7. H.E. Jackson and J.E. Lynn
Phys. Rev. 127, 461 (1962)

8. F.W.K. Firk, J.E. Lynn and M.C. Moxon
Nucl. Phys. 41, 614 (1963)

9. J.B. Garg, J. Rainwater, J.S. Peterson and W.W. Havens
Phys. Rev. 134, B 985 (1964)

10. M. Asghar, C.M. Chaffey and M.C. Moxon
Nucl. Phys. 85, 305 (1966)

11. L.M. Bollinger and G.E. Thomas
Phys. Rev. 171, 1293 (1968)

12. N.W. Glass, A.D. Schelberg, L.D.Tatro
Proc. 2nd Conf. non Neutron Cross sections and Technolgy,
Washington (1968) Vol.I, p. 573

13. Yu.V. Ryabov, So Don Sik, N. Chikov and N. Janeva
Dubna preprint P 3-4992 (1970)

14. G. Carraro and W. Kolar
Proc. Conf. on Neutron cross Sections and Technology
Knoxville (1971) p. 701

15. G. Rohr, H. Weigmann and J. Winter
Proc. IAEA Helsinki Conf. (1970) Vol.I, paper CN _ 26/18, page 413

16. H. Malecki, L.B. Pikelner and I.M. Salamatin
Journ. At. Energy 32, 45 (1972)

17. F. Rahn, H.S. Camarda, G. Hacken, W.W. Havens, H.I. Liou, J. Rainwater,
M. Slagowitz, S. Wynchank
Phys. Rev., 6 C, 1854 (1972)

18. F. Corvi, G. Rohr and H. Weigmann
Proc. Conf. on Neutron Cross Sections and Technology
Washington (1975) Vol. 2, p. 733

19. Y. Nakajima, A. Asami, M. Mizumoto, T. Fuketa and H. Takekoshi
Proc. Conf. Neutron Cross Sections and Technology
Washington (1975) Vol. 2, p. 738

20. H.I. Liou and R. E. Chrien
Nucl. Sci. Eng. 62, 463 (1977)

21. D.K. Olsen, G. de Saussure, R.B. Perez, E.G. Silver. F.C. Difilippo,
R.W. Ingle and H. Weaver
Nucl. Sci. Eng. 62, 479 (1977)
D.K. Olsen : private communication

22. M.G. Silbert and D.W. Bergen
Phys. Rev. C 4, 220 (1971)

23. R.C. Block, R.W. Hockenbury, R.E. Slovacek, E.B. Bean and D.S. Cramer
Phys. Lett. 31, 247 (1973)

24. J.A. Wartena, H. Weigmann and E. Migneco
Proc. Conf. Neutron Cross Sections and Technology
Washington (1975) Vol. 2, page 597

25. J. Blons, C. Mazun and D. Paya
Proc. Conf. Neutron Cross Sections and Technology
Washington (1975) Vol. 2, page 642

26. R.E. Slovacek, D.S. Cramer, E.B. Bean, J.R. Valentine, R.W. Hockenbury
R.C. Block
Nucl. Sci. Eng. 62, 455 (1977)

27. F.C. Difilippo, R.B. Perez, G. de Saussure, D.K. Olsen and R.W. Ingle
Nucl. Sci. Eng. 63, 153 (1977)

28. G. de Saussure, D.K. Olsen, R.B. Perez, F.C. Difilippo
Report ORNL/TM-6152 (1978)

29. Report NEANDC(E) 1634 (1975)
Specialists Meeting on Resonance Parameters of Fertile Nuclei and ^{239}Pu,
Saclay, May 1974

30. Report BNL - NCS - 50451, ENDF-217 (1975)
Seminar on ^{238}U Resonance Capture, Brookhaven, March 1975

31. F. Poortmans, E. Cornelis, L. Mewissen, G. Rohr, R. Shelley, T.van der Veen, G. Vanpraet and H. Weigmann
Int. Conf. on the Interaction of Neutrons and Nuclei, Lowell, July 1976, p. 1246

32. F. Poortmans, E. Cornelis, L. Mewissen, G. Rohr, R. Shelley, T.van der Veen, G. Vanpreat and H. Weigmann
Intern. Conf. on Neutron Physics, Kiev, April 1977, unpublished

33. P. Staveloz, F. Poortmans, L. Mewissen, E. Cornelis
Nucl. Sci. Eng. 66, 349 (1978)

34. L.A. Rayburn and E.O. Wollan
Nucl. Phys. 61, 381 (1965)

35. R.L. Macklin, private communication

36. W. Kolar, IBM 360 and IBM 1800 , Versions of the shape and area analysis programs of S.A. Atta and J.A. Harvey, Report EUR 4760 C, 1972

37. G. de Saussure, D.K. Olsen, R.B. Perez,
Nucl. Sci. Eng. , 61, 496 (1976)

38. A. Bignami, C. Coceva and R. Simonini
Monte Carlo Calculations for the Moderator of the pulsed Neutron Target of the Geel Linac, report EUR 5157 e, 1974

39. F.N. Fröhner, Report GA - 6906 (1966)

Table 1. Experimental Details.

^{238}U

	TRANSMISSION	CAPTURE	SCATTERING
Energy range	9 eV - 4.3 keV	20 eV - 6 keV	15 eV - 1 keV
Flight path length	60 m	60 m	30 m
Burst width	23 ns	23 ns	23 ns
Channel width	20 ns - 640 ns	10 ns - 640 ns	20 ns - 640 ns
Detectors	four ^{3}He gas.scint.	two C_6F_6 scint.	six He gas.scint.
Cut off filter	^{10}B	^{10}B	^{10}B
Samples	$7.48\ 10^{-5}$ at/b $1.61\ 10^{-3}$ $3.78\ 10^{-3}$ $1.009\ 10^{-2}$ $3.481\ 10^{-2}$	$1.311\ 10^{-5}$ at/b $5.527\ 10^{-5}$ $1.61\ 10^{-3}$ $6.31\ 10^{-3}$ $1.01\ 10^{-2}$	$1.32\ 10^{-5}$ at/b $5.53\ 10^{-5}$ $1.00\ 10^{-3}$ $1.01\ 10^{-2}$

Table 2. RESONANCE PARAMETERS FOR ^{238}U

E_o (eV)	Γ_n (meV)	Γ_γ (meV)	E_o (eV)	Γ_n (meV)	Γ_γ (meV)
** 4.41 ± 0.01	.000110 ± .000002		322.81 ± 0.22	0.057 ± 0.02	
** 6.67 ± 0.02	1.500 ± 0.01	24.2 ± 0.6	332.06 ± 0.23	0.063 ± 0.02	
10.23 ± 0.02	.001670 ± .000040		337.27 ± 0.23	0.110 ± 0.02	
11.30 ± 0.02	.000420 ± .000070		347.71 ± 0.25	79.900 ± 4.00	22.7 ± 0.3
** 16.30 ± 0.04	.000050 ± .000010		351.80 ± 0.25	0.250 ± 0.02	
19.57 ± 0.02	.001170 ± .000130		372.82 ± 0.27	0.030 ± 0.02	
20.90 ± 0.01	10.200 ± 0.10	23.2 ± 0.6	376.88 ± 0.28	1.110 ± 0.05	
36.81 ± 0.03	34.100 ± 0.50	22.9 ± 0.3	395.22 ± 0.30	0.072 ± 0.02	
63.54 ± 0.02	0.016 ± 0.002		397.51 ± 0.30	6.580 ± 0.30	
66.06 ± 0.02	23.900 ± 0.80	24.0 ± 0.4	408.08 ± 0.31	0.150 ± 0.07	
80.76 ± 0.03	1.810 ± 0.08		410.12 ± 0.31	20.600 ± 0.80	24.4 ± 0.6
83.69 ± 0.03	0.014 ± 0.001		433.91 ± 0.34	10.500 ± 0.50	23.5 ± 0.6
89.25 ± 0.04	0.099 ± 0.003		439.61 ± 0.35	0.280 ± 0.02	
93.17 ± 0.04	0.006 ± 0.001		448.52 ± 0.36	0.050 ± 0.02	
102.60 ± 0.04	70.000 ± 2.00	24.3 ± 0.4	453.95 ± 0.36	0.435 ± 0.02	
111.31 ± 0.05	0.010 ± 0.002		457.69 ± 0.37		
116.88 ± 0.05	25.000 ± 1.50	22.8 ± 0.6	463.07 ± 0.37	6.310 ± 0.49	23.5 ± 1.2
125.00 ± 0.06	0.026 ± 0.003		467.08 ± 0.38		
145.68 ± 0.07	0.930 ± 0.03		478.27 ± 0.39	4.400 ± 0.13	
152.41 ± 0.07	0.050 ± 0.005		481.86 ± 0.40		
159.03 ± 0.08	0.020 ± 0.006		485.18 ± 0.40	0.170 ± 0.03	
160.85 ± 0.08	0.095 ± 0.003		488.77 ± 0.40	0.940 ± 0.07	
165.28 ± 0.08	3.400 ± 0.12		498.98 ± 0.42	0.140 ± 0.05	
173.16 ± 0.09	0.050 ± 0.006		518.54 ± 0.15	50.800 ± 5.00	23.4 ± 0.6
189.65 ± 0.10	164.000 ± 3.00	23.1 ± 0.7	523.55 ± 0.15	0.260 ± 0.03	
194.77 ± 0.11	0.050 ± 0.01		532.61 ± 0.15	0.060 ± 0.03	
200.67 ± 0.11	0.070 ± 0.007		535.44 ± 0.15	44.000 ± 3.00	23.8 ± 0.3
203.12 ± 0.11	0.040 ± 0.007		542.60 ± 0.16	0.250 ± 0.04	
208.48 ± 0.12	48.600 ± 2.70	23.7 ± 0.7	550.81 ± 0.16	0.088 ± 0.04	
214.86 ± 0.12	0.083 ± 0.01		556.40 ± 0.16	0.890 ± 0.07	
218.40 ± 0.12	0.035 ± 0.007		580.30 ± 0.17	41.800 ± 2.00	25.0 ± 0.5
224.60 ± 0.13	0.020 ± 0.01		584.66 ± 0.17	0.080 ± 0.04	
237.34 ± 0.14	25.700 ± 1.50	25.0 ± 0.6	595.21 ± 0.18	85.000 ± 3.00	23.2 ± 0.3
242.74 ± 0.15	0.196 ± 0.01		607.04 ± 0.18	0.300 ± 0.05	
253.88 ± 0.16	0.115 ± 0.02		615.98 ± 0.18	0.140 ± 0.04	
257.17 ± 0.16	0.014 ± 0.006		620.17 ± 0.19	31.000 ± 1.00	23.4 ± 0.4
263.95 ± 0.16	0.275 ± 0.02		624.41 ± 0.19	0.700 ± 0.10	
273.62 ± 0.17	25.000 ± 1.30	22.5 ± 0.6	628.76 ± 0.19	6.300 ± 0.30	
275.13 ± 0.17	0.190 ± 0.02		633.55 ± 0.19	0.180 ± 0.09	
282.44 ± 0.18	0.100 ± 0.01		634.84 ± 0.19		
290.97 ± 0.19	17.000 ± 0.50	22.6 ± 0.6	635.86 ± 0.19		
311.26 ± 0.21	1.050 ± 0.05		661.30 ± 0.20	127.700 ± 4.00	24.3 ± 0.4

Table 2 Continued

E_o (eV)	Γ_n (meV)	Γ_γ (meV)	E_o (eV)	Γ_n (meV)	Γ_γ (meV)
668.77 ± 0.20	0.180 ± 0.06		982.61 ± 0.34	0.090 ± 0.05	
678.00 ± 0.21	0.740 ± 0.08		984.43 ± 0.34	0.150 ± 0.05	
681.88 ± 0.21	0.050 ± 0.03		* 991.65 ± 0.34	360.000 ± 20.00	
693.24 ± 0.21	42.400 ± 2.00	23.5 ± 0.5	1003.71 ± 0.35		
698.41 ± 0.22	0.236 ± 0.06		1011.80 ± 0.35	1.900 ± 0.10	
708.49 ± 0.22	22.600 ± 1.50	23.3 ± 0.6	1023.20 ± 0.36	8.700 ± 0.40	
710.73 ± 0.22	1.150 ± 0.07		1029.40 ± 0.36	2.300 ± 0.12	
713.79 ± 0.22	0.230 ± 0.06		1033.80 ± 0.36	0.750 ± 0.08	
721.80 ± 0.23	1.900 ± 0.07		1047.60 ± 0.37	0.350 ± 0.07	
730.29 ± 0.23	1.000 ± 0.06		1054.80 ± 0.37	94.000 ± 5.00	22.8 ± 0.5
732.70 ± 0.23	2.120 ± 0.08		1063.10 ± 0.38	0.750 ± 0.07	
735.13 ± 0.23	0.170 ± 0.04		1068.00 ± 0.38	1.250 ± 0.10	
743.24 ± 0.24	0.350 ± 0.05		1074.40 ± 0.38	0.900 ± 0.10	
756.37 ± 0.24	0.510 ± 0.05		1082.20 ± 0.39	1.590 ± 0.12	
765.27 ± 0.24	8.300 ± 0.40		1095.60 ± 0.39	2.300 ± 0.15	
771.13 ± 0.25	0.120 ± 0.06		1099.00 ± 0.40	21.400 ± 2.00	
772.84 ± 0.25	0.140 ± 0.07		1103.30 ± 0.40	2.300 ± 0.12	
779.50 ± 0.25	2.250 ± 0.10		1109.50 ± 0.40	32.500 ± 1.50	
786.18 ± 0.25	0.120 ± 0.04		1119.30 ± 0.41	0.500 ± 0.10	
787.54 ± 0.25	0.460 ± 0.03		1131.90 ± 0.41	4.230 ± 0.25	
791.03 ± 0.26	7.160 ± 0.20		1140.70 ± 0.42	224.000 ± 10.00	23.8 ± 0.8
796.29 ± 0.26			1145.80 ± 0.42	0.010 ± 0.005	
798.29 ± 0.26			1148.90 ± 0.42	0.300 ± 0.10	
800.79 ± 0.26			1152.70 ± 0.42	0.600 ± 0.15	
808.37 ± 0.26	0.350 ± 0.06		1155.30 ± 0.42	0.850 ± 0.10	
821.74 ± 0.27	64.000 ± 2.50	22.5 ± 0.6	1159.90 ± 0.43	0.730 ± 0.10	
828.54 ± 0.27	0.160 ± 0.03		1168.00 ± 0.43	87.000 ± 5.00	24.2 ± 0.5
834.63 ± 0.27	0.080 ± 0.04		1177.40 ± 0.43	75.000 ± 3.00	
846.83 ± 0.28	0.950 ± 0.10		1195.30 ± 0.44	104.000 ± 5.00	
851.19 ± 0.28	67.000 ± 3.00	24.0 ± 1.0	1202.20 ± 0.45	0.560 ± 0.08	
856.25 ± 0.28	83.900 ± 7.00	23.5 ± 1.0	1211.50 ± 0.45	9.800 ± 0.40	
859.70 ± 0.28	0.420 ± 0.04		1220.30 ± 0.46	0.600 ± 0.20	
866.68 ± 0.29	5.700 ± 0.30		1230.70 ± 0.46	0.400 ± 0.20	
891.64 ± 0.30	0.800 ± 0.10		1233.70 ± 0.46	0.400 ± 0.12	
* 905.25 ± 0.30	54.200 ± 2.00		1245.40 ± 0.47	254.000 ± 7.00	22.5 ± 0.8
910.27 ± 0.31	1.400 ± 0.08		1250.20 ± 0.47	0.300 ± 0.15	
925.34 ± 0.31	16.000 ± 1.00		1251.80 ± 0.47	0.400 ± 0.20	
937.21 ± 0.32	150.600 ± 4.00	23.5 ± 0.7	1261.30 ± 0.48	0.200 ± 0.10	
941.13 ± 0.32	0.700 ± 0.10		1267.50 ± 0.48	30.900 ± 1.40	25.3 ± 1.3
958.65 ± 0.33	203.300 ± 6.00	23.5 ± 1.0	1273.50 ± 0.48	32.000 ± 1.50	22.4 ± 1.3
964.52 ± 0.33	0.280 ± 0.06		1276.50 ± 0.48	0.700 ± 0.35	
977.54 ± 0.34	0.760 ± 0.08		1278.40 ± 0.49	0.700 ± 0.35	

Table 2 Continued

E_o (eV)	Γ_n (meV)	Γ_γ (meV)	E_o (eV)	Γ_n (meV)	Γ_γ (meV)
1284.00 ± 0.49	0.400 ± 0.20		1756.40 ± 0.75	140.500 ± 6.00	
1285.70 ± 0.49	0.400 ± 0.20		1776.70 ± 0.76	0.650 ± 0.20	
1289.40 ± 0.49	0.200 ± 0.10		1782.90 ± 0.77	652.000 ± 30.00	
1296.50 ± 0.49	0.100 ± 0.06		1798.00 ± 0.78	3.500 ± 0.40	
1299.10 ± 0.50	3.630 ± 0.40		1808.80 ± 0.78	20.500 ± 2.00	
1317.50 ± 0.51	5.600 ± 0.40		1824.00 ± 0.79	0.700 ± 0.15	
1331.90 ± 0.51	1.360 ± 0.15		1835.20 ± 0.80	0.400 ± 0.20	
1361.20 ± 0.53	0.400 ± 0.20		1846.60 ± 0.81	11.000 ± 1.00	
1386.20 ± 0.54	0.200 ± 0.10		1869.00 ± 0.82	2.800 ± 0.30	
1387.60 ± 0.54	0.080 ± 0.05		1881.50 ± 0.83	1.400 ± 0.20	
1394.20 ± 0.55	195.000 ± 10.00	24.0 ± 0.8	1894.90 ± 0.84	1.600 ± 0.20	
1405.90 ± 0.55	73.000 ± 3.00	25.6 ± 0.8	1903.30 ± 0.84	41.500 ± 3.00	25.0 ± 1.0
1417.60 ± 0.56	3.800 ± 0.25		1913.80 ± 0.85	6.200 ± 1.00	
1420.30 ± 0.56	9.000 ± 1.00		1917.60 ± 0.85	40.000 ± 3.00	23.5 ± 1.5
1428.40 ± 0.57	28.500 ± 1.40	25.5 ± 1.0	1926.90 ± 0.86	0.920 ± 0.30	
1438.70 ± 0.57	0.440 ± 0.10		1943.00 ± 0.87	0.600 ± 0.20	
1444.60 ± 0.57	14.400 ± 1.20		1954.40 ± 0.87	4.400 ± 0.20	
1447.90 ± 0.58	1.000 ± 0.30		1969.60 ± 0.88	810.000 ± 20.00	
1455.50 ± 0.58	0.150 ± 0.09		1974.90 ± 0.89	452.000 ± 20.00	
1457.10 ± 0.58	0.240 ± 0.10		1991.10 ± 0.90	1.600 ± 0.40	
1474.20 ± 0.59	125.000 ± 5.00	23.7 ± 0.6	2002.90 ± 0.90	0.700 ± 0.20	
1487.90 ± 0.60	0.170 ± 0.09		2024.10 ± 0.92	234.000 ± 15.00	23.7 ± 1.0
1504.80 ± 0.61	0.170 ± 0.09		2031.00 ± 0.92	44.700 ± 3.30	25.1 ± 1.2
1510.90 ± 0.61	0.660 ± 0.15		2049.70 ± 0.93	2.400 ± 0.40	
1523.00 ± 0.62	246.500 ± 10.00	23.6 ± 1.5	2053.40 ± 0.94	0.900 ± 0.20	
1528.50 ± 0.62	0.750 ± 0.15		2063.90 ± 0.59	0.250 ± 0.15	
1535.20 ± 0.62	0.890 ± 0.30		2072.10 ± 0.59	2.740 ± 0.20	
*1547.70 ± 0.63	4.170 ± 0.20		2081.00 ± 0.59	1.600 ± 0.20	
1550.90 ± 0.63	3.600 ± 0.40		2086.40 ± 0.60	5.600 ± 1.50	
1555.90 ± 0.64	0.330 ± 0.10		2089.00 ± 0.60	23.600 ± 2.00	
1565.90 ± 0.64	6.500 ± 0.65		2096.80 ± 0.60	22.300 ± 2.30	
1568.90 ± 0.64	1.200 ± 0.24		2104.30 ± 0.60	1.400 ± 0.15	
1591.90 ± 0.66	1.200 ± 0.24		2110.90 ± 0.61	0.600 ± 0.30	
1598.30 ± 0.66	410.000 ± 30.00	22.3 ± 0.7	2114.60 ± 0.61	1.500 ± 0.50	
1623.10 ± 0.67	114.000 ± 5.00	22.5 ± 0.7	2121.80 ± 0.61	0.250 ± 0.12	
1638.60 ± 0.68	55.000 ± 3.00	23.2 ± 0.7	2124.70 ± 0.61	4.500 ± 0.40	
1662.90 ± 0.70	220.000 ± 10.00	24.2 ± 0.8	2141.20 ± 0.62	1.000 ± 0.50	
1673.90 ± 0.70	0.090 ± 0.03		2146.10 ± 0.62	85.000 ± 6.00	24.2 ± 1.1
1689.30 ± 0.71	108.000 ± 4.00	23.8 ± 0.7	2153.30 ± 0.62	287.000 ± 10.00	24.3 ± 0.8
*1710.30 ± 0.72	95.000 ± 10.00		2173.20 ± 0.63	2.300 ± 0.20	
1723.30 ± 0.73	19.800 ± 1.60	22.1 ± 2.0	2179.50 ± 0.63	0.800 ± 0.40	
1746.10 ± 0.75	1.700 ± 0.20		2187.00 ± 0.63	592.000 ± 20.00	24.1 ± 1.0

Table 2 Continued

E_o (eV)	Γ_n (meV)	Γ_γ (meV)	E_o (eV)	Γ_n (meV)	Γ_γ (meV)
2201.90 ± 0.64	110.000 ± 7.00		2751.40 ± 0.85	38.000 ± 3.00	
2216.10 ± 0.64	3.500 ± 0.30		2763.40 ± 0.86	19.000 ± 1.50	
2241.60 ± 0.65	1.200 ± 0.30		2767.80 ± 0.86	3.000 ± 0.40	
2260.30 ± 0.66	118.000 ± 6.00	25.4 ± 1.0	2774.60 ± 0.86	1.500 ± 0.60	
2266.70 ± 0.66	240.000 ± 15.00		2779.10 ± 0.86	1.300 ± 0.40	
2272.10 ± 0.66	3.800 ± 0.30		2788.10 ± 0.87	13.700 ± 2.00	
2282.40 ± 0.67	186.000 ± 9.00		2800.20 ± 0.87	5.500 ± 0.50	
2297.20 ± 0.67	6.400 ± 0.60		2807.10 ± 0.87	11.000 ± 2.00	
2316.50 ± 0.68	19.500 ± 2.00		2812.10 ± 0.87	5.500 ± 0.50	
2328.20 ± 0.69	0.700 ± 0.40		2816.20 ± 0.88	1.500 ± 0.70	
*2339.30 ± 0.69	8.500 ± 2.00		2824.00 ± 0.88	2.000 ± 1.00	
2354.00 ± 0.70	56.000 ± 5.00		2830.00 ± 0.88	20.200 ± 2.00	
2356.50 ± 0.70	72.000 ± 5.00		2846.60 ± 0.89	0.600 ± 0.30	
2369.60 ± 0.70	7.100 ± 0.75		2865.80 ± 0.90	221.000 ± 13.00	22.0 ± 1.4
2392.60 ± 0.71	31.300 ± 2.50		2877.80 ± 0.90	2.100 ± 0.30	
2398.70 ± 0.71	6.100 ± 0.40		2883.50 ± 0.90	626.000 ± 30.00	24.6 ± 1.4
2402.50 ± 0.71	5.000 ± 1.00		2897.90 ± 0.91	17.000 ± 2.00	
2411.90 ± 0.72	6.500 ± 0.70		2919.20 ± 0.92	7.600 ± 0.80	
2418.50 ± 0.72	1.200 ± 0.40		2924.00 ± 0.92	5.000 ± 2.00	
2427.60 ± 0.72	158.000 ± 10.00		2926.00 ± 0.92	10.000 ± 3.00	
2447.20 ± 0.73	233.000 ± 15.00	23.5 ± 1.2	2934.20 ± 0.92	42.400 ± 4.60	23.6 ± 1.5
2447.90 ± 0.73	0.400 ± 0.20		2946.40 ± 0.93	2.500 ± 1.00	
2456.40 ± 0.73	16.800 ± 2.00		2957.40 ± 0.93	22.000 ± 3.00	
2489.70 ± 0.75	109.000 ± 6.00	24.5 ± 1.3	2968.20 ± 0.94	3.800 ± 0.50	
2502.60 ± 0.75	4.000 ± 0.40		2989.70 ± 0.95	7.200 ± 0.70	
2521.90 ± 0.76	19.000 ± 4.00		3004.40 ± 0.95	109.000 ± 8.00	24.9 ± 1.5
2548.30 ± 0.77	703.000 ± 30.00		3029.10 ± 0.96	130.000 ± 8.00	
2559.90 ± 0.77	270.000 ± 15.00		3044.20 ± 0.97	4.000 ± 0.60	
2581.80 ± 0.78	391.000 ± 16.00		3060.30 ± 0.98	32.000 ± 4.00	24.0 ± 3.0
2598.00 ± 0.79	727.000 ± 42.00	22.5 ± 1.1	3072.60 ± 0.98	1.000 ± 0.30	
2606.20 ± 0.79	3.200 ± 0.40		3082.10 ± 0.99	1.700 ± 0.40	
2612.50 ± 0.80	4.900 ± 0.50		3089.40 ± 0.99	4.000 ± 1.00	
2620.50 ± 0.80	44.000 ± 5.00		3104.20 ± 1.00	3.000 ± 1.50	
*2633.60 ± 0.80	4.800 ± 0.50		3110.20 ± 1.00	249.000 ± 16.00	
2637.60 ± 0.81	3.000 ± 0.50		3129.30 ± 1.01	3.700 ± 2.00	
2654.70 ± 0.81	1.000 ± 0.30		3134.60 ± 1.01	10.000 ± 4.00	
2659.50 ± 0.81	5.000 ± 1.20		3149.40 ± 1.01	116.000 ± 9.00	23.2 ± 1.4
2672.70 ± 0.82	269.000 ± 16.00	24.0 ± 1.4	3170.80 ± 1.02	11.200 ± 1.50	
2683.00 ± 0.82	2.500 ± 0.60		3179.50 ± 1.03	108.000 ± 7.00	
2697.10 ± 0.83	28.000 ± 3.00		3189.40 ± 1.03	117.000 ± 8.00	21.5 ± 2.0
2702.40 ± 0.83	1.500 ± 1.00		3206.40 ± 1.04	86.000 ± 7.00	
2718.00 ± 0.84	157.000 ± 11.00		3220.70 ± 1.04	11.900 ± 1.20	

Table 2 Continued

E_o (eV)	Γ_n (meV)	Γ_γ (meV)	E_o (eV)	Γ_n (meV)	Γ_γ (meV)
3227.00 ± 1.05	25.000 ± 4.50		3743.30 ± 1.27	0.800 ± 0.40	
3240.60 ± 1.05	1.700 ± 0.50		3746.20 ± 1.28	0.800 ± 0.40	
3249.50 ± 1.06	24.500 ± 2.00	22.5 ± 2.5	3759.70 ± 1.28	2.000 ± 0.40	
3264.40 ± 1.06	3.500 ± 2.00		*3765.80 ± 1.28	122.000 ± 10.00	
3268.30 ± 1.06	12.000 ± 1.50		3782.50 ± 1.29	481.000 ± 30.00	24.0 ± 2.2
3274.40 ± 1.07	25.000 ± 10.00		3791.90 ± 1.30	2.900 ± 0.60	
3280.20 ± 1.07	277.000 ± 15.00		3810.10 ± 1.30	0.650 ± 0.50	
3298.90 ± 1.08	13.000 ± 1.30		3826.30 ± 1.31	4.500 ± 0.70	
3313.00 ± 1.08	163.000 ± 10.00		3833.00 ± 1.32	15.500 ± 1.50	
3322.70 ± 1.09	125.000 ± 10.00	22.3 ± 2.0	3858.80 ± 1.33	623.000 ± 40.00	
3334.50 ± 1.09	95.000 ± 10.00	23.9 ± 1.8	3873.30 ± 1.33	165.000 ± 12.00	
3342.20 ± 1.10	4.100 ± 0.60		3879.90 ± 1.34	2.900 ± 0.60	
3356.60 ± 1.10	114.000 ± 10.00	23.6 ± 1.5	3897.50 ± 1.35	11.300 ± 3.00	
3367.50 ± 1.11	0.900 ± 0.50		3902.90 ± 1.35	285.000 ± 25.00	24.3 ± 2.5
3379.50 ± 1.11	8.500 ± 1.60		3915.40 ± 1.35	85.000 ± 10.00	22.4 ± 2.5
3383.00 ± 1.11	4.500 ± 1.00		3928.60 ± 1.36	14.500 ± 2.00	
3390.50 ± 1.12	27.000 ± 3.00		3931.00 ± 1.36	14.000 ± 3.00	
3400.40 ± 1.12	8.500 ± 1.20		3935.00 ± 1.36	12.400 ± 3.00	
3409.50 ± 1.13	218.000 ± 14.00		3940.50 ± 1.37	195.000 ± 20.00	23.9 ± 2.5
3418.70 ± 1.13	4.400 ± 0.60		3949.60 ± 1.37	4.000 ± 1.00	
3436.90 ± 1.14	356.000 ± 18.00	23.9 ± 1.5	3955.70 ± 1.37	105.000 ± 11.00	
3458.70 ± 1.15	688.000 ± 28.00	24.8 ± 2.0	3993.50 ± 1.39	3.000 ± 1.50	
3486.20 ± 1.16	92.000 ± 7.00		4009.90 ± 1.40	4.000 ± 1.00	
3496.10 ± 1.16	15.500 ± 2.20		4014.90 ± 1.40	2.600 ± 0.80	
3512.60 ± 1.17	1.900 ± 0.50		4025.70 ± 1.40	1.400 ± 0.70	
3515.40 ± 1.17	1.600 ± 0.50		4040.50 ± 1.41	69.000 ± 11.00	
3523.60 ± 1.18	2.000 ± 0.50		4064.70 ± 1.42	23.500 ± 4.00	
3529.40 ± 1.18	6.800 ± 1.00		4081.20 ± 1.43	3.800 ± 1.00	
3562.50 ± 1.19	240.000 ± 19.00		4084.40 ± 1.43	4.000 ± 1.00	
3574.70 ± 1.20	432.000 ± 20.00		4091.30 ± 1.44	88.000 ± 6.00	
3596.20 ± 1.21	54.000 ± 7.00		4099.90 ± 1.44	1.700 ± 1.00	
3624.20 ± 1.22	9.000 ± 4.20		4104.60 ± 1.44	2.000 ± 1.00	
3630.60 ± 1.22	470.000 ± 50.00		*4125.90 ± 1.45	45.000 ± 6.00	
3638.40 ± 1.23	8.100 ± 0.80		4133.00 ± 1.46	17.000 ± 3.00	
3654.30 ± 1.23	3.000 ± 1.00		4149.00 ± 1.46	4.300 ± 1.20	
3662.40 ± 1.24	2.800 ± 0.60		*4167.50 ± 1.47	276.000 ± 30.00	
3674.50 ± 1.24	5.200 ± 0.60		4180.30 ± 1.48	30.000 ± 6.00	
3684.30 ± 1.25	4.300 ± 1.00		4202.80 ± 1.49	4.000 ± 2.00	
3693.70 ± 1.25	456.000 ± 30.00		4211.90 ± 1.49	33.000 ± 6.00	
*3717.70 ± 1.26	154.000 ± 10.00		4227.00 ± 1.50	10.000 ± 2.00	
3726.30 ± 1.27	8.300 ± 1.00		4260.30 ± 1.52	32.000 ± 6.00	
3734.80 ± 1.27	195.000 ± 13.00				

* doublet

** Γ_n from BNL 325

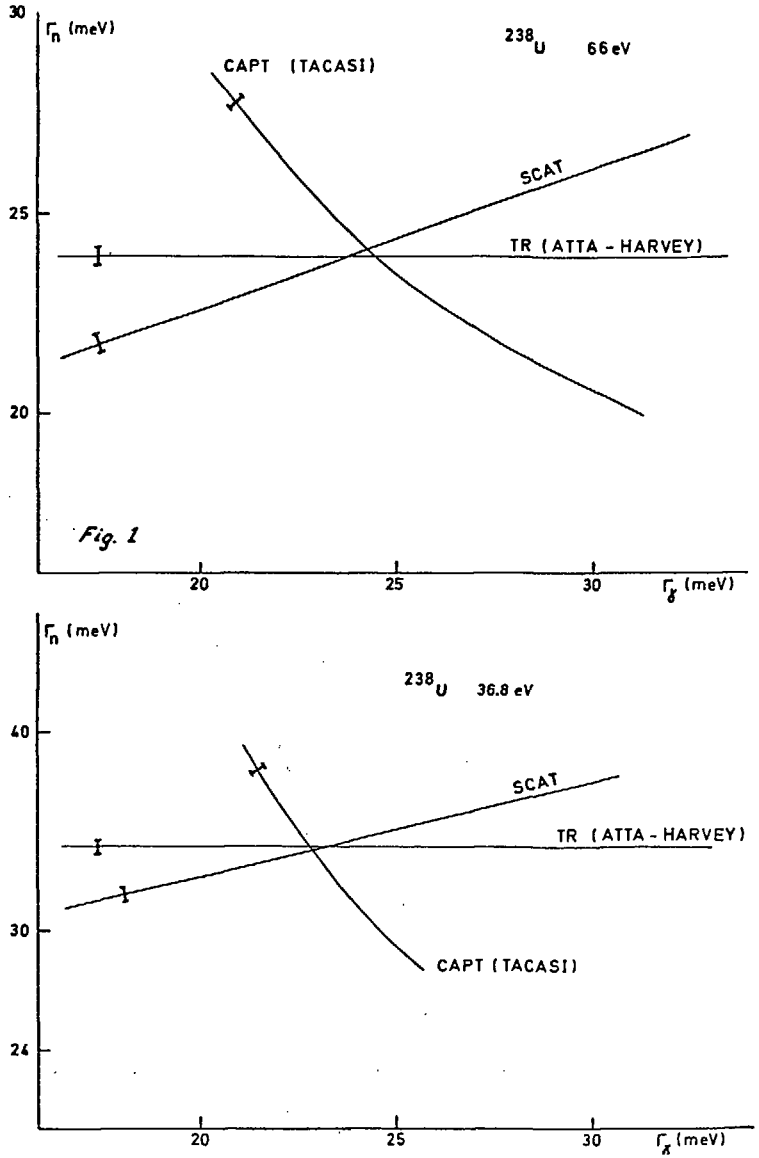

Fig. 1 example of area analysis of capture, scattering and transmission data for two resonances at 66 eV and 36.8 eV

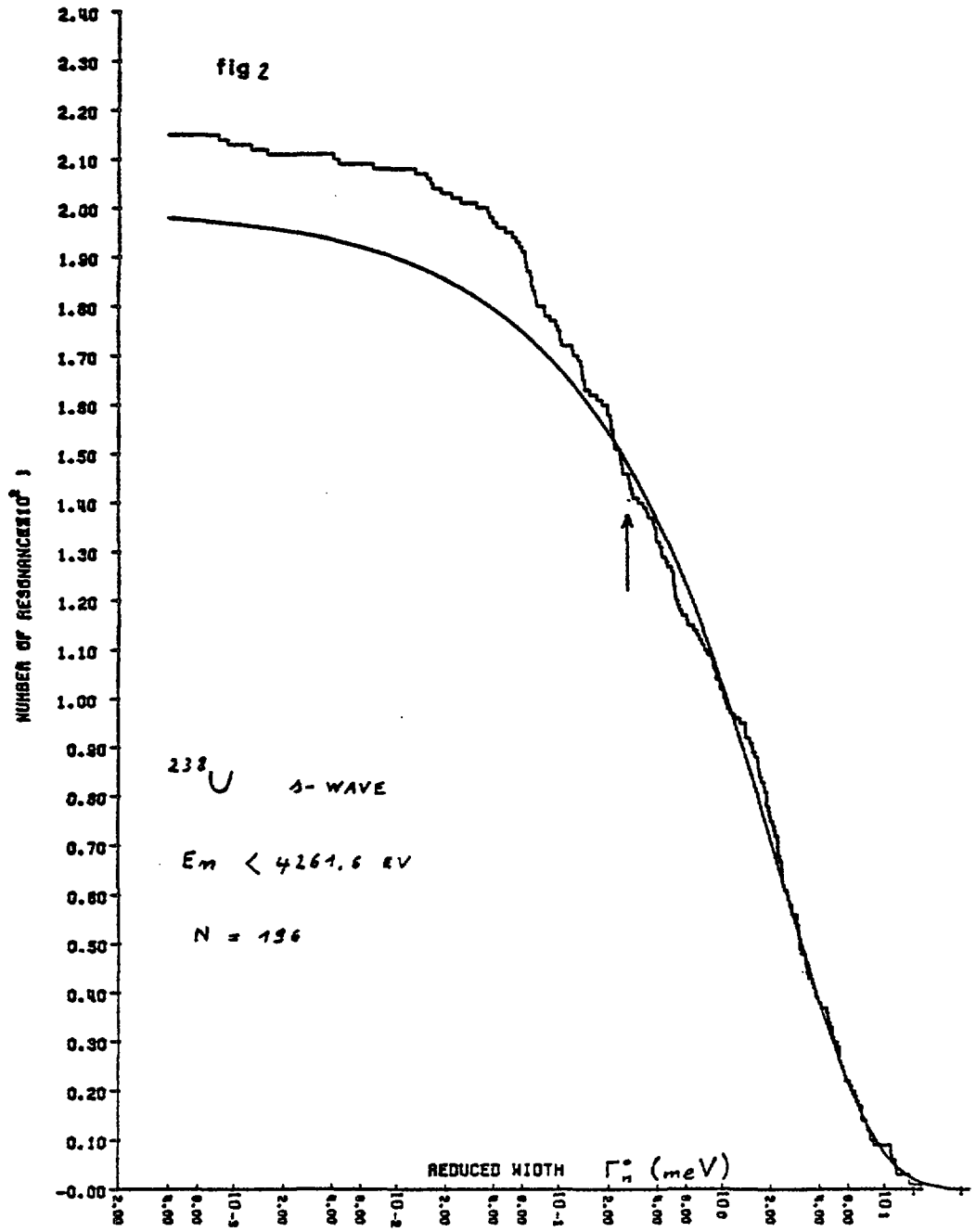

Fig. 2 integral distribution of reduced neutron widths Γ_n^o for the s-wave resonances.
The full line is the integral Porter-Thomas distribution obtained by fitting the experimental distrubition above the bias Γ_n^o = 0.25 meV.

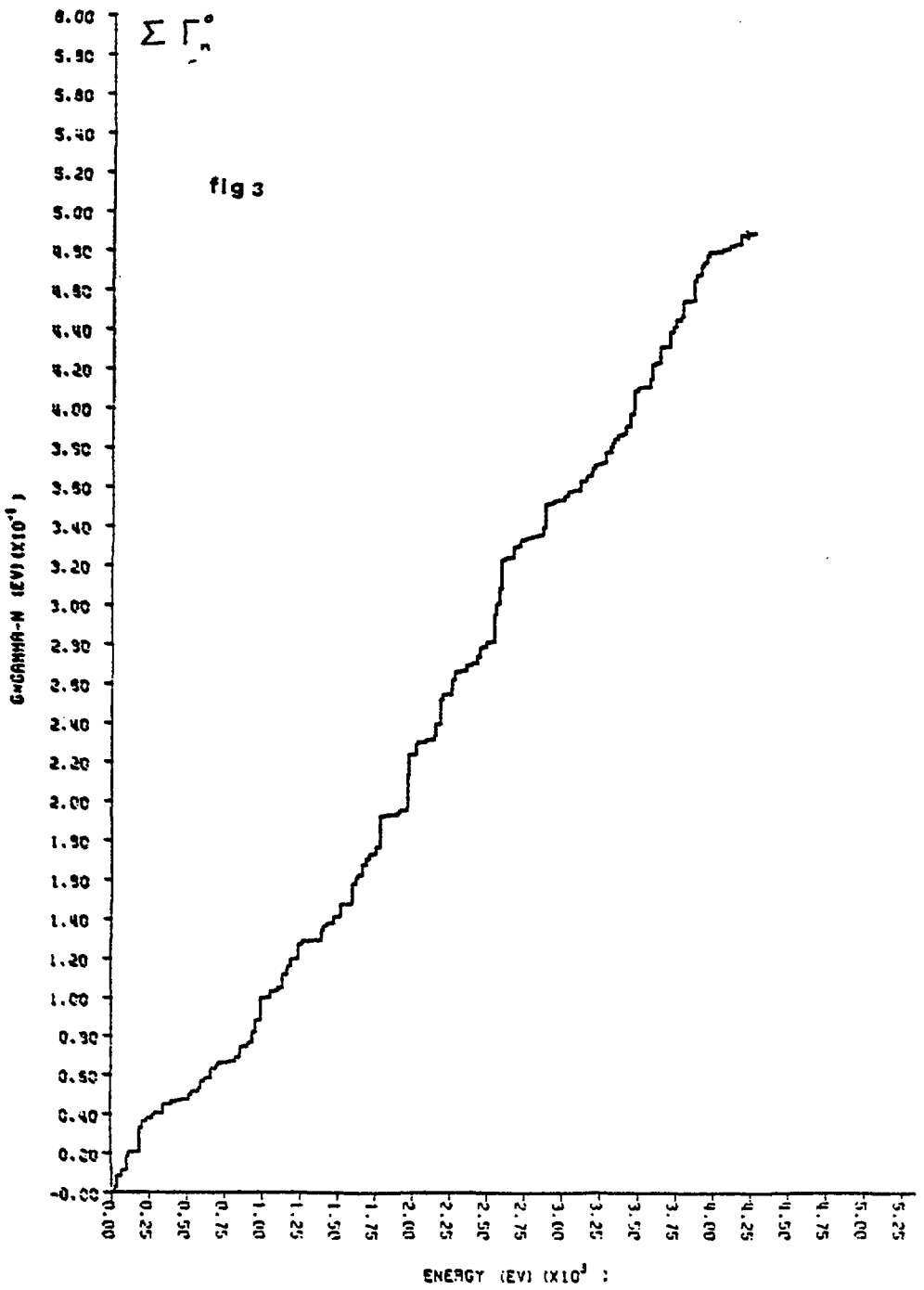

Fig. 3 sum of reduced neutron widths Γ_n^o versus neutron energy.

The Neutron Capture Cross-section of U-238 from 0.01 to 10 eV

M. C. Moxon and J. E. Jolly

Nuclear Physics Division, A.E.R.E., Harwell, Didcot, Oxon., U.K.

Introduction

Thermal reactors have been the subject of study for many years and there is a long standing minor discrepancy between calculation and measurement of the reactor parameters. This discrepancy can be attributed to many factors but is generally thought to be due to errors in the neutron energy dependence of the capture cross-sections of U-235 and U-238 in the energy region below ∿6 eV. There are many measurements of the energy dependence of the U-235 cross-section but surprisingly there is no published measurement of the U-238 capture cross-section, although Liou and Chrien[1] have published values of the capture cross-section of U-238 derived from the neutron energy dependence of the intensities of individual gamma-rays, following neutron capture using a Ge(Li) detector.

Several years ago we carried out neutron capture measurements on samples of depleted and natural uranium oxide in the energy region from ∿100 eV to ∿0.01 eV. These measurements were carried out using the plain uranium target of the 45 MeV Harwell electron linac. The analysis was abandoned at an early stage due to poor signal to background (e.g. ∿1 to 10 at 2 eV and ∿1 to 1 at 0.2 eV) and the lack of adequate analysis programs.

The recent renewed interest in the low energy U-238 capture cross-section by reactor designers and lack of published data led to a request to carry out further analysis of the data. This involved modifications to the resonance analysis program REFIT[2] to enable it to carry out calculations for oxide samples. The use of the program REFIT enables us to adjust the background and deduce that the capture cross-section below a few eV could be represented by a set of recommended resonance parameters using a multilevel formalism.

Measurements

The measurement of a partial cross-section (or rather the corresponding yield curve) is more difficult than the measurement of the total cross-section An accurate knowledge of the energy dependence of the incident neutron flux and the relative efficiency of the capture detector, together with corrections for finite sample size and multiple interactions of scattered neutrons, are the minimum requirement for the calculation of the partial cross-section from the observed data.

In neutron capture measurements a sample is placed in the neutron beam and gamma-ray detectors placed outside the beam. The count rate S(t) from the gamma-ray detector due to the fraction of neutrons $Y_\gamma(t)$ being captured in the sample, at time t following the neutron burst is

$$S(t) = \varepsilon_\gamma . \phi(t) . Y_\gamma(t) \qquad (1)$$

where ε_γ is the efficiency of the gamma-ray detector for detecting a neutron capture event in the sample and $\phi(t)$ is the neutron flux incident on the sample at time t.

With the condition that the energy resolution is narrower than any structure in the cross-section the relationship between the yield and capture cross-section is

$$Y_\gamma(t) = (1 - e^{-n\sigma_T(E)}) \frac{\sigma_\gamma(E)}{\sigma_T(E)} + M_s(t) \qquad (2)$$

where $\sigma_T(E)$ and $\sigma_\gamma(E)$ are the total and capture cross-sections respectively at a neutron energy E corresponding to the time-of-flight t, n is the sample thickness and $M_s(t)$ is the capture yield from neutrons that are initially scattered and captured on subsequent collisions.

(a) The gamma-ray detector

There are two main requirements for a gamma-ray detector for neutron capture measurements. The first is that its efficiency for detecting a neutron capture event should be independent of the mode of the prompt gamma-ray cascade following the capture event. The second is that the detector should be insensitive to the scattered neutrons.

The type of detector used in these measurements is fully described in references 3 and 4. In this class of detector the efficiency is

proportional to the total prompt gamma-ray energy emitted when a neutron is captured and is essentially independent of the details of the gamma-ray cascade.

The detector consists of a thick cylinder of Li_2CO_3 that converts the gamma-rays to Compton electrons. The electrons are detected by a 0.5 mm thick sheet of plastic scintillator and photon multiplier. The Li_2CO_3 not only acts as a gamma-ray to electron converter but also absorbs the scattered neutrons through the reaction $^6Li(n,\alpha)T$ in which no gamma-rays are emitted. Measurement of the neutron detection efficiency of this detector has shown it to be less than 10^{-4} of that for detecting a neutron capture event in uranium. In the low energy measurement on uranium, as the ratio of scattering to capture never exceeds 100 to 1, corrections for the detection of the scattered neutrons were neglected.

(b) Flight Path

A 4.58 m flight path was used for these measurements and is shown in Figure 1. The flight path viewed a plain air-cooled uranium target. A 25 mm thick slab of polyethylene was used to moderate the fast neutrons down to the neutron energy range of interest. The neutron beam was reduced from the 150 mm diameter at the neutron source to 60 mm at the sample by two 1 mm long reactor grade graphite collimators. The collimator nearest the sample was lined with Li_2CO_3 and in addition two lead collimators each 150 mm long were used to reduce the gamma-ray flux reaching the detector.

The time-of-flight data were recorded with the on-line equipment associated with the PDP-11 computer[5]. Measurements on each uranium sample took between 1 and 4 days, and 4 days were needed to measure the neutron spectra using the $^{10}B_2O_3$ sample. In order to keep the power below the maximum permitted for the target of 500 watts, an electron pulse width of 0.5 microseconds and a pulse repetition frequency of only 48 Hz was used.

(c) Samples

Initial measurements were carried out on a highly depleted metallic sample of uranium which unfortunately was shown to contain impurities. The sample had a higher thermal capture than expected for U-238 and resonance peaks were seen at ~0.1, ~0.65, ~1.3 and ~8 eV. The peaks at 0.1 eV and 8 eV could be associated with samarium at a level of impurity of ~100 ppm. This amount of samarium could account for most of the high thermal cross-section. The peaks at 0.65 and 1.3 eV indicate the presence of iridium. As iridium is used to harden the platinum crucible it could have been leached out during preparation of the metallic sample. These measurements indicated that very high purity uranium was required. Scintered discs of uranium oxide were the quickest and easiest way of obtaining some samples of pure uranium for this experiment. The presence of oxygen in the sample gave additional problems in the analysis of the data due to the increase of multiple scattering events.

The samples of natural and depleted uranium oxide were prepared at Harwell by Mr. F. Leach of Metallurgy Division. Pure powdered U_3O_8 was compressed and fired into a disc of diameter 50 mm, at the same time reducing the oxide to UO_2. These discs were then ground down to the required thickness.

The result of a chemical analysis on one of the depleted discs carried out after the neutron measurement is given in Table 1. The mass analysis using alpha spectrometry is also given in Table 1. The thickness of the samples used in these measurements is given in Table 2.

(d) Background Determination

In all neutron time-of-flight measurements the determination of the background is frequently the most difficult and least understood part of the measurement. The background can be broken down into three major components.

1. A constant component measured when the machine is off, due to local activity cosmic rays and very long lived activity from the sample, the latter being the major component in this case.
2. A time independent component coming from the neutron source due to long lived activity produced in the source. This can be either gamma-rays, or neutrons, or both. This part, together with the local activity, is measured by a 200 μsec timing gate at a delay of 10 milliseconds.
3. A time dependent component, which is the most difficult to measure. One part of this component is due to the 2.2 MeV gamma-rays from neutron capture in the moderator and has an exponential decay with a half life of between 20 and 30 μsecs. The other part of the time dependent component is due to the decay of the fast neutron burst after scattering into the detector assembly and the surrounding shielding by the sample.

(i) 'Black' Resonance Technique

The time dependent background associated with the measurements was determined using the 'black' resonance filter technique. In this technique samples of materials that have large resonances are placed in the neutron beam. The samples are thick enough for the transmission in the energy region around the resonances to be negligible. Two sets of filters were made up, each consisting of 1.5 mm Ta, 0.2 mm Co, 1.5 mm Mn, 0.2 mm In and 1.5 mm Cd. The capture measurements require at least four sets of data to determine the true capture rate from a given sample. They are:

1. sample in the detector and an open neutron beam
2. sample in the detector and first set of resonance filters in the neutron beam
3. sample in the detector and second set of resonance filters in the neutron beam
4. sample in the detector and both sets of resonance filters in the neutron beam

This sequence of filter changes was repeated about every 30 minutes. In this measurement equal times were spent at each filter position. In addition sets of measurements were carried out on the thicker natural and depleted samples with a 0.1 mm Rh sample permanently in the neutron beam; this gives a background point in the region of the 1.1 eV resonance.

The observed counts C(I,N) in channel N corresponding to a time-of-flight t from a sample for section I of the data are given below

$$C(I,N) = (S(t)\ T_I(t) + aF_I + b(t)G_I)\ M_I + J_I\tau \qquad (3)$$

where S(t) is given by equation (1), $T_I(t)$ is the transmission of the samples in the beam, 'a' is the machine time independent background, the time dependent background is b(t), τ is the background due to local activity and sample, M_I is the neutron flux monitor over the period J_I of the run spent in position I, F_I and G_I are the attenuation factors for the filter or filters in the neutron beam for the machine constant and time dependent background respectively. In the case of the open beam data $T_I(t)$, F_I and G_I are unity and in the minimum of the transmission dips due to 'black' resonances $T_I(t)$ is taken to be zero. As the background can only be determined at the 'black' resonances, several functions of time were parameterised to interpolate and extrapolate on the measured data. Simultaneous fits were carried out to find the parameters of the following equations and the attenuation factors for the background data.

$$b(t) = \beta e^{-\lambda t}\ t^{-\gamma} \qquad (4a)$$
$$= \beta t^{-\gamma} \qquad (4b)$$
$$= \beta/t + \gamma e^{-\lambda t} \qquad (4c)$$
$$= \beta/t + \gamma/t^2 + \Delta/t^3 \qquad (4d)$$

It was assumed that the attenuation factors are exponential in form, i.e.

$$F_3 = F_1 * F_2, \quad G_3 = G_1 * G_2 \qquad (5)$$

In the appendix it is shown that this type of extrapolation will underestimate the background for the open beam data when more than one component is present, e.g. gamma-rays and neutrons with a wide energy range. When the signal to background is large, the error due to the underestimation of the background can be allowed for at a later stage in the analysis.

Figures 2 and 3 show the total observed counts versus time-of-flight for the two samples of depleted uranium. The lower two solid lines are the least square fit to the 'black' resonance points at times greater than 100 μsec.

The upper solid line is the extrapolated curve assuming exponential attenuation and equation (4c). (These curves were used to calculate an observed capture yield from the data). Due to the poor energy resolution at times less than 100 μsec the resonance dips due to the filters did not have zero transmission. Assuming exponential attenuation, the open beam background was calculated from the 'non-black' resonances after correction for the transmitted signal and the time independent background. These points indicated that the assumed curves did not account for all the background in the open beam at times less than ∿150 μsec.

(ii) Adjustment of the Background Using REFIT

In the analysis program, REFIT, the background can be adjusted in order to obtain the best set of resonance parameters from either capture or transmission data. Figure 4 shows a fit to the 36, 20 and 6.7 eV resonances.

In this fit only the background adjustment has been determined using the resonance parameters given in Table 4. These parameters were taken from references 6 and 7. Only minor changes to the resonance parameters were indicated when both the background and resonance parameters were adjusted in a fit to the data. Fits assuming the background to be zero produce parameters ∿1.5 standard deviations from the given ones but very high values of chi-squared per degree of freedom, mainly arising from the poor fits to the wings of the resonances, i.e. the regions where errors in the background will give a large contribution to chi-squared.

This background adjustment to the observed capture yield was converted to counts per channel and is plotted as the dashed curve on Figures 2 and 3. In the region at times less than 150 μsec the dashed curve is above that obtained from the extrapolated 'black' resonance data but in general agreement with the data obtained from the resonance dip in that region.

In the energy region below 4 eV a calculation of the capture cross-section was carried out and the parameters of the first negative energy resonance were adjusted to give the recommended capture cross-section of 2.73 b at 0.0253 eV. These parameters were then used together with parameters for U-235 and U-234 in REFIT to obtain an adjustment to the background from ∿2 eV to ∿0.3 (i.e. 250 μsec < T < 700 μsec). This proved to be almost a constant fractional increase on the extrapolated background of ∿5% for the thin sample (see Fig. 2) and ∿7% for the thick sample (see Fig. 3). The background below ∿0.3 eV (i.e. T > 700 μsec) is assumed to follow the same shape as determined from the 'black' resonance data but increased in magnitude by the factor determined in the energy region 2 eV to 0.3 eV. This assumption had to be made because the program REFIT does not take into account solid state effects in calculating multiple scattering effects and these are much more important in the neutron energy region below 0.3 eV.

Measurements with samples of lead and graphite show there were no additional capture yields due to the scattered neutrons.

(e) Neutron Flux and Normalisation Measurements

The time dependence of the neutron flux incident on the sample was determined from a measurement of the count rate from a $^{10}B_2O_3$ sample, placed in the sample position, detecting the 480 keV gamma-ray from the $^{10}B(n,\alpha\gamma)^7Li$ reaction with the capture detector. The cross-section for this reaction is known to better than 3% below 100 keV[8,9] and varies smoothly with neutron energy over the region of interest. Details of the $^{10}B_2O_3$ sample are given in Table 3.

The relative yield for a uranium sample can simply be obtained from the ratio of the counts from the uranium sample multiplied by the $(n,\alpha\gamma)$ reaction yield from the ^{10}B sample divided by the counts from the $^{10}B_2O_3$ sample. This relative yield can be normalised at the peak of the 6.7 eV resonance.

It can be seen from equation (2) that if the product of the sample thickness and the total cross-section is much greater than unity, the yield is approximately the ratio of the capture to total cross-section. This condition is easily met in the peaks of the low energy resonances. Calculations using the program REFIT for the 6.7 eV resonance showed that for the samples used in this experiment the peak yield was near to unity and almost independent of the resonance parameters and resolution function. In the case of the resonances at 20, 36 and 60 eV the peak yields were not independent of the resolution function parameters. In fact the resonances at 60 eV and 102 eV were used to determine the values of the main parameters used in the resolution function.

The samples of natural uranium were only used to obtain the relative efficiency of detecting neutron fission and capture events in the U-235 to that of neutron capture in U-238.

The measured efficiency together with the abundance of U-235 in our depleted samples gives a contribution of 0.9 bs to the observed data at thermal energy.

Results

Figures 5 and 6 show our observed yield divided by sample thickness together with the calculated curve over the energy range 0.01 to 10.0 eV. As can be seen after the background correction, the observed data in the energy region above 0.3 eV for both samples are in reasonable agreement with the calculation using the resonance parameters given in Table 4. The resonance parameters below 100 eV are taken from reference 7 and those above

partly from reference 7 and the evaluation given in reference 8. The differences below 0.3 eV are not thought to be genuine due to assumptions made in REFIT being invalid at the lower neutron energies. These assumptions are that the sample is a free gas at a given effective temperature and that all neutron scattering is isotropic in the centre of mass frame. All these assumptions lead to an overestimation of the multiple scattering correction and are 20% at 0.2 eV and 55% at 0.025 eV, for the thickest sample of depleted U-238.

Conclusion

On the basis of our analysis we believe the capture cross-section of U-238 is well represented by the resonance parameters given in Table 4. The present data do not exclude the possibility that the cross-section may be higher than that given by the resonance parameters in the energy region 1 to 6 eV.

These measurements do not meet the reactor requirements (i.e. ±3% or ±30 mbs, whichever is the larger). New measurements are required of the energy dependence of the capture cross-section of U-238. In carrying out these measurements we would like to have several very pure highly depleted metallic uranium samples, ideally with a U-235 content of less than 50 ppm, and an absence of elements with high capture cross-sections in the thermal and eV region (e.g. B, Rh, Ag, In, Rare earths, Au, etc.).

References

1. Liou H. I. and Chrien R. E., Nuc. Sci. and Eng. 62 (1977) 463.
2. Moxon M. C., REFIT A least squares fitting program for analysis of neutron transmission and capture data, to be published as an AERE report.
3. Moxon M. C. and Rae E. R., Nuc. Instr. and Meth. 221 (1963) 445.
4. Moxon M. C., Thesis London University (1968).
5. Morris D. V., UKAEA Report AERE-R 7556 (1973).
6. Haste T. J., Moxon M. C. and Jolly J. E., UKAEA Report AERE-R 8966 (1979).
7. Moxon M. C., Proc. Specialists Meeting on Resonance Parameters of Particle Nuclei and Pu-239, Saclay (1974) page 159.
8. Sowerby M. G., Patrick B. H., Uttley C. A. and Diment K. M., J. Nuc. Energy 24 (1970) 323.
9. Sowerby M. G., J. Nuc. Energy 20 (1966) 135.

Table 1 Chemical and mass analysis of a depleted uranium dioxide sample.

(a) CHEMICAL ANALYSIS

Uranium content	88.3±0.1%
Theoretical for UO_2	88.15%
Hydrogen content	2.1±0.5 ppm by weight
Carbon not measurable	
Rare earths not detected	

(b) ALPHA SPECTROMETRY

	Mass Ratio
U-235/U-238	$(9.02\pm0.36) \times 10^{-4}$
Value given by suppliers	6.9×10^{-4}
U-234/U-238	$(1.61\pm0.03) \times 10^{-6}$
No value given by suppliers	

Table 2 Thickness of uranium dioxide samples.

Sample	Thickness a/b
U depleted	$(4.3662\pm0.0175) \times 10^{-3}$
U depleted	$(1.051\pm0.0052) \times 10^{-2}$
U natural	$(1.6697\pm0.0066) \times 10^{-2}$
U natural	$(3.4108\pm0.0137) \times 10^{-3}$

Table 3 Details of B-10 sample used to measure the neutron flux.

Details of standard $^{10}B_2O_3$ sample

Isotopic composition of boron sample			
^{10}B 0.9532±0.00013 ^{11}B 0.0468±0.00013			
Spectrographic analysis			
Element	%	Element	%
Si	0.04	Be	<0.005
Pb	0.04	Mo	<0.005
Al	0.03	Ni	<0.005
Fe	0.02	Bi	<0.005
Cu	0.01	Co	<0.01
Mg	<0.005	Ag	<0.01
Mn	<0.005	Ga	<0.01
Sn	<0.005	Ge	<0.01
Cd	<0.02	Cr	<0.02
As	<0.1	Sb	<0.1
Zr	<0.1	V	<0.1
Ti	<0.1		
diameter	80 mm		
thickness	4.41 mm (1.345±0.0079) x 10^{-2} atoms per barn		
density	1.8074±0.0017 gram/cc		

Table 4 U-238 resonance parameters used in the analysis of the data.

(a) s-wave resonances

Nucleus radius = 0.9183×10^{-12} cm		
Resonance Energy eV	Neutron Width eV	Radiation Width eV
-14.000	0.196900E-02	0.214000E-01
6.668	o.150700E-02	0.235400E-01
10.241	0.159000E-05	0.235800E-01
20.877	0.101800E-01	0.224400E-01
36.692	0.344200E-01	0.240300E-01
66.076	0.256900E-01	0.234600E-01
80.762	0.179400E-02	0.235800E-01
89.217	0.847000E-04	0.235800E-01
102.582	0.695700E-01	0.235800E-01
116.929	0.251700E-01	0.235800E-01
145.630	0.847690E-03	0.240000E-01
165.290	0.319040E-02	0.179920E-01
189.620	0.171800E+00	0.238280E-01
208.420	0.496960E-01	0.223300E-01
237.280	0.266530E-01	0.231170E-01
242.660	0.155170E-03	0.240000E-01
273.560	0.249920E-01	0.232860E-01
290.900	0.149790E-01	0.226030E-01
311.100	0.100050E-02	0.240000E-01
347.680	0.773250E-01	0.226120E-01
376.720	0.111480E-02	0.240000E-01
397.430	0.595840D-02	0.249100E-01
410.080	0.188230E-01	0.216460E-01
433.930	0.921520E-02	0.215410E-01
463.000	0.501770E-02	0.185940E-01
478.070	0.339830E-02	0.350000E-01
518.190	0.457300E-01	0.243390E-01
535.110	0.422380E-01	0.243050E-01
579.830	0.311310E-01	0.236860E-01
594.760	0.817850E-01	0.226800E-01
619.610	0.294890E-01	0.230540E-01
628.260	0.612550E-02	0.240000E-01
660.810	0.121160E+00	0.253720E-01
692.820	0.381140E-01	0.235450E-01
707.930	0.212500E-01	0.243640E-01
721.200	0.128280E-02	0.240000E-01
731.950	0.148070E-02	0.240000E-01
764.690	0.630850E-02	0.170000E-01
778.810	0.143810E-02	0.240000E-01
790.440	0.593640E-02	0.150000E-01
821.110	0.588400E-01	0.235930E-01
850.700	0.573140E-01	0.275480E-01
855.820	0.816470E-01	0.236060E-01
867.120	0.390080E-02	0.240000E-01
904.640	0.472980E-01	0.249190E-01
909.500	0.108330E-02	0.240000E-01
924.620	0.935380E-02	0.250000E-01
936.560	0.138620E+00	0.241170E-01
940.100	0.309680E-03	0.240000E-01
958.020	0.171480E+00	0.223110E-01

TABLE 4

(b) p-wave resonances

$a = 0.8366 \times 10^{-12}$ cm		
Resonance Energy eV	Neutron Width eV	Radiation Width eV
4.418	0.123000E-06	0.235800E-01
11.310	0.437000E-06	0.235800E-01
16.243	0.530000E-07	0.240000E-01
19.559	0.113000E-05	0.235800E-01
45.176	0.855680E-06	0.240000E-01
49.456	0.680000E-06	0.240000E-01
57.738	0.480000E-06	0.240000E-01
63.532	0.562370E-05	0.240000E-01
83.559	0.666270E-05	0.240000E-01
92.975	0.300000E-05	0.240000E-01
121.600	0.596020E-05	0.240000E-01
124.220	0.139720E-04	0.240000E-01
152.400	0.370460E-04	0.240000E-01
158.900	0.101800E-04	0.240000E-01
173.100	0.324490E-04	0.240000E-01
202.300	0.394270E-04	0.240000E-01
215.000	0.396920E-04	0.240000E-01
253.900	0.988880E-04	0.240000E-01
255.400	0.604570E-04	0.240000E-01
257.100	0.198500E-04	0.240000E-01
263.770	0.215160E-03	0.240000E-01
275.800	0.797150E-04	0.240000E-01
282.300	0.614780E-04	0.240000E-01
295.000	0.300230E-04	0.240000E-01
337.200	0.504430E-04	0.240000E-01
351.800	0.806330E-04	0.240000E-01
354.700	0.296820E-04	0.240000E-01
407.600	0.822910E-04	0.240000E-01
439.520	0.262220E-03	0.240000E-01
453.880	0.399700E-03	0.240000E-01
488.520	0.511150E-03	0.240000E-01
498.900	0.825540E-04	0.240000E-01
523.200	0.199460E-03	0.240000E-01
542.300	0.514650E-04	0.240000E-01
555.820	0.729550E-03	0.240000E-01
605.910	0.310350E-03	0.240000E-01
623.630	0.694820E-03	0.240000E-01
668.400	0.249610E-03	0.240000E-01
676.920	0.842010E-03	0.240000E-01
712.500	0.253580E-03	0.240000E-01
729.600	0.638650E-03	0.240000E-01
742.780	0.403060E-03	0.240000E-01
755.820	0.413800E-03	0.240000E-01
808.170	0.508320E-03	0.240000E-01
815.300	0.198300E-03	0.240000E-01
832.400	0.257960E-03	0.240000E-01
846.510	0.661780E-03	0.240000E-01
890.820	0.826870E-03	0.240000E-01
932.200	0.305580E-03	0.240000E-01
964.900	0.199830E-03	0.240000E-01
976.850	0.644690E-03	0.240000E-01

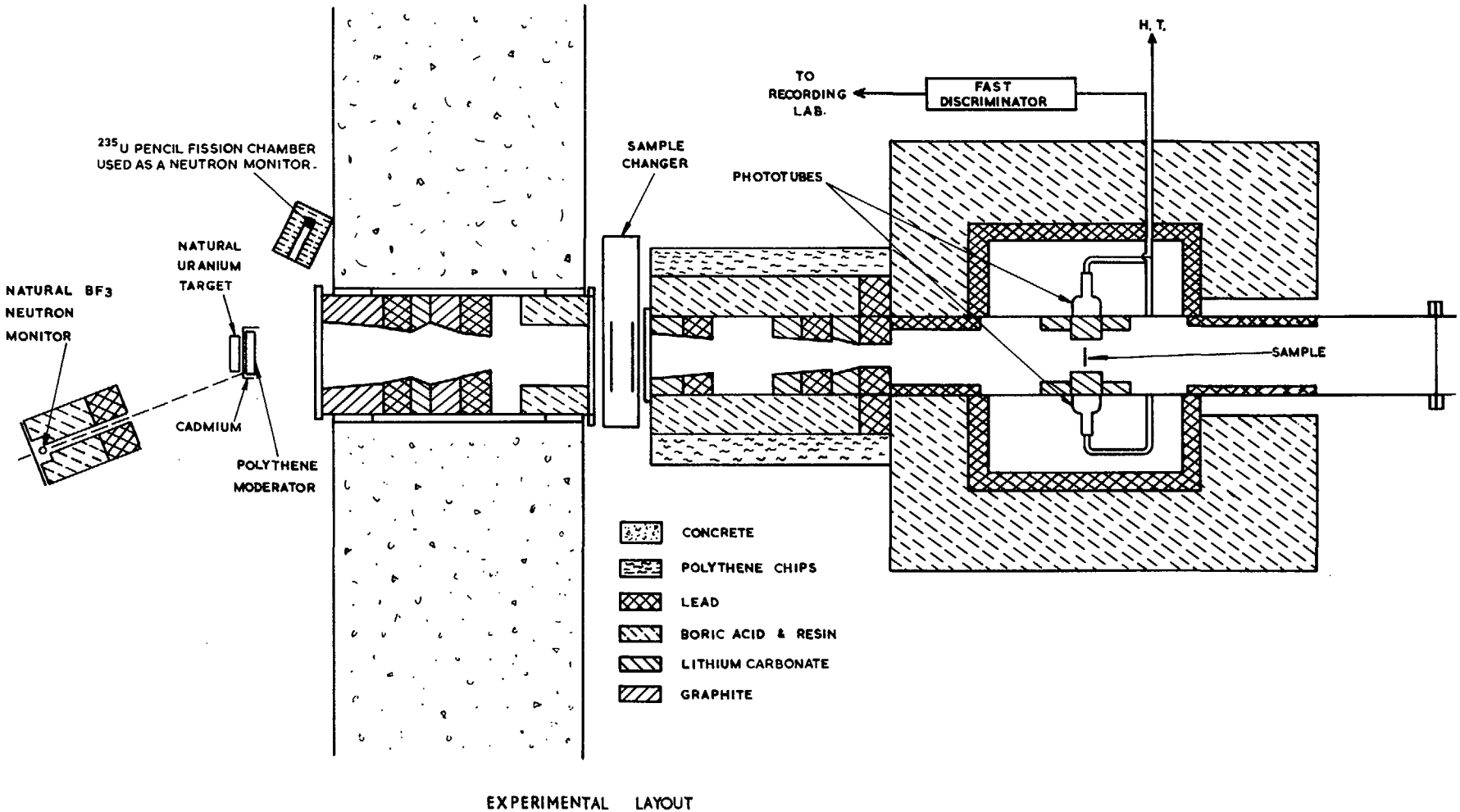

Figure 1 Layout of the 4.58 m flight path.

observed data

⊙ 'black' resonance background data

* open beam background points calculated from resonance dips after correction for transmitted signal

Curve 1 fitted background curve for two sets of resonance filters in the neutron beam

Curve 2 fitted background curve for a single set of resonance filters in the neutron beam

Curve 3 exponential extrapolation of curves 1 and 2 to give the background for the open beam data

Curve 4 corrected background curve for the open beam data using the least square fitting program REFIT.

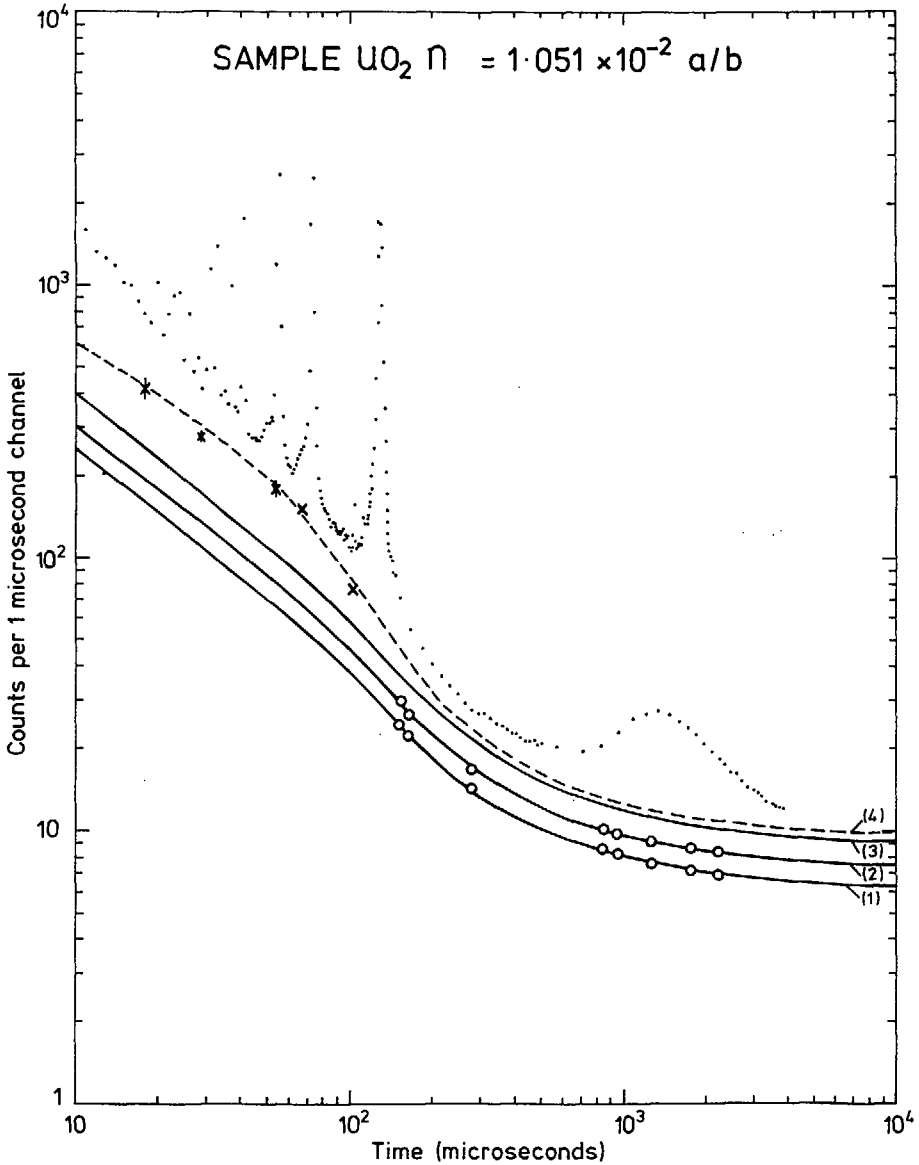

Figure 2 The observed count rate as a function of time-of-flight for the sample UO_2, n = 1.05 x 10^{-2} a/b

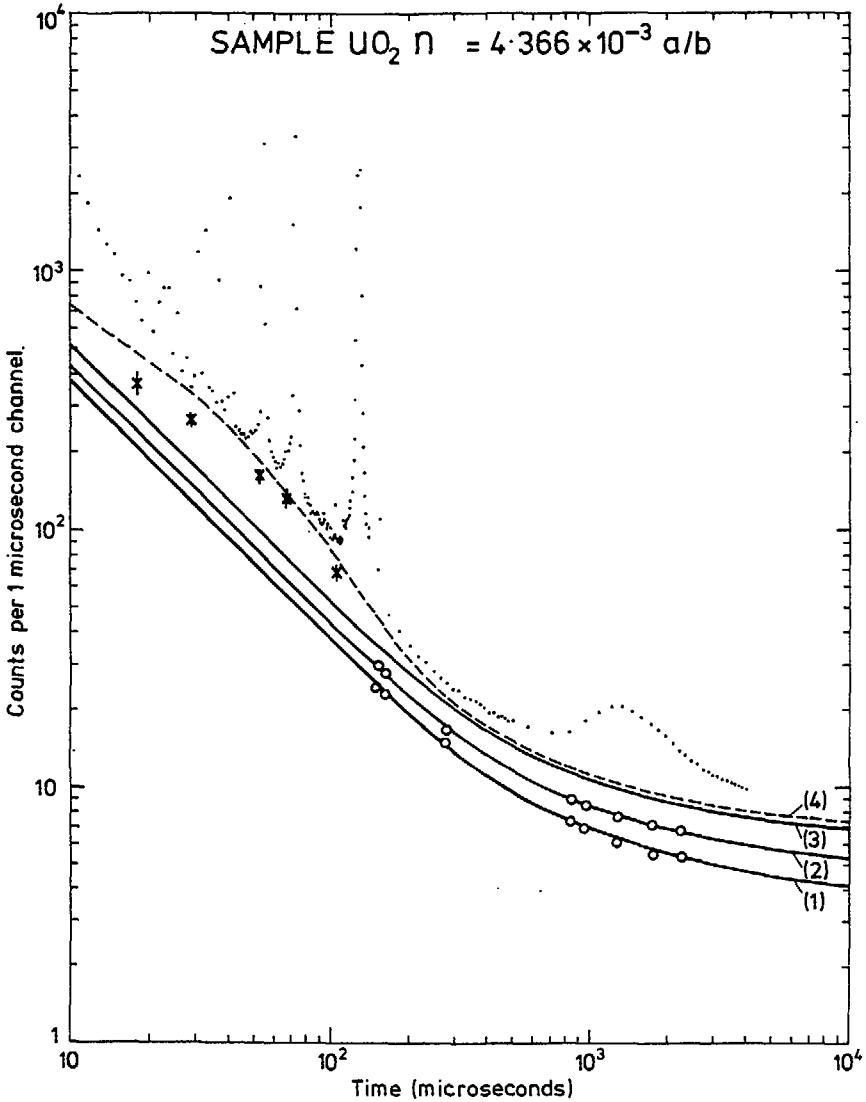

Figure 3 The observed count rate as a function of time-of-flight for the sample of UO_2, n = 4.366 x 10^{-3} a/b (see Figure 2 above for details).

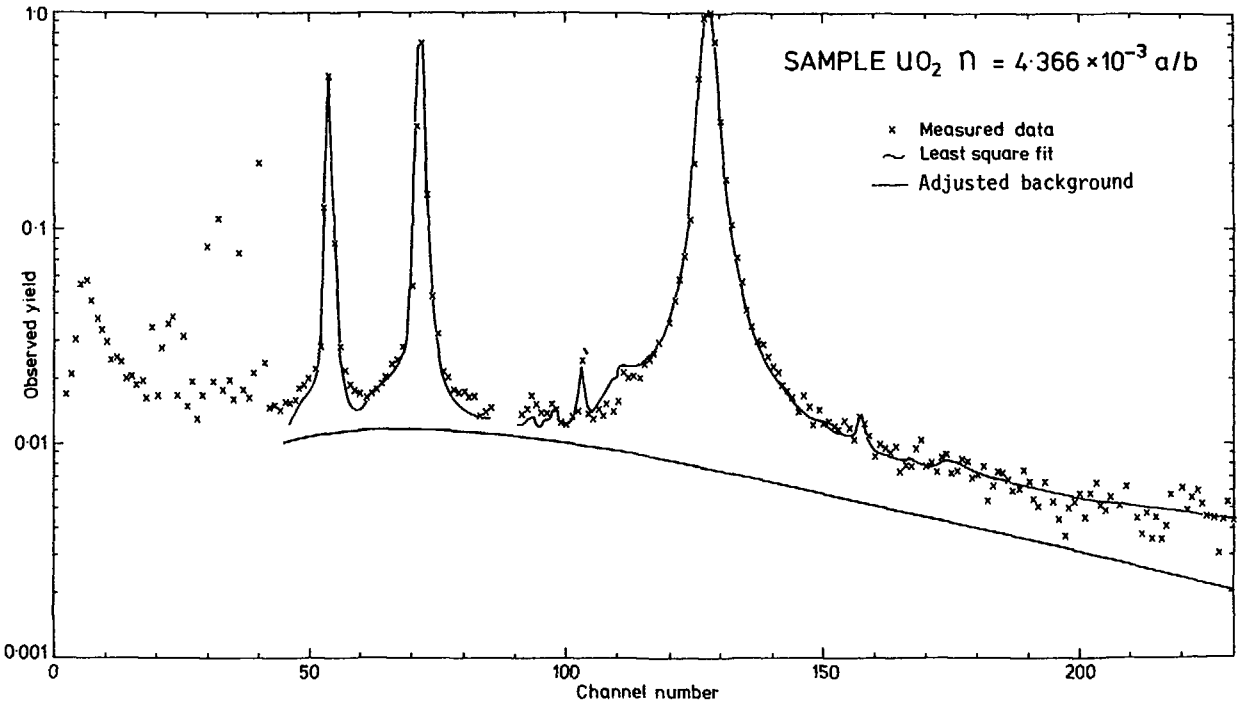

Figure 4 The least square fit to adjust the background in the time region below 200 μsec.

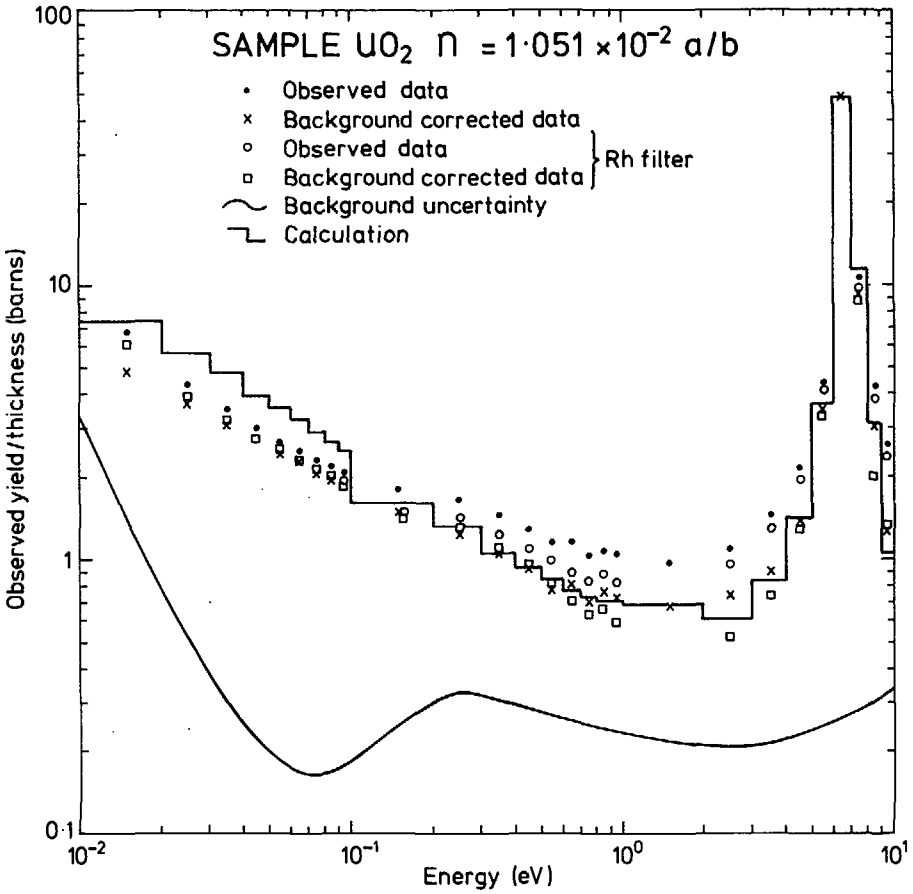

Figure 5 The calculated and observed capture yield divided by sample thickness ($n = 1.051 \times 10^{-2}$ a/b).

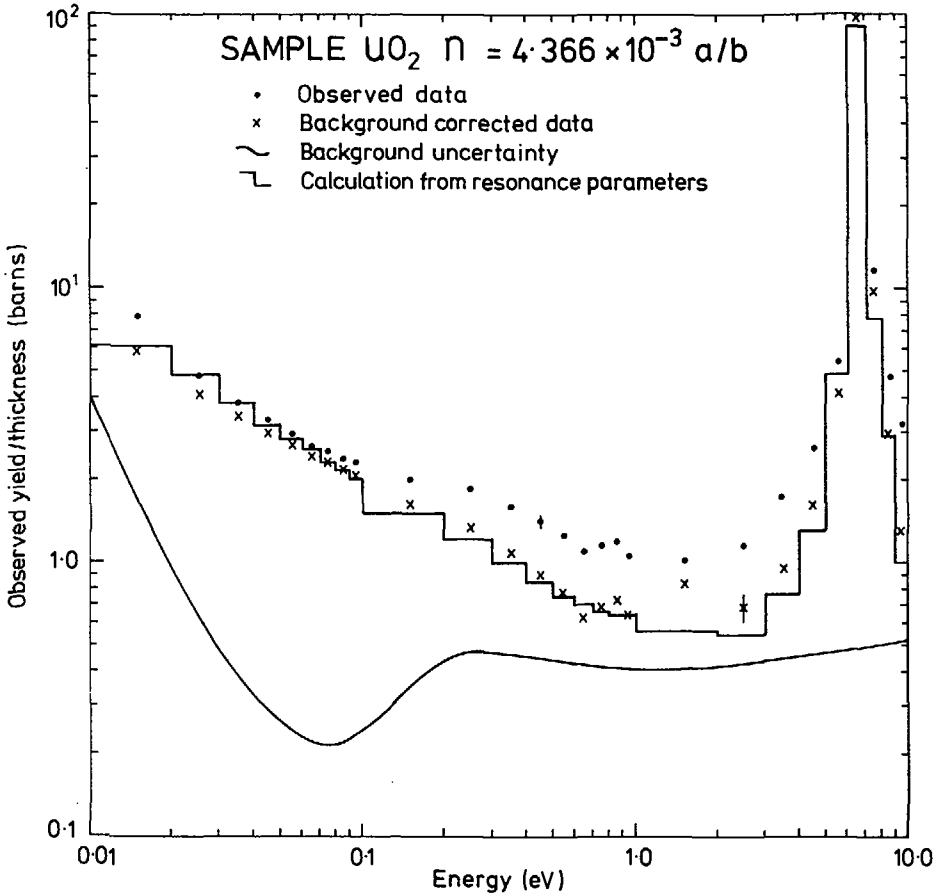

Figure 6 The calculated and observed capture yield divided by sample thickness ($n = 4.366 \times 10^{-5}$ a/b).

Appendix

If the background consists of the components α_i with attenuation factor T_i, the observed value for the open beam is β_0 for a single set of filters β_1 and for two sets of filters β_2, and are given by the following

$$\beta_0 = \sum_{i=1}^{k} \alpha_i \quad (A1)$$

$$\beta_1 = \sum_{i=1}^{k} \alpha_i T_i \quad (A2)$$

$$\beta_2 = \sum_{i=1}^{k} \alpha_i T_i^2 \quad (A3)$$

If we assume exponential attenuation of the observed values, $_1$ and $_2$ the ratio R given in equation (A4) should be unity

$$R = \beta_1^2/\beta_2\beta_0 \quad (A4)$$

If there are several components with different attenuations R will be less than unity and is shown as follows:

$$1-R = 1-(\Sigma_i \alpha_i T_i)^2/((\Sigma_i \alpha_i T_i^2)(\Sigma_i \alpha_i)) \quad (A5)$$

$$= \frac{\Sigma_i(\Sigma_{J, i\neq J} \alpha_i \alpha_J (T_J - T_i)^2)}{(\Sigma_i \alpha_i T_i^2)(\Sigma \alpha_i)} \quad (A6)$$

The RHS of equation (A6) is positive and hence R is always less than unity, i.e. this technique underestimates the background when more than one component is present in the measurement.

U-238 Unresolved Resonance Parameters

M. G. Sowerby and N. J. Bee*
Nuclear Physics Division, A.E.R.E., Harwell, Didcot, Oxon., U.K.

1. Introduction

The unresolved resonance region, which for U-238 extends from ~4 keV to ~150 keV, is the energy range where the resonances are not overlapping (and hence self-shielding is important in reactor calculations) but experimental resolution is inadequate to determine the parameters of individual resonances. This energy range is particularly important for fast reactors. Barre and Khairallah[1] have shown, for example, that ~50% of U-238 captures occur in the 4 to 100 keV energy range in the inner core of a 1200 MWe fast reactor.

The main aims of any unresolved resonance parameter evaluation are two fold

(1) to enable the infinitely dilute cross-sections to be calculated as a function of neutron energy

(2) to allow the self-shielding factors to be calculated as a function of reactor temperature and core composition.+

The effective cross-section $\tilde{\sigma}_{gi\chi}$ for reaction χ of isotope i in group g is then given by

$$\tilde{\sigma}_{gi\chi} = f_{gi\chi} \times \sigma^{\infty}_{gi\chi}$$

where $f_{gi\chi}$ is the self-shielding factor and $\sigma^{\infty}_{gi\chi}$ is the infinitely dilute cross-section.

In many countries fast reactor group cross-sections are adjusted to fit integral data; in others the evaluated differential data are chosen so that measured and calculated integral reactor parameters are in "agreement".

---

*Imperial College, London attached to A.E.R.E., Harwell

+This problem will not be discussed in this paper. The reader is referred to Rowlands (paper presented to this meeting) for further information.

There is, however, general agreement that reactor integral measurements imply a U-238 capture cross-section about 12% (or two standard deviations) below broad resolution differential measurements. This problem was discussed at the previous Specialist Meeting on "Resonance Parameters of Fertile Nuclei and Pu-239" held at Saclay in 1974. The meeting noted in the conclusions[2] that the values of self-shielding factors f are only weakly dependent on resonance parameters. It was therefore concluded that if the usual assumptions were made about mean resonance parameters and distributions then it was impossible to find a set of resonance parameters that will decrease the self-shielded capture cross-section $\tilde{\sigma}_{gi\gamma}$ without decreasing $\sigma^{\infty}_{gi\gamma}$. It was suggested that possible explanations of the discrepancy could include

(1) systematic errors in either the differential measurements of the capture cross-section (i.e. σ^{∞}_{γ}) or in reactor measurements or in their interpretation

(2) systematic faults in the adjustment procedure; for example other cross-sections used in the interpretation may be erroneous

(3) some new physical effect in the U-238 resonance parameters (for example a correlation between the neutron and capture widths Γ_n and Γ_γ; or different Γ_γ's for s and p-wave resonances).

The aim of this paper is to review the state of our knowledge of the U-238 unresolved resonance parameters. In order to do this it is necessary first to summarise the situation at the 1974 Specialist Meeting.

2. Knowledge of parameters at the time of the 1974 Specialist Meeting

Before reviewing the knowledge in 1974 it is worthwhile noting that in the U-238 unresolved energy range we have to consider s, p and d-wave interactions (l = 0, 1 and 2) though the d-wave contribution is sufficiently small that we can limit discussion to the s and p-wave contributions (the value of the d-wave strength function and mean radiation width are usually assumed to be the same as the s-wave values). For U-238 the s-wave interactions form compound nuclear states with spin and parity $J = \frac{1}{2}^+$ while for p-waves the values are $\frac{1}{2}^-$ and $3/2^-$. For each of these spin states an unresolved resonance parameter evaluation must provide the following information which can vary with incident neutron energy:

(a) the mean value of the reduced neutron width (or alternatively the strength function) and the distribution function of the widths

(b) the mean value of the total radiation width and the distribution function of the widths

(c) the mean level spacing and the distribution of level spacings.

Other information such as the effective scattering radius and the nuclear radius for use in the calculation of penetrability are also required.

The distribution functions for widths and spacings have been discussed extensively in the literature (see for example Lynn[3]) and there is a general concensus that:

(1) the level spacing distribution is in good agreement with the Wigner form

(2) the reduced neutron width distribution is a χ^2 distribution with the number of degrees of freedom (ν) being 1 or 2 depending on whether or not the spin state can be formed for both channel spins $I + \frac{1}{2}$ and $I - \frac{1}{2}$ (for $\nu = 1$ the distribution is of course the Porter-Thomas distribution)

(3) the total capture widths have a narrow distribution about their mean value (similar to a χ^2 distribution with ν very large) and it is usually assumed that the capture width is a constant.

Table 1 lists the main techniques that have been used to obtain the average resonance parameters needed in evaluations of the unresolved region. A number of assumptions that have usually been made in the analysis of the results are listed below:

(a) the average level spacing D_J is related to the spin J as follows

$$D_J = \frac{D_o}{2J+1} \exp\left(\frac{J(J+1)}{2\sigma^2}\right)$$

where D_o is a constant and σ is approximately 6

(b) for a given l wave the strength function is assumed to be independent of J

(c) the value of the radiation width Γ_γ is assumed to be independent of J and l.

Table 2, which was given by Sowerby[10], lists the average resonance parameters obtained from some pre-1974 experiments and analyses. The most striking differences are in the values of the p-wave strength function where the analysis of transmission data gives values about 60% higher than other techniques. However, it can also be seen that none of the other parameters, except the effective potential scattering radius, are consistent within ±10%.

Table 3[10] gives the average unresolved resonance parameters used in some pre-1974 evaluations. There is considerable variation in the values chosen and on the whole they are all consistent with the typical "experimental" values given in Table 2. The calculated average capture cross-sections, which are also given in 2 energy ranges, show a large spread and one would expect significant discrepancies in the calculated total cross-sections and other parameters based on these data.

It was concluded in 1974 therefore that

(1) the average resonance parameters in U-238 are not well known and improved data are required

(2) insufficient checks have been made to date to see that evaluations fit all the data that are available

(3) in the future evaluators should check that the resolved and unresolved data on U-238 are consistent with

(a) average capture cross-section data
(b) average total cross-section data
(c) average transmission data for thick samples (including variation with sample temperature)
(d) average self-indication ratio data and their variation with transmission sample temperature.

3. Work done since 1974

(a) Resolved resonance parameters

Though this paper is not concerned with resolved resonance parameter data, improvements to the data in this region have implications in the unresolved region. New resolved region data have been obtained at a number of laboratories and most of these were taken into account by de Saussure et al[15] in their detailed evaluation of the 0 to 4 keV energy range which is included in ENDF-B V. An evaluation of this energy range has also been performed in Japan for JENDL-2. Though the results of this are given in a JENDL file, only a limited amount of documentation is available. Both evaluations include fission widths.

Table 4 gives the more important conclusions from the evaluation of de Saussure et al and also gives the modifications suggested by Keyworth and Moore[16] in their review. It is now generally agreed that the value of $\langle\Gamma_\gamma\rangle$ is ∿23.5 meV. The value of $0.944\pm0.025 \times 10^{-12}$ cm for the effective potential scattering radius given by de Saussure et al is the result of careful measurement and analysis at Oak Ridge by Olsen et al[17]. It is somewhat higher than the value of $0.9185\pm0.014 \times 10^{-12}$ cm obtained by Lynn[8]. The values of the p-wave strength function deduced by Lynn and Uttley et al (see Table 2) are correlated with the value of the scattering radius.

If the correct value of the scattering radius is 0.944×10^{-12} cm then their estimated p-wave strength function is likely to be below 2.5×10^{-4}. Uttley et al show that if the effective scattering radius changes from 0.9185×10^{-12} cm to 0.944×10^{-12} cm then their fitted value of S_1 reduces to $\sim 1.9 \times 10^{-4}$. It would therefore appear that the p-wave strength function of $1.9\ (\pm0.2) \times 10^{-4}$ is a reasonable global fit to all the data. There is still some doubt about the values of the mean level spacings. It seems reasonable however to accept the modifications of Keyworth and Moore to the de Saussure et al evaluation and hence the best value of the s-wave level spacing is 20.9 eV.

(b) Measurements in the unresolved energy range

A number of measurements have been performed which give improved data in this energy range. Basically these are of three types:

(1) measurements of capture cross-sections
(2) transmission measurements with samples of various thickness and in some cases with heated samples
(3) measurements of fission cross-sections.

There is also a little information on the inelastic scattering cross-section to the first level in U-238 at 45 keV. The fission cross-section is on average small throughout the "unresolved energy region" and for most practical purposes it can be forgotten.

The capture cross-section data above 10 keV were recently reviewed by Poenitz[18]. He concludes that most measurements are within a ±5% range except the measurements of de Saussure et al[19] which are higher and Moxon[20] which are lower. Poenitz considers that the error in the capture cross-section is ∿±5% and this agrees with the values given in ENDF-B V. Between 4 and 10 keV the errors given in ENDF-B V are similar. The recent data do not solve the discrepancy in U-238 capture between integral and differential data and, because the U-238 capture cross-section in the unresolved region is so important, improved measurements are required. As has been stated by de Saussure[21] new measurements should attempt to reduce the corrections for background,efficiency variations and multiple scattering by stressing new approaches and better techniques.

Evaluations of the capture cross-section tend to ignore the large fluctuations (up to ∿20%) that are known to exist in the unresolved energy region[22,23]. Similar structures are known to occur in the total cross-section and there is a need to understand the origin of these fluctuations - are they due to local fluctuations in Γ_n or D? Melkonian et al[24] have shown that in the resolved region there are fluctuations in Γ_n^o. Unless these fluctuations are correctly represented errors will occur in calculated self-screening factors.

As far as transmission data are concerned there have been significant improvements in the data; Olsen et al[25] have performed high resolution accurate transmission measurements through samples of various thickness covering the energy range 0.88 to 100 keV, Haste and Sowerby[26] have made measurements of the average transmission of heated UO_2 samples in the energy range 10 eV to 200 keV and Brugger and co-workers[27,28] have measured the transmission of U-238 in various chemical forms as a function of sample temperature for energy bands at 2, 24 and 144 keV.

Brugger and Aminfar[28] have analysed their transmission data by generating a ladder of resonances which have a set of average resonance parameters. The cross-sections deduced from the ladder were then Doppler broadened using an ideal gas model which incorporated an effective temperature to account for zero state vibrations and an effective mass to account for chemical binding. It was found necessary to include the effective mass so that one particular ladder of resonances will fit all the measurements in one energy band. A change in the effective mass is also needed to fit the observed step in transmission when U is melted. There is a need for further analysis of these results because if the present conclusions are correct there may be errors in the current Doppler broadening calculations. In particular it is recommended that the measurements at 2 keV be analysed using the known resonance parameters.

The transmission data are at present being analysed by Bee[29] who has devised a method for estimating the s-wave strength function in the energy range where self-shielding is important. Some estimates are shown in Fig. 1 together with values of the s and p-wave strength functions that have been used in the two latest evaluations in the unresolved region for ENDF-B V and JENDL-2. These attempts to estimate s-wave strength functions in the unresolved energy range are an important step in an evaluation in the unresolved region because the calculation of correct self-screening factors requires that the total cross-section be correctly divided up into its various ℓ wave components.

The total cross-section in the unresolved region is an important quantity but it is difficult to measure because of self-screening effects. However, the data of Olsen et al[25] can be used to provide an estimate which agrees reasonably well in the region of overlap between 6 and 100 keV with the data of Uttley et al[7]. From these data it would appear that the average total cross-section is known to better than ∿±4% over the whole of the unresolved energy range.

(c) Evaluations in the unresolved region

Three new evaluations* have been performed in the unresolved region since 1974 for the KEDAK-3, ENDF-B V and JENDL-2 nuclear data libraries. These evaluations are of course constrained by the procedures

*Two new evaluations for ENDF/B IV and JENDL-1 have also been performed but these will be neglected as they have been superceded.

of the libraries and therefore any comments should not be considered to be a criticism of the evaluators.

The KEDAK-3 evaluation was performed by Fröhner and is reported in reference 30; the values of the parameters are given in Table 5. These parameters were determined as follows. For ℓ=0 the values are maximum likelihood estimates derived from the individual resonance parameters in the resolved region with due account of missing levels. The p-wave strength function was determined by a least squares fit to the evaluated total cross-section data; this was primarily based on the data of Carraro and Kolar[6] and Uttley et al[7] below and above 14 keV respectively. The other parameters were then chosen to make the calculated cross-section fit the evaluated capture cross-section. It should be noted that in this evaluation the average resonance parameters are independent of neutron energy and fluctuations in the average cross-sections are not represented by the resonance parameters.

The ENDF-B V evaluation was performed in the unresolved region by Pennington et al[31] and covers the energy range 4 keV to 149 keV. Average parameters are given at 36 energy points over this energy range and for given values of ℓ and J most of these are independent of neutron energy; Table 6 gives the values of the energy independent parameters. The competitive widths ($\bar{\Gamma}_{comp}$) are included so that inelastic scattering to the first level at 45 keV is represented. The values of $\bar{\Gamma}_n^o$ for p-waves and $\bar{\Gamma}_{comp}$ vary with neutron energy with the values being chosen to fit the evaluated capture and inelastic scattering cross-sections respectively. The values of s and p-wave strength functions given by the evaluation are plotted below 100 keV in Fig. 1. The values of total cross-sections calculated from the evaluation are not a reasonable fit to the measured data above ∿20 keV; the discrepancy at 60 keV is ∿8%. The evaluation method ensures that all the structure in the evaluated capture cross-section appears in the p-wave strength function.

The JENDL-2 evaluation considers the unresolved region to extend from 4 keV to 50 keV and average parameters are given at 21 energy points over this energy range for the same values of ℓ and J as ENDF-B V. The values of the s and p-wave strength functions, which are plotted in Fig. 1, were determined by adjusting their values (keeping their ratio constant) so as to reproduce smooth evaluations of the measured capture and total cross-sections. Table 7 gives some of the other parameters.

It is clear by comparing the evaluations and from Fig. 1 that:

(1) the evaluations do not represent the fine structure in the total cross-section (or capture cross-section)

(2) the values of $\bar{\Gamma}_\gamma$ are in good agreement as are the values of $\bar{D}$ at ∿4 keV

(3) these values of $\bar{\Gamma}_\gamma$ and $\bar{D}$ are in good agreement with the best values deduced in the resolved region

(4) the values of the s-wave strength function used in ENDF-B V are higher than the estimates by Bee below 12 keV. Reasonable agreement with the smoothed total cross-section data is achieved because a small value (0.89×10^{-12} cm) is used for the effective scattering radius

(5) the value of the d-wave strength function used in ENDF-B V is a factor ∿2.5 higher than in the other evaluations.

(d) The adequacy of the ENDF-B V format in the unresolved region

The ENDF-B format is widely used throughout the world and it is pertinent to ask if the format is adequate. In the unresolved energy range the format only allows the cross-sections to be described by the Breit-Wigner single level formalism but the average parameters can be given at 250 energy points. This number is probably sufficient to describe the known structure in the cross-sections but the use of the single level formalism can lead to problems if the data are not used in the way intended. For instance, the creation of single level resonance ladders can be expected to produce the same kind of end effect bias and frequent negative scattering cross-sections that are seen when the single level representation is used in the resolved region.

The problems of the ENDF-B unresolved resonance formalism have been considered in detail by de Saussure and Perez[32] and some of their comments are given in the rest of this section. The central question is whether or

not the ENDF-B representation leads to a correct estimate of resonance self-shielding. Ultimately this question will have to be answered by comparing computed self-shielding factors as a function of energy temperature and dilution with the values derived from experiments but as far as is known this has not been done.

As far as the ENDF-B V U-238 evaluation is concerned de Saussure and Perez consider that there is no theoretical or logical justification of the model used in the unresolved region although this model conforms to usual ENDF-B procedures. From the theoretical point of view, there is no reason to expect the variation in the locally averaged cross-section to be due entirely to a variation in the locally averaged $\ell=1$ reduced neutron widths. There is no reason either to expect a small sample of the reduced neutron widths to have a Porter-Thomas distribution around their locally averaged values.

The model is also logically inconsistent. By specifying average resonance parameters and their distributions, we specify only the probability distribution of the average cross-sections, not the actual values. By fitting the local reduced neutron widths to the locally averaged values of the capture cross-section, on the other hand, we imply that the most probable value of the average cross-section is the actual value. Furthermore the magnitude of the fluctuations of the locally averaged capture cross-section is determined by the width of the averaging intervals and there is no compelling rationale for selecting these widths. The widths of the averaging intervals should probably be interpreted as being of the same order of magnitude as the intervals between successive energy points at which the average parameters are defined; these intervals vary considerably in magnitude.

Because of the lack of theoretical justification and because of these logical inconsistencies, the model should be viewed at best as an ad hoc parameterization of the average capture cross-section. Because of the way it is constructed, the model will reproduce exactly the evaluated locally averaged capture cross-sections but there is no reason to expect it to provide correct values of the self-shielding factors, since the parameterization is not unique and since no self-shielding information was utilized.

In order to check the uncertainties that arise in self-screening factors due to these effects de Saussure and Perez[32] have performed a series of calculations at 4 keV. In these the ENDF-B V evaluation was used but the s-wave strength function was allowed to vary over an acceptable range (±40%) and the p-wave strength function was then selected so that the average capture cross-section was unchanged. Table 8 gives the values of the self-screening factors obtained as a function of dilution cross-section (σ_0) and temperature. It can be seen that the 40% change in S_0 corresponds to a change in the self-screening factor (f_γ) of ~±10% for a dilution of 10b and an uncertainty of the same magnitude in the change in f_γ between 1000K and 2000K. It should also be noted that the changes in S_0 correspond to changes in the average total cross-section and hence these results show that good knowledge of the average total cross-section and/or the s-wave strength function should improve the accuracy of values of f_γ and $\tilde{\sigma}_\gamma$ calculated from resonance parameters.

Rowlands[33] has done some calculations of the values of $\tilde{\sigma}_\gamma$ averaged over the energy range 0.5 to 25 keV using a reference set of average resonance parameters and 4 other sets where changes were made to one parameter. The results are given in Table 9 and these together with the data given in Table 8 lead to the conclusion that the present errors in the unresolved resonance parameters lead to significant uncertainties in the self-shielding factors. This means that

(a) the accuracy of values of $\tilde{\sigma}_\gamma$ deduced using the formula $\tilde{\sigma}_\gamma = f_\gamma \sigma_\gamma^\infty$ is poorer than the accuracy of σ_γ^∞

and (b) it is not sufficient to perform integral measurements of $\tilde{\sigma}_\gamma$ for a limited number of experimental conditions because if one wishes to use these to determine $\tilde{\sigma}_\gamma$ for some other condition (e.g. temperature) then accurate values of f_γ are needed.

It follows, therefore, that the reactor physicist always requires a good description of the unresolved resonance parameters irrespective of the method he uses to determine $\tilde{\sigma}_\gamma$. The use of the data adjustment method where group cross-sections are adjusted to fit integral data does <u>not</u> remove this need.

The above discussion tends to contradict a conclusion[2] reached in the previous specialist meeting that the self-shielding factors are only weakly dependent on the assumed resonance parameters if the usual assumptions are made about the parameters and their distributions. Based upon this it was felt in 1974 that the discrepancy between integral and differential measurements of the U-238 capture cross-section was unlikely to be caused by errors in f_γ due to errors in the unresolved resonance parameters unless these have unexpected properties. It is now clear that some of the errors in these parameters are larger than previously thought (e.g. the values of S_o deduced by Bee[29] between 4 and 10 keV are significantly below the value of 1×10^{-4} usually assumed) and so the discrepancy could in part be due to errors in self-screening factors. More work needs to be done to extract the local values of the parameters to clear up this point.

de Saussure and Perez have also tested the ENDF-B V unresolved region methodology by applying it to the energy range 1 - 4 keV where resolved resonance parameters are available. The results are given in Table 10 where $\sigma_{n\gamma}f$ and $\sigma_{n\gamma}f^*$ are the self-screened cross-section values calculated by the unresolved region and resolved region methodologies respectively. It can be seen that the values significantly differ even when the averaging intervals are 1 keV. If there are similar differences in the unresolved region then part of the discrepancy between integral and differential capture cross-section data could be due to this.

There is obviously a need to improve the ENDF-B methodology for treating the unresolved region. A number of methods have been given by de Saussure and Perez:

(1) "ladder" of artificial resonances selected to fit data using a forced sampling technique

(2) using directly cross-sections obtained in high resolution methods

(3) representing the data by the probability table method

(4) parameterization of the resonance self-shielding factors.

4. Discussion and Conclusions

It is clear that a considerable amount of work has been performed since the last review of the unresolved resonance region of U-238 was made in 1974. The capture cross-section data are now known to ±5% over the whole of the unresolved energy range (4 to 150 keV). This is only a marginal improvement since 1974 and the discrepancy between integral measurements of U-238 capture and values calculated from differential data still exists. Of course this could be due to incorrect calculation of self-screening factors but there is still a need for more differential measurements. As recommended previously by de Saussure[21] the new measurements should attempt to reduce the corrections that have to be applied to the experimental data by using new approaches and better techniques.

The average total cross-section now appears to be known to ±4% over the whole energy range and a series of good measurements of transmission through a range of sample thicknesses are available, some being done with heated samples. The transmission data of Brugger and Aminfar[28], however, require further analysis because if the present analyses are correct the gas model of Doppler broadening could be wrong. In particular their data at 2 keV require analysis using the available resolved resonance parameters.

Little attention has been paid in this review to the fission cross-section, which is small, or to the inelastic scattering cross-section to the first level at 45 keV. This latter cross-section is large in magnitude reaching about 0.7 barns at 150 keV but it is probably known to sufficient accuracy that resulting errors in calculated self-shielding factors are small.

From the resolved region there are now reasonable estimates of a number of parameters, i.e.

Level spacing of s-wave resonances = 20.9±1.5 eV

$\langle\Gamma_\gamma\rangle$ for s-wave resonances = 23.5 meV

effective scattering radius (s-wave) = $0.944\pm0.025 \times 10^{-12}$ cm

p-wave strength function = $1.9\pm0.2 \times 10^{-4}$

The data on level spacings for p-waves are consistent with the formula $D_J = \frac{D_o}{2J+1}$

However, we do not know if $\langle\Gamma_\gamma\rangle$ for p-waves is the same as $\langle\Gamma_\gamma\rangle$ for s-waves as Γ_γ has not been determined for a p-wave resonance. Such a determination could be very valuable.

The present analyses of the unresolved region often assume that the unresolved parameters are constant or they only vary slowly with neutron energy. However, it is known that there is significant structure in the cross-sections in the unresolved region and the effects of the structure on the calculation of self-shielding factors require further investigation.

de Saussure and Perez[32] have investigated the methodology of the ENDF-B V U-238 unresolved region evaluation and considered its adequacy.

They conclude that improvements are required and have listed some possible methods.

It is clear that the average unresolved resonance parameters and in particular the local values of these parameters are not well known. Work is required to improve this situation and it should be noted that these data are required irrespective of whether or not the method of data adjustment is used to improve the accuracy of production of integral properties. Bee[29] has started an analysis and his results, which give estimates of the s-wave strength function in the region where self-screening is important, look promising. The parameters deduced in any analysis must be checked to see that they are consistent with

(a) average capture cross-section data

(b) average total cross-section data

(c) average transmission data for thick samples (including variation with sample temperature)

(d) average self-indication ratio data and their variation with transmission sample temperature.

The checks against (c) and (d) are particularly important as they will give some commentary on the calculated shielding factors.

5. Acknowledgements

The authors would like to thank Dr. M. S. Coates, Mr. M. C. Moxon and Dr. B. H. Patrick for the help given in the preparation of this paper. Miss E. M. Bowey and Mr. D. A. J. Endacott have provided assistance with computing and this is gratefully acknowledged.

References

(1) Barré J. Y. and Khairallah A., NEANDC(E)163U, Page 19 (1975).

(2) NEANDC(E)163U, Page 6 (1975).

(3) Lynn J. E., The Theory of Neutron Resonance Reactions, Clarendon Press, Oxford (1968).

(4) Rahn F., Camarda H. S., Hacken G., Havens W. W. Jnr., Liou H. I., Rainwater J., Slagowitz M. and Wynchank S., Phys. Rev. C6 (1972) 1854.

(5) Rohr G., Weigmann H. and Winter J., Nuclear Data for Reactors 1, 413 (1970).

(6) Carraro G. and Kolar W., CONF 710301, Page 70 (1971).

(7) Uttley C. A., Newstead C. M. and Diment K. M., Nuclear Data for Reactors 1, 165, IAEA Vienna (1967).

(8) Lynn J. E., Proc. Phys. Soc. 82 (1963) 903.

(9) Moxon M. C., M.Sc. Thesis (1968).

(10) Sowerby M. G., NEANDC(E)163U, Page 183 (1975).

(11) Pitterle T. A. and Durston C., Private Communication (1971).

(12) James M. F., Private Communication (1974). See also EANDC 90L.

(13) Schmidt J. J., KFK 120 (1966).

(14) Abagyan L. P., Abramov A. I., Nikolaev M. N., Stavisskii Yu. Ya. and Tolstikov V. A., INDC(CCP)11/U (1971).

(15) de Saussure G., Olsen D. K., Perez R. B. and Difilippo F. C., Progress in Nuclear Energy 3 (1979) 87.

(16) Keyworth G. A. and Moore M. S., Proc. Conf. on Neutron Physics and Nuclear Data, Harwell, September 1978, Page 241.

(17) Olsen D. K., de Saussure G., Perez R. B., Silver E. G., Difilippo F. C., Ingle R. W. and Weaver H., Nucl. Sci. Eng. 62 (1977) 479.

(18) Poenitz W. P., BNL-NCS-51123 Section B, Page XII.1 (1980).

(19) de Saussure G., Silver E. G., Perez R. B., Ingle R. and Weaver H., Nucl. Sci. Eng. 51 (1973) 385.

(20) Moxon M. C., AERE-R 6074 (1969).

(21) de Saussure G., BNL-NCS-51123 Section B, Page III.1 (1979).

(22) Spencer R. R. and Kaeppeler F., NBS Special Publication 425, Page 620 (1975).

(23) Perez R. B. and de Saussure G., NBS Special Publication 425, Page 623 (1975).

(24) Melkonian E., Felvinci J. P. and Havens W. W. Jnr., NBS Special Publication 425, Page 742 (1975).

(25) Olsen D. K., de Saussure G., Perez R. B., Difilippo F. C., Ingle R. W. and Weaver H., Nucl. Sci. Eng. 69 (1979) 202.

(26) Haste T. J. and Sowerby M. G., J. Phys. D, 12 (1979) 1203.

(27) Brugger R. M. and Tsang F. Y., Proc. Conf. on Neutron Physics and Nuclear Data, Harwell, September 1978, Page 343.

(28) Brugger R. M. and Aminfar H., Private Communication (1981).

(29) Bee N. J., Paper to be presented at this meeting.

(30) Goel B. and Weller F., KFK 2386/111 (1977).

(31) See BNL-NCS-17541 (ENDF 201) Page 92-238-1 (1979) also ANL/NDM-32 (1977).

(32) de Saussure G. and Perez R. B. to be published in Annals of Nuclear Energy.

(33) Rowlands J. L., BNL-NCS-51363, P.23 (1981).

Table 1

Methods of obtaining data on unresolved resonance parameters

Method	Assumptions	Data obtained
A Analysis of resolved resonance data	The average values of parameters in the resolved region are the same as the unresolved region when known energy dependence allowed for	s and p-wave strength functions (S_0 and S_1) s and p-wave level spacings and hence D_0 $\langle\Gamma_\gamma\rangle$ for s-waves scattering radius R' for s-waves
B Analysis of average total cross-section data	Values of S_0 and R'	p and d-wave strength functions (S_1 and S_0) Dimensionless quantity for p-waves (R_1^∞) which allows for the effect of distant levels
C Analysis of thick sample average transmission data	Values of D_0, $\langle\Gamma_\gamma\rangle$ S_0 and distribution of s-wave neutron widths are assumed	S_1 and R'
D Analysis of average capture cross-section measurements	Values of S_0 and S_2 are assumed plus distribution of neutron widths	$\frac{\langle\Gamma_\gamma\rangle}{D_0}$ for s-waves $\frac{\langle\Gamma_\gamma\rangle}{D_0}$ for p-waves S_1 The values $\frac{\langle\Gamma_\gamma\rangle}{D_0}$ for s-waves and S_1 are strongly correlated

Table 2

Data obtained from typical experiments and analyses (pre 1974)

Experiment	Type	s-wave level spacing (eV)	S_0	Effective potential scattering radius (fm)	S_1	$\langle\Gamma_\gamma\rangle$ meV	Comment
Rahn et al[4]	A	20.8	$1.08\pm0.10 \times 10^{-4}$	9.6 ± 0.3	$\sim 1.4 \times 10^{-4}$	22.9 ±0.5 (stat) ±0.9 (syst)	Analysis to divide levels into s and p populations
Rohr et al[5]	A					24.64 ± 0.85	
Carraro and Kolar[6]	A	17.8 ± 0.9	1.13 ± 0.13				Assumes all resonances <2 keV produced by s-wave neutrons
Uttley et al[7]	B		Assumed to be 1.0×10^{-4}	Assumed to be 9.185	$2.47^{+0.16}_{-0.28} \times10^{-4}$		
Lynn[8]	C	Assumed to be 18.0	Assumed to be 1.0×10^{-4}	9.185 ± 0.14	$2.5\pm0.4 \times10^{-4}$	Assumed to be 27	
Moxon[9]	D		1.0 ± 0.3		1.59 ± 0.45	$\langle\Gamma_\gamma\rangle/D_0 = 5.7\pm0.9 \times 10^{-4}$ (s-wave) $= 5.8\pm1.2 \times 10^{-4}$ (p-wave)	If s-wave level spacing = 20.8 eV $\langle\Gamma_\gamma\rangle$ = 23.7 meV

Table 3

Comparison of evaluations of unresolved resonance parameters (pre 1974)

Quantity \ Evaluation	ENDF-B III[11]	James for UK SDR-GENEX evaluation[12]	Schmidt[13]	Abagyan et al[14]
S_o	1.05×10^{-4} but varied by up to 15% below 10 keV	0.93×10^{-4}	0.90×10^{-4}	0.91×10^{-4}
S_1	Variable between 1.337×10^{-4} and 1.932×10^{-4}	1.58×10^{-4}	2.5×10^{-4}	2.0×10^{-4}
s-wave level spacing	Variable decreasing from 20 to 18.59 eV from 4 to 45 keV	22.5 eV	20.8 eV	20.4 eV
p-wave level spacing J = 1/2 J = 3/2	 As s-wave Variable decreasing from 10.98 to 10.21 eV from 4 to 45 keV	 22.5 eV 11.25 eV	 20.8 eV 11.4 eV	
s-wave scattering radius (R')	9.184×10^{-13} cm	9.1843×10^{-13}	9.18×10^{-13} cm	
radius used for calculating penetrability	8.401×10^{-13} cm	8.3662×10^{-13}	9.18×10^{-13} cm	
$\langle \Gamma_\gamma \rangle$	23.5 meV	23.0 meV	24.8 meV	24.3 meV
Comment	Parameters chosen to reproduce average capture cross-section	Parameters chosen to give shielded cross-sections required to fit reactor measurements	Parameters chosen from the types of experiments listed in Table 1	Parameters chosen from resolved resonance data
Average calculated capture cross-section* 5-6 keV 10-20 keV	 0.972 0.645	 0.885 0.547	 1.138 0.736	 1.04 0.68

*Values in last column from INDC(CCP)-11/U. Otherwise data in EANDC 90L quoted.

Table 4

Some recent data from resolved resonance analysis

Reference	Data
de Saussure et al[15] (evaluation)	s-wave level spacing 24.8±2 eV s-wave strength function energy interval (keV) S_0 ($\times 10^{-4}$) 0 - 0.5 1.006 0.5 - 1 1.004 1 - 1.5 0.927 1.5 - 2 1.566 2 - 2.5 0.988 2.5 - 3 1.461 3 - 3.5 1.172 3.5 - 4 1.221 0 - 4 1.168 effective potential scattering radius $0.944\pm0.025 \times 10^{-12}$ cm $S_1 = 1.93\pm0.5 \times 10^{-4}$ (below 1500 eV) p-wave level spacing 8.91±0.1 eV (below 800 eV) $\langle\Gamma_\gamma\rangle$ 23.23 meV (23.5 meV used where no measurements)
Keyworth and Moore[16] (review)	s-wave level spacing 20.9±1.5 eV $S_0 = 1.134\pm0.1 \times 10^{-4}$ $S_1 = 1.70\pm0.51 \times 10^{-4}$ p-wave level spacing 7.25±0.52 eV

Table 5

Unresolved resonance parameters in KEDAK-3

ℓ	J	$\bar{\Gamma}_\gamma$ (eV)	$\bar{D}$ (eV)	$\bar{\Gamma}_n^o$ (eV)	$\bar{\Gamma}_n^o/\bar{D}$	ν_f	ν_n
0	1/2	0.024	20.2	1.879×10^{-3}	0.93×10^{-4}	0	1
1	1/2	0.024	20.2	3.64×10^{-3}	1.8×10^{-4}	0	1
1	3/2	0.024	10.17	1.879×10^{-3}	1.8×10^{-4}	0	1
2	3/2	0.024	10.17	0.946×10^{-3}	0.93×10^{-4}	0	1
2	5/2	0.024	6.83	0.635×10^{-3}	0.93×10^{-4}	0	1

The nuclear radius is taken to be 0.93×10^{-12} cm

Table 6

Unresolved resonance parameters in ENDF-B V

ℓ	J	$\bar{\Gamma}_\gamma$ (eV)	$\bar{D}$ (eV)	$\bar{\Gamma}_n^o$ (eV)	$\bar{\Gamma}_f$ (eV)	$\bar{\Gamma}_{comp}$ (eV)	ν_n	ν_f	ν_{comp}
0	1/2	0.0235	20.0	2.1×10^{-3}	0	varies+	1	0	2
1	1/2	0.0235	20.0	χ_i*	0	varies+	1	0	1
1	3/2	0.0235	10.0	1/2 χ_i*	0	varies+	1	0	2
2	3/2	0.0235	10.0	2.5×10^{-3}	0	varies+	1	0	1
2	5/2	0.0235	6.667	1.667×10^{-3}	0	varies+	1	0	2

The effective scattering radius is taken as 0.890×10^{-12} cm

*The values χ_i vary with neutron energy but $\bar{\Gamma}_n^o$ (for $\ell = 1$ J = 3/2) always half the value of $\bar{\Gamma}_n^o$ (for $\ell = 1$ J = 1/2)

+The values of $\bar{\Gamma}_{comp}$ are zero below 45.18 keV

Table 7

Unresolved resonance parameters in JENDL 2

ℓ	J	$\bar{\Gamma}_\gamma$	$\bar{D}$	$\bar{\Gamma}_n^o$	$\bar{\Gamma}_f$	$\bar{\Gamma}_{comp}$	ν_n	ν_f	ν_{comp}
0	1/2	V*	V	V	0.0	V	1	0	2
1	1/2	V	V	V	0.0	V	1	0	1
1	3/2	V	V	V	0.0	V	1	0	2
2	3/2	V	V	V	0.0	V	1	0	1
2	5/2	V	V	V	0.0	V	1	0	1

*V means that the value is energy dependent

For $\bar{\Gamma}_\gamma$ the values are independent of ℓ and J and vary between 23.524 meV at 4 keV and 23.803 meV at 50 keV.

For $\bar{D}$ values are related with a $\frac{\bar{D}(E)}{2J+1}$ dependence. The s-wave level spacing varies between 19.83 eV at 4 keV to 17.94 eV at 50 keV.

The $\bar{\Gamma}_n^o$ values for ℓ = 1 J = 1/2 are twice those for ℓ = 1 J = 3/2.

For ℓ = 2 the values of $\bar{\Gamma}_n^o/\bar{D} = 1 \times 10^{-4}$.

The effective scattering radius is given as 0.936×10^{-12} cm.

Table 8

U-238 capture self-shielding factors at 4 keV

ENDF-B V values s-wave strength function (S_0) = 1.05×10^{-4}
p-wave strength function (S_1) = 0.775×10^{-4}
$\langle\sigma_{n\gamma}\rangle$ = 0.92615 b
$\langle\sigma_{nT}\rangle$ = 17.95 b

S_0	S_1	$\langle\sigma_{nT}\rangle$ b	σ_0 = 1 b	T = 300 K σ_0 = 10 b	σ_0 = 100 b
0.63	1.22	15.5	0.60±0.01*	0.68±0.01	0.88±0.02
0.84	0.96	16.8	0.55±0.01	0.64±0.01	0.85±0.02
1.05	0.78	18.0	0.52±0.01	0.60±0.01	0.83±0.02
1.26	0.64	19.4	0.48±0.01	0.57±0.01	0.81±0.02
1.47	0.53	20.7	0.46±0.01	0.55±0.01	0.79±0.02
				T = 1000 K	
0.63	1.22	15.5	0.70±0.01	0.77±0.01	0.92±0.01
0.84	0.96	16.8	0.66±0.01	0.73±0.01	0.91±0.01
1.05	0.78	18.0	0.62±0.01	0.70±0.01	0.89±0.01
1.26	0.64	19.4	0.59±0.01	0.67±0.01	0.88±0.01
1.47	0.53	20.7	0.56±0.01	0.65±0.01	0.86±0.01
				T = 2000 K	
0.63	1.22	15.5	0.76±0.01	0.82±0.01	0.95±0.01
0.84	0.96	16.8	0.72±0.01	0.72±0.01	0.93±0.01
1.05	0.78	18.0	0.69±0.01	0.76±0.01	0.92±0.01
1.26	0.64	19.4	0.66±0.01	0.74±0.01	0.91±0.01
1.47	0.53	20.7	0.63±0.01	0.71±0.01	0.90±0.01

*The errors in the self-screening factors are absolute statistical errors from Monte Carlo calculations. The uncertainty in the ratio or difference of two values is much smaller than implied by these errors

Table 9

(a) Calculated U-238 capture cross-sections averaged over the energy range 0.5 to 25 keV

Parameter Set	σ_γ^∞ (barns)	$\tilde{\sigma}_\gamma$ (barns) for σ_o = 30 b			
		300°K	1500°K	2700°K	3900°K
Standard	2.5221	0.9392	1.2450	1.3915	1.4933
Γ_γ changed	2.5849	0.9577	1.2701	1.4198	1.5238
D changed	2.6990	1.0299	1.3750	1.5390	1.6525
S_o changed	2.6507	0.9657	1.2967	1.4631	1.5819
S_1 changed	2.5901	0.9703	1.2781	1.4251	1.5270

(b) Average resonance parameters used in the calculations

Parameter	Standard Value	Changed Value	Per Cent Change
Γ_γ	23 meV	24 meV	+ 4.3
D	22.5 eV	20 eV	- 11.1
S_o	0.9289×10^{-4}	1.1611×10^{-4}	+ 25
S_1	1.729×10^{-4}	1.9788×10^{-4}	+ 14.4

Table 10

1-4 keV treated as unresolved region using ENDF-B V methodology

E eV	EL-EH eV	$\langle\sigma_{n\gamma}\rangle$ b	p-wave strength function x10^{-4}	σ_o = 10 b			σ_o = 50 b			σ_o = 100 b		
				$\sigma_{n\gamma}f$	$\sigma_{n\gamma}f^*$	Ratio	$\sigma_{n\gamma}f$	$\sigma_{n\gamma}f^*$	Ratio	$\sigma_{n\gamma}f$	$\sigma_{n\gamma}f^*$	Ratio
1000	900-1100	3.044	4.74	1.075	0.852	1.26	1.535	1.257	1.22	1.818	1.525	1.19
1250	1100-1400	2.113	0.50	0.651	0.676	0.96	1.001	1.000	1.00	1.222	1.209	1.01
1500	1400-1600	1.912	1.07	0.708	0.771	0.92	1.026	1.059	0.97	1.216	1.231	0.99
1700	1600-1800	2.087	3.41	0.971	0.737	1.32	1.303	1.068	1.22	1.486	1.281	1.16
1950	1800-2100	1.442	2.76	0.558	0.742	0.75	0.818	0.941	0.87	0.965	1.045	0.92
2250	2100-2400	1.610	2.17	0.824	0.797	1.03	1.081	1.042	1.04	1.215	1.178	1.03
2500	2400-2600	1.640	2.97	0.915	0.671	1.36	1.169	0.919	1.27	1.295	1.070	1.21
2750	2600-2900	1.256	1.12	0.660	0.802	0.82	0.865	0.955	0.91	0.970	1.032	0.94
3000	2900-3100	0.985	1.27	0.464	0.712	0.65	0.646	0.827	0.78	0.738	0.878	0.84
3250	3100-3400	1.455	3.04	0.911	0.932	0.98	1.123	1.133	0.99	1.220	1.231	0.99
3500	3400-3600	1.216	1.86	0.755	0.646	1.16	0.933	0.823	1.13	1.016	0.921	1.10
3750	3600-3800	1.099	1.40	0.681	0.659	1.03	0.843	0.795	1.06	0.919	0.872	1.05
3900	3800-4000	1.094	1.54	0.699	0.699	1.00	0.856	0.836	1.02	0.927	0.909	1.02
	900-2100*			3.963	3.779	1.05	5.683	5.325	1.07	6.707	6.291	1.07
	2100-3100*			2.863	2.983	0.96	3.761	3.743	1.00	4.218	4.158	1.01
	3100-4000*			3.046	2.936	1.04	3.755	2.587	1.05	4.082	3.933	1.04
	900-4000*			9.872	9.698	1.02	13.199	12.655	1.04	15.007	14.425	1.04

*Summation of values

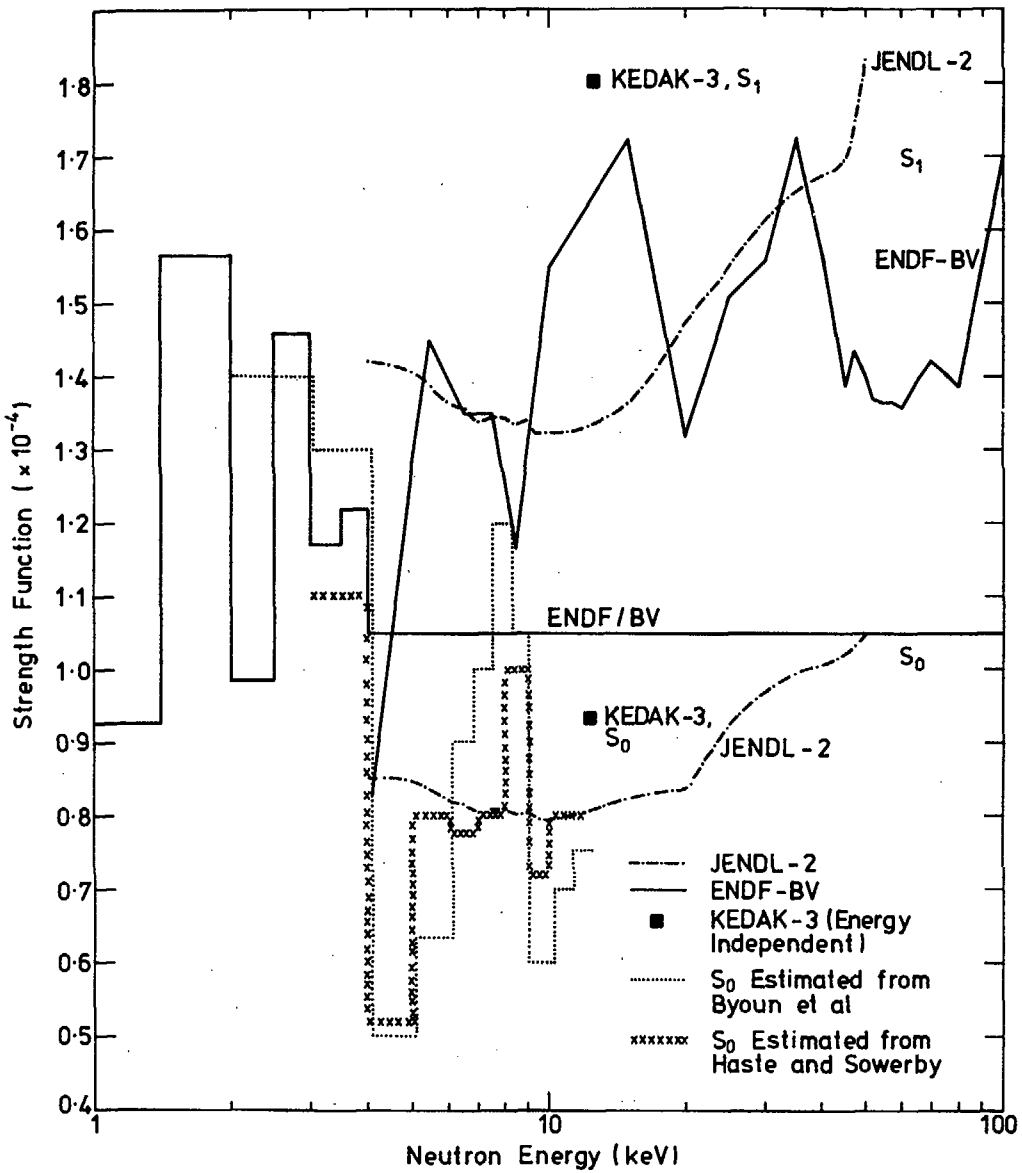

Figure 1

THE VARIATION OF STRENGTH FUNCTIONS WITH NEUTRON ENERGY

Parity Assignment of the Pronounced Structure in the Radiative Capture of Neutrons by ^{238}U Below 100 keV.

M.S. Moore* and F. Corvi
Joint Research Centre, Central Bureau for Nuclear Measurements, Steenweg op Retie, 2440 Geel, Belgium

and

L. Mewissen and F. Poortmans
Centre d'Etude de l'Energie Nucléaire, C.E.N./S.C.K., 2400 Mol, Belgium

Abstract

Some years ago, Perez and de Saussure reported evidence for intermediate structure in the radiative capture cross section of ^{238}U. More recently, these and additional data, obtained by a different experimental technique but which showed the same non-statistical behavior, were analyzed by Perez et al. under the assumption that the structure could be attributed to doorway states in the $p^{1/2}$ neutron channel. In the present paper, we report the results of an experimental determination of the parity of the structure, using neutron capture-gamma ray spectroscopy. We find that much of the structure below 50 keV appears to be due to s-wave interactions. The magnitude of the fluctuations is much larger than can be calculated with the usual unresolved-resonance treatment unless the average neutron and radiative-capture widths are correlated. We show that such an apparent correlation can arise as a result of multiple-scattering enhancement of radiative capture in the samples used, and conclude that the evidence for intermediate structure in the capture of neutrons by ^{238}U is not yet firmly established.

---

* Scientific Visitor to CBNM from Los Alamos National Laboratory

I. Introduction

At the conference on Nuclear Cross Sections and Technology in 1975, Perez and de Saussure[1] noted that there are pronounced fluctuations in the average radiative capture cross section of ^{238}U that are much larger than would be expected from Porter-Thomas fluctuations in the neutron widths. They suggested that these fluctuations might constitute evidence for intermediate structure. In 1979, Perez et al.[2] addressed the problem in more detail. They incorporated additional data by Macklin, obtained by a different experimental technique[3] but which showed the same fluctuations, and applied a number of statistical tests that indicated the existence of non-statistical behavior. They then showed that a modulated strength function in the $p^{1/2}$ neutron channel could provide an explanation of the structure. These results have far-reaching implications. If intermediate structure exists and is important for (^{238}U + n), then, following Müller and Rohr[4] and Kerouac,[5] it should be taken into account for all the actinides, including the fissile species. If the structure is due to doorway states, then the channel-capture mechanism of Lane and Lynn[6] suggests that the neutron and radiative-capture widths may be correlated. It is thus of interest to establish the properties of the structure, and in particular to answer the following two questions: 1) Is the structure due to p-wave interactions, which are responsible for about 2/3 of the capture at 40 keV? 2) Does the structure imply correlated widths?

We addressed this second question as part of a study of practical implications of intermediate structure in ^{235}U and ^{238}U.[7] We concluded that, using the usual statistical treatment of unresolved resonances, the structure in ^{238}U capture seems to require that the neutron and radiative-capture widths be correlated. However, in the present study, we show that such an apparent correlation may be due to the inadequacy of multiple-scattering corrections to the data.

II. Experimental Method and Analysis

Noting that all the lowest-lying levels in ^{239}U have even parity, Corvi et al.[8] suggested that one could measure the intensity of primary transitions feeding these levels relative to transitions to all levels and deduce the parity of resonances in (^{238}U + n), using the property that E1 transitions are on the average much more intense than M1 and E2. Corvi's method was used successfully in assigning 57 resonances as p-wave.
The method cannot be used for assigning all resonances simply because of Porter-Thomas fluctuations in the partial widths for the few most energetic primary transitions. (Only two such transitions are possible for $p^{1/2}$ resonances, and four for $p^{3/2}$ resonances.)

For a determination of the parity of the intermediate structure reported by Perez et al, these fluctuations are negligible. In fact, in a typical 400 eV energy interval there are about twenty $s^{1/2}$ and $p^{1/2}$ resonances, and about forty $p^{3/2}$. If the structure is due to p-wave resonances in which the highest energy primary transitions occur with their expected intensity, the method should give a reliable estimate of the relative p-wave contribution. (One estimates the variance as 4/40 for $p^{1/2}$; 4/160 for $p^{3/2}$).

To investigate the parity of the average capture cross section of ^{238}U in the neutron energy range from 5 to 100 keV, a measurement was performed at the electron linear accelerator laboratory (GELINA) at the Central Bureau for Nuclear Measurements at Geel, Belgium. A 3 mm thick metallic sample of ^{238}U was placed in the neutron beam at a flight path of 30 m. The sample was viewed by a 6" x 7" dia. NaI(Tl)

γ-ray spectrometer placed 20-30 cm away from the sample, outside the neutron beam, and shielded from scattered neutrons by at least 10 cm of borated polyethylene and borated paraffin. Capture gamma spectra were collected as a function of neutron time of flight. The spectra were divided into three gamma-ray energy intervals : 1.5 - 3.5 MeV (LOW BIAS data, representative of transitions from resonances of both parities), 4.3 - 5.2 MeV (HIGH BIAS data, representative of transitions from p-wave structure), and > 5.2 MeV (BACKGROUND data, to give the scattered neutron contribution).

The scattered neutron background was found to be featureless and therefore was ignored. The time-of-flight spectra corresponding to the LOW BIAS and HIGH BIAS data were first averaged over 400-eV intervals, as done by Perez et al. Then a fluctuation analysis was carried out by subtracting from each point a running eleven-interval average. Parity assignments were made by comparing the relative intensity of the HIGH BIAS to that of the LOW BIAS data.

As a check we were able to confirm most of the parity assignments made by Corvi et al. in the resonance region as shown in Table I and we even extended the range of resolved resonances over which parity assignments could be made to 4 keV.

The results are summarized in Fig. 1 where the fluctuations of the LOW BIAS data are superposed on the modulated strength function fit of Perez et al.

A parity assignment is given on top of most of the peaks present in the capture cross section. The conclusions to be drawn are two-fold : firstly the structure observed by Perez et al. is confirmed, secondly the most prominent peaks below 50 keV are found to be due primarily to s-wave interactions, since they do not involve the highest energy transitions.

III. Multiple Scattering Enhancement of the Capture Yield.

Our finding that the structure in the capture cross sections below 50 keV is mainly due to s-wave interactions is in contrast with the surmise of Perez et al, who foresee a set of doorway states in the $p^{1/2}$ neutron channel. Furthermore such a structure can not be explained by doorway states in the $s^{1/2}$ entrance channel. In fact, in the whole energy range under consideration here the neutron widths of s-wave resonances are on the average much larger than the radiation width. This results in the average capture being roughly proportional to the total radiation width alone : therefore even a considerable local enhancement of the neutron strength function has little effect on the capture cross section. This simple fact was confirmed by a series of calculations of the observed fluctuations[7] using the prescribed unresolved resonance treatment of ENDF/B that allows an energy-dependent average neutron width but assumes a Porter-Thomas distribution within the averaging interval. We found it impossible to obtain a consistent fit to the fluctuations in the capture cross section and to the total cross section measured by Olsen et al.,[9] unless the neutron and radiative-capture widths are correlated. Such an apparent correlation could arise from a purely experimental effect: multiple scattering enhancement of the observed capture, which is particularly important for s-wave resonances that are strongly asymmetric in scattering.

It should be noted that multiple scattering corrections are treated differently in the resolved and unresolved resonance regions. In the resolved region, one uses initial values of the resonance parameters to calculate energy-dependent Doppler-broadened cross sections from which the relative interaction probabilities can be calculated as a function of energy and scattering angle, the final resonance parameters being determined by an iterative process. In the unresolved range, a Porter-Thomas distribution of neutron widths about the average is generally assumed, and the interaction probabilites corrected for width fluctuations are used to calculate a multiple-scattering correction that varies smoothly with neutron energy.

In order to determine whether these differences in approach give significantly different estimates for the multiple-scattering enhancement, we chose one particular-

ly strong s-wave resonance clump, that at 37 keV, for further study. The high-resolution total-cross-section measurements of Olsen et al.[9] appear to confirm our conclusion that this region is dominated by several particularly strong s-wave resonances. We carried out an R-function fit to these data in the region between 36.5 and 38.0 keV, using the MULTI code developed by Auchampaugh,[10] in order to obtain a set of typical resonance parameters that would describe the data. The typical parameters are listed in Table II. The fits we obtained are shown in Figs. 2 and 3, Fig. 2 being the fit to the measured total cross section and Fig. 3 being the 300K Doppler broadened cross section that is appropriate for the multiple scattering calculations.

We then carried out a calculation of the energy-dependent capture yield in this energy region using a hybrid code in which the "resolved-resonance parameters" of Table II were used to describe the s-wave interactions and the usual unresolved resonance treatment described above was used for p-wave interactions. In this calculation, the capture yield with and without multiple scattering enhancement was tabulated, in order to determine the magnitude of the effect, for various sample thicknesses used in the measurements.

The results of this exercise showed that a surprisingly strong energy dependence of the multiple-scattering enhancement can be expected. In the case of our experiment such an enhancement ranges from 16 to 24% within the 37 keV clump, and is about 10% away from this clump. One of the data sets considered by Perez et al.[1,2] is that of de Saussure et al.[11], who calculated a correction of 3.8% for multiple scattering and self screening for their thickest sample between 30 and 40 keV. This is in good agreement with the value we obtain at energies far away from the 37 keV clump, yet within the clump, the calculated multiple-scattering enhancement of the capture yield can be as large as 10% for this same sample thickness.

The importance of such an effect can therefore provide an explanation for at least part of the fluctuations observed in the capture yield of ^{238}U.

While the present results do not preclude the existence of intermediate structure in the capture cross section of ^{238}U, they do suggest that further study may be needed. Before one applies statistical tests to determine whether the magnitude of the fluctuations is outside the range expected from statistical theory, either an improved multiple-scattering treatment is required, or the data used should have been obtained only with samples so thin that this effect is negligible.

References

1. R. B. Perez and G. de Saussure, in "Nuclear Cross Sections and Technology," NBS Spec. Pub. 425, Vol. II, p. 623 (1975).
2. R. B. Perez, G. de Saussure, R. L. Macklin, and J. Halpern, Phys. Rev. C20, 528 (1979).
3. R. L. Macklin, Nucl. Inst. Methods 91, 79 (1971).
4. K. N. Müller and G. Rohr, Nucl. Phys. A164, 97 (1971).
5. G. J. Kerouac, in "Nuclear Cross Sections and Technology," NBS. Spec. Pub. 425, Vol. I, p. 338 (1975).
6. A. M. Lane and J. E. Lynn, Nucl. Phys. 17, 553, 586 (1960); see also J. E. Lynn, "Theory of Neutron Resonance Reactions," Clarendon Press, (1968), p. 326; A. M. Lane, in "Statistical Properties of Nuclei," Plenum Press (1972), p. 271.
7. M. S. Moore, in "1980 Advances in Reactor Physics and Shielding," Amer. Nucl. Soc., Inc. (1980), p. 656.
8. F. Corvi, G. Rohr, and H. Weigmann, in "Nuclear Cross Sections and Technology," NBS Spec. Pub. 425, Vol. II, p. 733 (1975).

9. D. K. Olsen, G. de Saussure, R. B. Perez, F. C. Difilippo, R. W. Ingle, and H. Weaver, Nucl. Sci. Eng. 69, 202 (1979); see also ORNL/TM 5915 (1977).

10. G. F. Auchampaugh, USAEC Report LA-5473-MS (1974).

11. G. de Saussure, E. G. Silver, R. B. Perez, R. Ingle, and H. Weaver, Nucl. Sci. Eng. 51, 385 (1973), see also ORNL/TM 4059 (1973).

Table I. Energies, in eV, of resolved resonances in (^{238}U + n) assigned as p-wave from the present study and from Corvi et al. (shown with an asterisk). Assignments of Corvi et al. that were not confirmed in the present study are designated by a double asterisk.

63.51**	439.74*	828.75*	1289.3	2049.0	3378.3
83.68*	448.36	940.94	1317.0*	2063.3	3383.8
89.29*	498.88*	964.45*	1332.0**	2071.4	3522.3
98.17	523.33*	977.36**	1387.1**	2215.4	3528.5
124.98*	542.71*	1029.1*	1417.5*	2294.0	3636.9
158.95	550.98*	1047.3*	1454.8	2296.5	3654.2
200.71*	556.24*	1067.7*	1486.8	2397.8	3683.2
203.11*	560.12	1074.1*	1510.6*	2401.8	3724.7
214.85*	584.46	1081.7*	1534.9*	2527.1	3791.1
218.32*	615.75*	1095.2*	1550.6**	2606.6	3809.2
224.97	624.20*	1102.9*	1568.5	2658.6	3825.7
242.71*	668.41*	1131.4*	1672.7	2682.8	3927.9
253.89*	677.74*	1152.7*	1745.7	2945.3	
263.93*	698.21*	1155.1*	1768.6	3043.8	
275.11*	710.59*	1184.8	1797.5	3072.3	
282.43*	713.77*	1201.4	1834.2	3081.1	
322.86	732.46*	1219.9*	1893.9	3169.8	
337.25*	743.14	1230.1*	1925.4	3264.1	
351.86*	779.31*	1252.0**	1990.0	3267.5	
372.84*	787.33*	1277.0*	2000.7	3341.2	

Table II. A typical set of "resolved-resonance parameters" that can be used to describe the unresolved s-wave structure in the total cross section of (^{238}U + n) near 37 keV. The radiative capture width is assumed to be 0.02 eV for all resonances.

E_o(keV)	Γ_n(eV)	E_o(keV)	Γ_n(eV)	E_o(keV)	Γ_n(eV)	E_o(keV)	Γ_n(eV)
36.510	0.004	36.910	0.004	37.222	0.555	37.605	0.004
36.530	0.004	36.920	0.941	37.232	0.105	37.625	0.445
36.550	0.462	36.930	0.512	37.250	0.171	37.635	0.527
36.570	0.004	36.947	0.004	37.265	0.135	37.662	0.004
36.590	0.004	36.970	1.332	37.285	0.004	37.682	0.004
36.615	0.375	36.980	0.232	37.305	0.004	37.700	0.040
36.635	0.004	36.994	0.004	37.325	0.004	37.720	0.004
36.665	0.285	37.010	0.040	37.345	0.004	37.740	0.004
36.685	0.004	37.030	0.004	37.365	0.166	37.760	0.004
36.700	0.285	37.060	0.345	37.390	0.932	37.785	0.324
36.710	0.347	37.065	0.206	37.410	0.475	37.805	0.004
36.732	0.004	37.080	2.964	37.430	0.846	37.825	0.004
36.752	0.004	37.090	0.154	37.440	0.077	37.838	0.303
36.777	0.040	37.110	0.004	37.450	0.697	37.868	0.004
36.797	0.004	37.135	1.356	37.470	1.049	37.888	0.004
36.817	0.004	37.145	0.430	37.505	0.241	37.908	0.004
36.837	0.004	37.160	0.004	37.515	0.298	37.933	0.628
36.857	0.004	37.180	0.214	37.545	0.004	37.948	0.418
36.875	0.582	37.198	0.402	37.565	0.004	37.968	0.004
36.885	0.795	37.205	1.062	37.585	0.040	37.988	0.004

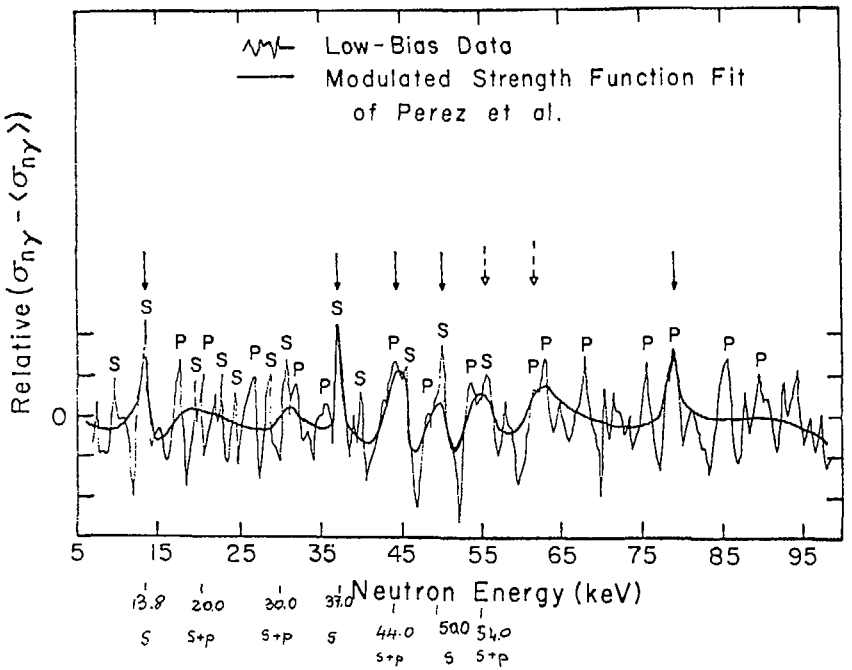

Fig. 1

Parity assignments of relative fluctuations in the capture cross section of (^{238}U + n). The fluctuations were determined by binning the data in 400 eV bins, and subtracting from each point a running eleven-bin average. Parity assignments were made by the method of Corvi et al. by the relative intensity of primary transitions to levels near the ground state of ^{239}U as a p-wave signature. The smooth curve shows a schematic representation of the intermediate structure proposed by Perez et al. described in the text.

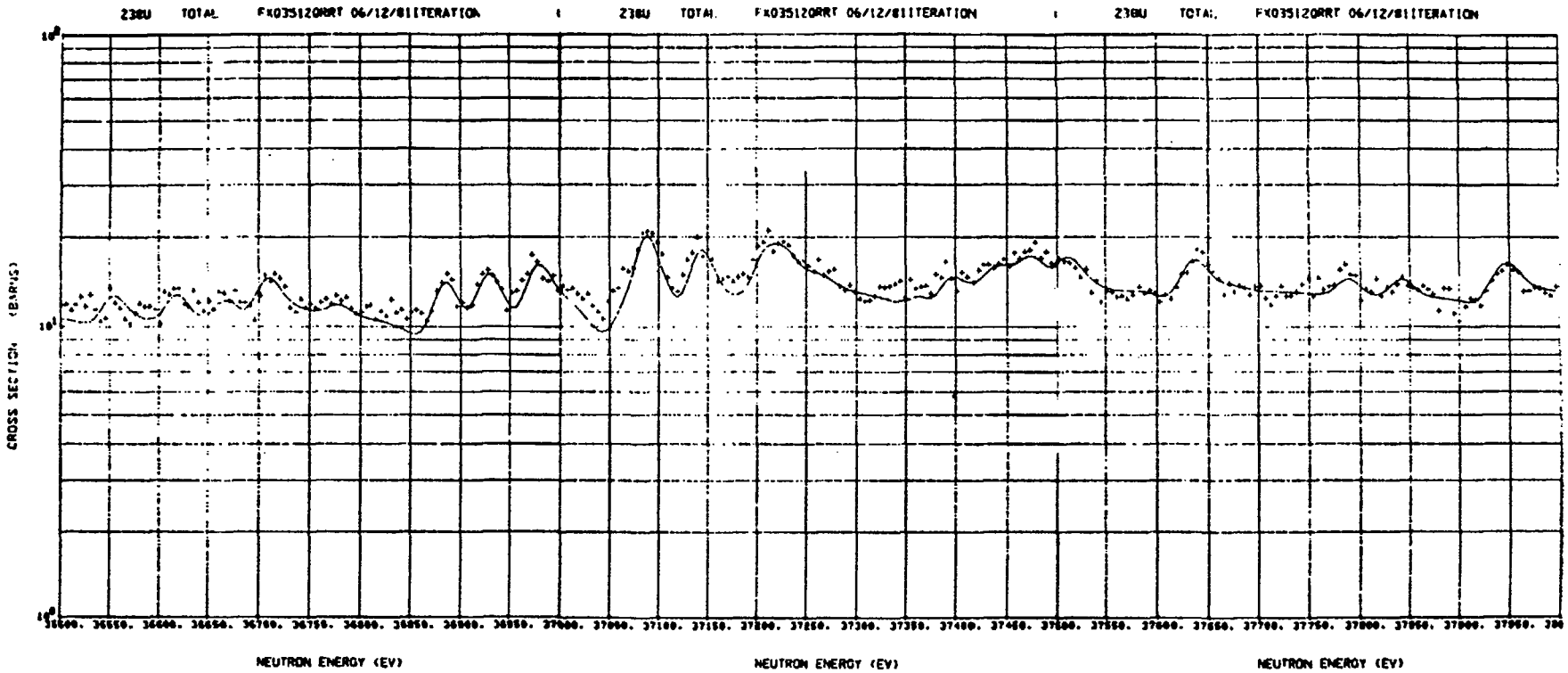

Fig. 2 Representation of the total cross section of (^{238}U + n) measured by Olsen et al. between 36.5 and 38.0 keV. The smooth curve is a resolution-broadened least-squares R-function fit to the data, which gave the parameters listed in Table II.

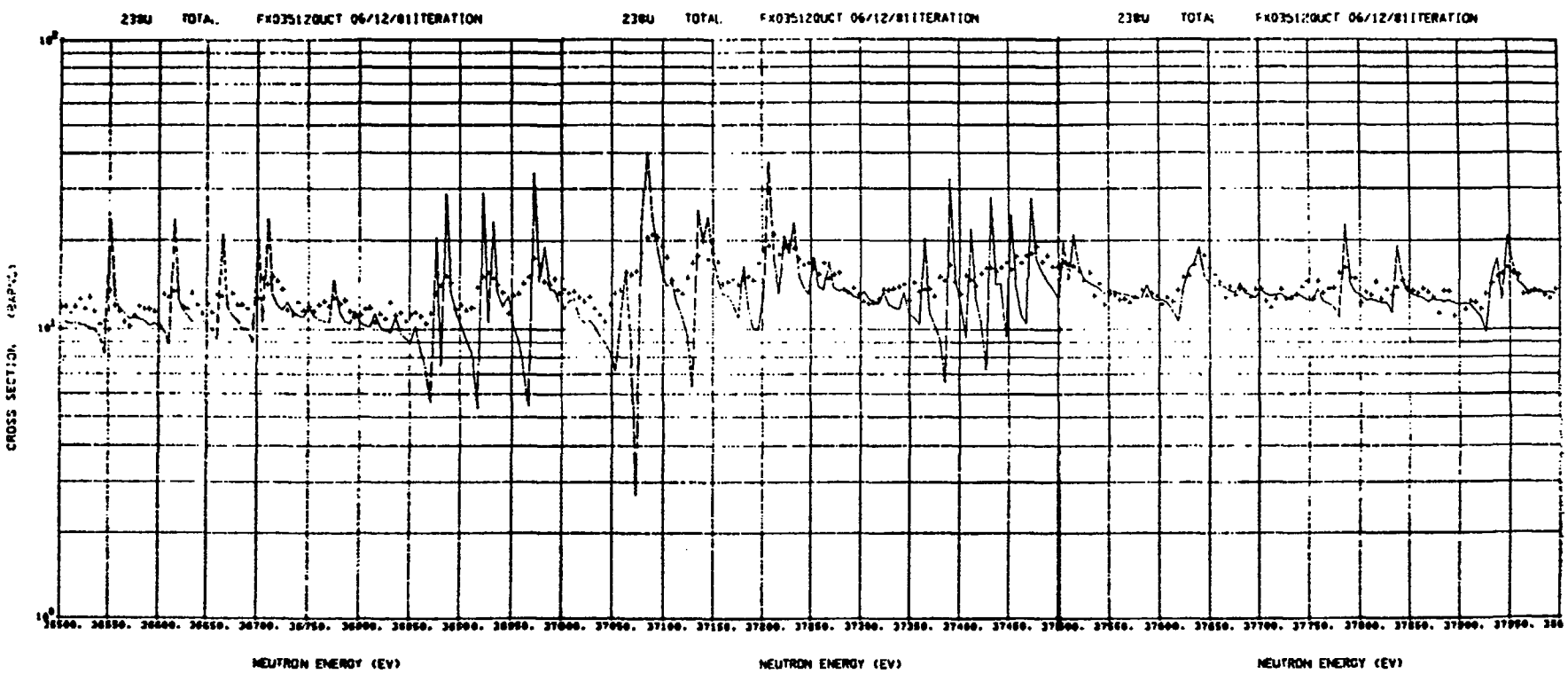

Fig. 3 Representation of the total cross section of (^{238}U + n) measured by Olsen et al. between 36.5 and 38.0 keV. The smooth curve shows the R-function calculated energy dependence that would be observed with perfect resolution using the parameters of Table II.

Review of ^{240}Pu and ^{242}Pu Resolved Resonance Parameters

H. Weigmann

ABSTRACT

The present status of the knowledge of resolved resonance parameters of ^{240}Pu and ^{242}Pu is reviewed. Apart from a few specific problems which are addressed to in detail, this knowledge is adequate to satisfy the requirements for practical purposes.

I. INTRODUCTION

The two isotopes ^{240}Pu and ^{242}Pu have many common features : the level density, the neutron strength functions, and the average radiative widths are of the same order of magnitude, both isotopes have fission thresholds at about 600 keV neutron energy, and both show the characteristic intermediate structure in sub-barrier fission cross sections. Nevertheless, not only experimental, but also evaluation work has rarely been done simultaneously for both isotopes. Moreover, our knowledge of the resonance parameters of the two nuclei has experienced a rather different history. Therefore, in the present paper the two isotopes will also be treated separately, in section II and III, respectively. For each nucleus, in sub-section 1 a short review and some general references will be given, sub-section 2 will discuss special low energy resonances and their relation to the thermal cross section, sub-section 3 will deal with the bulk of resonances for each isotope, in sub-section 4 the statistical properties of the resonances will be discussed, and sub-section 5 will deal with fission parameters. Finally, in section IV some general conclusions will be drawn.

II. ^{240}Pu

1. General Review

The history of our knowledge of the resonance parameters of ^{240}Pu has been characterized by surprising developments. Not only has ^{240}Pu been one of the first nuclei for which intermediate structure in sub-barrier fission had been detected; it has also typified the difficulties encountered in the analysis of these data (see sub-section I.5). Moreover, the resonance parameters like neutron and capture widths have been subject to important changes in the corse of time.

The first extensive measurements in the resonance region were in the late 60's [1-3] , followed by full evaluations [4,5] . Soon afterwards, a careful measurement of the parameters of the 20.45 eV resonance performed at Harwell [6] led to a renormalization of the older capture data [6,7] which then showed good agreement with another more recent measurement [8] . The status of the revised parameters is summarized and discussed in detail in an earlier review [9] . Most of what has been said in ref.[9] is still valid, with the exception of the discussion of fission parameters which have been superceded by very accurate new measurements [10] . More recent reviews have been given in connection with evaluations by Goel and Krieg [11] and, for the ENDF/B-V evaluation, by Weston and Wright [12] .

2. The 1.056 eV Resonance

The low energy region and the thermal cross sections are dominated by the very strong resonance at 1.056 eV neutron energy. The most precise value of the thermal capture cross section has been obtained by Lounsbury et al. [13] to be

$$\sigma_{n\gamma}\,(\text{therm}) = (289.5 \pm 1.4)\ \text{b}$$

The contribution to this cross section from the higher energy resonances is about 1 barn. If one assumes that the contribution from bound states does not exceed a few barns either, the thermal cross section value fixes the product of the neutron and capture widths of the 1.056 eV resonance to about 1%. Experimental data on the individual parameters were rather discrepant, however, with neutron widths ranging from 2.06 to 2.4 meV and radiative widths from 28.7 to about 38 meV. Most evaluators [4,5,12] have favoured neutron widths around 2.3 meV and radiative widths around 33 meV. Preliminary results from new extensive measurements at BNL [14] yield

$$\Gamma_n = (2.32 \pm 0.06)\ \text{meV} \qquad \Gamma_\gamma = (32.4 \pm 1.0)\ \text{meV}$$

in close agreement with the evaluations [4,5,12] and with the thermal cross section.

3. Resolved Resonance Parameters

The numerical values of the revised neutron and capture widths from Harwell [6] and Geel [9] are given in ref. [9] . Together with the parameters from RPI [8] , these three sets of experimental data form the main data basis for resolved resonance parameters of ^{240}Pu. In the range of overlap, i.e. up to 665 eV neutron energy, they are in acceptable agreement with each other. In this range, most evaluators [11,12,15] , including Weston and Wright in their evaluation for ENDF/B-V, adopt weighted averages of the parameters from these three sets. At higher energies, the neutron widths from Geel [2] are the only parameters available and are adopted for the evaluations.

4. Statistical Properties of Resonances

There is a general consensus between different evaluators with respect to the average resonance parameters.

For the average level spacing, values between 12.7 eV and 13.5 eV are found [9,16,17] . In a recent systematic analysis [18] the level spacings of actinides have been obtained by fitting a Porter-Thomas distribution to the reduced neutron widths above a predefined bias, thus correcting for missed levels or admixtures of p-wave levels in the set of resonances. In repeating the procedure for different bias values, the minimum bias above which the neutron width distribution

is unaffected by missed levels or p-wave resonances, is obtained, and the systematic uncertainty of the method is estimated. The case of ^{240}Pu is shown in Fig.1. The smooth curve corresponds to a level spacing of 13 eV. This value is also listed in Table 1 together with other average resonance parameters for both, ^{240}Pu and ^{242}Pu.

The remaining parameters for ^{240}Pu given in Table 1 have been taken over from ref. [9]; the apparent change of the p-wave strength function is due only to the fact that the value of ref.[9] was given for a channel radius of 9.1 fm, whereas for the value of Table 1 we have used a channel radius of 8.44 fm, in accord with present convention [19].

According to Weston and Wright [12] the average resonance parameters of ref.[9] well reproduce the experimental average capture cross section of Weston and Todd [20], and have therefore been adopted for ENDF/B-V. Very similar values have also been given by several other authors [11,16,17].

5. Fission Parameters

The analysis [21,9] of the earlier sub-barrier fission measurements [21] suffered from the fact that the largest fission width within each cluster of sub-barrier resonances remained essentially undetermined, because for these resonances the fission width exceeded by far the neutron width, and thus the resonance area was essentially independent of the fission width. Only the later measurement of Auchampaugh and Weston [10] allowed, due to its improved neutron energy resolution, a shape analysis of those resonances and showed that their fission widths were as large as a few eV. Fig.2 shows the data for the cluster around 780 eV neutron energy. The widths of the resonances at 791, 811, and 820 eV are determined by the resolution which at 800 eV is $\approx$ 1.6 eV. It can be seen from the figure that the 782 eV resonance is slightly broader.

Fission widths for resonances between 600 eV and 2860 eV neutron energy are given in ref.[10]. Rough averages of the parameters $\Gamma^{\downarrow}$ and $\Gamma^{\uparrow}$, including the $\Gamma^{\downarrow}$ -value derived from the parameters of the almost degenerate 1405-eV doublett, are

$$\Gamma^{\downarrow} \approx 1.5 \text{ eV} \qquad \Gamma^{\uparrow} \approx 2.5 \text{ eV}$$

With these rather large values of $\Gamma^{\downarrow}$ and $\Gamma^{\uparrow}$, it is probable that no class II levels have escaped detection, and the average class II spacing is

$$D_{II} = (450 \pm 50) \text{ eV}$$

Apart from the resonances with fission widths enhanced by the intermediate structure effect, the remaining resonances are expected to possess a "background" fission width due to direct tunneling through both barriers according to

$$\Gamma_f \text{ (backgr.)} = D_I/8\pi . P_A P_B$$

Extracting the penetrabilities P_A and P_B from the above estimates for $\Gamma^{\downarrow}$ and $\Gamma^{\uparrow}$,

$$P_A = 2\pi \, \Gamma^{\downarrow} / D_{II} \qquad P_B = 2\pi \, \Gamma^{\uparrow} / D_{II}$$

one obtaines as an expectation value for the "background" fission width

$$\Gamma_f \text{ (backgr.)} = 0.38 \text{ meV}$$

which compares reasonably well to the measured "background" fission width [10] of 0.4 meV, as well as to the fission widths of the three lowest energy resonances at 1.056 eV, 20.45 eV, and 38.32 eV, which are 0.006, 0.23 and 0.11 meV, respectively [9].

III. ^{242}Pu

1. General Review

Our knowledge of the resonance parameters of ^{242}Pu has developed more smoothly than was the case for ^{240}Pu, but, as will be discussed below, the present status is less satisfying than that of ^{240}Pu.

There have been essentially three extensive measurements in the resonance region [22-24], two of which have, however, only partly been analysed.

The number of essentially complete evaluations is rather large [25-29,17]. Only one extensive measurement of the sub-barrier fission cross section has been reported until now [30], but fission widths obtained by combining these data with the analysis of other resonance parameter measurements are given in ref. [22,24].

2. Thermal Region and Lowest Energy Resonances

The accurate measurements of the thermal cross sections by Young and Reeder [31] and Young et al.[32] have been generally adopted. The lowest positive energy resonance at 2.67 eV neutron energy essentially accounts for the thermal cross sections, if its radiative width is adjusted to 26 meV [25]. On the other hand, Menapace et al. [27] choose to use a smaller radiative width, equal to the average radiative width of the higher energy resonances, and add a bound state at - 13.3. eV to account for the thermal cross section. However, these small differences in the interpretation of the thermal data should not cause any trouble.

3. Resolved Resonance Parameters

Of the three extensive measurements in the resonance region, the one by Poortmans et al. [22] is the most complete one. It comprises capture, elastic scattering, and total cross section measurements, and resonance analysis has been carried out up to 1290 eV neutron energy. The high resolution transmission measurements of Simpson et al. [23] with metal samples cooled to liquid nitrogen temperature, have only been analysed up to 500 eV neutron energy. Within this energy range, the neutron widths of ref. [22,23] agree very well, but the capture widths of ref. [23] are on the average larger than those of ref. [22]. However, at the lowest neutron energies, where the transmission data should give the most reliable capture widths, the Γ_γ-values of ref. [23] are lower than on the average, and more close to ref. [22]. The extensive transmission measurements of Auchampaugh and Bowman [24] have only been analysed for those resonances between 590 eV and 3840 eV

neutron energy which in the sub-barrier fission measurement [30] have shown a non-zero fission yield. For several of the resonances in the range of overlap, disturbing discrepancies are found between the neutron widths of ref. [22,24] , which cannot be resolved at present.

Most evaluations adopt either the resolved resonance parameters of Poortmans et al. because they are based on the most complete set of measurements [28], or in the range of overlap use a weighted average of the three extensive measurements [15,27,29] .

4. Statistical Properties of Resonances

There is considerable confusion with respect to the average level spacing of ^{242}Pu. Roughly speaking, level spacings given in the literature fall into two groups, namely values around 17 to 18 eV [18,22,27] and values between 12.4 and 14.2 eV [17,25,28,29] . The reason for the problem may be seen from Fig.3, which shows the measured neutron width distribution and a Porter-Thomas distribution fitted to the measured one above a bias of 0.08 meV, yielding a level spacing of 17.5 eV [18] .

There is clearly a surplus of levels with small reduced neutron widths which, if the level spacing of 17.5 eV ought to be correct, had to be explained as being due to p-wave resonances. More precisely, 10 out of the 24 resonances with $\Gamma_n^o \leq 0.15$ meV would have to be assigned p-wave. In Table 2, these 24 resonances are listed together with their reduced neutron widths for s-wave as well as p-wave assignment(for the p-wave reduced widths a channel radius of 8.46 fm has been used). In the last column of the table, the 13 resonances with the smallest Γ_n^1 are indicated by (1).

Table 3 serves to show that the assumption that all of these 13 resonances are in fact p-wave, is compatible with a reasonable p-wave strength function: assuming a p-wave strength function of $S_1 = 2.5 \cdot 10^{-4}$, and a p-wave level spacing of $D_1 = 6$ eV (from the s-wave level spacing of 17.5 eV and a spin cut-off parameter of $\sigma^2 = 36$), the average reduced p-wave width is $< g\Gamma_n^1 > = 4.5$ meV, and the expected total number of p-wave resonances in the energy range under consideration, is 215. Among the 13 levels marked by (1) in Table 2, there are 2, 7 and 13 with $g\Gamma_n^1 / < g\Gamma_n^1 >$ larger than 7, 4 and 1.5, respectively, corresponding to a fraction of the total number of p-wave levels as indicated in column 3 of Table 3. In column 4 of that table, the corresponding fraction as expected from the Porter-Thomas distribution, is given. As can be seen, the observed fraction never significantly exceeds the expected one. Thus the assumption that even 13 (instead of the 10 required) of the weak levels of Table 2 are indeed p-wave, is compatible with a reasonable p-wave strength function.

We thus recommend a level spacing of 17.5 eV, and this value is again listed in Table 1 together with other average resonance parameters for ^{242}Pu, which we will shortly comment on :

There is no problem with respect to the s-wave strength function with literature values [17,22,27-29] concentrating around the figure given in Table 1.

Values for the p-wave strength function as obtained from fits to the average capture cross section in the unresolved resonance region are given in ref. [27,28,33]; the value of Table 1 is a rough average of these.

There is some spread in the values given for the average capture width, due to the above-mentioned differences in the experimental data of ref.[22,23] . Most evaluations [27-29] adopt values between 22 and 25 meV. Fits to the average capture cross section [27,33] result in radiative widths of the same order; however they have been obtained using comparatively low values for the level spacing.

The differences in the average level spacings and radiative widths of ^{240}Pu and ^{242}Pu are qualitatively explainable by the different neutron binding energies.

5. Fission Parameters

The sub-barrier fission cross section has been measured with high statistical precision with an underground nuclear explosion as the pulsed neutron source [30] . As mentioned above, these data have been analysed in the course of resonance parameter analysis of total cross section measurements [24] . The analysis meets the characteristic difficulty mentioned already in connection with the older analysis of the ^{240}Pu fission data, i.e. for the resonance with the largest fission width within each cluster only a lower limit to the fission width is obtained. Moreover, there is the well-known ambiguity in the interpretation due to the fact that the parameters Γ^A and Γ^B are interchangeable. In fact, the cluster around 762 eV neutron energy has also been analysed in connection with the resonance parameter studies of ref. [22] and there the data have been interpreted as being due to a class II state with a large fission width. Due to the inclusion of radiative capture data in the analysis of ref. [22], a more precise value of the fission width of the 762 eV resonance could be obtained. However, the data are not sufficiently complete in order to extract class II resonance parameters with the necessary reliability. A new sub-barrier fission measurement is presently under way at Geel. Although it aims mainly at a high resolution measurement of the fission cross section in the higher keV energy range, some additional information on the low energy resonances may be obtained as well.

IV. CONCLUSION

In conclusion, we may state that our knowledge of the resonance parameters of ^{240}Pu and ^{242}Pu is to the most part adequate for practical purposes. Particularly noteworthy is the improved knowledge of the 1.056 eV resonance parameters of ^{240}Pu due to the new measurements at BNL [14] .

In the case of ^{242}Pu the following problems still exist :

1. There are some uncertainties in the capture widths of ^{242}Pu resonances, due to discrepancies between the experimental data of ref. [22,23] . Also,the neutron widths of a few resonances are strongly discrepant in ref. [22,24] . These discrepancies should be resolved by additional measurements.

2. Most evaluations for ^{242}Pu need to be updated with respect to the average level spacing and possibly also to quantities derived when using a low value for the level spacing.

REFERENCES

[1] M. Asghar, M.C. Moxon and N.J. Pattenden, Nuclear Data For Reactors, IAEA, Vienna 1966

[2] W. Kolar and K.H. Böckhoff, J. Nucl. En. 22 (1968) 299.

[3] H. Weigmann and H. Schmid, J. Nucl. En. 22 (1968) 317.

[4] J.P. L'Heriteau and P. Ribon, CEA-N-1273/EANDC(E) 126 AL (1970).

[5] M. Caner and S. Yiftah, IA-1243 (1972).

[6] M.C. Moxon, Private Communication 1972.

[7] H. Weigmann and J.P. Theobald, J. Nucl. En. 26 (1972) 643.

[8] R.W. Hockenbury, W.R. Moyer and R.C. Block, Nucl. Sci. Eng. 49 (1972) 153.

[9] H. Weigmann, G. Rohr and F. Poortmans, NEANDC(E) 163 U (1975) 219.

[10] G.F. Auchampaugh and L.W. Weston, Phys. Rev. C12 (1975) 1850.

[11] B. Goel and B. Krieg, KfK 2386/3 (1979) 15.

[12] L.W. Weston and R.Q. Wright, Nuclear Cross Sections For Technology, NBS Special Publication 594 (1980) 464.

[13] M. Lounsbury, R.W. Durham and G.C. Hanna, Nuclear Data For Reactors, IAEA, Vienna 1970, Vol.I p. 287.

[14] H.I. Liou and R.B. Chrien, Private Communication 1981.

[15] S.F. Mughabghab and D.I. Garber, BNL-325, Third Edition, Vol.I (1973).

[16] G.V. Antsipov, V.A. Konshin and E.Sh. Sukhovitskij, Proc. Third All-Union Conf. on Neutron Physics, Kiev 1975, p. 21

[17] F.H. Fröhner, U. Fischer and H. Jahn, NEANDC(E) 202 U (1979), Vol. V, 31

[18] H. Weigmann, Proc. Int. Conf. on Neutron Physics and Nuclear Data, Harwell 1978, p. 969.

[19] M.R. Bhat, Brookhaven Nat. Lab. Report BNL 50296 (1971).

[20] L.W. Weston and J.H. Todd, Nucl. Sci. Eng. 63 (1977) 143.

[21] E. Migneco and J.P. Theobald, Nucl. Phys. A112 (1968) 603.

[22] F. Poortmans, G. Rohr, J.P. Theobald, H. Weigmann and G.J. Vanpraet, Nucl. Phys. A207 (1973) 342.

[23] O.D. Simpson, F.B. Simpson, H.G. Miller, J.A. Harvey and N.W. Hill, Oak Ridge Nat. Lab. Report ORNL-4844 (1973), p. 90.

[24] G.F. Auchampaugh and C.D. Bowman, Phys. Rev. C7 (1973) 2085.

[25] M. Caner and S. Yiftah, IA-1275 (1973)

[26] F. Mann and R.E. Schenter, HEDL-TME 77-54 (1977)

[27] E. Menapace, M. Motta and A. Ventura, Proc. Specialists Meeting on Nuclear Data of Plutonium and Americium Isotopes for Reactor Applications, BNL 50991 (1979), p. 251

[28] G.V. Antsipov, L.A. Bakhanovich, V.A. Konshin, V.M. Maslov, G.B. Norogovskij, E.Sh. Sukhovitskij and Yu.V. Porodzinskij, INDC (CCP)-150/LJH (1979), p.1

[29] M. Kawai and T. Murata, NEANDC(J)-61/U (1979), p. 58

[30] G.F. Auchampaugh, J.A. Farrell and D.W. Bergen, Nucl. Phys. A171 (1971) 31

[31] T.E. Young and S.D. Reeder, Nucl. Sci. Eng. 40 (1970) 389.

[32] T.E. Young, F.B. Simpson and R.E. Tate, Nucl. Sci. Eng. 43 (1971) 341.

[33] R.W. Hockenbury, A.J. Sanislo and N.N. Kaushal, Nuclear Cross Sections and Technology, NBS Special Publication 534 (1975) 584.

Table 1 Average Resonance Parameters of ^{240}Pu and ^{242}Pu

	^{240}Pu	ref.	^{242}Pu	ref.
D [eV]	13.0 ± 0.7	18	17.5 ± 1.0	18
$\bar{\Gamma}_\gamma$ [meV]	30.8 ± 1.0	9 , 12	24 ± 2	27 - 29
R_e [fm]	8.44		8.46	
S_0	$\left(1.04 \begin{smallmatrix} +0.14 \\ -0.12 \end{smallmatrix}\right) \cdot 10^{-4}$	9 , 12	$(0.9 \pm 0.1) \cdot 10^{-4}$	22,27-29
S_1	$(2.56 \pm 0.24) \cdot 10^{-4}$	9 , 12	$\approx 2.6 \cdot 10^{-4}$	27,28,33

Table 2. ^{242}Pu Resonances with small Γ_n^o

E_{res} [eV]	Γ_n^o [meV]	$g\Gamma_n^l$ [meV]	remark
14.60	0.016	320.	
22.57	0.060	776.	
40.95	0.070	499.	
88.45	0.070	231.	
141.43	0.010	20.7	(1)
163.5	0.041	73.3	
210.0	0.029	40.4	
219.3	0.020	26.6	(1)
264.5	0.022	24.3	(1)
271.95	0.010	10.7	(1)
274.75	0.010	10.6	(1)
281.05	0.008	8.3	(1)
327.6	0.028	25.0	(1)
379.63	0.014	10.8	(1)
396.1	0.13	96.0	
399.9	0.09	65.8	
425.15	0.0134	9.2	(1)
473.7	0.044	27.2	(1)
494.75	0.012	7.1	(1)
665.0	0.105	46.2	
727.6	0.12	48.3	
761.2	0.14	53.8	
824.5	0.10	35.5	(1)
1117.	0.15	39.4	(1)

Table 3. Fraction F of resonances with $g\Gamma_n^l / \langle g\Gamma_n^l \rangle$ larger than X

X	number of reson. (experim.)	F (experim.)	F (Porter-Thomas)
7	2	$9.3 \cdot 10^{-3}$	$8.2 \cdot 10^{-3}$
4	7	0.033	0.046
1.5	13	0.060	0.22

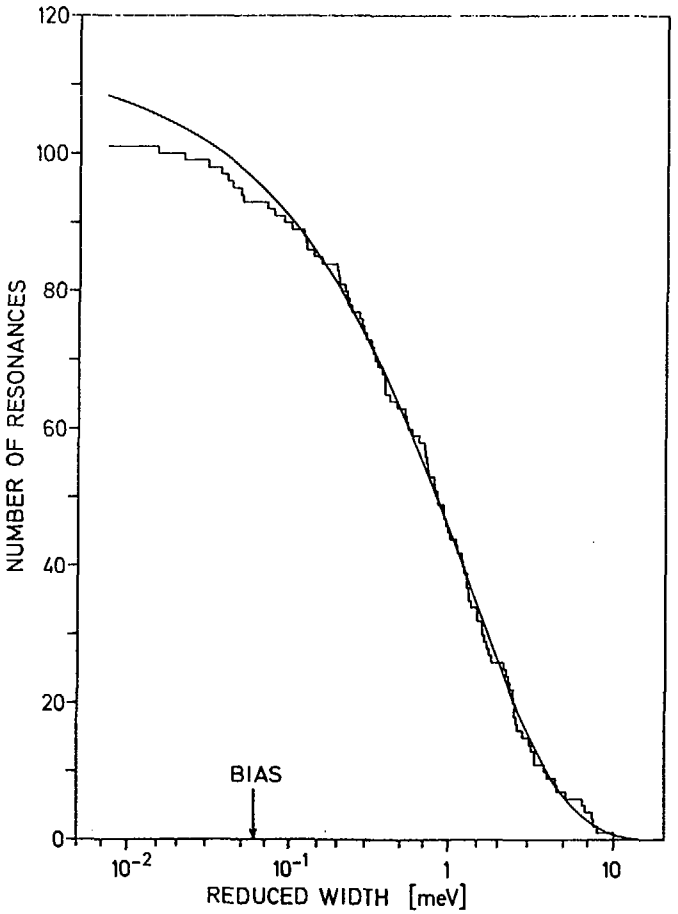

Fig. 1 : Fit of the neutron width distribution of ^{240}Pu resonances for a determination of the average level spacing.

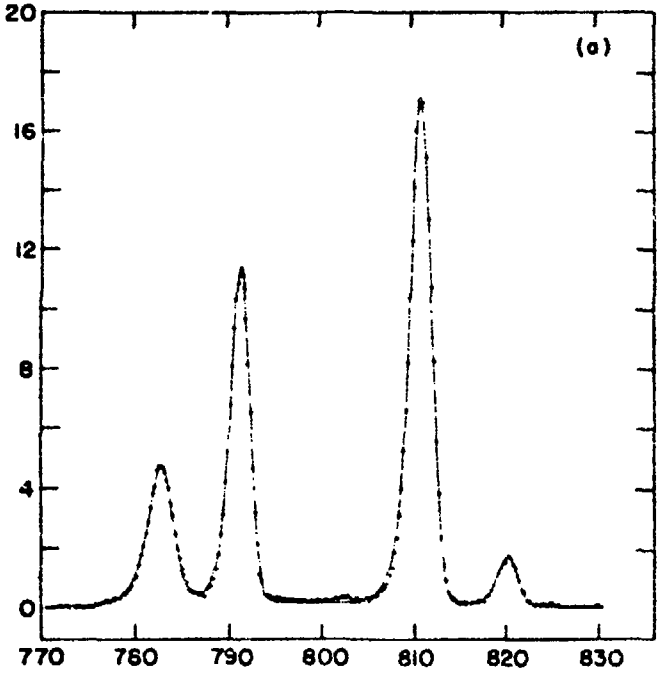

Fig. 2 : The fission cross section of ^{240}Pu in the region of the first sub-barrier fission cluster around 782 eV neutron energy ; after Auchampaugh and Weston [10].

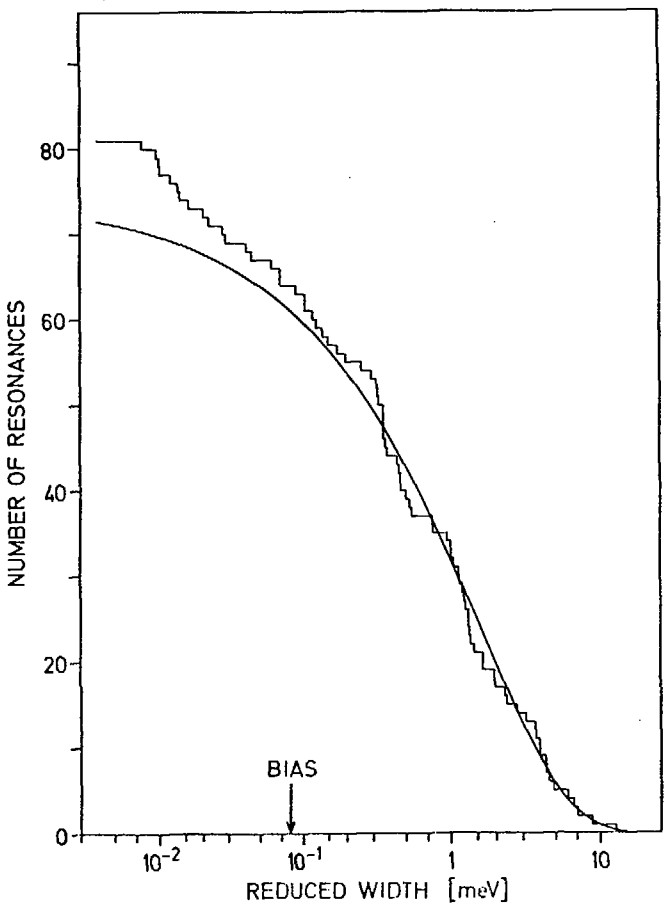

Fig. 3 : Fit of the neutron width distribution of ^{242}Pu resonances for a determination of the average level spacing. The surplus of resonances with small reduced widths is interpreted as being due to p-wave levels.

Review of the ^{240}Pu and ^{242}Pu Unresolved Resonance Region

K. Wisshak, F. Käppeler

Kernforschungszentrum Karlsruhe GmbH
Institut für Angewandte Kernphysik
P.O.B. 3640, D-7500 Karlsruhe
Federal Republic of Germany

F.H. Fröhner

Kernforschungszentrum Karlsruhe GmbH
Institut für Neutronenphysik und Reaktortechnik
P.O.B. 3640, D-7500 Karlsruhe
Federal Republic of Germany

ABSTRACT

Recent measurements and evaluations of neutron cross sections for ^{240}Pu and ^{242}Pu in the unresolved resonance region are reviewed. The most conspicuous data gaps could be closed during the last few years but a number of discrepancies between different sets of experimental data and between data and nuclear reaction theory remain problematic.

I. INTRODUCTION

The present review on neutron data of ^{240}Pu and ^{242}Pu in the unresolved resonance region considers total, capture and fission cross sections. For our purposes the unresolved resonance region will be defined as ranging from 1 to 500 keV for capture and from 10 to 500 keV for fission. Data on total cross sections are supposed to be of interest in the energy range from 10 keV to 5 MeV. The reason for these rather high upper limits are the possible checks on total cross section and subthreshold fission cross section data at low keV energies by judging the overlap with high energy data.

 In the first part experimental data will be presented together with a brief description of the different neutron sources and experimental techniques. In case of total and capture cross sections the available experiments are so scarce that they can be discussed completely. In case of fission cross sections a restriction is made to recent measurements (published in final form since 1978) because earlier data have been reviewed in detail by Patrick [1] at the Brookhaven meeting in 1978. These data are supposed to be encorporated already in presently used evaluations.

In the second part a brief review is given of the respective evaluations. The methods for the calculation of average total, capture and fission cross sections are discussed. The unresolved resonance parameters used as input are compared and the corresponding cross section curves are presented. A number of discrepancies is identified where further experimental or evaluation effort is needed.

II. EXPERIMENTAL DATA

The most relevant parameters characterizing the individual measuremehts are compiled in Tables I-IV. The first and second columns of these tables list the authors and the status of the respective work which is quoted as final if the data have been published in a scientific journal including a discussion of systematic uncertainties. Measurements published in conference proceedings are considered as preliminary since in most cases the allocated space did not allow for a detailed presentation of the systematic uncertainties. Columns 3 to 5 contain information on neutron sources, experimental methods and detectors as well as sample characteristics. These are the most important parameters characterizing cross section measurements which may allow to judge specific advantages and drawbacks and to elucidate how independent the individual results are as far as systematic uncertainties are concerned. The energy range, the obtained accuracy and the type of normalization are given in the last columns of the tables.

a) Total Cross Sections

Total cross sections of ^{240}Pu have been published by three groups [2,3,4] as shown in Table I. In general, white neutron spectra were used at low energies and monoenergetic neutrons at high energies. Monoenergetic neutrons in connection with the time-of-flight (TOF) technique are preferable to a measurement in dc mode since it allows for a more accurate determination of possible backgrounds. Very different detectors have been utilized in the experiments. An essential feature in transmission measurements is the homogeneity of the sample. Here, thin metallic samples offer much better conditions than oxide powder samples which in addition require a sizeable correction for the oxygen cross section. The most accurate data are those of Poenitz et al. [4] which were obtained in a simultaneous measurement of several isotopes including a carbon reference sample as an important check. In addition, these data have been corrected for resonance self-shielding which caused a non-negligible shift at low energies. A comparison to the other data is made in Fig. 1. Above 100 keV good agreement is found for all data sets, while a 13 % discrepancy is found at 40 keV which is well outside the quoted uncertainties. Very recently, a measurement has been performed by Gwin et al. [5]. These data are not yet available but the final publication is in preparation.

In case of ^{242}Pu only two data sets [3,6] exist which cover a different energy region. Again, there are large differences in the quality of the sample material which emphasizes that less weight should be given to the results of Ref. 3. The respective data are shown in Fig. 2.

b. Capture Cross Sections

The capture cross section of ^{240}Pu has been measured by three groups [7,8,9,10] as shown in Table II. In two cases white spectra from an electron linear accelerator (LINAC) were utilized whereas in the third experiment a Van de Graaff served as a neutron source In the second case very short flight

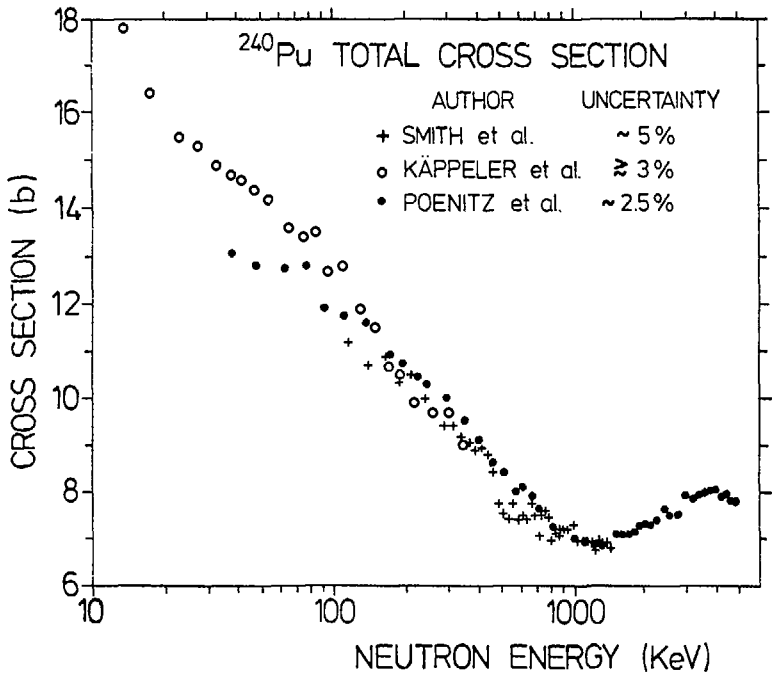

Fig. 1 Total cross section measurements on ^{240}Pu in the unresolved resonance region (1 keV - 5 MeV).

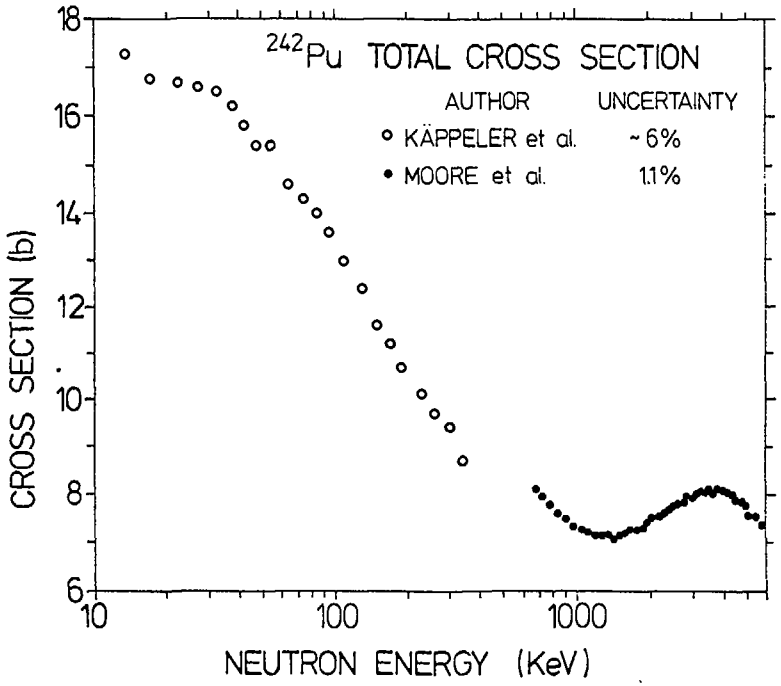

Fig. 2 Total cross section measurements on ^{242}Pu in the unresolved resonance region (1 keV - 5 MeV).

TABLE I Compilation of the Total Cross Section Measurements on ^{240}Pu and ^{242}Pu in the Unresolved Resonance Region (1 keV - 5 MeV)

Authors	Reference Year Status	Neutron Source	Method/Detector	Sample composition thickness enrichment	Energy Range (keV)	Uncertainty (%)
			^{240}Pu			
Smith et al.	2 1972 final	Van de Graaff dc current $^{7}Li(p,n)$ monoenergetic neutrons	BF_3 counter E_n < 650 keV proton recoil detector E_n > 650 keV	metal ~0.04 a/b 98.7 %	100-1500	5.
Käppeler et al.	3 1979 preliminary	Van de Graaff pulsed: 250 kHz, 1 ns $^{7}Li(p,n)$ white spectrum TOF, 5.0 m flight path	lithium-loaded glass scintillator	PuO_2 0.165 a/b 98.3 %	10-370	$\gtrsim$3. not discussed in detail
Poenitz et al.	4 1981 final	Tandem Dynamitron pulsed: 0.5-2 MHz, 1 ns $^{7}Li(p,n)$ white spectrum: 30-250 keV, monoenergetic: 200 keV-4.8 MeV TOF, 7.8 m flight path	black neutron detector E_n < 2 MeV hydrogeneous scintillator with PSD E_n > 1 MeV	metal 0.072 a/b 98.3 %	30-4800	2.8
Gwin et al.	5 publication in preparation				2 eV-6000	
			^{242}Pu			
Käppeler et al.	3 1979 preliminary	same as ^{240}Pu	same as ^{240}Pu	PuO_2 0.146 a/b 77.2 %	10-370	$\gtrsim$5.8 not discussed in detail
Moore et al.	6 1980 preliminary	Spallation Source 800 MeV p on Ta pulsed: 1.25 kHz 1.5 ns white spectrum TOF, 31.8 m flight path	NE 110 plastic scintillator	metal 0.076 a/b 99.91 %	700-170 MeV	1.1 for E_n < 5 MeV

TABLE II Compilation of the Capture Cross Section Measurements on ^{240}Pu and ^{242}Pu in the Unresolved Resonance Region (1-500 keV)

Authors	Reference Year Status	Neutron Source	Method/Detector	Sample composition thickness enrichment	Energy Range (keV)	Normalization	Uncertainty (%)
			^{240}Pu				
Hockenbury et al.	7 1972 final	LINAC pulsed: 480 Hz, 100 ns white spectrum TOF, 25.6 m flight path	liquid scintillator tank high/low bias technique to separate fission	? 1.3×10^{-3} a/b ~97 %	6.-28.	using transmission of s-wave resonance with $\Gamma_\gamma >> \Gamma_n$ at 92.5eV and black resonance technique at 20.46 eV and 60.2 eV(gold) rel. flux: $^{10}B(n,\alpha)$	8.
Weston and Todd	8 1977 final	LINAC pulsed: white spectrum TOF, 20 and 85 m flight path	C_6F_6 scintillator pulse height weighting technique NE 213 with PSD fission neutron detector to separate fission (norm. at thermal)	PuO_2 1.1×10^{-4} a/b (2g) 5.0×10^{-4} a/b (9g) 98.3 %	200.eV-350.	at thermal (0.02-0.03 eV) and black resonance technique at 1.06 eV rel. Flux: $^{10}B(n,\alpha)$ <2 keV $^{6}Li(n,\alpha)$>2 keV	7.-8. (0.2-80. keV) 9.-20. (>80. keV)
Wisshak and Käppeler	9,10 1978/79 final	Van de Graaff pulsed: 2.5 MHz, 1 ns $^{7}Li(p,n),T(p,n)$ white spectrum TOF, 0.068-0.135 m flight path	Moxon-Rae-detector graphite converter NE 213 with PSD fission neutron detector to separate fission (norm via ^{235}U)	PuO_2 9.8×10^{-4} a/b (3.1 g) 9.5×10^{-4} a/b (3.0 g) 98.3 %	10.-250.	$^{240}Pu/^{197}Au$ and $^{240}Pu/^{238}U$ ratio measured	4.-6. (20.-60. keV) 6.-10. (10.-20. keV >60. keV)
			^{242}Pu				
Hockenbury et al.	11 1975 preliminary	same as ^{240}Pu	same as ^{240}Pu	metal 7.76 g 92.6 %	6.-70.	using transmission of 5 resonances Γ_n measured Γ_γ from lit. rel. Flux: $^{10}B(n,\alpha)$	$\gtrsim$6 not discussed in detail
Wisshak and Käppeler	9,10 1978/79 final	same as ^{240}Pu	same as ^{240}Pu	PuO_2 3.33×10^{-3} a/b (10.7 g) 2.72×10^{-3} a/b (8.7 g) 77.2 %	10.-250.	$^{242}Pu/^{197}Au$ and $^{242}Pu/^{238}U$ ratio measured	6.-8. (20.-60. keV) 8.-12. (10.-20. keV >60. keV)

paths of only 7-13 cm were used which allowed for a high neutron flux at the sample position. Consequently, the experimental signal-to-background ratio was up to one order of magnitude better than in LINAC experiments. This method is restricted, however, to a limited energy range from 10 to 250 keV.

The capture gamma rays were measured with three different detectors. Two methods have been applied to separate capture from fission events and in addition, different normalization procedures have been used. Therefore the various results as displayed in Fig. 3 can be considered to be completely independent from each other. For easier comparison the experimental ratios of Wisshak and Käppeler [9,10] which were obtained in five independent runs under different experimental conditions, have been converted to absolute cross sections using the gold data from ENDF/B-V and the ^{238}U data from KEDAK 4. These cross sections were then averaged over the same energy intervals as given by Weston and Todd [8] by weighting each point according to its uncertainty. The resulting values, shown in Fig. 3 as dotted bars, are in good agreement with Ref. 8 between 50 and 200 keV. Between 10 and 50 keV a 10 % discrepancy is found which is still compatible with the quoted uncertainties. In the region of overlap, the agreement between the data of Hockenbury et al. [11] and Wisshak and Käppeler [9] is quite good.

Two additional remarks need to be made on the data of Wisshak and Käppeler concerning recent experimental refinements and some misunderstandings in the literature:
(i) In the original publications [9,10] the systematic uncertainty due to deviations of the Moxon-Rae detector efficiency from an ideal linear increase with gamma ray energy was neglected. As recently

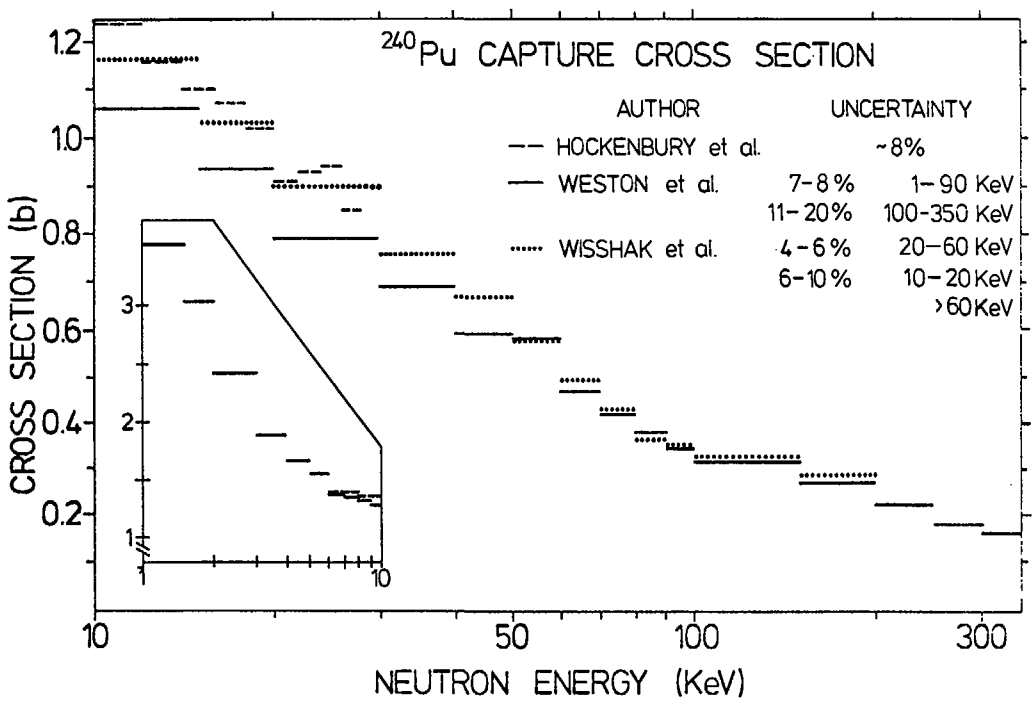

Fig. 3 Capture cross section measurements on ^{240}Pu in the unresolved resonance region (1 - 500 keV).

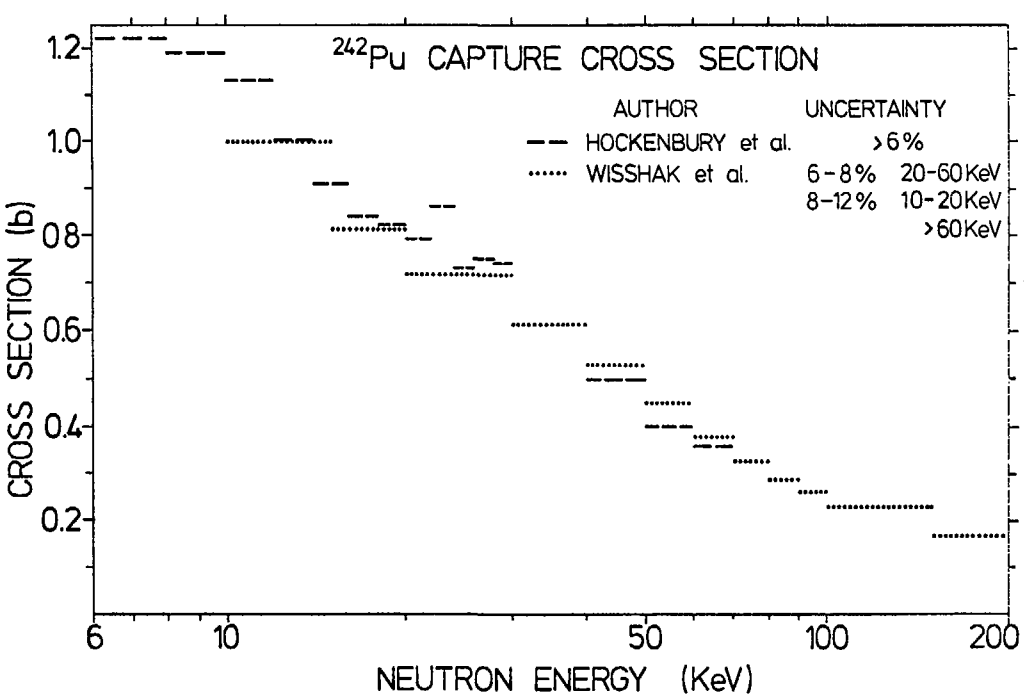

Fig. 4 Capture cross section measurements on ^{242}Pu in the unresolved resonance region (1-500 keV).

shown [12], this effect caused a 2.7 % decrease of the experimental capture cross section ratio in a measurement of ^{241}Am relative to gold. A correction of about the same size, which will be calculated in the near future, may be expected for the measurements of ^{240}Pu and ^{242}Pu relative to gold, too. Furthermore, the systematic uncertainty due to flight path uncertainties has been underestimated for the data points at highest energy in Refs. 9,10. Therefore, an additional systematic uncertainty of 5 % and 10 % has to be assigned to the two points with highest energy in each of the experimental runs, respectively. These wrong uncertainties together with the fact that only selected points have been considered, led Weston and Wright [13] to the conclusion that there is a disturbing difference in shape to their own data. As is obvious from Fig. 3 this is not the case.

(ii) A possible inconsistency in the data of Wisshak and Käppeler [9] was supposed by Poenitz [14]. He calculated the ratio $\sigma_\gamma(^{238}U)/\sigma_\gamma(^{197}Au)$ from the $\sigma_\gamma(Pu)/\sigma_\gamma(^{238}U)$ and $\sigma_\gamma(Pu)/\sigma_\gamma(^{197}Au)$ ratios (Tables V and VI in Ref. 9) and found different values than given in Table IV of Ref. 9. In addition, he stated that the $\sigma_\gamma(^{238}U)/\sigma_\gamma(^{197}Au)$ values derived in this way scattered by ∿20 % which would be inconsistent with the quoted systematic uncertainties. In this argumentation he obviously overlooked that the measurements relative to gold and uranium have been carried out in separate runs for each of the plutonium isotopes (see Table II of Ref. 9). Therefore, in calculating the ratio $\sigma_\gamma(^{238}U)/\sigma_\gamma(^{197}Au)$ from these values, the entire statistical and systematic uncertainty of the plutonium spectra of both runs has to be taken into account. This uncertainty does not cancel out as one would expect for the case that the ratios relative to uranium and gold were measured simultaneously in the same run. If treated in this correct way, the calculated data derived for $\sigma_\gamma(^{238}U)/\sigma_\gamma(^{197}Au)$ have a rather large statistical uncertainty which is compatible with the observed scatter.

In case of ^{242}Pu there are only two data sets [9,10,11] which were measured with the same techniques as discussed already for ^{240}Pu. The results are plotted in Fig. 4, the data of Wisshak and Käppeler being averaged in the same way as described above. A remarkably good agreement is found for the two measurements.

To our knowledge, no other measurements on the capture cross section of these plutonium isotopes are presently under way.

a) Fission Cross Sections

Most recent experiments on ^{240}Pu and ^{242}Pu are fission cross section measurements. In Table III those experiments on ^{240}Pu are compiled which have been published in final form since the Brookhaven meeting in 1978 or which are not yet included in the review given there by Patrick [1]. Van de Graaff and LINAC accelerators have been used for neutron production. Measurements have been performed with white neutron spectra as well as with monoenergetic neutrons in pulsed and dc mode. As a significant background due to the high spontaneous fission rate is present in all experiments, the use of monoenergetic neutrons from a pulsed accelerator seems to be preferable to subtract this background correctly. Unfortunately, as the source strength is limited in this case, such measurements have been performed with high accuracy only above threshold. Another approach to overcome background problems is the use of very short flight paths [15] as mentioned already for the capture measurements.

In most of the present experiments fission events were registered via fragment detection. Here, the threshold method [14] offers considerable advantages since no absolute determinations are required for sample masses and detector efficiencies which both are difficult to perform with high accuracy. Another important feature concerns special detector designs [17] which allow for an effective alpha suppression to reduce background due to pile-up signals from these highly alpha active samples. Another significant parameter is the sample thickness since above ∿0.1 mg/cm² the energy loss of the fission fragments starts to spoil the pulse-height discrimination against alpha particles. These problems have been avoided in a measurement which has been performed in the subthreshold region via fission neutron detection [15]. This allows the use of gram amounts of sample material and therefore high statistical accuracy even in a region with very low cross section. The related systematic uncertainties are very different from those encountered with fragment detection and hence these results yield complementary and independent information on the fission cross section.

TABLE III Compilation of Recent Fission Cross Section Measurements on ^{240}Pu in the Unresolved Resonance Region (1o-500 keV) (Older Measurements are Compiled in Ref. 1)

Authors	Reference Year Status	Neutron Source	Method/Detector	Sample mass thickness enrichment	Energy Range (MeV)	Measured Parameter	Normalization	Uncertainty (%)
Behrens et al.	14 1978 final	LINAC pulsed: 1440 Hz, 10 ns white spectrum TOF, 15.7 m flight path	ionization chamber back to back geometry threshold method	25. mg 0.05 mg/cm^2 98.48 % 40 mg 0.08 mg/cm^2 85.3 % U 14.5 % Pu	0.1 - 34.0 1.75-4.0	$^{240}Pu/^{235}U$ shape $^{240}Pu/^{238}U$ absolute	$^{238}U/^{235}U$	2.3-8 (0.1-0.5 MeV) 2.1-2.5 (0.5-10 MeV)
Wisshak and Käppeler	15 1978 final	Van de Graaff pulsed: 2.5 MHz, 1 ns $^7Li(p,n),T(p,n)$ white spectrum TOF, 0.068-0.135 m flight path	NE 213 with PSD fission neutron detector	9.8 x 10^{-4} a/b (3.1 g) 9.5 x 10^{-4} a/b (3.0 g) 98.3 %	0.01-0.25	$^{240}Pu/^{235}U$ absolute		7-10
Kupriyanov et al.	16 1979 final	Van de Graaff dc current $^7Li(p,n)$, T(p,n) D(d,n) monoenergetic neutrons	ionization chamber back to back geometry threshold method	? ? 99.49 % ? ? 92.7 % ^{240}Pu 6.7 % ^{239}Pu	0.1 - 7.4 0.9 - 3.0 5 points	$^{240}Pu/^{235}U$ shape $^{240}Pu/^{239}Pu$ absolute	$^{239}Pu/^{235}U$	2.2-4.8 (0.1-0.5 MeV) 2.1-2.3 (0.5-6 MeV)
Budtz-Jørgensen and Knitter	17 1981 final	Van de Graaff pulsed: 2.5 MHz 1.5 ns $^7Li(p,n)T(p,n)$ D(d,n) monoenergetic neutrons TOF, 0.06-0.11 m flight path LINAC pulsed: 800 Hz, 4.4 ns white spectrum TOF, 9.0 m flight path	ionization chamber special design for alpha suppression back to back geometry	0.3/1.5 mg 0.05/0.24 mg/cm^2 98.5 %	0.2-10.0 0.01-0.3	$^{240}Pu/^{235}U$ absolute $^{240}Pu/^{235}U$ absolute		3.9-20. (0.2-0.6 MeV) 3.3-3.9 (0.6-10. MeV) ~6.5
Weston and Todd	18,19 1979 publication in preparation				0.01-0.10 0.05-20.	^{240}Pu absolute $^{240}Pu/^{235}U$ absolute		
Meadows	20 1981 submitted for publication	Tandem Dynamitron pulsed: $^7Li(p,n)$, D(d,n) monoenergetic neutrons	ionization chamber back to back geometry	four samples 0.07-0.33 mg 0.015-0.066 mg/cm^2 89.6 - 98.4 %	0.34-9.56 2.0-3.0 five points	$^{240}Pu/^{235}U$ shape $^{240}Pu/^{235}U$ absolute		4.3-5.4 (0.3-0.5 MeV) 1.1-2.0 (0.8-9.5 MeV)

In all recent measurements the fission cross sections have been determined relative to ^{235}U. The results are shown in Fig. 5. In the subthreshold region the data of Wisshak and Käppeler [15] have been averaged in the same way as described for the capture cross sections. For easier comparison the high resolution data of Budtz-Jørgensen and Knitter have been averaged over the same energy intervals. In general, both data sets differ by ∿20 % which is outside the quoted uncertainties. The most striking difference occurs between 80 and 90 keV where the data differ by a factor two. The higher cross section was also found by Behrens et al. [21] but this energy region was not included in their final publication [14]. The existing discrepancy in the subthreshold fission cross section of ^{240}Pu will probably be solved by the data of Weston and Todd[18] which are to be published in the near future[19].

In the energy range from 350 to 500 keV agreement is found between the data of Behrens[14] and Kupriyanov[16] within the respective uncertainties, while there is a ∿10 % difference around 300 keV. The cross sections of Budtz-Jørgensen and Knitter[17] are systematically lower between 450 and 500 keV but agree with both other data sets at lower energies within the given uncertainties. The very recent results from Meadows[18] are also 10-15 % lower than the results of Behrens. This discrepancy could be explained by a difference in the energy scales of ∿25 keV which, however, would be far outside the quoted accuracy of the energy calibrations.

For ^{242}Pu three new measurements are available. The experimental methods are identical to those described for ^{240}Pu. Important features of the measurements

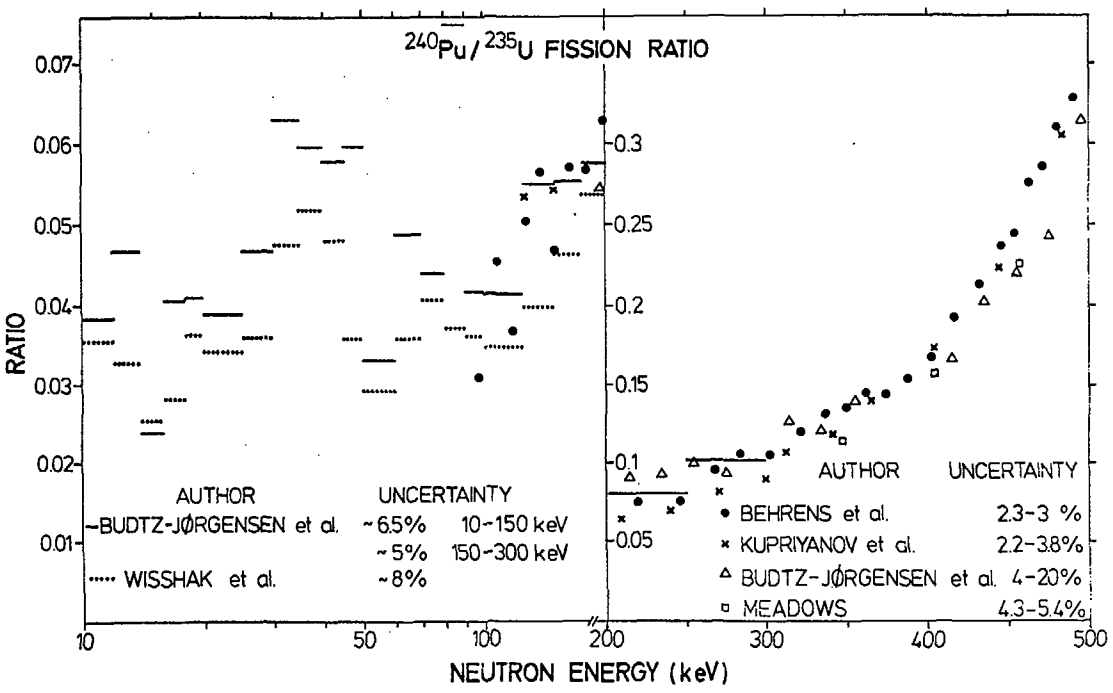

Fig. 5 Recent fission cross section measurements on ^{240}Pu in the unresolved resonance region (10-500 keV).

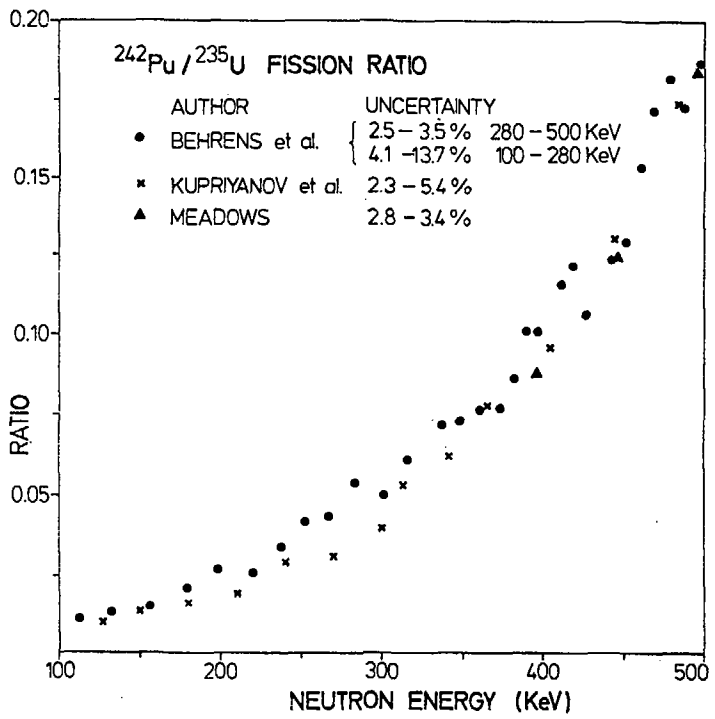

Fig. 6 Recent fission cross section measurements on ^{242}Pu in the unresolved resonance region (10-500 keV).

are listed in Table IV and the results are shown in Fig. 6. In the energy range from 300 to 500 keV the data of Kupriyanov et al. are about 6-8 % lower than the values of Behrens et al. This discrepancy is still larger between 200 and 300 keV. The lower values are supported by the data of Meadows[22] which are slightly lower than both other data sets. These discrepancies in the threshold region may again be explained by an uncertainty in the energy calibration.

New measurements of the ^{242}Pu fission cross section are planned in Geel[23] in the energy range from 100 eV up to 10 MeV.

III. EVALUATIONS

The more recent evaluations of unresolved resonance cross sections for ^{240}Pu and ^{242}Pu to be considered are those reported for ENDF/B-V [24,25], ENDF/BRC [26,27], JENDL-1 and -2 [28,29,30], the Soviet evaluated file [31,32] SOKRATOR and KEDAK-4 [33].

The situation with regard to this evaluation work can be characterized briefly by stating that the most conspicuous gaps in experimental data have been closed in recent years. For instance, total cross section data exist now all the way down to a few keV, thanks to measurements at ANL and KfK [3,4] and subthreshold fission data for ^{240}Pu were measured down to the resolved resonance region at Geel and KfK [15,17]. At the same time evaluation methods have progressed from mere drawing of eye-guide curves to coherent calculation of all relevant cross sections from nuclear models, with average parameters from resolved resonances incorporated as a-priori information in the data fits. This utilization of nuclear reaction theory has already uncovered apparent systematic errors in some of the experimental data.

a) Total cross sections

Mainly two methods are being employed for ^{240}Pu and ^{242}Pu total cross section computation in the unresolved resonance region, viz.

(1) level-statistical calculations with energy-averaged expressions from resonance theory, based on average resonance parameters;
(2) optical-model calculations, based on a suitable complex potential.

The first of these is used up to energies between 45 and 500 keV with various degrees of rigor for ENDF, JENDL, SOKRATOR and KEDAK. The second method is used, with suitable overlap, at higher energies, as low down as 10 keV at Bruyères-le-Châtel (and in KfK work[33]).

Since the KEDAK level statistical calculations have not been reported so far, but appear to represent the state of the art we describe them briefly. The average total cross section for each reaction channel $c \equiv \{J\ell s\}$ ($\ell = 0,1,2,3$) is calculated from the practically rigorous R-matrix expressions

$$\langle\sigma_c\rangle = 2\pi\lambda_c^2 g_c (1-\mathrm{Re}\langle U_{cc}\rangle), \tag{1}$$

$$\langle U_{cc}\rangle = e^{-2i\phi_c} \frac{1-\bar{R}_{cc}L_c^{o*}}{1-\bar{R}_{cc}L_c^{o}}, \tag{2}$$

$$\bar{R}_{cc} = R_c^{\infty} + i\pi s_c \tag{3}$$

(see Ref. 34,35). The hard-sphere phases $\phi_c = \phi_\ell$ and the $L_c^o = L_\ell - B_c$ are computed from the recursion relations

$$\phi_o = k_c a_c, \phi_\ell = \phi_{\ell-1} - \arg(L_{\ell-1} - \ell) \tag{4}$$

$$L_o = ik_c a_c, \; L_\ell = -\ell - \frac{(k_c a_c)^2}{L_{\ell-1} - \ell} \tag{5}$$

with the conventions $a_c = a = (1.23\, A^{1/3} + 0.80)$ fm for the channel radius and $B_c = -\ell$ for the boundary parameter.

TABLE IV Compilation of Recent Fission Cross Section Measurements on ^{242}Pu in the Unresolved Resonance Region (10-500 keV) (Older Measurements are Compiled in Ref. 1)

Authors	Reference Year Status	Neutron Source	Method/Detector	Sample	Energy Range	Measured Parameter	Normalization	Uncertainty
Behrens et al.	14 1978 final	LINAC pulsed: 1440 Hz, 10 ns white spectrum TOF, 15.7 m flight path	ionization chamber back to back geometry	55 mg 0.15 mg/cm^2 99.87 %	0.1-34.0	$^{242}Pu/^{235}U$ shape		3.1-10. (0.1-0.5 MeV) 2.3-3. (0.5-10. MeV)
			threshold method	40 mg 0.11 mg/cm^2 25.2 % ^{239}Pu 74.8 % ^{242}Pu	1.75-4.0	$^{242}Pu/^{239}Pu$ absolute	$^{239}Pu/^{235}U$	
Kupriyanov et al.	16 1979 final	Van de Graaff dc current $^7Li(p,n)$,T(p,n), D(d,n) monoenergetic neutrons	ionization chamber back to back geometry	? ? 99.92 %	0.1-7.4	$^{242}Pu/^{235}U$ shape		2.3-5.7 (0.1-0.5 MeV)
			threshold method	? ? 94.1 % ^{242}Pu 5.8 % ^{239}Pu	0.9-3.0 5 points	$^{242}Pu/^{239}Pu$ absolute	$^{239}Pu/^{235}U$	2.2-3.0 (0.5-7.4 MeV)
Meadows	22 1979 final	Tandem Dynamitron pulsed: $^7Li(p,n)$, D(d,n) monoenergetic neutrons	ionization chamber back to back geometry	? ? 99.7 % and 90.2 %	0.4 - 9.8	$^{242}Pu/^{235}U$ absolute		3. (0.4-0.5 MeV) 1.6-1.9 (0.5-9.8 MeV)
Weigmann et al.	23 1981 measurement in progress	LINAC			100 eV-10 MeV			

In the case of ^{240}Pu the strength functions $S_\ell = 2k_c a_c s_c \sqrt{1\ eV/E}$ and distant-level parameters R^∞_ℓ for ℓ = 2,3 were taken from a calculation by Fischer [36] who had established a spherical optical potential for actinides by fitting ^{238}U total elastic and inelastic cross sections for ^{238}U between 50 keV and 10 MeV. The quantities S_ℓ and R^∞_ℓ for ℓ = 0 and 1 were fitted with the code FITACS to measured total cross sections. Values determined in the resolved resonance region (S_o, $R^\infty_o = 1-R'/a_c$) or taken from Fischer's work (S_1, R^∞_1) were fed into the fit as a-priori information via Bayes' theorem (see Ref. 37). Fig. 7 shows that the resulting curve fits the data of Poenitz et al. [4] quite well whereas it is in conflict with those of Käppeler et al. [3] below 100 keV. The same is true for the curve calculated by Jary et al. [27] with a deformed optical potential. The JENDL curve which is closest to the KfK data is not calculated from a nuclear model but a mere eye guide interpolation. Also the ENDF/B-IV curve is not directly obtained from the unitarity-based expression (1) or from an optical model but rather as the sum of all partial cross sections. Comparing the theoretical curves and the data one is led to the conclusion that the KfK measurement was afflicted by some uncrecognized systematic error at energies below 100 keV.

The situation is similar for ^{242}Pu, see Fig. 8. The ENDF/B-IV curve is computed with a spherical optical model, the ENDF/BRC curve with a deformed optical potential, the Minsk curve with approximate level-statistical expressions and the KEDAK curve with the expressions given above. The steeper rise of the BRC curve below 40 keV seems to be due to the adoption of older

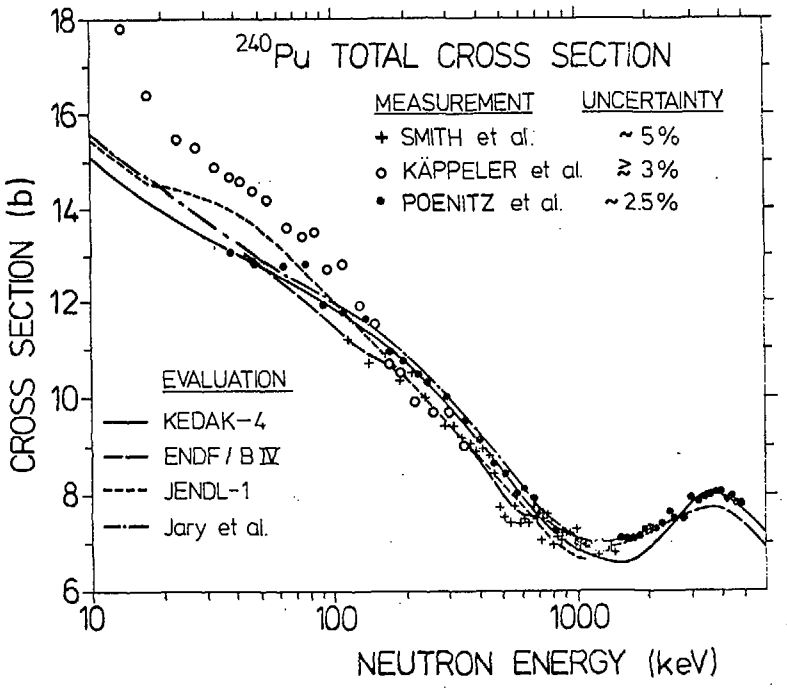

Fig. 7 Evaluations of the ^{240}Pu total cross section in the unresolved resonance region in comparison with experimental data.

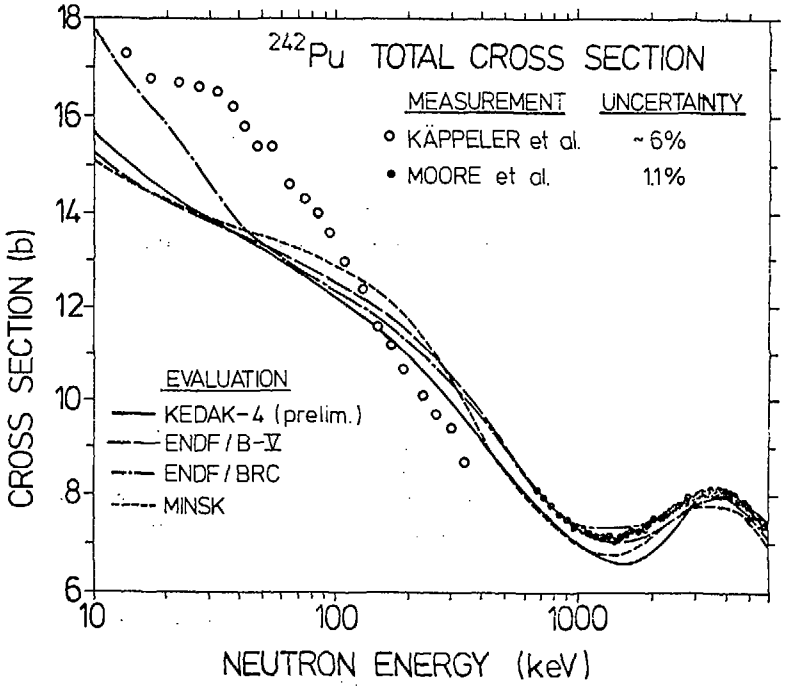

Fig. 8 Evaluations of the ^{242}Pu total cross section in the unresolved resonance region in comparison with experimental data.

ENDF/B-IV data there. Again reaction theory seems to indicate systematic errors in the KfK measurements at low energies. The preliminary KEDAK evaluation is based on Fischer's results [36] and statistical analysis of the resolved resonances. Fischer's results were adopted down to 200 keV and the level-statistical calculation below 200 keV was forced to join them smoothly. The data of Moore et al. [6] show, however, that this calculation is about 3-5 % low, whereas both the ENDF/B-V and ENDF/BRC curves reproduce the data quite well, differing among themselves by less than 2 % above 40 keV. Below that energy the BRC curve shows the unphysical deviation from other calculations mentioned already. In order to clarify the situation new transmission data below 500 keV down to 40 keV or lower are needed with an accuracy of better than 5 %.

b) Capture cross sections

The Hauser-Feshbach approach with width fluctuation correction is practically universally adopted for the computation of neutron capture cross sections in the unresolved resonance region. The necessary neutron transmission coefficients are either taken from level-statistical theory or from optical-model calculations. The capture transmission coefficients are essentially calculated as ratio of radiative width and level spacing, the values of these latter being taken from statistical analysis of s-wave levels in the resolved resonance region and translated to other reaction channels by means of the usual assumptions on spin and parity dependence.

We illustrate this with the level-statistical approach employed in KEDAK evaluation work up to 100 or 200 keV. The neutron transmission coefficients are taken as those following from eq. (2) in the absence of direct processes, viz.

$$T_c \equiv 1 - |\langle U_{cc} \rangle|^2 = \frac{4\pi s_c P_c}{|1-\bar{R}_{cc} L_c^o|^2} , \qquad (6)$$

where $P_c = \mathrm{Im}\, L_\ell$ is the well-known centrifugal-barrier penetrability. The denominator represents multi-level interference. The transmission coefficients for radiation channels are taken as

$$T_\gamma = 2\pi \frac{\langle \Gamma_\gamma \rangle}{D_c} . \qquad (7)$$

The energy dependence of D_c is taken as that of the Gilbert-Cameron composite level-density formula [38] with the spin cut-off calculated according to $\sigma^2 = (6/\pi^2) \langle m^2 \rangle \sqrt{aU}$, where a and U are the a parameter in the Fermi gas formula and the effective excitation energy. The mean square of the magnetic quantum numbers is taken as $\langle m^2 \rangle = 0.24\, A^{2/3}$ (Ref. 39). This prescription for D_c is also used to calculate the energy dependence of $\langle \Gamma_\gamma \rangle$ in E1 (electric dipole) approximation with a giant-dipole resonance form factor. The Bethe formula (see Ref. 38)

$$D_c^{-1} \propto \exp\left[-\frac{J^2}{2\sigma^2}\right] - \exp\left[-\frac{(J+1)^2}{2\sigma^2}\right] \qquad (8)$$

is used to relate the various D_c to the s-wave level spacing which is taken from the resolved resonance region (after correction for missing levels). The radiation widths of levels with positive and negative parity can be separately adjusted in FITACS calculations, any J dependence of $\langle \Gamma_\gamma \rangle$ is neglected. Competition of inelastic and fission channels is fully taken into account. Width fluctuations are calculated as Dresner quadratures [40] with Moldauer's recent prescription for the effective numbers of degrees of freedom [41]. Other groups use similar prescriptions. For instance Konshin and co-workers employ two superposed giant dipole resonances for these deformed nuclei but neglect fission competition.

The various evaluations for ^{240}Pu are shown in Fig. 9. All follow the measured data quite closely, the Minsk curve fitting best below 25 keV, the KEDAK and ENDF curves above 100 keV. The ENDF/BRC curve is systematically low. For ^{242}Pu the evaluations are all very close together (Fig. 10). It must be said, however, that at least the KEDAK curve is generated from level-statistical theory only up to the first inelastic threshold at 44.7 keV (marked by an arrow). Above 44.7 keV it is a mere eye guide curve through the data [33]. Our calculations were always higher there by 10-20 %, indicating that the measured data are systematically low or that the

average resonance parameters (Γ_γ/D) are at fault. The preliminary KEDAK results favour the radiation width given by Poortmans et al. [42], $\langle\Gamma_\gamma\rangle = 21.9 \pm 1.4$ meV, over the value of Ref. 43, $\langle\Gamma_\gamma\rangle = 30 \pm 5$ meV. This is seen from Table V where the average parameters recommended in the various evaluations for total and capture cross section computation are collected.

c) Fission cross sections

The calculation of subthreshold fission cross sections for actinides is still under development and the methods are quite diverse. The greatest problem is a lack of convenient but adequate recipes for the estimation of transition state densities at the saddle point for the various reaction channels. The resolved resonance region can only furnish information on s-wave channels but for the various p-, d-, channels one must try to use theory in some simplified way. The approach of the Minsk group, as documented in Ref. 32, will serve as an illustration. The transmission factors are taken as sums over fission barrier penetrabilities,

$$T_f = 2\pi \frac{\langle\Gamma_f\rangle}{D_c} = \sum_{c'} P_{c'}, \qquad (c': \text{fission channels only}) \qquad (9)$$

with summation over all accessible transition states at the saddle point.

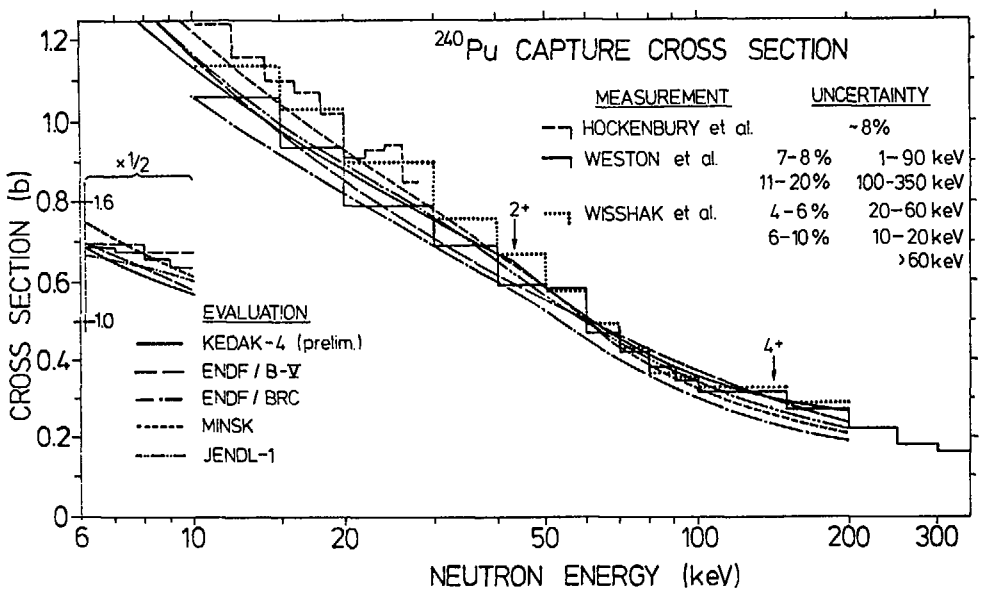

Fig. 9 Evaluations of the ^{240}Pu capture cross section in the unresolved resonance region in comparison with experimental data.

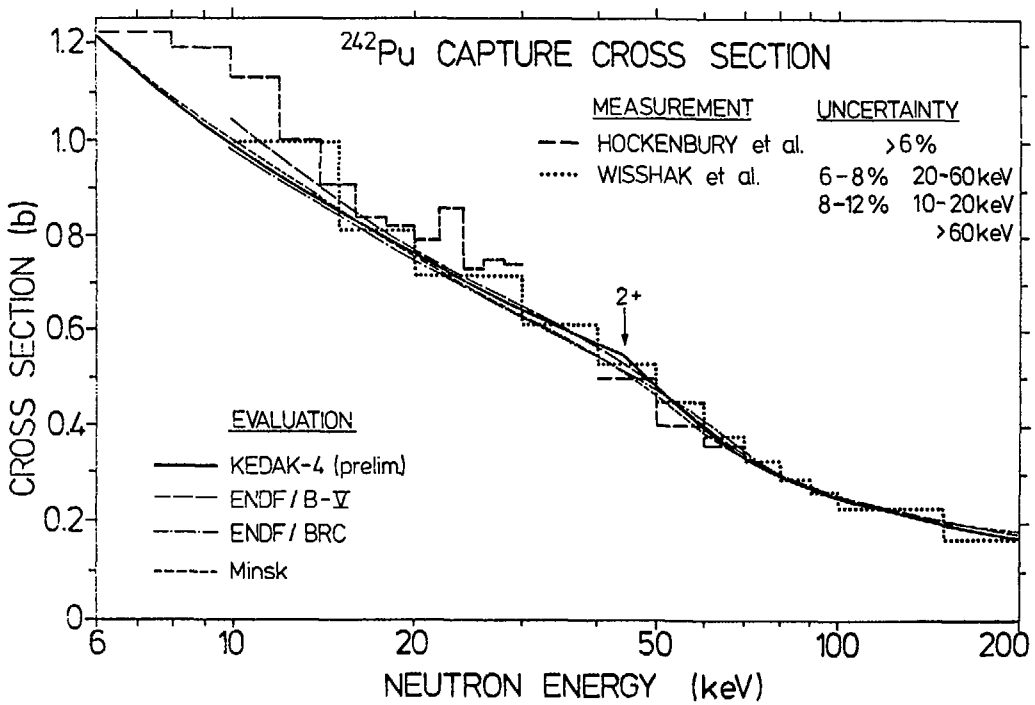

Fig. 10 Evaluations of the ^{242}Pu capture cross section in the unresolved resonance region in comparison with experimental data.

TABLE V Average parameters given in recent evaluations

Target Nucleus	S_o (10^{-4})	S_1 (10^{-4})	D_o (eV)	$\langle\Gamma_\gamma\rangle$ (meV)	$\langle\Gamma_\gamma\rangle/D$ (10^{-3})	Evaluation	Ref.
^{240}Pu	1.10	3.07	13.5	29.5	2.19	ENDF/B-IV	25
	1.04	2.66	13.6	29.5	2.17	JENDL-1	28
	0.88	1.67				JENDL-2	30
	1.00	2.31	13.6	30.8	2.26	Jary et al.	27
	1.10	2.8	13.5	30.7	2.27	Antsipov et al.	31
	1.02[a]	1.98[a]	13.1	32.5	2.48	KEDAK-4(prelim.)	this work
^{242}Pu	1.15	2.7	15.0	25.0	1.67	Menapace et al.	49
	0.85		13.04	24.2	1.86	JENDL-2	29,30
	0.813	1.24	16.5	23.4	1.42	ENDF/B-V	24,25
	1.00	2.63	16.5	27	1.64	ENDF/BRC	26,27
	0.91	2.5	14.23	22.6	1.59	Antsipov et al.	32
	1.05[b]	2.00[b]	12.6	22.5	1.80	KEDAK-4 (prelim.)	this work

a) for $R_o^\infty = -0.09$, $R_1^\infty = 0.13$

b) for $R_o^\infty = -0.11$, $R_1^\infty = 0.16$

The P_c, are calculated for a double-humped barrier by combining the Hill-Wheeler penetrabilities [44]

$$P_x = [1 + e^{-2\pi(E_x-E)/(\hbar\omega_x)}]^{-1} \quad , \quad x = A,B \qquad (10)$$

for the two barriers A and B according to prescriptions given by Gaj et al. [45] and Tyapin et al. [46],

$$P = \frac{P_A P_B}{\sqrt{1-(1-P_A)(1-P_B)}} \quad . \qquad (11)$$

Because not enough information exists on the E_A, $\hbar\omega_A$, E_B, $\hbar\omega_B$ for all transition states that can be reached from the various compound states formed by s-, p-, d-wave reactions one simplifies drastically. The ensemble of transition states is replaced by a single representative one. Its barrier characteristics are then used for all compound states. The enhanced fluctuation of fission widths due to the cluster structure of subthreshold fission resonances was described as follows. The number of degrees of freedom, ν_f, for the fission width χ^2 distributions were taken as equal to 2J+1 except for s-wave levels for which ν_f=1 was used. The average widths of these local distributions were then subjected to the Lorentzian-type behaviour predicted by theory across the resonance clusters. The resulting overall distributions were finally obtained by Monte Carlo sampling and used to calculate the width fluctuation corrections. The Bruyères-le-Châtel group used transition state spectra due to Thomet [47] for ^{240}Pu, due to Back [48] for ^{242}Pu, with double-humped barriers. KEDAK calculations below 200 keV and ENDF/B-V use only one single-hump barrier for all level sequences. The resulting shape of the subthreshold cross section is, however, quite comparable to that from the more sophisticated BRC and Minsk calculations, at least for ^{242}Pu. Figs. 11 and 12 show the various results. It is ovbious that improvements both in experimental data and computational methods are desirable in the subthreshold region.

IV. CONCLUSIONS

The following improvements in experimental data appear most important in the unresolved resonance range:

- improved total cross section data below 100 keV for ^{240}Pu, below 500 keV for ^{242}Pu;
- check on the capture cross section data of ^{242}Pu above 50 keV where at least KEDAK calculations with level-statistical theory seem to indicate 10-20 % higher cross sections than the measurement (while reproducing the ^{240}Pu data quite well);
- improved values of $\langle\Gamma_\gamma\rangle$ for ^{240}Pu and of D(ℓ=0) for both ^{240}Pu and ^{242}Pu;
- improved subthreshold fission data for both ^{240}Pu and ^{242}Pu.

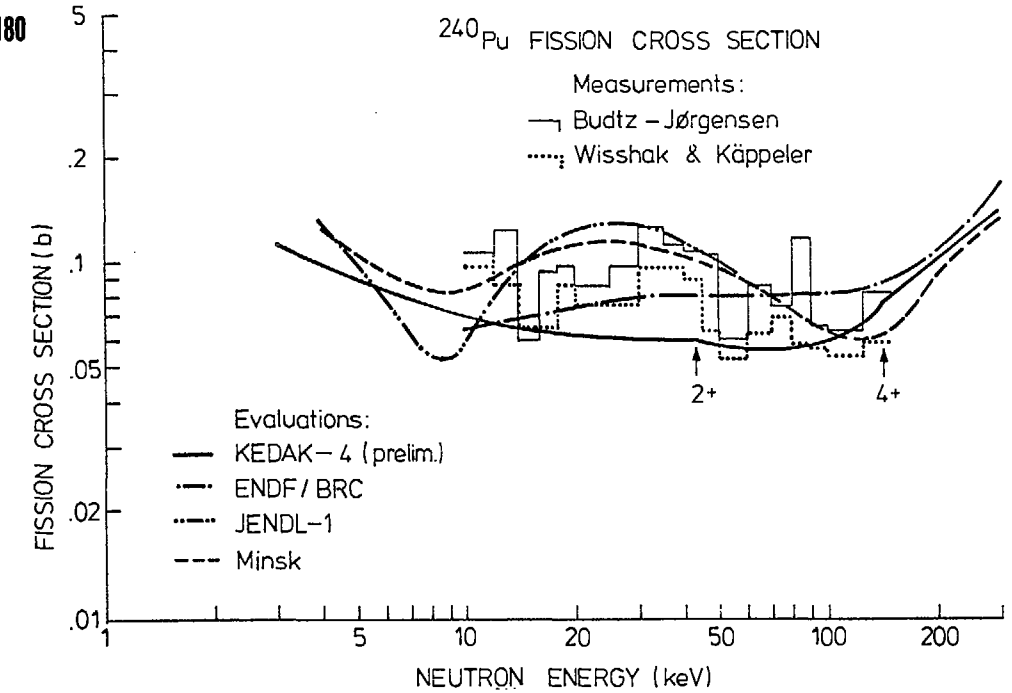

Fig. 11 Evaluations of the ^{240}Pu fission cross section in the unresolved resonance region in comparison with experimental data.

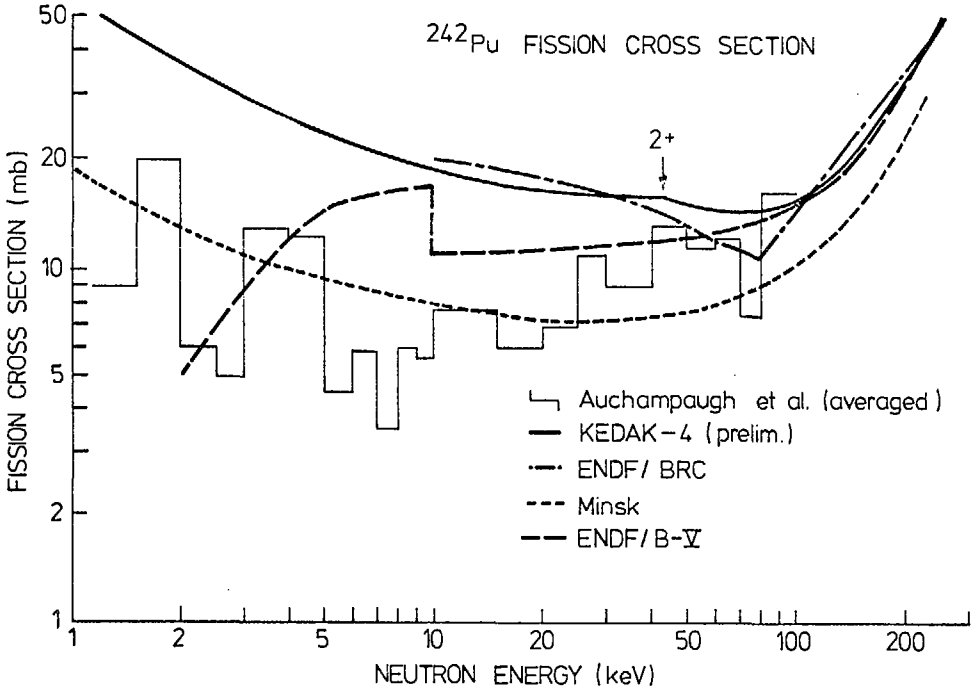

Fig. 12 Evaluations of the ^{242}Pu fission cross section in the unresolved resonance region in comparison with experimental data.

The computational methods are most dependable for the calculation of total cross sections if results from global optical-model potentials are refined to reproduce local trends. The achieveable accuracy at present seems to be of order ± 3 % above 50 keV. At lower energies it may be equally good with the best theoretical methods, but this remains to be confirmed by better experimental data. Capture cross section computation appears possible with an accuracy of the order of 10-20 % depending mainly on how good the ratio $\langle\Gamma_\gamma\rangle/D$ is defined by resolved resonance data and how well its energy dependence can be calculated over the whole range considered here. The subthreshold fission cross section calculations are least dependable since good recipes for the estimation of barrier characteristics and especially transition state densities for the various compound level series are not available. Thus eye-guide lines to good data may at present be equally good as calculated curves. Progress in this field can best be achieved by improvements in the theory of transition states at the saddle point and especially their level densities for the various spins and parities.

ACKNOWLEDGEMENTS

The authors wish to acknowledge the assistance of all those who made their unpublished or preliminary results available for this review. Discussions with H. Jahn and U. Fischer on reaction theory are gratefully acknowledged.

REFERENCES

1 B.H. PATRICK, Proc. Specialists Meeting on Nuclear Data of Plutonium and Americium Isotopes for Reactor Applications, Brookhaven, November 20-21, 1978, BNL 50991, p. 133, Brookhaven National Laboratory, Upton N.Y. (1979).

2 A.B. SMITH, P. LAMBROPOULOS, and J.F. WHALEN, Nucl. Sci. Eng. 47 (1972) 19.

3 F. KÄPPELER, L.D. HONG, and H. BEER, Proc. Specialists Meeting on Nuclear Data of Plutonium and Americium Isotopes for Reactor Applications, Brookhaven, November 20-21, 1978, BNL 50991, p. 49, Brookhaven National Laboratory, Upton, N.Y. (1979).

4 W.P. POENITZ, J.F. WHALEN, and A.B. SMITH, Nucl. Sci. Eng. 78 (1981) 333.

5 R. GWIN et al., Private Communications from L.W. Weston (1981).

6 M.S. MOORE, P.W. LISOWSKI, G.L. MORGAN, G.F. AUCHAMPAUGH, and R.E. SHAMU, Proc. Conf. Nuclear Cross Sections for Technology, Knoxville, October 22-26, 1979, NBS Spec. Publ. 594, p. 703, National Bureau of Standards, 1980.

7 R.W. HOCKENBURY, W.R. MOYER, and R.C. BLOCK, Nucl. Sci. Eng. 49 (1972) 153.

8 L.W. WESTON and J.H. TODD, Nucl. Sci. Eng. 63 (1977) 143.

9 K. WISSHAK and F. KÄPPELER, Nucl. Sci. Eng. 66 (1978) 363.

10 K. WISSHAK and F. KÄPPELER, Nucl. Sci. Eng. 69 (1979) 39.

11 R.W. HOCKENBURY, A.J. SANISLO, and N.N. KAUSHAL, Proc. Conf. on Nuclear Cross Sections and Technology, Washington, D.C., March 3-7, 1975, NBS Spec. Publ. 425, Vol. II, p. 584, National Bureau of Stand., 1975.

12 K. WISSHAK, J. WICKENHAUSER, F. KÄPPELER, G. REFFO, and F. FABBRI, submitted for publication to Nucl. Sci. Eng.

13 L.W. WESTON and R.Q. WRIGHT, Proc. Conf. Nuclear Cross Sections for Technology, Knoxville, October 22-26, 1979, NBS Spec. Publ. 594, p. 464, National Bureau of Standards, 1980.

14 J.W. BEHRENS, R.S. NEWBURY, and J.W. MAGANA, Nucl. Sci. Eng. 66 (1978) 433.

15 K. WISSHAK and F. KÄPPELER, Nucl. Sci. Eng. 69(1979) 47.

16 V.M. KUPRIYANOV, B.I. FURSOV, B.K. MASLENNIKOV, V.M. SURIN, and G.N. SMIRENKIN, Atomnaya Energiya 46 (1979) 35.

17 C. BUDTZ-JØRGENSEN and H.H. KNITTER, accepted for publ. in Nucl. Sci. Eng.

18 L.W. WESTON, Proc. Spec. Meeting on Nuclear Data of Plutonium and Americium Isotopes for Reactor Applications, Brookhaven, November 20-21, 1978, BNL 50991, p. 1 Brookhaven National Laboratory, Upton N.Y. (1979).

19 L.W. WESTON, Private Communication (1981).

20 J.W. MEADOWS, submitted for publication to Nucl. Sci. Eng.

21 J.W. BEHRENS, J.C. BROWNE, and G.W. CARLSON, UCID-17047 Lawrence Livermore Laboratory 1976.

22 J.W. MEADOWS, Nucl. Sci. Eng. 68 (1979) 360.

23 H. WEIGMANN, Private Communications (1981).

24 D.G. MADLAND and P.G. YOUNG, Proc. Spec. Meet. on Nucl. Data for Reactor Applications, BNL 50991, Brookhaven (1978) p. 189.

25 R. KINSEY (ed.), report BNL-NCS-17541 (=ENDF-201) Brookhaven (1979).

26 J. JARY, Ch. LAGRANGE and C. PHILIS, Proc. Spec. Meet. on Nucl. Data for Plutonium and Americium Isotopes for Reactor Applications, BNL 50991, Brookhaven (1978) p. 83.

27 J. JARY, Ch. LAGRANGE, C. PHILIS, J. SALVY, Report CEA-N-2084, Bruyères-le-Châtel (1979).

28 S.-I. IGARASI, T. NAKAGAWA, Y. KIKUCHI, T. ASAMI, and T. NARITA, Report JAERI 1261 (1079).

29 S. KIKUCHI (ed.), Report NEDANC(J)-61/U (1979).

30 H. MATSUNOBU, Y. KANDA, M. KAWAI, T. MURATA, and Y. KIKUCHI, Nucl. Cross Sections for Technology, NBS Spec. Public. 594, Washington (1980), p. 715.

31 G.V. ANTISPOV, V.A. KONSHIN, E.Sh. SUKHOVITSKY, Third Kiev Conference on Neutron Physics, II, p. 21, Kiev (1975), English translation: report INDC(CCP)-77/U (1976).

32 G.V. ANTSIPOV, L.A. BAKHANOVICH, V.A. KONSHIN, V.M. MASLOV, G.B. MOROGOVSKIJ, E.Sh. SUKHOVITSKY, Yu. V. PORODZINSKY, Report INDC(CCP)-150/LJH (1980).

33 B. GOEL, Proc. Spec. Meet. on Nucl. Data of Plutonium and Americium Isotopes for Reactor Applications, Brookhaven (1978), p. 177; F.H. FRÖHNER and B. GOEL, unpublished work.

34 A.M. LAUE and R.G. THOMAS, Rev. Mod. Phys. 30(1958) 257.

35 F.H. FRÖHNER, Nuclear Theory for Applications, IAEA-SMR-43, Trieste (1978), p. 59.

36 U. FISCHER, report KfK 2907 (1980).

37 F.H. FRÖHNER, Proc. Conf. Nucl. Data Eval. Methods, BNL-NCS-51363, Brookhaven (1981) p. 375.

38 A. GILBERT and A.G.W. CAMERON, Can. J. Phys. 43 (1965) 1446.

39 U. FACCHINI and E. SAETTA-MANICHELLA, Energia Nucleare 15 (1968) 54.

40 L. DRESNER, Report CU-175 (1957) p. 71, cf. also E. LYNN; The Theory of Neutron Resonance Reactions, Oxford (1968) p. 230.

41 P. MOLDAUER, Nucl. Phys. A344 (1980) 185.

42 F. POORTMANS, G. ROHR, J.P. THEOBALD, H. WEIGMANN, and G.J. VANPRAET, Nucl. Phys. A207 (1973) 342.

43 G.F. AUCHAMPAUGH and C.D. BOWMAN, Phys. Rev. C7 (1973) 2085.

44 D.L. HILL and J.A. WHEELER, Phys. Rev. 89 (1953) 1102.

45 E.V. GAJ, A.V. IGNATYUK, N.S. ROBOTNOV, G.N. SMIRENKIN, Yad. Fiz. 10 (1969) 542.

46 A.S. TYAPIN, V.E. MARSHALKIN, Yad. Fiz. 18 (1973) 277.

47 P. THOMET, report CEA-R-4631 (1974).

48 B.B. BACK et al, Report LA-UR-74-798 (1974).

49 E. MENAPACE, M. MOTTA, and A. VENTURA, Proc. Spec. Meeting on Nucl. Data of Plutonium and Americium Isotopes for Reactor Appl., BNL-50991, Brookhaven (1978) p. 251.

The Relationship between the Nuclear Doppler and Self–Shielding Effects and the Local s–Wave Strength Function in ^{238}U

N. J. Bee †

Department of Mechanical Engineering,

Imperial College of Science and Technology,
London, England.

September 1981

Abstract

If neutron transmission is averaged over an energy interval containing many resonances, the effective total cross section, σ_T^{eff} calculated from this average transmission depends on the sample thickness, n, and the effective temperature, θ. It is shown here that in the case of ^{238}U, to a first approximation σ_T^{eff} depends only the variable $n/\sqrt{\theta}$. There is therefore a simple mathematical relationship in this case between the nuclear Doppler, $(\partial\sigma_T^{\text{eff}}/\partial\theta)$, and self-shielding, $(\partial\sigma_T^{\text{eff}}/\partial n)$, effects. It is found that when exact values of σ_T^{eff} are calculated numerically from resonance "ladders", the deviations from $n/\sqrt{\theta}$ scaling are small. Also there is a region where σ_T^{eff} depends linearly on $\ln(n/\sqrt{\theta})$, and the gradient here can be used to determine the local s-wave strength function. A review is then presented of experimental measurements of σ_T^{eff} in different energy regions and they are analysed to give values for the local s-wave strength function. Abrupt reductions of this function are observed at 4 keV and 9 keV.

† attached to
Nuclear Physics Division,
A.E.R.E., Harwell,
Oxfordshire, England.

1. Introduction

In order to describe the nuclear reactions in a fast reactor and how they depend on temperature, a knowledge of self-shielding factors is required (L. P. Abagyan *et al.* 1964). A considerable amount of effort over many years by many workers has been devoted to providing data to calculate these factors. The work of this paper is specifically concerned with ^{238}U, which produces the largest contribution to the Doppler effect in a typical reactor.

At energies below 4 keV in ^{238}U compound nuclear resonances are clearly observed in neutron transmission and capture measurements. Resonance parameters can be extracted (see de Saussure *et al.* 1978) and the temperature dependence of the experimental results is well understood in terms of multi-level R–matrix theory (see Chapter 11 of Lynn 1968), and Doppler broadening according to the free gas model. The effect of crystalline binding is taken into account by the use of an effective temperature, following Lamb (1939). Having found resonance parameters self-shielding factors can be calcuated at different temperatures and with different dilution cross sections by programs such as those of Cullen (1980).

Above 4 keV there is still a considerable amount of transmission data for different sample thicknesses and at different temperatures (see for example de Saussure *et al.* 1977, Byoun *et al.* 1972, Vankov *et al.* 1971, Tsang & Brugger 1979, and Haste & Sowerby 1978). There is also capture data (Poenitz 1980). None of this data shows any significant change of form at 4 keV, but above this energy there is not sufficient infomation to extract resonance parameters, and so different techniques to predict self-shielding factors from data must be used. These techniques can also be used below 4 keV, and should be checked in this region against the resonance parameter method. They may even prove to be a simpler description of ^{238}U in this resolved region. The descriptions that have been used to date fall into two categories.

The first involves generating resonance parameters from assumed probability distributions (Brissenden & Durston 1965). Average transmissions (see Haste & Sowerby 1978, Tsang & Brugger 1979, and Byoun *et al.* 1972), and other quantities that can be measured experimentally can then be calculated numerically. When a satisfactory fit is obtained (this may involve selecting one particular set of parameters), these can be used to calculate self-shielding factors as in the resolved region.

The second approach is the one currently used in the ENDF description of the ^{238}U unresolved region. The resonance parameters are regarded not as having a discrete set of values but as occupying a continuum, with a probability weighting associated with each point in this continuum. Predictions made in this way are accurate provided the quantity being predicted depends on a large number of resonance parameters. It should be noted that this is not true for average transmissions of extremely thick samples, as these are dominated by the minimum total cross section rather than any form of average. However in most cases of physical interest the predictions are accurate. They are comparatively simple in form, depending on only a few parameters which describe the probability weighting. Such formulae have been used for many years and can be derived directly by treating the nucleus like an optical scattering body, with no direct reference being made to the compound nucleus bound states (see Roy & Nigam 1967).

In particular, for the case of average neutron transmission with which this paper is mainly concerned, one can construct comparatively simple analytical formulae which predict the statistical average of the energy averaged transmission, where this average is over a large number of random selections of the resonance parameters from the assumed distributions. If a sufficient number of resonances is included in the energy average, then deviations from this statistical average should be small. These formulae express this average value in terms of just a few parameters, which, when there is no self-shielding, are simply strength functions (see Lynn 1968, p. 215). As self-shielding increases other parameters have to be introduced (see Table II of Byoun *et al.* 1972). When there is considerable self-shielding Lynn (1963) reports the relevant parameters to be s– and p-wave strength functions, and the mean s-wave level spacing and radiation width. In physical terms the assumption being made in all these cases is that average transmission is not dependent on details of the resonance distributions such as whether a p-wave resonance happens to coincide with the interference minimum of an s-wave resonance, but only on average behaviour.

The main object of the work reported here is to justify the use of this second approach, despite the pessimistic conclusions presented in Section 3 of Haste & Sowerby (1978). If this can be done, it should be possible to obtain certain average resonance parameters (in particular the local s-wave strength function), from average transmission data at different sample thicknesses and temperatures. These can then be used in the calculation of self-shielding factors, if these are expressed in terms of the same parameters.

2. The high temperature limit of the Doppler broadened MLBW cross section

De Saussure *et al.* (1976) have found that the Multi-level Breit–Wigner (MLBW) form of the nuclear cross section together with a "picket fence" extension of resonances outside the resolved region is adequate to describe the ^{238}U total cross section in the resolved energy region. Using this formalism in the unresolved region allows us to write

$$\sigma_T = \sum_l \sigma_T^l \tag{2.1}$$

$$\sigma_T^l = \sigma_p^l + \sum_r \sigma_0^r \left(\frac{1}{1+x_r^2} + \frac{a^r x_r}{1+x_r^2} \right). \tag{2.2}$$

Here the total cross section has been written as a sum of components with definite orbital angular momentum l. Each of these can be expressed as the sum of a potential term and a series of Breit–Wigner terms.

The potential term is given by the expression

$$\sigma_p^l = (2l+1)\frac{4\pi}{k^2} \sin^2 \varphi_l , \tag{2.3}$$

where the wave number k is given by

$$k = \sqrt{\frac{2mE}{\hbar^2}} \left(\frac{M}{M+m} \right),$$

E being the laboratory energy of the incident neutron, m its mass and M the mass of the target nucleus. The potential scattering phase shift φ_l has the simple value ka, where a is the nuclear radius, for $l = 0$.

The Breit–Wigner term corresponding to a resonance r has a peak height given by

$$\sigma_0^r = \frac{4\pi}{k^2} g_J \frac{\Gamma_{nr}}{\Gamma_r} (\cos 2\varphi_l + B_r), \tag{2.4}$$

where g_J is the statistical spin weighting factor ($= J + \frac{1}{2}$ when the target nucleus has spin 0), Γ_{nr} is the neutron width and Γ_r the total width of resonance r. The term is centred at E_r, with

$$x_r = \frac{2}{\Gamma_r} (E - E_r), \tag{2.5}$$

and has an interference term whose coefficient is

$$a^r = \frac{\sin 2\varphi_l + C_r}{\cos 2\varphi_l + B_r}. \tag{2.6}$$

B_r and C_r take into account multi-level effects

$$B_r = \frac{1}{2} \sum_{s \neq r} \frac{\Gamma_{ns}(\Gamma_r + \Gamma_s)}{(E_r - E_s)^2 + \frac{1}{4}(\Gamma_r + \Gamma_s)^2} \tag{2.7}$$

$$C_r = \sum_{s \neq r} \frac{\Gamma_{ns}(E_r - E_s)}{(E_r - E_s)^2 + \frac{1}{4}(\Gamma_r + \Gamma_s)^2}. \tag{2.8}$$

Eqn. (2.2) expresses the total cross section as the sum of Breit–Wigner terms. If the energy dependence of the quantities other than x_r is neglected, and if it is assumed that the Doppler width is much less than the resonance energies Doppler broadening can be performed easily,

$$\sigma_T^l \simeq \sigma_p^l + \sum_r \sigma_0^r \frac{\sqrt{\pi}}{\beta_r} \left\{ \mathscr{R}\, \omega \left(\frac{x_r}{\beta_r} + \frac{i}{\beta_r} \right) + a^r \mathscr{I}\, \omega \left(\frac{x_r}{\beta_r} + \frac{i}{\beta_r} \right) \right\}, \tag{2.9}$$

where

$$\beta_r = \frac{2\Delta}{\Gamma_r}, \tag{2.10}$$

and

$$\Delta = \sqrt{4k_B \theta E m / M}. \tag{2.11}$$

The quantity k_B is Boltzman's constant, and θ is the effective absolute temperature, taking into account the effect of crystalline binding (see Lamb 1939). $\mathscr{R}$, $\mathscr{I}$ are real and imaginary parts, and $\omega(z)$ is the complex error function discussed in Chapter 7 of Abramowitz & Stegun (1970), and defined by

$$\omega(z) = \frac{i}{\pi} \int_{-\infty}^{\infty} \frac{e^{-t^2}\, dt}{z - t} \tag{2.12}$$

$$= e^{-z^2} + \frac{2i}{\sqrt{\pi}} F(z), \tag{2.13}$$

where $F(z)$ is Dawson's integral

$$F(z) = e^{-z^2} \int_0^z e^{t^2}\, dt. \tag{2.14}$$

For ^{238}U in the region where the Doppler effect is significant $\beta_r \sim 20$ at room temperature, and is much larger than this at the higher temperatures of interest in reactor safety studies. The quantity i/β_r is therefore small and σ_T^l can be approximated by setting it to zero

$$\sigma_T^l \simeq \sigma_p^l + \sum_r \sigma_0^r \frac{\sqrt{\pi}}{\beta_r} \left\{ e^{-x_r^2/\beta_r^2} + a^r \frac{2}{\sqrt{\pi}} F\left(\frac{x_r}{\beta_r} \right) \right\}. \tag{2.15}$$

3. The $n/\sqrt{\theta}$ scaling property of effective average total cross sections

When performing an experiment it is always important to extract from the data quantities which do not depend on the detail of the experiment. Results from different experimenters using different equipment and techniques can then be compared. In the case of neutron transmission results must be independent of the energy resolution function. In the resolved region such results can be the standard transmission area for sets of resonances or, if more processing is done, resonance parameters. In the unresolved region, by definition there is not sufficient data to determine resonance parameters and transmission areas cannot be obtained correctly either. The best that can be done is to average the transmission over energy regions containing many resonances. The region should be large enough to make both the wing corrections arising from the partial inclusion of resonances and the dependence on resolution function small. The region, however, must not be too big otherwise the potential scattering cross section could not be treated as constant over it, and much data would be unnecessarily discarded.

In a suitable energy region σ_T can be written in the form of the preceding section

$$\sigma_T = \sigma_c + \sum_r \sigma_r \,, \tag{3.1}$$

where σ_c is a potential scattering term with the effect of distant levels included, σ_r is a Breit–Wigner cross section, and $\sum_r$ only includes resonances inside the energy region being considered.

If energy averaging over the region of width W is denoted by $\langle\ \rangle$ we can write

$$\langle T \rangle = \left\langle e^{-n\sigma_T} \right\rangle = e^{-n\sigma_c} \left\langle e^{-n\sum_r \sigma_r} \right\rangle \tag{3.2}$$

$$= e^{-n\sigma_c} \left\{ 1 - n\frac{1}{W}\sum_r \int \sigma_r dE + \frac{n^2}{2!}\frac{1}{W}\left(\sum_r \int \sigma_r^2 dE + \sum_{r\neq s} \int \sigma_r \sigma_s dE \right) \right.$$

$$\left. - \frac{n^3}{3!}\frac{1}{W}\left(\sum_r \int \sigma_r^3 dE + \sum_{\substack{r,s,t \\ \text{not all equal}}} \int \sigma_r \sigma_s \sigma_t \, dE \right) + \ldots \right\} . \tag{3.3}$$

From now on the cross terms in this equation will be neglected. Those that involve resonances with the same J,l values are small because the Wigner level spacing distribution predicts a small probability for two resonances to be close enough to have a subtantial overlap. Those with different J,l values are also small if the Doppler width is much less than the level spacing. Neglecting these terms allows the right hand size of Eqn. (3.3) to be summed to give

$$\langle T \rangle = e^{-n\sigma_c} \left(1 - \frac{1}{W}\sum_r A_E^r \right) , \tag{3.4}$$

where A_E^r is the standard transmission area function

$$A_E^r = \int_{-\infty}^{\infty} \left(1 - e^{-n\sigma_r} \right) dE \,. \tag{3.5}$$

The limits of integration here have been extended to infinity and the resulting wing correction neglected. This is because wing corrections from different resonances have different signs and average to zero. Eqn. (3.4) has also been obtained by Lynn (1963), where he explicitly evaluates correction terms and finds them to be negligible.

Using the high temperature limit of the Breit–Wigner form for σ_r, Eqn. (3.5) can be written

$$A_E^r = \Delta \int_{-\infty}^{\infty} \left[1 - \exp - \left\{ \frac{n\sigma_0^r \sqrt{\pi}\Gamma_r}{2\Delta} \left(e^{-\xi^2} + a^r \frac{2}{\sqrt{\pi}} F(\xi) \right) \right\} \right] d\xi \,. \tag{3.6}$$

As $\Delta \propto \sqrt{\theta}$, A_E/n depends on the variable $n/\sqrt{\theta}$ in the high temperature limit. The next paragraph discusses the extent to which this is true at temperatures of physical interest.

It is convenient to define the normalised area function A_n so that its value for small n is unity,

$$A_n = \frac{2}{\pi n \sigma_0^0 \Gamma_n} A_E \,,$$

where $\sigma_0^0 = 4\pi g_J / k^2$. It is plotted against the logarithm of $n\sigma_0^0\Gamma_n / 2\Delta$ in Fig. 3.1 (a), (b) and (c). for an s-wave resonance. Three values of the interference parameter a are considered, namely $a = 0$, $a = 0.28$ and $a = 0.41$. The latter two are the values taken by a at 5 keV and 10 keV respectively, if the effect of resonance-resonance interference on the interference minima of s-wave resonances is neglected. Two values of the temperature parameter have been considered; $\beta = 16$, corresponding to room temperature, and $\beta = \infty$. In the abscissa region shown in Fig. 3.1, which is the region of interest in most experiments, increasing the temperature by a factor of four from room temperature, and therefore doubling β, changes A_n by ~0.02 at fixed $n/\sqrt{\theta}$. This is ~10% of the change that would occur at fixed n, and this gives an indication of the accuracy of $n/\sqrt{\theta}$ scaling. It should be noted from Fig. 3.1 that for thin samples the Doppler effect is independent of a, whereas for thick samples, when the effect is caused by the filling in of s-wave interference dips, there is a strong dependence on the size of these dips and therefore a. $\langle T \rangle$ can therefore be written in the form

$$\langle T \rangle = e^{-n\sigma_c} \left| 1 - n f(n/\sqrt{\theta}) \right| . \tag{3.7}$$

Provided Δ is much less than the level spacing, nf will be small and Eqn. (3.7) can be written

$$\langle T \rangle = \exp \left\{ -n \left[\sigma_c + f(n/\sqrt{\theta}) \right] \right\} , \tag{3.8}$$

and the effective average total cross section is simply

$$\sigma_T^{\text{eff}} = \sigma_c + f(n/\sqrt{\theta}) \,. \tag{3.9}$$

If σ_T^{eff} has this simple form there is a simple relationship between the Doppler and self-shielding effects

$$\theta \frac{\partial \sigma_T^{\text{eff}}}{\partial \theta} = -\frac{1}{2} n \frac{\partial \sigma_T^{\text{eff}}}{\partial n} \,, \tag{3.10}$$

or, if sample expansion is allowed

$$\frac{d\sigma_T^{\text{eff}}}{d\theta} = -\left(\frac{1}{2}\frac{1}{\theta} + 2a_\theta \right) n \frac{\partial \sigma_T^{\text{eff}}}{\partial n} \,, \tag{3.11}$$

where a_θ is the linear thermal expansion coefficient.

Numerical tests of Eqn. (3.10) described in Section 5 show that the two sides of this equation typically differ by about 5%.

4. The determination of the local s-wave strength function from effective average total cross section data

In order to analyse experimental data in a given energy region certain assumptions about the resonances in that region have to be made. In contrast to situation when evaluating average capture and the self-shielding factors, nothing need be known about the Γ_γ's of the included resonances. This is because the high temperature limit of the average transmission given by Eqn. (3.4) has the interesting property that it is independent of these quantities.

A further simplification can be made if multi-level effects are ignored. Lynn (1963) has shown that these are of order

$$-\frac{\pi^3}{k^2}\left(\frac{\Gamma_n}{D}\right)^2 \sim 60 \text{ m barns},$$

which is a small though not insignificant quantity. If this is done a is the same for all resonances, and the average transmission of Eqn. (3.4) is then independent of the energy distribution of the resonances. This is because overlap effects in the average transmission have been neglected.

As a result the only assumption that must be made is concerned with the local distribution of the Γ_n's. At this point Lynn (1963) uses the distribution of Porter & Thomas (1956). This has been criticised by de Saussure & Perez (1981), who argue that there is no reason to expect a small sample of reduced neutron widths to have a Porter–Thomas distribution around their locally averaged value. Fig. 4.1 shows the effect of self-shielding on average transmission when this distribution is used, and Figs. 3.1 (a), (b) and (c) correspond to the use of a delta function distribution. It can be seen that the gradients of the corresponding linear regions (which will prove to be of use later) are similar, and they are therefore insensitive to the distribution used. However, the large n behaviour is highly sensitive, as it depends on a few large resonances.

Using the Porter–Thomas distribution allows us to write in the high temperature limit

$$\langle T\rangle = e^{-n\sigma_c}\left\{1-\sum\frac{\rho\Delta}{\sqrt{2\pi}}\int_0^\infty dx\frac{e^{-x/2}}{\sqrt{x}}\int_{-\infty}^{\infty}d\xi\left(1-\exp\left\{\frac{-n\sigma_0^0\bar{\Gamma}_n x\sqrt{\pi}}{2\Delta}\left[e^{-\xi^2}+a\frac{2}{\sqrt{\pi}}F(\xi)\right]\right\}\right)\right\}, \quad (4.1)$$

where $x=\Gamma_n/\bar{\Gamma}_n$, $\bar{\Gamma}_n$ is the mean neutron width, ρ is the mean level density, $\sigma_0^0=4\pi g_J/k^2$ and $a=2ka$. The sum is over the different l,J values for the resonances.
Performing the x integration gives

$$\langle T\rangle = e^{-n\sigma_c}\left[1-\sum\rho\Delta\int_{-\infty}^{\infty}d\xi\left\{1-\left(1+\frac{2n\sigma_0^0\bar{\Gamma}_n\sqrt{\pi}}{2\Delta}\left[e^{-\xi^2}+a\frac{2}{\sqrt{\pi}}F(\xi)\right]\right)^{-1/2}\right\}\right] \quad (4.2)$$

$$= e^{-n\sigma_c}\left[1-n\frac{\pi}{2}\sigma_0^0\rho\bar{\Gamma}_n G\left(\frac{n\sigma_0^0\bar{\Gamma}_n}{2\Delta}\right)\right], \quad (4.3)$$

where

$$G(v)=\frac{1}{\pi v}\int_{-\infty}^{\infty}d\xi\left\{1-\frac{1}{\sqrt{1+2v\sqrt{\pi}\left[e^{-\xi^2}+(2a/\sqrt{\pi})F(\xi)\right]}}\right\}. \quad (4.4)$$

$G(v)$ is shown in Fig. 4.1 for $a=0$, $a=0.28$, and $a=0.41$, the latter two being the values taken by a for ^{238}U at 5 and 10 keV respectively. G is not defined if the argument of the square root becomes negative for any ξ; this happens when v exceeds a critical value.

It is found that the second term in the braces of Eqn. (4.3) is small, so we can write

$$\sigma_T^{\text{eff}}=\sigma_c+\sum\frac{\pi}{2}\sigma_0^0\rho\bar{\Gamma}_n G\left(\frac{n\sigma_0^0\bar{\Gamma}_n}{2\Delta}\right). \quad (4.5)$$

For resonances with $l>0$ the corresponding argument of G in Eqn. (4.5) is small. G can then be approximated by unity, and σ_c is then effectively changed by a constant amount. Thus only s-wave resonances contribute significantly to the Doppler and self-shielding effects.

By fitting Eqn. (4.5) to data both the s-wave strength function $\rho\bar{\Gamma}_n/\sqrt{(E(eV)}$, and $\bar{\Gamma}_n$ can be obtained. In particular it can be seen from Fig. 4.1 that there is a wide region where G depends linearly on the logarithm of its argument. For $a\approx 0$ the gradient is -0.15 per factor 2 change in argument (or, more briefly, "per octave"), for $a=0.28$ it is -0.17, and for $a=0.41$ it is -0.23. By measuring the corresponding gradient from graphs such as Fig. 6.2, it is straightforward to make an estimate of the s-wave strength function using Eqn. (4.5)

$$S=\frac{g\sqrt{E}}{12.93\,r}, \quad (4.6)$$

where S is the s-wave strength function in units of 10^{-4}, g is the gradient of σ_T^{eff} against $\ln(n/\sqrt{\theta})$ in barns/octave, E is the energy on keV and r is the theoretically calculated gradient of G referred to above.

5. Numerical calculation of σ_T^{eff} at different sample thicknesses and temperatures.

The work described here is a continuation of that reported in Section 3 of Haste & Sowerby (1978), although several changes have been made. It was decided to replace the computer program AVTRAN by several other programs which together perform the same task.

The first of these, GENERATE, is a newly written program to generate sets of resonance parameters from the Porter–Thomas (1956) reduced neutron width distribution and the Wigner level spacing distribution. In contrast to the corresponding step in AVTRAN, only s-wave resonance parameters are generated, because it is only these that contribute significantly to the self-shielding and Doppler effects. This considerably simplifies the calculations to be performed.

Another difference is that the generated parameters are permanently stored. ENDF format is used (see Kinsey 1979), and an unique "MAT" number is assigned to each set, together with several lines,of descriptive comments. Table 5.1 describes several of the sets used.

"MAT" number	Energy region (keV)	Expectation value of neutron width (eV)	Expectation value of resonance spacing (eV)	Input for random number generator (FC01AS in Harwell Subroutine Library)
11	3.8 – 5.2	.134	20	(1234, 4321)
12	3.8 – 5.2	.134	20	(1666, 6661)
13	3.8 – 5.2	.067	20	(1666, 6661)
14	3.8 – 5.2	.067	20	(1357, 7531)
17	3.8 – 5.2	.1	20	(1247, 7431)
20	8.8 – 10.2	.195	20	(395, 6789)
21	8.8 – 10.2	.0975	20	(3397, 4041)
22	8.8 – 10.2	.1463	20	(31415,92653)
30	3.7 – 5.3	.134	20	(10101,10101)
31	3.7 – 5.3	.134	20	(2358, 6395)
32	3.7 – 5.3	.067	20	(27818,28305)
33	3.7 – 5.3	.067	20	(11685,12671)
1262	3.0 – 4.0			

Table 5.1 A description of various sets of resonance parameters for which σ_T^{eff} has been calculated

These can readily be inspected later to calculate local strength functions in limited energy regions, and to check whether the resonances have any features such as the presence of excessively large resonances near an energy boundary used later.

The second step in predicting effective average total cross sections is the calculation of the pointwise Doppler broadened total cross section from the resonance parameters. This can be performed by any of the programs available around the world, provided simple ENDF interfacing programs are written for the input and output files. ENDF output from these programs is again permanently stored and can be viewed at any magnification by the newly written program GRAPH. In this way checks can easily be made that different programs produce the same cross section and that enough energy points have been used to specify it satisfactorily. To date SIGAR (Story 1981), the two programs RECENT and SIGMA1 (Cullen 1980), and a section of the original AVTRAN (Lynn 1964) have been used. Test runs show that the cross sections produced by RECENT and SIGMA1 are in resonable agreement with the results of SIGAR. SIGAR was used to obtain most of the results of this section.

The final step, namely the calculation of σ_T^{eff} from pointwise cross sections is performed by a new program SIGMAEFF which evaluates σ_T^{eff} exactly for any specified energy region, assuming that the pointwise Doppler broadened cross section is linearly interpolable.

Fig. 5.1 shows some typical predictions of σ_T^{eff} for different sample thicknesses, n, and absolute temperatures θ. The abscissa is the logarithm of $n / \sqrt{\theta / \theta_0}$, where θ_0 is 300 K. The hree energy regions shown are, (a) 4–5 keV, (b) 9–10 keV, and (c) 18–20 keV. The local s-wave strength function is shown on the graphs. The effect of p-wave resonances is simply to add a constant to σ_T^{eff}, so they have not been included in calculations. The mean level spacing for the s-wave resonances, $\bar{D}$, was taken to be 20 eV, the nuclear radius, a, was assumed to have the ENDF/B–1V value of 9.184 fm, and the radiation width of all resonances, Γ_γ, was assigned the value 23 meV. It can be seen that $n/\sqrt{\theta}$ scaling holds to about 10%, but is better when resonances are weak. Table 5.2 and Fig. 5.2 compare predictions made of the local s-wave strength function made using Eqn. (4.6) with the true values calculated from the resonance parameters. Fig. 5.3 is similar except that resonance parameters from the ^{238}U ENDF/B–1V file were used, instead of stochastically generated ones. It can be concluded that that Eqn. (4.6) is valid to within about 10%.

"MAT" number	Actual s-wave strength function in units of 10^{-4}	Gradient of linear region of σ_T^{eff} against $\ln(n/\sqrt{\theta})$ (barns/octave)	Predicted s-wave strength function in units of 10^{-4}	Error (%)
11	1.217	1.188 ± 1%	1.147	–5.8
12	1.174	1.165 ± 1%	1.124	–4.3
13	0.445	0.420 ±10%	0.406	–8.8
14	0.510	0.527 ± 1%	0.509	–0.2
17	0.869	0.868 ±.1%	0.837	–3.7
20	0.984	0.750 ±10%	1.050	+6.5
21	0.493	0.338 ±10%	0.474	–3.9
22	0.695	0.522 ±35%	0.732	+5.3
30	0.906	0.917 ± 1%	0.885	–2.3
31	1.115	1.089 ± 1%	1.051	–5.7
32	0.537	0.570 ± 5%	0.549	+2.2

Table 5.2 Comparison of predicted and actual local s-wave strength functions for different sets of resonances at several energies.

Fig. 5.4 shows a comparison of σ_T^{eff} calculated from Eqn. (4.3) and from resonance parameters directly using SIGAR for the resonance set with "MAT" number 13, at 5 keV. Agreement can be seen to be very good up to a sample thickness of about 0.2 atoms/barn. Fig. 5.5 shows a similar comparison at 2 keV using resonance parameters taken from ENDF/B-IV.

6. Experimental measurements of the temperature variation of ^{238}U effective average total cross sections.

In this section the results from some experiments designed to measure the Doppler and self-shielding effects in ^{238}U are briefly reviewed. Five experiments, (a) to (e), are considered. The first uses filters to select neutron energy; the others use neutron time-of-flight techniques. The sample temperature is varied in all except experiment (e).

The data in each case are fitted using equation Eqn. (4.5). However the measurements are not sufficiently accurate, particularly in the thin sample region, to determine $\tilde{D}$, so this parameter was not varied but given a constant value 20 eV. Values of σ_c and the local s-wave strength function were obtained, and do not depend significantly on the assumption about $\tilde{D}$. The theoretical curves are not defined when n exceeds a critical value, so fitting must be done with points where n is less than this value (which in most cases is ~ 0.2 atoms/barn). Above this value σ_T^{eff} depends on the largest resonances present, not the overall probability distribution.

a). Tsang & Brugger (1979), and Brugger & Aminfar (1981)

In these experiments neutrons were selected by filters to have energies of 2 ± 0.35 keV, 24 ± 0.9 keV and 144 ± 12 keV. At 144 keV it is difficult to measure the very small Doppler and self-shielding effects. The other two sets of data are shown in Fig. 6.1, where the measured values of σ_T^{eff} for different sample thicknesses, n, and for three of the temperatures used, θ, are plotted against $\ln(n/\sqrt{\theta/\theta_0})$, where θ_0 is 303K. The data shown in Fig. 6.1 (a) is at 24 keV.

This figure also shows a theoretical fit using Eqn. (4.5) with a local s-wave strength function of 0.71×10^{-4} and $\sigma_c = 11.37$ barns.

For the more recent data taken at 2 keV, shown in Fig. 6.1 (b), a similar analysis indicates a local s-wave strength function of 0.87×10^{-4}, and $\sigma_c = 12.44$ barns.

b). Byoun, Block & Semler (1979)

The results from this experiment are available from the NEA data bank at Saclay. The data were taken on the Rensselaer Polytechnic Institute Linear Accelerator at temperatures up to 1000 K. Fig. 6.2 shows typical resuls for an energy bin extending from 3.058 to 4.129 keV. Discrepancies from $n/\sqrt{\theta}$ scaling appear to be within 0.2 barns. The error bars shown here have been estimated from the statistical fluctuations of the results. The theoretical curve shown is obtained with an s-wave strength function of 1.3×10^{-4}, and $\sigma_c = 13.4$ barns. Fig. 6.3 shows the results of similar analyses in different bins spanning the 2 to 12 keV region. There are significant drops at 4 keV and 9 keV.

c). Haste & Sowerby (1978)

This experiment was performed on the Harwell Linear Accelerator. Count loss corrections were not performed on these data, so only cross section differences between thick samples as temperature varies are reliably predicted. Typical results are shown in Fig. 6.4. Using the gradients of these curves the s-wave strength function can be calculated, using Eqn. (4.6). The results are shown in Fig. 6.3, which again shows significant drops at 4 and 9 keV. The 2 to 3 keV result is not shown, as the linear region for the σ_T^{eff} against $\ln(n/\sqrt{\theta})$ occurs for low n values where the cross section is not accurately determined.

d). Vankov *et al.* (1971)

This data has been averaged in much wider energy bins than that of later experiments, and so is not suitable for detecting local fluctuations of the s-wave strength function. However $n/\sqrt{\theta}$ scaling is approximately satisfied, as can be seen from graphs such as the one reproduced here as Fig. 6.5. The theoretical fit shown was produced using an s-wave strength function of 1.0×10^{-4} and $\sigma_c = 11.3$ barns.

e). Olsen *et al.* (1977)

This data, taken at the Oak Ridge National Laboratory, is available from the National Nuclear Data Center at Brookhaven National Laboratory. It is transmission data taken at four sample thicknesses, but only at room temperature. It has been averaged, and an estimate of the local s-wave strength function is similar to that shown in Fig. 6.3, except for a peak at 6 to 7 keV, which is not present in the other data.

7. Conclusions

By considering the high temperature limit of the work of Lynn (1963), when all the resonances have the same width, governed by the temperature, it has been shown that, to a good approximation, the contribution of the resonances to the effective average total cross section, σ_T^{eff}, over an energy region containing many resonances, depends only on $n/\sqrt{\theta}$. This dependence has a fixed functional form at a given energy, the form being altered in scale not shape by changes in local s-wave strength function and level spacing. Changes in energy, however, do alter the shape, as these are associated with changes in resonance-potential interference. This simple description of σ_T^{eff} curves has been found to be accurate to about ± 0.1 barns at 5 keV, ± 0.2 barns at 10 keV, and ± 0.5 barns at 24 keV.

Between 5 and 20 keV, σ_T^{eff}, when plotted against the logarithm of $n/\sqrt{\theta}$ is found to have a linear region and the gradient here can be used to predict a value for the local s-wave strength function. These values are systematically $\sim$ 5% too low, and have a similar statistical error, but they are sufficiently accurate to detect structure in the ^{238}U local s-wave strength function, which is found to have statistically significant drops at 4 and 9 keV, in three sets of data.

If increased accuracy is required, violation of $n/\sqrt{\theta}$ scaling would have to be taken into account explicitly, and many other correction terms would have to be evaluated. However, the

equations derived in this paper at least act as a starting point for more detailed studies, and may prove to be adequate for the needs of reactor physicists.

Acknowledgements

The author would like to thank many members of the Linear Accelerator Group at Harwell, in particular Dr. M. G. Sowerby for supervising this work, and for his many useful suggestions. Specific mention should also be made of Mr. M. C. Moxon and Dr. D. B. Syme for their valuable discussions. Mr. M. B. Bailey and Mr. D. M. James have benn very helpful in tackling some of the many numerical and analytical problems that have arisen during the course of the work reported here, and thanks should also go to Dr. E. Gryntakis of the N.E.A. data bank for providing much of the experimental data analysed here.

The Computer Science and Systems Division at Harwell has provided excellent technical support both for the computational work that has been done, and for the typesetting of this document, for which M. J. Hopper's TSSD system was used.

Finally, I would like to acknowledge the encouragement, support and advice of Dr. J. E. Lynn and Dr. M. S. Coates at Harwell. It was their work in arranging the E.M.R. contract, in association with Dr. A. H. Goddard of Imperial College of Science and Technology, London, which enabled this work to be financed.

References

Abramowitz M. & Stegun I. A. (1965). *Handbook of Mathematical Functions*. Dover.

Abagyan L. P. *et al.* (1964). *Group Constants for Nuclear Reactor Calculations* (I. I. Bondarenko, Ed., translated by Conultants Bureau, New York, 1964).

Brissenden R. J. & Durston C. (1965). *The Calculation of Neutron Spectra in the Doppler Region*, in ANL–7050 p. 51.

Brugger R. M. & Aminfar H. (1981). An invited paper to be presented at the Joint IAEA/NEA Consultants Meeting on Uranium and Plutonium Resonance Parameters, Vienna, September 28 – October 2, 1981.

Byoun T. Y., Block R. C. & Semler T. (1972). *Proc. National Topical Meeting on New Developments in Reactor Physics Shielding, Kiamesha Lake, New York, September 12–15 1972*. (USAEC) p. 115.

Carraro G. & Kolar W. (1970). *Proc. Int. Conf. Nuclear Data for Reactors, Helsinki* IAEA-CN–26/116 **1**, 403. IAEA, Vienna.

Cullen D. E. (1980). *Lawrence Livermore Laboratory Report* UCRL–50400.

Haste T. J. & Sowerby M. G. (1978). *Atomic Energy Research Establishment Report* AERE-R 8961.

Kinsey R. (1979). *ENDF–102 Data Formats and Procedures for the Evaluated Nuclear Data File, ENDF*, National Nuclear Data Center, Brookhaven National Laboratory Associated Universities Inc. BNL-NCS–50496.

Lamb W. E. (1939). *Phys. Rev.* **55**, 190.

Lynn J. E. (1963). *Proc. Phys. Soc.* **82**, 903.

Lynn J. E. (1964). Private communication.

Lynn J. E. (1968). *The Theory of Neutron Resonance Reactions*. Clarendon Press, Oxford.

Olsen D. K., Saussure G. de, Perez R. B., Difilippo F.C., Ingle R.W. & Weaver H. (1977). *Oak Ridge National Laboratory Report* ORNL/TM–5915.

Poenitz W. P. (1980). BNL-NCS–51123.

Porter C. E. & Thomas R. G. (1956). *Phys. Rev.* **104**, 483.

Roy R. R. & Nigam B. P. (1967). *Nuclear Physics*. Wiley, New York.

Saussure G. de, Olsen D. K. & Perez R. B. (1976). *Nucl. Sci. Eng.* **61**, 496.

Saussure G. de, Olsen D. K., Perez R. B. & Difilippo F.C. (1978). *Oak Ridge National Laboratory Report* ORNL/TM–6152.

Saussure G. de & Perez R. B. (1981). Paper presented at the American Nuclear Society Meeting, June 7–12, 1981, Miami, Florida.

Story J. (1981). Private communication.

Tsang F. Y. & Brugger R. M. (1979). *Nucl. Sci. Eng.* **72**, 52.

Vankov A. A., Grigoriev Yu. V., Nikolaev M. N., Filippov W., Bochmer B., Collatz S. & Pickelner L.B. (1971). INDC (CCP)–16/L (translation by IAEA) p. 49.

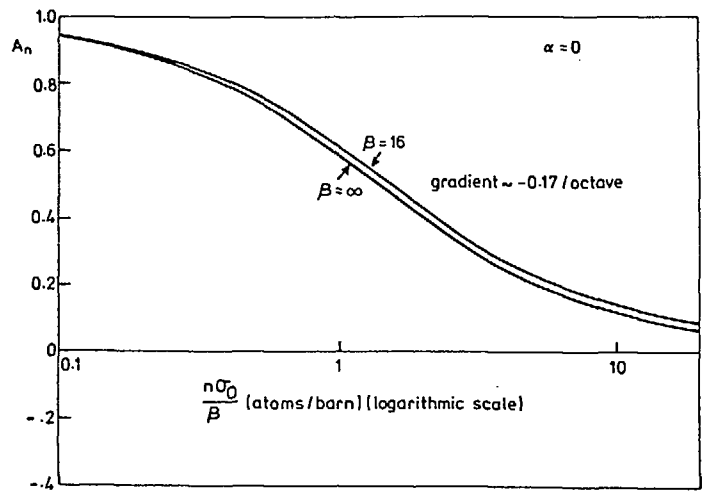

Fig. 3.1 (a)

A plot of the normalised area function, A_n, against the logarithm of $n\sigma_0^0\Gamma_n / 2\Delta$ for $\alpha = 0$ (corresponding to no interference).

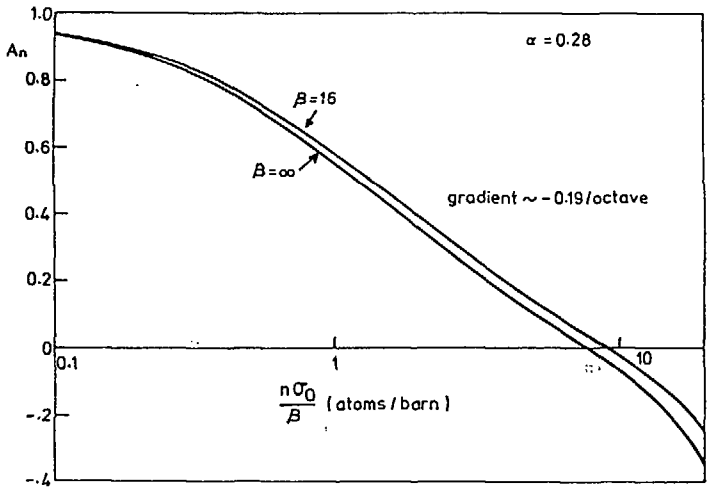

Fig. 3.1 (b)

A plot of the normalised area function, A_n, against the logarithm of $n\sigma_0^0\Gamma_n / 2\Delta$ for $\alpha = 0.28$ (corresponding to the interference at 5 keV).

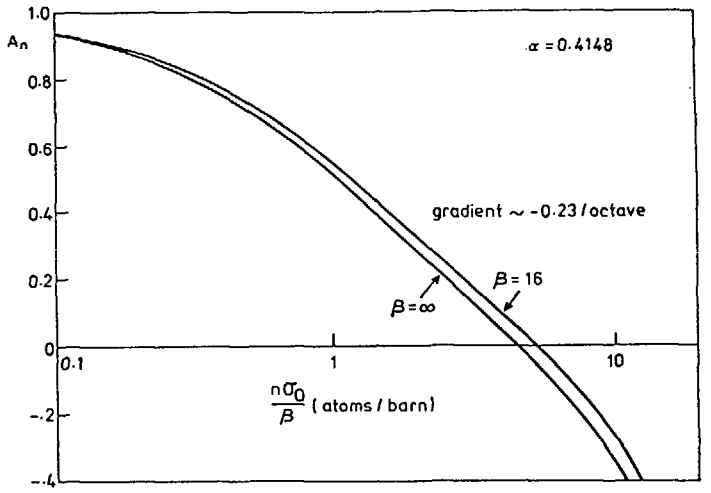

Fig. 3.1 (c)

Plots of the normalised area function, A_n, against the logarithm of $n\sigma_0^0\Gamma_n / 2\Delta$ for $\alpha = 0.4148$ (corresponding to 10 keV).

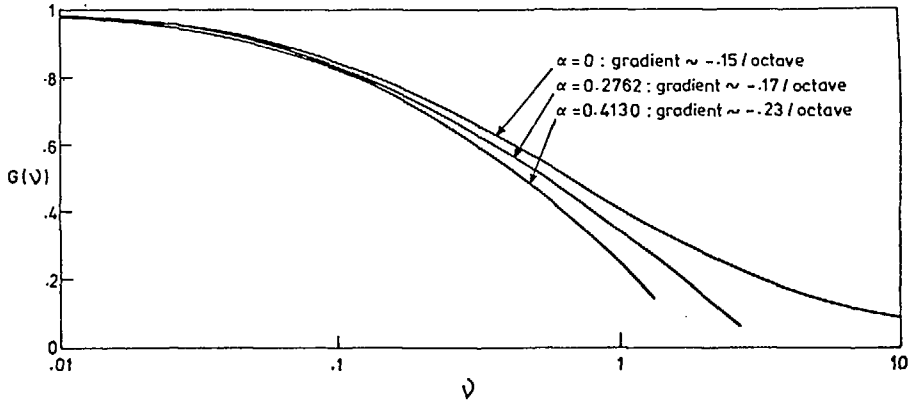

Fig. 4.1

The normalised Porter–Thomas weighted area function in the infinite temperature limit.

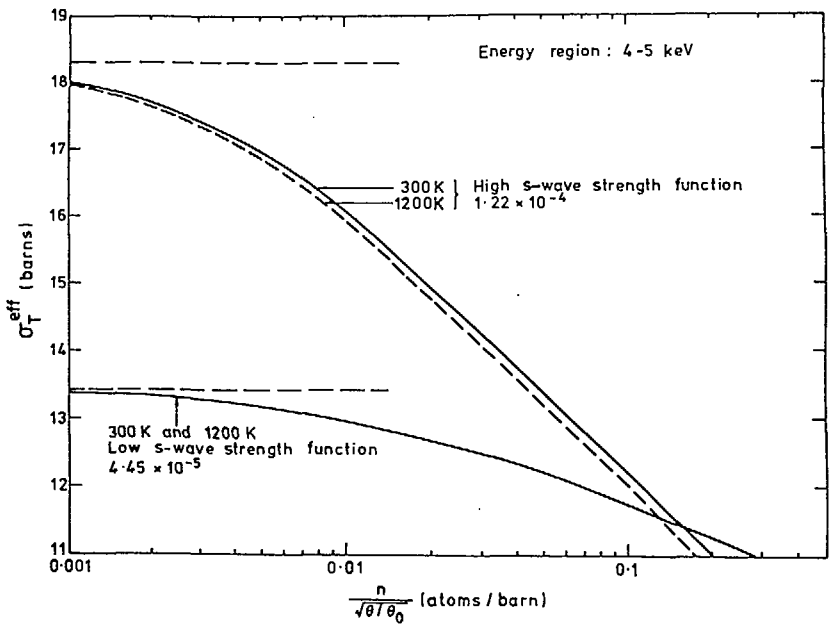

Fig. 5.1 (a)

Predictions from numerical computer calculations of the dependence of the effective average total cross section of ^{238}U on sample thickness, temperature and assumed local s-wave strength function, from 4 to 5 keV.

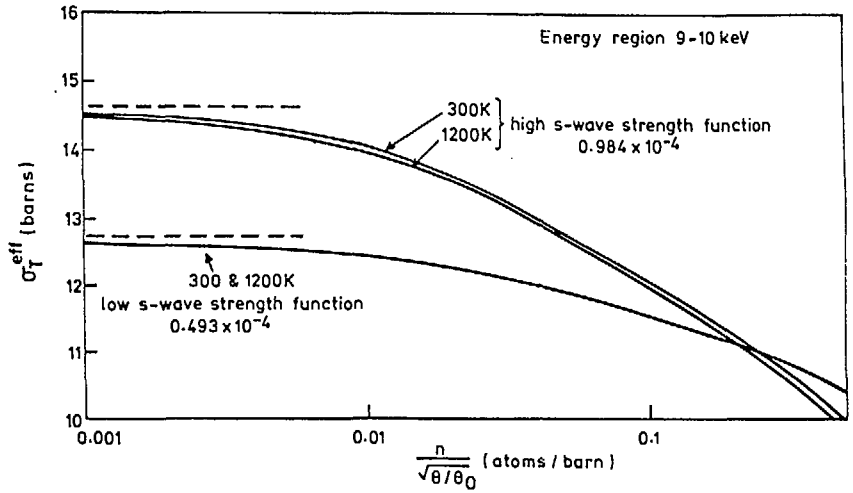

Fig. 5.1 (b)

Predictions from numerical computer calculations of the dependence of the effective average total cross section of ^{238}U on sample thickness, temperature and assumed local s-wave strength function, from 9 to 10 keV.

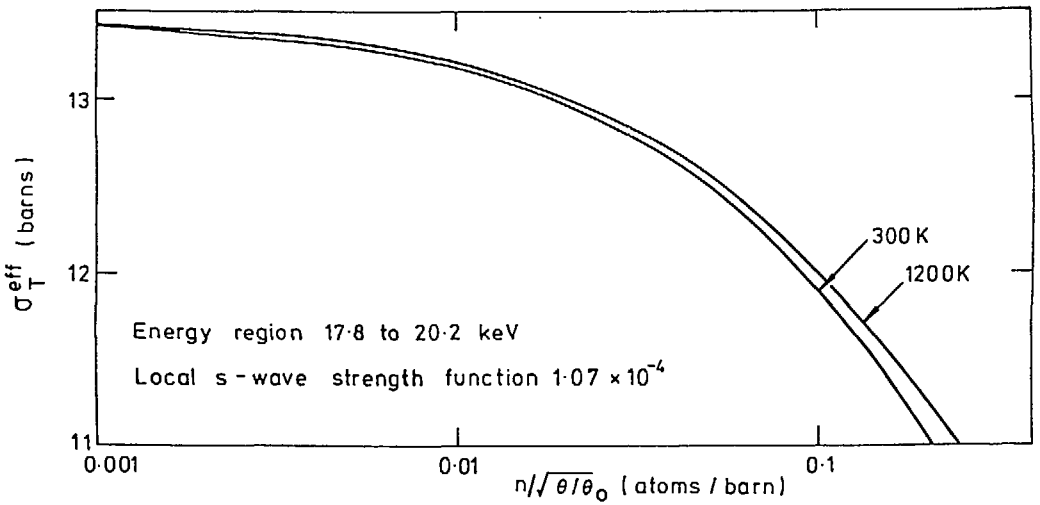

Fig. 5.1 (c)

Predictions from numerical computer calculations of the dependence of the effective average total cross section of ^{238}U on sample thickness, temperature and assumed local s-wave strength function, from 18 to 20 keV.

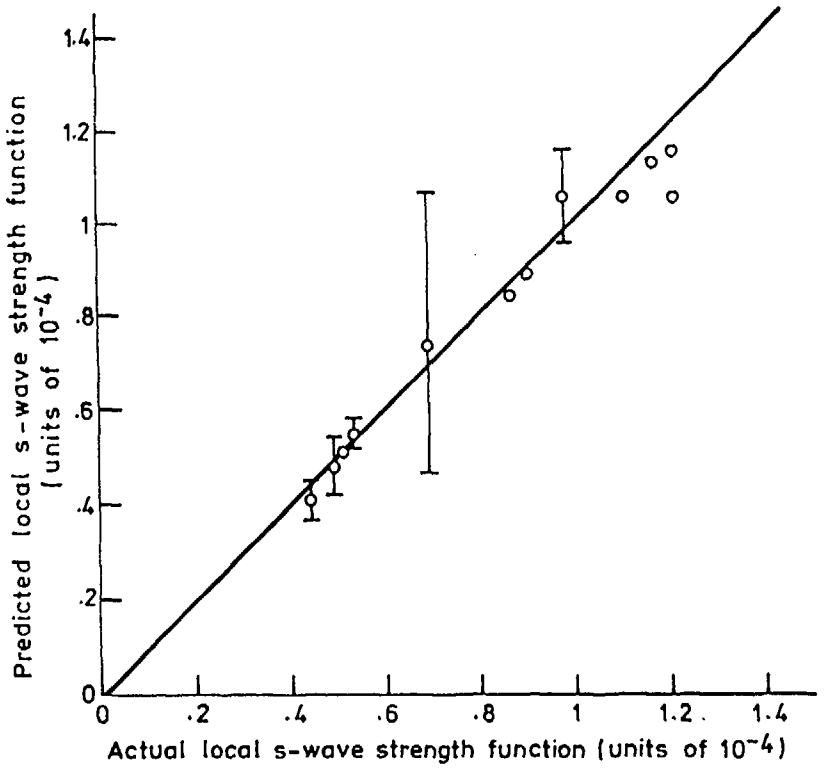

Fig. 5.2

Comparison of predicted and actual local s-wave strength functions for different sets of resonances at several energies.

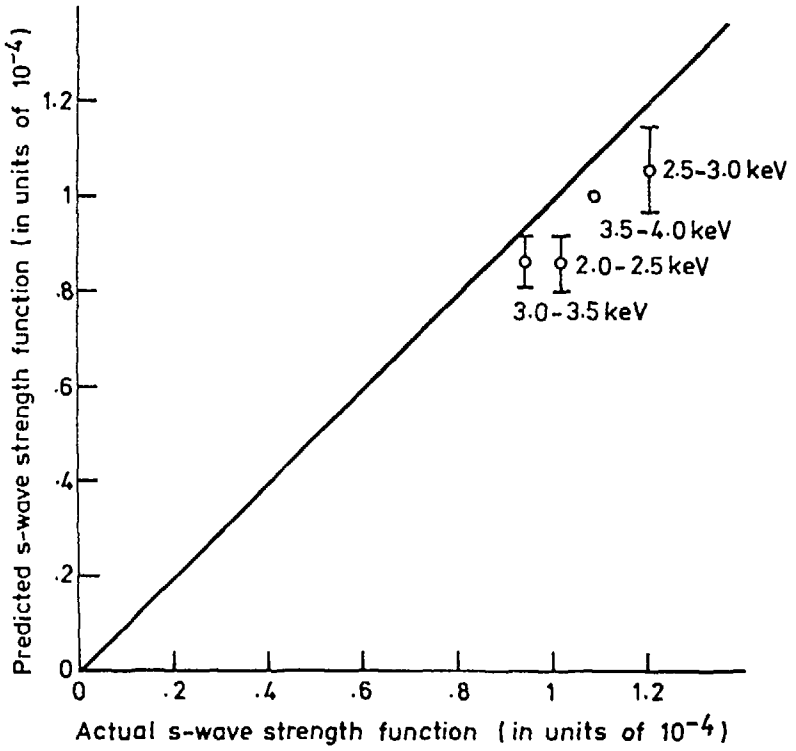

Fig. 5.3

Comparison of predicted and actual local s-wave strength functions for different energy regions using resonances specified by ENDF/B-IV for ^{238}U.

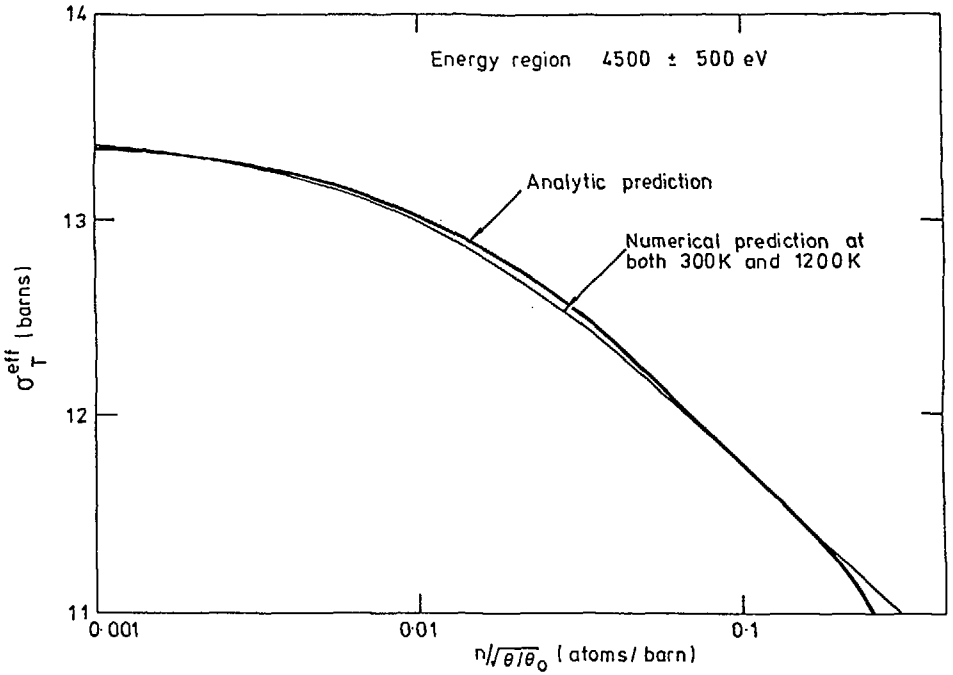

Fig. 5.4

Comparison of σ_T^{eff} calculated from equation (4.3) and from resonance parameters directly using SIGAR for the resonance set with "MAT" number 13 at 5 keV.

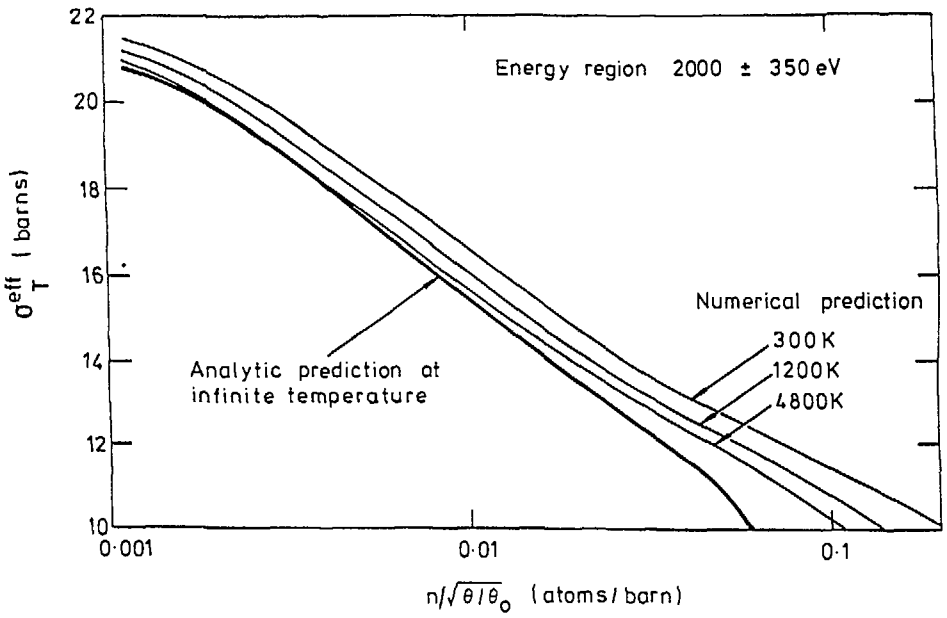

Fig. 5.5

Comparison of σ_T^{eff} calculated from equation (4.3) and from resonance parameters directly using SIGAR for resonances in the energy region 2 ± 0.35 keV from ENDF/B-IV.

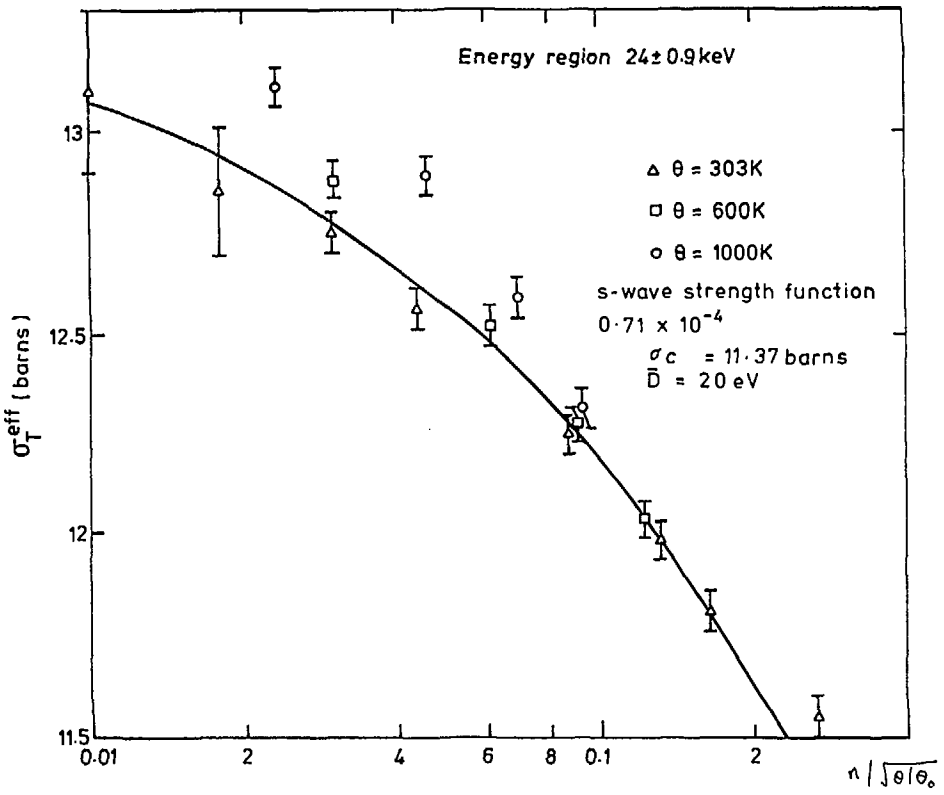

Fig. 6.1 (a)

The effective average total cross section of ^{238}U at different sample thicknesses and temperatures as measured by Tsang & Brugger (1979) using neutrons filtered to 24 ± 0.9 keV.

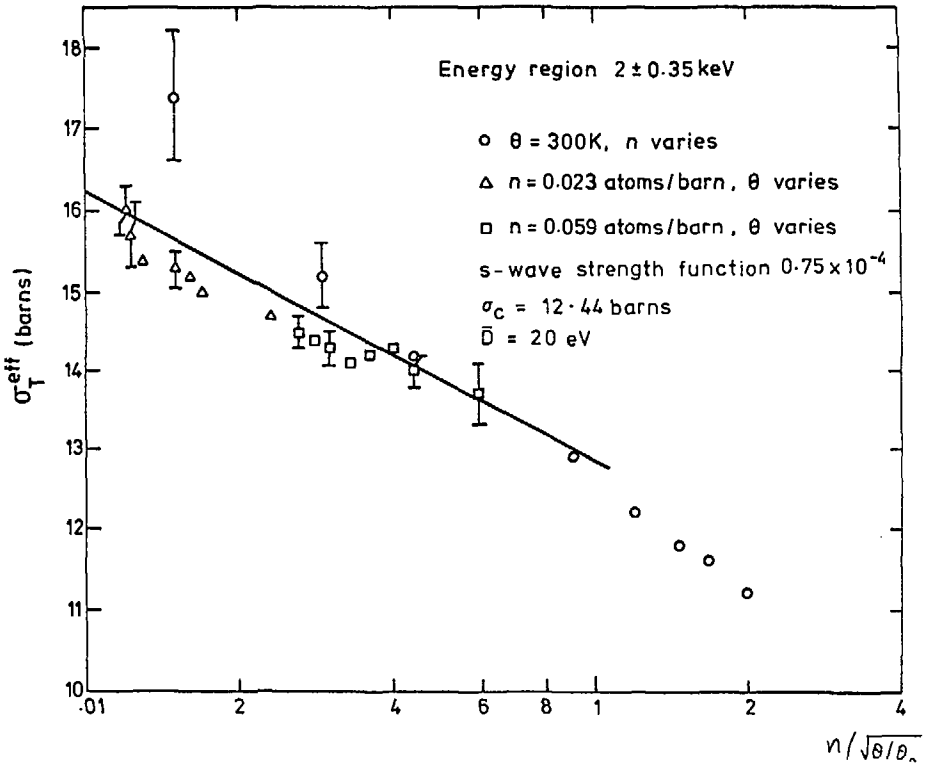

Fig. 6.1 (b)

The effective average total cross section of ^{238}U at different sample thicknesses and temperatures as measured by Brugger & Aminfar (1981) using neutrons filtered to 2 ± 0.35 keV.

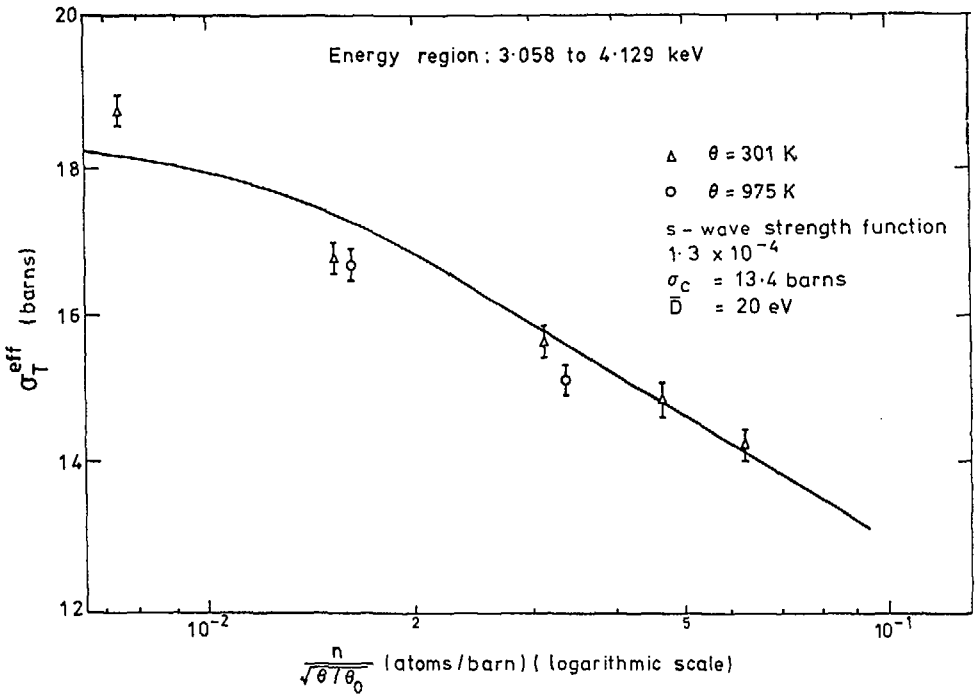

Fig. 6.2

The effective average total cross section of ^{238}U at different sample thicknesses and temperatures from data taken by Byoun *et al.* (1979), using neutrons selected by time-of-flight from 3.058 to 4.129 keV.

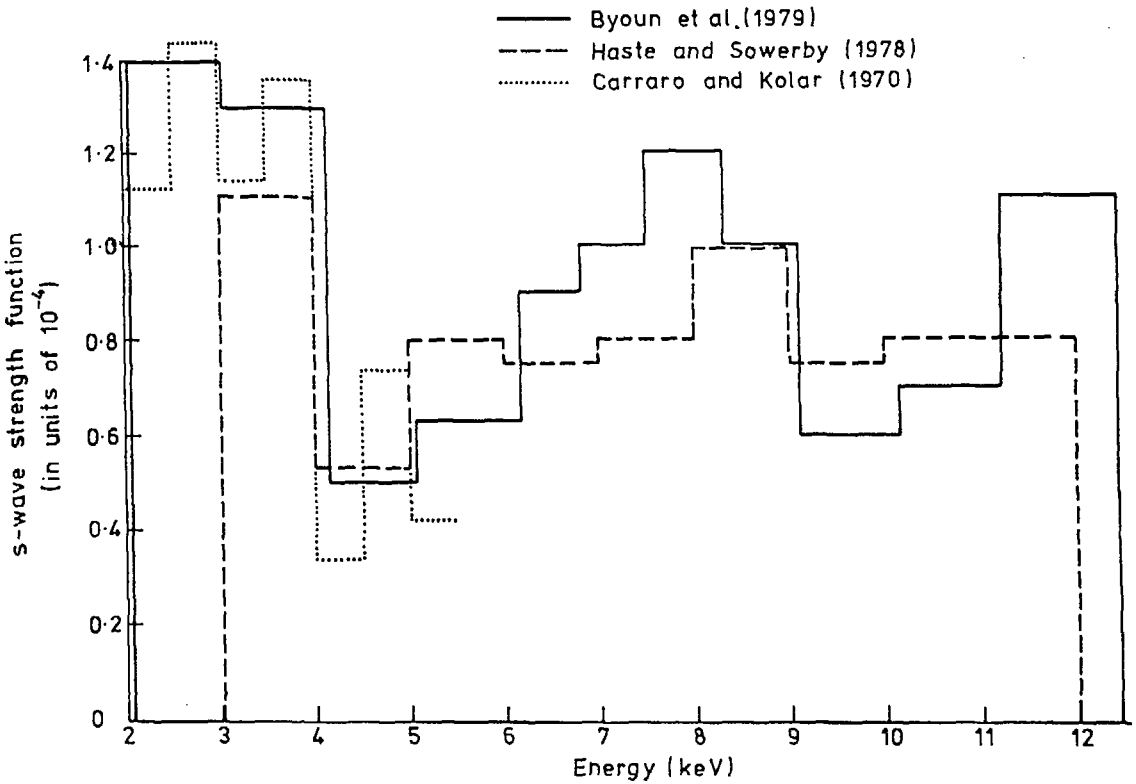

Fig. 6.3

The local s-wave strength function of ^{238}U from 3 to 12 keV, calculated using the techniques of this paper, from data taken by Byoun *et al.* (1979) and Haste & Sowerby (1978). A prediction from resolved resonance parameters by Carraro & Kolar (1970) is also shown.

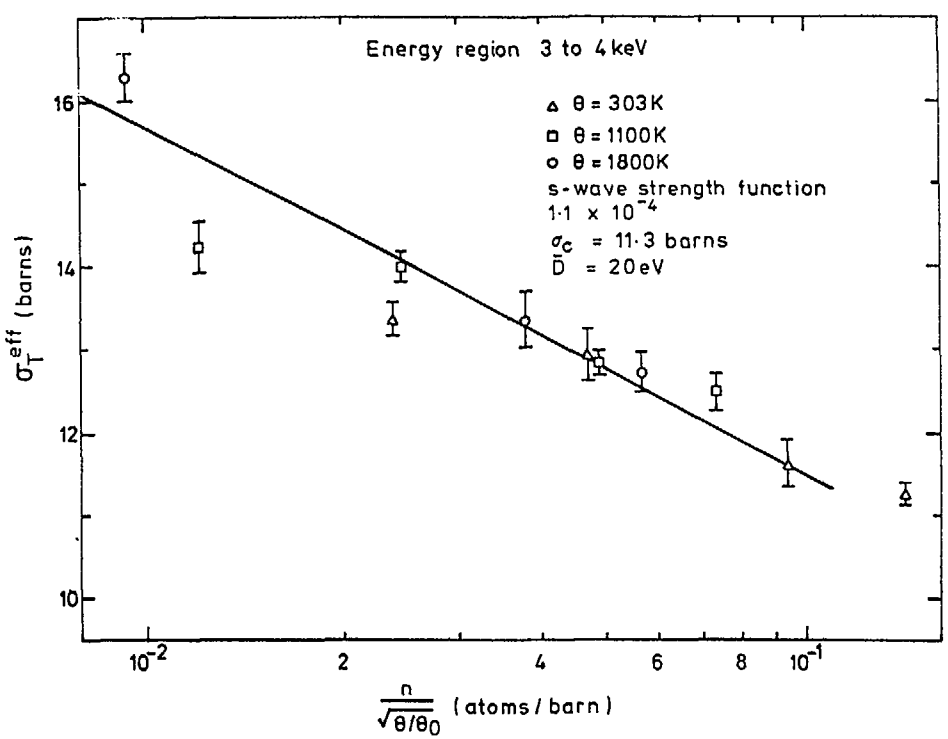

Fig. 6.4

The effective average total cross section of ^{238}U at different sample thicknesses and temperatures from data taken by Haste & Sowerby (1978), using neutrons selected by time-of-flight from 3 to 4 keV. Count loss corrections were not performed on the data.

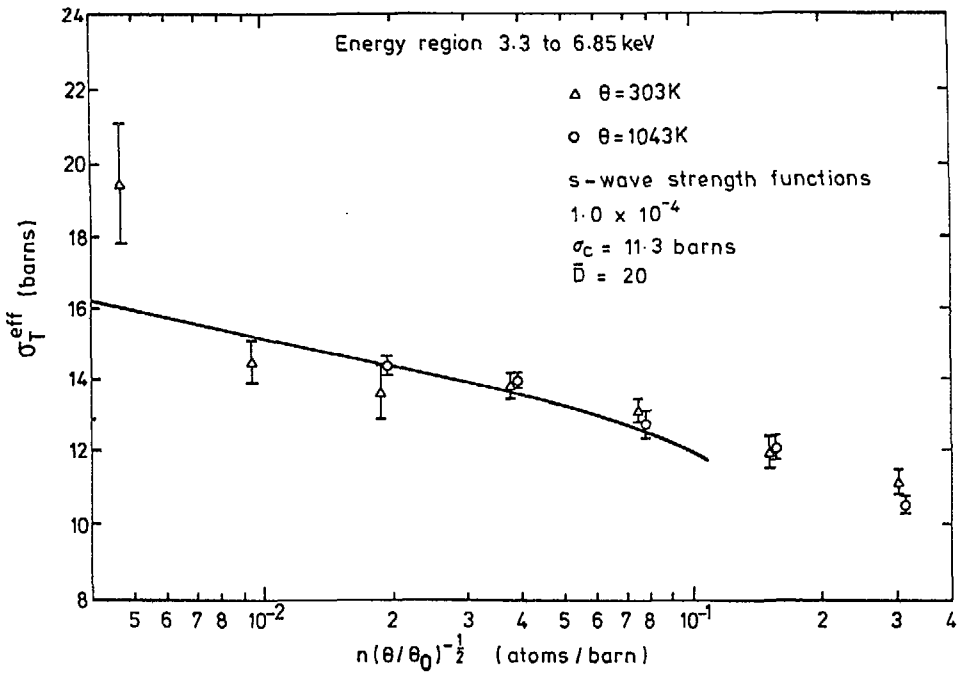

Fig. 6.5

The effective average total cross section of ^{238}U at different sample thicknesses and temperatures from data taken by Vankov *et al.* (1971), using neutrons selected by time-of-flight from 3.30 to 6.85 keV.

Comparison of Uranium and Plutonium Group Averaged Cross Sections and Staircase Plots

by

D.E. Cullen and O. Schwerer

Prepared for presentation at the IAEA Consultants meeting on Uranium and Plutonium Isotopes, 28 Sep. - 2 Oct. 1981

Summary

Unshielded and self-shielded cross sections are presented in the ABBN 26 group structure for the isotopes: ^{235}U, ^{238}U, ^{239}Pu, ^{240}Pu, ^{241}Pu and ^{242}Pu from the currently used data libraries: ENDF/B-V, JENDL-II, SOKRATOR and KEDAK-IV. Results are only presented in the resolved resonance region. In order to estimate the current disagreement between these libraries, average variations from the mean value are presented.

In addition to group averages, staircase plots for each sequence of resonances are presented.

Introduction

This paper is intended to present an estimate of the current differences between a variety of currently used evaluation libraries, namely: ENDF/B-V[1], JENDL-II[2], SOKRATOR[3] and KEDAK-IV[4], in the resolved resonance region of the isotopes: ^{235}U, ^{238}U, ^{239}Pu, ^{240}Pu, ^{241}Pu and ^{242}Pu.

One approach to estimating the current accuracy of data for these isotopes would be to examine the measurer assigned uncertainties for the currently measured experimental data. However, in this paper we will only examine evaluated data and in this way hopefully consider not only the value judgements of the experimentalists, but also the value judgements of the evaluators and we will attempt to see if the available experimental data is generally accepted and interpreted in the same manner in a variety of current evaluated data libraries. In this way we will attempt to estimate the total uncertainty that users of evaluated data may expect to encounter between different evaluations.

If we assume that the data in each of these evaluated data libraries was independently evaluated and all had the same experimentally measured data available during the evaluation process, then by examining the differences between various evaluations we can define the difference in the data, not only due to a lack or disagreement between experimental data, but also due to interpretation of the data by the evaluators. These differences reflect what a user of this set of evaluated libraries may expect to encounter in any application due to the use of one of these libraries, as opposed to using one of the other libraries of this set of libraries.

What to compare?

Since we are discussing the resolved resonance region of uranium and plutonium isotope it might seem natural to simply compare the resonance parameters. However, since we are interested in estimating the differences in the actual evaluated cross section data this approach is not particularly useful. This is because it is possible to obtain very similar cross sections using very different sets of resonance parameters, or resonance formalisms; e.g. single vs. multi-level. It is also possible to obtain very different cross sections using the same set of resonance parameters, but different resonance formalisms; e.g. single vs. multi-level. Examples of where this occurs will be given later in this work.

A more practical base for comparison is to compare multigroup cross sections and staircase plots. In actual applications, depending on the composition and geometry involved, multigroup cross sections will vary from the optically thin, or infinitely dilute, unshielded limit,[5]

$$\langle \Sigma_\lambda \rangle_G = \int_{E_G}^{E_{G+1}} \Sigma_\lambda(E) S(E) dE \Big/ \int_{E_G}^{E_{G+1}} S(E) dE \qquad (1)$$

to the optically thick, totally self-shielded limit,[5]

$$\langle \tilde{\Sigma}_\lambda \rangle_G = \int_{E_G}^{E_{G+1}} \frac{\Sigma_\lambda(E) S(E) dE}{\Sigma_T(E)} \Big/ \int_{E_G}^{E_{G+1}} \frac{S(E) dE}{\Sigma_T(E)} \qquad (2)$$

where

$\langle \Sigma_\lambda \rangle_G$ - the group average cross section in energy group G for reaction i; i = total, elastic, capture, etc.

$S(E)$ - energy dependent weighting spectrum. Since we will only be interested in the resolved resonance region a 1/E weighting spectrum will be used.

$\Sigma_\lambda(E)$ - energy dependent cross section for reaction i

$\Sigma_T(E)$ - energy dependent total cross section

E_G, E_{G+1} - lower and upper energy limits of group G.

The two limiting cases of the unshielded and totally shielded cross sections will be used as indications of agreement or disagreement between the four evaluated libraries considered in this work. The unshielded cross section is a good indication of normalization, since multiplying the energy dependent cross section $\Sigma_\lambda(E)$ by a scalar factor over the energy range E_G to E_{G+1} leads directly to a change in the group average cross section $\langle\Sigma_\lambda\rangle_G$ by the same scalar factor. As an indicator of cross section shape dependence, rather than presenting the self-shielded cross section, we will present self-shielding f-factors which are defined as the ratio of the self-shielded to unshielded cross section,

$$f_G = \frac{\langle\tilde{\Sigma}_\lambda\rangle_G}{\langle\Sigma_\lambda\rangle_G} = \frac{\int_{E_G}^{E_{G+1}} \frac{\Sigma_\lambda(E)S(E)dE}{\Sigma_T(E)} \Big/ \int_{E_G}^{E_{G+1}} \frac{S(E)dE}{\Sigma_T(E)}}{\int_{E_G}^{E_{G+1}} \Sigma_\lambda(E)S(E)dE \Big/ \int_{E_G}^{E_{G+1}} S(E)dE} \qquad (3)$$

Since the cross sections $\Sigma_\lambda(E)$ and $\Sigma_T(E)$ appear in both numerator and denominator of this expression f-factors are completely independent of normalization. However, f-factors are sensitive indicators of the amount and magnitude of structure in the cross sections. Generally if the total cross section is fairly smooth the f-factor will be close to unity. As the amount of structure in the cross section increases the f-factor tends to decrease and for materials with a large number of resonances the f-factors can be quite small[5,6]. Later in this work it will be shown that for several of the isotopes considered here the f-factors are only about 0.02, indicating that the self-shielded cross section is only about 2% of the unshielded cross section (see: Tables IV and V). Agreement between the unshielded cross sections and f-factors for an evaluation of an isotope from one evaluated library and the corresponding quantities from a second evaluated library generally is a strong indication that in any application a user will obtain similar solutions using the cross sections from either evaluation. However it should be stressed that agreement between these quantities is merely an indicator and it does not guarantee that both evaluations will yield similar solutions.

Since it is widely used both in experimental measurements [7,8] as well as in applications [5] the ABBN twenty-six (26) group structure will be used to present comparisons. However, for each evaluation, of each isotope results will only be presented for those energy groups which lie completely below the upper energy limit of the resolved resonance region.

Besides the unshielded and shielded cross sections a third basis of comparison will be staircase plots for each l sequence of resonances, for each isotope, for each library. In these staircase plots we will plot the number of resonances of a given l sequence below energy E versus the energy E. These staircase plots will be used as a simple compact means of comparing average resonance spacings. In order to allow comparison between the staircase plots for several different evaluations of the same isotope on a single plot the staircase plots presented herein are a somewhat stylized version of the tradition staircase plot, in the sense that we have drawn smooth curves in an attempt to only show the important trends in the plots.

Evaluated Libraries

Table I presents a brief summary of the evaluations considered in this work. For each isotope, in each library Table I defines: the year of the evaluation (as an indication of what experimental data the evaluator had available at the time of the evaluation), the energy limits of resolved and unresolved resonance energy ranges, the number and type of resolved resonances and the number of energies at which unresolved resonance parameters are tabulated (as an indication of the amount of detail presented in the unresolved resonance region).

In order to reduce all of this evaluated data to comparable multigroup form the various libraries were treated as follows,

ENDF/B-V

Permission was obtained to use the ENDF/B-V data [1] for these isotopes over the energy range up to 40 keV. At the IAEA this data was linearized [9], the resonance and background contributions combined to define energy dependent cross sections [10], the shielded and unshielded group averaged cross sections were calculated, using a 1/E weighting spectrum [11]. All of the following ENDF/B-V results correspond to the results of this multigroup calculation.

JENDL-II

This data was converted to energy dependent form in the ENDF/B format [2] and then sent to the IAEA. At the IAEA shielded and unshielded group averaged cross sections were calculated, using a 1/E weighting spectrum [11]. All of the following JENDL-II results correspond to the results of this multigroup calculation.

SOKRATOR

The evaluations for ^{239}Pu, ^{241}Pu and ^{242}Pu were obtained[3] in the ENDF/B format. At the IAEA the evaluations for ^{235}U and ^{240}Pu were converted [12] from the SOKRATOR to the ENDF/B format. A SOKRATOR evaluation for ^{238}U was not available in the ENDF/B format. All evaluations were linearized [9], the resonance and background contributions combined to define energy dependent cross sections [10], the shielded and unshielded group averaged cross sections were calculated, using a 1/E weighting spectrum[11]. For ^{239}Pu and ^{241}Pu the results of this multigroup calculation did not agree with the results published by the evaluators [13]. Therefore for ^{239}Pu and ^{241}Pu the following SOKRATOR results are those published by the evaluators [13]. For ^{235}U, ^{240}Pu and ^{242}Pu the following SOKRATOR results are the results of the multigroup calculation performed at the IAEA.

KEDAK-IV

This data was sent to the IAEA in energy dependent form [4]. It was converted to the ENDF/B format and then shielded and unshielded group averaged cross sections were calculated, using a 1/E weighting spectrum [11]. All of the following KEDAK-IV results correspond to the results of this multigroup calculation.

In all cases the following results correspond to the cold (nominally 0 C) data; i.e. the data has not been Doppler broadened.

Presentation of Results

Tables II and III present tabulated comparisons of the total, capture and fission cross sections for each of the six isotopes, from each of the four data libraries, for each energy group up to the upper energy limit of the resolved resonance region. Similarly Tables IV and V present tabulated comparisons of the corresponding total, capture and fission self-shielding f-factors. Within each group, for each reaction the average of the libraries was calculated and Tables VI and VII define the per-cent variation of each library cross section from the average. Tables VIII and IX present similar results for the f-factors.

Figures I-VII present staircase plots for each isotope, for each l sequence. For the six isotopes considered results are presented for the s wave (l = 0) resonances and in addition for ^{238}U, results are presented for the p wave (l = 1) resonances.

Discussion of Results

235U

The comparison of cross sections shows a close agreement between ENDF/B-V, JENDL-II and SOKRATOR. The KEDAK-IV cross sections are considerably lower in the 0.465 to 1.0 eV group. Table X compares the total widths of the first few resonances of each evaluation. From Table 8 we can see that the difference in the 0.465 to 1.0 eV group is primary due to the smaller 121 milli-eV total width used by KEDAK-IV, for the 0.29 eV resonance compared to the 135 milli-eV total width used by all of the other evaluations.

The agreement between ENDF/B-V, JENDL-II and SOKRATOR is excellent in average cross section, f-factor and staircase plot over the entire energy range (figure I). The KEDAK-IV cross sections are slightly lower than ENDF/B-V and JENDL-II. The latter result is somewhat surprising since the staircase plot (Figure I) shows that the KEDAK-IV evaluation uses a resonance spacing that is approximately 30% less than that used by ENDF/B-V or JENDL-II. However, in Table X we see that the KEDAK-IV resonances are generally narrower than the ENDF/B-V resonances.

238U

The comparison of cross sections and f-factors show a close agreement between ENDF/B-V, JENDL-II and KEDAK-IV (see: Tables II and IV). Examination of the staircase plots for s and p wave resonances (figures II and III) show that although ENDF/B-V and KEDAK-IV use approximately the same total number of resonances (444 vs. 442) they differ in assignment of l values for about 18% of the resonances.

239Pu

The comparison of total and fission cross sections and f-factors show good agreement. In the 1 - 2.15 eV range there is a disagreement between the capture cross sections; ENDF/B-V and KEDAK-IV suggest approximately 7.7 barns, while JENDL-II and SOKRATOR are lower at 4.65 and 5.07 barns respectively. The staircase plot (figure IV) indicates all evaluations are using essentially the same resonance spacing.

240Pu

The comparison of cross sections shows agreement except above 100 eV where ENDF/B-V and JENDL-II yield similar results and SOKRATOR and KEDAK-IV yield similar results, but the ENDF/B-V and JENDL-II are consistently higher than the SOKRATOR and KEDAK-IV results. Comparison of f-factors above 100 eV shows wide variation between evaluations. The reason for this disagreement is the difference in the cross section structure between the various evaluations above 100 eV. The staircase plot (figure V) indicates that all of the evaluations are using similar resonance spacings.

241Pu

The total cross sections in the 0.215-0.465 eV range have a spread of about 16% between evaluations of the total cross sections, 18% for the capture and fission. A comparison of the evaluated energy dependent total cross sections in this energy range with the available experimental data shows that both SOKRATOR and JENDL-II reproduce accurately the measurement of Young (1974) [14], whereas the ENDF/B-V peak value is about 4%, and the peak value of the KEDAK evaluation is significantly higher (about 15%). For all other energy ranges there is good agreement between cross sections and f-factors for the various evaluations. The staircase plot (figure VI) shows a spread in resonance spacing of approximately 10%.

242Pu

In the 2.15 - 4.65 eV range JENDL-II, SOKRATOR and KEDAK-IV yield very similar results for the total cross section of approximately 1475 barns, whereas ENDF/B-V yields a value of 1738 barns, almost 18% higher. The agreement between cross sections is good over all other energy ranges. There are large differences between the f-factors, particularly in the 100 - 465 eV range. The staircase plot (figure VII) indicates all evaluations used very similar resonance spacing.

Conclusions

Comparison of group averaged cross sections, self-shielding f-factors and staircase plots for each resonance sequence within the resolved resonance region for evaluations of ^{235}U, ^{238}U, ^{239}Pu, ^{240}Pu, ^{241}Pu and ^{242}Pu from the ENDF/B-V, JENDL-II, SOKRATOR and KEDAK-IV libraries, generally show good agreement. Comparisons and deviations from averages are provided to allow the user to decide if the agreement is good enough to meet the needs of any given application.

Acknowledgements

The authors thank P. Hemmig, DOE, for providing the ENDF/B-V data, S. Igarasi, JAERI, for providing the JENDL-II data, F. Froehner, Karlsruhe, for providing the KEDAK-IV data and V. Konshin, Minsk, for providing the SOKRATOR data. This was truly an international effort that could not have been accomplished without help from all of these individuals. The authors thank Edith Lanka for typing this report in such a timely and accurate manner.

References

[1] P. HEMMIG, DOE, Private Communication (1981).
[2] S. IGARASI, JAERI, Private Communication (1981).
[3] V. KONSHIN, Minsk, Private Communication (1981).
[4] F. FROEHNER, Karlsruhe, Private Communication (1981)
[5] I.I. BONDERENKO, Group Constants for Nuclear Reactor Calculations, Consultants Bureau, New York, (1964).
[6] E.F. PLECHATY, D.E. CULLEN, R.J. HOWERTON and J.R. KIMLINGER, UCRL-50400, Vol. 16, Rev. 2, Lawrence Livermore Laboratory (1978).
[7] R. L. BRAMBLETT and J.B. CZIRR, Nuc. Sci. and Eng. 35, 350 (1969).
[8] T. BOKALOV et al., pp. 692, Knoxville (1979).
[9] D.E. CULLEN, UCRL-50400, Vol. 17, part A, Rev. 2, Lawrence Livermore Lab. (1979).
[10] D.E. CULLEN, UCRL-50400, Vol. 17, part C, Lawrence Livermoe Lab. (1979).
[11] D.E. CULLEN, UCRL-50400, Vol. 17, part D, Lawrence Livermore Lab. (1979).
[12] V.G. PRONYAEV, NDS, IAEA - Private Communication (1981).
[13] G.V. ANTSIPOV, V.A. KONSHIN and E.S. SUKHOVITSKI, Nuclear Constants for Plutonium Isotopes, Science and Technology, Minsk (1981).
[14] T.E. YOUNG, Idaho Nucl. Corp., Priv. Comm. to NNDC Brookhaven (1974), data file EXFOR-10406 dated 1974-07-24.

TABLE I

SUMMARY OF RESONANCE REGIONS

ISOTOPE	ENDF/B-V	JENDL-II	SOKRATOR	KEDAK-IV
U-235				
EVAL. YEAR	1977	?	1975	?
RESOLVED	1-82 EV: 130 S SLBW	1-100 EV: 148 S SLBW	1-100 EV: 208 S MLBW	?-100 EV: 199 S ?
UNRESOLVED	82-25 KEV :137 ENERGIES	100-30 KEV: 28 ENERGIES	100-100 KEV: 81 ENERGIES	?
U-238				
EVAL. YEAR	1977	?	EVALUATION	?
RESOLVED	1-4000 EV: 164 S MLBW : 280 P MLBW	0-4 KEV: 187 S MLBW : 265 P MLBW	NOT AVAILABLE	?-3993 EV: 189 S ? : 253 P ?
UNRESOLVED	4-25 KEV: 36 ENERGIES	4-50 KEV: 21 ENERGIES		?
PU-239				
EVAL. YEAR	1976	?	1980	?
RESOLVED	1-301 EV: 128 S SLBW	1-598 EV: 257 S MLBW	0-500 EV: 260 S MLBW	?-658 EV: 258 S ?
UNRESOLVED	301-25 KEV: 94 ENERGIES	598-30 KEV: 34 ENERGIES	500-100 KEV: 35 ENERGIES	?
PU-240				
EVAL. YEAR	1977	?	1975	?
RESOLVED	0-3910 EV: 201 S MLBW	0-4 KEV: 268 S MLBW	1-1000 EV: 70 S MLBW	?-3990 EV: 204 S ?
UNRESOLVED	3910-40 KEV: 16 ENERGIES	4-40 KEV: 28 ENERGIES	1-150 KEV: 28 ENERGIES	?
PU-241				
EVAL. YEAR	1977	?	1979	?
RESOLVED	2.873-100 EV: 83 S A-A	1-100 EV: 92 S SLBW	1-100 EV: 112 S A-A	?-160 EV: 123 S ?
UNRESOLVED	100-40.2 KEV: 32 ENERGIES	100-30 KEV: 22 ENERGIES	100-100 KEV: 32 ENERGIES	?
PU-242				
EVAL. YEAR	1978	?	1979	?
RESOLVED	0-986 EV: 68 S SLBW	0-1290 EV: 95 S MLBW	0-1000 EV: 70 S MLBW	?-495 EV: 37 S ?
UNRESOLVED	986-10 KEV: 5 ENERGIES	NONE	1-200 KEV: 28 ENERGIES	?

TERMINOLOGY

SLBW	= SINGLE-LEVEL BREIT-WIGNER PARAMETERS
MLBW	= MULTI-LEVEL BREIT-WIGNER PARAMETERS
A-A	= ADLER-ADLER PARAMETERS
ENERGIES	= NUMBER OF ENERGIES AT WHICH UNRESOLVED PARAMETERS ARE GIVEN
S OR P	= NUMBER OF S OR P WAVE RESOLVED RESONANCES

NOTE: (1) ALL EVALUATIONS USE ENERGY DEPENDENT UNRESOLVED PARAMETERS.
(2) THE ENERGY LISTED FOR KEDAK-IV IS THE ENERGY OF THE LAST RESOLVED RESONANCE.

TABLE II

U-235: COMPARISON OF GROUP AVERAGES (BARNS)

ENERGY GROUP	TOTAL				CAPTURE				FISSION			
EV	ENDF/B	JENDL	SOKRATOR	KEDAK	ENDF/B	JENDL	SOKRATOR	KEDAK	ENDF/B	JENDL	SOKRATOR	KEDAK
THERMAL	699.92	700.37	701.27	703.01	98.89	96.42	102.15	99.94	586.54	586.58	580.06	590.83
0.215-0.465	206.69	204.71	208.29	193.31	34.42	32.86	34.55	33.71	158.24	156.36	154.27	147.68
0.465-1.0	86.69	87.66	88.03	70.46	7.95	7.12	7.40	8.28	65.32	66.08	64.56	51.10
1.0-2.15	60.89	62.17	62.37	57.46	12.38	13.17	11.64	11.89	35.95	35.95	40.80	35.05
2.15-4.65	35.50	36.18	36.53	32.76	6.98	7.61	7.19	6.83	17.11	16.94	20.69	16.17
4.65-10.0	96.60	98.88	96.01	96.19	37.20	41.43	42.09	36.51	48.36	46.43	45.83	50.06
10.0-21.5	108.05	107.31	107.85	105.73	44.67	49.90	47.15	46.42	51.14	45.33	51.46	48.35
21.5-46.5	79.31	82.67	88.04	78.34	23.90	27.44	28.42	24.45	43.09	43.12	49.92	42.55
46.5-100		66.53	63.14	65.57		18.82	17.37	17.31		34.54	35.82	36.63

U-238: COMPARISON OF GROUP AVERAGES (BARNS)

	TOTAL				CAPTURE				FISSION			
	ENDF/B	JENDL	SOKRATOR	KEDAK	ENDF/B	JENDL	SOKRATOR	KEDAK	ENDF/B	JENDL	SOKRATOR	KEDAK
THERMAL	11.61	11.59		11.68	2.71	2.71		2.73	0.0	0.0		0.0
0.215-0.465	9.68	9.65		9.78	0.807	0.813		0.815	0.0	0.0		0.0
0.465-1.0	9.41	9.38		9.54	0.587	0.593		0.595	0.0	0.0		0.0
1.0-2.15	9.17	9.15		9.42	0.476	0.484		0.486	0.0	0.0		0.0
2.15-4.65	8.94	8.92		9.17	0.646	0.666		0.637	0.0	0.0		0.0
4.65-10.0	190.93	189.78		189.45	170.91	170.46		170.10	0.0	0.0		0.0
10.0-21.5	131.73	131.53		129.49	86.75	86.64		86.34	0.0002	0.0001		0.0
21.5-46.5	145.82	143.56		144.92	54.96	55.42		55.38	0.0	0.0		0.0
46.5-100	41.91	42.21		41.82	16.57	16.37		16.55	0.0	0.0		0.0
100-215	90.68	90.76		90.78	20.03	20.06		20.04	0.0	0.0		0.0
215-465	22.28	22.15		22.05	4.53	4.50		4.45	0.0005	0.0004		0.0
465-1000	23.37	23.19		22.98	3.37	3.32		3.25	0.0009	0.0009		0.0
1000-2150	22.19	22.22		22.20	1.90	1.85		1.72	0.0003	0.0003		0.0

PU-239: COMPARISON OF GROUP AVERAGES (BARNS)

	TOTAL				CAPTURE				FISSION			
	ENDF/B	JENDL	SOKRATOR	KEDAK	ENDF/B	JENDL	SOKRATOR	KEDAK	ENDF/B	JENDL	SOKRATOR	KEDAK
THERMAL	1023.7	1023.7	1018.6	1026.1	270.99	270.99	267.20	271.36	744.68	744.68	744.00	748.14
0.215-0.465	2760.9	2760.9	2782.5	2760.1	1105.30	1105.30	1091.70	1105.50	1643.70	1643.30	1679.40	1643.50
0.465-1.0	154.3	152.5	155.07	154.29	44.34	42.54	42.82	44.33	98.68	98.68	101.34	98.70
1.0-2.15	41.79	37.58	39.35	41.95	7.69	4.65	5.07	7.73	24.14	23.03	24.74	24.27
2.15-4.65	21.35	22.59	21.54	21.41	1.14	1.42	1.58	1.15	11.04	11.93	11.03	11.09
4.65-10.0	69.50	67.52	69.80	69.71	26.35	24.98	23.47	26.42	34.74	34.56	36.21	34.85
10.0-21.5	181.99	178.97	174.38	182.52	66.75	71.14	63.81	66.92	104.49	97.65	98.38	104.79
21.5-46.5	67.39	68.78	67.91	67.58	34.06	36.03	33.36	34.15	22.37	22.28	21.38	22.43
46.5-100	110.60	115.29	116.60	110.90	37.16	37.94	36.70	37.26	56.51	60.25	61.26	56.65
100-215	51.23	50.34	49.60	51.31	17.11	17.30	15.06	17.15	18.80	18.89	19.45	18.83
215-465		40.09	38.95	41.61		13.01	11.17	12.67		12.74	13.02	12.99

TABLE III

PU-240: COMPARISON OF GROUP AVERAGES (BARNS)

ENERGY GROUP	TOTAL				CAPTURE				FISSION			
EV	ENDF/B	JENDL	SOKRATOR	KEDAK	ENDF/B	JENDL	SOKRATOR	KEDAK	ENDF/B	JENDL	SOKRATOR	KEDAK
THERMAL	292.48	291.48	290.26	290.34	290.90	289.91	288.67	291.40	0.0573	0.0679	0.0510	0.0614
0.215-0.465	163.65	159.75	163.54	160.74	163.30	159.47	163.21	164.29	0.0308	0.0341	0.0289	0.0321
0.465-1.0	1189.8	1191.8	1240.4	1191.2	1149.4	1141.4	1194.5	1157.2	0.208	0.222	0.211	0.210
1.0-2.15	9740.	10567.	10086.	9737.6	9077.1	9719.8	9363.8	9089.0	1.636	1.873	1.657	1.639
2.15-4.65	23.79	24.09	21.40	23.19	8.98	8.82	8.77	8.86	0.0211	0.0028	0.0024	0.0025
4.65-10.0	10.89	10.79	9.13	10.10	0.867	0.879	0.776	0.787	0.0005	0.0010	0.0001	0.0001
10.0-21.5	41.87	36.04	40.68	41.25	31.30	26.30	30.91	31.36	0.225	0.192	0.669	0.223
21.5-46.5	121.63	116.38	112.34	116.45	71.39	71.81	68.27	70.62	0.181	0.505	0.236	0.284
46.5-100	106.53	100.76	101.85	105.23	43.40	43.66	42.41	43.53	0.0293	0.309	0.154	0.605
100-215	55.12	54.60	53.26	54.70	24.73	25.53	24.05	24.33	0.0153	0.334	0.130	0.153
215-465	32.08	31.46	29.87	30.62	9.44	9.50	7.84	7.76	0.0050	0.221	0.055	0.0509
465-1000	24.43	24.33	23.52	23.84	5.56	5.50	4.83	4.78	0.244	0.408	0.262	0.207
1000-2150	22.24	22.28		21.80	3.30	3.23		2.59	0.187	0.306		0.117

PU-241: COMPARISON OF GROUP AVERAGES (BARNS)

	TOTAL				CAPTURE				FISSION			
	ENDF/B	JENDL	SOKRATOR	KEDAK	ENDF/B	JENDL	SOKRATOR	KEDAK	ENDF/B	JENDL	SOKRATOR	KEDAK
THERMAL	1392.8	1395.0	1389.0	1393.5	363.03	364.65	362.80	366.77	1019.8	1020.0	1015.0	1016.9
0.215-0.465	1245.0	1188.7	1196.5	1380.6	389.97	356.40	398.86	428.48	842.00	820.50	784.34	941.72
0.465-1.0	77.84	72.93	82.52	74.87	22.86	18.22	15.21	15.03	43.22	43.93	52.98	50.37
1.0-2.15	43.75	40.16	41.07	33.73	6.25	3.64	2.80	2.76	26.79	26.93	26.37	22.42
2.15-4.65	196.00	194.38	180.30	198.52	69.76	69.90	54.20	77.50	112.53	115.84	116.36	112.80
4.65-10.0	302.65	290.51	283.07	261.01	40.10	33.07	26.48	34.82	248.52	246.14	239.38	215.91
10.0-21.5	225.84	227.48	198.14	232.37	69.75	72.79	43.11	66.54	137.32	138.19	138.55	149.37
21.5-46.5	90.49	89.36	90.54	104.38	13.35	13.51	10.09	15.42	64.48	62.66	61.99	76.47
46.5-100	62.88	65.74	64.25	70.68	11.80	11.35	10.02	12.92	37.93	40.62	39.34	44.46

PU-242: COMPARISON OF GROUP AVERAGES (BARNS)

	TOTAL				CAPTURE				FISSION			
	ENDF/B	JENDL	SOKRATOR	KEDAK	ENDF/B	JENDL	SOKRATOR	KEDAK	ENDF/B	JENDL	SOKRATOR	KEDAK
THERMAL	26.97	26.77	26.88	27.35	19.24	18.54	18.64	19.04	0.0010	0.122	0.0	0.0
0.215-0.465	14.26	14.52	14.68	14.86	6.85	6.63	6.71	6.83	0.0003	0.0355	0.0	0.0001
0.465-1.0	13.45	13.84	14.00	14.09	6.59	6.40	6.49	6.61	0.0002	0.0255	0.0	0.0001
1.0-2.15	20.55	21.18	21.53	21.77	16.01	15.67	16.10	16.60	0.0001	0.0249	0.0	0.0001
2.15-4.65	1738.3	1473.7	1484.5	1471.4	1561.0	1355.8	1367.6	1357.6	0.0001	0.917	0.0	0.0001
4.65-10.0	12.95	12.51	11.03	13.17	0.735	0.706	0.701	0.708	0.0001	0.0071	0.0	0.0001
10.0-21.5	12.03	12.04	10.51	12.56	1.63	1.62	1.62	1.63	0.0001	0.0078	0.0	0.0001
21.5-46.5	13.32	13.61	12.37	14.04	4.48	4.46	4.74	4.50	0.0001	0.0130	0.0	0.0001
46.5-100	114.54	114.72	113.46	114.35	33.18	35.63	33.01	39.83	0.0742	0.0695	0.0670	0.0645
100-215	30.24	31.24	30.04	33.09	10.11	10.33	10.30	11.99	0.0645	0.0254	0.0240	0.0231
215-465	32.15	33.43	31.28	34.14	5.77	6.01	6.14	6.44	0.0207	0.0249	0.0180	0.0177
465-1000		28.76	27.03	26.59		4.01	4.01	4.76		0.0979	0.0055	0.0178

TABLE IV

U-235: COMPARISON OF GROUP AVERAGES (F FACTORS)

ENERGY GROUP	TOTAL				CAPTURE				FISSION			
EV	ENDF/B	JENDL	SOKRATOR	KEDAK	ENDF/B	JENDL	SOKRATOR	KEDAK	ENDF/B	JENDL	SOKRATOR	KEDAK
THERMAL												
0.215-0.465	0.939	0.940	0.940	0.903	0.905	0.903	0.915	0.871	0.941	0.942	0.941	0.902
0.465-1.0	0.983	0.990	0.983	0.971	0.973	0.979	0.964	0.970	0.981	0.990	0.981	0.966
1.0-2.15	0.719	0.742	0.755	0.730	0.653	0.693	0.667	0.630	0.647	0.670	0.723	0.684
2.15-4.65	0.721	0.719	0.738	0.745	0.578	0.566	0.566	0.565	0.597	0.597	0.690	0.667
4.65-10.0	0.354	0.361	0.379	0.376	0.262	0.256	0.265	0.266	0.288	0.314	0.382	0.344
10.0-21.5	0.390	0.397	0.361	0.347	0.258	0.269	0.249	0.223	0.389	0.407	0.379	0.347
21.5-46.5	0.446	0.455	0.384	0.437	0.304	0.334	0.270	0.293	0.392	0.401	0.357	0.388
46.5-100		0.525	0.473	0.506		0.381	0.345	0.344		0.441	0.406	0.445

U-238: COMPARISON OF GROUP AVERAGES (F FACTORS)

	TOTAL				CAPTURE				FISSION			
	ENDF/B	JENDL	SOKRATOR	KEDAK	ENDF/B	JENDL	SOKRATOR	KEDAK	ENDF/B	JENDL	SOKRATOR	KEDAK
THERMAL												
0.215-0.465	1.0	1.0		1.0	1.	1.		1.	1.	1.		0.
0.465-1.0	1.0	1.0		1.0	1.	1.		1.	1.	1.		0.
1.0-2.15	1.0	1.0		1.0	1.	1.		1.	1.	1.		0.
2.15-4.65	1.0	1.0		1.0	0.994	0.993		1.	1.	1.		0.
4.65-10.0	0.0681	0.0689		0.0694	0.0255	0.0263		0.0265	0.0283	0.0293		0.
10.0-21.5	0.0678	0.0672		0.0680	0.0171	0.0172		0.0174	0.0153	0.0155		0.
21.5-46.5	0.0765	0.0772		0.0747	0.0297	0.0300		0.0309	0.0628	0.0484		0.
46.5-100	0.234	0.230		0.228	0.0430	0.0426		0.0427	0.0350	0.0350		0.
100-215	0.120	0.117		0.109	0.0431	0.0435		0.0451	0.0518	0.0526		0.
215-465	0.528	0.533		0.520	0.0886	0.0880		0.0871	0.0983	0.0987		0.
465-1000	0.410	0.413		0.394	0.121	0.121		0.121	0.171	0.171		0.
1000-2150	0.413	0.407		0.401	0.212	0.185		0.188	0.129	0.124		0.

PU-239: COMPARISON OF GROUP AVERAGES (F FACTORS)

	TOTAL				CAPTURE				FISSION			
	ENDF/B	JENDL	SOKRATOR	KEDAK	ENDF/B	JENDL	SOKRATOR	KEDAK	ENDF/B	JENDL	SOKRATOR	KEDAK
THERMAL												
0.215-0.465	0.590	0.590		0.590	0.573	0.573		0.573	0.598	0.598		0.598
0.465-1.0	0.743	0.725		0.743	0.700	0.655		0.700	0.736	0.727		0.736
1.0-2.15	0.949	0.954		0.949	0.903	0.907		0.903	0.945	0.946		0.945
2.15-4.65	0.981	0.992		0.981	0.930	0.983		0.930	0.973	0.989		0.973
4.65-10.0	0.309	0.315		0.309	0.149	0.153		0.149	0.276	0.282		0.276
10.0-21.5	0.204	0.185		0.204	0.133	0.121		0.133	0.188	0.168		0.188
21.5-46.5	0.225	0.224		0.225	0.107	0.120		0.107	0.159	0.162		0.159
46.5-100	0.339	0.316		0.339	0.177	0.157		0.177	0.370	0.349		0.370
100-215	0.411	0.431		0.412	0.202	0.259		0.202	0.369	0.377		0.369
215-465		0.497		0.469		0.270		0.200		0.464		0.443

TABLE V

PU-240: COMPARISON OF GROUP AVERAGES (F FACTORS)

ENERGY GROUP	TOTAL				CAPTURE				FISSION			
EV	ENDF/B	JENDL	SOKRATOR	KEDAK	ENDF/B	JENDL	SOKRATOR	KEDAK	ENDF/B	JENDL	SOKRATOR	KEDAK
THERMAL												
0.215-0.465	0.992	0.993	0.992	0.992	0.992	0.993	0.992	0.992	0.993	0.994	0.992	0.993
0.465-1.0	0.350	0.339	0.338	0.347	0.357	0.347	0.346	0.356	0.360	0.355	0.346	0.362
1.0-2.15	0.0179	0.0164	0.0166	0.0179+	0.0153	0.0138	0.0144	0.0153+	0.0156	0.0146	0.0150	0.0159+
2.15-4.65	0.875	0.875	0.855	0.864	0.762	0.766	0.742	0.749	0.812	0.845	0.828	0.831
4.65-10.0	0.989	0.987	0.988	0.988	0.948	0.943	0.943	0.942	0.987	0.987	0.998	0.989
10.0-21.5	0.213	0.239	0.187	0.195	0.0355	0.0378	0.0319	0.0336+	0.0308	0.0346	0.0277	0.0312+
21.5-46.5	0.0660	0.0679	0.0635	0.0534+	0.0227	0.0226	0.0217	0.0253+	0.0272	0.0228	0.0302	0.0269+
46.5-100	0.0859	0.0893	0.0801	0.0724+	0.0335	0.0330	0.0313	0.0375+	0.0367	0.0332	0.0292	0.0348+
100-215	0.207	0.244	0.195	0.209	0.0560	0.124	0.0488	0.0513+	0.0546	0.535	0.0507	0.0526+
215-465	0.349	0.362	0.293	0.299	0.227	0.241	0.0725	0.0816+	0.0840	0.763	0.0769	0.0822+
465-1000	0.415	0.433	0.383	0.126	0.230	0.295	0.107	0.192	0.142	0.408	0.147	1.123
1000-2150	0.477	0.483		0.0984+	0.343	0.427		0.541	0.180	0.504		0.197

PU-241: COMPARISON OF GROUP AVERAGES (F FACTORS)

ENERGY GROUP	TOTAL				CAPTURE				FISSION			
EV	ENDF/B	JENDL	SOKRATOR	KEDAK	ENDF/B	JENDL	SOKRATOR	KEDAK	ENDF/B	JENDL	SOKRATOR	KEDAK
THERMAL												
0.215-0.465	0.444	0.428		0.458	0.461	0.479		0.445	0.427	0.398		0.458
0.465-1.0	0.910	0.923		0.832	0.864	0.835		0.746	0.913	0.943		0.829
1.0-2.15	0.990	0.994		0.997	0.977	0.983		0.991	0.990	0.994		0.998
2.15-4.65	0.324	0.305		0.264	0.145	0.141		0.107	0.357	0.356		0.326
4.65-10.0	0.708	0.711		0.648	0.627	0.667		0.511	0.706	0.704		0.655
10.0-21.5	0.238	0.333		0.309	0.150	0.305		0.198	0.218	0.295		0.313
21.5-46.5	0.495	0.528		0.527	0.405	0.476		0.415	0.423	0.445		0.479
46.5-100	0.464	0.515		0.455	0.299	0.396		0.281	0.358	0.404		0.364

PU-242: COMPARISON OF GROUP AVERAGES (F FACTORS)

ENERGY GROUP	TOTAL				CAPTURE				FISSION			
EV	ENDF/B	JENDL	SOKRATOR	KEDAK	ENDF/B	JENDL	SOKRATOR	KEDAK	ENDF/B	JENDL	SOKRATOR	KEDAK
THERMAL												
0.215-0.465	1.	1.	1.	1.	1.	1.	1.	1.	1.	1.	1.	1.
0.465-1.0	1.	1.	1.	1.	1.	1.	1.	1.	1.	1.	1.	1.
1.0-2.15	0.889	0.893	0.880	0.887	0.830	0.832	0.821	0.824	1.028	0.946	1.028	1.027
2.15-4.65	0.0262	0.0290	0.0270	0.0301+	0.0177	0.0196	0.0186	0.0200+	0.929	0.0292	0.928	0.934
4.65-10.0	0.988	0.990	0.988	0.990	0.916	0.924	0.914	0.924	0.992	0.985	0.993	0.995
10.0-21.5	0.890	0.891	0.938	0.897	0.198	0.196	0.304	0.212	1.	0.655	1.	1.
21.5-46.5	0.682	0.694	0.809	0.699	0.0984	0.0994	0.160	0.103	1.099	0.306	1.023	1.095
46.5-100	0.0902	1.	0.178	0.103	0.0340	0.0329	0.0464	0.0357+	0.0343	0.0627	0.0522	0.0358+
100-215	0.336	0.357	0.525	0.359	0.0538	0.0546	0.117	0.0606+	0.0634	0.109	0.153	0.0561+
215-465	0.223	0.323	0.552	0.337	0.102	0.0856	0.246	0.0947+	0.179	0.123	0.305	0.0863+
465-1000		0.400	0.665	0.934		0.117	0.441	0.854		0.193	0.341	0.880

TABLE VI

U-235: CROSS SECTION PER-CENT DEVIATION FROM AVERAGE

ENERGY GROUP	TOTAL				CAPTURE				FISSION			
EV	ENDF/B	JENDL	SOKRATOR	KEDAK	ENDF/B	JENDL	SOKRATOR	KEDAK	ENDF/B	JENDL	SOKRATOR	KEDAK
THERMAL	-0.17	-0.11	0.02	0.27	-0.46	-2.95	2.82	0.59	0.09	0.10	-1.01	0.82
0.215-0.465	1.69	0.72	2.48	-4.89	1.58	-3.02	1.96	-0.52	2.66	1.44	0.09	-4.19
0.465-1.0	4.18	5.35	5.79	-15.32	3.41	-7.38	-3.74	7.71	5.76	6.99	4.53	-17.27
1.0-2.15	0.28	2.38	2.71	-5.37	0.90	7.33	-5.13	-3.10	-2.67	-2.67	10.46	-5.11
2.15-4.65	0.73	2.66	3.65	-7.04	-2.41	6.40	0.52	-4.51	-3.48	-4.44	16.71	-8.79
4.65-10.0	-0.33	2.02	-0.94	-0.75	-5.36	5.40	7.08	-7.12	1.45	-2.60	-3.86	5.01
10.0-21.5	0.76	0.07	0.57	-1.40	-5.03	6.09	0.24	-1.31	4.22	-7.62	4.87	-1.47
21.5-46.5	-3.39	0.71	7.25	-4.57	-8.26	5.33	9.09	-6.15	-3.54	-3.47	11.75	-4.75
46.5-100		2.23	-2.98	0.75		5.53	-2.60	-2.93		-3.15	0.44	2.71

U-238: CROSS SECTION PER-CENT DEVIATION FROM AVERAGE

	TOTAL				CAPTURE				FISSION			
	ENDF/B	JENDL	SOKRATOR	KEDAK	ENDF/B	JENDL	SOKRATOR	KEDAK	ENDF/B	JENDL	SOKRATOR	KEDAK
THERMAL	-0.14	-0.32		0.46	-0.25	-0.25		0.49				
0.215-0.465	-0.24	-0.55		0.79	-0.57	0.16		0.41				
0.465-1.0	-0.67	-0.67		1.02	-0.79	0.23		0.56				
1.0-2.15	-0.83	-1.05		1.87	-1.24	0.41		0.83				
2.15-4.65	-0.78	-1.00		1.78	-0.56	2.51		-1.95				
4.65-10.0	0.46	-0.14		-0.32	0.25	-0.02		-0.23				
10.0-21.5	0.62	0.47		-1.09	0.20	0.07		-0.27				
21.5-46.5	0.73	-0.83		0.11	-0.53	0.30		0.23				
46.5-100	-0.17	0.55		-0.38	0.44	-0.77		0.32				
100-215	-0.07	0.02		0.04	-0.07	0.08		-0.02				
215-465	0.54	-0.05		-0.50	0.82	0.15		-0.96				
465-1000	0.82	0.04		-0.86	1.71	0.20		-1.91				
1000-2150	-0.06	0.08		-0.01	4.20	1.46		-5.67				

PU-239: CROSS SECTION PER-CENT DEVIATION FROM AVERAGE

	TOTAL				CAPTURE				FISSION			
	ENDF/B	JENDL	SOKRATOR	KEDAK	ENDF/B	JENDL	SOKRATOR	KEDAK	ENDF/B	JENDL	SOKRATOR	KEDAK
THERMAL	0.07	0.07	-0.43	0.30	0.32	0.32	-1.09	0.45	-0.09	-0.09	-0.18	0.37
0.215-0.465	-0.19	-0.19	0.59	-0.22	0.30	0.30	-0.93	0.32	-0.53	-0.56	1.63	-0.54
0.465-1.0	0.17	-1.00	0.67	0.16	1.91	-2.22	-1.58	1.89	-0.67	-0.67	2.00	-0.65
1.0-2.15	4.04	-6.44	-2.04	4.44	22.35	-26.01	-19.33	22.99	0.40	-4.22	2.89	0.94
2.15-4.65	-1.71	3.99	-0.84	-1.44	-13.80	7.37	19.47	-13.04	-2.06	5.83	-2.15	-1.62
4.65-10.0	0.53	-2.33	0.97	0.84	4.13	-1.28	-7.25	4.41	-1.00	-1.51	3.19	-0.68
10.0-21.5	1.41	-0.28	-2.83	1.70	-0.60	5.93	-4.98	-0.35	3.12	-3.63	-2.91	3.42
21.5-46.5	-0.77	1.27	-0.01	-0.49	-0.99	4.74	-3.02	-0.73	1.15	0.75	-3.32	1.42
46.5-100	-2.42	1.71	2.87	-2.16	-0.28	1.81	-1.52	-0.01	-3.68	2.70	4.42	-3.44
100-215	1.21	-0.55	-2.02	1.36	2.73	3.87	-9.58	2.97	-1.01	-0.54	2.41	-0.86
215-465		-0.31	-3.15	3.46		5.92	-9.06	3.15		-1.37	0.80	0.57

TABLE VII

PU-240: CROSS SECTION PER-CENT DEVIATION FROM AVERAGE

ENERGY GROUP	TOTAL				CAPTURE				FISSION			
EV	ENDF/B	JENDL	SOKRATOR	KEDAK	ENDF/B	JENDL	SOKRATOR	KEDAK	ENDF/B	JENDL	SOKRATOR	KEDAK
THERMAL	0.46	0.12	-0.30	-0.27	0.23	-0.11	-0.53	0.41				
0.215-0.465	1.07	-1.34	1.00	-0.73	0.45	-1.91	0.40	1.06				
0.465-1.0	-1.12	-0.96	3.08	-1.01	-0.97	-1.66	2.92	-0.30				
1.0-2.15	-2.92	5.33	0.53	-2.94	-2.53	4.37	0.55	-2.40				
2.15-4.65	2.91	4.21	-7.43	0.31	1.30	-0.42	-0.99	0.03				
4.65-10.0	6.48	5.50	-10.73	-1.25	4.81	6.26	-6.20	-4.87				
10.0-21.5	4.78	-9.81	1.80	3.23	4.45	-12.24	3.15	4.65				
21.5-46.5	4.22	-0.27	-3.74	-0.21	1.23	1.83	-3.19	0.14				
46.5-100	2.84	-2.73	-1.68	1.58	0.35	0.95	-1.94	0.65				
100-215	1.29	0.33	-2.13	0.51	0.28	3.53	-2.47	-1.34				
215-465	3.46	1.46	-3.67	-1.25	9.32	10.02	-9.21	-10.13				
465-1000	1.66	1.25	-2.12	-0.79	7.60	6.43	-6.53	-7.50				
1000-2150	0.60	0.78		-1.39	8.55	6.25		-14.80				

PU-241: CROSS SECTION PER-CENT DEVIATION FROM AVERAGE

	TOTAL				CAPTURE				FISSION			
	ENDF/B	JENDL	SOKRATOR	KEDAK	ENDF/B	JENDL	SOKRATOR	KEDAK	ENDF/B	JENDL	SOKRATOR	KEDAK
THERMAL	0.02	0.17	-0.26	0.07	-0.35	0.09	-0.42	0.67	0.18	0.20	-0.29	-0.10
0.215-0.465	-0.61	-5.11	-4.49	10.21	-0.88	-9.41	1.38	8.91	-0.61	-3.14	-7.41	11.16
0.465-1.0	1.04	-5.33	7.11	-2.82	28.21	2.19	-14.69	-15.70	-9.25	-7.76	11.24	5.76
1.0-2.15	10.26	1.22	3.51	-14.99	61.81	-5.76	-27.51	-28.54	4.54	5.08	2.90	-12.52
2.15-4.65	1.92	1.08	-6.24	3.23	2.83	3.04	-20.11	14.24	-1.62	1.27	1.73	-1.38
4.65-10.0	6.45	2.18	-0.44	-8.20	19.28	-1.63	-21.23	3.58	4.65	3.64	0.80	-9.09
10.0-21.5	2.21	2.95	-10.33	5.17	10.63	15.45	-31.62	5.54	-2.51	-1.89	-1.64	6.04
21.5-46.5	-3.42	-4.62	-3.36	11.41	1.97	3.19	-22.93	17.78	-2.89	-5.63	-6.64	15.17
46.5-100	-4.56	-0.22	-2.49	7.27	2.41	-1.50	-13.04	12.13	-6.55	0.08	-3.07	9.54

PU-242: CROSS SECTION PER-CENT DEVIATION FROM AVERAGE

	TOTAL				CAPTURE				FISSION			
	ENDF/B	JENDL	SOKRATOR	KEDAK	ENDF/B	JENDL	SOKRATOR	KEDAK	ENDF/B	JENDL	SOKRATOR	KEDAK
THERMAL	-0.08	-0.82	-0.42	1.32	1.99	-1.72	-1.19	0.93				
0.215-0.465	-2.19	-0.41	0.69	1.92	1.41	-1.85	-0.67	1.11				
0.465-1.0	-2.85	-0.04	1.12	1.77	1.03	-1.88	-0.50	1.34				
1.0-2.15	-3.33	-0.36	1.28	2.41	-0.53	-2.64	0.03	3.14				
2.15-4.65	12.73	-4.43	-3.73	-4.58	10.67	-3.88	-3.04	-3.75				
4.65-10.0	4.31	0.77	-11.16	6.08	3.16	-0.91	-1.61	-0.63				
10.0-21.5	2.08	2.16	-10.82	6.58	0.31	-0.31	-0.31	0.31				
21.5-46.5	-0.11	2.06	-7.24	5.29	-1.43	-1.87	4.29	-0.99				
46.5-100	0.24	0.40	-0.71	0.07	-6.30	0.61	-6.78	12.47				
100-215	-2.93	0.28	-3.57	6.22	-5.36	-3.30	-3.58	12.24				
215-465	-1.83	2.08	-4.49	4.24	-5.25	-1.31	0.82	5.75				
465-1000		4.73	-1.57	-3.17		-5.87	-5.87	11.74				

TABLE VIII

U-235: F FACTOR PER-CENT DEVIATION FROM AVERAGE

ENERGY GROUP	TOTAL				CAPTURE				FISSION			
EV	ENDF/B	JENDL	SOKRATOR	KEDAK	ENDF/B	JENDL	SOKRATOR	KEDAK	ENDF/B	JENDL	SOKRATOR	KEDAK
THERMAL												
0.215-0.465	0.91	1.02	1.02	-2.96	0.72	0.50	1.84	-3.06	1.02	1.13	1.02	-3.17
0.465-1.0	0.13	0.84	0.13	-1.09	0.15	0.77	-0.77	-0.15	0.15	1.07	0.15	-1.38
1.0-2.15	-2.38	0.75	2.51	-0.88	-1.17	4.88	0.95	-4.65	-4.99	-1.62	6.17	0.44
2.15-4.65	-1.33	-1.61	0.99	1.95	1.63	-0.48	-0.48	-0.66	-6.39	-6.39	8.19	4.59
4.65-10.0	-3.67	-1.77	3.13	2.31	-0.10	-2.38	1.05	1.43	-13.25	-5.42	15.06	3.61
10.0-21.5	4.35	6.22	-3.41	-7.16	3.30	7.71	-0.30	-10.71	2.23	6.96	-0.39	-8.80
21.5-46.5	3.60	5.69	-10.80	1.51	1.25	11.24	-10.07	-2.41	1.95	4.29	-7.15	0.91
46.5-100		4.72	-5.65	0.93		6.82	-3.27	-3.55		2.40	-5.73	3.33

U-238: F FACTOR PER-CENT DEVIATION FROM AVERAGE

	TOTAL				CAPTURE				FISSION			
	ENDF/B	JENDL	SOKRATOR	KEDAK	ENDF/B	JENDL	SOKRATOR	KEDAK	ENDF/B	JENDL	SOKRATOR	KEDAK
THERMAL												
0.215-0.465	0.0	0.0		0.0	0.0	0.0		0.0				
0.465-1.0	0.0	0.0		0.0	0.0	0.0		0.0				
1.0-2.15	0.0	0.0		0.0	0.0	0.0		0.0				
2.15-4.65	0.0	0.0		0.0	-0.17	-0.27		0.44				
4.65-10.0	-1.02	0.15		0.87	-2.30	0.77		1.53				
10.0-21.5	0.20	-0.69		0.49	-0.77	-0.19		0.97				
21.5-46.5	0.48	1.40		-1.88	-1.66	-0.66		2.32				
46.5-100	1.45	-0.29		-1.16	0.55	-0.39		-0.16				
100-215	4.05	1.45		-5.49	-1.82	-0.91		2.73				
215-465	0.19	1.14		-1.33	0.80	0.11		-0.91				
465-1000	1.07	1.81		-2.88	0.0	0.0		0.0				
1000-2150	1.47	0.00		-1.47	8.72	-5.13		-3.59				

PU-239: F FACTOR PER-CENT DEVIATION FROM AVERAGE

	TOTAL				CAPTURE				FISSION			
	ENDF/B	JENDL	SOKRATOR	KEDAK	ENDF/B	JENDL	SOKRATOR	KEDAK	ENDF/B	JENDL	SOKRATOR	KEDAK
THERMAL												
0.215-0.465	0.00	0.00		0.00	0.0	0.0		0.0	0.00	0.00		0.00
0.465-1.0	0.81	-1.63		0.81	2.19	-4.38		2.19	0.41	-0.82		0.41
1.0-2.15	-0.18	0.35		-0.18	-0.15	0.29		-0.15	-0.04	0.07		-0.04
2.15-4.65	-0.37	0.74		-0.37	-1.86	3.73		-1.86	-0.55	1.09		-0.55
4.65-10.0	-0.64	1.29		-0.64	-0.89	1.77		-0.89	-0.72	1.44		-0.72
10.0-21.5	3.20	-6.41		3.20	3.10	-6.20		3.10	3.68	-7.35		3.68
21.5-46.5	0.15	-0.30		0.15	-3.89	7.78		-3.89	-0.62	1.25		-0.62
46.5-100	2.31	-4.63		2.31	3.91	-7.83		3.91	1.93	-3.86		1.93
100-215	-1.67	3.11		-1.44	-8.60	17.19		-8.60	-0.72	1.44		-0.72
215-465		2.90		-2.90		14.89		-14.89		2.32		-2.32

TABLE IX

PU-240: F-FACTOR PER-CENT DEVIATION FROM AVERAGE

ENERGY GROUP	TOTAL				CAPTURE				FISSION			
EV	ENDF/B	JENDL	SOKRATOR	KEDAK	ENDF/B	JENDL	SOKRATOR	KEDAK	ENDF/B	JENDL	SOKRATOR	KEDAK
THERMAL												
0.215-0.465	-0.03	0.08	-0.03	-0.03	-0.03	0.08	-0.03	-0.03				
0.465-1.0	1.89	-1.31	-1.60	1.02	1.56	-1.28	-1.56	1.28				
1.0-2.15	4.07	-4.65	-3.49	4.07	4.08	-6.12	-2.04	4.08				
2.15-4.65	0.89	0.89	-1.41	-0.37	0.96	1.49	-1.69	-0.76				
4.65-10.0	0.10	-0.10	0.00	0.00	0.42	-0.11	-0.11	-0.21				
10.0-21.5	2.16	14.63	-10.31	-6.47	2.31	8.93	-8.07	-3.17				
21.5-46.5	5.26	8.29	1.28	-14.83	-1.63	-2.06	-5.96	9.64				
46.5-100	4.85	9.00	-2.23	-11.63	-0.96	-2.44	-7.46	10.86				
100-215	-3.16	14.15	-8.77	-2.22	-20.03	77.08	-30.31	-26.74				
215-465	7.14	11.13	-10.05	-8.21	45.96	54.96	-53.38	-47.53				
465-1000	22.33	27.63	12.90	-62.86	11.65	43.20	-48.06	-6.80				
1000-2150	35.20	36.90		-72.11	-21.51	-2.29		23.80				

PU-241: F-FACTOR PER-CENT DEVIATION FROM AVERAGE

ENERGY GROUP	TOTAL				CAPTURE				FISSION			
EV	ENDF/B	JENDL	SOKRATOR	KEDAK	ENDF/B	JENDL	SOKRATOR	KEDAK	ENDF/B	JENDL	SOKRATOR	KEDAK
THERMAL												
0.215-0.465	0.15	-3.46		3.31	-0.14	3.75		-3.61	-0.16	-6.94		7.09
0.465-1.0	2.44	3.90		-6.34	6.01	2.45		-8.47	2.01	5.36		-7.37
1.0-2.15	-0.37	0.03		0.34	-0.68	-0.07		0.75	-0.40	0.00		0.40
2.15-4.65	8.85	2.46		-11.31	10.69	7.63		-18.32	3.08	2.79		-5.87
4.65-10.0	2.76	3.19		-5.95	4.21	10.86		-15.07	2.57	2.28		-4.84
10.0-21.5	-18.86	13.52		5.34	-31.09	40.12		-9.04	-20.82	7.14		13.68
21.5-46.5	-4.19	2.19		2.00	-6.25	10.19		-3.94	-5.79	-0.89		6.68
46.5-100	-2.93	7.74		-4.81	-8.09	21.72		-13.63	-4.62	7.64		-3.02

PU-242: F-FACTOR PER-CENT DEVIATION FROM AVERAGE

ENERGY GROUP	TOTAL				CAPTURE				FISSION			
EV	ENDF/B	JENDL	SOKRATOR	KEDAK	ENDF/B	JENDL	SOKRATOR	KEDAK	ENDF/B	JENDL	SOKRATOR	KEDAK
THERMAL												
0.215-0.465	0.0	0.0	0.0	0.0	0.0	0.0	0.0	0.0				
0.465-1.0	0.0	0.0	0.0	0.0	0.0	0.0	0.0	0.0				
1.0-2.15	0.20	0.65	-0.82	-0.03	0.39	0.64	-0.70	-0.33				
2.15-4.65	-6.68	3.29	-3.83	7.21	-6.72	3.29	-1.98	5.40				
4.65-10.0	-0.10	0.10	-0.10	0.10	-0.38	0.49	-0.60	0.49				
10.0-21.5	-1.55	-1.44	3.76	-0.77	-12.97	-13.85	33.63	-6.81				
21.5-46.5	-5.41	-3.74	12.21	-3.05	-14.58	-13.72	38.89	-10.59				
46.5-100	-73.69	191.72	-48.07	-69.95	-8.72	-11.68	24.56	-4.16				
100-215	-14.77	-9.45	33.16	-8.94	-24.76	-23.64	63.64	-15.24				
215-465	-37.84	-9.97	53.87	-6.06	-22.77	-35.19	86.26	-28.30				
465-1000		-39.93	-0.15	40.24		-75.10	-6.17	81.70				

TABLE X

U-235: COMPARISON OF RESONANCE PARAMETERS

ENDF/B-V			JENDL-II			SOKRATOR			KEDAK-IV		
EV	J	GAM-TOT	EV	J	GAM-TOT	EV	J	GAM-TOT	EV	J	GAM-TOT
									-19.19	3	0.137
									-14.16	4	0.160
-1.49	3.5	0.23768	-1.49	3.5	0.24588	-1.49	4	0.2377			
0.29	3.5	0.135	0.273	3.5	0.135	0.29	3	0.135	0.285	3	0.121
1.14	3.5	0.1508	1.14	3.5	0.162	1.14	4	0.1508	1.144	4	0.142
2.035	3.5	0.0447	2.035	3.5	0.0480	2.035	3	0.0447	2.033	3	0.0457
2.92	3.5	0.22	2.84	3.5	0.191	2.92	4	0.22	2.762	4	0.109
3.147	3.5	0.1396	3.14	3.5	0.113	3.156	3	0.1396	3.150	3	0.138
3.609	3.5	0.0844	3.61	3.5	0.084	3.626	4	0.0844	3.613	4	0.0878
									4.20	3	0.235
4.848	3.5	0.0396	4.85	3.5	0.039	4.850	4	0.0396	4.845	4	0.0389
5.448	3.5	0.0901	5.45	3.5	0.090	5.511	4	0.7310	5.50	4	0.435
5.60	3.5	0.642	5.60	3.5	0.125						
6.21	3.5	0.231	6.21	3.5	0.269	6.211	3	0.231	6.21	3	0.167
6.38	3.5	0.048	6.39	3.5	0.0492	6.382	4	0.045	6.38	4	0.0462
7.07	3.5	0.064	7.08	3.5	0.0611	7.07	4	0.064	6.95	3	0.365

FIGURE 1

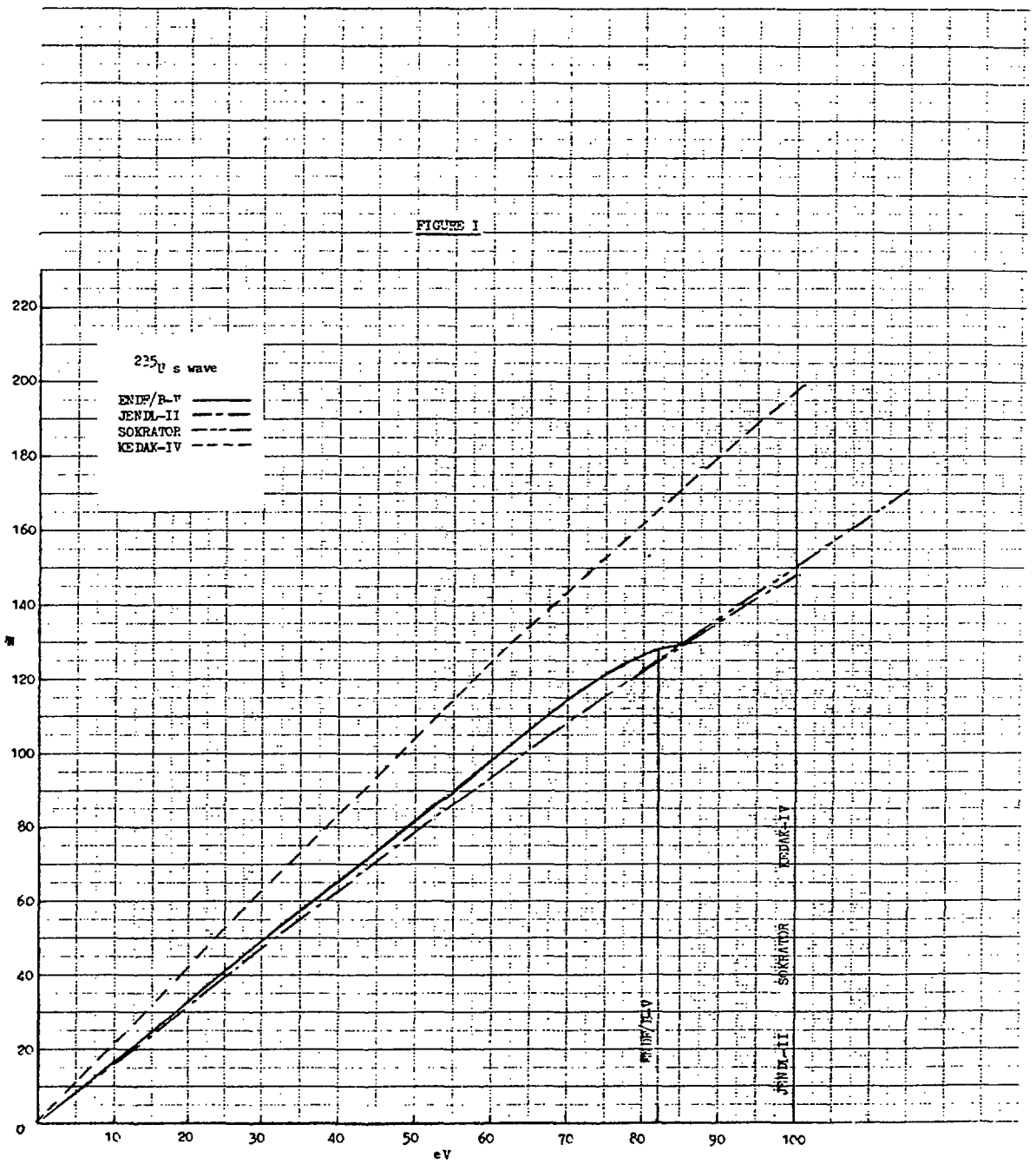
^{235}U s wave
ENDF/B-V
JENDL-II
SOKRATOR
KEDAK-IV
η
eV
ENDF/B-V
JENDL-II
SOKRATOR
KEDAK-IV

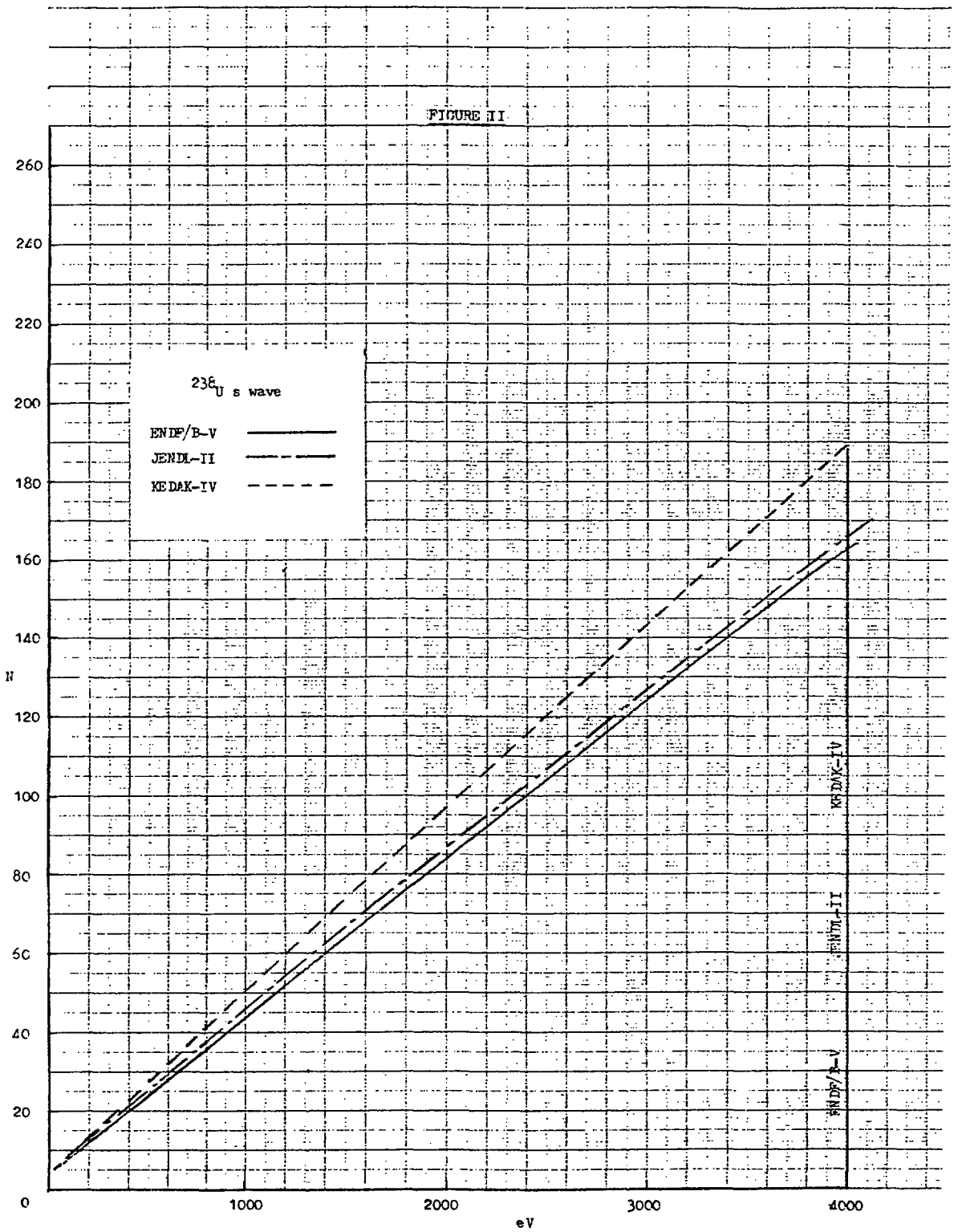
FIGURE II
^{238}U s wave
ENDF/B-V
JENDL-II
KEDAK-IV
N
eV
0
20
40
60
80
100
120
140
160
180
200
220
240
260
1000
2000
3000
4000

FIGURE III

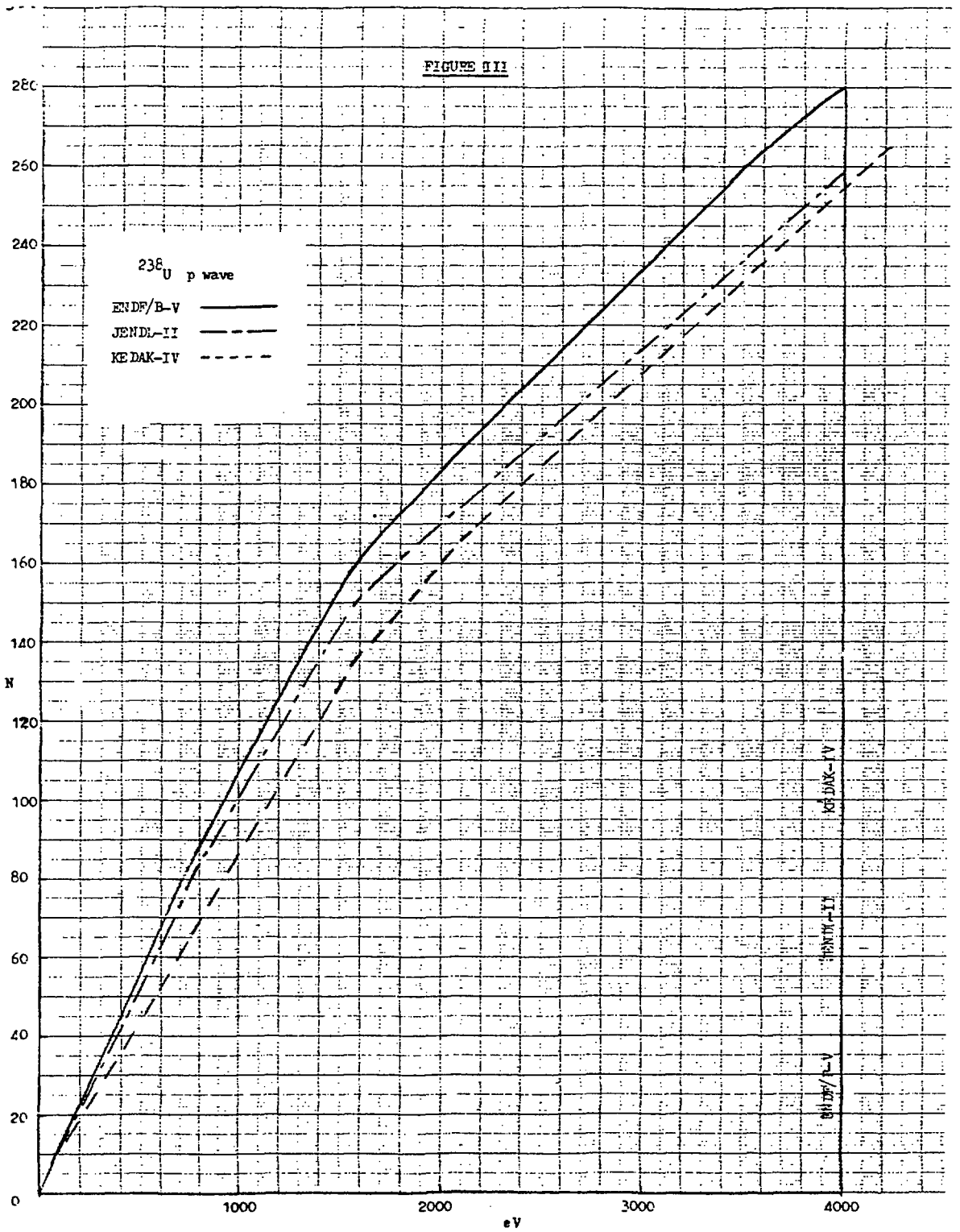
^{238}U p wave
ENDF/B-V
JENDL-II
KEDAK-IV
N
eV
0
20
40
60
80
100
120
140
160
180
200
220
240
260
280
1000
2000
3000
4000

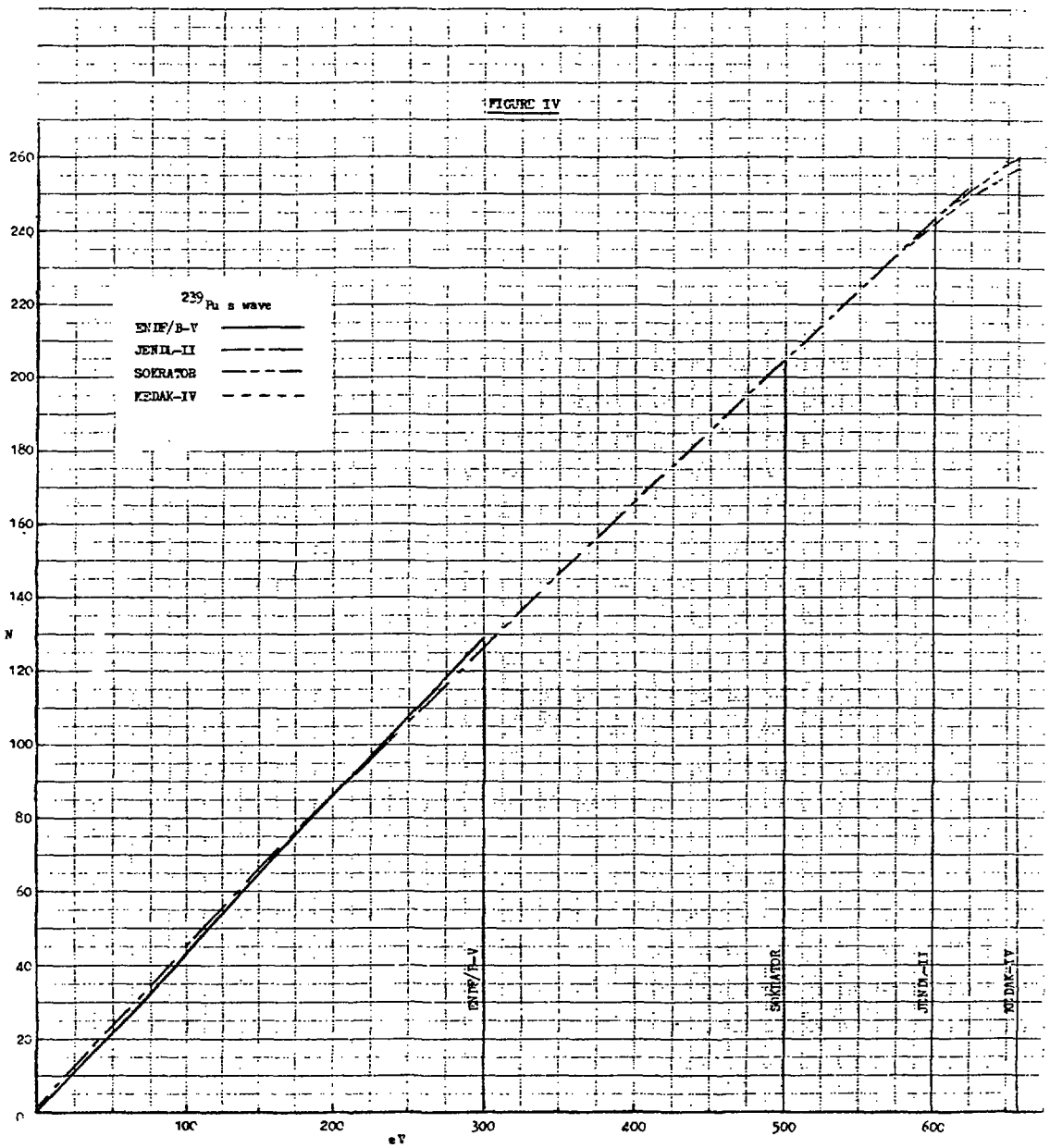
FIGURE IV
239Pu s wave
ENDF/B-V
JENDL-II
SOKRATOR
KEDAK-IV
N
eV
260
240
220
200
180
160
140
120
100
80
60
40
20
0
100
200
300
400
500
600
ENDF/B-V
SOKRATOR
JENDL-II
KEDAK-IV

FIGURE V

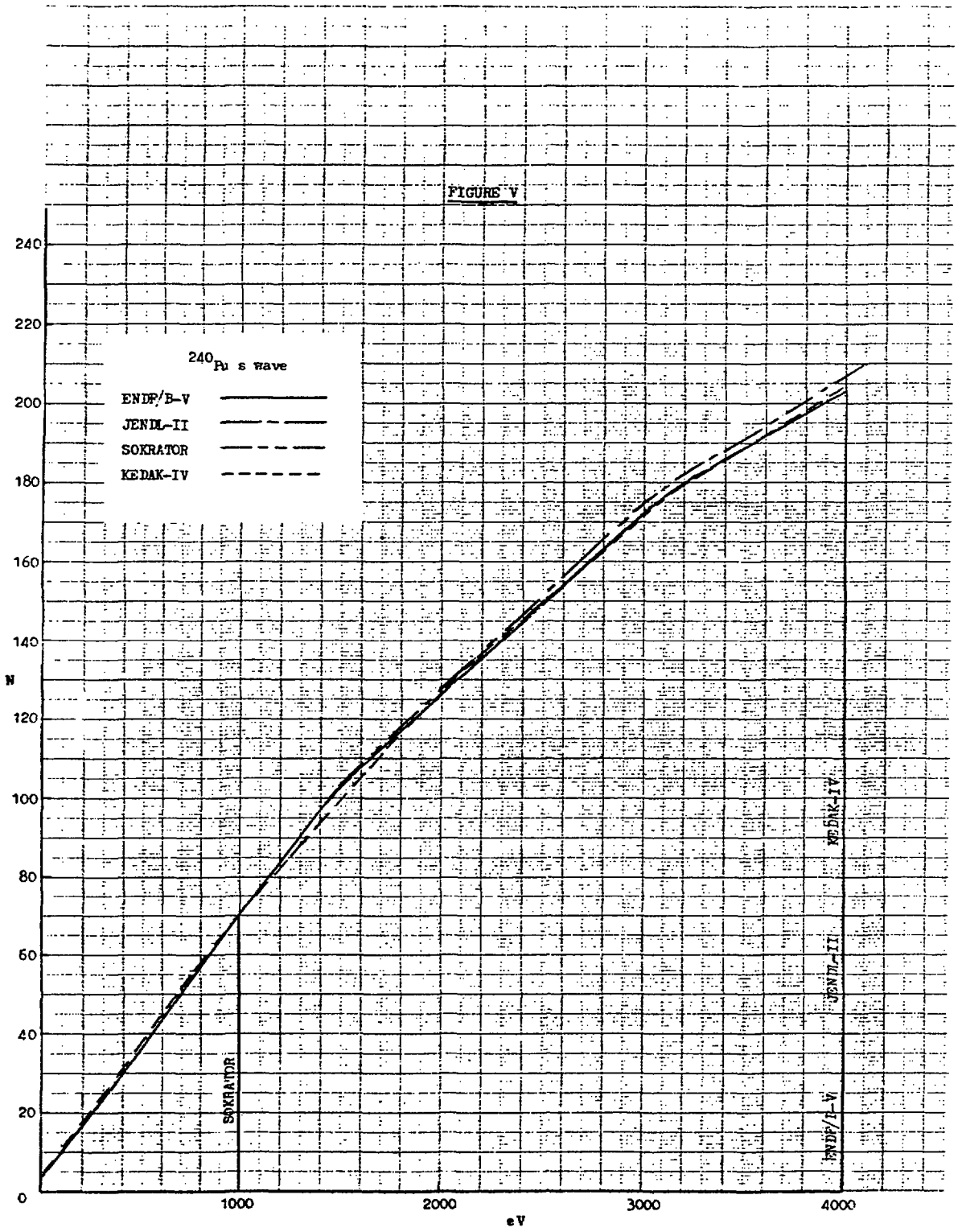
^{240}Pu s wave
ENDF/B-V
JENDL-II
SOKRATOR
KEDAK-IV
N
eV
0
20
40
60
80
100
120
140
160
180
200
220
240
1000
2000
3000
4000
SOKRATOR
ENDF/B-V
JENDL-II
KEDAK-IV

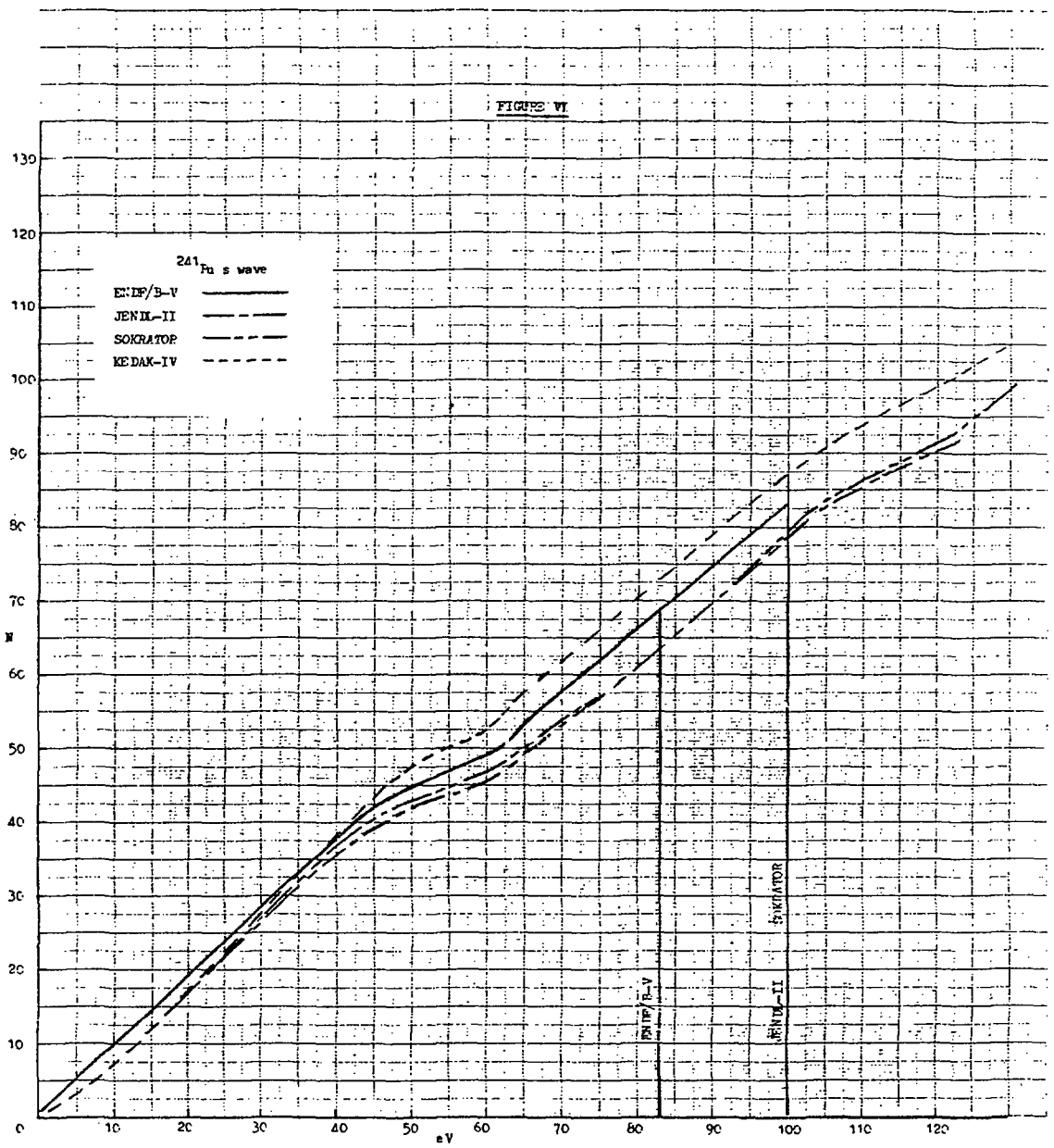
FIGURE VI
^{241}Pu s wave
ENDF/B-V
JENDL-II
SOKRATOR
KEDAK-IV
130
120
110
100
90
80
70
60
50
40
30
20
10
0
10
20
30
40
50
60
70
80
90
100
110
120
eV
ENDF/B-V
JENDL-II
SOKRATOR

FIGURE VII

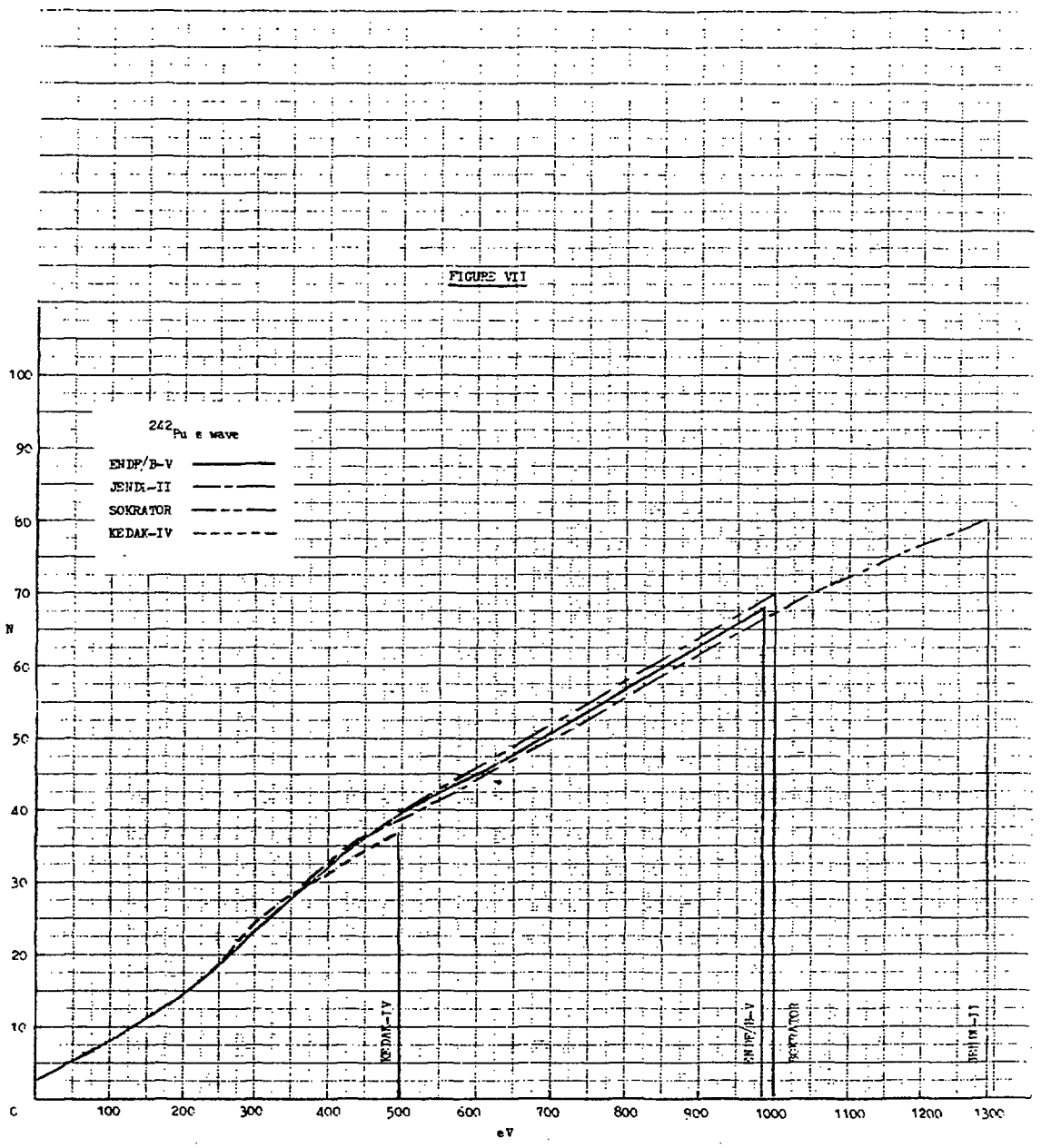
^{242}Pu s wave
ENDF/B-V
JENDL-II
SOKRATOR
KEDAK-IV
N
eV
0
10
20
30
40
50
60
70
80
90
100
100
200
300
400
500
600
700
800
900
1000
1100
1200
1300
KEDAK-IV
ENDF/B-V
SOKRATOR
JENDL-II

Comparison of the ENDF/B-V and SOKRATOR Evaluations of ^{235}U, ^{239}Pu, ^{240}Pu and ^{241}Pu at Low Neutron Energies

G. de Saussure and R. Q. Wright

ABSTRACT

The U.S. and U.S.S.R.'s most recent evaluations of ^{235}U, ^{239}Pu, ^{240}Pu and ^{241}Pu are compared over the thermal region and over the first few resonances. The two evaluations rest on essentially the same experimental data base and the differences reflect different approaches to the representation of the cross sections or different weightings of the experimental results. It is found that over the thermal and resolved ranges the two evaluations are very similar. Some differences in approaches are briefly discussed.

I. INTRODUCTION

In this paper we present a brief comparison of the U.S. evaluation ENDF/B-V and the USSR evaluation SOKRATOR of the nuclides ^{235}U, ^{239}Pu, ^{240}Pu and ^{241}Pu, over the thermal energy region and over the first few resolved resonances.[1-8] The emphasis is on comparing methods of representing the evaluated cross sections since the comparison of evaluated and measured resonance parameters is the subject of other papers at this meeting.

The SOKRATOR evaluations were "translated" into the ENDF/B-V format by the Nuclear Data Section of the IAEA.[9] This ENDF/B Version of SOKRATOR forms the basis for the comparison presented here. In the next few sections we discuss successively the file structure, the scattering radius, the cross sections below 1 eV, and the resolved resonance region. General comments on the cross-section representations are collected in the concluding section. For ease in presentation and for conciseness, much of this comparison is presented in tabular and graphical form.

*Research sponsored by the Division of Reactor Research and Technology, U.S. Department of Energy, under contract W-7405-eng-26 with the Union Carbide Corporation.

II. COMPARISON OF THE ENDF/B-V AND SOKRATOR FILE STRUCTURES

The general file structures for ^{235}U, ^{239}Pu, ^{240}Pu and ^{241}Pu are compared in Tables I to IV. All the SOKRATOR evaluations, as well as the ^{235}U and ^{239}Pu ENDF/B-V evaluations, represent the cross sections below 1 eV with point data (MF=3). In the ENDF/B-V representation of ^{241}Pu this pointwise description extends to 2.873 eV, whereas in the ENDF/B-V representation of ^{240}Pu the resolved resonance region starts at 10^{-5} eV.

The ENDF/B-V and SOKRATOR representations of the ^{235}U, ^{239}Pu and ^{240}Pu cross sections over the resolved resonance range use Breit-Wigner resonance parameters. The ENDF/B-V representation of the ^{241}Pu cross sections over the resolved resonance region (2.873 to 100 eV) uses the Adler-Adler formalism whereas the corresponding SOKRATOR evaluation uses a "modified Adler-Adler representation" which is incompatible with ENDF/B formats as will be shown in Section VI. In the ENDF/B-V representation of the ^{235}U and ^{239}Pu cross sections over the resolved resonance region the resonance contributions are supplemented by a point-data file (MF=3). In all the SOKRATOR evaluations this point data file vanishes over the resonance region.

The SOKRATOR ^{235}U evaluation has an alternate representation of the resolved range in terms of "modified Adler-Adler parameters."[5]

As can be seen from Tables I to IV, the unresolved representation in the SOKRATOR evaluations extends to 100 or 150 keV (except for ^{239}Pu, where no unresolved parameters are given). The unresolved resonance range for ENDF/B-V extends to 25 keV for ^{235}U and ^{239}Pu and to 40 keV for ^{240}Pu and ^{241}Pu. Since the ENDF/B-V and SOKRATOR formats for the unresolved resonance range are not compatible,[5] this range will not be discussed here.

III. THE ENDF/B-V AND SOKRATOR SCATTERING RADIUS

The values of the scattering radius, AP, in the ENDF and SOKRATOR evaluations differ by 10 to 15% for the four isotopes considered. The scattering radius in the ENDF evaluations is derived from the relation:

$$AP=\left(\frac{\sigma_p}{4\pi}\right)^{1/2} \qquad (1)$$

where σ_p is the potential scattering cross section. For instance, in the ^{235}U ENDF/B-V evaluation the scattering radius, $AP=0.957\times10^{-12}$ cm, was obtained by (1) from the value σ_p=11.7b recommended by F. Poortmans *et al.*[10] on the basis of their measurement of the scattering cross section of ^{235}U below 100 eV.[11]

The values of the scattering radius given in the SOKRATOR evaluations are smaller and are probably computed from an expression relating the scattering radius to the mass number A such as:[12]

$$AP = (.123A^{1/3} + .08) \times 10^{-12} \text{ cm} \qquad (2)$$

IV. ENDF/B-V AND SOKRATOR EVALUATIONS IN THE THERMAL ENERGY REGION

The ENDF/B-V and SOKRATOR evaluations of ^{235}U, ^{239}Pu, ^{240}Pu and ^{241}Pu in the thermal energy region are compared in Tables V-IX and in Figs. 1-16.

As can be seen from the figures, except for the scattering cross sections of the fissile isotopes, the two evaluations are fairly consistent. This agreement is not surprising, since both evaluations are based in part on the result of the periodic evaluations of the thermal parameters of the fissile nuclei performed by an international team of experts under the sponsorship of the IAEA Nuclear Data Section.[13-15]

The scattering cross sections of these heavy nuclei are difficult to measure, particularly at low energy where Bragg scattering and extinction are important. Most evaluated scattering cross sections are compiled from resonance parameters, except for the SOKRATOR ^{235}U evaluation where the scattering cross section shows considerable structure and was probably obtained directly from a measurement (Fig. 2).

For a more precise comparison of the evaluations in the thermal region it is convenient to parameterize the cross sections with the 2200 m/s value, σ_o, and the Westcott g-factor[16] at 294 K.

The values of σ_o and g for the four isotopes are compared in Tables V to VIII and are generally consistent to within a few percent, except for the ^{240}Pu fission cross section, which is only of the order of 50 mb, and the ^{235}U and ^{239}Pu scattering cross sections, also relatively small.

The thermal parameters for the fission and capture cross sections of the fissile isotopes are compared with results of other evaluations[13,14,17,18] in Table IX. The ENDF/B-V ^{235}U thermal region is based on the work of Leonard *et al.*[17] The ENDF/B-V thermal parameters are consistent (within quoted errors) with the 1975-IAEA values,[14] except for g_γ for ^{235}U and ^{239}Pu. The SOKRATOR evaluations of ^{235}U and ^{239}Pu have somewhat smaller fission cross sections and somewhat larger capture cross sections. As discussed

by Lemmel,[15] there are still unexplained discrepancies in the "best values" of the thermal parameters, and the differences between the ENDF/B-V and SOKRATOR evaluations reflect different interpretations of the probable cause of these discrepancies.

V. ENDF/B-V AND SOKRATOR EVALUATIONS IN THE RESOLVED RANGES

The ENDF and SOKRATOR evaluated ^{235}U Breit-Wigner resonance parameters for levels up to 20 eV are compared in Table X. In general corresponding resonance parameters agree within 10% or better. SOKRATOR assigns a J-value to each level, and these assignments are consistent with the spin determination of Moore *et al.*,[19] based on the measurements with polarized beams and polarized targets of Keyworth *et al.*[20] The ENDF/B-V evaluation assigns a fictitious J=3.5 to all levels. Both the ENDF and SOKRATOR evaluations represent the cross sections up to 20 eV with about 30 levels, whereas Moore *et al.*[19] observe between 40 and 50 levels in the same interval.

As is well known, the asymmetries in the resonance shape of the fissile nuclides cannot be represented accurately with the Breit-Wigner formalism.[21-23] The ENDF/B-V supplements the resonance description of the cross sections with "smooth files" (MF=3), which are the differences between the evaluated cross sections and the Breit-Wigner representations. These "smooth files" include considerable structure and to a large extent negate the advantages of a resonance representation; these files must be numerically Doppler broadened and self-shielded. Figure 17 shows the "smooth file" for the ^{235}U fission cross section.

In the SOKRATOR evaluations these "smooth files" vanish over the resonance region, so that the resonance asymmetries are not correctly described in the ^{235}U evaluation using Breit-Wigner parameters. SOKRATOR also has a representation of the ^{235}U resonance region, using "modified Adler-Adler parameters," but this representation is incompatible with ENDF/B formats as will be discussed in the next section.

The ENDF and SOKRATOR evaluated ^{239}Pu Breit-Wigner resonance parameters for levels up to 25 eV are compared in Table XI. As in the case of ^{235}U these parameters agree within 10% or better for the more important levels. As for ^{235}U, the ENDF/B-V representation is supplemented by a "smooth file" (MF=3) which is not "smooth". The MF=3 contribution to the ^{239}Pu fission cross section is illustrated in Fig. 18.

The ENDF and SOKRATOR evaluated ^{240}Pu Breit-Wigner resonance parameters for levels up to 100 eV are compared in Table XII. The values of the neutron and capture widths are mostly consistent to within 10% or better. The values of the fission widths differ by factors of 5 or even 10! But these fission widths are very small and hence difficult to measure. The ENDF/B-V values of the fission widths of the first three levels were obtained from the evaluation of Weigmann *et al.*[24] and the levels for which no measurements of the fission width had been made were assigned a fission width of 20 meV. The fission widths of SOKRATOR were obtained from an area analysis of the data of Byers *et al.*[25] and Migneco *et al.*[26] For the important level at 1.058 eV, the neutron and capture widths of the two evaluations differ by about 3% but the capture cross sections below 0.1 eV, proportional to the product of these two widths, are fully consistent.

The resolved range of ^{241}Pu is represented by Adler-Adler parameters in the ENDF/B-V evaluation, and by "modified Adler-Adler parameters" in the SOKRATOR evaluation. As discussed in the next section, these two

formalisms are not compatible, so that a meaningful comparison of resonance parameters cannot be made.

VI THE SOKRATOR MODIFIED ADLER-ADLER FORMALISM

In the resonance region, some SOKRATOR evaluations[5,8] use a "modified Adler-Adler formalism" in which a reaction cross section is represented by:

$$\sigma_{n,r}(E) = \frac{2.6\times10^6}{E} \sum_{i=1}^{N} \left(G_i^{(r)} \psi(x,\theta) + H_i^{(r)} \chi(x,\theta) \right) \tag{3}$$

where N is the number of resonances taken into account, $G_i^{(r)}$ and $H_i^{(r)}$ are the modified Adler-Adler parameters for the i-th level and the r-th reaction and $\psi(x,\theta)$ and $\chi(x,\theta)$ are the Voight profiles[27,28] for,

$$x = \frac{\mu - E}{\nu} \quad \text{and} \quad \theta = 2\frac{\nu}{\Delta}$$

where μ is the resonance energy, ν the resonance half-width and Δ the Doppler width. If the Doppler broadening is negligible, the first Voigt profile becomes:

$$\psi(x,\infty) = \frac{1}{1+x^2} = \frac{\nu^2}{(\mu-E)^2 + \nu^2} . \tag{4}$$

If we consider a single level (H=0) and no broadening, expression (3) reduces to:

$$\sigma_{n,r}(E) = \frac{2.6\times10^6}{E} G^{(r)} \frac{\nu^2}{(\mu-E)^2 + \nu^2} . \tag{5}$$

By identifying (5) with the single-level Breit-Wigner formula we see that for a single level $G^{(r)}$ reduces to:

$$G^{(r)} \simeq g \frac{\Gamma_n \Gamma_r}{\Gamma^2} \tag{6}$$

In the ENDF/B formulation,[29] as in the original Adler-Adler formulation,[30] the reaction cross section is represented by:

$$\sigma_{n,r}(E) = \frac{2.6\times10^6}{4\,E^{1/2}} \left(\frac{A+1}{A}\right)^2 \sum_{i=1}^{N} \left(\frac{G^*}{\nu} \psi + \frac{H^*}{\nu} \chi \right) \tag{7}$$

where we use G* and H* for the "regular Adler-Adler parameters. Using (4), for a single level and no broadening, (7) reduces to:

$$\sigma_{n,r}(E) = \frac{2.6\times10^6}{4\,E^{1/2}} \left(\frac{A+1}{A}\right)^2 G^* \frac{\nu}{(\mu-E)^2 + \nu^2} . \tag{8}$$

By identifying (8) with the single-level Breit-Wigner formula we see that, for a single level G* reduces to:

$$G^* \simeq 2g\Gamma_n^\circ \frac{\Gamma_r}{\Gamma} . \tag{9}$$

It is clear, from comparing (3) with (7) that the cross sections in the modified Adler-Adler formalism and in the standard Adler-Adler formalism do not have the same energy dependance. As can be seen from (6), taking the modified Adler-Adler parameters as constant corresponds to neglecting the $E^{1/2}$-dependence of the neutron width due to the s-wave penetration factor.

Because of this difference in energy dependence it is not very meaningful to compare the ENDF Adler-Adler parameters to the SOKRATOR modified Adler-Adler parameters.

VII. CONCLUSION

The ENDF and SOKRATOR evaluations of the low energy cross sections of the four isotopes examined are fairly consistent. The scattering radius of the SOKRATOR evaluations are systematically lower by 10 to 15% than those of ENDF and are not consistent with low energy potential scattering cross

section data. The ENDF and SOKRATOR values of the fission and capture thermal parameters of the fissile isotopes are consistent within a few percent. The ENDF/B-V values are consistent, within quoted uncertainties, with the 1975 IAEA evaluation.[14] The SOKRATOR values tend to be lower in fission and higher in capture. Since the SOKRATOR values of $\bar{\nu}$ also tend to be lower than those of ENDF, SOKRATOR's computed criticality constants should be lower than those computed with ENDF/B-V.

Both ENDF/B-V and SOKRATOR represent the cross sections of the important nuclides ^{235}U and ^{239}Pu in the resolved resonance range, with Breit-Wigner parameters. This is somewhat surprising since it has been known, for more than twenty years, that the Breit Wigner resonance formula is a poor approximation for the fissile nuclides, even at low energies.[21-23] Several practical multilevel formalisms have been developed for the purpose of representing the low-energy cross sections of the fissile isotopes.[30-32] Several resonance analysis codes are available.[33,34] The ENDF/B procedures manual[30] recommends that the low-energy cross sections of the fissile isotopes be analysed with the Reich-Moore formalism,[32] because it is unitary and yields R-matrix resonance parameters. The Reich-Moore representation can then be converted into an equivalent Adler-Adler representation by partial expansion,[35,36] for ease in Doppler broadening. Unfortunately for ENDF/B-V, the recommended procedure has been followed only for ^{233}U, and it has not been followed in any of the SOKRATOR evaluations examined here.

Finally, the "modified Adler-Adler formalism" used in some SOKRATOR evaluations is not compatible with the "standard Adler-Adler formalism."[30] For a single level it does not reduce to the correct energy dependence of the cross sections; but viewed as an arbitrary parameterization it may permit an adequate representation of the cross sections of the fissile nuclides.

ACKNOWLEDGMENTS

The authors are indebted to J. R. Knight for considerable help in generating the comparison plots and to L. Stewart and L. W. Weston for several helpful comments.

REFERENCES

1. ENDF/B-V file for ^{235}U (MAT-1395); principal evaluator: M. R. Bhat (BNL); see also R. Kinsey, ENDF/B Summary Documentation; ENDF-201 (1979) and M. R. Bhat, Evaluation of ^{235}U Neutron Cross Section and Gamma Ray Production Data for ENDF/B-V, BNL-NCS-51184 (1980).
2. ENDF/B-V file for ^{239}Pu (MAT-1399); principal evaluators: E. Kujawski (GEFBRD), L. Stewart (LASL) and R. Labauve (LASL); see also R. Kinsey, ENDF/B Summary Documentation, ENDF-201 (1979) and E. Kujawski *et al.*, Evaluation of ^{239}Pu data for ENDF/B-V, GEFR-00247 (1977).
3. ENDF/B-V file for ^{240}Pu (MAT-1380); revised for version V by L. W. Weston and R. Q. Wright; see also R. Kinsey, ENDF/B Summary Documentation, ENDF-201 (1979) and L. W. Weston and R. Q. Wright, "Evaluation of Fission and Capture Cross Sections of ^{240}Pu and ^{241}Pu for ENDF/B-V," Nuclear Cross Sections for Technology, NBS Special Publication 594 p. 464 (1980).
4. ENDF/B-V file for ^{241}Pu (MAT-1381); evaluators: L. W. Weston (ORNL), R. Q. Wright (ORNL) and R. J. Howerton (LLL); see also R. Kinsey, ENDF/B Summary Documentation, ENDF-201 (1979) and reference 3 above.
5. SOKRATOR file for ^{235}U in ENDF/B-V Format (MAT-9210); evaluators: V. A. Konshin, G. V. Antsipov *et al.*, see also G. V. Antsipov *et al.*, Yadernije Konstanty 20, part 2 (1975) and INDC (CCP) 78/U (1976).
6. SOKRATOR file for ^{239}Pu in ENDF/B-V format (MAT-9420); Evaluators: V. A. Konshin, G. V. Antsipov *et al.*, see Bulletin of Nuclear Data Centre (1974).

7. SOKRATOR file for ^{240}Pu in ENDF/B-V Format (MAT-9430); Evaluators: V. A. Konshin *et al.*, see Report INE-564, Minsk, 1975 and Proc. of the 1975 Kiev Conference.

8. SOKRATOR file for ^{241}Pu in ENDF/B-V Format (MAT-2024); Principal Evaluators: V. A. Konshin, E. S. Sukhovitskii and G. V. Antsipov (1979).

9. The authors are indebted to Drs. V. Pronyaev and O. Schwerer of the IAEA-NDS for providing the SOKRATOR files in the ENDF/B-V format.

10. F. Poortmans *et al.*, "Scattering Cross Section of ^{235}U below 100 eV, Determination of Γ_n and J of Resonances," Nuclear Data for Reactors, Helsinki 1970 (IAEA), Vol. I p. 449.

11. J. R. Smith and R. C. Young, "^{235}U Resonance Parameters for ENDF/B-III," ENDF-161 (1971).

12. D. L. Hill, Encyclopedia of Physics (Ed. S. Flügge), Vol. 39, p. 178 (1956).

13. G. C. Hanna *et al.*, Atomic Energy Rev. 7, 4, 3 (1969).

14. H. D. Lemmel, Conf. Nuclear Cross Sections and Technology, Washington, D. C., I, 286 (1975).

15. H. D. Lemmel, Symp. Neutron Standards and Applications, Gaithersburg, MD, 170 (1977).

16. C. H. Westcott, "A Study of the Accuracy of g-Factors for Room-Temperature Maxwellian Spectra for U and Pu Isotopes," AECL-3255, Atomic Energy of Canada, Ltd., Chalk River (1969).

17. B. R. Leonard, Jr., D. A. Kottwitz and J. K. Thompson, "Evaluation of the Neutron Cross Sections of ^{235}U in the Thermal Energy Region," EPRI-NP-167 (1976).

18. B. R. Leonard, Jr. and J. K. Thompson, "Evaluation of the Thermal Cross Sections of ^{239}Pu and ^{241}Pu," EPRI-NP-1763 (1981).

19. M. S. Moore *et al.*, *Phys. Rev.* *C118*, 1328 (1978).

20. G. A. Keyworth *et al.*, *Phys. Rev.* *C8*, 2352 (1973).

21. F. J. Shore and V. L. Sailor, *Phys. Rev.* *112*, 191 (1958).

22. M. S. Moore and C. W. Reich, *Phys. Rev.* *118*, 718 (1960).

23. E. Vogt, *Phys. Rev.* *118*, 724 (1960).

24. H. Weigmann, G. Rohr and F. Poortmans, "An Evaluation of ^{240}Pu Resonance Parameter Data," Specialist Meeting on Resonance Parameters of Fertile Nuclei and ^{239}Pu, Saclay, 20-22 May 1974, NEANDC(E) 163 U p. 219, (1975).

25. D. H. Beyers, B. C. Diven and M. G. Silbert, "Capture and Fission Cross Sections of ^{240}Pu," Neutron Cross Section Technology, Washington, D. C., March 22-24, 1966, CONF-660303, 2, 903 (1966).

26. E. Migneco and J. P. Theobald, "Resonance Grouping Structure in Neutron Induced Subthreshold Fission of ^{240}Pu," Neutron Cross Sections and Technology, Washington, D. C., March 4-7, 1968, NBS Special Publication 299, I, 527 (1968).

27. W. Voigt, S. B. Bayer Akad. Wiss., 603 (1912).

28. L. Dresner, Resonance Absorption in Nuclear Reactors, p. 36, (Pergamon Press, 1960).

29. Data Formats and Procedures for ENDF, revised by R. Kinsey 1979, ENDF-102 (1979).

30. D. B. Adler and F. T. Adler, "Neutron Cross Sections in Fissile Elements," ANL-6792, 695 (1963).

31. E. Vogt, *Phys. Rev.* *112*, 203 (1958).

32. C. W. Reich and M. S. Moore, *Phys. Rev.* *111*, 929 (1958).

33. G. F. Auchampaugh, "MULTI, A Fortran Code for Least-Squares Shape Fitting of Neutron Cross-Section Data Using the Reich-Moore Multilevel Formalism," LA-5473-MS, LASL (1974).

34. H. Derrien and M. Alix, CEA-N-1554, Commissariat a l'Energie Atomique, France, 1972).

35. F. Froehner in "Neutron Physics and Nuclear Data" p. 306, Harwell (1978); OECD/IAEA.

36. F. Froehner, "New Techniques for Multilevel Cross Section Calculation and Fitting," Proceedings on the Conference on Nuclear Data Evaluation Methods and Procedures, BNL-NCS-51464, I, 375 (1981).

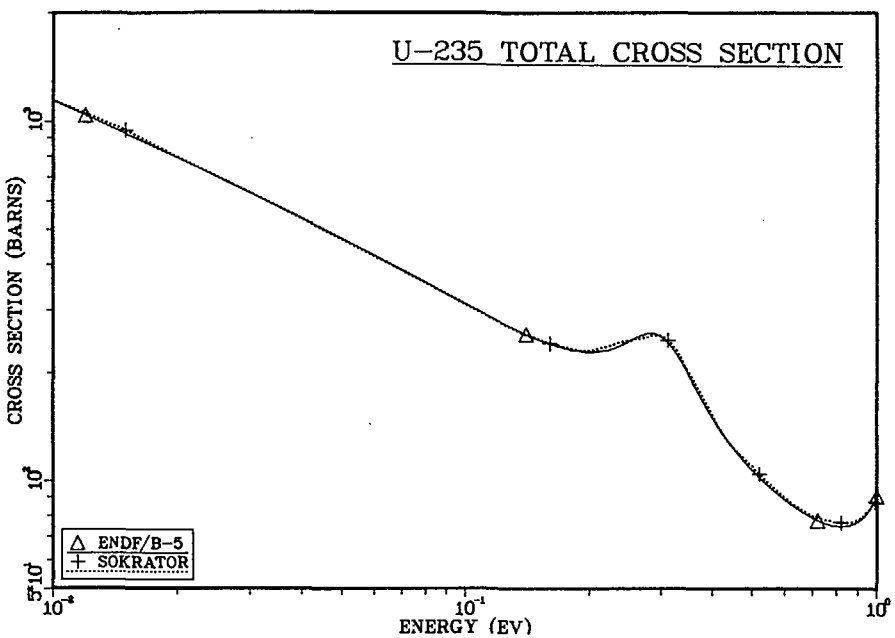

Fig. 1. Comparison of the ENDF/B-V and SOKRATOR Evaluations of the ^{235}U total cross sections below 1.0 eV.

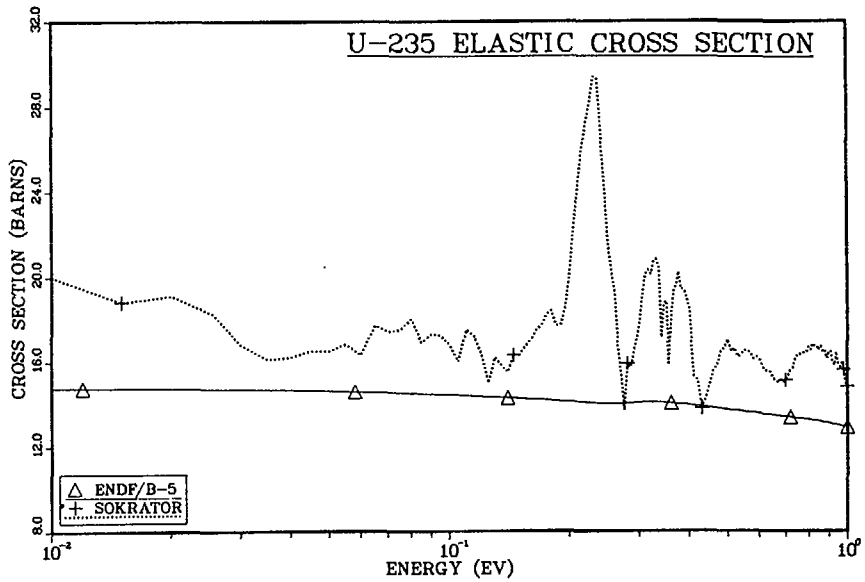

Fig. 2. ^{235}U scattering.

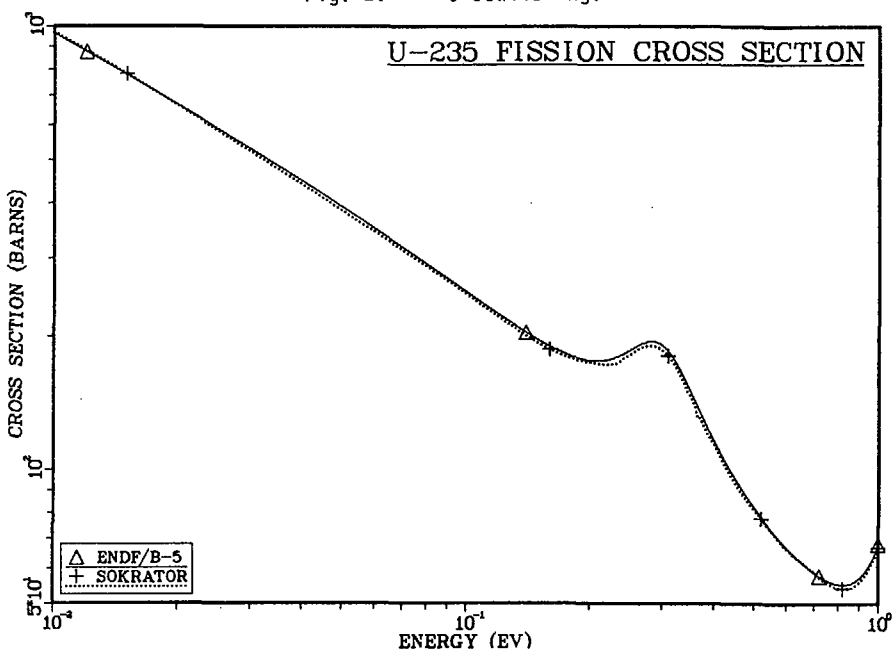

Fig. 3. ^{235}U fission.

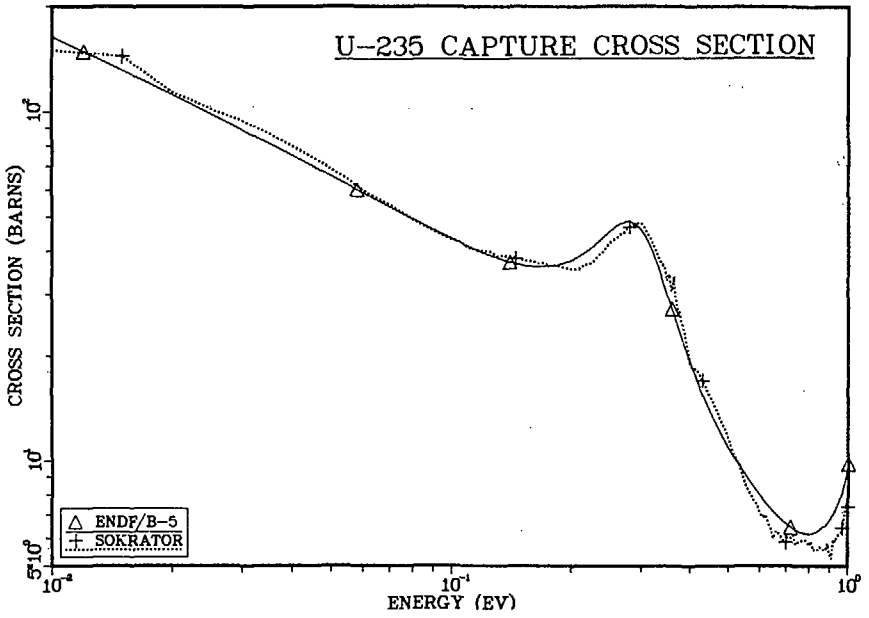

Fig. 4. ^{235}U capture.

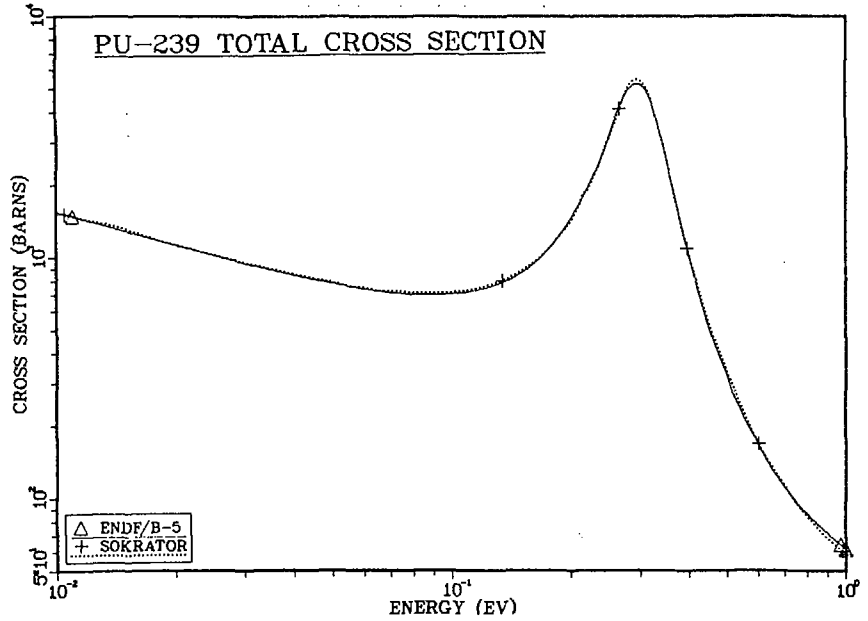

Fig. 5. ^{239}Pu total.

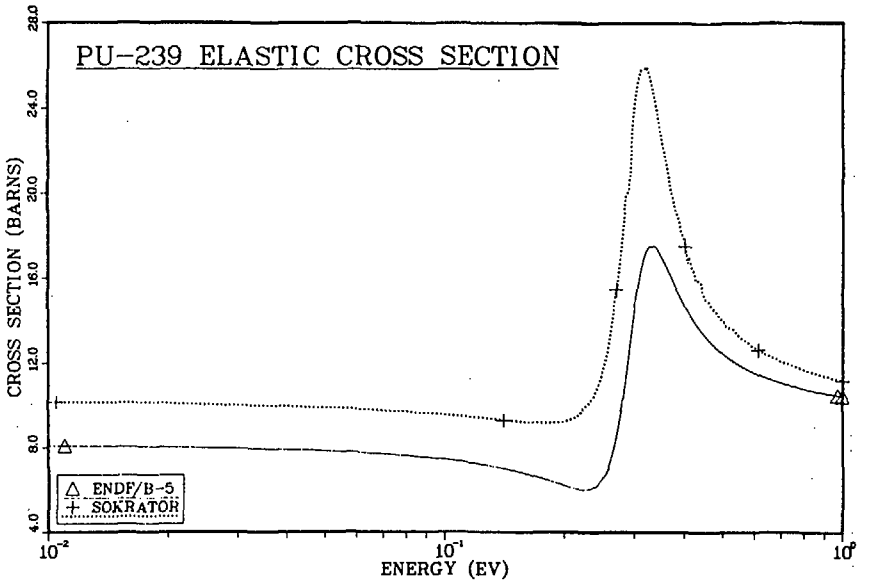

Fig. 6. ^{239}Pu scattering.

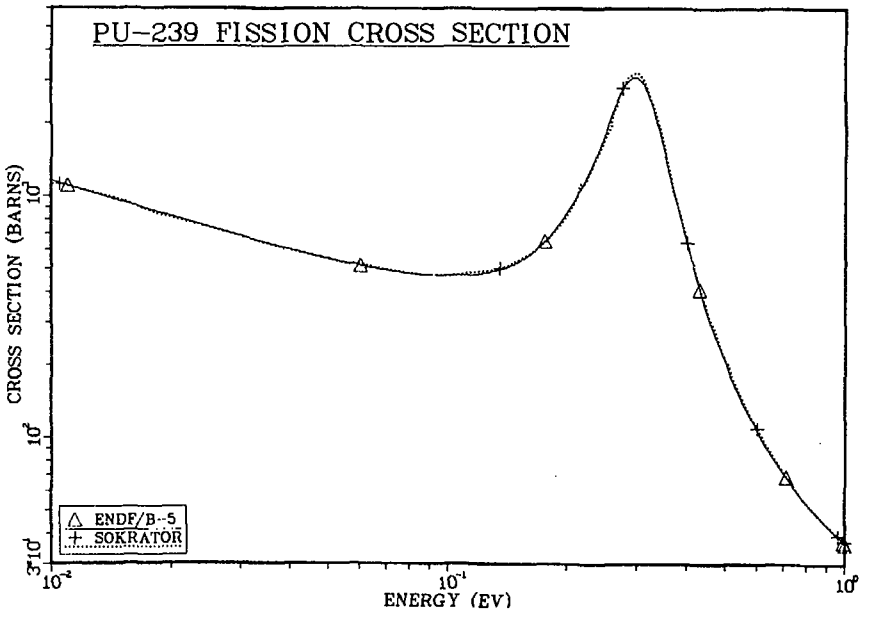

Fig. 7. ^{239}Pu fission.

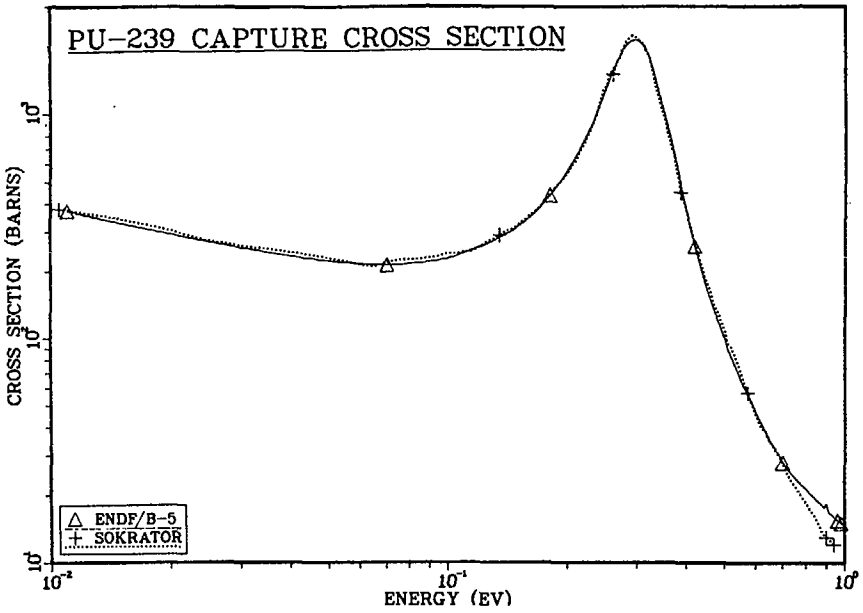

Fig. 8. ^{239}Pu capture.

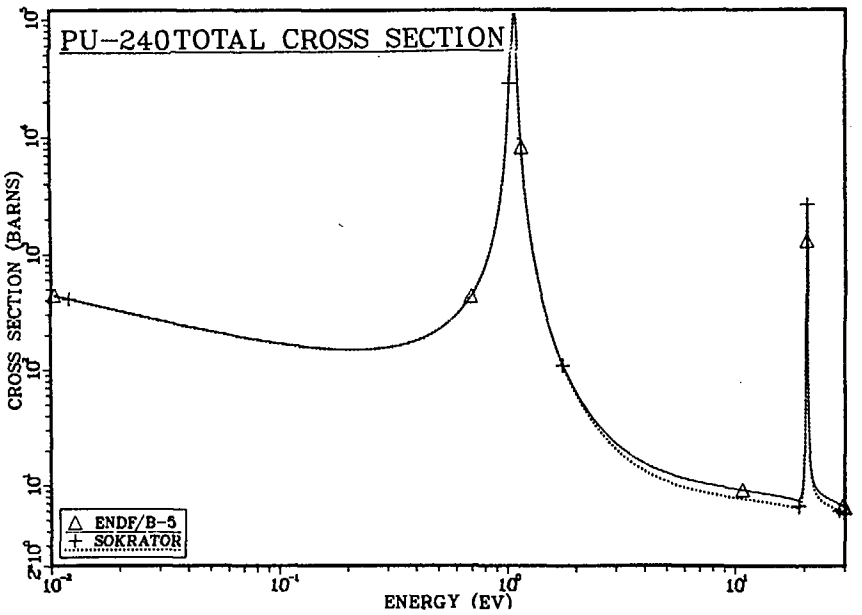

Fig. 9. ^{240}Pu total.

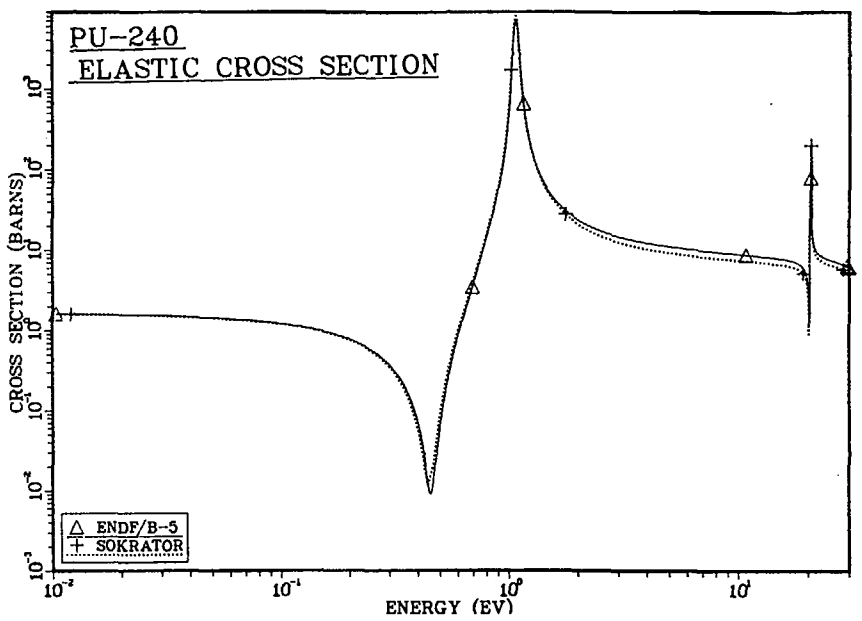

Fig. 10. ^{240}Pu scattering.

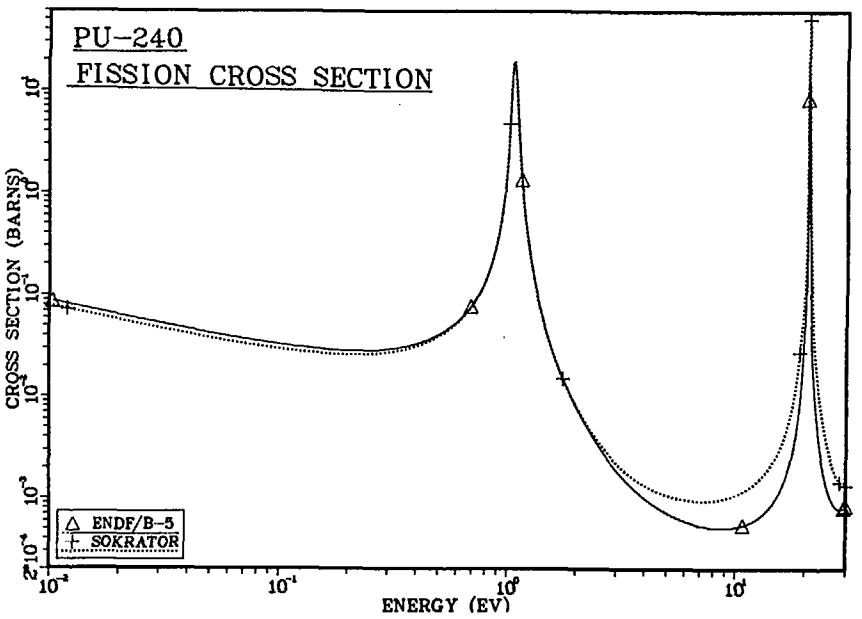

Fig. 11. ^{240}Pu fission.

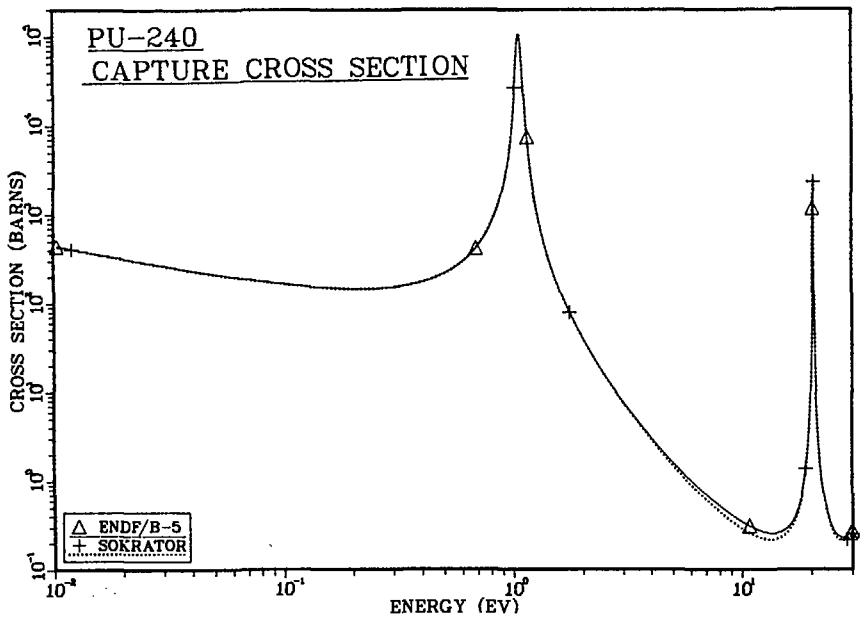

Fig. 12. ^{240}Pu capture.

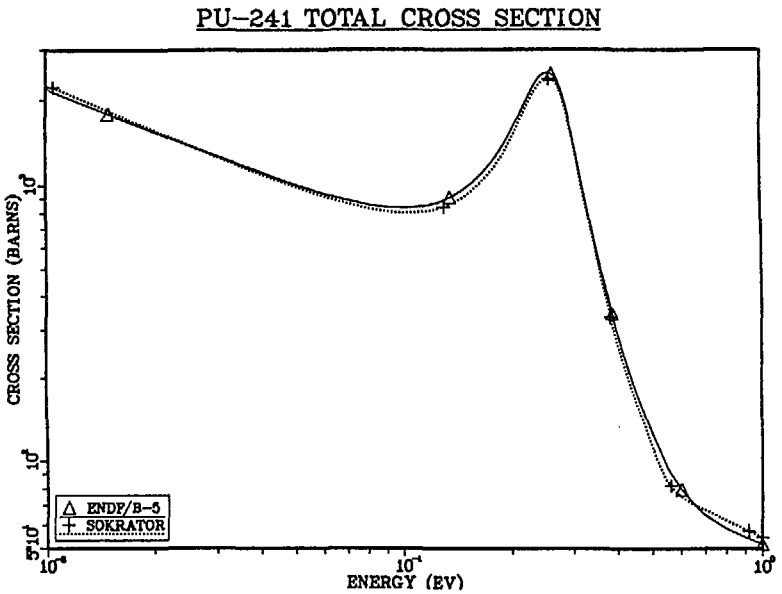

Fig. 13. ^{241}Pu total.

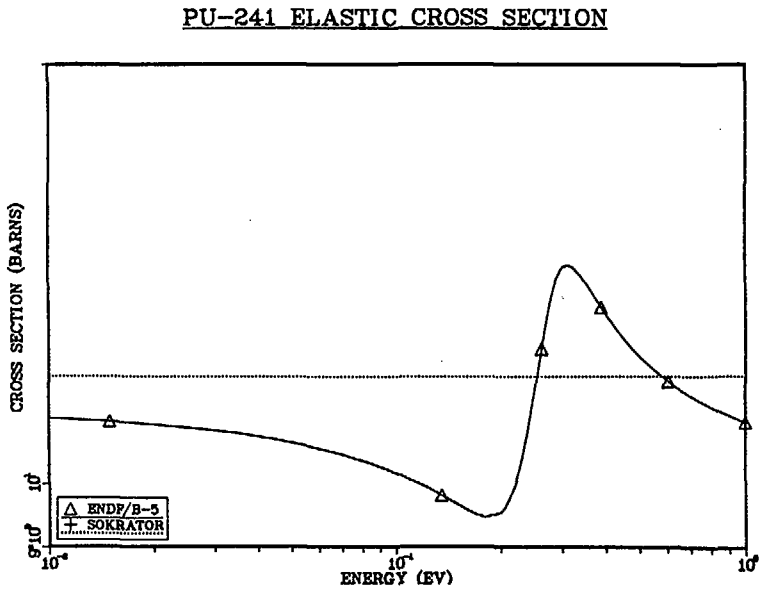

Fig. 14. ^{241}Pu scattering.

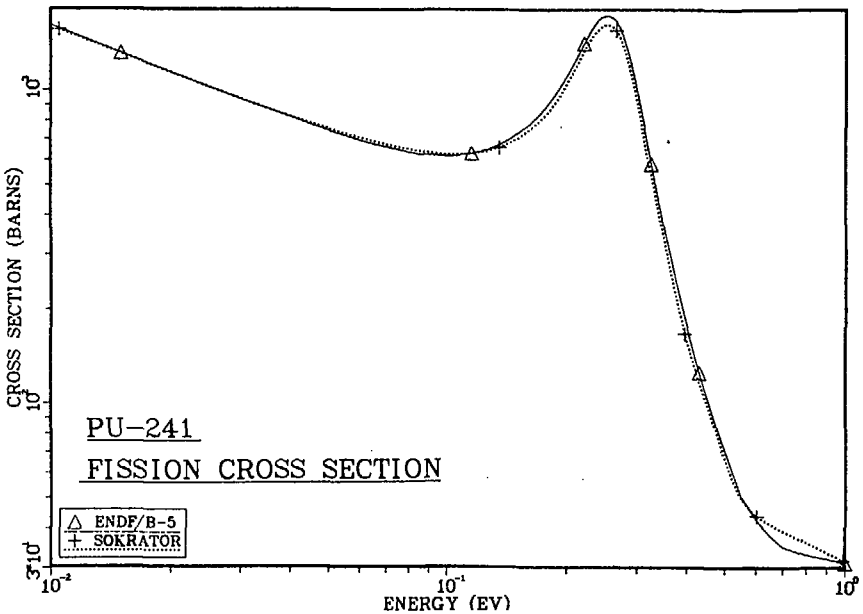

Fig. 15. ^{241}Pu fission.

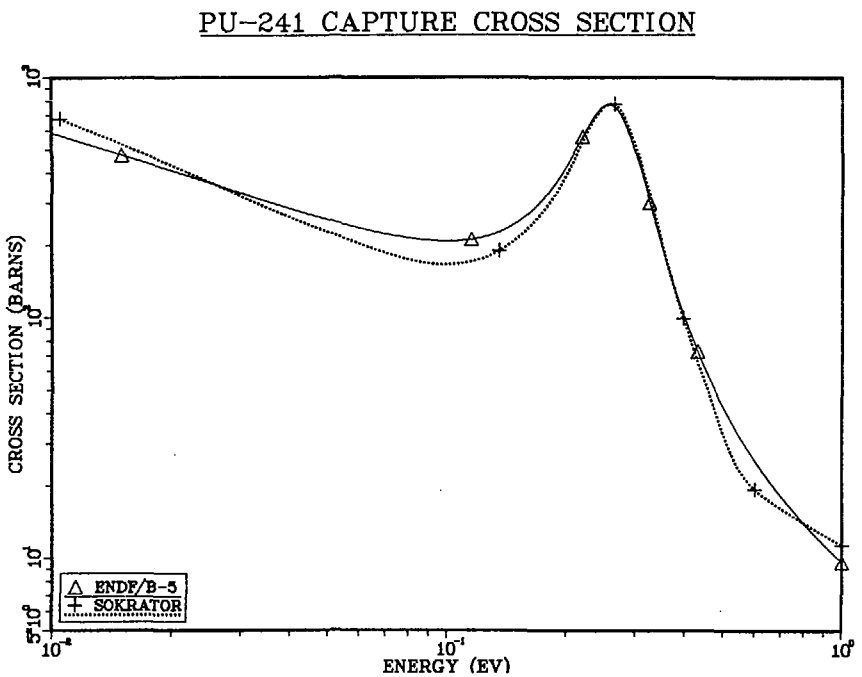

Fig. 16. ^{241}Pu capture.

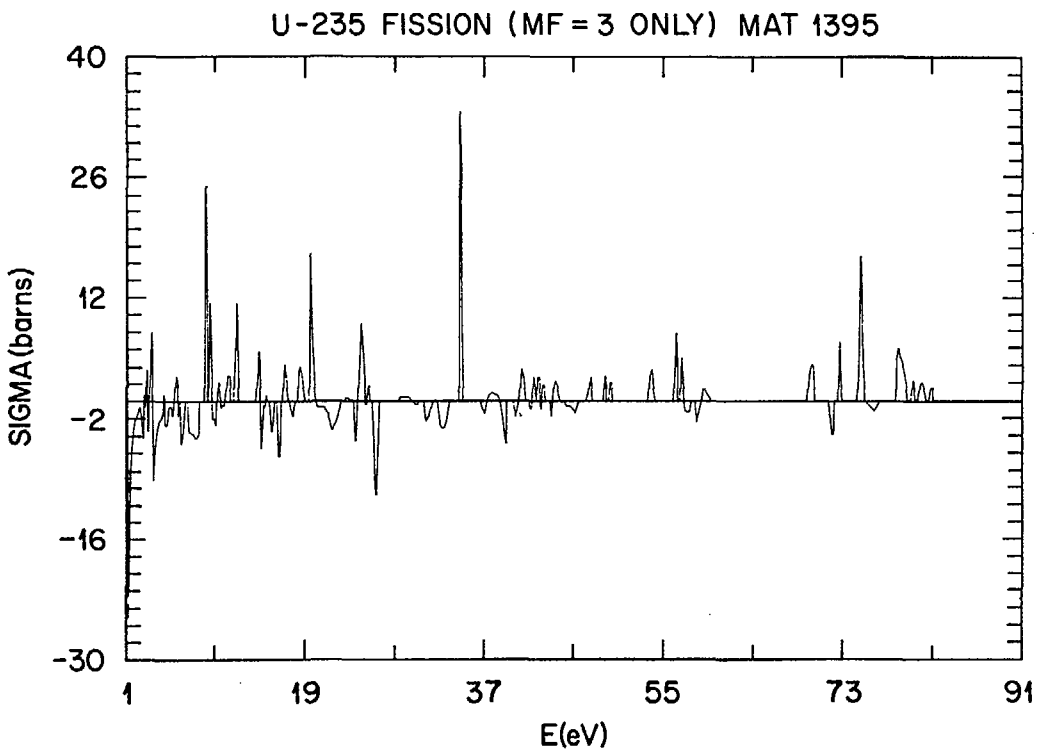

Fig. 17. The "smooth" contribution (MF=3) to the ENDF/B-V ^{235}U fission cross section in the resolved resonance range. This contribution must be added to the Breit-Wigner resonance contribution (MF=2) to obtain the evaluated fission cross section.

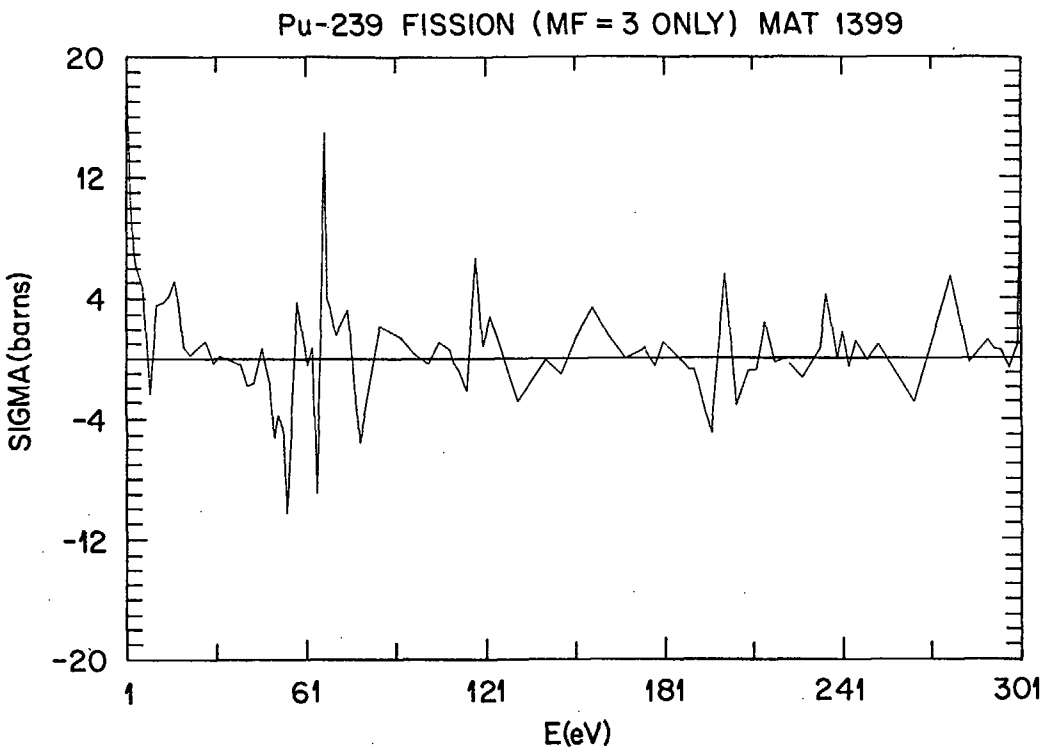

Fig. 18. The "smooth" contribution (MF=3) to the ENDF/B-V ^{239}Pu fission cross section in the resolved resonance range. This contribution must be added to the Breit-Wigner resonance contribution (MF=2) to obtain the evaluated fission cross section.

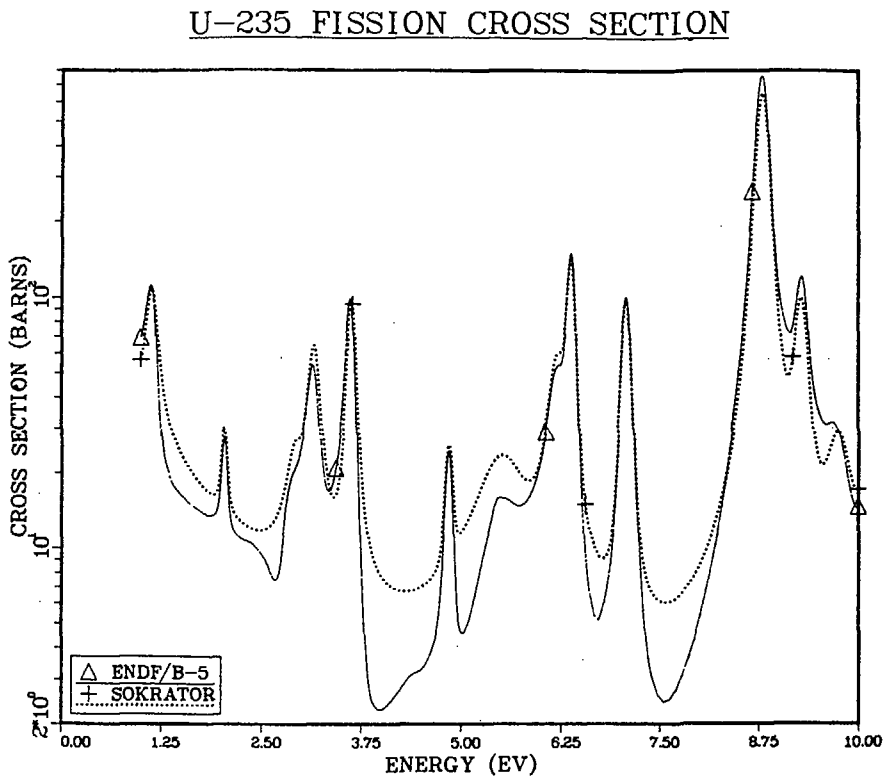

Fig. 19. Comparison of the ENDF/B-V and SOKRATOR evaluations of the ^{235}U fission cross section from 1.0 to 10.0 eV.

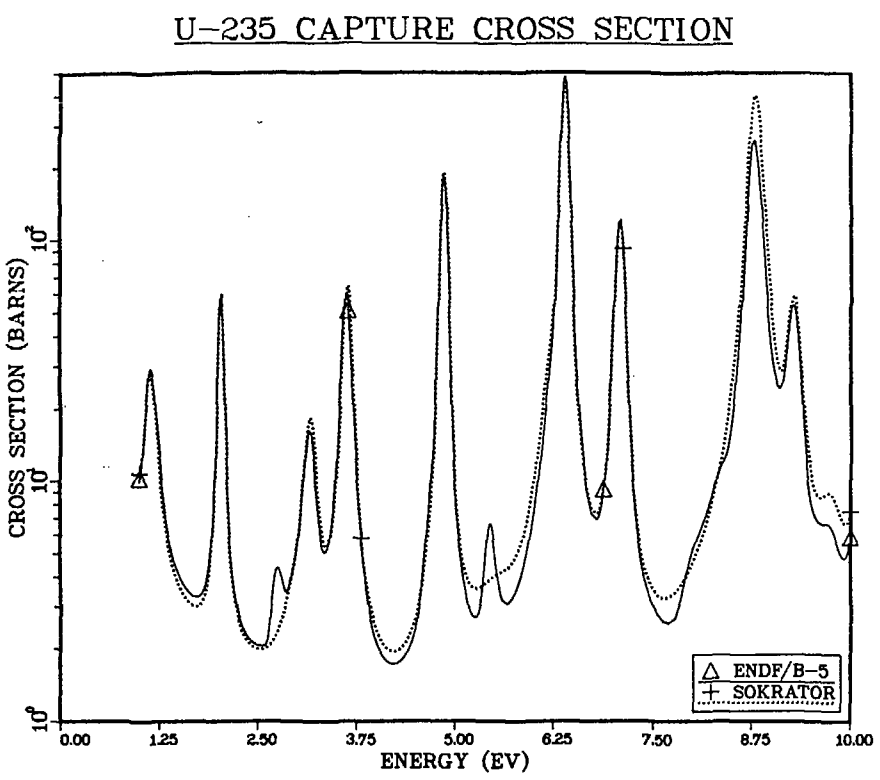

Fig. 20. Comparison of the ENDF/B-V and SOKRATOR evaluations of the ^{235}U capture cross section from 1.0 to 10.0 eV.

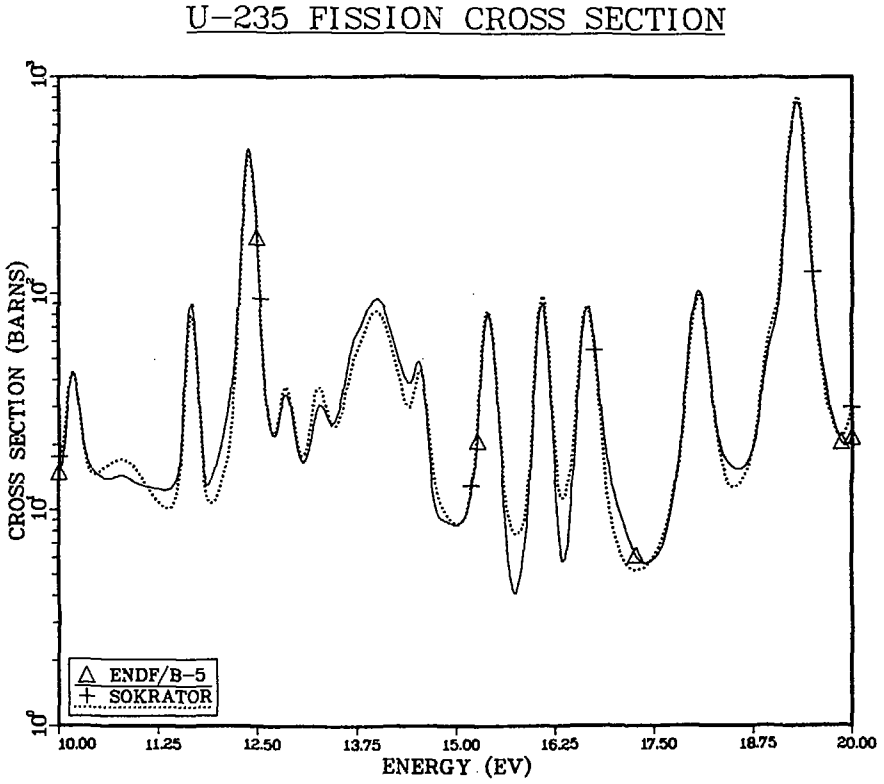

Fig. 21. Comparison of the ENDF/B-V and SOKRATOR evaluations of the ^{235}U fission cross section from 10.0 to 20.0 eV.

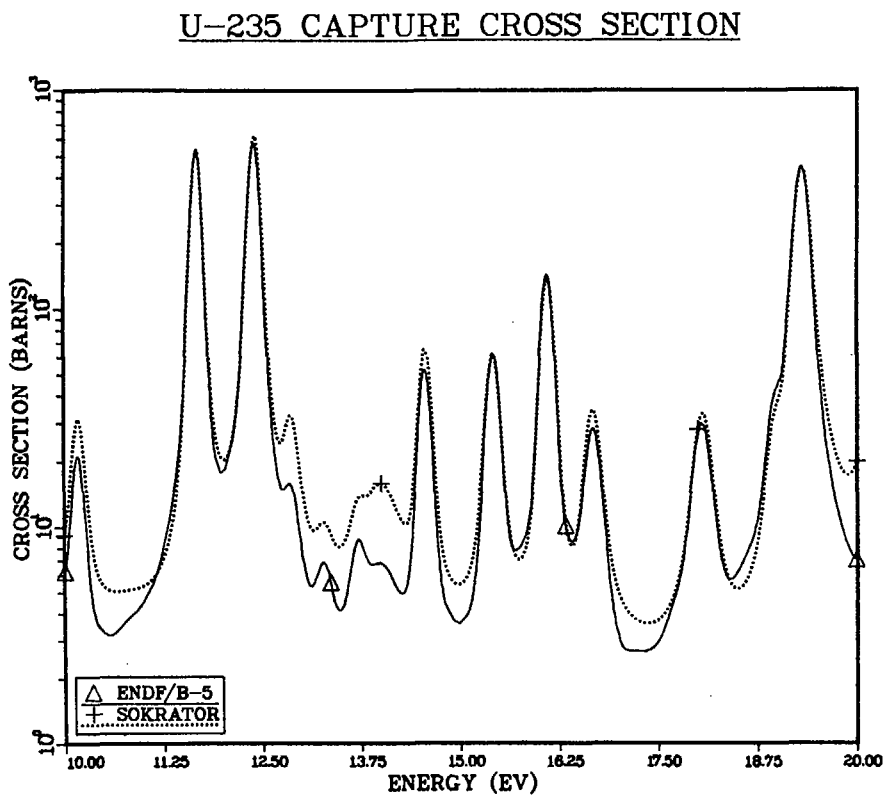

Fig. 22. Comparison of the ENDF/B-V and SOKRATOR evaluations of the ^{235}U capture cross section from 1.0 to 10.0 eV.

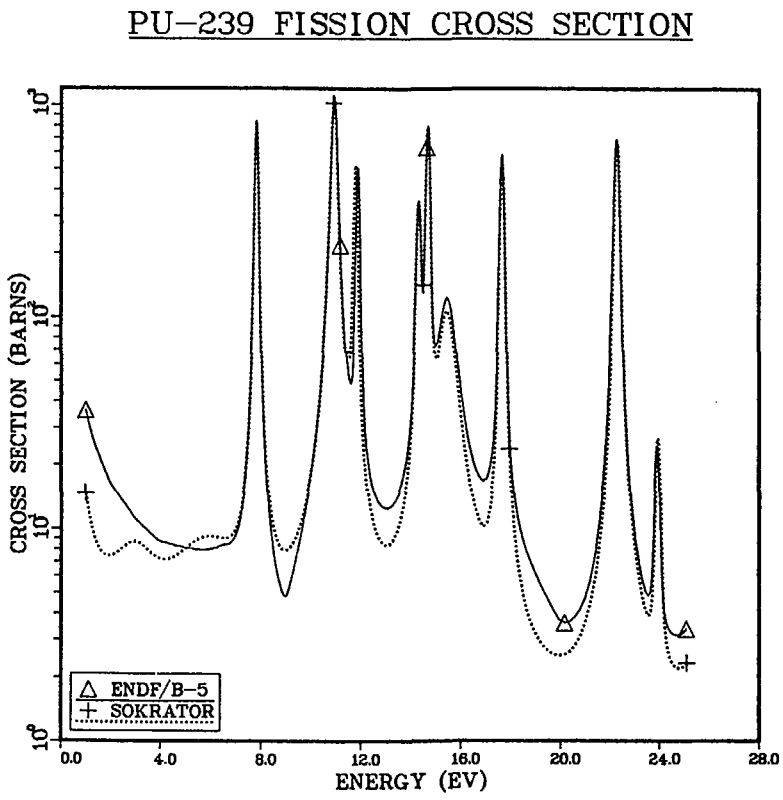

Fig. 23. Comparison of the ENDF/B-V and SOKRATOR evaluations of the ^{239}Pu fission cross section from 1.0 to 25.0 eV.

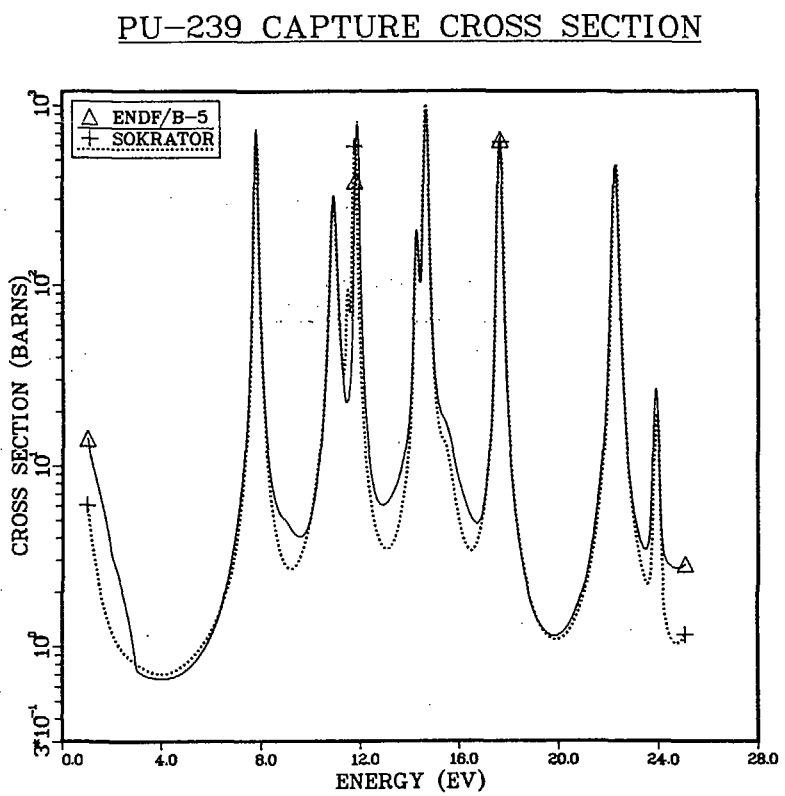

Fig. 24. Comparison of the ENDF/B-V and SOKRATOR evaluations of the ^{239}Pu capture cross section from 1.0 to 25.0 eV.

Table I. Comparison of the ENDF/B-V and SOKRATOR ^{235}U Evaluations

File Structure	ENDF/B-V	SOKRATOR
MAT Number (^{235}U)	1395	9210
AWRI: (Target Mass)/(Neutron Mass)	233.025	233.0
AP: Scattering Radius (10^{-12} cm)	0.95663	0.8391
Resolved Range (eV)	1 - 82	1 - 100
LRF, Formalism Employed	1, SLBW	2, MLBW[a]
Number of Levels	130	208
Unresolved Range (eV)	82 - 25000	100 - 100000
Range for MF=3 ≠ 0.0 (eV)	10^{-5} - 2x10^{7}	10^{-4} - 1.0 100 - 1.5x10^{7}

[a]Modified Adler-Adler parameters also available.

Table II. Comparison of the ENDF/B-V and SOKRATOR ^{239}Pu Evaluations

File Structure	ENDF/B-V	SOKRATOR
MAT Number (^{239}Pu)	1399	9420
AWRI: (Target Mass)/(Neutron Mass)	237.0	237.0
AP: Scattering Radius (10^{-12} cm)	.90094	.905
Resolved Range (eV)	1 - 301	1 - 500
LRF, Formalism Employed	1, SLBW	2, MLBW
Number of Levels	128	210
Unresolved Range (eV)	301 - 25000	No URR
Range for MF=3 ≠ 0.0 (eV)	10^{-5} - 2..10^{7}	10^{-4} - 1. 500. - 1.5.10^{7}

Table III. Comparison of the ENDF/B-V and SOKRATOR ^{240}Pu Evaluations

File Structure	ENDF/B-V	SOKRATOR
MAT Number (^{240}Pu)	1380	9430
AWRI: (Targer Mass)/(Neutron Mass)	237.992	238.0
AP: Scattering Radius (10^{-12} cm)	.9184	.8578
Resolved Range (eV)	10^{-5} - 3910.	1 - 1000.
LRF, Formalism Employed	2, MLBW	2, MLBW
Number of Levels	201	70
Unresolved Range (eV)	3910 - 40000	1000 - 150000
Range for MF=3 ≠ 0.0 (eV)		10^{-3} - 1.0
	200 - 2.10^7	4318 - $1.5.10^7$

Table IV. Comparison of the ENDF/B-V and SOKRATOR ^{241}Pu Evaluations

File Structure	ENDF/B-V	SOKRATOR
MAT Number (^{241}Pu)	1381	2024
AWRI: (Target Mass)/(Neutron Mass)	238.978	238.986
AP: Scattering Radius (10^{-12} cm)	.933	.845
Resolved Range (eV)	2.873 - 100.	1. - 100.
LRF, Formalism Employed	4, Adler	4, Modif. Adler
Number of Levels	83	112
Unresolved Range (eV)	100. - 40200	100. - 10^5
Range for MF=3 ≠ 0.0 (eV)	10^{-5} - 2.873	10^{-4} - 1.0
	4020 - $2.0.10^7$	$1.0.10^5$ - $1.5.10^7$

Table V. Comparison of the ENDF/B-V and SOKRATOR ^{235}U Evaluations

Thermal Region	ENDF/B-V	SOKRATOR
MAT Number (^{235}U)	1395	9210
Energy Range Below Resolved Range (eV)	10^{-5} - 1.	10^{-4} - 1
Temperature (K)	0	293
Number of (E, σ) - points	219	149
INT, Interpolation	5. Log-Log	2, Lin-Lin
Cross Sections at .0253 eV (b)		
MT=1 Total	696.633	697.5
MT=2 Scattering	14.713	18.3
MT=18 Fission	583.54±1.7	577.7
MT=102 Capture	98.38±.76	101.5
Westcott g-factors at 293 K		
MT=1	.9811	.9818
MT=2	1.1220	1.0686
MT=18	.9775	.9807
MT=102	.9823	.9716

Table VI. Comparison of the ENDF/B-V and SOKRATOR ^{239}Pu Evaluations

Thermal Region	ENDF/B-V	SOKRATOR
MAT Number (^{239}Pu)	1399	9420
Energy Range Below Resolved Range (eV)	10^{-5} - 1.	10^{-4} - 1.
Temperature (K)	0	293
Number of (E, σ) points	219	143
INT, Interpolation	Lin-Lin	Lin-Lin
Cross Sections at .0253 eV (b).		
MT=1 Total	1019.9	1024.5
MT=2 Scattering	8.002	10.036
MT=18 Fission	741.7	740.4
MT=102 Capture	270.2	274.1
Westcott g-factors at 293 K		
MT=1	1.0755	1.0780
MT=2	1.1025	1.1123
MT=18	1.0548	1.0545
MT=102	1.1307	1.1402

Table VII. Comparison of the ENDF/B-V and SOKRATOR ^{240}Pu Evaluations

Thermal Region	ENDF/B-V	SOKRATOR
MAT Number (^{240}Pu)	1380	9430
Energy Range Below Resolved Range (eV)	No L.E.R.	10^{-3} - 1
Temperature (K)		293
Number of (E, σ) points		95
INT, Interpolation		2, Lin-Lin
Cross Sections at .0253 eV (b)		
MT=1 Total	292.04	289.32
MT=2 Scattering	1.555	1.540
MT=18 Fission	.0572	.0508
MT=102 Capture	290.43	287.73
Westcott g-factors at 293 K		
MT=1	1.0269	1.0165
MT=2	1.0489	1.0461
MT=18	1.0245	1.0254
MT=102	1.0268	1.0164

Table VIII. Comparison of the ENDF/B-V and SOKRATOR ^{241}Pu Evaluations

Thermal Region	ENDF/B-V	SOKRATOR
MAT Number (^{241}Pu)	1381	2024
Energy Range Below Resolved Range (eV)	10^{-5} - 2.873	10^{-4} - 1.0
Temperature (K)	0	293
Number of (E, σ) points	121	140
INT, Interpolation	5, Log-Log and 2	2 Lin-Lin
Cross Sections at .0253 eV (b)		
MT=1 Total	1387.0	1390.0
MT=2 Scattering	11.0	12.0
MT=18 Fission	1015.0	1015.0
MT=102 Capture	361.4	363.0
Westcott g-factors at 293 K		
MT=1	1.0445	1.0417
MT=2	1.1044	1.1284
MT=18	1.0459	1.0465
MT=102	1.0378	1.0296

Table IX. The 2200 m/s Fission and Capture Cross Sections and the Value of ν_T for ^{235}U, ^{239}Pu, and ^{241}Pu

	ENDF/B-V	SOKRATOR	IAEA-69[a]	IAEA-75[b]	Leonard-76/81[c]
^{235}U σ_{nf}	583.54±1.7	577.7	580.2±1.8	583.5±1.3	583.54±1.7
$\sigma_{n\gamma}$	98.38±.76	101.5	98.3±1.1	97.4±1.6	98.38±.76
g_f	.9775	.9807	.9766±.0016	.976±.002	.9775±.0011
g_γ	.9823	.9716	.991	1.003±.018	.9823±.0014
ν_T	2.437	2.408	2.423±.007	2.416±.005	
^{239}Pu σ_{nf}	741.7	740.4	741.6±3.1	744.0±2.5	754.84±4.5
$\sigma_{n\gamma}$	270.2	274.1	271.3±2.6	267.2±3.3	273.75±2.7
g_f	1.0548	1.0545	1.0548±.0030	1.0555±.0024	1.05353±.0015
g_γ	1.1307	1.1402	1.131	1.151 ±.015	1.13872±.011
ν_T	2.891	2.880	2.880 ±.009	2.862 ±.008	
^{241}Pu σ_{nf}	1015.0	1015.0	1007.3±7.2	1015±7	1003.8
$\sigma_{n\gamma}$	361.4	363.0	368.1±7.8	362±6	364.66
g_f	1.0459	1.0465	1.0486±.0053	1.0442±.0048	
g_γ	1.0378	1.0296	1.008	1.025 ±.016	
ν_T	2.953	2.924	2.934 ±.012	2.924 ±.010	

[a] G. C. Hanna *et al.* Atomic Energ. Rev. 7, 4, 3 (1969).

[b] H. D. Lemmel, Conf. Nuclear Cross Sections and Technology, Washington, D. C., I, 286, 1975.

[c] B. R. Leonard *et al.* EPRI-NP-167 (1976) and EPRI-NP-1763 (1981).

Table X. Comparison of the ENDF/B-V and SOKRATOR ^{235}U Evaluations

3. Resonance parameters below 20 eV.

E_o(eV)	2g Γ_n (meV)		Γ_f (meV)		Γ_γ (meV)		J
(approximate)	ENDF	SOKRATOR	ENDF	SOKRATOR	ENDF	SOKRATOR	SOKRATOR
-1.49	3.682	3.677	207.0	212.25	27.0	22.258	4
.29	.00302	.00302	99.0	100.74	36.0	34.26	3
1.14	.01516	.01397	116.2	115.25	34.6	35.55	4
2.04	.00739	.00739	98.14	101.64	34.9	34.52	3
2.92	.00485	.00729	200.0	209.12	20.0	10.87	4
3.15	.0224	.0265	106.37	107.00	33.2	32.58	3
3.61	.0456	.0468	50.637	49.504	33.7	34.83	4
4.85	.0604	.0618	3.587	3.245	35.9	36.29	4
5.5	.0034		30.117		60.0		
5.6	.0333	.0639	621.89	671.78	20.0	59.27	4
6.21	.0638	.0804	187.36	165.62	43.5	65.19	3
6.38	.268	.247	9.548	9.569	35.0	35.0	4
7.08	.127	.123	28.233	28.238	35.6	35.6	4
8.78	1.123	1.157	91.0	75.4	31.2	46.9	4
9.28	.164	.145	75.0	69.3	35.6	41.6	4
9.75	.0530	.0534	237.0	211.8	32.0	47.2	3
10.2	.0619	.0687	62.5	54.7	38.0	45.8	4
10.8	.0933	.1137	868.0	856.1	67.0	69.9	4
11.7	.627	.617	6.25	5.52	40.4	41.2	4
12.4	1.262	1.296	27.5	25.285	34.5	36.5	3
12.9	.0531	.0813	86.0	63.97	33.5	55.5	4
13.3	.0393	.0552	122.8	131.79	28.6	19.6	4
13.7	.0370	.0259	93.5	86.28	30.4	37.6	3
14.0	.537	.508	470.0	431.6	26.0	64.3	3
14.6	.115	.126	20.9	17.4	35.2	38.7	3
15.4	.237	.247	43.3	48.5	35.3	36.3	4
16.1	.361	.375	18.617	22.5	31.4	33.2	4
16.7	.237	.270	100.89	87.4	32.1	32.3	4
18.1	.385	.371	125.0	116.6	35.0	37.9	3
19.0	.116	.116	55.0	62.0	50.0	37.9	4
19.3	3.194	3.388	60.179	66.102	34.8	35.9	4

Table XI. Comparison of the ENDF/B-V and SOKRATOR ^{239}Pu Evaluations

3. Resonance Parameters Below 25 eV

E_o(eV)	J		2g Γ_n(meV)		Γ_f(meV)		Γ_γ(meV)	
	ENDF	SOK	ENDF	SOKRATOR	ENDF	SOKRATOR	ENDF	SOKRATOR
-.22	0		.0235		500.		40.0	
.296	0	0	.121	.123	60.	61.2	39.0	37.4
3.0		1/2		.020		1958.		43.3
5.9		1/2		.094		3259.		43.3
7.8	1	1	1.228	1.147	45.8	48.2	40.2	38.8
10.9	1	1	2.799	2.648	153.1	156.6	44.2	42.2
11.5		1/2		.085		10.4		41.2
11.8	1	1	1.521	1.339	24.4	29.0	40.6	37.0
14.3	1	1	.898	.864	65.1	67.0	35.9	34.0
14.7	1	1	2.685	2.839	30.2	20.2	36.8	38.8
15.5	0	0	1.060	.934	683.3	648.9	39.0	50.0
17.7	1	1	2.538	2.450	33.5	32.4	38.5	40.6
22.3	1	1	3.924	2.714	69.4	61.8	46.7	44.2
23.9	0	1	.136	.128	32.6	40.0	37.4	30.0

Table XII. Comparison of the ENDF/B-V and SOKRATOR ^{240}Pu Evaluations

3. Resonance Parameters Below 100 eV

E(eV)	$g\Gamma_n$(meV)		Γ_f(meV)		Γ_γ(meV)	
	ENDF	SOKRATOR	ENDF	SOKRATOR	ENDF	SOKRATOR
-14.45	18.83		.009		31.0	
1.058[a]	2.280	2.354	.0060	.0057	33.3	32.2
20.46	2.65	2.65	.23	.70	32.2	32.2
38.32	17.36	17.00	.11	.09	26.5	26.5
41.62	16.69	14.40	.02	.11	30.2	32.0
66.62	54.17	51.00	.02	.04	29.2	28.5
72.78	21.45	21.50	.02	.22	27.5	28.6
90.77	12.85	13.00	.02	.08	38.3	30.7
92.51	3.12	3.20	.02	.20	29.5	30.7

[a] $g\Gamma_n\Gamma_\gamma$ for level at 1.058 eV: ENDF 75.92 meV^2
SOKRATOR 75.89 meV^2

Table XIII. Comparison of Evaluated ^{238}U Neutron and Capture Widths

E_o(eV)	6.67	20.9	36.7	66.0	80.7	102.5	10.2
			Neutron Widths (meV)				
BNL-325(65)	1.52 ±.02	8.5 ±.5	31.0 ±.9	25.0 ±1.2	2.0 ±.2	68.0±3	.0014
BNL-325(73)	1.52 ±.02	8.7 ±.5	32.0 ±1	26.0 ±1.5	2.0 ±.2	70.0±3	.00156
MOXON(74)	1.510±.009	8.9 ±.175	31.6 ±.5	24.0 ± .4	1.96 ±.07	70.8±.4	.00156
ENDF/B-IV(75)	1.50	8.8	31.1	25.3	2.0	71.0	.00156
ENDF/B-V(77)	1.510±.015	10.12±.10	33.9 ±.4	24.6 ± .4	1.91 ±.04	71.6±.4	.00167
KEDAK(81)	1.495	9.94	33.64	24.61	1.907	71.64	.001674
JENDL-2(81)	1.50	10.1	33.3	24.9	1.87	70.9	.00159
BNL-325(81)	1.50 ±.02	10.04±.20	34.0 ±.4	24.0 ±1.0	1.9 ±.1	70 ±3	.00165
			Capture Widths (meV)				
BNL-325(65)	26.0 ±2	26.0 ±4	26.0 ±4	24.0 ± 2	21.0 ±15	24.0±3	
BNL-325(73)	26.0 ±2	25.0 ±3	25.0 ±2	22.0 ± 2		26.0±2	
MOXON(74)	26.9 ±.37	25.7 ±1.0	26.55±1.20	23.56± .76	21.17 ±8.9	25.78±.94	
ENDF/B-IV(75)	25.6	26.8	26.0	23.5	23.5	26.0	23.5
ENDF/B-V(77)	22.5 ±.6	23.1 ±.5	22.9 ±.3	23.7 ± .3	24.2 ±1.2	24.4 ±.3	23.5
KEDAK(81)	23.7	23.67	23.64	23.69	24.17	24.41	23.5
JENDL-2(81)	23.7	23.0	23.5	22.9	24.4	25.1	23.6
BNL-325(81)	22.8 ±.6	23.5 ±.8	23.5 ±.3	23.6 ±.1	25 ±1	24.5 ±.7	

Table XIV. Comparison of Evaluated ^{240}Pu Neutron and Capture Widths (meV)

E_o(eV)	ENDF/B-V		SOKRATOR		KEDAK		JENDL-2		BNL-325(1981)	
	$g\Gamma_n$	Γ_γ	$g\Gamma_n$	Γ_γ	$g\Gamma_n$	Γ_γ	$g\Gamma_n$	Γ_γ	$g\Gamma_n$	Γ_γ
1.058	2.280	33.3	2.345	32.2	2.280	33.3	2.440	29.6	2.32	32.4
20.46	2.65	32.2	2.65	32.2	2.65	32.2	2.20	30.0	2.65	32.2
38.32	17.36	26.5	17.00	26.5	17.00	28.5	17.00	30.0	17.3	29.4
41.62	16.69	30.2	14.40	32.0	15.50	31.0	15.50	33.0	16.7	(31.0)
66.62	54.17	29.2	51.00	28.5	53.20	30.5	50.0	31.0	54.0	31.0
72.78	21.45	27.5	31.50	28.6	21.00	29.5	21.00	32.0	21.4	28.5
90.77	12.85	38.3	13.00	30.7	13.00	31.5	12.80	29.5	12.8	27.5
92.51	3.12	29.5	3.20	30.7	3.10	30.5	3.20	29.5	3.10	(31.0)
$g\Gamma_n\Gamma_\gamma$ (meV^2) (1.058 eV)	75.92		75.89		75.92		72.22		75.17	

Table XV. Comparison of Evaluated ^{242}Pu Neutron and Capture Widths (meV)

E_o(eV)	ENDF/B-5		SOKRATOR		KEDAK		JENDL-2	
	$g\Gamma_n$	Γ_γ	$g\Gamma_n$	Γ_γ	$g\Gamma_n$	Γ_γ	$g\Gamma_n$	Γ_γ
2.67	2.325	22.0	1.970	25.5	1.937	26.0	1.970	25.4
14.6	.061	23.4	.061	22.6	.061	28.0	.061	24.2
22.57	.29	23.0	.31	22.6	.29	20.0	.286	20.0
40.95	.45	27.0	.47	22.6	.448	29.0	.451	29.0
53.46	52.0	21.2	52.2	21.2	51.25	29.0	51.95	23.9
66.70	4.5	23.0	4.4	23.0	4.94	22.0	4.578	22.5
88.45	.66	23.4	.53	22.6	.66	28.0	.64	24.2
107.32	17.0	21.0	17.0	21.2	17.64	28.0	16.99	21.5

Table XVI. Thermal Parameters of the Fissile Nuclei

		ENDF/B-V	SOKRATOR	KEDAK	IAEA-69	IAEA-75
^{235}U	σ_{nf}	583.54±1.7	577.7	580.9	580.2±1.8	583.5±1.3
	$\sigma_{n\gamma}$	98.38±.76	100.5	98.21	98.3±1.1	97.4±1.6
	g_f	.9775	.9807	.9831	.9766±.0016	.976±.002
	g_γ	.9823	.9716	.9832	.991	1.003±.018
	ν_T	2.437	2.408	2.423	2.423 ±.007	2.416±.005
	η_{th}	2.084	2.051	2.073	2.068	2.062
^{239}Pu	σ_{nf}	741.7	740.4	742.3	741.6±3.1	744.0±2.5
	$\sigma_{n\gamma}$	270.2	274.1	270.15	271.6±2.6	267.2±3.3
	g_f	1.0548	1.0545	1.0535	1.0548±.0030	1.0555±.0024
	g_γ	1.1307	1.1402	1.1284	1.131	1.131 ±.015
	ν_T	2.891	2.880	2.885	2.880 ±.009	2.862 ±.008
	η_{th}	2.079	2.057	2.076	2.069	2.057
^{241}Pu	σnf	1015.0	1015.0	1011.7	1007.3±7.2	1015 ±7
	σn_γ	361.4	363.0	364.8	368.1±7.8	362 ±6
	g_f	1.0459	1.0465	1.0265	1.0486±.0053	1.0442±.0048
	g_γ	1.0378	1.0296	1.0107	1.008	1.025 ±.016
	ν_T	2.953	2.924	(2.934)	2.934 ±.012	2.924 ±.010
	η_{th}	2.182	2.163	(2.165)	2.171	2.166

ADDENDUM

Drs. F. Froehner (KFK, Germany) and S. Igarasi (JEARI, Japan) have recently provided the IAEA/NDS with evaluated resonance parameters from the German data file KEDAK-III and from the Japanese data file JENDL-2. These parameters were forwarded to us by Drs. Pronyaev and Schwerer of the IAEA/NDS. On the basis of these new data the comparison of evaluations can be extended to include these new parameter sets.

Evaluated neutron and capture widths of the seven first large levels of ^{238}U are listed in Table XIII. There is a high degree of consistency in the evaluations performed in the past five years, and significant changes from evaluations older than 1976, particularly in the capture widths of the first three levels listed and in the neutron widths of the levels at 20.9 and 36.7 eV.

The resonance parameters of the eight first large levels of ^{240}Pu are compared in Table XIV. In the last line of the Table, the products $g\Gamma_n\Gamma_\gamma$ of the widths of the first level are also given. The capture cross section in the thermal region is nearly proportional to this product. Even though the evaluated values of the neutron (and capture) widths of the first level differ, the products $g\Gamma_n\Gamma_\gamma$ are quite consistent, except for JENDL-2.

The resonance parameters of the eight first large levels of ^{242}Pu are compared in Table XV. Except for the ENDF/B-V values of the parameters of the first level and the larger capture widths evaluated by KEDAK-III, the several evaluations are consistent. The ENDF/B-V parameters of the first levels were modified from the BNL-325 (1974) evaluation so as to preserve the cross section values and shapes in the thermal region as described by Young *et al.* (Nucl. Sci. and Eng. 43, 341, 1971).

The thermal parameters of the fissile nuclei, from the 1969 and 1975 IAEA evaluations, and from the files ENDF/B-V, SOKRATOR, and KEDAK-III are compared in Table XVI. The KEDAK evaluated value of ν_τ for ^{241}Pu could not be found and was assigned arbitrarily the 1969 IAEA value ν_τ=2.934, since the KEDAK-III values of ν_τ for the other two isotopes are consistent with that evaluation. We note that the ENDF/B-V values for ν_τ and $\eta=\nu_\tau\, g_f\sigma_{nf}/(g_f\sigma_{nf}+g_\gamma\sigma_{n\gamma})$ are 1% or 2% higher than those of the other evaluations. This is in part caused by an ENDF/B-V reevaluation of the standard, ν for ^{252}Cf, based on the results of recent unpublished measurements.

Comparison of Strength Functions and Average Level Spacing for U and Pu Isotopes

V. Pronyaev, D.E. Cullen
Nuclear Data Section
International Atomic Energy Agency

Introduction

The strength functions and the average distance between levels of compound nuclei are two main parameters which determine the values of fluctuating (compound) part of cross-sections in the unresolved resonance region. But comparison of different evaluations in this energy region based on the unresolved resonance parameters themselves is a difficult task, because the same average cross sections and even fluctuations near average may be obtained in different ways. For example: one can present the cross section in the elastic scattering channel as the sum of the potential scattering and the scattering via compound nucleus with energy dependent or independent neutron strength functions. A different division between this two parts can give similar results for the average cross sections and self-shielding factors. Because of this the conclusion about consistency of different evaluations can be best given by means of comparison of average cross sections and the results of transmission and self-indication measurements; it is difficult to draw any conclusions simply by looking only at average parameters.

There are some other reasons which hamper the analysis and comparison of cross-sections in the unresolved resonance region. Many experimental and a few theoretical works show that the cross sections in the unresolved resonance region for heavy nuclei can have fluctuations, the nature of which is different from the usual statistical fluctuations described in the frame work of the statistical model of compound nuclear reactions. Such intermediate structures in the cross section can be connected with door-way states, that is the states with relatively simple (in comparison with the compound nuclear states) structure and having much larger widths than the compound nucleus states. Many results of measurements of the cross sections with high resolution in the unresolved resonance region for heavy fissile and fertile isotopes show a strong energy dependence. Transmission curves in this energy region confirm a strong energy dependence.

Most theoretical calculations of the neutron strength functions were done using an optical model. The reduced neutron strength functions which can be obtained in these calculations, taking into account strong channel coupling scheme, have in general a very weak energy dependence. As was found in some coupled channel calculations by Konshin's group [1], the reduced neutron strength function S_o can change smoothly in the energy range from hundreds of eV to hundreds of keV by about 20%. These changes are connected with broad structure in the cross sections.

Important results concerning the energy dependence of neutron strength functions for heavy nuclei were obtained in the so called semi-microscopical approaches by Soloviev [2]. Soloviev's calculations demonstrated that the neutron strength functions can have more complicated structure and stronger fluctuations in energy dependence than the result from the use of simple spherical optical model predictions. But because these calculations do not include the calculations of total widths and contain some averaging it is difficult to determine exactly the real widths of the intermediate structures in the cross sections which we can observe in the unresolved resonance region. Microscopical calculations in the shell model approach to nuclear reactions, which were done for some light and closed-shell nuclei, have shown the existence of intermediate structures in the unresolved resonance region [3] which cannot be described by the usual statistical model of compound nuclear reactions.

Semi-microscopical calculations of level density for heavy nuclei by Soloviev and co-workers [4] have shown that there can be

some deviations from predictions of the usual Fermi-gas model, which is often used for decomposition of D_{obs} between states with different spins and parities.

Comparisons

The tables and figures given in this paper contain the results of intercomparison of average parameters and values of cross sections for a series of current evaluations. As we stressed earlier the question of consistency between different evaluations can best be given in terms of comparison of calculated average cross sections and transmission data (but not from comparison of parameters). Below we discuss the consistency of different evaluations for each isotope separately.

^{235}U

The average resonance parameters in the unresolved resonance region for different ^{235}U evaluations are given in Table I. The reduced neutron width as well as the reduced neutron strength functions have strong energy dependence in all cases. There are differences between JENDL-2 and ENDF/B-V on one side and SOKRATOR on the other in the subdivision of the cross-section between the potential scattering and the compound nuclear parts although the difference between the averaged total, fission and capture crosssection from different files does not exceed 6%. The new integral like measurements of Vertebnyi [5] supports the subdivision given in the ENDF/B-V and JENDL-2 libraries. Fig. 1 shows the comparison of the energy dependence of the reduced neutron strength function S_o for ^{235}U taken from JENDL-2 (dot-dashed line) and SOKRATOR (thin line) libraries. Figures 2-4 present comparison of the group averaged total, fission and capture cross-sections in the unresolved resonance region. The designations for different libraries are the same as for Fig. 1 and in addition, the dashed-dashed line represent the results from ENDF/B-V library. It should be noted that the ENDF/B-V fission cross-section is 4-6% lower than the fission cross section in the JENDL-2 and old SOKRATOR evaluation.

^{238}U

The average resonance parameters for ^{238}U in different libraries are presented in Table II and the total and capture cross-sections in the unresolved resonance region are given in Fig. 5 and 6. The ENDF/B-V total and capture cross-sections are a little higher than in JENDL-2 library (up to 10%) in the energy range from 5 to 20 keV.

^{239}Pu

The comparison of the average resonance parameters for ^{239}Pu and corresponding cross sections is given in Table III and Fig. 7-9. There is good consistency between different evaluations for all cross sections and energies except below 0.5 keV where the JENDL-2 library gives resolved resonance parameters while ENDF/B-V and SOKRATOR use unresolved resonance parameters. The α-value for energy group 0.215 to 0.465 keV is 25% higher in ENDF/B-V library than in SOKRATOR.

^{240}Pu, ^{242}Pu

The evaluated data for ^{240}Pu and ^{242}Pu (Tables IV and V, Fig. 10-15) have a large spread. The general trend is that JENDL-2 evaluated total cross-section is approximately 10-15% higher than SOKRATOR data and 10-20% higher than ENDF/B-V. The reason for these differences is that the JENDL-2 evaluations probably take into account the results of recent Kaeppeler measurements [6]. Generally although the total and partial cross-sections can have some

structure in the unresolved resonance region, the cross sections predicted by non-spherical optical model, with suitable adjusted parameters, on the average degree well with experimental points. The results of Kaeppeleris total cross section measurements [6] are in strong contradiction with such calculations by Fisher [7] and Lagrange [8] as well as the general trend on the A-dependence shown by Fisher [7]. In addition, there are some indications based on the results of the measurements by Young et al. [9] that the SOKRATOR and ENDF/B-V evaluations for ^{242}Pu underestimate a little the total cross-section in the energy range 1-10 keV. The spread in the capture cross-section between different evaluations in the case of ^{242}Pu is 30% in the energy range 1-5 keV.

^{241}Pu

There is a good consistency between the results of different evaluations for total and all partial cross-sections (Table VI, Fig. 14-16). This consistency would appear to be due to a lack of the experimental data for this nucleus. Some discrepancies exist between the capture cross-sections in the ENDF/B-V library on one side and SOKRATOR and JENDL-2 on the other in the energy range 0.1-0.5 keV.

General Conclusions

More attention must be paid to the total, capture and fission cross section measurements in the energy region 0.1-1 keV for fissile and 1-10 keV for fertile plutonium isotopes. These regions are transitional between resolved resonance region and region of overlapping levels. The cross section in these regions have strong intermediate structure. The methods of representation of the cross sections in these regions must provide correct description not only of the average cross sections but also the results of transmission and self-indication measurements.

REFERENCES

1. Antsipov, G.V. et al., INDC(CCP)-166/GHJ (1981) p. 23
2. Malov, L.A. et al., Nucl. Phys. A270 (1976) 87
3. Payne, G.L., Phys. Rev. 174 (1968) 1227
4. Soloviev, V.G. et al., Nucl Phys. A224 (1974) pp. 396, 411
5. Vertebnyi, V.P. et al., 80Kiev, 2 (1980) 254
6. Kaeppeler, F., KFK-2686 (1978) 27
7. Fisher, U., KFK-2907 (1980)
8. Lagrange, C.H. et al., NEANDC(E) 198 "L" (1980)
9. Young, T.E. et al., Nucl. Sci. Eng. 40 (1970) 389

Table I. Average Parameters for ^{235}U in Unresolved Resonances Region

Parameter / Evaluation (year)	Unresolved resonance energy region Emin,keV	Emax,keV	$\langle D \rangle_{\ell=0}$ eV	$\langle \Gamma_n^o \rangle_{\ell=0}$ meV	$\langle \Gamma_\gamma \rangle$ meV	S_o x10^4	S_1 x10^4	S_2 x10^4	a, fm	Background cross section
SOKRATOR	0.1	100	0.61	strong energy dependence	40.69	strong energy dependence		-	8.391	no
JENDL-2	0.1	30	0.567	strong energy dependence	45.0	strong energy dependence		-	9.5663	yes
ENDF/B-V	0.082	25	0.438	strong energy dependence	35.0	strong energy dependence		-	9.566	yes
BNL-325 (1973)			0.63±0.06			0.92±0.10	1.8±0.3			

Table II. Average Parameters for ^{238}U in Unresolved Resonances Region

Parameter / Evaluation (year)	Unresolved resonance energy region Emin,keV	Emax,keV	$\langle D \rangle_{\ell=0}$ eV	$\langle \Gamma_n^o \rangle_{\ell=0}$ meV	$\langle \Gamma_\gamma \rangle$ meV	S_o x10^4	S_1 x10^4	S_2 x10^4	a, fm	Background cross section
JENDL-2	4	50	19.83	1.69	23.5	0.8536	1.42	1.0	9.36	yes
BNL-325 (1973)			17.7±0.7			1.1±0.1	1.7±0.3			
ENDF/B-V (1980)	4	149	20	2.1	23.5	1.05	strong energy dependence	2.5	8.9	yes

Table III. Average Parameters for ^{239}Pu in Unresolved Resonances Region

Evaluation (year) \ Parameter	Unresolved resonance energy region Emin,keV	Emax,keV	$\langle D \rangle_{\ell=0}$ eV	$\langle \Gamma_n^o \rangle_{\ell=0}$ meV	$\langle \Gamma_\gamma \rangle$ meV	S_o x10^4	S_1 x10^4	S_2 x10^4	a, fm	Background cross section
SOKRATOR (1980)	0.3	100	2.38±0.06	strong energy dependence	43.3	1.03±0.05	2.3±0.3		8.4337	no
JENDL-2	0.598	30	2.93	strong energy dependence	41.5	strong energy dependence		-	9.054	yes
ENDF/B-V (1976)	0.301	25	2.30	strong energy dependence	41.6	strong energy dependence		-	9.054	yes
BNL-325 (1973)			2.3±0.1			1.3±0.1	2.3±04			

Table IV. Average Parameters for ^{240}Pu in Unresolved Resonances Region

Evaluation (year) \ Parameter	Unresolved resonance energy region Emin,keV	Emax,keV	$\langle D \rangle_{\ell=0}$ eV	$\langle \Gamma_n^o \rangle_{\ell=0}$ meV	$\langle \Gamma_\gamma \rangle$ meV	S_o x10^4	S_1 x10^4	S_2 x10^4	a, fm	Background cross section
SOKRATOR (1975)	1	150	13.5±.5	1.485	30.7	1.1±.16	2.8±0.4	1.1	8.578	no
BNL-325 (1973)			13.6±0.4			0.94±0.09				
JENDL-2	4	40	12.6	1.31	29.5	1.04	3.03	1.0	9.184	yes
ENDF/B-V (1977)	3.91	40	12.7	1.32	31.0	1.04	2.20	-	9.184	no

Table V. Average Parameters for ^{242}Pu in Unresolved Resonances Region

Evaluation (year)	Unresolved resonance energy region Emin,keV	Emax,keV	$\langle D \rangle_{\ell=0}$ eV	$\langle \Gamma_n^o \rangle_{\ell=0}$ meV	$\langle \Gamma_\gamma \rangle$ meV	S_o x10^4	S_1 x10^4	S_2 x10^4	a, fm	Background cross section
SOKRATOR (1978)	1	200	14.233±0.536	1.30±0.20	22.61±0.65	0.91±0.15	2.5	0.91	9.7409	no
ENDF/B-V	0.986	10	16.5	1.342	23.4	0.813	1.15	-	9.228	yes
JENDL-2	no unresolved resonance parameters; point wise representation									
BNL-325 (1973)			16.5±0.5	1.50		0.9±0.1				

Table VI. Average Parameters for ^{241}Pu in Unresolved Resonances Region

Evaluation (year)	Unresolved resonance energy region Emin,keV	Emax,keV	$\langle D \rangle_{\ell=0}$ eV	$\langle \Gamma_n^o \rangle_{\ell=0}$ meV	$\langle \Gamma_\gamma \rangle$ meV	S_o x10^4	S_1 x10^4	S_2 x10^4	a, fm	Background cross section
ENDF/B-V	0.1	40.2	0.935	strong energy dependence	43	strong energy dependence		-	9.33	no
SOKRATOR (1980)	0.1	100	1.34	(J=2) 0.358 (J=3) 0.275	43	1.16	2.0	-	8.45	no
JENDL-2	0.1	30	0.8498	strong energy dependence	40	strong energy dependence		-	9.8	yes
BNL-325 (1973)			1.0±0.1			0.99±0.14				

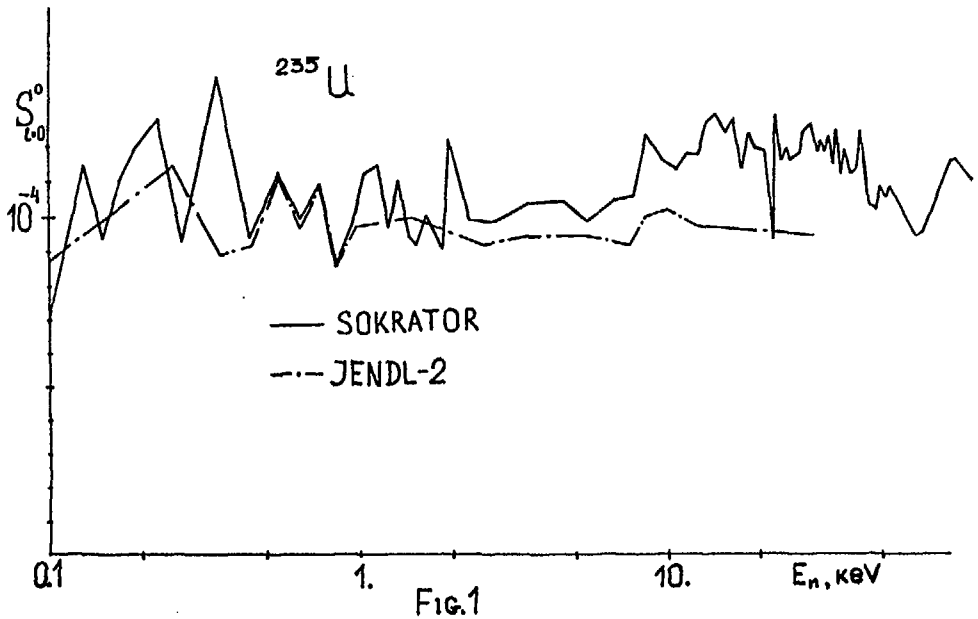

Fig.1

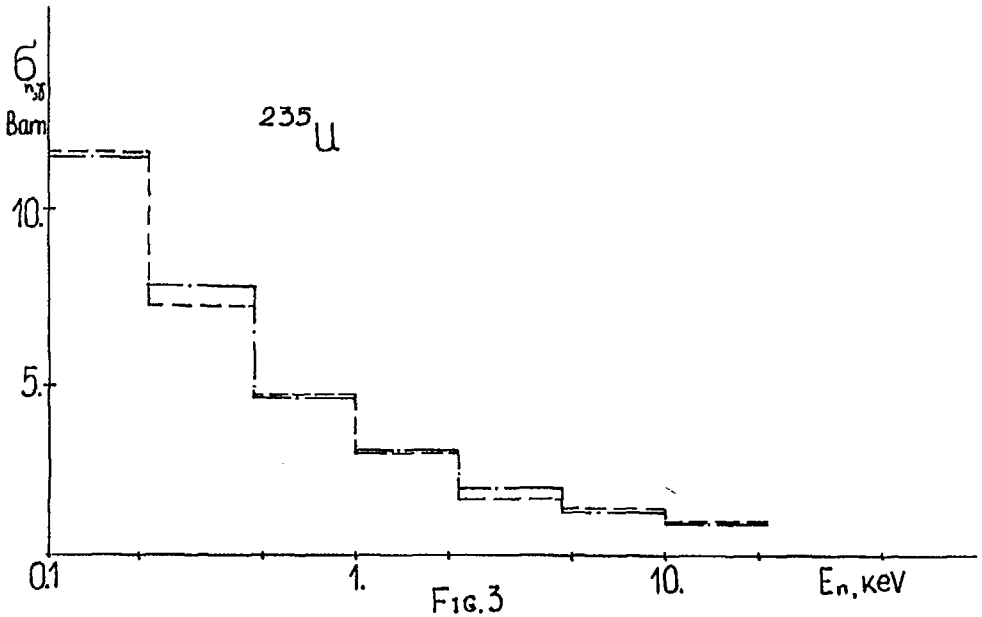

Fig.3

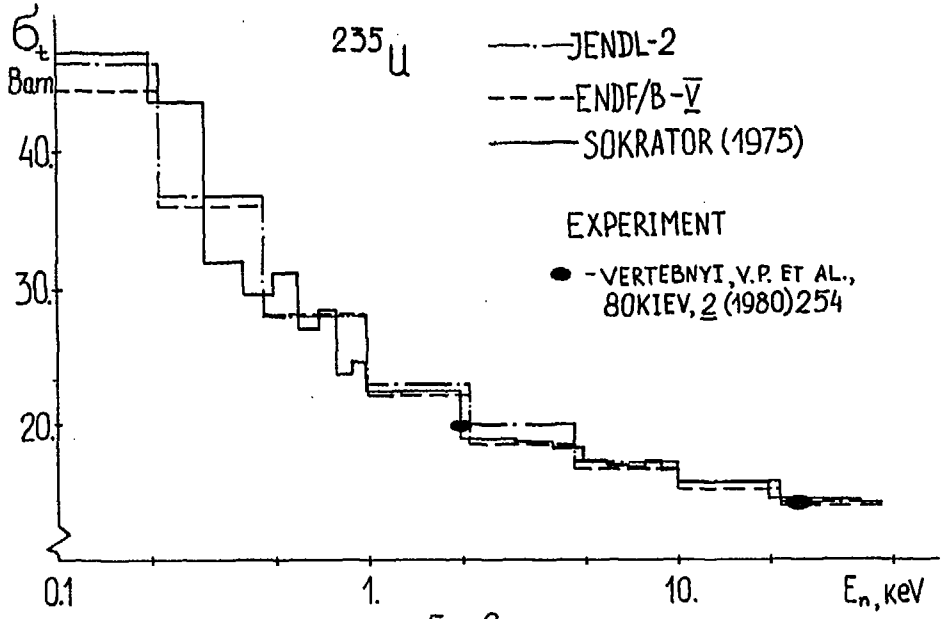

Fig.2

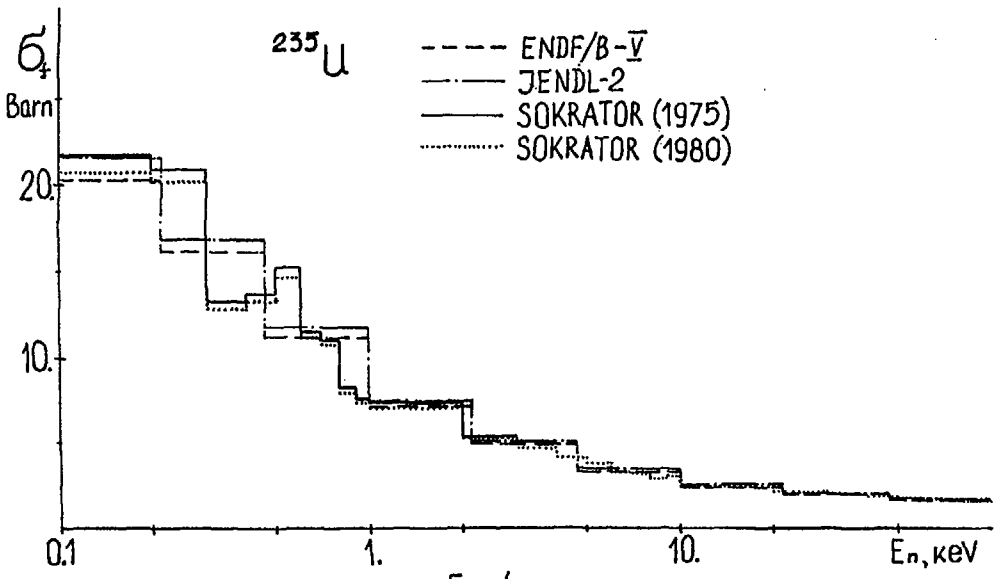

Fig.4

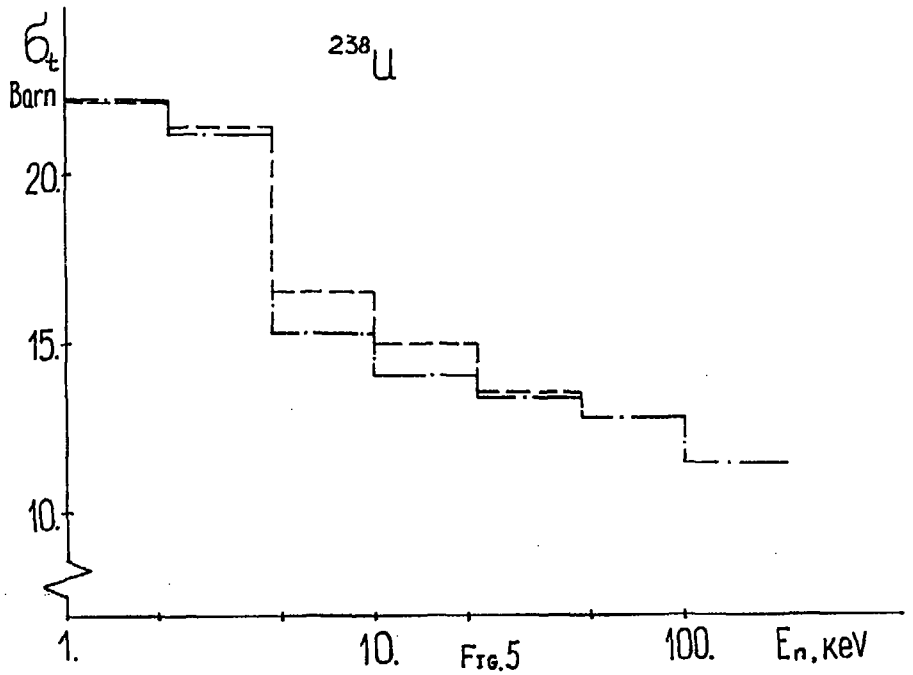

Fig.5

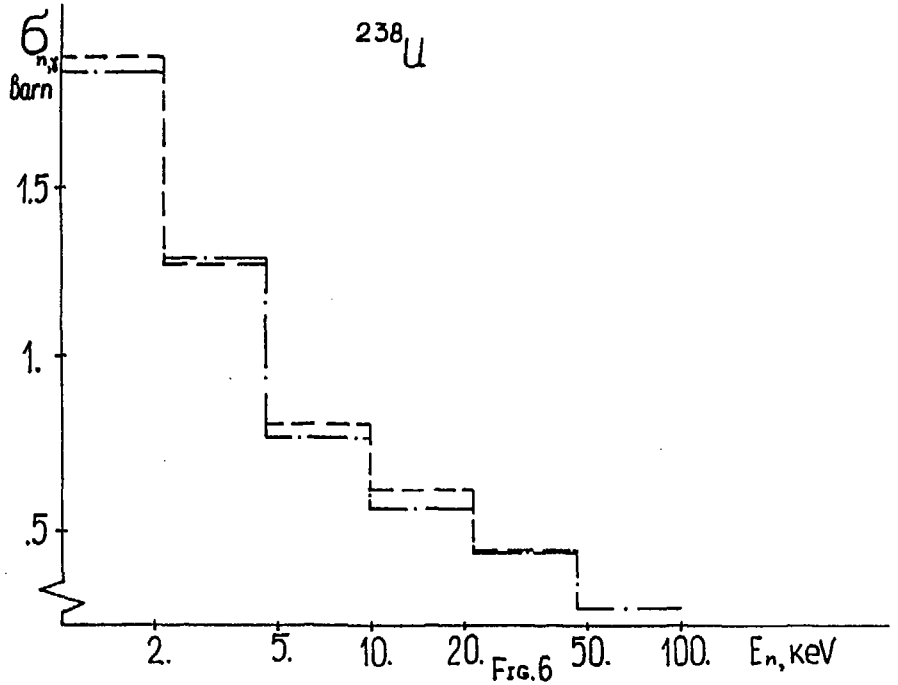

Fig.6

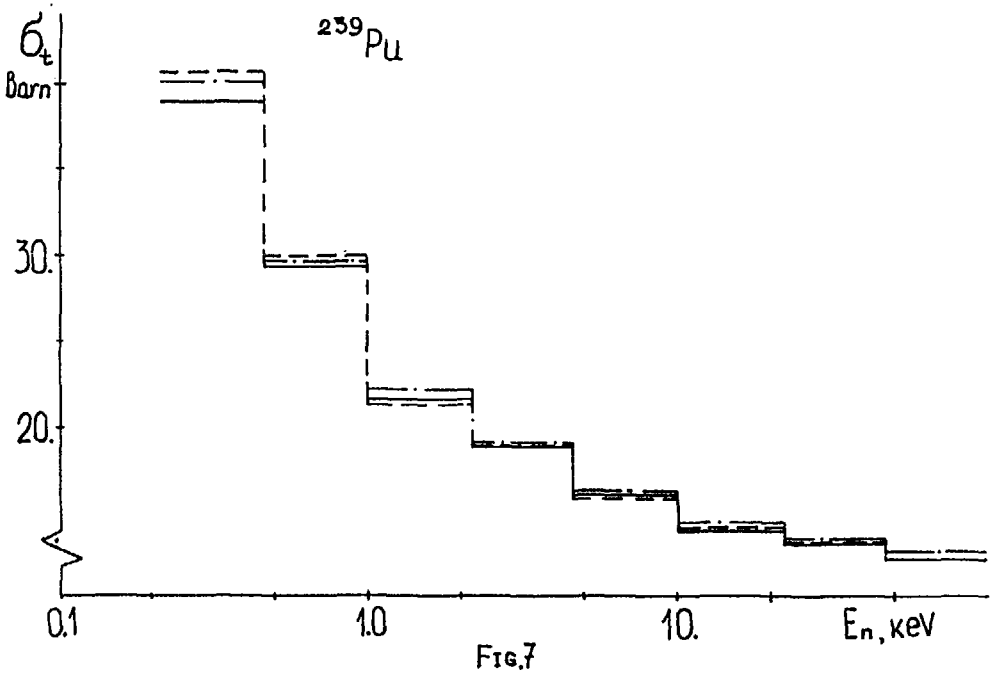

Fig.7

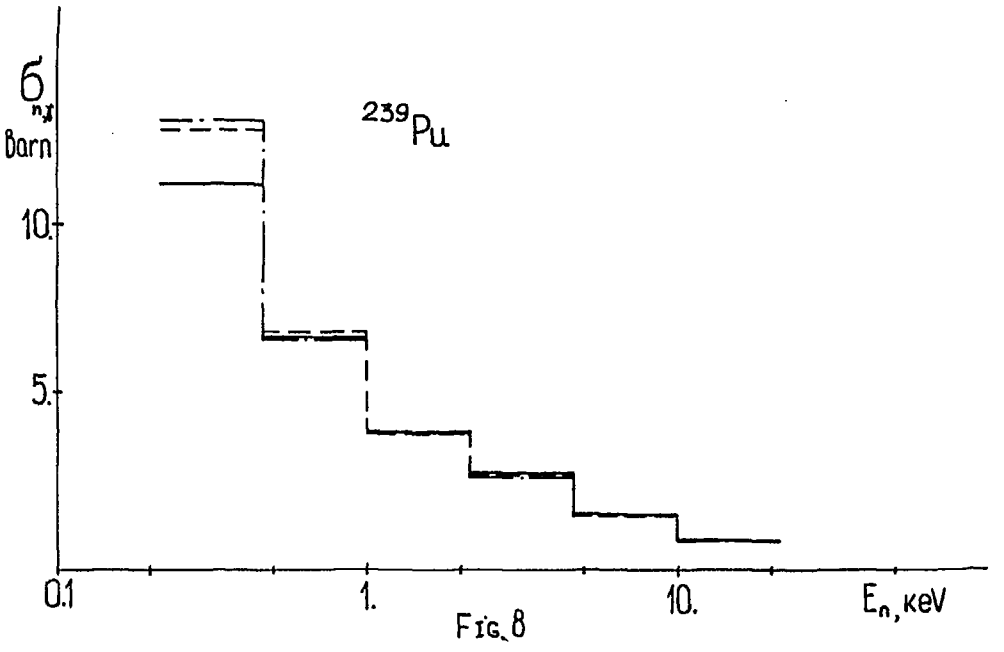

Fig.8

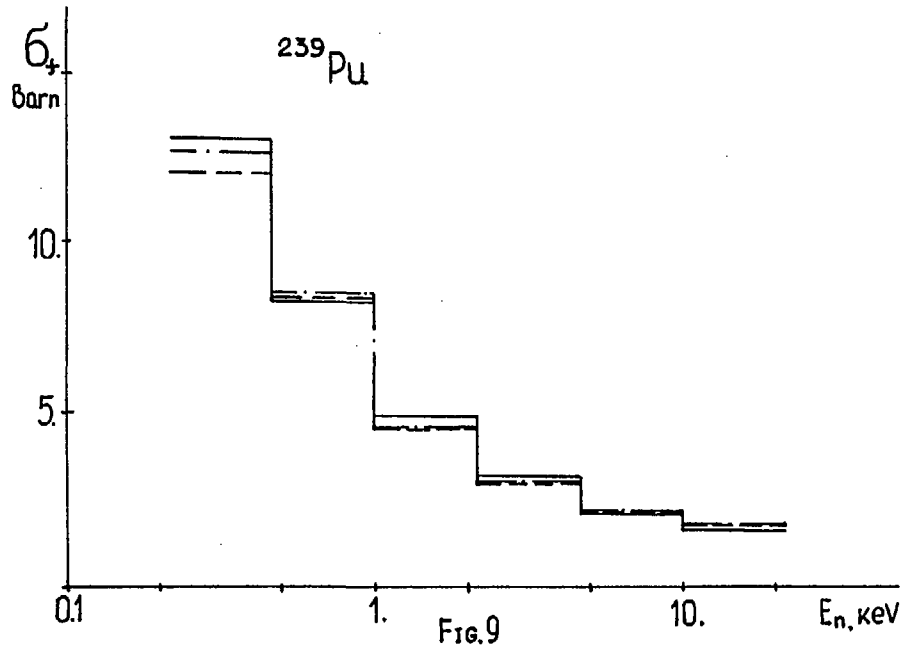

Fig. 9

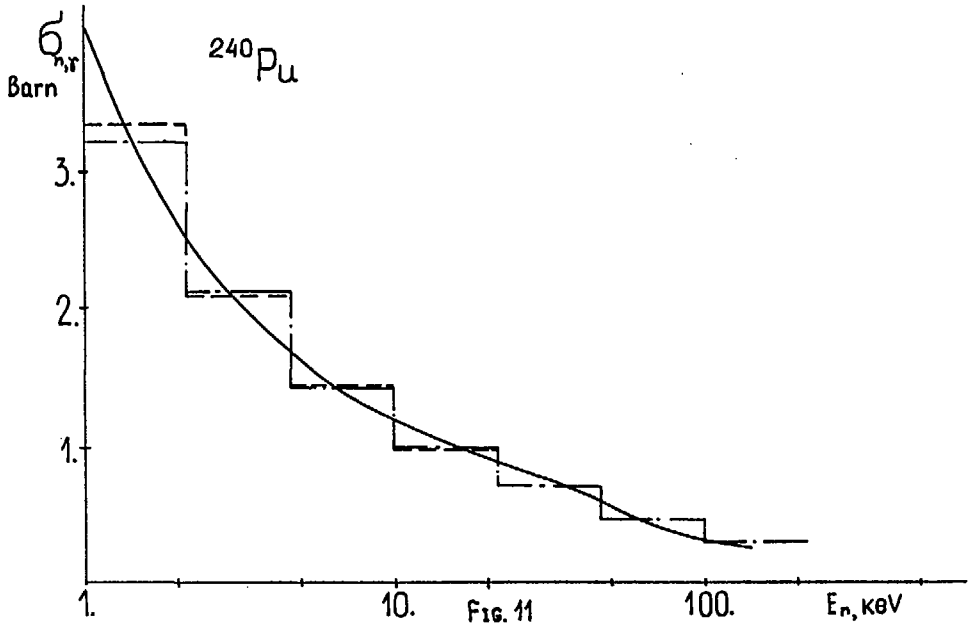

Fig. 11

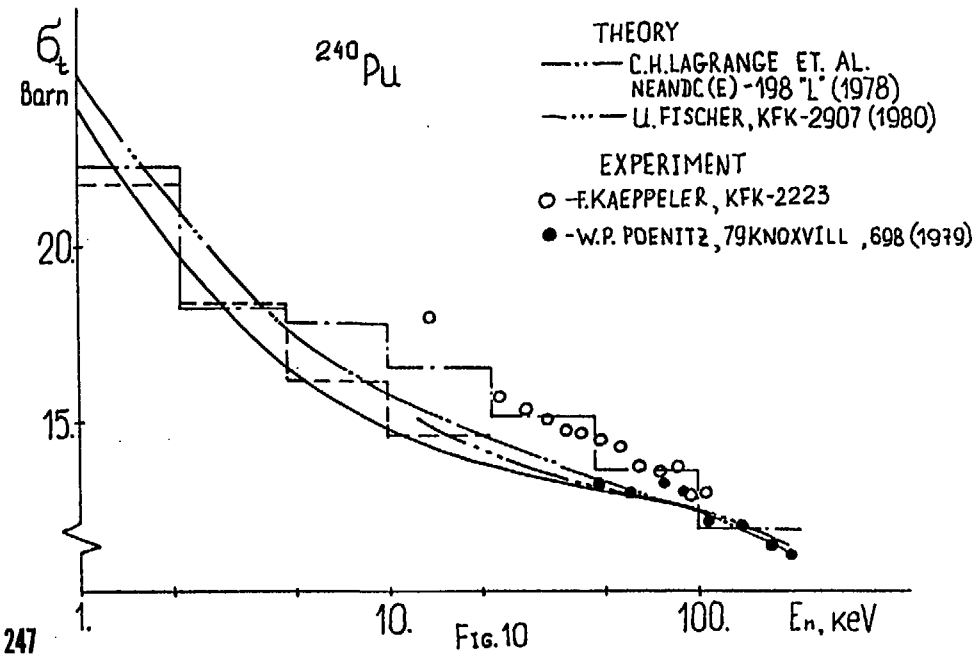

Fig. 10

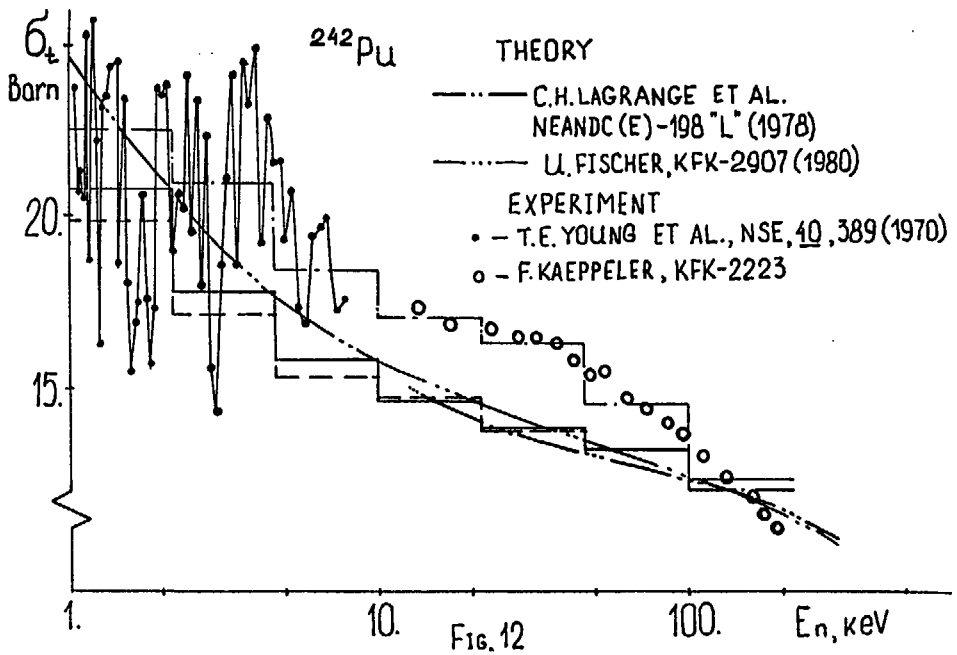

Fig. 12

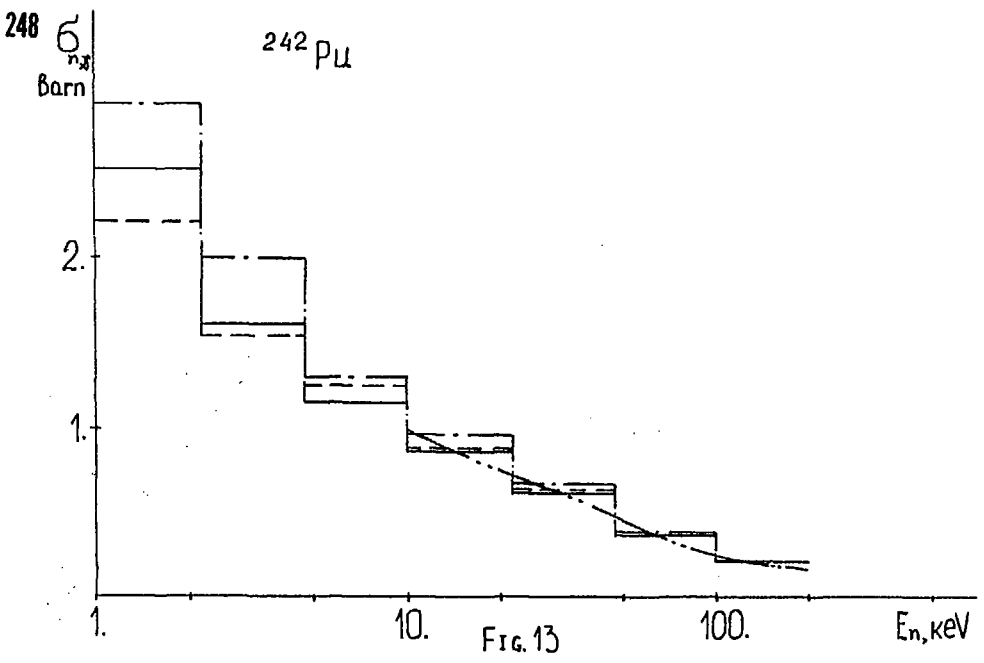

FIG. 13

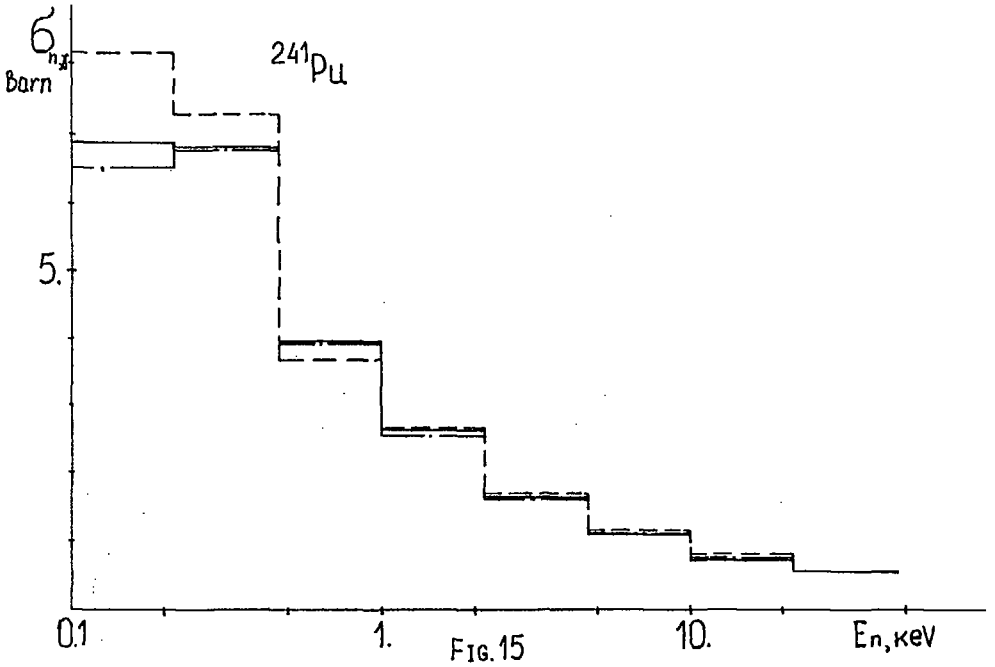

FIG. 15

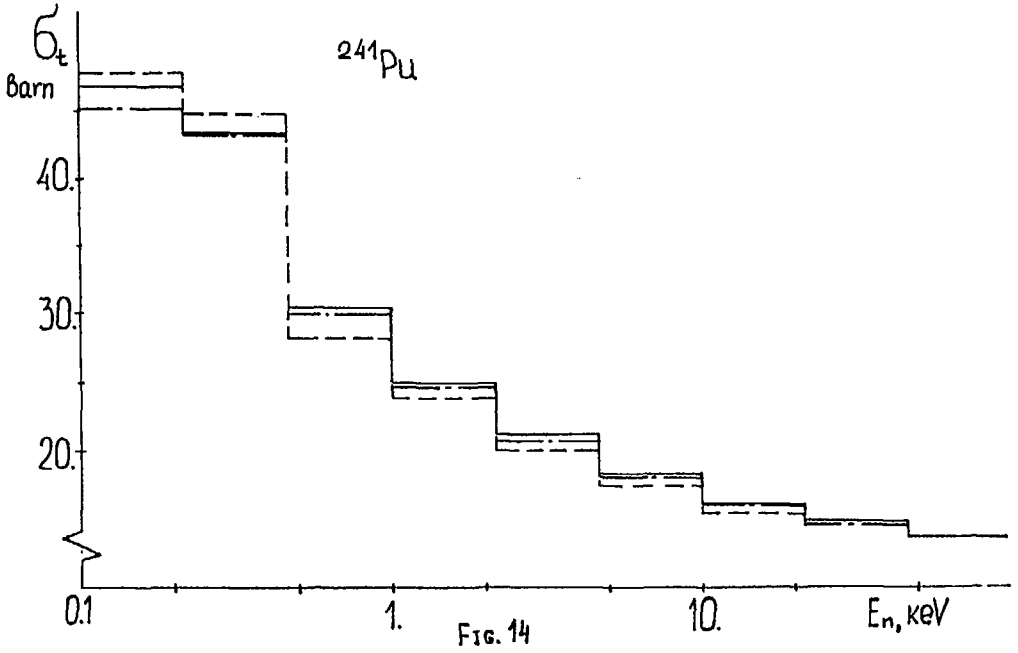

FIG. 14

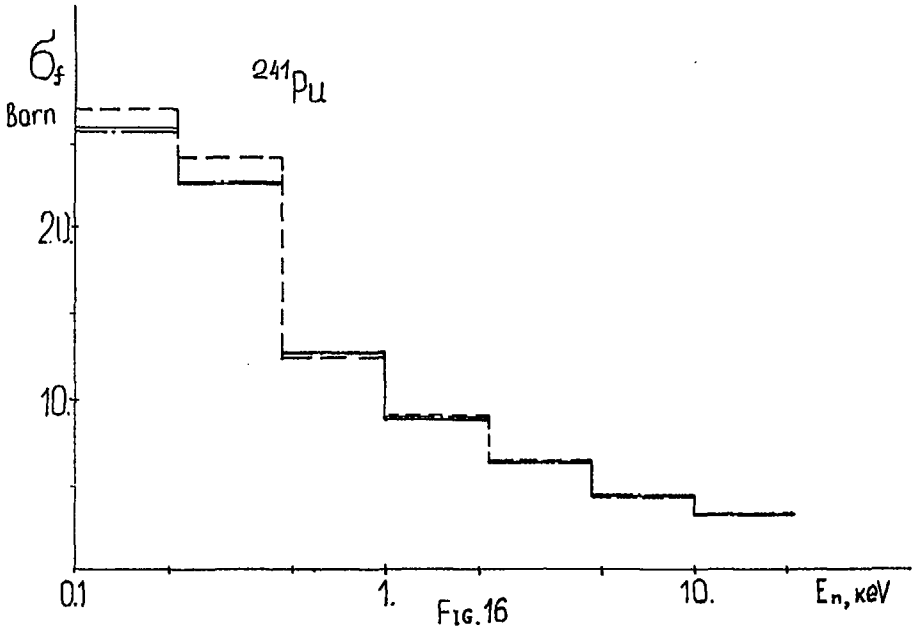

FIG. 16

NEA Nuclear Data Committee

Intercomparison of methods used to determine average resonance parameters

(Coordinated by Dr. P. Ribon, CEN Saclay, France)

The 1979 meeting of NEA Nuclear Data Committee endorsed a proposal to carry out a benchmark intercomparison study of methods used to determine average parameters from resolved resonance parameters. The report NEANDC-(E)213"AL", sent out in September 1980 (First part: Generation of test data) and March 1982 (Second part: Results and their interpretation) showed important systematic discrepancies between the sets of solutions obtained by physicists using essentially the same approach to the calculation of average level spacings, strength functions and radiation widths in the two hypothetical nuclei for which artificially generated resonance parameters were supplied.

A workshop will be held at the NEA Data Bank on 15th and 16th October 1981 for participants in this exercise. The aim of the workshop is to identify the origin of the discrepancies between different solutions; in order to provide a clearer basis for discussion, a second exercise has been distributed to the original participants, and to a small number of other physicists in NEA and IAEA countries who did not submit solutions but who regularly carry out calculations of this kind. Data has been sent for calculating two cases each, at three levels of complexity in calculation:

(a) two cases of pure reduced neutron width distributions (the only quantity to be determined is $\langle \Gamma_n^o \rangle$).

(b) two cases of resolved resonance parameters, without any experimental effect.

(c) two cases of pseudo-experimental resonance parameters sets, similar to case 1 of the previous exercise, but without the correlations introduced by a programming error into the data for the previous exercise.

It was clear from discussions during the analysis of the previous exercise that the methods used are not all fully prescribed, and that results may depend on the way in which physicists apply their judgement, for example in defining the neutron width threshold to exclude p-wave resonances.

Five solutions have so far been sent or firmly promised for examination at the October meeting, from:

Dr. F. Froehner	KFK Karlsruhe, FRG
Dr. Y. Guy	Israel
Dr. M. Moore	LANL, USA
Dr. G. Rohr	CBNM, Geel (EEC)
Dr. H. Weigmann	CBNM, Geel (EEC)

It is expected that eight or ten physicists in all, with their solutions to this and the earlier problem, will attend the workshop, and that it will be possible to make clear recommendations about programs giving good results, and about the approach to be taken in order to obtain consistent results in use.

FIRST PART: GENERATION OF DATA

P.RIBON, CEN SACLAY

ABSTRACT

In order to check the methods used by different laboratories to determine the average parameters by analysing sets of resolved resonance parameters, an exercise is proposed: to analyse artificially generated sets of resonance parameters.This paper describes how these parameters have been generated. The calendar for carrying out this benchmark is defined.

Following discussions at various international meetings, and a recommendation from the last NEANDC meeting, we propose the following exercise : sets of resonance parameters have been theoritically generated and modified to take into account experimental effects. These sets are available for analysis by voluntary physicists, who will determine the values of the average parameters.

These sets of resonance parameters are obtained by the following process: values of average parameters are chosen (and kept secret). From these values we generated individual resonance parameters, then total cross sections, then transmissions, affected by experimental effects. These transmissions have been analysed as if nothing (exept experimental conditions) was known; from the shape analysis sets of "pseudo-experimental" resonance parameters are provided for analysis.

This paper presents the purpose of this study, the conditions of generation of the pseudo-experimental sets, the suggested cases, and the calendar for the programme.

I. PURPOSE

It has appeared that there are great discrepancies between the values of $\overline{D}(l=0)$ determined by different laboratories from the analysis of the same set of experimental data (resonance parameters). The differences in results may be due to:

- -differences in methods used to analyse the sets of data;
- -personnal bias of the physicists involved.

At the PETTEN meeting on "FISSION PRODUCT NUCLEAR DATA ", E.FORT (Fo 77) suggested the organization of an international exercise: a few sets of resonance parameters are generated, with the double condition to satisfy known statistical laws and to include experimental effects; these sets will be available for analysis to laboratories on a voluntary basis and the results compared.

Following discussions at the "SPECIALIST MEETING ON NEUTRON CROSS SECTION OF FISSION PRODUCT NUCLEI", held at BOLOGNA (Bo80),we propose 6 sets of data.

II-CONDITIONS OF GENERATION OF THE STATISTICAL SETS OF RESONANCE PARAMETERS

1-Generation of the level energies. Sets of values distributed in the Gaussian Orthogonal Ensemble (GOE) are obtained by the diagonalisation of symmetric random matrices.

1-1.The matrix elements are randomly generated according to normal laws characterized by: $\langle e_{\lambda\lambda'} \rangle = 0 \qquad \sigma^2_{\lambda,\lambda'\neq\lambda} = 1 \qquad \sigma^2_{\lambda\lambda} = 2$

1-2.The matrices have been diagonalised by the subroutine DERUGI (Ng74), based upon the GIVENS-RUTISHAUSER method. It appeared as the fastest of 3 possible subroutines,the computing time being about $2*N^3$ µs with a IBM 360-91 computer. The comparison with the 2 other subroutines proved that DERUGI provides about 10 exact figures when N=200, and 8 or 9 when N=500, which is amply sufficient.

1-3.As a fact the average spacing of eigenvalues is distributed according to the WIGNER semi-circle law (Wi55,Po60); it is equal to $\pi/\sqrt{N}$ at the center of the distribution, but increases at the ends. As suggested by the BOLOGNA group (Co79), the distribution has been corrected, the eigenvalues x being replaced by :

$$x' = \frac{x}{2}\sqrt{1 - \frac{x^2}{4N}} + \sqrt{N}\ \sin^{-1}\frac{x}{2\sqrt{N}}$$

For security, in order to avoid ends effects, we still rejected 15 to 20 % of eigenvalues at each end of the distribution.

1-4.The agreement of some of these sets with statistical laws has been checked: there is no significant departure. Amongst other controls, to study the sensitivity of these sets to random error over D, we applied a random fluctuation with standard deviation:

$$\sigma = 0.05\ \overline{D} = 0.05\ \pi/\sqrt{N}$$

to the eigenvalues x. The resulting distribution of D show no significant perturbation, and there was almost no variation in the Δ3 value (Dy63).

2-Generation of the neutron widths.

They are generated according to the X^2 law with one degree of freedom per entrance channel (PORTER and THOMAS distribution).A control indicates that a 10% error in $\overline{\Gamma}n$ values does not disturb significantly the distribution (a maximum likehood analysis of the distribution of 200 neutron widths shows a 1 or 2 % effect on $\overline{\Gamma}n$ and $\overline{D}$).

3-Generation of radiation widths.

They are also generated according a X^2 law, but with a ν value between 20 and 100. For practical reasons,the X^2 distribution is approximated by a normal law with variance equal to $2/\nu$. No special control has been applied.

III-CONDITIONS OF GENERATION OF THE "EXPERIMENTAL" TRANSMISSIONS

1-The total cross section is computed with the BREIT AND WIGNER single level formulae:

$$\sigma_t = 4\pi R^2 + 4\pi \lambda^2 \sum_{\lambda} g_\lambda \frac{\Gamma_{n\lambda}}{\Gamma_\lambda} \frac{1}{1+X^2_\lambda} + 8\pi \lambda R \sum_{\lambda(\ell=o)} g_\lambda \frac{\Gamma_{n\lambda}}{\Gamma_\lambda} \frac{X_\lambda}{1+X^2_\lambda}$$

the total width being assumed constant. The same formulae has been used for a least squares analysis.

2-The transmissions were computed as: $T=\exp(-n\sigma_t)$

At this step, we made an approximation: resolution broadening should be applied to the transmission. In order to improve the rapidity of the least squares analysis, we applied this resolution broadening to the cross section: this can be justify by the preponderance of the Doppler broadening.

The thicknesses used are:

- case 1 : n=0.15, 0.03, 0.006 atom/barn (3 thicknesses);
- case 5 : n=0.05, 0.01, 0.002 atom/barn (3 thicknesses).

3-The total resolution is then the sum of 3 contributions: Doppler broadening, neutron slowing down and electronic widths. As the Doppler broadening is preponderant and uniform over the considered energy ranges, the two other contributions were also assumed uniform. The values adopted are given in table 1.

4-The channel width was defined as a function of the resolution. It is equal to k standard deviation of the resolution function, with:

case 1 :	k=1.2	below ~650 eV;
	k=1.0	up to ~1800 eV;
	k=0.8	above.
case 5	k=1.2	below ~30 eV;
	k=0.8	up to ~60 eV;
	k=0.6	up to ~120 eV;
	k=0.4	above.

5-Statistical fluctuations. Every transmission data point has been affected by a random fluctuation, with a standard deviation ε equal to:

$$\varepsilon = 0.004 + 0.013\ T$$

It corresponds to a counting rate of 6000 counts/channel for T great, and to a background between 5 and 10 %.

IV-ANALYSIS OF DATA

In order to be as close as possible of a true experiment, it was decided to analyse these data by a least square fit. This has been done in collaboration with H.DERRIEN.

1-The old SACLAY least square fitting programme (Ri67) was modified in order to save time:

-the resolution function was suppressed (see III-2),the resolution being included in the the Doppler effect;

-the cross section formulae was simplified (see III-1);

-a fastest subroutine was used for the PSI-PHI functions (Ri79);

-many other modifications were applied to the programme itself to avoid useless computation.

As a result of these modifications, the computation time was greatly reduced: as an example, for case 1A, between 2310 and 2600 eV, (1323 data points), a computation with 3 iterations, 37 resonances and 40 free parameters lasted 10 s on a IBM 3033 computer.

These programme modifications made the preparation of this exercise feasible.

2-Results.The analysis was made as if nothing was known (exept thicknesses and the resolution function). The results are, for each identified resonance:

-the resonance energy E

-the total width Γt

-the product $2\,g\,\Gamma n$

The errors given are those resulting from the computation. No error is given when the parameter was not adjusted by the least square fitting.

The identification of resonances was made by eye, by comparison of the theoritical and "experimental" curves (which were plotted at every computation). In a few cases abnormally large values of the total width were taken as another reason to introduce a new resonance.

All resonances were treated as "s" wave resonances. Nevertheless, some noticeable disagreements appeared for nuclei 1 : the treatment of a few resonances as "p" wave resonance improve the fit. These cases are indicated in the results.

V-THE 6 PROPOSED CASES

Our first idea was to propose 5 very different nuclei. At the BOLOGNA meeting it was pointed out that it would then be impossible to distinguish between random and systematic disagreements. This is why we propose only 2 nuclei, but with 3 cases for each (each case having slightly different average parameters). They are:

-nucleus 1 : A~100, odd, I=1/2; there are about 300 resonances up to 5 keV.

-nucleus 5 : A~150, odd, I=5/2; there are about 150 resonances up to 300 eV.

VI-AVERAGE PARAMETERS TO BE DETERMINED

The main value to be determined is: $\bar{D}(l=0)$

also, but subsidiary, the strength functions and the radiative widths.

VII-AGENDA OF ACTIONS

Data are available upon request through the channel of the 4 nuclear data centers. Participating laboratories are requested to fill the form included, (eventually several forms if they do several analysis differing by methods, or by energy range; but they must clearly state the values they recommend), and to send it back before the end of NOVEMBER 1980 either to:

Pierre RIBON, CEN SACLAY, BP N°2, 91190 GIF-sur-YVETTE, FRANCE
or to:

Peter JOHNSTON, NEA Nuclear Data Bank, BP N°9, 91190 GIF-sur-YVETTE, FRANCE

A report,comparing results with the "truth", will be prepared and distributed to participants in January 1981.

CONCLUSION The BOLOGNA meeting shows a convergence between the methods used by several laboratories. Nevertheless no laboratory has checked its methods (except, to a certain extent,the BOLOGNA group-Co79). The analysis of the 6 sets of data is a good opportunity to test these methods. Of course we know that we did not reproduce exactly reality: but we feel that the main defect of these data is to be clean, and they are only representative of the best experimental data available.

The continuation of this action will depend upon the degree of agreement or of disagreement that it will reveal.

TABLE 1 Values of the standard deviation characterizing the resolution.

		Case 1 (A 100)	Case 5 (A 150)
Doppler Broadening	Effective Temperature	97 °K	300 °k
	Standard Deviation	$0.130\sqrt{E/A}$	$0.227\sqrt{E/A}$
Slowing down, length fluctuation	Exemple of length resolution	2.5 cm at 100 m	
	Standard deviation	$0.20\ 10^{-5}\ E$	
Electronics widths	Exemple of nominal resolution	13 ns at 100 m	
	Standard deviation	$1.5\ 10^{-6}\ E^{3/2}$	

Times in µs, energies in eV.
Nominal resolution: half width of a triangular distribution.

REFERENCES

Bo80 Proceedings of the "Specialists' meeting on neutron cross section of fission product nuclei", edited by C.CCCEVA and G.C.PANINI, NEANDC(E) 209 L, 1980

Co79 C.CCCEVA and M.STEFANCN, "Experimental aspects of the statistical theory of nuclear spectra fluctuations", Nucl. Phys. A 315(1979)1.

Dy63 F.J.DYSON and M.L.MEHTA, "Statistical theory of the energy levels of complex systems-IV", J. Math. Phys. 4,701(1963)

Ng74 H.NGUYEN NGCC, "Specification d'emploi des sous-programmes de la rubrique valeur et vecteurs propres", CISI, Octobre 1974.

Po60 C.E.PORTER and N.ROSENZWEIG, "Statistical properties of atomic and nuclear spectra", Ann. Acad. Scien. Fennicae, 44(1960).

Ri79 P.RIBON, "Programme de calcul des fonctions PSI et PHI", unpublished(1979).

St79 M.STEFANCN, "Description of a statistical method of analysis of neutron resonance data", unpublished.

Wi55 E.P.WIGNER, Ann.of Math 62,548(1955); 65,203(1957);67,325(1958).

DETERMINATION OF AVERAGE PARAMETERS FROM THEORITICALLY GENERATED SETS OF RESOLVED RESONANCES PARAMETERS

LABORATORY :

NAME OF PHYSICIST(S) having done the analysis :

METHODS USED TO ANALYSE THE DATA:
-Principle:

-Reference (if any) :

REMARKS ABOUT THE DATA :

COMMENTS ABOUT THE RESULTS (reasons for limiting the energy range,estimation of lost resonances,...):

RESULTS

CASE	1A	1B	1C	5A	5B	5C
Energy range retained :						
$\overline{D}$ (l=0)						
S0 (10^{-4})						
S1 (10^{-4})						
(Γ_γ,....)						

To be sent back to P.RIBON (CEN SACLAY) or to P.JOHNSTON (NEA DATA BANK)

SECOND PART : RESULTS AND THEIR INTERPRETATION

P. RIBON AND P. JOHNSTON

ABSTRACT

In order to check the methods used by different laboratories to determine average parameters by analysing sets of resolved resonance parameters, an exercise was proposed: to analyse artifically generated sets of resonance parameters. The first part of this paper describes how these parameters were generated. This second part presents the results obtained from several laboratories, and tries to identify the origin of observed discrepancies.

- - - - - - - -

Following discussions at various international meetings, and a recommendation from the last NEANDC meeting, the following exercise was proposed: sets of resonance parameters have been theoretically generated and modified to take into account experimental effects. These sets have been analysed by several physicists, who have determined the values of the average parameters.

The first part of this report, NEANDC(E)213AL, described the conditions of generation of the data. This second part deals with the solutions contributed by nine physicists from six laboratories. We shall consider here only the average parameters: the full list of the values of the exact sets of individual resonance parameters is available on request from Dr. Ribon, and from the NEA Data Bank.

I. The participating physicists

Solutions have been received from:

M. Caner, SOREQ, Israel
H. Derrien, CEN, Cadarache, France
E. Fort, CEN, Cadarache, France
F.H. Fröhner, KFK (Karlsruhe), F.R. Germany
H. Gruppelaar, ECN Petten, the Netherlands
Y.S. Gur, SOREQ, Israel
M.S. Moore, LASL (Los Alamos), USA
G. Rohr, CBNM Geel, Euratom
H. Weigmann, CBNM Geel, Euratom

The contributions are identified by the letters A to I assigned randomly.

Table 1 - Theoritical values
(i.e. average values introduced in the computation).

Case	1A	1B	1C	5A	5B	5C
$\overline{D}$ (l = 0)	44.09	36.67	38.91	1.850	1.425	1.811
$\overline{D}$ (J) - J = 0	170.	140.	150.			
J = 1	59.54	49.68	52.5	6.546	5.141	6.245
J = 2	39.43	33.77	34.79	4.196	3.261	4.059
J = 3				3.310	2.531	3.269
J = 4				2.938	2.200	2.984
S^0 (10^{-4})	0.42	0.41	0.45	2.2	2.5	1.8
S^1 "	5.1	5.5	6.0	1.0	1.0	0.8
$\overline{\Gamma}_\gamma$ (l = 0)	0.159	0.165	0.151	0.072	0.080	0.075
$\overline{\Gamma}_\gamma$ (l = 1)	←	0.130	→			
ν (Γ_γ)	←	60	→	←	80	→

Table 2 - True values
(i.e average values resulting from the random generation of resonance parameters)

Energy range	5200	5210	5240	319.9	319.9	310.0
$\overline{D}$ (l = 0)	43.70	36.43	39.10	1.849	1.428	1.824
$\overline{D}_{(J)}$ J = 0^+/J = 0^-	167.7/162.5	140.8/137.1	149.7/141.6			
J = 1^+/J = 1^-	59.09/59.09	49.15/49.62	52.93/52.40	/6.53	/5.08	/6.08
J = 2^+/J = 1^-	/39.69	/34.05	/34.70	4.21/4.21	3.26/3.26	4.08/4.03
J = 3^+/J = 3^-				3.30/3.33	2.53/2.56	3.30/3.30
J = 4^+/J = 4^-				/2.91	/2.24	/3.01
S^0 (10^{-4})	0.415	0.415	0.453	2.22	2.47	1.785
" (J = 0^+/J = 1^+)	0.401/0.419	0.388/0.424	0.443/0.456			
" (J = 2^+/J = 3^+)				2.24/2.21	2.51/2.43	1.83/1.75
S^1	5.05	5.32	5.64	1.02	1.01	0.795
$\overline{\Gamma}_\gamma$ (l = 0)	0.158	0.165	0.150	0.073	0.081	0.076
" (J = 0^+.J = 1^+)	0.167/0.155	0.175/0.161	0.161/0.147			
$\overline{\Gamma}_\gamma$ (l = 1)	0.132	0.132	0.131	0.071	0.079	0.074

II. The exact average values

Table 1 gives the values of the average parameters which were introduced in the computation of the synthesised parameter sets. Due to statistical fluctuations, the average values of each set of chosen generated individual resonance parameters are slightly different: they are given in Table 2.

These values, that we shall hereafter call the "true values", have been determined over the entire energy range. They would be slightly different if we considered a different energy range, as is illustrated by the following table:

Values of $\bar{D}$ (l=0) for nuclei 1

Theoretical value	43.09 eV	36.67 eV	38.91 eV
"True value", i.e. all resonances "s" up to 5200 eV	43.70 "	36.43 "	39.10 "
All resonances "s" up to 1800 eV	43.90 "	37.50 "	40.00 "
All resonances "s" up to Em, mid-energy between 2 resonances "s" around 1800 eV:			
Em	1793. "	1809. "	1793. "
$D_{(Em)}$	43.73 "	37.69 "	39.84 "

This table shows that 1% to 3% differences are expected in values on $\bar{D}(l=0)$ and are not significant.

III. The results

The results are given in Tables 3 and 4. A quick look shows a great dispersion of some recommended values ($\bar{D}(l=0)$ for nuclei 1). In order to clarify the order of magnitude and the origin of this dispersion, we calculate:

- the ratio of the recommended value to the true value;
- the average of the three ratios (for nuclei 1, 2 and 3);
- the standard deviation characterising the distribution of these three ratios.

Results are given in Table 5. They show that the disagreements are systematic, as the standard deviations are small compared with the differences between unity and the average ratios.

For nucleus 1 the results of D are included in Table 3, but have not been retained in Table 5 as the large discrepancy probably results from a misunderstanding.

IV. Comments about the submitted solutions

It was suggested to physicists that they comment on the data. We noted two observations:

- From H. Weigmann: "In case 1, I would repeat the measurements with a better resolution in order to identify the stronger s and p wave levels by their interference properties. With this large S^1 there should be no problem".

We remark, however, that this experiment 1 was assumed to be done with a cooled sample (T_{eff} = 97 = °K), and that nevertheless the Doppler broadening was predominent up to ~4keV. At 3600 eV for instance.

Resolution due to:

Doppler broadening: $\delta E = 0.130 \sqrt{\frac{E}{A}} = 0.78$ eV

Slowing down: $\delta E = 0.20 \ 10^{-3} E = 0.72$ eV

Electronics width: $\delta E = 1.5 \ 10^{-6} E^{3/2} = 0.32$ eV

- From G. Rohr: "Data are not realistic.

For nuclei with large S^1/S^o ratio, as it is the case for 1A, 1B and 1C, parity assignments (experimentally) have been done (BNL 325).

Our method has not been developed for these cases."

We always feared that our data were not realistic, and we would welcome more specific explanations from G. Rohr on why, according to him, these data are not realistic.

V. Methods used to analyse the data

The methods used to determine $\bar{D}$ and S^1 can be assigned to 2 categories:

1. The number of resonances in the energy range ΔE is determined from the staircase N = f(E) (used as a first guess) corrected by an attribution of the orbital momentum of resonances based upon experimental evidence (if any), sometimes by using BAYES theorem, and corrected by the missing level estimator method.

   The strength function is determined from:

   $$S^1 = \frac{1}{2l+1} \frac{1}{\Delta E} \sum g \Gamma_n^o$$

   Belonging to this method are analyses B, D, F. It is also used by E as a complement to the second method.

Table 3 - Results for nuclei 1

	Energy range	Nuclei 1 - A $\bar{D}(\ell=0)$	$\bar{D}(\ell=1)$	$s^0(10^{-4})$	$s^1(10^{-4})$	$\bar{\Gamma}_\gamma(\ell=0)$	Nuclei 1 - B $\bar{D}(\ell=0)$	$\bar{D}(\ell=1)$	$s^0(10^{-4})$	$s^1(10^{-4})$	$\bar{\Gamma}_\gamma(\ell=0)$	Nuclei 1 - C $\bar{D}(\ell=0)$	$\bar{D}(\ell=0)$	$s^0(10^{-4})$	$s^1(10^{-4})$	$\bar{\Gamma}_\gamma(\ell=0)$	Remarks
Theoritical value		14.09	20.82	0.42	5.1	0.159	36.67	17.58	0.41	5.5	0.165	38.91	18.36	0.45	6.0	0.151	
True value	5200	13.70	20.72	0.415	5.05	0.158	36.43	17.60	0.415	5.3	0.165	39.10	18.19	0.453	5.6	0.150	
	A	5200	39.±4.		$0.42^{+0.06}_{-0.04}$		0.157±0.008	31.±3.		$0.45^{+0.06}_{-0.04}$		0.164±0.007	31±3.		$0.48^{+0.05}_{-0.05}$		0.167±0.012	smaller E range for Γ_γ
	B	5200	18.9±5.6	21.4±2.0	0.408±0.008	5.7±0.5		39.1±4.8	17.8±1.4	0.414±0.009	6.49±0.53		41.±5.3	18.8±1.5	0.449±0.008	6.63±0.56		error on S^1: only the error of determination
	C	1800	15.±3.		$0.56^{+0.15}_{-0.11}$	10.±2.5		36.±2.		$0.54^{+0.13}_{-0.11}$	8.5±2.0		38.±2.		$0.59^{+0.13}_{-011}$	10.5±2.5		ΔE = 5200 for S^1
D	1	5000	22.3		0.44	0.02	0.172	19.8		0.45	0.02	0.169	20.1		0.49	0.02	0.156	
D	2	5000	21.7		0.44	0.02	0.172	19.4		0.45	0.02	0.169	19.8		0.49	0.02	0.156	
D	3		16.9		0.24		0.167	14.1		0.18		0.163	16.2		0.21		0.165	E range = 50 resonances
D	4		15.2		0.24		0.177	13.8		0.18		0.163	17.7		0.21		0.165	E range = 50 resonances
D	5		24.8		0.45	0.02	0.174	22.7		0.48	0.02	0.172	22.4		0.50	0.02	0.156	
D	C(R)	5000	17.8		0.49		0.165	15.8		0.50		0.162	16.4		0.54		0.158	Recommended
E	1	2990/2840	35.4±1.8		0.35±0.025	8.3		33.5±1.7		0.33±0.025	5.75		32.7±1.8		0.389±0.027	7.1		
E	2	530 to 3000	35.8±2.5		0.38±0.04	8.3		31.±2.		0.305±0.04	5.75		33.± 2.3		0.399±0.040	7.1		
	F	1500	33.0±3.2		0.60±0.18			30.8±2.9		0.55±0.14			38.± 3.8		0.56± 0.15			
	G	5189						34.5±5.0	18.5	0.43	4.9							
	H	2600	32.±3.		0.34±0.06	6.		28.±3.		0.35±0.06	7.		30.± 3.		0.37±0.06	8.		
	I						0.175±0.010					0.170±0.008					0.165±0.007	

Table 4 - Results for nuclei 5

		Energy range	Nuclei 5 - A $\overline{D}(\ell = o)$	Nuclei 5 - A $S^o(10^{-4})$	Nuclei 5 - A $\overline{\Gamma}_\gamma(\ell = o)$	Nuclei 5 - B $\overline{D}(\ell = o$	Nuclei 5 - B $S^o(10^{-4})$	Nuclei 5 - B $\overline{\Gamma}_\gamma(\ell = o)$	Nuclei 5 - C $\overline{D}(\ell = o)$	Nuclei 5 - C $S^o(10^{-4})$	Nuclei 5 - C $\overline{\Gamma}_\gamma(\ell = o$	Remarks
Theoritical value			1.850	2.2	0.072	1.425	2.5	0.080	1.811	1.8	0.075	
True value		320 - 310	1.849	2.22	0.073	1.428	2.47	0.081	1.824	1.785	0.076	
Results from	A	320	2.02±0.08	$2.23^{+0.30}_{-0.24}$	0.075±0.005	1.56±0.05	$2.52^{+0.34}_{-0.28}$	0.079±0.007	1.90±0.09	$1.81^{+0.25}_{-0.19}$	0.081±0.006	smaller E renge for Γ_γ
	B	320	1.95±0.15	2.23±0.03		1.54±0.11	2.55±0.04		1.98±0.16	1.80±0.03		
	C	320	1.85±0.10	2.24±0.3		1.52±0.08	2.53±0.3		1.92±0.10	1.81±0.25		
	D 1	300	2.27	2.24	0.077	1.84	2.53	0.087	2.20	1.81	0.081	
	D 2(R)	300	2.15	2.24	0.077	1.79	2.53	0.087	2.13	1.81	0.081	recommended
	D 3		2.16	1.84	0.074	1.56	2.47	0.081	2.21	1.36	0.079	ΔE for
	D 4		2.04	1.85	0.074	1.51	2.59	0.081	2.04	1.37	0.079	50 resonances
	D 5		1.96	2.33	0.078	1.56	2.65	0.088	1.84	1.92	0.082	
	E	81/140/199	1.89±0.10	2.15±0.20		1.58±0.07	2.50±0.16		1.98±0.12	1.76±0.14		
	F	320	1.93±0.09	2.25±0.33		1.52±0.07	2.56±0.38		1.94±0.09	1.82±0.27		
	G	180				1.95±0.29	2.10					
	H	320	1.88±0.14	2.3 ±0.3		1.55±0.10	2.6±0.3		1.92±0.15	1.8±0.3		* same result with ΔE = 160 eV
	I				0.077±0.002			0.087±0.002			0.082±0.002	

Table 5 - Average ratio of X(evaluated) / X(true)
and dispersion around this average (standard deviation)

Result from	$\overline{D}$ (ℓ = o)		S(ℓ = o)(10^{-4})		$\Gamma_{\dot{y}}$(ℓ = o)		S(ℓ = 1)
	Nuclei 1	Nuclei 5	Nuclei 1	Nuclei 5	Nuclei 1	Nuclei 5	Nuclei 1
A	0.845 ± 0.050	1.075 ± 0.029	1.052 ± 0.037	1.013 ± 0.008	1.034 ± 0.069	1.023 ± 0.046	
B	1.089 ± 0.026	1.073 ± 0.016	0.991 ± 0.008	1.015 ± 0.015			1.18 ± 0.06
C	1.015 ± 0.038	1.039 ± 0.034	1.317 ± 0.027	1.016 ± 0.008			1.82 ± 0.19
D		1.195 ± 0.051	1.196 ± 0.008	1.016 ± 0.008			
E	0.838 ± 0.017	1.071 ± 0.044	0.911 ± 0.026	0.989 ± 0.022	1.026 ± 0.039	1.065 ± 0.010	1.20 ± 0.10
F	0.857 ± 0.109	1.057 ± 0.012	1.336 ± 0.105	1.022 ± 0.013			
G	0.947	1.366	1.036	0.83			
H	0.756 ± 0.021	1.052 ± 0.034	0.826 ± 0.014	1.032 ± 0.023			1.19 ± 0.13
I					1.079 ± 0.043	1.069 ± 0.013	

2. The number of levels and $\langle g\Gamma_n^o \rangle$ are determined by a maximum likelihood analysis of the distribution of $g\Gamma_n^o$. This method is used by A, C, E, F, H with slight differences: only the values above a given threshold are analysed (C, E, G(?), H); or the distribution also described p wave resonances (A).

3. Γ_γ was determined as:

$$\Gamma_\gamma = \Gamma_t - 2g\Gamma n \quad \text{by D and I.}$$

The subtraction of $2g\Gamma_n$ instead of Γ_n has the effect of introducing a systematic bias increasing Γ_γ.

Annex 1 gives more details about the methods as given by the authors.

It has to be noted that none of the contributors uses any form of statistics of the level spacing.

VI. The origin of discrepancies

We can summarise Table 5 as follows:

Average parameter	Nucleus-	Range of solutions (relative to "true values")
$\bar{D}(l=0)$	1	-24% to +10%
	2	+ 4% to +20%
s^o	1	-17% to +34%
	2	- 1% to + 3%
s^1	1	+20% and +80%
$\Gamma_\gamma(l=0)$	1	+ 2% to + 7%

Bearing in mind that:

- these errors are systematic
- the data are about the best presently available and do not present any kind of systematic error,

we observe that the results obtained by a good sampling of skilled laboratories are discrepant.

Is this discrepancy linked to the method? It does not appear so. Despite the fact that the sample is small, the disagreements for B, D, F (method 1) are of the same order as those for A, C, H (method 2 alone).

We conclude that the systematic bias introduced in the data analysis is due to the physicist and to the codes that he used, rather than to the principle of the method.

Conclusions

The extent of participation in this intercomparison was not large, bearing in mind that there are very many groups of physicists working in laboratories and who publish average parameters derived by methods relevant to this exercise. Nevertheless, we do consider that the participation is a good sample of the more experienced groups working in the field.

The discrepancies between submitted solutions are such as to strongly suggest that physicists have too much confidence in the correctness of their particular applications of the principal methods. The systematic discrepancies are larger than the uncertainties given by the authors.

In view of the importance of derived average parameters we do recommend that this intercomparison should be followed up within the framework of NEANDC. It does not however seem obvious that a large specialist meeting (10+ participants), with a duration of a few days, would be fruitful.

The discrepancies seem to lie in the detailed application of the methods, rather than in the theoretical approach used. For this reason there is a better chance of resolving differences in application in much smaller working meetings in an environment where the codes can be run and compared at a detailed level. Working visits to laboratories and very small working group meetings with only a few directly concerned physicists are most likely to be of value.

This exercise has shown the value of "benchmarks", particularly where the true values are not known to the participants. We suggest that NEANDC should sponsor similar exercises in other fields, as this does seem to be a good way of bringing to the attention of physicists the dangers in over-confidence in their applications of analysis and calculational methods.

References provided by:

- F.H. Fröhner: Code STARA
  - Nuclear Theory for Applications, IAEA-SMR-43, Trieste 1980, p.90 (=KFK 2669, 1978, p.63).
  - Proc. Spec. Meeting on Neutron Cross Sections of Fiss. Prod. Nuclei, NEANDC(E)209L, Bologna 1979, p.145.
- H. Gruppelaar: Code CAVE (modified version)
  - G. Delfini and H. Gruppelaar: "Maximum likelihood analysis of resolved resonance parameters for some fission product nuclides", NEANDC(E)209"L", p.169(1979).
- Author D:
  - Gyulassy-Perkins (NSE, 53,4,pp.482-486(1974)).

Annex 1

1-B The procedure is as follows:

1) Using typical average parameters for A = 100 or 150, calculate the probability that each resonance is p-wave.

2) Set the probability to one if shape analysis (or other evidence) requires that resonance to be p-wave.

3) Set the probability to zero if the resonance is very large but not required to be p-wave by shape analysis or other evidence.

4) Form the sums in the missing-level estimator using the s-wave probability when solving for the s-wave density and the p-wave probability when solving for the p-wave density. This is a new feature of the method: each small resonance is partially counted in both sums.

5) Obtain new average parameters and iterate steps 1-4 until the input and output parameters are the same.

Unfortunately, the solution is not unique in your exercise for A = 100. The problem is in step 3 above: how large is "very large"? If we set a threshold equal to some of the smallest of your levels required to be p-wave, we get far too many s-wave levels. If we set no threshold, we get far too many p-wave levels. I finally arbitrarily set the threshold such that the relative s-wave to p-wave level density was 4:9, the expected value for a spin 1/2 target. Hopefully, the uncertainties assigned to the solutions are large enough to include possible deviations from the expected 4:9 ratio.

Let me also note that the quantities reported in the table are local averages. The strength functions have lower relative uncertainties than the spacings, under the assumption that your analysis preserves the total area even when resonances may be unresolved.

I-C Method:

Fit of part of neutron width distribution above predefined bias for Γ_n^o. Variation of bias to check sensitivity of results to bias values used. In case of small p-wave strength function S_1, fit with Porter-Thomas distribution for s-wave levels alone. In case of large S_1, fit with superposition of distributions for s- and p-wave levels (assuming a ratio of s- and p-wave level densities according to usual spin dispersion); this gives estimate of S_1, too.

This is a very simple-minded method which certainly is not comparable to the much more involved procedures nowadays in vogue. However, I felt it useful to include it in the comparison, in order to find out how much worse this simple method really is.

I-D Enclosed are six different evaluations of the data based mainly on the Gyulassy-Perkins paper (NSE 53, 4, pp 482-486 (1974)) recommended also by ENDF/B (ENDF-102, Data Formats and Procedures for the ENDF/B, Oct. 1975).

In Evaluation#1, the entire "experimental" data is analysed according to the above mentioned paper, for D(o), s0 and s1. Γ_γ is obtained assuming "undetermined J ", i.e. J=I and $g_J = \frac{1}{2}$ so that $2g\Gamma_n \cong \Gamma_n$ and $\langle \Gamma_\gamma \rangle = \langle \Gamma_t - (2g\Gamma_n) \rangle$.

In evaluation #2 it is assumed that resonances with Γ_n^o less than the (Γ_n^o minimum) of the experimental data were "lost". The probability of these small resonances (i.e. with $\Gamma_n^o \leq (\Gamma_n^o$ minimum)) is estimated assuming $P(\Gamma)d\Gamma = e \times p\left(-\frac{\Gamma}{2\langle\Gamma\rangle}\right)\left(\frac{\pi\Gamma}{2\langle\Gamma\rangle}\right)^{-\frac{1}{2}}$ and the mean level spacing is corrected accordingly. Somewhat smaller $\overline{D(o)}$ values than in evaluation 1 were obtained, as expected.

In evaluation #3 the 50 lowest resonances were taken from each ladder. They were analysed as in evaluation #1. It was found out that in these limited samples the $\overline{D(o)}$ values are smaller than in the larger samples for cases 1A,B,C, and are practically the same for cases 5A,B,C.

In evaluation #4 the 50 lowest resonances are analysed as in evaluation # 2, estimating the number of "lost" resonances, and correcting the values.

In both evaluations #3 and #4 we noted that the strength functions, $\mathcal{O}$, are much smaller than those of evaluation #1 and #2 for cases 5 A,B,C.

In evaluation #5 we used a "cut-off" method, where only resonances with $\Gamma_n^o > (\Gamma_n^o$ cutoff) are considered, assuming that all resonancess with $\Gamma_n^o > (\Gamma_n^o$ cutoff) are presented in the "experimental" data and estimating the number of lost resonances from the assumed $P(\Gamma_n^o)$ distribution. We got rather high D(o) values for cases 1 A,B,C, and reasonable values for cases 5 A,B,C,.

In evaluation #6, which concerns cases 1 A,B,C, only, the D(o) values are estimated with corrections for lost resonances as in evaluation #2, but assuming that all resonances are S - resonances, and NOT

as declared by the "experimentalist". This is based mainly on the discrepancies between D(o) obtained from the lower 50 resonances of the ladders (evaluations 3 and 4) and those obtained from the whole ladder (evaluations 1 and 2). The much smaller $D(\phi)$ values obtained from the lower parts of the ladders can not be explained just by estimating the number of lost resonances, which is about 2% of the population for the whole ladder. We rather assumed that the "lost" S - resonances are really those declared as p - resonances.

Thus we got evaluation#6 for cases 1 A,B,C, which, together with evaluation#2 for cases 5 A,B,C, is the one to which we subcribe.

I-E Principle of the method:

- Maximum likelihood applied to truncated $g\Gamma_n$ distributions
- missing level estimator which uses the properties of the Porter-Thomas distribution
- utilisation of Porter-Thomas distribution to calculate partial integrated with limits equal to $10 < g\Gamma n >$, $< g\Gamma n >$, $0.5 < g\Gamma n >$, $0.2 < g\Gamma n >$, ...
- the BAYES criteria has to be eliminated.

1-F Methods used to analyse the data:

Principle: The method used separates large s-wave resonances from all other resonances by means of the Bayes' theorem. The number of small s-wave resonances lost in this procedure is estimated assuming a Porter-Thomas distribution of the reduced neutron widths. The uncertainty of the method is determined using a large number of different resonance parameter sets, produced in a statistical fashion using Porter-Thomas and Wigner distribution for the widths and level spacing respectively.

ORGANISATION FOR ECONOMIC COOPERATION AND DEVELOPMENT

NUCLEAR ENERGY AGENCY NUCLEAR DATA COMMITTEE (NEANDC)

Intercomparison of methods used to determine average parameters from resolved resonance parameters

Introduction

The 1979 meeting of NEA Nuclear Data Committee endorsed a proposal to carry out a benchmark intercomparison study of methods used to determine average parameters from resolved resonance parameters. The report NEANDC(E)213"AL", sent out in September 1980 (First part : generation of test data) and March 1981 (Second part : results and their interpretation) showed important systematic discrepancies between the sets of solutions obtained by physicists using essentially the same approach to the calculation of average level spacings, strength functions and radiation widths in the two hypothetical nuclei for which artificially generated resonance parameters were supplied. It was agreed at the April 1981 meeting of NEANDC that a workshop should be held at the NEA Data Bank in October 1981 for the participants in this intercomparison.

The aim of the workshop is to identify the origin of the discrepancies between different solutions; in order to provide a clearer basis for discussion, a second exercise is being distributed to the original participants, and to a small number of other physicists who did not submit solutions but who regularly carry out calculations of this kind and may wish to join the exercise now. Intending participants will be asked to send in advance of the meeting their solutions, a detailed account of the calculational route followed, and tape copies of the source files for the programs used.

The second calculation exercise

Data for calculating two cases each, of three stages of complexity in calculation, are being sent separately to participants in the previous exercise:

(a) two cases of pure reduced neutron width distributions (the only quantity to be determined is $< \Gamma_n^o >$).

(b) two cases of resolved resonance parameters, without any experimental effect.

(c) two cases of pseudo-experimental resonance parameter sets, similar to case 1 of the previous exercise (account has been taken of Dr. Weigmann's comments).

It is hoped that obtaining consistent results for (a) will present no problem. Possible differences in the results obtained for (b) and (c) should allow it to be established whether the discrepancies are due to the way in which contamination by p-wave resonances is allowed for, or whether they result from the treatment of experimental effects.

It was clear from discussions during the analysis of the previous exercise that most of the methods used are not fully prescribed, but that the physicist must apply his judgement in choosing input parameters (such as neutron width threshold) for the calculation. These choices, and the reasons for them, should be presented clearly in the notes accompanying the solution. Where possible, the effect on the results of varying these choises should be investigated.

The following material should be sent to arrive before 1st October 1981, to:

Dr. Pierre RIBON
DEDR-DRE-SERMA
Centre d'Etudes Nucléaires de Saclay
91191 Gif-sur-Yvette CEDEX
(France)

- Solutions and the author's detailed comments.

- The program source files including all subroutines and a sample test case with results.
  If programs are submitted in time, it is hoped to implement them on an IBM computer, and to run some test cases during the two-day meeting where it appears desirable for a good understanding of calculation procedures.

Queries about the calculation exercise should be addressed to Dr. Ribon. As participation in the workshop will be very limited, we do not think it appropriate to preserve anonymity within it, though it can if necessary be restored in any publication resulting from it.

Participation

Participation in the workshop is restricted to scientists nominated, in the case of OECD Member countries, by national representatives on NEANDC. The International Atomic Energy Agency is invited to submit nominations for a limited number of participants from non-OECD countries. All intending participants should have submitted solutions to one of the two exercises. Overall participation will be strictly limited to 12-15 persons.

Nominations should be sent to :

Dr. N.A. TUBBS
NEA Data Bank
91191 Gif-sur-Yvette CEDEX
(France) Telex: 690920

with a copy to Dr. P. Ribon at the address above.

V. Contributed papers

In the following section the full text of the contributed papers are enclosed in the order in which they were received (see: III. List of working papers).

DIFFERENCES IN THE DOPPLER BROADENING OF NEUTRON RESONANCES IN CRYSTALS AND GAS STUDIED AT THE 6.7 EV RESONANCE OF ^{238}U

A. Meister, D. Pabst[+], L.B. Pikelner[+], W. Pilz[+], D. Seeliger, K. Seidel, R. Tschammer[+]

Technical University Dresden, GDR
[+]Joint Institute for Nuclear Research Dubna, USSR

The search for the chemical (isomer) shift of neutron resonances required a careful study of Doppler broadening of the resonance in different crystal lattices. Transmission spectra were measured with time-of-flight technique at the pulsed fast reactor IBR-30 and a procedure was made which allowed the determination of differences between the spectra of U - metal, UO_2, UF_4, UO_3 and $UO_2(NO_3)_2 \cdot 6 H_2O$.

The differences in the Doppler broadening can not be described with the commonly used free-gas model. The interpretation is possible with an expression for the weighted normal-mode frequency spectrum of the crystal oscillations of $g(h\nu) = a_1 \delta(h\nu - h\nu_1) + a_2 \delta(h\nu - h\nu_2)$

In the paper the cross section behaviour in the region of the 6.7 eV resonance of ^{238}U with Doppler broadening taking into account crystalline binding is compared with that of the free-gas model (temperature parameter is taken equal to the sample temperature as well as to the effective Lamb-corrected temperature) for Uranium-metal and UO_3 at 300 K and 600 K. The influence on resonance parameters is discussed.

1. Introduction

The hyperfine interaction between the electrons of an atom and the protons of the nucleus should cause an energy shift of the observed neutron resonances between different chemical compounds of the atom (different electron density at the nucleus) if the nuclear mean-square charge radius $\langle r^2 \rangle$ is changed by the capture of a neutron. The determination of this energy shift could permit to deduce $\langle r^2 \rangle$ values of highly (by the neutron binding energy) excited states.

However not about the results of $\langle r^2 \rangle$ obtained for $^{238}U+n$ [1] may be reported in this paper but some results are presented, which have been important for the analysis of the measurement: the different Doppler broadening of low-lying Uranium resonance in different chemical compounds.

2. Experiment

The time-of-flight arrangement for the measurement of transmission spectra in the beam of the pulsed fast reactor IBR-30 with booster [2] is shown in Fig. 1.

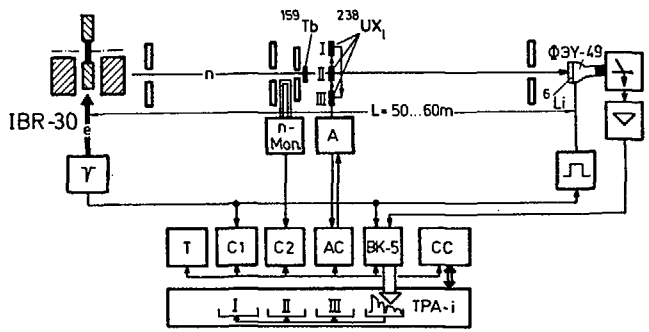

Fig. 1: Experimental arrangement
IBR-30,e: pulsed reactor with booster;
$^{238}UX_1$: samples with Uranium compounds;
^{159}Tb: reference sample;
ФЭУ-49,^{6}Li: neutron detector;
TPA-i: minicomputer as processor;
CC: Camac crate controller;
BK-5: time coder;
C1, C2: counter;
AC, A: sample changer

The measuring procedure is concentrated on equal experimental conditions for the three samples (I, II, III) containing different chemical compounds of Uranium. Several special tests are carried out during the experiment to guarantee the stability of the whole experimental procedure. For instance, the measurement is divided in cycles of short-time runs, after every of which stability of beam and equipment are tested and only those spectra accumulated for which all required conditions are fulfilled. The mean pulse density in the detector - direct memory access tract is up to $5 \cdot 10^5 s^{-1}$. Differences between transmission spectra, accumulated during about 10 h, are shown in Fig. 2 and Fig. 3 for three and two samples respectively after elimination of the resonance position shift.

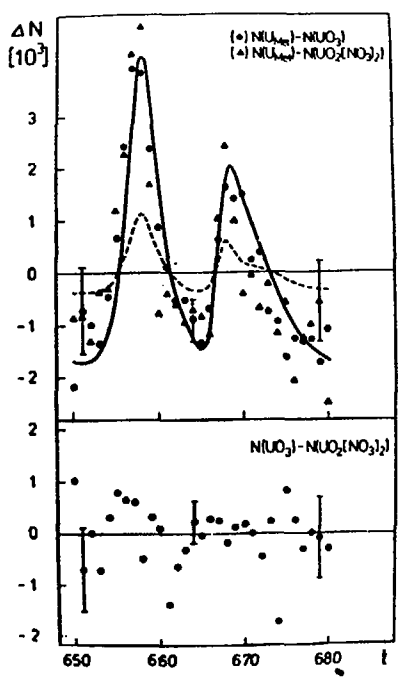

Fig. 2:

Differences of transmission spectra between the indicated sample pairs with $1.19 \cdot 10^{21}$ nuclei/cm² at room temperature. The width of the time channels t is 2.5 μs. The full line corresponds to $\langle \epsilon \rangle_U / kT = 1.080$ for UO_3 and $UO_2[NO_3]_2$, the dashed line to $\langle \epsilon \rangle_U / kT = 1.038$, whereas for metal in all cases $\langle \epsilon \rangle_U / kT = 1.015$ is used.

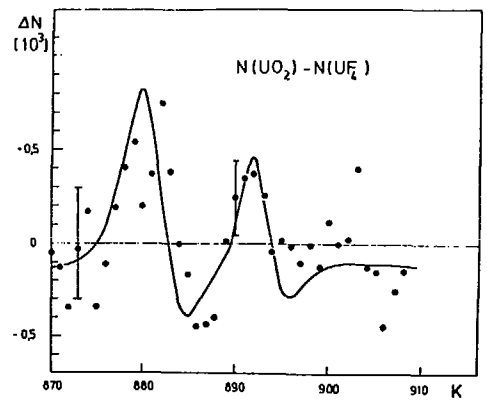

Fig. 3: The same as Fig. 2, but for the pair UO_2 - UF_4 with $0.552 \cdot 10^{21}$ nuclei/cm² and a time channel width of 2.0 μs. $\langle \epsilon \rangle_U / kT$ has been choosen 1.023 for UO_2 and 1.034 for UF_4 respectively

3. Interpretation

These measurements and additional ones with the compounds mentioned above at higher temperatures, with changed sample thickness, and small temperature differences between the samples [1] could not be interpreted with the commonly used model for the description of Doppler broadening, the free-gas model, where, following Lamb [3], on the place of the sample temperature effective temperature parameters T_{eff} in the expression of the Doppler width are used which correspond to the mean energy per degree of freedom of the Uranium atom oscillations in the crystal lattice

$$\langle \epsilon \rangle_U \quad \text{by} \quad \langle \epsilon \rangle_U = k\, T_{eff} \qquad (1)$$

However, sufficient agreement is obtained, as the Fig. 2 and Fig. 3 show, if the crystalline binding of the atoms is taken into account by an weighted normal - mode frequency spectrum of the oscillations of the following type [4]

$$g(h\nu) = a_1 \cdot \delta(h\nu - h\nu_1) + a_2 \cdot \delta(h\nu - h\nu_2) \qquad (2)$$

The parameters in this expression act in first order only in the following combination

$$\langle \epsilon \rangle_U = \frac{1}{2} \int_0^\infty d(h\nu) \cdot h\nu \cdot g(h\nu) \cdot \coth(h\nu/2kT), \qquad (3)$$

values of which could be obtained for the studied compounds from the measured differences [1] and are given inserted in the figure captions. For metal, a crystal with atoms of one type only, the parameters are choosen according to Ref. [4] with $a_1 = 1.0$, $a_2 = 0.0$, and $h\nu_1 = 0.011$ eV, which corresponds to $\langle \epsilon \rangle_U = 1.015$ kT at a sample temperature of T = 300 K.

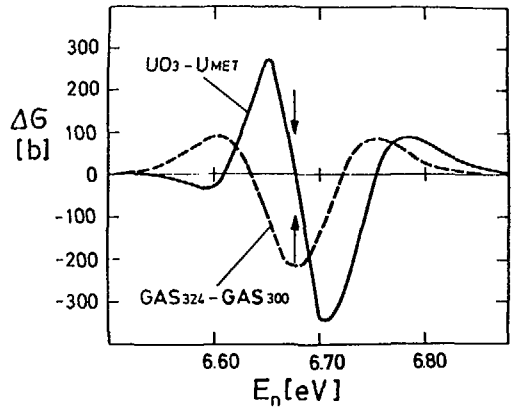

Fig. 4: Cross section differences between UO_3 and Uranium metal at T = 300 K if the Doppler broadening of the resonance is calculated with a crystal oscillator treatment by (2) (full line) and with effective temperature gas model (T_{eff} = 324 K, dashed line). The bars indicate the resonance maximum.

4. Comparision of gas model predictions with a crystal oscillator treatment

The largest differences occur between UO_3 and Uranium metal. For this pair in Fig. 4 the results of both models are compared directly. There are qualitativ differences, above all the gas model doesn't reproduce the asymmetric behaviour relatively to the resonance maximum.

Group cross sections employed in reactor calculations, are integrals over certain energy (lethargy) intervals with (in this energy region) Doppler broadened resonances in the kernel. An asymmetric behaviour on the energy scale in contrast to a symmetric one (gas model, Ψ-χ functions) should in principle have an influence.

In Fig. 5 differences and quotients of the resonance cross sections between both procedures are shown directly. As ecpected, for metal with the lowest Debye temperature they are small, for UO_3 about five times larger. The other compounds are placed between these examples, according to their $\langle \epsilon \rangle_U/kT$ - values. The use of T_{eff} instead of T in the gas model reduces slightly the asymmetry only. An enhancement of the temperature by a factor of two reduces the deviations to almost the half.

To extimate the influence of the different Doppler broadening procedures on the determination of resonance parameters with the usually used least - square fit, a Doppler broadened resonance expression with the parameters of UO_3 in (2) is fitted by variation

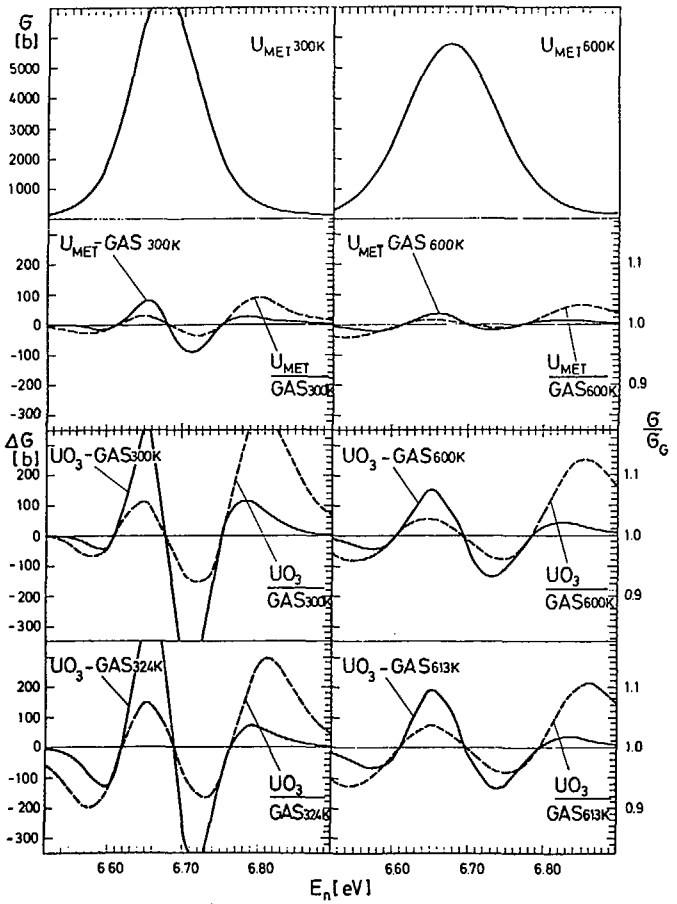

Fig. 5: Resonance cross sections, differences (full lines) and quotients (dashed lines) between crystal oscillator treatment and gas model with T = 300 K and T_{eff} = 324 K as well as T = 600 K and T_{eff} = 613 K respectively.

of Γ_n and Γ to the resonance form of the free gas model with T = 300 K. The fitted parameters differ from the reference one in the gas model procedure by 4 % and 0.4 % in the case of Γ and Γ_n respectively. At the temperature for which experimental data are fitted, a different Doppler broadening procedure is only another parametrization with changed values for Γ and Γ_n. However, in the order of magnitude as the differences to the gas model are diminished with increasing temperature (Fig. 5) the values of Γ and Γ_n should become temperature dependent in the case of the gas model.

References

[1] Seidel, K. et al., Comm. of the JINR Dubna, P3-11740 (1978), P3-11741 (1978), P3-11742 (1978), P3-80-135 (1980). Meister, A. et al., Nucl.Phys. A 362 (1981) 187.

[2] Golikov, V.V. et al., Comm. of the JINR Dubna, 3-5736 (1971).

[3] Lamb, W.E., Phys.Rev. 55 (1939) 190.

[4] Jackson, H.E. and J.E. Lynn, Phys. Rev. 127 (1972) 461.

ESTIMATE OF AVERAGE LEVEL SPACING AND S-WAVE NEUTRON STRENGTH FUNCTION FOR ^{241}Pu RESONANCE DATA

C. Bonifazzi and E. Menapace

Comitato Nazionale Energia Nucleare, C.S.R. "E.Clementel", Bologna (Italy)

The statistical analysis of neutron resonance parameters developed in refs [2,3]) was applied to the same set of data of ^{241}Pu neutron resonances quoted in ref. [1]). The ^{241}Pu is a fissile not even even nucleus and this makes it difficult to meet the applicability conditions of the method, i.e. the possibility to find a reasonable threshold for $g\Gamma_n$ above which all resonances are observed. In fact a non negligible overlapping probability is to be expected between s-wave neutron resonances of different spin; furthermore the strong interference terms prevent a correct statistical description of the experimental resolution of close doublets.

The maximum likelihood estimation method, refs [2,3]) was applied to the Montecarlo simulation of the set of data for different values of the threshold on $g\Gamma_n^o$ and of the one on the spacing of close doublets. This allowed to study the bias introduced by a finite experimental resolution in the maximum likelihood estimate of the average spacing D.

The results of the analysis of the experimental set of data assuming that no resonance is missed due to overlapping are given in figs 1.a) and 1.b) (open circles) for different observability thresholds $\eta(E)$ on $g\Gamma_n$ value.

The threshold function $\eta_o(E) = \sqrt{E}$ was deduced from the experimental data and allowed to vary by a multiplicative factor α.

One can see that above $\alpha = 0.3$ the data are rather stable with $D = 1.0$ (eV) and $\langle g\Gamma_n^o \rangle = 0.118$ (meV)$^{\frac{1}{2}}$. The increasing D value for $\alpha < 0.3$ is due to the missed s-wave resonances above the threshold.

The dotted lines represent the standard deviations of Montecarlo simulation, with $D = 1.0$ (eV) and $\langle g\Gamma_n^o \rangle = 0.118$ (meV)$^{\frac{1}{2}}$ as population averages, without loss of levels due to the finite resolution of doublets. In this case no appreciable bias is present.

The situation changes if one allows for a finite resolution considering each doublet with spacing less than λ as a singlet resonance. The threshold function λ is introduced to consider the overlapping effect and is chosen to be a constant over the total energy range.

The results of simulation performed taking into account the density of resonances with spin $J^\pi = 2^+$ and $= 3^+$ are shown in fig. 1.c) where the estimated D value averaged over 20 simulated experiments is plotted against λ. Apart from statistical fluctuations one can see that the estimated D is affected by a bias toward larger values which increases almost linearly with λ. In fact the two s-wave neutron resonance sequences make the Wigner level repulsion less effective than the case of an even even nucleus with only one resonance sequence. In this case the bias in D estimate would go to zero more rapidly with λ.

It is very difficult to find the real value of λ from experimental information and measured parameters, ref. [1]). The Montecarlo simulations performed by the authors estimate the missed resonances, because unresolved doublets, as 9% of the total number. This estimate corresponds to $\lambda \approx 0.15$ in fig. 1c) which seems reasonable with the cross section energy dependence. The corresponding correction on the estimated D gives

$$\langle D \rangle = 0.91 \pm 0.05 \quad \text{eV}$$

where a possible variation of λ between 0.1 and 0.2 is included in the estimate of error. Comparing this value with the estimate $\langle D \rangle = 0.83$ (eV) given in ref. [1]) one can have an idea of the kind of agreement one can obtain using different methods of analysis in cases like the present one of ^{241}Pu, in which no clear statistical assumption can be made about spurious experimental effects (see ref. [4])).

The estimated value of neutron strength function is obviously the same as ref. [1]), i.e. $S_o = 1.18 \times 10^{-4}$, because the unresolved doublets affect the estimate of $\langle g\Gamma_n^o \rangle$ and D in a correlated way so that the value of S_o is practically unchanged.

The authors wish to thank Drs. H. Derrien, M. Motta and M. Stefanon for helpful suggestions and stimulating discussion.

References

1) I. Blons and H. Derrien, Le Journal de Phisique 37 (1976).
2) C. Ccceva and M. Stefanon, Nuclear Physics A315 (1979) 1.
3) M. Stefanon, Nuclear Instruments and Methods 174 (1980) 243.
4) M. Stefanon, Proc. Spec. Meet. on F.P. Neutron Cross Sections, Eds. C. Coceva, G.C. Panini, Bologna, December 12-14, 1979.

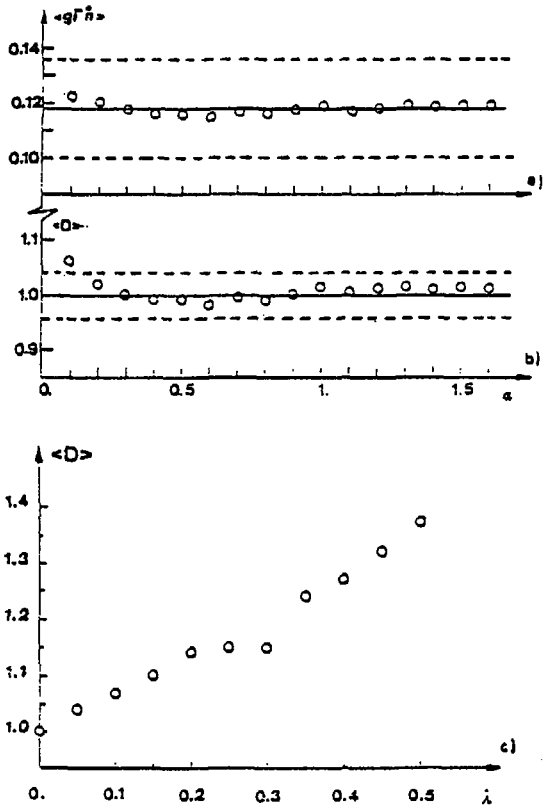

fig. 1

DOPPLER MEASUREMENTS OF ^{238}U

By

Robert M. Brugger*†°

Habib Aminfar*‡

Abstract

The effect on the total cross section of self-shielding of resonances of ^{238}U as the samples become thicker has been measured for 2, 24 and 144keV neutrons. The effect of Doppler broadening of these shielded resonances as the temperature increases has been measured for 2keV neutrons. These measurements have been made for ^{238}U in the chemical forms of solid metal, liquid metal, U_3O_8, UO_2 and UC. The measured changes in cross sections have been fit by a model having a ladder of nuclear resonances which are Doppler broadened by an ideal gas model. The gas model not only includes an effective temperature to account for zero state vibrational motions at lower temperatures, but also includes an effective mass to account for chemical binding. While most of the curves show a change in cross section vs temperature that is continuous, a step change was observed in the total cross section of U metal when the metal was melted.

*Nuclear Engineering Department, University of Missouri, Columbia, Missouri.
†Physics Department and Research Reactor Facility, University of Missouri, Columbia, Missouri.
°Present address: Physics Division, Los Alamos National Laboratory.
‡Mansour Ave. near bridge, Tabriz, Iran.

I. Introduction

In a previous experiment (1) the effective average total corss section EATSC of ^{238}U was measured. EATSC was defined as that cross section σ that was determined from $T = \exp(-n\sigma)$ when T is the transmission that is measured, and n is the number of U atoms per cm^2. In these experiments, first the effect of resonance self-shielding on EATSC was measured as n was increased. The measurements were at 300K for samples of ^{238}U metal and $^{238}U_3O_8$, and T ranged from 0.97 to 0.1. The measurements were made for bands of neutrons centered at 24 and 144 keV and with band widths of 2 and 24keV. Since O has no resonances in these bands, its effect could be directly subtracted from the cross section at all n. The total cross section of O was taken from ENDF/B.

^{238}U has hundreds of resolved and unresolved resonances in these bands which produce self-shielding as n increases and the measurements showed the self-shielding. They also showed that the EATSC of ^{238}U in metal is different from that of ^{238}U in U_3O_8. Both are smaller than σ(ENDF/B) at large n but approach σ(ENDF/B) as the n's approach zero.

The next set of measurements in the experiment of reference 1 determined EATSC for ^{238}U in metal and in U_3O_8 as the temperature was increased to 1000K. Here the n's were values which gave T ≅ 0.5. The data show an increase in EATSC as the temperature increases. An empirical fit to the data from both sets of experiments was achieved when the resonances of ^{238}U were defined by a single set of nuclear parameters, and an ideal gas model was used to account for Doppler broadening. In the ideal gas model the temperature was the effective temperature T_{eff} of Lamb (2), but for the mass, an effective mass M_{eff} was required to account for chemical binding.

In the experiments reported here (3) the previous experiments have been extended to:

- o a band of 2keV neutrons
- o an upper temperature of 1450K
- o samples of UO_2 and UC

The band of 2keV neutrons extends the energy range one decade lower to where the resonances in ^{238}U are better resolved and to where the Doppler effect is more pronounced. The temperature was pushed up to 1450K for U metal to see if EATSC changed on melting. UO_2 and UC were added as samples to include the other chemical forms of U that are being considered as fuel for fast reactors.

The next section briefly reviews the experiments; the third section presents the data; and section IV includes discussions and conclusions.

II. Experiment

The experimental arrangement was the same as in reference 1 and is described in detail in reference 3. Total cross sections were determined by measuring the transmissions of samples in good geometry. The Si filter passing 144keV neutrons and the Fe filter passing 24keV neutrons have been described before (4). A Sc filter passing 2keV neutrons was developed for this experiment (5). The uniqueness of the Sc filter at the University of Missouri Research Reactor is that it includes separated isotopes of ^{54}Fe and ^{60}Ni to improve the beam purity. The band widths of these three filtered beams are 24keV, 2keV and 0.7keV, respectively.

The samples were either placed on a platform that could be oscillated to perform "sample in"/"sample out" measurements, or were placed in a furnace for heating. Collimators defined the beam before and after the sample to prevent diffusion and multiple scattering from effecting the results. A Hansen McKibben-type long counter was used to detect the transmitted neutrons.

Each filtered beam had some flux of gamma-rays accompanying the neutrons. These gamma-rays were used to simultaneously measure, as the samples were heated, the change in density of the sample. Then a correction for density change was made to the neutron transmission so that changes in EATSC reflect only the broadening and self-shielding of resonances and not a change in n/cm^2 of the sample.

Several tests were run to verify the method. Neutron cross sections of well characterized materials, such as Al and C, were measured. These agreed with ENDF/B values. Using the gamma-rays the density of graphite was measured as a function of temperature. This agreed with published values. The EATSC of graphite was measured as a function of temperature. This did not change with temperature which agreed with the fact that C has no resonances between 2 and 144keV. Using the gamma-rays, the density changes of the solid U metal, liquid U metal, U_3O_8, UO_2 and UC were measured as a function of temperature. These agreed with published data. Figure 1 shows the data for the density change measured for solid and liquid U metal. All the tests indicated that the experiment was working as intended.

To fit the EATSC data once it had been obtained, the U3R program was obtained from ANL (6). This program uses averaged nuclear parameters as input and calculates ladders of resonances to represent the cross section. An ideal gas model was used to Doppler broaden the resonances before transmissions were calculated. The transmissions for given thicknesses were averaged over the energy bands. The averaged transmission was then used to calculate an EATSC for each thickness.

III. Data

Figures 2, 3 and 4 show the EATSC measured at 300K for ranges of thicknesses. These data show the effect of self-shielding of resonances. The data approach the ENDF/B value of the cross section for thin samples where there are too few nuclei to produce shielding. The EATSC drops as the samples are thickened and self-shielding increases. The cross section for O and C have been removed by subtraction. One notes that the EATSC's for ^{238}U do not fall on a single curve but forms a curve for each of the compounds.

The curves of Figures 2, 3 and 4 were calculated using the U3R program. The set of nuclear parameters used in these calculations are listed in Table I along with the set that was used to fit the data of reference 1. In Table II are given the Debye temperatures, from which T_{eff} can be calculated, and the M_{eff}'s that were used to produce the curves. The only satisfactory fits to all the data when using a single set of nuclear parameters required that both a T_{eff} and M_{eff} be used in the ideal gas model to represent Doppler broadening.

Figures 5, 6, 7 and 8 show the EATSC data measured as a function of temperature for samples of U metal, U_3O_8, UO_2 and UC for neutrons of 2keV. The lines are again fits using the U3R program with the ideal gas model and the parameters of Tables I and II.

For the metal, a step in EATSC was observed at the melting point. This is similar to what was observed for Sn metal (7). To describe the step with the U3R program required that an M_{eff} = 100-150amu be used in the calculations.

IV. Discussion and Conclusions

The data measured in this experiment and presented in section III show similar effects as were observed in reference 1. The EATSC's measured as a function of thickness show self-shielding as the samples thicken, and the amount of self-shielding is different depending upon whether the U is bound as a metal, or as an oxide, or as a carbide. The EATSC's measured as a function of temperature show a Doppler effect, and the magnitude of the change in EATSC is different depending upon whether the U is bound as a metal, or as an oxide, or as a carbide. Both self-shielding and Doppler effect are more pronounced for 2keV neutrons than for 24keV neutrons or for 144keV neutrons. At the melting point a step in EATSC of U metal was measured. This behavior of EATSC for U indicates that the Doppler broadening of the resonances of ^{238}U are effected by chemical binding.

As in reference 1 a model to describe the cross section of ^{238}U was used which treats the resonances in the

TABLE I

Nuclear Parameters of ^{238}U Resonances Used to Fit the Data

	Reference 1	This Work
R x 10^{-12}(cm)	0.94	0.94
Γ_T (eV)	0.019	0.019
S-Wave	l=0 J=1/2	
S	0.943 x 10^{-4}	0.995 x 10^{-4}
Γ_n^o (eV)	1.961 x 10^{-3}	2.1 x 10^{-3}
<D> (eV)	20.8	21.1
P-Wave	l=1 J=1/2	
S		
Γ_n^o (eV)	3.409 x 10^{-3}	3.409
<D> (eV)	20.8	20.8
P-Wave	l=1 J=3/2	
S		
Γ_n^o (eV)	1.7 x 10^{-3}	1.7 x 10^{-3}
<D> (eV)	10.4	10.4

TABLE II

Comparison of Effective Mass and Debye Temperature of ^{238}U Metal, U_3O_8, UO_2 and UC

Compound	Effective Mass (amu)	Debye Temperature (K)	Reference	Methods of Debye Temperature Determination
^{238}U Metal (liquid)	100-150	260	This Work	Doppler Effect Measurement
^{238}U Metal (solid)		210	12	X-ray Diffraction
	238	260	1	Doppler Effect Measurement
	238	260	This Work	Doppler Effect Measurement
U_3O_8		516	12	X-ray Diffraction
	400	545	1	Doppler Effect Measurement
	835	505	This Work	Doppler Effect Measurement
UO_2		620	13	X-ray Diffraction
	600	590	This Work	Doppler Effect Measurement
UC		265	14	X-ray Diffraction
		366	14	X-ray Diffraction
	400	265	This Work	Doppler Effect Measurement

energy bands as a ladder of resonances having a set of averaged nuclear parameters. These resonances were then Doppler broadened using an ideal gas model which incorporated not only a T_{eff} to account for zero state vibrations, but a M_{eff} to account for chemical binding. For any energy band the nuclear parameters should be the same for ^{238}U in any chemical form. Thus, for example, one cannot have two sets of nuclear parameters to fit U in metal and U in UO_2. Since $T_{eff} \rightarrow T_{real}$ as T_{real} increases and approaches the Debye temperature, T_{eff} shows no variation for U in metal as compared to U in UO_2 at higher temperatures. This says that T_{eff} cannot be adjusted to fit both U metal and UO_2 data for example. Therefore, it was found necessary to introduce an M_{eff} to have some parameter in the ideal gas model that would permit fitting of the data.

An adjustable M_{eff} also allowed fitting of the step in the solid U metal to liquid U metal data. An M_{eff} <238amu does not seem realistic; it shows only that an adjustable parameter is needed. To approach more realistic values, all the data need to be refit with a new set of nuclear parameters and larger M_{eff}'s for all samples. However, the present fit is an empirical description that fits all the data.

Other evidence of similar behavior of the Doppler effect would help to confirm the empirical approach of this paper. Criticality measurements of fast reactor assemblies (10) have found a consistent error in the calculated to measured value of the ^{238}U activation reaction rate. Brugger and Loyalka (11) have made simple calculations of the activation reaction rate and observed a difference which depends upon the chemical form of the ^{238}U near the activation foil. Detailed reaction rate calculations using sophisticated reactor codes should now be performed to follow up on these suggestions.

Acknowledgements

This research was partially supported by the National Science Foundation. The authors thank Argonne National Lab and Los Alamos National Lab for providing the samples.

References

1. F. Y. Tsang and R. M. Brugger, Nucl. Sci. & Engr. 72, 52 (1979).

2. W. E. Lamb, Phy. Rev. 55, 190 (1939).

3. H. Aminfar, "Doppler Measurements of ^{238}U", Ph.D. Dissertation, Nuclear Engineering Department, University of Missouri, Columbia, Missouri 65211, July (1981).

4. F. Y. Tsang and R. M. Brugger, Nucl. Inst. & Methods 134, 441 (1975).

5. H. Aminfar and R. M. Brugger, Nucl. Inst. & Methods, accepted for publication (1981).

6. J. M. Otter, R. C. Lewis and L. B. Levitt, U3R Computer Code, AT(04-3)-824 (1972).

7. F. Y. Tsang and R. M. Brugger, Nucl. Sci. & Engr. 74, 34 (1980).

8. Reactor Handbook - Materials USAEC, McGraw-Hill Book Company, Inc., New York (1955).

9. J. H. Gillus, "Uranium", Metallurgy of Rarer Materials-8, London, Butterworth (1963).

10. P. J. Collins, H. F. McFarland, C. L. Beck, M. J. Lineberry, S. G. Carpenter, G. A. Ducat, J. M. Gasidlo and R. W. Goin, "Fast Reactor Physics 1979", Vol. II lAEASM-244/70, 57 (1980).

11. R. M. Brugger and S. K. Loyalka, Proceedings of the Annual ANS Meeting, San Francisco, November (1981).

12. P. W. Powell and Y. W. Touloukian, Science 181, 994 (1973).

13. G. Dolling, R. A. Cowley and A. D. Woods, Canadian Journal of Physics 43, 1397 (1965).

14. R. Colella, D. Dragone and A. Merlevi, Phy. Stats. Sol. 36, 135 (1969).

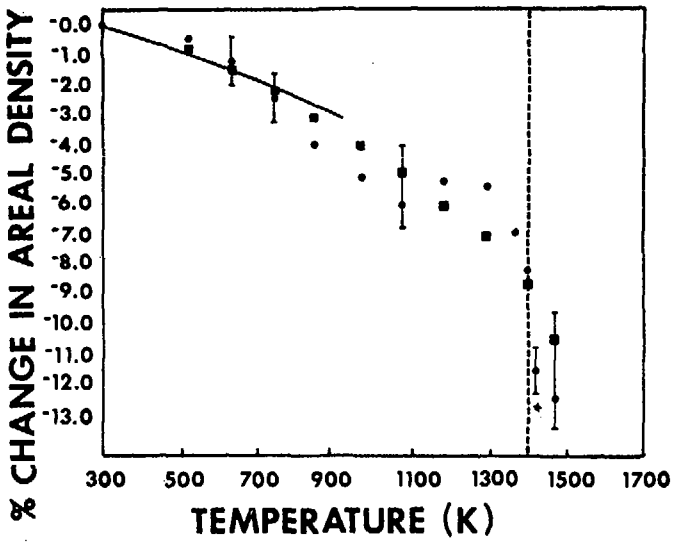

1. The percent change in area density as measured for the samples of ^{238}U metal. The vertical dashed line is the melting point of U metal. The solid line is calculated from linear expansion coefficient data from references 8 and 9. The points ● are for the sample having n=0.059 nuclei/barn and ■ for n=0.023 nuclei/barn. The ★ is calculated for liquid U of density 16.63g/cm^3.

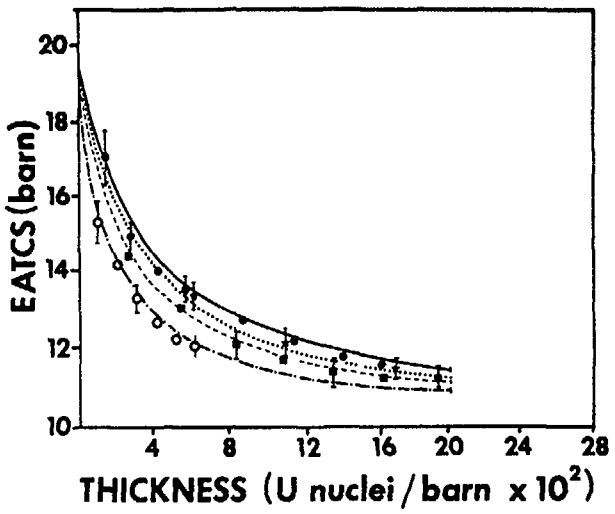

2. The EATCS of ^{238}U as metal (●, —), U_3O_8 (○, —·—), UO_2 (■, - - -) and UC (★, •••). The samples were at 300K and the neutron band was centered at 2keV. The curves are from U3R calculations.

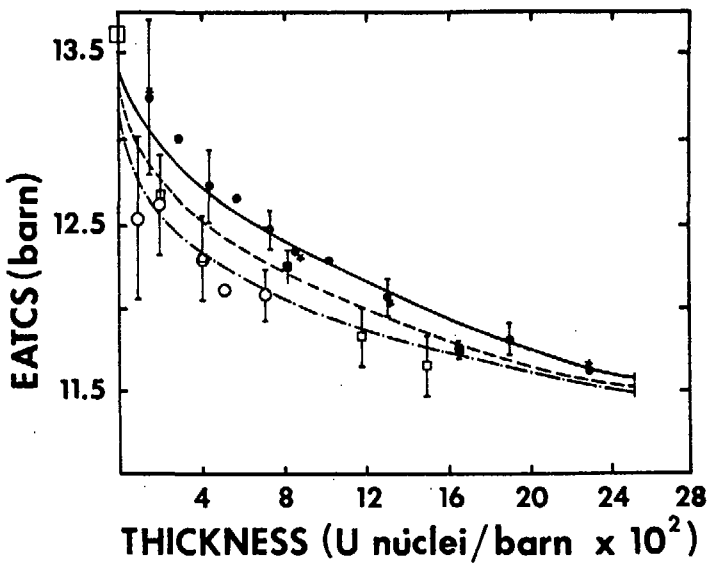

3. The EATCS of ^{238}U as metal (●,——), U_3O_8 (○,—·—), UO_2 (■,---), metal from reference 1 (★), U_3O_8 from reference 1 (□) and ENDF/B-IV (☐). The samples were at 300K and the neutron band was centered at 24keV. The curves are from U3R calculations.

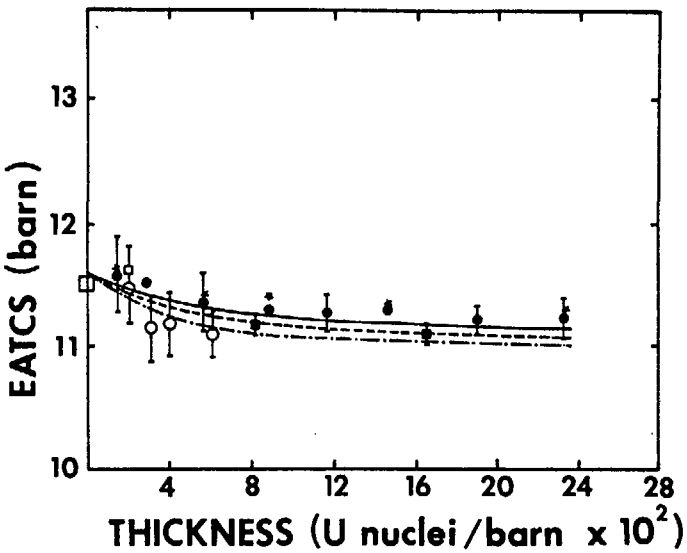

4. The EATCS of ^{238}U as metal (●,——), U_3O_8 (○,—·—), UO_2 (■,---), metal from reference 1 (★), U_3O_8 from reference 1 (□) and ENDF/B-IV (☐). The samples were at 300K and the neutron band was centered at 144keV. The curves are from U3R calculations.

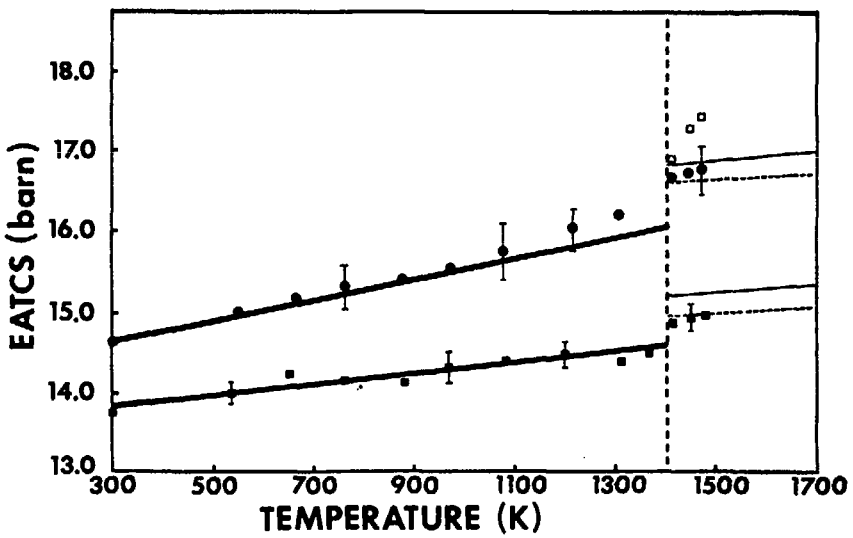

5. The EATCS of ^{238}U metal for 2keV neutrons. The points ● are for n=0.23 nuclei/barn, ■ are for n=0.059 nuclei/barn and □ are for n=0.022 nuclei/barn. The lines are from U3R calculations where ▬ is for M_{eff}=238amu, - - - is for M_{eff}=150amu and —— is for M_{eff}=100amu. The vertical dashed line is the melting point of U metal.

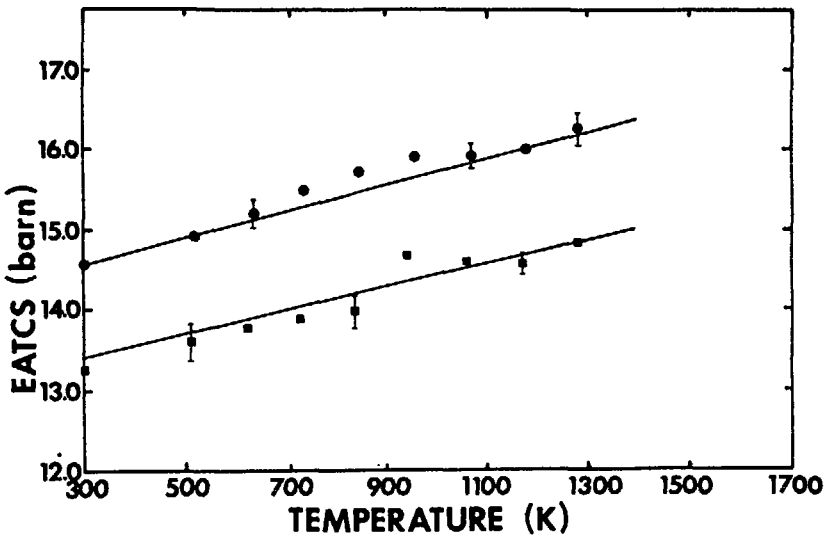

6. The EATCS of ^{238}U in U_3O_8 for 2keV neutrons. The points ● are for n=0.021 U nuclei/barn and ■ are for n=0.0303 U nuclei/barn. The lines are from U3R calculations where M_{eff}=835amu.

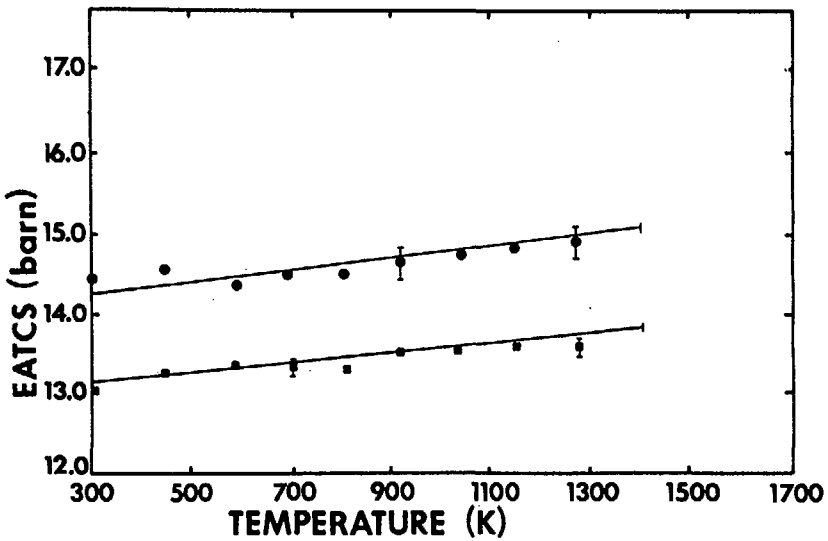

7. The EATCS of ^{238}U in UO_2 for 2keV neutrons. The points ● are for n=0.0265 U nuclei/barn and ■ are for n=0.0538 U nuclei/barn. The lines are from U3R calculations where M_{eff}=600amu.

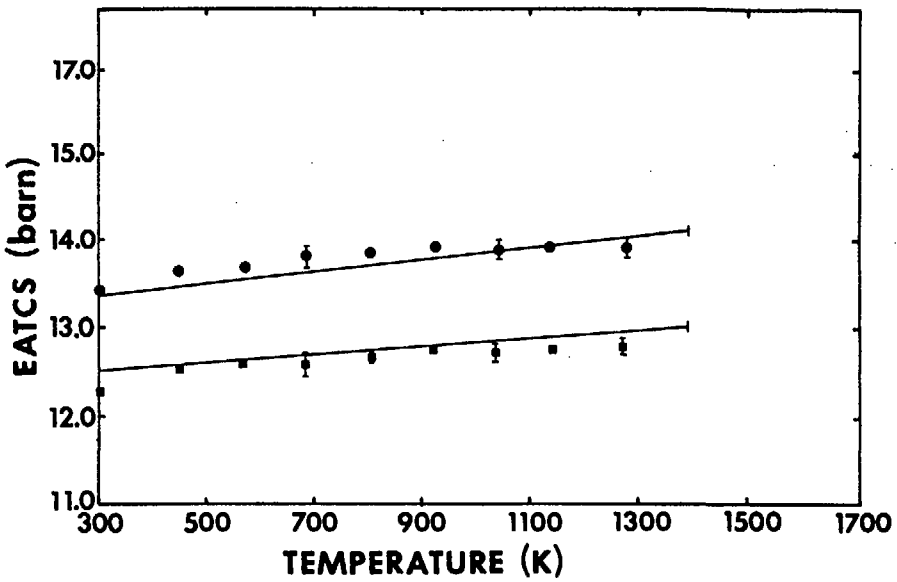

8. The EATCS of ^{238}U in UC for 2keV neutrons. The points ● are for n=0.0603 U nuclei/barn and ■ for n=0.110 U nuclei/barn. The lines are from U3R calculations where M_{eff}=400amu.

Evaluation of Resonance Parameters of ^{238}U, ^{240}Pu and ^{242}Pu

T. Nakagawa*, A. Zukeran** and M. Kawai***
Japanese Nuclear Data Committee, Japan Atomic Energy Research Institute

Abstract

The evaluation of the resolved resonance parameters of ^{238}U, ^{240}Pu and ^{242}Pu was performed for the second version of Japanese Evaluated Nuclear Data Library JENDL-2. In this work, all the resonance parameters measured so far were compiled and examined. The evaluation was made by mainly using recent measurements for each isotope. The presently evaluated resonances are 183 s-wave and 265 p-wave resonances up to 4.73 keV for ^{238}U, 267 s-wave resonances up to 5.69 keV for ^{240}Pu and 95 s-wave resonances up to 1.89 keV for ^{242}Pu. For ^{238}U and ^{240}Pu, negative resonances were also recommended. The multi-level Breit-Wigner formula was applied, and the their resolved resonance regions were chosen to be from 10^{-5} eV to 4 keV for ^{238}U and ^{240}Pu and from 10^{-5} eV to 1.29 keV for ^{242}Pu. Furthermore, background cross sections were determined to correct the cross sections calculated from the evaluated resonance parameters.

1. Introduction

The first version of Japanese Evaluated Nuclear Data Library JENDL-1[1] was released in 1977. In JENDL-1, the resolved resonance parameters of ^{238}U and ^{240}Pu were mainly taken from ENDF/B-IV[2] because our own evaluation work had not been completed. The data of ^{242}Pu were not contained in JENDL-1.

New experimental data of resonance parameters for these three nuclides have been accumulated after the compilation of JENDL-1. For ^{238}U, low lying resonances were particularly investigated, because benchmark tests[3] for thermal reactors indicated that the underprediction of criticality was due to too large capture widths of the low lying resonances. Transmission measurements were carried out also at various laboratories in wide energy ranges. New measurements of the sub-threshold fission were also performed for ^{238}U, ^{240}Pu and ^{242}Pu. These new data are different from the evaluated parameters adopted in JENDL-1 more or less. This indicates the necessity for a new evaluation work of resolved resonance parameters for JENDL-2.

Our evaluation work of resolved resonance parameters was started around 1975. At first, measured resonance parameters were compiled by using the Resonance Parameter Storage and Retrieval System REPSTOR[4]. Evaluation was performed on the basis of these compiled data. The present evaluation of resonance parameters was mainly based on the recent experiments. The evaluation and results are described in this paper. The results are tabulated in Appendix. The presently evaluated data were compiled in JENDL-2 with ENDF/B format[5].

2. Evaluation of Resolved Resonance Parameters

2.1 Uranium-238

At the time of the JENDL-1 compilation, the most reliable evaluated data were those by McCrosson[6] for ENDF/B-IV who took account of data measured until about 1973. Many new experiments, however, have been made by various experiments since then.

In the present evaluation, the resolved resonance parameters measured until 1980[7-44] were compiled by using REPSTOR. By comparing them with one another, it was found that there were discrepancies among resonance energies and parameters. The present evaluation was carried out as follows.

Resonance energy

Systematic discrepancies were found in resonance energies reported by various experimenters. These discrepancies can be interpreted in

* Japan Atomic Energy Research Institute
** Energy Research Laboratory, Hitachi, Ltd.
*** Nippon Atomic Industry Group, Ltd.

terms of systematic errors of flight-path length and initial time delay in time-of-flight spectrometers. Neutron energies are represented as follows by using flight-path length L(m), time of flight t(sec) and initial time delay t_0 (sec),

$$E(eV) = \left(\frac{72.2977\ L}{t - t_0}\right)^2. \quad (1)$$

A systematic error of E caused by errors of L and t_0 can be written as

$$\Delta E(eV) = \frac{2\Delta L}{L} E + \frac{2\Delta t_0}{72.2977\ L} E^{3/2} . \quad (2)$$

In the present evaluation, measured resonance energies were compared with those of Olsen et al.[39] which were adopted as standards. An example of energy discrepancies between Rahn et al.[28] and Olsen et al. is shown in Fig. 1 where these discrepancies were reproduced by Eq. (2) with the least squares method. The solid curves in Fig. 1 give the fitted one and one standard deviations. After correction of resonance energies in each measurement by using Eq. (2), the resonance energies were averaged over all the measurements in order to obtain an evaluated value. In the present work, resonance levels reported by neither Poortmans et al.[38], Olsen et al.[36,39] nor Nakajima[44] were abandoned.

Finally we adopted 187 s-wave resonances including 4 negative ones and 265 p-wave resonances in the energy range from -113 eV to 4728.0 eV. The energy range where the cross sections are calculated from the resonance parameters was selected to be from 10^{-5} eV to 4 keV.

Neutron and capture widths

The neutron and capture widths were determined by taking account of resonance areas. In the case of ^{238}U, the resonance areas can be approximated as follows, because the sub-threshold fission widths are negligibly small.

(1) Thin sample transmission area

$$A_1 = 2\pi^2\lambda^2\, g\Gamma_n . \quad (3)$$

(2) Thick sample transmission area

$$A_2 = 2\pi\lambda \sqrt{g\Gamma_n(\Gamma_n + \Gamma_\gamma)} . \quad (4)$$

(3) Thin sample capture area

$$A_3 = 2\pi^2\lambda^2\, g\Gamma_n\Gamma_\gamma/(\Gamma_n + \Gamma_\gamma) . \quad (5)$$

(4) Thin sample scattering area

$$A_4 = 2\pi^2\lambda^2\, g\Gamma_n^2/(\Gamma_n + \Gamma_\gamma) . \quad (6)$$

For a certain resonance energy, these relations are essentially expressed as

$$a_1 = \Gamma_n, \quad (3')$$

$$a_2 = \sqrt{\Gamma_n(\Gamma_n + \Gamma_\gamma)} , \quad (4')$$

$$a_3 = \Gamma_n\Gamma_\gamma/(\Gamma_n + \Gamma_\gamma), \quad (5')$$

$$a_4 = \Gamma_n^2/(\Gamma_n + \Gamma_\gamma). \quad (6')$$

In the present evaluation, the values of a_1, a_2, a_3 and a_4 were calculated from the reported values of Γ_n and Γ_γ for each measurement. The values of a_1, a_2, a_3 and a_4 are less discrepant than the values of Γ_n and Γ_γ among the different measurements. Then, averaged values of a_1, a_2, a_3 and a_4 were obtained, by giving especially high weights to new data measured after 1977. The best values of Γ_n and Γ_γ were so obtained as to minimize the following sum of squares of residuals.

$$I = w_1[\langle a_1\rangle - \Gamma_n]^2 + w_2[\langle a_2\rangle - \sqrt{\Gamma_n(\Gamma_n + \Gamma_\gamma)}\ ]^2 + w_3[\langle a_3\rangle - \frac{\Gamma_n\Gamma_\gamma}{\Gamma_n + \Gamma_\gamma}\ ]^2 + w_4[\langle a_4\rangle - \frac{\Gamma_n^2}{\Gamma_n + \Gamma_\gamma}]^2, \quad (7)$$

where w_1, w_2, w_3 and w_4 are weights for residuals, and $\langle a_1\rangle$, $\langle a_2\rangle$, $\langle a_3\rangle$ and $\langle a_4\rangle$ stand for averaged values of a_1, a_2, a_3 and a_4, respectively. Figure 2 shows an example of the evaluation of Γ_n and Γ_γ of a resonance at 66.01 eV. Measured resonance parameters are shown in the figure together with errors, and four solid curves give the relations between Γ_n and Γ_γ corresponding to $\langle a_1\rangle$, $\langle a_2\rangle$, $\langle a_3\rangle$ and $\langle a_4\rangle$. In this example, the best values of Γ_n and Γ_γ were determined to be 24.9 and 22.9 meV, respectively. This method was applied to determine the neutron and capture widths of all the resonances where more than one experiments existed.

As the results of the present work, smaller capture widths were obtained for the low lying s-wave resonances on the basis of small values in recent measurements. An average capture width obtained from the present parameters is (23.6 ± 1.9) meV which agrees well with (23.5 ± 1.2) meV which is a weighted average of the reported values.

Sub-threshold fission width

The sub-threshold fission widths were determined from the fission resonance areas measured by Difilippo et al.[43] Finally, a total of 28 s-wave resonances were given their sub-threshold fission widths.

Effective scattering radius and formula

Olsen et al.[39] analyzed their transmission data with a shape analysis code by the multi-level Breit-Wigner formula in various energy intervals and obtained effective scattering radii for those intervals. We adopted the multi-level Breit-Wigner formula and the effective scattering radius of 9.48 fm obtained by averaging the values of Olsen et al. below 2.2 keV.

Correction of calculated cross sections

In order to take account of contributions from negative resonances, four s-wave resonances were added artificially. The first negative resonance was located at -41 eV and its neutron width was determined so as to reproduce at 0.0253 eV the capture cross section of (2.7 ± 0.02) barns, the elastic scattering cross section of (8.90 ± 0.16) barns and the total cross section of (11.60 ± 0.16) barns recommended in BNL-325 3rd edition[45].

Contributions from the resonances lying outside of the presently considered resonance range (truncation effects) were taken into account by using the picket-fence model. The truncation effects were approximated by

$$\Delta\sigma_{tot} = \frac{4\pi}{k^2} S_0\sqrt{E}\left[\frac{\langle\Gamma\rangle}{4}\,\frac{E^+ - E^- + D}{(E^+-E+0.5D)(E-E^-+0.5D)}\right.$$

$$\left. - \frac{1}{2}\ln\left(\frac{E-E^-+0.582D}{E^+-E+0.582D}\right)kR\right], \qquad (8)$$

$$\Delta\sigma_{cap} = \frac{\pi}{k^2} S_0\sqrt{E}\,\langle\Gamma_\gamma\rangle\,\frac{E^+ - E^- + D}{(E^+-E+0.5D)(E-E^-+0.5D)}, \qquad (9)$$

$$\Delta\sigma_{el} = \Delta\sigma_{tot} - \Delta\sigma_{cap}, \qquad (10)$$

where E^+ and E^- are the upper and lower limit energies, respectively, of the presently considered resonances. Equation (8) was derived by de Saussure et al.[46] and Eq. (9) was obtained in this work with the same procedure. The following values were applied to calculate Eqs. (8), (9) and (10).

$S_0 = 1.1 \times 10^{-4}$, $D = 23.92$ eV,

$E^+ = 4278.0$ eV, $E^- = -113.0$ eV,

$R = 9.48$ fm, $\langle\Gamma_\gamma\rangle = 23.5$ meV.

It was found out from a ploting of cumulative numbers of p-wave resonances that the number of p-wave resonances decreased above 1.5 keV. Taking account of contributions from the missed p-wave resonances, the capture cross section above 1.5 keV was corrected by adding small background cross section calculated by the following equation.

$$\Delta\sigma_{cap} = 3.2 \times 10^{-3}\sqrt{E} - 4.8126\,\frac{1}{\sqrt{E}}. \qquad (11)$$

Figure 3 shows an example of the comparison of the calculated total cross section with measured one. The solid curve shows the present value and the dashed curve JENDL-1. Table 1 lists the thermal properties of the present results. The resonance integral of the capture cross section agrees with the recommended value within the quoted error. The thermal fission cross section also agrees with measured values of $(3 \pm 5) \times 10^{-6}$ barns by Silbert and Bergen[25] and $(2.7 \pm 0.3) \times 10^{-6}$ barns by Slovacek et al.[37]

2.2 Plutonium-240

JENDL-1 adopted the resonance parameters of ENDF/B-IV[2] up to 3.91 keV, which used the multi-level Breit-Wigner formula in order to avoid

the negative values of the elastic scattering cross section. The parameters were given for 201 s-wave resonances including a negative resonance at -4.099 eV, 20 of which were given the sub-threshold fission widths. The present evaluation of ^{240}Pu resonance parameters was made by using all the experimental data[47-66] reported so far.

Resonance energy

The resonance energy of the lowest level was determined to be 1.056 eV on the basis of the measurement by Pattenden and Rainey[51]. The other resonance energies above 20 eV were based on the transmission measurement by Kolar and Böckhoff[58]. A negative resonance at -4.099 eV was taken from ENDF/B-IV. Finally a total of 268 resonances from -4.099 eV to 5.692 keV were adopted, and the resolved resonance energy region was defined to be from 10^{-5} eV to 4 keV.

Neutron and capture widths

The resonance parameters of the first resonance at 1.056 eV were taken from the total cross section measurement made by Pattenden and Rainey, and those of the negative resonance from the ENDF/B-IV evaluation.

The neutron and capture widths of resonances from 20 eV to 500 eV were based on the experimental data by Hockenbury et al.[63] which agree with those by Kolar and Böckhoff. For the resonances from 500 eV to 5.7 keV, the neutron widths obtained by Kolar and Böckhoff were adopted. For the resonances whose capture widths were not reported, the value of 29.5 meV was assumed by averaging the data of Hockenbury et al. This assumed value is higher than the average value of 23.2 meV obtained by Weigmann and Schmid[59]. Weigmann and Theobald[64], however, reanalyzed the experimental data by Weigmann and Schmid, and obtained the higher average capture width of (32 $\pm$ 2) meV. The ENDF/B-IV evaluation also assumed the value of 29.5 meV.

Sub-threshold fission width

The sub-threshold fission widths were taken from the measured data by Auchampaugh and Weston[66] in the energy range of 500 eV to 10 keV with the ORELA neutron facility. They obtained the sub-threshold fission widths for 82 resonances with the area and shape analyses by assuming the neutron widths deduced by Kolar and Böckhoff. Furthermore, Auchampaugh and Weston estimated the minimum fission width $\Gamma_{f,min}$ with the formula[66,67] by Gai et al. in terms of the penetrabilities through the inner and outer fission barriers,

$$\Gamma_{f,min} = \frac{1}{2}\,\pi\,\left(\frac{\Gamma^{\downarrow}\Gamma^{\uparrow}}{D_{II}}\right)^{2} D_I, \qquad (12)$$

where $\Gamma^{\downarrow} = \frac{P_A}{2\pi}\,D_{II}$, $\Gamma^{\uparrow} = \frac{P_B}{2\pi}\,D_{II}$,

P_A, P_B = penetrabilities for the inner and outer barriers,

D_I, D_{II} = average class-I and class-II level spacing.

Auchampaugh and Weston obtained the $\Gamma_{f,min}$ value of (0.22 $\pm$ 0.17) meV which was a little higher than 0.20 meV of the ENDF/B-IV value. These 82 sub-threshold fission widths and the minimum fission width of 0.22 meV were used in the present work.

Correction of calculated cross sections

The average capture cross section is compared in Table 2 with the measured data by Weston and Todd[68]. The differences between them were corrected by applying the background cross sections.

The multi-level Breit-Wigner formula was adopted together with the effective scattering radius of 9.184 fm which is the same as that of ENDF/B-IV. Figure 4 shows the fission cross sections calculated from the present and ENDF/B-IV parameters as well as experimental data. The capture and fission cross sections at 0.0253 eV and their resonance integrals are compared with the recommended values of BNL-325 3rd edition in Table 1. All the values are in agreement with the recommended ones in the quoted errors.

2.3 Plutonium-242

In the case of ^{242}Pu, resolved resonance parameters are given to

only eleven levels up to 390 eV in ENDF/B-IV[2]. They were evaluated on the basis of the data[69-74] measured until 1971. After the ENDF/B-IV evaluation, several new measurements were performed. Bergen and Fullwood[75] measured the sub-threshold fission cross section by using nuclear explosion and obtained the fission widths of 23 resonances lying from 53.4 to 788.2 eV. Poortmans et al.[76] determined Γ_n and Γ_γ of 72 levels from 2.68 eV to 1286 eV on the basis of the scattering capture and transmission data measured with the CBNM linac. Harvey et al.[77], Hockenbury et al.[78] and Auchampaugh and Bowman[79] obtained Γ_n values of resonances from 22.57 eV to 494.75 eV, from 205.0 eV to 382.4 eV and from 595.2 eV to 3836 eV, respectively, by using their transmission data. Auchampaugh and Bowman gave also the sub-threshold fission widths on the basis of another measurement[80] of the sub-threshold fission cross section.

In the present evaluation, the measured data mentioned above were compiled together with old ones by using REPSTOR and examined, and a complete set of resolved resonance parameters was determined up to 1891 eV. The multi-level Breit-Wigner formula was applied.

Resonance energy

Resonance energies up to 1891 eV were taken from the recommended values of BNL-325 3rd edition[45], but the resolved resonance energy region was determined to be from 10^{-5} eV to 1290 eV because resonance parameters were not given between 1290 to 1700 eV.

Neutron and capture widths

The neutron and capture widths were determined by averaging the measured values. The obtained neutron widths are close to those of Poortmans et al.[76] and Auchampaugh and Bowman[79]. For the resonances whose capture widths were not measured, the value of 24.2 meV was applied.

Sub-threshold fission width

The sub-threshold fission widths were deduced from the fission areas given by Bergen and Fullwood[75] and by Auchampaugh and Bowman[79]. In order to give the sub-threshold fission widths to the resonances whose fission widths were not measured, an average was taken over the resonances locating outside an intermediate fission resonance near 750 eV. The average value of 0.116 meV was thus obtained in the energy range from 200 to 900 eV, and was applied in this energy region. For the other energy regions, Γ_f = 0.05 meV was assumed, by taking account of the neutron energy dependence of the sub-threshold fission width near the intermediate fission resonance.

Correction of calculated cross sections

Using the resonance parameters thus obtained and the effective scattering radius of 9.6 fm recommended in BNL-325 3rd edition, the cross sections were calculated. It was found that the thermal capture cross section agreed well with the experimental values[70,73,74,81,82], and the thermal fission cross section fell below the experimental upper limit of 0.2 barns. The elastic scattering and total cross sections, however, were lower than recommended values of BNL-325 3rd edition. We corrected them by adding the background cross sections of 0.67 barns so as to reproduce the measured data of the elastic[83] and total cross sections[73,74].

Table 1 shows comparison of thermal cross sections and resonance integrals with values recommended in BNL-325 3rd edition. The present resonance integral for capture agrees well with the BNL-325 data and the measured data by Young et al.[73,74], and the value for fission is slightly larger than the BNL-325 recommendation. Figure 5 displays the total cross section in the energy range of 1 eV to 100 eV. The present result shown with a thick solid line slightly underestimates the total cross section at off-resonance energies. The same problems are also found in the other evaluations. This disagreement may be diminished by the adjustment of the scattering radius. The evaluated fission cross sections are shown in Fig. 6 below 10 keV. There are very large discrepancies among the present results, ENDF/B-V[84], KEDAK-3[85] and ENDL-78[86]. Particularly the present fission cross section is higher than the others by an order of magnitude below 0.5 eV as seen in Fig. 6.

Average resonance parameters were obtained from the presently evaluated parameters below 500 eV which were regarded as s-wave resonances. They are D_0 = 13.04 eV, S_0 = 0.85 × 10^{-4} and $\overline{\Gamma}_\gamma$ = 24.2 meV.

3. Concluding Remarks

The evaluation of the resolved resonance parameters of ^{238}U, ^{240}Pu and ^{242}Pu was performed for the second version of Japanese Evaluated Nuclear Data Library JENDL-2 by using all the experimental data reported so far. The evaluated parameters are listed in Appendix. The multi-level Breit-Wigner formula was adopted to avoid the negative values in the elastic scattering cross section.

The neutron and capture widths of ^{238}U were determined by applying the least squares method to resonance areas. The capture widths of the low lying resonances became smaller than those of ENDF/B-IV. The evaluated fission widths were based on the measured fission areas. The resonance energies were determined by averaging the values of recent measurements after correction of their systematic errors. Finally 183 s-wave and 265 p-wave resonances were recommended up to 4.73 keV.

A total of 267 resonances up to 5.69 keV were recommended for ^{240}Pu. Their sub-threshold fission widths were obtained by taking account of the ORELA measurement by Auchampaugh and Weston. The resonance parameters of ^{242}Pu were determined for 95 resonances up to 1.89 keV. Their neutron and capture widths were obtained by averaging the measured values, and the sub-threshold fission widths were given to all the resonances on the basis of measured fission areas. All the resonances were assigned as s-wave resonances for ^{240}Pu and ^{242}Pu. This seems improbable taking account of the situation of ^{238}U. Probably some p-wave resonances were misassigned as s-wave ones and some p-wave resonances might be missing.

The energy region where the cross sections are calculated from the parameters were determined to be from 10^{-5} eV to 4 keV for ^{238}U and ^{240}Pu, and from 10^{-5} eV to 1.29 keV for ^{242}Pu. The background cross sections were also evaluated in order to reproduce well the measured cross sections. The thermal fission and capture cross sections and their resonance integrals agree with the recommended values in BNL-325 3rd edition.

The authors thank to the members of Working Group on Heavy-Nuclide Nuclear Data for their useful discussion during the present work.

References

1) Igarasi, S., Nakagawa, T., Kikuchi, Y., Asami, T. and Narita, T.: "Japanese Evaluated Nuclear Data Library, Version-1, --JENDL-1--", JAERI 1261 (1979).
2) Compiled by Garber, D.: "ENDF/B Summary Documentation", ENDF-201 (1975).
3) Edited by Pearlstein, S.: "Seminar on ^{238}U Resonance Capture", BNL-NCS-50451 (1975).
4) Nakagawa, T.: "Computer Codes for Neutron Data Evaluation", JAERI-M 8163, 51 (1979) [in Japanese].
5) Garber, D., Dunford, C. and Pearlstein, S.: "Data Formats and Procedures for the Evaluated Nuclear Data File, ENDF", ENDF-102 (1975).
6) McCrosson, F. J.: "Evaluation of ^{238}U cross sections for ENDF/B-IV", Seminar on ^{238}U Resonance Capture, BNL-NCS-50451, p. 122 (1975).
7) Harvey, J. A., Hughes, D. J., Carter, R. S. and Pilcher, V. E.: Phys. Rev. 99, 10 (1955).
8) Lynn, J. E. and Pattenden, N. J.: "The Slow Neutron Cross Sections of the Uranium Isotopes", Proc. of the International Conference on the Peaceful Uses of Atomic Energy, Geneva (1955), vol. 4, 210.
9) Fluharty, R. G., Simpson, F. B. and Simpson, O. D.: Phys. Rev. 103, 1778 (1956).
10) Levin, J. S. and Hughes, D. J.: Phys. Rev. 101, 1328 (1956).
11) Bollinger, L. M., Cote, R. E., Dahlberg, D. A. and Thomas, G. E.: Phys. Rev. 105, 661 (1957).
12) Radkevich, I. A., Vladimirsky, V. V. and Sokolovsky, V. V.: J. Nucl. Energy 5, 107 (1957).
13) Leonard,Jr. B. R. and Odegaaden, R. H.: "Sub-threshold Fission - ^{236}U, ^{238}U, ^{240}Pu, ^{241}Pu, ^{231}Pa", HW-67219 (1960).
14) Rosen, J. L., Desjardins, J. S., Rainwater, J. and Havens,Jr. W. W.: Phys. Rev. 118, 687 (1960).
15) Jackson, H. E. and Lynn, J. E.: Phys. Rev. 127, 461 (1962).
16) Moxon, M. C. and Mycock, C. M.: Qouted from BNL 325 (2nd edition).
17) Firk, F. W. K., Lynn, J. E. and Moxon, M. C.: Nucl. Phys. 41, 614 (1963).
18) Garg, J. B., Rainwater, J., Peterson, J. S. and Havens,Jr. W. W.: Phys. Rev. 134, B985 (1964).

19) Asghar, M., Chaffey, C. M. and Moxon, M. C.: Nucl. Phys. 85, 305 (1966).

20) Bollinger, L. M. and Thomas, G. E.: Phys. Rev. 171, 1293 (1968).

21) Glass, N. W., Schelberg, A. D., Tatro, L. D. and Warren, J. H.: "^{238}U Neutron Capture Results from Bomb Source Neutrons", Proc. of the Second Conference on Neutron Cross Sections and Technology, Washington (1968), Vol. 1, 573.

22) Carraro, G. and Kolar, W.: "Neutron Widths of ^{238}U from 60 eV to 5.7 keV", Proc. of the Conference on Nuclear Data for Reactors, Helsinki (1970), Vol. 1, 403.

23) Rohr, G., Weigmann, H. and Winter, J.: "Resonance Parameters from Neutron Radiative Capture in ^{238}U", Proc. of the Conference on Nuclear Data for Reactors, Helsinki (1970), Vol. 1, 413.

24) Carraro, G. and Kolar, W.: "Total Neutron Cross Section Measurements of ^{238}U", Proc. of the Third Conference on Neutron Cross Section and Technology, Knoxville (1971), Vol. 2, 701.

25) Silbert, M. G. and Bergen, D. W.: Phys. Rev. C4, 220 (1971).

26) Wasson, O. A., Chrien, R. E., Slaughter, G. G. and Harvey, J. A.: Phys. Rev. C4, 900 (1971).

27) Malecki, H., Pikel'ner, L. B., Salamatin, M. and Sharapov, F. I.: Atomnaya Energiya 32, 49 (1972).

28) Rahn, F., Camarda, H. S., Hacken, G., Hevens,Jr. W. W., Liou, H. I., Rainwater, J., Slagowitz, M. and Wynchank, S.: Phys. Rev. C6, 1854 (1972).

29) Block, R. C., Hockenbury, R. W., Slovacek, R. E., Bean, E. B. and Cramer, D. S.: Phys. Rev. Letters 31, 247 (1973).

30) de Saussure, G., Silver, E. G., Perez, R. B., Ingle, R. and Weaver, H.: Nucl. Sci. Eng. 51, 385 (1973).

31) Ceulemans, H.: "Resonance Scattering Cross-Section of ^{238}U below 220 eV", Proc. of the Specialist Meeting on Resonance Parameters of Fertile Nuclei and ^{239}Pu, Saclay (1974), 145.

32) Corvi, F., Rohr, G. and Weigmann, H.: "p-wave Assignment of ^{238}U Resonances", Proc. of a Conference on Nuclear Cross Sections and Technology, Washington (1975), Vol. 2, 732.

33) Wartena, J. A., Weigmann, H. and Migneco, E.: "On Sub-barrier Fission in ^{238}U", Proc. of a Conference on Nuclear Cross Sections and Technology, Washington (1975), Vol. 2, 597.

34) Difilippo, F. C., Perez, R. B., de Saussure, G., Olsen, D. K. and Ingle, R. W.: Nucl. Sci. Eng. 63, 153 (1977).

35) Liou, H. I. and Chrien, R. E.: Nucl. Sci. Eng. 62, 463 (1977).

36) Olsen, D. K., de Saussure, G., Perez, R. B., Silver, E. G., Difilippo, F. C., Ingle, R. W. and Weaver, H.: Nucl. Sci. Eng. 62, 479 (1977).

37) Slovacek, R. E., Cramer, D. S., Bean, E. B., Valentine, J. R., Hockenbury, R. W. and Block, R. C.: Nucl. Sci. Eng. 62, 455 (1977).

38) Poortmans, F., Cornelis, E., Mewissen, L., Rohr, G., Shelley, R., van der Veen, T., Vanpraet, G. and Weigmann, H.: "Cross Sections and Neutron Resonance Parameters for ^{238}U below 4 keV", Proc. of the International Conference on the Interactions of Neutrons with Nculei, Lowell (1976), 1264.

39) Olsen, D. K., de Saussure, G., Perez, R. B., Difilippo, F. C., Ingle, R. W. and Weaver, H.: Nucl. Sci. Eng. 69, 202 (1979).

40) Stavealoz, P., Poortmans, F., Mewissen, L. and Cornelis, E.: Nucl. Sci. Eng. 66, 349 (1978).

41) Block, R. C., Harris, D. R., Kim, S. H. and Kobayashi, K.: "^{238}U Resonance Self-Indication Capture Measurements and Analysis", EPRI NP-996 (1979).

42) Haste, T. J. and Moxon, M. C.: "Resonance Parameters of ^{238}U below a Neutron Energy of 520 eV", Proc. of an International Conference on Neutron Physics and Nuclear Data, Harwell (1978), 337.

43) Difilippo, F. C., Perez, R. B., de Saussure, G., Olsen, D. K. and Ingle, R. W.: Phys. Rev. C21, 1400 (1980).

44) Nakajima, Y.: Ann. Nucl. Energy 7, 25 (1980).

45) Mughabghab, S. F. and Garber, D. I.: "Neutron Cross Sections Vol. 1, Resonance Parameters", BNL-325, 3rd Edition Vol. 1 (1973).

46) de Saussure, G., Olsen, D. K. and Perez, R. B.: Nucl. Sci. Eng. 61, 496 (1976).

47) Estwood, T. A., Baerg, A. P., Bigham, C. B., Brown, F., Cabell, M. J., Grummitt, W. E., Roy, J. C., Roy, L. P. and Schuman, R. P.: "Radiochemical Methods Applied to the Determination of Cross Sections of Reactor Interest", Proc. of the Second United Nations International Conference on the Peaceful Uses of Atomic Energy, Geneva (1958), Vol. 16, 54.

48) Fields, P. R., Ryle, G. L., Inghram, M. G., Diamond, H., Studier, M. H. and Manning, W. H.: Nucl. Sci. Eng. 1, 62 (1956).

49) Roose, H., Cooper, W. A. and Tattersall, R. B.: "The Use of the Pile Oscillator in Thermal Reactor Problems", Proc. of the Second United Nations International Conference on the Peaceful Uses of Atomic Energy, Geneva (1958), Vol. 16, 34.

50) Halperin, J. H., Oliver, J. O. and Pamerance, H. S.: J. Inorg. Nucl. Chem. 9, 1 (1959).

51) Pattenden, N. J. and Rainey, V. S.: J. Nucl. Energy 11, 14 (1959).

52) Block, R. C., Slaughter, G. G., Pattenden, N. J. and Harvey, J. A.: "The ORNL Fast-Chopper Time-of-Flight Neutron Spectrometer", Proc. of IAEA Symposium on Pile Neutron Research, Vienna (1960), 535.

53) Block, R. C., Slaughter, G. G. and Harvey, J. A.: Nucl. Sci. Eng. 8, 112 (1960).

54) Cabell, M. J. and Wilkins, M.: J. Inorg, Nucl. Chem. 28, 2467 (1966).

55) Lounsbury, M., Durham, R. W. and Hanna, G. C.: "Measurements of Alpha and Fission Cross Section Ratios for U-233, U-235 and Pu-239 at thermal Energies", Proc. of the Conference on Nuclear Data for Reactors, Helsinki (1970), Vol. 1, 287.

56) Ramakrishina, D. V. S. and Navalkar, M. P.: "Determination of Resonance Parameters of Pu-240 using a Crystal Spectrometer", Proc. of the Conference on Nuclear Data for Reactors, Helsinki (1970),

57) Asghar, M., Moxon, M. C. and Pattenden, N. J.: "Neutron Resonance Parameters of ^{240}Pu", Proc. of Conference on Nuclear Data for Reactors, Paris (1966), Vol. 2, 145.

58) Kolar, W. and Böckhoff, K. H.: J. Nucl. Energy 22, 299 (1968).

59) Weigmann, H. and Schmid, H.: J. Nucl. Energy 22, 317 (1968).

60) Migneco, E. and Theobald, J. P.: "Resonance Grouping Structure in Neutron Induced Sub-threshold Fission of Pu-240", Proc. of the Second Conference on Neutron Cross Sections and Technology, Washington (1968), Vol. 1, 527.

61) Cao, M. G., Migneco, E., Theobald, J. P. and Wartena, J. A.: "Scattering Cross Section of Pu-240", Proc. of the Second Conference on Neutron Cross Sections and Technology, Washington (1968), Vol. 1, 513.

62) Asghar, M., Moxon, M. C. and Pattenden, N. J.: "Neutron Capture Measurements in the Resonance Parameters of Pu-240", EANDC(UK) 103AL (1968).

63) Hockenbury, R. W., Moyer, W. R. and Block, R. C.: Nucl. Sci. Eng. 49, 153 (1972).

64) Weigmann, H. and Theobald, J. P.: J. Nucl. Energy 26, 643 (1972).

65) Moxon, M. C.: private communication to Weigmann, H. and Theobald, J. P., see Ref. 64.

66) Auchampaugh, G. F. and Weston, L. W.: Phys. Rev. C12, 1850 (1975).

67) Lynn, J. E.: "Structure in Sub-threshold Fission Modes", AERE-R 5891 (1968).

68) Weston, L. W. and Todd, J. H.: Nucl. Sci. Eng. 63, 143 (1977).

69) Egelstaff, P. A., Gayther, D. B. and Nicholson, K. P.: J. Nucl. Energy 6, 303 (1958).

70) Coté, R. E., Bollinger, L. M., Barnes, R. F. and Diamond, H.: Phys. Rev. 114, 505 (1959).

71) Pattenden, N. J.: "Slow Neutron Transmission Measurements on Pu-242", Proc. of the International Conference on the study of Nuclear Structure with Neutrons, Antwerp (1965), 93.

72) Auchampaugh, G. F., Bowman, C. D., Coops, M. S. and Fultz, S. C.: Phys. Rev. 146, 840 (1966).

73) Young, T. E. and Reeder, S. D.: Nucl. Sci. Eng. 40, 389 (1970).

74) Young, T. E., Simpson, F. B. and Tate, R. E.: Nucl. Sci. Eng. 43, 341 (1971).

75) Bergen, D. W. and Fullwood, R. R.: Nucl. Phys. A163, 577 (1971).

76) Poortmans, F., Rohr, G., Theobald, J. P., Weigmann, H. and Vanpraet, G. J.: Nucl. Phys. A207, 342 (1973).

77) Harvey, J. A., Hill, N. W., Benjamin, R. W., Ahlfeld, C. E., Simpson, F. B., Simpson, O. D. and Miller, H. G.: "Neutron Total Cross Section of ^{248}Cm and ^{242}Pu from 0.5 to 5000 eV", ORNL-4844, 90 (1973).

78) Hockenbury, R. W., Sanislo, A. J. and Kaushal, N. N.: "KeV Capture Cross Section of ^{242}Pu", Proc. of Fourth International Conference on Nuclear Cross Sections and Technology, Washington (1975), 584.

79) Auchampaugh, G. F. and Bawman, C. D.: Phys. Rev. C7, 2085 (1973).

80) Auchampaugh, G. F., Farrell, J. A. and Bergen, D. W.: Nucl. Phys. A171, 31 (1971).

81) Durham, R. W. and Molson, F.: Can. J. Phys. 48, 716 (1970).

82) Butler, J. P., Lousbury, M. and Merritt, J. S.: Can. J. Phys. 35, 147 (1957).

83) Lander, G. H. and Mueller, M. H.: Acta Crystallographica B27, 2284 (1971).

84) Mann, F. M. and Schenter, R. E.: "HEDL Evaluation of Actinide Cross Sections for ENDF/B-V", HEDL-TME 77-54 (1977).

85) Goel, B.: Contribution to the NEANDC Specialist Meeting on Nuclear Data of Higher Plutonium and Americium Isotopes for Reactor Applications, BNL (1978).

86) Howerton, R. J. and MacGregor, M. H.: "The LLL Evaluated Nuclear Data Library (ENDL) Descriptions of Individual Evaluations for Z = 0 - 98", UCRL-50400, Vol. 15, Part D (1978).

Table 1 Comparison of thermal properties*

Isotope	Quantity	BNL-325 (3rd)	JENDL-2
^{238}U	σ_{cap}	2.70 ± 0.02	2.699
	σ_f		3.86×10^{-6}
	I_γ	275 ± 5	279
	I_f		2.05
^{240}Pu	σ_{cap}	289.5 ± 1.4	288.5
	σ_f	0.030 ± 0.045	0.0676
	I_γ	8013 ± 960	8454
	I_f		10.1
^{242}Pu	σ_{cap}	18.5 ± 0.4	18.43
	σ_f	<0.2	0.013
	I_γ	1130 ± 60	1117
	I_f	5	6.3

* All the values are given in barns.

Table 2 Background values for the ^{240}Pu capture cross section*

E (keV)	experiment[68] (E)	calculated (C)	E-C	adopted** background
0.1 -.0.3	8.71 ± 0.61	7.15	1.56	1.92
0.3 - 0.4	10.27 ± 0.72	8.00	2.27	
0.4 - 0.5	6.60 ± 0.46	6.24	0.36	0.80
0.5 - 0.6	7.14 ± 0.50	6.34	0.80	
0.6 - 0.7	5.09 ± 0.36	3.85	1.24	
0.7 - 0.8	2.63 ± 0.18	1.71	0.92	1.60
0.8 - 0.9	6.63 ± 0.46	3.73	2.92	
0.9 - 1.0	5.53 ± 0.39	4.55	0.98	
1.0 - 1.5	3.50 ± 0.25	2.44	1.06	1.04
1.5 - 2.0	3.03 ± 0.21	2.01	1.02	
2.0 - 3.0	2.42 ± 0.17	1.43	0.99	0.99
3.0 - 4.0	1.89 ± 0.13	0.798	1.092	1.092

* All the values are given in barns.

** Average values of (E-C) were adopted as background cross sections.

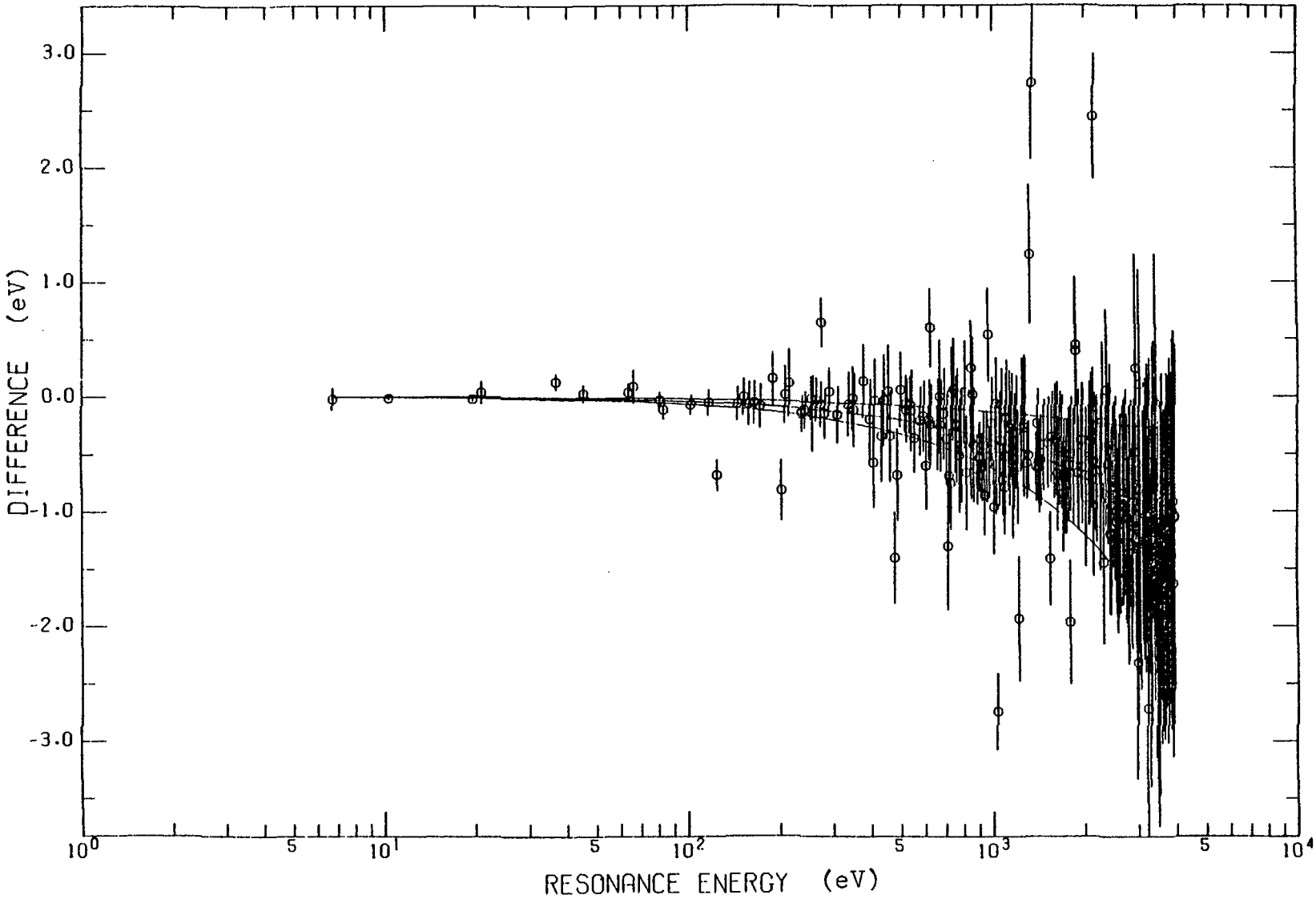

Fig. 1 Resonance energy discrepancies in ^{238}U between the measurements by Rahn et al. and by Olsen et al. Solid curves show the fitted values with the least squares method and its one standard deviations.

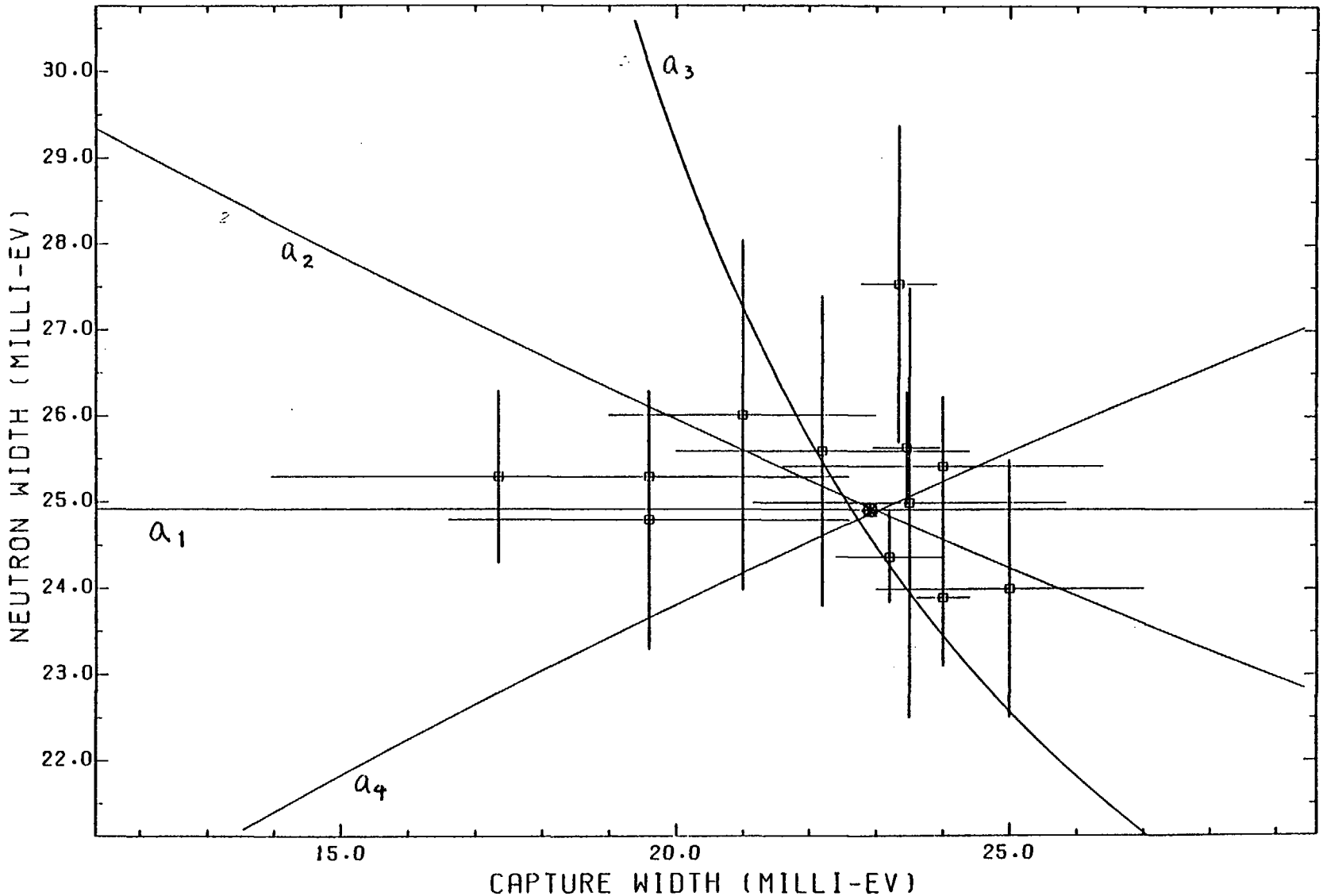

Fig. 2 Typical example of relations between neutron and capture widths of ^{238}U resonance at 66.01 eV. Four curves a_1, a_2, a_3 and a_4 represent the relations by Eqs. (3'), (4'), (5') and (6') , respectively, corresponding to the average values obtained from the reported resonance parameters.

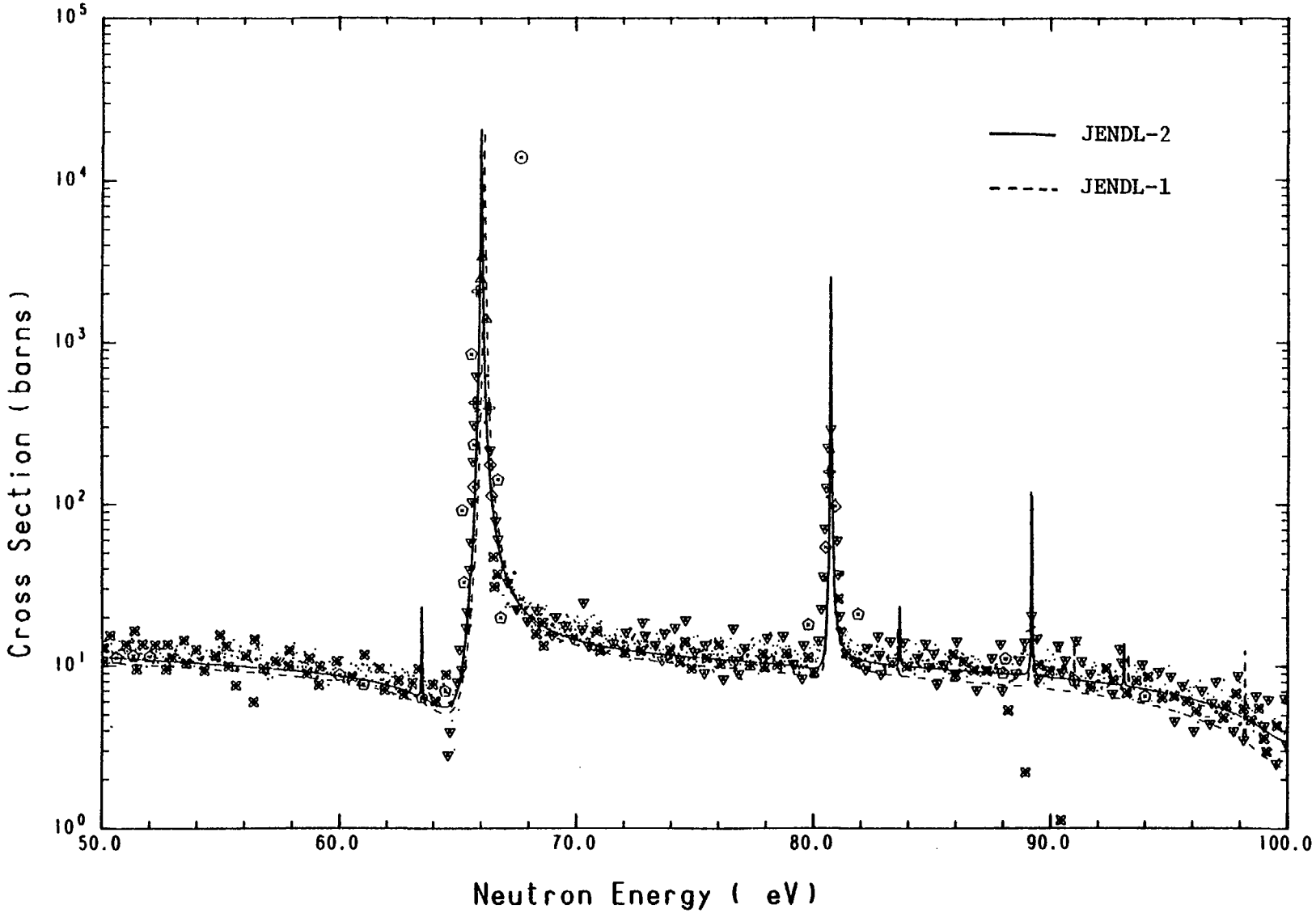

Fig. 3 Total cross sections of ^{238}U in the energy range from 50 eV to 100 eV.

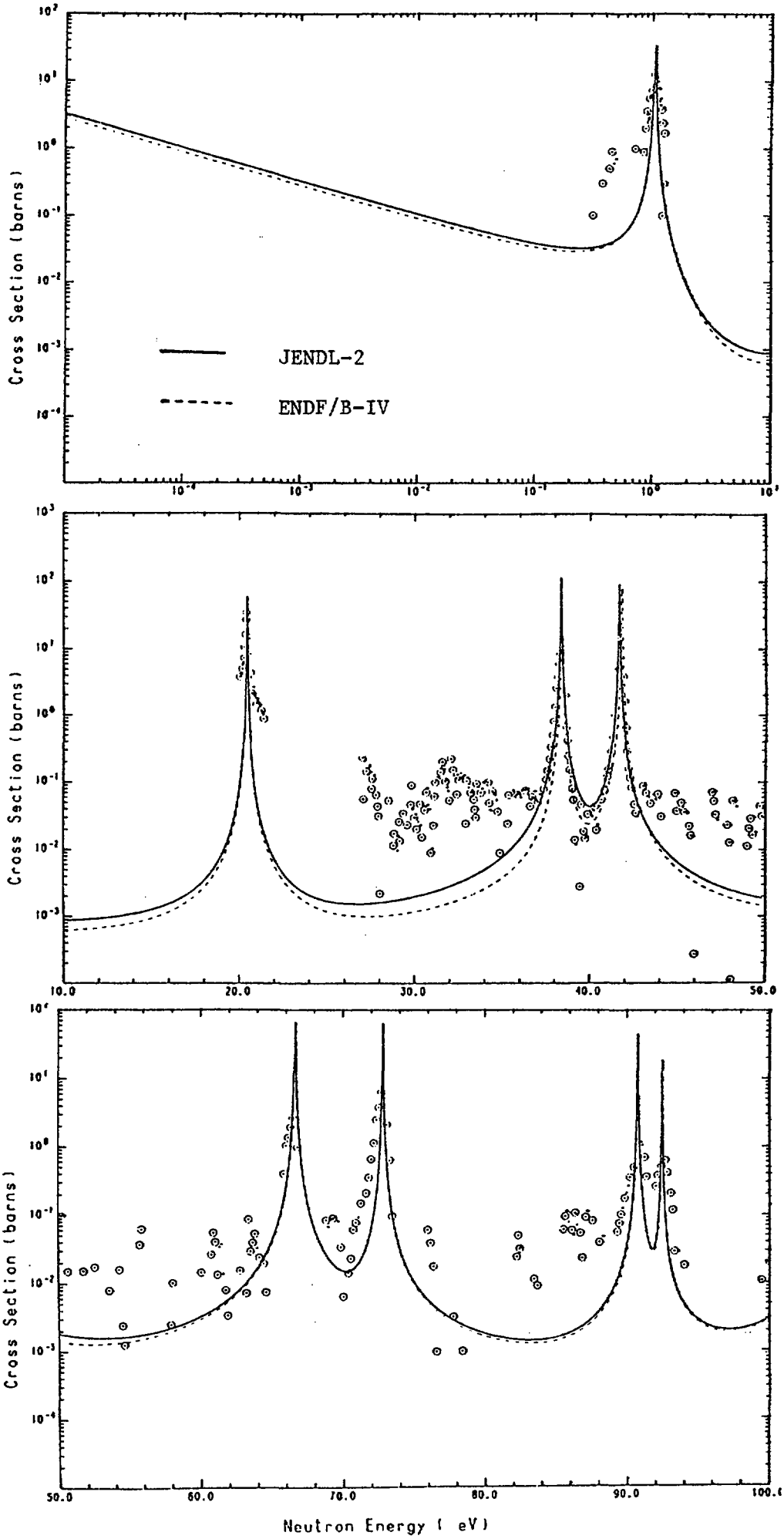

Fig. 4 Fission cross sections of ^{240}Pu up to 100 eV.

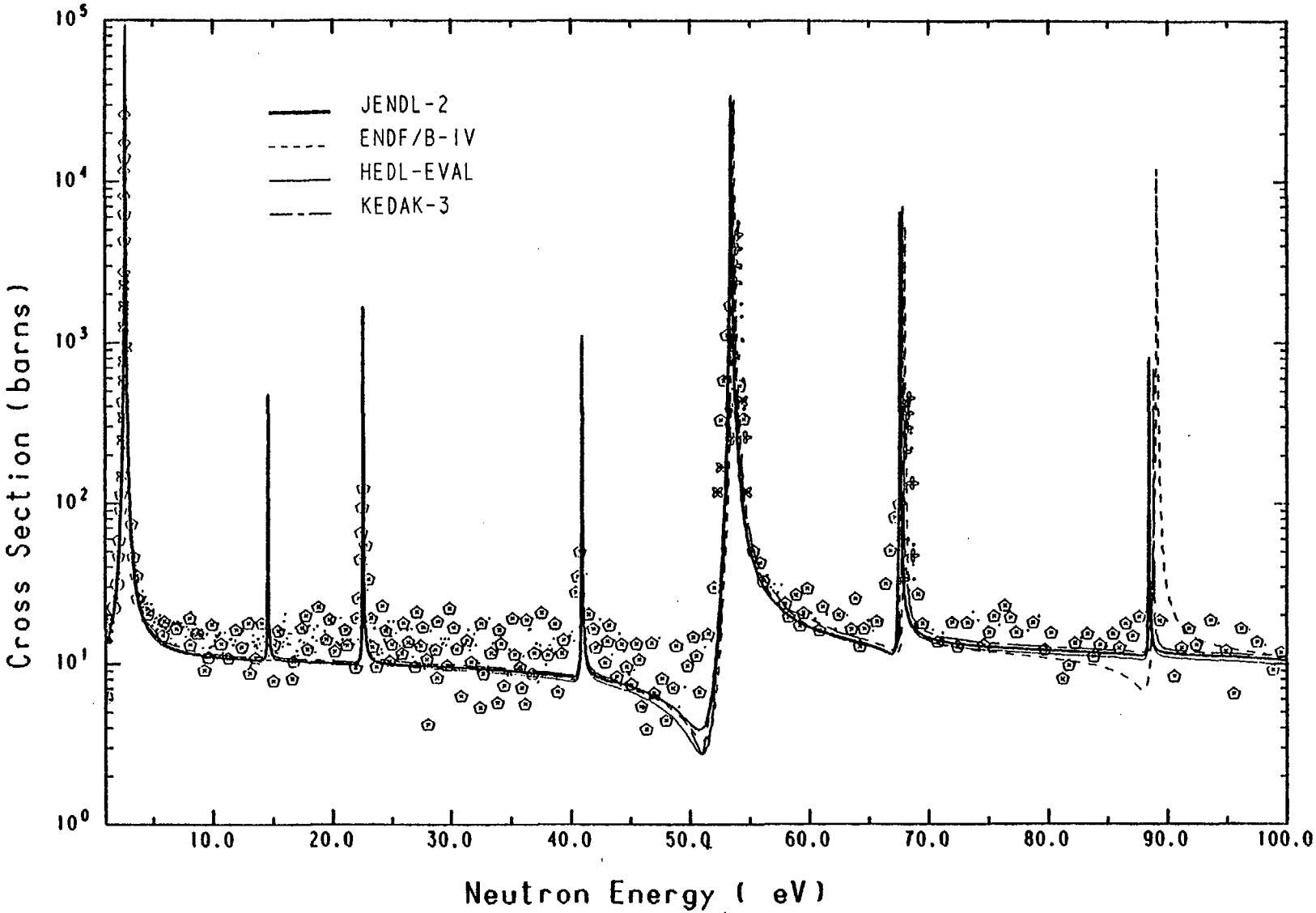

Fig. 5 Total cross sections of ^{242}Pu in the energy range from 1 to 100 eV.

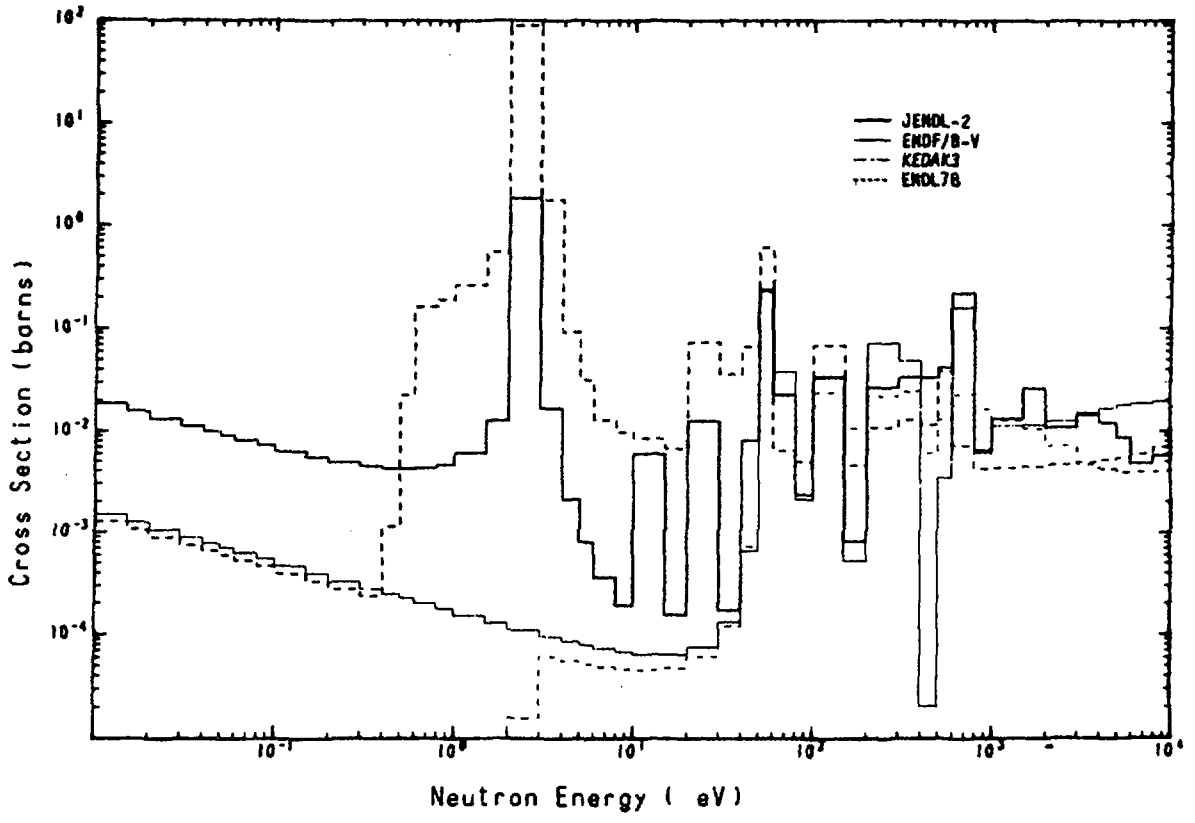

Fig. 6 Average fission cross sections of ^{242}Pu in the energy range from 0.01 eV to 10 keV.

ENERGY (EV)	L	J	TOTAL WIDTH (MEV)	NEUTRON WIDTH (MEV)	GAMMA WIDTH (MEV)	FISSION WIDTH (MEV)	REFERENCE
-113.0	0	0.5	51.5	28.0	23.5		JENDL-2
-89.0	0	0.5	48.5	25.0	23.5		JENDL-2
-65.0	0	0.5	44.5	21.0	23.5		JENDL-2
-41.0	0	0.5	35.35	11.85	23.5		JENDL-2
4.404	1	0.5	18.4001	1.11 -4	18.4		JENDL-2
6.672	0	0.5	25.2	1.5	23.7	9.2 -6	JENDL-2
10.235	1	0.5	23.6016	0.00159	23.6		JENDL-2
11.307	1	0.5	23.6004	3.69 -4	23.6		JENDL-2
16.28	1	0.5	23.6001	5.04 -5	23.6		JENDL-2
19.524	1	0.5	23.8014	0.00136	23.8		JENDL-2
20.864	0	0.5	33.1	10.1	23.0	4.8 -5	JENDL-2
36.671	0	0.5	56.8	33.3	23.5	1.2 -5	JENDL-2
45.176	1	0.5	27.0014	0.00136	27.0		JENDL-2
49.626	1	0.5	24.9009	9.22 -4	24.9		JENDL-2
63.504	1	0.5	23.9098	0.00978	23.9		JENDL-2
66.015	0	0.5	47.8001	24.9	22.9	5.1 -5	JENDL-2
80.729	0	0.5	26.2701	1.87	24.4	6.6 -5	JENDL-2
83.66	1	0.5	24.4104	0.0104	24.4		JENDL-2
89.219	1	0.5	24.0851	8.509-2	24.0		JENDL-2
93.109	1	0.5	24.4054	0.00538	24.4		JENDL-2
102.54	0	0.5	96.0	70.9	25.1	1.2 -5	JENDL-2
111.25	1	0.5	23.1084	0.00842	23.1		JENDL-2
116.87	0	0.5	48.7	25.6	23.1		JENDL-2
124.89	1	0.5	24.0206	0.0206	24.0		JENDL-2
133.29	1	0.5	23.4083	0.00835	23.4		JENDL-2
145.63	0	0.5	23.909	0.909	23.0		JENDL-2
152.41	1	0.5	24.0468	0.0468	24.0		JENDL-2
158.97	1	0.5	24.6134	0.0134	24.6		JENDL-2
160.8	1	0.5	23.605	0.005	23.6		JENDL-2
165.26	0	0.5	27.21	3.31	23.9		JENDL-2
173.18	1	0.5	23.8461	0.0461	23.8		JENDL-2
189.64	0	0.5	199.1	176.0	23.1	4.8 -5	JENDL-2
194.73	1	0.5	24.7455	0.0455	24.7		JENDL-2
200.68	1	0.5	24.1557	0.0557	24.1		JENDL-2
203.05	1	0.5	23.6344	0.0344	23.6		JENDL-2
208.47	0	0.5	71.8001	49.5	22.3	8.8 -5	JENDL-2
214.86	1	0.5	24.3595	0.0595	24.3		JENDL-2
218.37	1	0.5	23.5302	0.0302	23.5		JENDL-2
224.57	1	0.5	23.62	0.02	23.6		JENDL-2
237.34	0	0.5	50.7001	26.5	24.2	0.00006	JENDL-2
242.71	1	0.5	23.689	0.189	23.5		JENDL-2
253.89	1	0.5	23.507	0.107	23.4		JENDL-2
257.19	1	0.5	24.0176	0.0176	24.0		JENDL-2
263.94	1	0.5	23.868	0.268	23.6		JENDL-2
273.62	0	0.5	48.4	25.3	23.1		JENDL-2
275.2	1	0.5	23.792	0.192	23.6		JENDL-2
282.44	1	0.5	23.708	0.108	23.6		JENDL-2
290.96	0	0.5	39.6	16.5	23.1		JENDL-2
311.28	0	0.5	24.35	1.05	23.3		JENDL-2
322.85	1	0.5	22.0417	0.0417	22.0		JENDL-2
332.02	1	0.5	23.1518	0.0518	23.1		JENDL-2
337.27	1	0.5	23.708	0.108	23.6		JENDL-2
347.75	0	0.5	102.1	79.2	22.9	2.68 -4	JENDL-2
351.86	1	0.5	23.633	0.233	23.4		JENDL-2
372.91	1	0.5	24.34	0.04	24.3		JENDL-2
376.89	0	0.5	25.8502	1.25	24.6	2.05 -4	JENDL-2
395.33	1	0.5	21.4709	0.0709	21.4		JENDL-2
397.58	0	0.5	30.52	6.12	24.4		JENDL-2
408.15	1	0.5	23.8807	0.0807	23.8		JENDL-2
410.21	0	0.5	42.3	19.8	22.5		JENDL-2
434.04	0	0.5	33.86	9.76	24.1		JENDL-2
439.75	1	0.5	23.888	0.288	23.6		JENDL-2
448.5	1	0.5	23.9462	0.0462	23.9		JENDL-2
454.06	1	0.5	24.022	0.422	23.6		JENDL-2
463.14	0	0.5	28.6415	5.54	23.1	0.00147	JENDL-2
467.21	1	0.5	24.4613	0.0613	24.4		JENDL-2
478.4	0	0.5	27.8402	4.14	23.7	2.41 -4	JENDL-2
485.3	1	0.5	23.742	0.142	23.6		JENDL-2
488.87	1	0.5	24.614	0.814	23.8		JENDL-2
498.96	1	0.5	23.207	0.107	23.1		JENDL-2
518.33	0	0.5	73.0003	48.9	24.1	2.93 -4	JENDL-2
523.35	1	0.5	23.686	0.286	23.4		JENDL-2
532.44	1	0.5	23.1687	0.0687	23.1		JENDL-2
535.28	0	0.5	67.7004	43.6	24.1	3.67 -4	JENDL-2
542.41	1	0.5	25.452	0.152	25.3		JENDL-2
550.71	1	0.5	23.5855	8.549-2	23.5		JENDL-2
556.25	1	0.5	24.398	0.898	23.5		JENDL-2
580.08	0	0.5	61.6	36.5	25.1		JENDL-2
584.47	1	0.5	23.911	0.111	23.8		JENDL-2
595.01	0	0.5	108.901	85.8	23.1	0.0011	JENDL-2
606.73	1	0.5	23.564	0.264	23.3		JENDL-2
615.78	1	0.5	23.449	0.149	23.3		JENDL-2
619.95	0	0.5	53.5002	30.2	23.3	2.15 -4	JENDL-2
624.23	1	0.5	24.303	0.803	23.5		JENDL-2
628.53	0	0.5	30.2	6.3	23.9		JENDL-2
633.34	1	0.5	23.52	0.12	23.4		JENDL-2
661.14	0	0.5	150.9	126.0	24.9		JENDL-2

ENERGY (EV)	L	J	TOTAL WIDTH (MEV)	NEUTRON WIDTH (MEV)	GAMMA WIDTH (MEV)	FISSION WIDTH (MEV)	REFERENCE
668.55	1	0.5	23.706	0.206	23.5		JENDL-2
677.75	1	0.5	24.3	0.7	23.6		JENDL-2
681.67	1	0.5	22.6525	0.0525	22.6		JENDL-2
693.05	0	0.5	63.3	40.4	22.9		JENDL-2
698.14	1	0.5	24.392	0.292	24.1		JENDL-2
708.27	0	0.5	46.626	21.1	25.5	0.026	JENDL-2
710.52	1	0.5	25.85	1.05	24.8		JENDL-2
713.54	1	0.5	23.917	0.217	23.7		JENDL-2
721.58	0	0.5	26.49	1.76	23.7	1.03	JENDL-2
730.12	0	0.5	24.884	1.0	23.8	0.084	JENDL-2
732.48	1	0.5	26.38	1.78	24.6		JENDL-2
734.9	1	0.5	22.363	0.163	22.2		JENDL-2
743.14	1	0.5	23.759	0.359	23.4		JENDL-2
756.2	1	0.5	24.129	0.529	23.6		JENDL-2
765.05	0	0.5	31.0773	7.57	23.5	0.0073	JENDL-2
770.89	1	0.5	23.72	0.12	23.6		JENDL-2
772.6	1	0.5	23.74	0.14	23.6		JENDL-2
779.31	1	0.5	25.64	2.14	23.5		JENDL-2
785.9	1	0.5	26.35	0.15	26.2		JENDL-2
787.3	1	0.5	24.473	0.473	24.0		JENDL-2
790.82	0	0.5	30.24	6.84	23.4		JENDL-2
808.2	1	0.5	23.903	0.403	23.5		JENDL-2
821.56	0	0.5	88.9	65.3	23.6		JENDL-2
828.46	1	0.5	24.486	0.186	24.3		JENDL-2
833.86	1	0.5	25.2947	0.0947	25.2		JENDL-2
846.68	1	0.5	24.269	0.869	23.4		JENDL-2
850.99	0	0.5	86.9011	62.9	24.0	0.0011	JENDL-2
856.08	0	0.5	110.301	86.6	23.7	0.001	JENDL-2
859.44	1	0.5	24.114	0.414	23.7		JENDL-2
866.42	0	0.5	28.91	5.41	23.5		JENDL-2
891.23	1	0.5	24.197	0.697	23.5		JENDL-2
905.03	0	0.5	77.9	54.2	23.7		JENDL-2
910.01	1	0.5	24.85	1.35	23.5		JENDL-2
925.11	0	0.5	40.0	14.0	26.0		JENDL-2
932.66	1	0.5	23.029	0.229	22.8		JENDL-2
937.02	0	0.5	173.7	150.0	23.7		JENDL-2
940.84	1	0.5	24.557	0.657	23.9		JENDL-2
958.52	0	0.5	227.8	205.0	22.8		JENDL-2
964.58	1	0.5	24.404	0.304	24.1		JENDL-2
977.34	1	0.5	24.172	0.772	23.4		JENDL-2
982.32	1	0.5	23.69	0.09	23.6		JENDL-2
985.17	1	0.5	24.969	0.169	24.8		JENDL-2
991.63	0	0.5	407.2	378.0	29.2		JENDL-2
1003.67	1	0.5	28.107	0.107	28.0		JENDL-2
1011.44	1	0.5	25.46	1.86	23.6		JENDL-2
1022.96	0	0.5	31.25	8.45	22.8		JENDL-2
1029.12	1	0.5	25.81	2.31	23.5		JENDL-2
1033.38	1	0.5	23.833	0.733	23.1		JENDL-2
1047.27	1	0.5	23.897	0.397	23.5		JENDL-2
1054.45	0	0.5	117.8	94.6	23.2		JENDL-2
1062.69	1	0.5	24.387	0.787	23.6		JENDL-2
1067.68	1	0.5	25.02	1.12	23.9		JENDL-2
1074.07	1	0.5	24.323	0.923	23.4		JENDL-2
1081.7	1	0.5	25.25	1.55	23.7		JENDL-2
1095.18	1	0.5	25.88	2.28	23.6		JENDL-2
1098.62	0	0.5	45.2	21.4	23.8		JENDL-2
1102.9	1	0.5	25.84	2.24	23.6		JENDL-2
1109.08	0	0.5	58.0	34.6	23.4		JENDL-2
1118.97	1	0.5	23.221	0.521	22.7		JENDL-2
1131.37	1	0.5	27.61	3.71	23.9		JENDL-2
1140.35	0	0.5	258.701	235.0	23.7	0.0015	JENDL-2
1145.47	1	0.5	23.61	0.01	23.6		JENDL-2
1147.97	1	0.5	23.7	0.3	23.4		JENDL-2
1152.57	1	0.5	25.176	0.476	24.7		JENDL-2
1155.07	1	0.5	23.925	0.825	23.1		JENDL-2
1159.38	1	0.5	23.44	0.74	22.7		JENDL-2
1167.63	0	0.5	109.911	86.8	23.1	0.011	JENDL-2
1177.07	0	0.5	91.9	69.2	22.7		JENDL-2
1194.81	0	0.5	115.7	94.6	21.1		JENDL-2
1201.57	1	0.5	23.724	0.524	23.2		JENDL-2
1211.11	0	0.5	33.495	9.64	23.6	0.255	JENDL-2
1219.51	1	0.5	24.881	0.581	24.3		JENDL-2
1230.08	1	0.5	23.899	0.399	23.5		JENDL-2
1233.17	1	0.5	23.908	0.408	23.5		JENDL-2
1238.36	1	0.5	23.166	0.466	22.7		JENDL-2
1245.06	0	0.5	276.8	254.0	22.8		JENDL-2
1249.85	1	0.5	23.9	0.3	23.6		JENDL-2
1251.42	1	0.5	24.606	0.606	24.0		JENDL-2
1260.94	1	0.5	23.708	0.208	23.5		JENDL-2
1267.04	0	0.5	54.3041	29.6	24.7	0.0041	JENDL-2
1272.97	0	0.5	52.0	28.3	23.7		JENDL-2
1276.53	1	0.5	24.142	0.542	23.6		JENDL-2
1278.04	1	0.5	24.3	0.7	23.6		JENDL-2
1283.64	1	0.5	24.0	0.4	23.6		JENDL-2
1285.4	1	0.5	22.91	0.41	22.5		JENDL-2
1289.04	1	0.5	24.45	0.25	24.2		JENDL-2
1296.14	1	0.5	23.7	0.1	23.6		JENDL-2

ENERGY (EV)	L	J	TOTAL WIDTH (MEV)	NEUTRON WIDTH (MEV)	GAMMA WIDTH (MEV)	FISSION WIDTH (MEV)	REFERENCE
1298.69	0	0.5	27.09	3.49	23.6		JENDL-2
1310.99	1	0.5	23.125	0.225	22.9		JENDL-2
1317.01	1	0.5	28.29	4.99	23.3		JENDL-2
1324.85	1	0.5	22.915	0.315	22.6		JENDL-2
1331.48	1	0.5	25.05	1.35	23.7		JENDL-2
1361.21	1	0.5	25.706	0.506	25.2		JENDL-2
1386.15	1	0.5	27.329	0.329	27.0		JENDL-2
1387.22	1	0.5	23.68	0.08	23.6		JENDL-2
1393.81	0	0.5	235.2	211.0	24.2		JENDL-2
1405.43	0	0.5	98.2	72.8	25.4		JENDL-2
1416.92	1	0.5	27.47	3.47	24.0		JENDL-2
1419.76	0	0.5	32.66	9.16	23.5		JENDL-2
1428.01	0	0.5	53.9	28.5	25.4		JENDL-2
1438.3	1	0.5	23.941	0.441	23.5		JENDL-2
1444.05	0	0.5	37.7	15.0	22.7		JENDL-2
1447.65	1	0.5	24.95	1.15	23.8		JENDL-2
1455.1	1	0.5	26.504	0.204	26.3		JENDL-2
1456.7	1	0.5	23.84	0.24	23.6		JENDL-2
1473.82	0	0.5	144.9	121.0	23.9		JENDL-2
1487.04	1	0.5	27.025	0.225	26.8		JENDL-2
1504.3	1	0.5	27.83	0.23	27.6		JENDL-2
1508.1	1	0.5	23.9	0.4	23.5		JENDL-2
1510.53	1	0.5	25.044	0.844	24.2		JENDL-2
1522.7	0	0.5	268.8	245.0	23.8		JENDL-2
1527.86	1	0.5	24.394	0.794	23.6		JENDL-2
1534.79	1	0.5	24.086	0.786	23.3		JENDL-2
1547.18	1	0.5	27.81	3.81	24.0		JENDL-2
1550.3	1	0.5	28.18	3.18	25.0		JENDL-2
1555.38	1	0.5	23.14	0.34	22.8		JENDL-2
1565.45	0	0.5	28.97	5.67	23.3		JENDL-2
1568.23	1	0.5	24.87	1.27	23.6		JENDL-2
1591.52	1	0.5	24.77	1.17	23.6		JENDL-2
1597.89	0	0.5	400.1	378.0	22.1		JENDL-2
1622.67	0	0.5	123.3	101.0	22.3		JENDL-2
1638.07	0	0.5	73.8	50.8	23.0		JENDL-2
1646.69	1	0.5	22.775	0.475	22.3		JENDL-2
1662.45	0	0.5	248.1	224.0	24.1		JENDL-2
1672.74	1	0.5	24.6952	9.519-2	24.6		JENDL-2
1688.78	0	0.5	130.5	107.0	23.5		JENDL-2
1695.99	1	0.5	22.986	0.386	22.6		JENDL-2
1706.7	1	0.5	24.9	1.4	23.5		JENDL-2
1709.85	0	0.5	116.5	89.5	27.0		JENDL-2
1722.89	0	0.5	40.1	17.4	22.7		JENDL-2
1745.65	1	0.5	24.69	1.69	23.0		JENDL-2
1755.89	0	0.5	165.0	139.0	26.0		JENDL-2
1776.4	1	0.5	24.185	0.685	23.5		JENDL-2
1781.34	1	0.5	24.7	1.2	23.5		JENDL-2
1782.69	0	0.5	685.6	662.0	23.6		JENDL-2
1797.35	1	0.5	27.12	2.92	24.2		JENDL-2
1808.4	0	0.5	38.1	19.0	19.1		JENDL-2
1823.59	1	0.5	24.188	0.788	23.4		JENDL-2
1834.22	1	0.5	25.01	0.41	24.6		JENDL-2
1846.1	0	0.5	30.4	11.1	19.3		JENDL-2
1868.03	1	0.5	27.66	1.16	26.5		JENDL-2
1869.64	1	0.5	26.42	2.52	23.9		JENDL-2
1881.09	1	0.5	24.97	1.47	23.5		JENDL-2
1893.88	1	0.5	25.05	1.55	23.5		JENDL-2
1902.83	0	0.5	68.3	44.2	24.1		JENDL-2
1913.28	1	0.5	35.66	3.56	32.1		JENDL-2
1917.16	0	0.5	62.5	39.8	22.7		JENDL-2
1925.43	1	0.5	24.551	0.951	23.6		JENDL-2
1942.7	1	0.5	24.077	0.677	23.4		JENDL-2
1953.79	0	0.5	27.95	4.25	23.7		JENDL-2
1968.98	0	0.5	850.8	822.0	28.8		JENDL-2
1974.91	0	0.5	461.4	438.0	23.4		JENDL-2
1990.23	1	0.5	25.09	1.39	23.7		JENDL-2
2001.15	1	0.5	22.768	0.568	22.2		JENDL-2
2023.68	0	0.5	250.4	227.0	23.4		JENDL-2
2030.49	0	0.5	69.9	46.9	23.0		JENDL-2
2049.02	1	0.5	25.48	2.18	23.3		JENDL-2
2052.8	1	0.5	24.56	0.86	23.7		JENDL-2
2063.38	1	0.5	23.85	0.25	23.6		JENDL-2
2071.42	1	0.5	31.41	2.11	29.3		JENDL-2
2080.71	1	0.5	25.22	1.62	23.6		JENDL-2
2086.04	1	0.5	27.99	4.39	23.6		JENDL-2
2088.62	0	0.5	48.4	25.6	22.8		JENDL-2
2096.29	0	0.5	50.6	26.3	24.3		JENDL-2
2104.07	1	0.5	25.14	1.44	23.7		JENDL-2
2110.37	1	0.5	24.2	0.6	23.6		JENDL-2
2114.05	1	0.5	27.745	0.845	26.9		JENDL-2
2121.27	1	0.5	23.85	0.25	23.6		JENDL-2
2124.18	1	0.5	28.0	3.7	24.3		JENDL-2
2140.67	1	0.5	24.6	1.0	23.6		JENDL-2
2145.56	0	0.5	98.4	74.7	23.7		JENDL-2
2152.76	0	0.5	324.4	300.0	24.4		JENDL-2
2173.12	1	0.5	25.89	2.19	23.7		JENDL-2
2178.96	1	0.5	24.4	0.8	23.6		JENDL-2

ENERGY (EV)	L	J	TOTAL WIDTH (MEV)	NEUTRON WIDTH (MEV)	GAMMA WIDTH (MEV)	FISSION WIDTH (MEV)	REFERENCE
2186.58	0	0.5	615.2	591.0	24.2		JENDL-2
2201.26	0	0.5	130.2	105.0	25.2		JENDL-2
2215.44	1	0.5	27.02	3.42	23.6		JENDL-2
2241.41	1	0.5	26.32	1.02	25.3		JENDL-2
2259.7	0	0.5	134.3	109.0	25.3		JENDL-2
2266.54	0	0.5	256.0	234.0	22.0		JENDL-2
2270.15	1	0.5	27.58	3.88	23.7		JENDL-2
2281.92	0	0.5	209.0	188.0	21.0		JENDL-2
2293.95	1	0.5	24.8	1.3	23.5		JENDL-2
2296.56	1	0.5	30.41	5.61	24.8		JENDL-2
2315.93	0	0.5	43.1	19.1	24.0		JENDL-2
2327.28	1	0.5	30.24	1.14	29.1		JENDL-2
2334.83	1	0.5	26.86	1.66	25.2		JENDL-2
2338.59	1	0.5	32.35	8.65	23.7		JENDL-2
2352.75	0	0.5	83.4	55.2	28.2		JENDL-2
2355.73	0	0.5	102.0	77.9	24.1		JENDL-2
2368.75	1	0.5	30.38	5.78	24.6		JENDL-2
2383.87	1	0.5	24.0	0.5	23.5		JENDL-2
2384.94	1	0.5	26.6	2.0	24.6		JENDL-2
2391.98	0	0.5	54.1	30.1	24.0		JENDL-2
2397.8	1	0.5	29.9	5.2	24.7		JENDL-2
2401.82	1	0.5	28.22	4.42	23.8		JENDL-2
2411.24	0	0.5	29.93	5.63	24.3		JENDL-2
2418.17	1	0.5	26.169	0.969	25.2		JENDL-2
2426.89	0	0.5	180.7	157.0	23.7		JENDL-2
2446.7	0	0.5	246.6	223.0	23.6		JENDL-2
2447.31	1	0.5	24.0	0.4	23.6		JENDL-2
2455.75	0	0.5	41.3	17.3	24.0		JENDL-2
2489.18	0	0.5	129.4	105.0	24.4		JENDL-2
2502.22	1	0.5	27.45	3.85	23.6		JENDL-2
2521.49	0	0.5	43.3	19.0	24.3		JENDL-2
2527.08	1	0.5	24.4	0.9	23.5		JENDL-2
2548.19	0	0.5	761.5	738.0	23.5		JENDL-2
2559.59	0	0.5	301.7	278.0	23.7		JENDL-2
2581.15	0	0.5	470.6	447.0	23.6		JENDL-2
2597.61	0	0.5	783.7	761.0	22.7		JENDL-2
2606.23	1	0.5	26.95	3.25	23.7		JENDL-2
2612.02	1	0.5	28.53	4.93	23.6		JENDL-2
2620.05	0	0.5	71.9	48.1	23.8		JENDL-2
2632.73	1	0.5	28.64	4.44	24.2		JENDL-2
2636.85	1	0.5	26.56	2.86	23.7		JENDL-2
2654.08	1	0.5	24.6	1.0	23.6		JENDL-2
2658.73	1	0.5	27.97	4.17	23.8		JENDL-2
2672.22	0	0.5	312.0	288.0	24.0		JENDL-2
2682.61	1	0.5	26.22	2.32	23.9		JENDL-2
2696.5	0	0.5	55.2	31.2	24.0		JENDL-2
2701.95	1	0.5	25.93	1.93	24.0		JENDL-2
2717.33	0	0.5	200.6	177.0	23.6		JENDL-2
2750.74	0	0.5	65.6	41.7	23.9		JENDL-2
2762.66	0	0.5	42.7	18.9	23.8		JENDL-2
2766.69	1	0.5	27.13	3.23	23.9		JENDL-2
2774.55	1	0.5	25.14	1.54	23.6		JENDL-2
2778.46	1	0.5	24.9	1.3	23.6		JENDL-2
2787.43	0	0.5	39.6	15.0	24.6		JENDL-2
2799.52	1	0.5	29.43	5.13	24.3		JENDL-2
2806.38	0	0.5	34.8	10.2	24.6		JENDL-2
2811.62	1	0.5	29.05	5.05	24.0		JENDL-2
2815.93	1	0.5	25.05	1.35	23.7		JENDL-2
2823.35	1	0.5	25.6	2.0	23.6		JENDL-2
2829.32	0	0.5	44.4	20.8	23.6		JENDL-2
2845.95	1	0.5	24.2	0.6	23.6		JENDL-2
2865.39	0	0.5	240.2	218.0	22.2		JENDL-2
2877.57	1	0.5	26.04	2.24	23.8		JENDL-2
2882.78	0	0.5	632.4	608.0	24.4		JENDL-2
2897.23	0	0.5	41.7	17.8	23.9		JENDL-2
2918.38	1	0.5	30.86	6.86	24.0		JENDL-2
2922.92	1	0.5	29.97	5.07	24.9		JENDL-2
2925.57	1	0.5	31.45	6.85	24.6		JENDL-2
2933.65	0	0.5	62.4	38.3	24.1		JENDL-2
2945.37	1	0.5	25.98	2.08	23.9		JENDL-2
2956.93	0	0.5	46.3	21.8	24.5		JENDL-2
2967.52	1	0.5	27.39	3.79	23.6		JENDL-2
2988.56	1	0.5	30.39	6.59	23.8		JENDL-2
3003.62	0	0.5	146.7	122.0	24.7		JENDL-2
3014.99	1	0.5	24.88	1.18	23.7		JENDL-2
3024.7	1	0.5	27.9	4.4	23.5		JENDL-2
3028.61	0	0.5	160.7	137.0	23.7		JENDL-2
3043.72	1	0.5	27.69	3.49	24.2		JENDL-2
3059.64	0	0.5	57.2	32.9	24.3		JENDL-2
3072.14	1	0.5	25.18	1.08	24.1		JENDL-2
3081.21	1	0.5	25.34	1.74	23.6		JENDL-2
3088.71	1	0.5	27.21	3.51	23.7		JENDL-2
3103.55	1	0.5	26.37	2.07	24.3		JENDL-2
3109.91	0	0.5	253.6	230.0	23.6		JENDL-2
3130.16	1	0.5	26.72	3.12	23.6		JENDL-2
3133.86	1	0.5	33.11	8.91	24.2		JENDL-2
3149.03	0	0.5	136.6	113.0	23.6		JENDL-2

ENERGY (EV)	L	J	TOTAL WIDTH (MEV)	NEUTRON WIDTH (MEV)	GAMMA WIDTH (MEV)	FISSION WIDTH (MEV)	REFERENCE
3169.8	0	0.5	34.5	10.9	23.6		JENDL-2
3178.83	0	0.5	117.3	93.5	23.8		JENDL-2
3188.91	0	0.5	133.1	111.0	22.1		JENDL-2
3205.81	0	0.5	120.0	96.2	23.8		JENDL-2
3219.67	0	0.5	34.32	9.52	24.8		JENDL-2
3226.34	0	0.5	49.3	24.9	24.4		JENDL-2
3240.23	1	0.5	26.45	1.45	25.0		JENDL-2
3248.86	0	0.5	49.3	26.2	23.1		JENDL-2
3263.89	1	0.5	27.31	1.71	25.6		JENDL-2
3267.53	1	0.5	33.8	9.5	24.3		JENDL-2
3273.29	0	0.5	43.0	13.6	29.4		JENDL-2
3279.51	0	0.5	308.6	285.0	23.6		JENDL-2
3297.47	0	0.5	35.6	10.1	25.5		JENDL-2
3307.81	1	0.5	28.5	5.0	23.5		JENDL-2
3312.18	0	0.5	189.6	166.0	23.6		JENDL-2
3321.64	0	0.5	161.7	139.0	22.7		JENDL-2
3333.66	0	0.5	130.1	106.0	24.1		JENDL-2
3341.25	1	0.5	27.75	4.15	23.6		JENDL-2
3346.82	1	0.5	25.0	1.5	23.5		JENDL-2
3355.81	0	0.5	148.8	125.0	23.8		JENDL-2
3366.78	1	0.5	24.5	0.9	23.6		JENDL-2
3378.3	1	0.5	31.35	7.75	23.6		JENDL-2
3383.59	1	0.5	27.95	3.35	24.6		JENDL-2
3389.74	0	0.5	50.9	26.0	24.9		JENDL-2
3399.28	1	0.5	31.43	7.73	23.7		JENDL-2
3408.77	0	0.5	266.7	243.0	23.7		JENDL-2
3417.93	1	0.5	28.22	3.92	24.3		JENDL-2
3436.49	0	0.5	448.9	425.0	23.9		JENDL-2
3458.14	0	0.5	755.7	731.0	24.7		JENDL-2
3485.8	0	0.5	122.6	98.8	23.8		JENDL-2
3495.64	0	0.5	35.7	10.7	25.0		JENDL-2
3513.02	1	0.5	25.52	1.92	23.6		JENDL-2
3514.66	1	0.5	25.2	1.6	23.6		JENDL-2
3522.39	1	0.5	26.08	2.18	23.9		JENDL-2
3528.51	1	0.5	30.04	6.34	23.7		JENDL-2
3561.59	0	0.5	293.6	270.0	23.6		JENDL-2
3574.04	0	0.5	460.6	437.0	23.6		JENDL-2
3595.02	0	0.5	81.4	57.6	23.8		JENDL-2
3623.24	0	0.5	52.3	24.3	28.0		JENDL-2
3629.8	0	0.5	558.6	535.0	23.6		JENDL-2
3637.05	1	0.5	31.59	7.99	23.6		JENDL-2
3653.99	1	0.5	26.63	2.63	24.0		JENDL-2
3662.39	1	0.5	26.83	2.53	24.3		JENDL-2
3673.35	1	0.5	28.74	5.14	23.6		JENDL-2
3683.26	1	0.5	28.2	4.6	23.6		JENDL-2
3693.19	0	0.5	442.6	419.0	23.6		JENDL-2
3716.8	0	0.5	137.9	114.0	23.9		JENDL-2
3724.77	1	0.5	32.11	6.81	25.3		JENDL-2
3734.21	0	0.5	242.8	219.0	23.8		JENDL-2
3741.55	1	0.5	25.5	2.0	23.5		JENDL-2
3742.53	1	0.5	24.4	0.8	23.6		JENDL-2
3745.43	1	0.5	24.4	0.8	23.6		JENDL-2
3758.93	1	0.5	25.6	2.0	23.6		JENDL-2
3765.11	0	0.5	127.9	104.0	23.9		JENDL-2
3781.96	0	0.5	504.0	480.0	24.0		JENDL-2
3791.13	1	0.5	26.5	2.9	23.6		JENDL-2
3809.33	1	0.5	24.25	0.65	23.6		JENDL-2
3825.68	1	0.5	28.17	4.57	23.6		JENDL-2
3831.6	0	0.5	38.0	13.8	24.2		JENDL-2
3857.79	0	0.5	623.6	600.0	23.6		JENDL-2
3873.09	0	0.5	203.9	180.0	23.9		JENDL-2
3880.06	1	0.5	26.68	2.98	23.7		JENDL-2
3894.84	1	0.5	32.49	8.49	24.0		JENDL-2
3902.22	0	0.5	324.3	300.0	24.3		JENDL-2
3915.03	0	0.5	130.1	107.0	23.1		JENDL-2
3927.9	1	0.5	36.4	12.0	24.4		JENDL-2
3930.21	1	0.5	37.6	14.0	23.6		JENDL-2
3933.38	1	0.5	36.2	12.7	23.5		JENDL-2
3940.06	0	0.5	204.1	180.0	24.1		JENDL-2
3948.81	1	0.5	27.6	4.0	23.6		JENDL-2
3954.94	0	0.5	151.9	128.0	23.9		JENDL-2
3992.71	1	0.5	26.6	3.0	23.6		JENDL-2
4009.11	1	0.5	27.6	4.0	23.6		JENDL-2
4014.11	1	0.5	26.2	2.6	23.6		JENDL-2
4024.9	1	0.5	25.0	1.4	23.6		JENDL-2
4040.62	0	0.5	88.9	64.6	24.3		JENDL-2
4063.92	0	0.5	45.3	20.2	25.1		JENDL-2
4080.4	1	0.5	27.4	3.8	23.6		JENDL-2
4083.6	1	0.5	27.6	4.0	23.6		JENDL-2
4090.29	0	0.5	117.6	93.4	24.2		JENDL-2
4099.1	1	0.5	25.3	1.7	23.6		JENDL-2
4103.8	1	0.5	25.6	2.0	23.6		JENDL-2
4125.12	0	0.5	65.3	41.4	23.9		JENDL-2
4132.19	1	0.5	40.6	17.0	23.6		JENDL-2
4148.19	1	0.5	27.9	4.3	23.6		JENDL-2
4167.95	0	0.5	229.3	205.0	24.3		JENDL-2
4179.31	0	0.5	55.4	31.5	23.9		JENDL-2

ENERGY (EV)	L	J	TOTAL WIDTH (MEV)	NEUTRON WIOTH (MEV)	GAMMA WIOTH (MEV)	FISSION WIDTH (MEV)	REFERENCE
4201.99	1	0.5	27.6	4.0	23.6		JENDL-2
4210.72	0	0.5	62.9	38.4	24.5		JENDL-2
4225.52	1	0.5	33.6	10.0	23.6		JENDL-2
4258.76	0	0.5	55.8	31.2	24.6		JENDL-2
4299.54	0	0.5	162.0	138.0	24.0		JENDL-2
4307.04	0	0.5	134.3	110.0	24.3		JENDL-2
4325.15	0	0.5	106.0	81.3	24.7		JENDL-2
4371.0	0	0.5	176.1	152.0	24.1		JENDL-2
4435.55	0	0.5	124.5	100.0	24.5		JENDL-2
4511.74	0	0.5	607.4	583.0	24.4		JENDL-2
4543.45	0	0.5	117.8	93.1	24.7		JENDL-2
4567.76	0	0.5	68.1	43.6	24.5		JENDL-2
4594.67	0	0.5	48.3	22.8	25.5		JENDL-2
4632.17	0	0.5	52.1	27.6	24.5		JENDL-2
4662.9	0	0.5	170.2	146.0	24.2		JENDL-2
4705.73	0	0.5	356.1	332.0	24.1		JENDL-2
4727.89	0	0.5	43.8	19.4	24.4		JENDL-2

ENERGY (EV)	L	J	TOTAL WIDTH (MEV)	NEUTRON WIDTH (MEV)	GAMMA WIDTH (MEV)	FISSION WIDTH (MEV)	REFERENCE
-4.099	0	0.5	34.0582	4.0492	30.0	0.009	JENDL-2
1.056	0	0.5	32.0457	2.44	29.6	0.0057	JENDL-2
20.46	0	0.5	32.42	2.2	30.0	0.22	JENDL-2
38.34	0	0.5	47.22	17.0	30.0	0.22	JENDL-2
41.64	0	0.5	48.72	15.5	33.0	0.22	JENDL-2
66.66	0	0.5	81.22	50.0	31.0	0.22	JENDL-2
72.83	0	0.5	53.22	21.0	32.0	0.22	JENDL-2
90.78	0	0.5	42.52	12.8	29.5	0.22	JENDL-2
92.5	0	0.5	32.92	3.2	29.5	0.22	JENDL-2
105.05	0	0.5	78.72	43.0	35.5	0.22	JENDL-2
121.67	0	0.5	44.22	14.5	29.5	0.22	JENDL-2
130.9	0	0.5	30.41	0.19	30.0	0.22	JENDL-2
135.3	0	0.5	47.72	18.0	29.5	0.22	JENDL-2
151.9	0	0.5	44.12	14.4	29.5	0.22	JENDL-2
162.7	0	0.5	38.72	9.0	29.5	0.22	JENDL-2
170.1	0	0.5	44.82	15.1	29.5	0.22	JENDL-2
185.8	0	0.5	45.92	16.2	29.5	0.22	JENDL-2
192.2	0	0.5	30.52	0.3	30.0	0.22	JENDL-2
199.6	0	0.5	30.72	1.0	29.5	0.22	JENDL-2
239.3	0	0.5	42.82	13.1	29.5	0.22	JENDL-2
260.5	0	0.5	55.42	23.2	32.0	0.22	JENDL-2
287.1	0	0.5	155.22	125.0	30.0	0.22	JENDL-2
304.9	0	0.5	37.12	7.4	29.5	0.22	JENDL-2
318.5	0	0.5	35.92	6.2	29.5	0.22	JENDL-2
320.9	0	0.5	49.42	19.7	29.5	0.22	JENDL-2
338.4	0	0.5	37.12	7.4	29.5	0.22	JENDL-2
346.0	0	0.5	47.42	17.7	29.5	0.22	JENDL-2
363.7	0	0.5	67.72	32.5	35.0	0.22	JENDL-2
372.0	0	0.5	44.42	14.7	29.5	0.22	JENDL-2
405.0	0	0.5	137.72	108.0	29.5	0.22	JENDL-2
419.0	0	0.5	36.82	7.1	29.5	0.22	JENDL-2
446.2	0	0.5	32.42	2.2	30.0	0.22	JENDL-2
449.8	0	0.5	49.42	19.7	29.5	0.22	JENDL-2
466.4	0	0.5	33.12	3.4	29.5	0.22	JENDL-2
473.2	0	0.5	34.52	4.8	29.5	0.22	JENDL-2
493.9	0	0.5	38.32	8.6	29.5	0.22	JENDL-2
499.3	0	0.5	44.57	19.3	25.05	0.22	JENDL-2
514.3	0	0.5	67.22	31.0	36.0	0.22	JENDL-2
526.1	0	0.5	33.76	4.04	29.5	0.22	JENDL-2
530.8	0	0.5	30.42	0.7	29.5	0.22	JENDL-2
546.4	0	0.5	60.72	31.0	29.5	0.22	JENDL-2
553.2	0	0.5	49.92	20.2	29.5	0.22	JENDL-2
566.3	0	0.5	61.22	31.5	29.5	0.22	JENDL-2
584.1	0	0.5	30.86	1.14	29.5	0.22	JENDL-2
596.8	0	0.5	91.22	57.5	33.5	0.22	JENDL-2
608.0	0	0.5	45.945	22.685	23.2	0.06	JENDL-2
632.0	0	0.5	36.964	13.324	23.2	0.44	JENDL-2
637.0	0	0.5	34.98	11.61	23.2	0.17	JENDL-2
665.0	0	0.5	220.697	197.017	23.2	0.48	JENDL-2
678.6	0	0.5	50.018	26.038	23.2	0.78	JENDL-2
712.1	0	0.5	25.334	1.334	23.2	0.8	JENDL-2
743.0	0	0.5	27.209	1.009	23.2	3.0	JENDL-2
750.0	0	0.5	104.091	68.191	23.2	12.7	JENDL-2
759.0	0	0.5	30.681	6.061	23.2	1.42	JENDL-2
778.3	0	0.5	124.4	1.2	23.2	100.0	JENDL-2
782.4	0	0.5	1476.0	2.8	23.2	1450.0	JENDL-2
791.0	0	0.5	59.612	23.912	23.2	12.5	JENDL-2
810.5	0	0.5	248.955	214.155	23.2	11.6	JENDL-2
819.9	0	0.5	35.2981	10.9981	23.2	1.1	JENDL-2
845.6	0	0.5	34.31	10.18	23.2	0.93	JENDL-2
854.9	0	0.5	71.454	47.954	23.2	0.3	JENDL-2
876.5	0	0.5	38.071	13.911	23.2	0.96	JENDL-2
891.5	0	0.5	118.845	94.325	23.2	1.32	JENDL-2
904.0	0	0.5	45.819	21.949	23.2	0.67	JENDL-2
909.0	0	0.5	102.252	78.992	23.2	0.06	JENDL-2
915.3	0	0.5	59.756	35.996	23.2	0.56	JENDL-2
943.5	0	0.5	146.353	122.833	23.2	0.32	JENDL-2
958.4	0	0.5	94.888	71.498	23.2	0.19	JENDL-2
971.3	0	0.5	104.005	80.395	23.2	0.41	JENDL-2
979.2	0	0.5	31.496	7.196	23.2	1.1	JENDL-2
1001.8	0	0.5	122.449	98.129	23.2	1.12	JENDL-2
1024.1	0	0.5	34.72	5.0	29.5	0.22	JENDL-2
1041.6	0	0.5	36.919	12.589	23.2	1.13	JENDL-2
1045.7	0	0.5	33.72	4.0	29.5	0.22	JENDL-2
1072.6	0	0.5	132.917	109.407	23.2	0.31	JENDL-2
1099.8	0	0.5	107.654	84.204	23.2	0.25	JENDL-2
1115.7	0	0.5	32.32	2.6	29.5	0.22	JENDL-2
1129.0	0	0.5	73.295	49.395	23.2	0.7	JENDL-2
1134.0	0	0.5	30.535	6.735	23.2	0.6	JENDL-2
1143.0	0	0.5	63.89	40.57	23.2	0.12	JENDL-2
1159.0	0	0.5	45.609	22.129	23.2	0.28	JENDL-2
1185.5	0	0.5	180.817	157.317	23.2	0.3	JENDL-2
1191.0	0	0.5	138.461	114.921	23.2	0.34	JENDL-2
1208.9	0	0.5	86.239	62.909	23.2	0.13	JENDL-2
1228.0	0	0.5	39.72	10.0	29.5	0.22	JENDL-2
1236.5	0	0.5	35.04	11.25	23.2	0.59	JENDL-2
1255.01	0	0.5	101.864	76.874	23.2	1.79	JENDL-2

ENERGY (EV)	L	J	TOTAL WIDTH (MEV)	NEUTRON WIDTH (MEV)	GAMMA WIDTH (MEV)	FISSION WIDTH (MEV)	REFERENCE
1281.4	0	0.5	34.02	4.3	29.5	0.22	JENDL-2
1300.3	0	0.5	269.581	244.911	23.2	1.47	JENDL-2
1328.1	0	0.5	393.336	369.296	23.2	0.84	JENDL-2
1345.0	0	0.5	49.709	26.039	23.2	0.47	JENDL-2
1350.9	0	0.5	38.02	8.3	29.5	0.22	JENDL-2
1363.0	0	0.5	31.284	7.384	23.2	0.7	JENDL-2
1377.0	0	0.5	88.868	64.568	23.2	1.1	JENDL-2
1389.0	0	0.5	42.362	14.162	23.2	5.0	JENDL-2
1402.2	0	0.5	2028.44	5.24	23.2	2000.0	JENDL-2
1408.5	0	0.5	1524.29	1.09	23.2	1500.0	JENDL-2
1426.0	0	0.5	65.13	36.63	23.2	5.3	JENDL-2
1429.0	0	0.5	39.926	15.126	23.2	1.6	JENDL-2
1450.0	0	0.5	90.212	63.592	23.2	3.42	JENDL-2
1462.9	0	0.5	46.969	21.059	23.2	2.71	JENDL-2
1481.2	0	0.5	34.145	9.245	23.2	1.7	JENDL-2
1540.7	0	0.5	130.72	101.0	29.5	0.22	JENDL-2
1549.5	0	0.5	186.42	156.7	29.5	0.22	JENDL-2
1563.7	0	0.5	144.42	114.7	29.5	0.22	JENDL-2
1575.3	0	0.5	149.952	126.242	23.2	0.51	JENDL-2
1609.6	0	0.5	59.229	34.909	23.2	1.12	JENDL-2
1621.4	0	0.5	58.32	28.6	29.5	0.22	JENDL-2
1643.0	0	0.5	136.82	107.1	29.5	0.22	JENDL-2
1662.6	0	0.5	93.62	63.9	29.5	0.22	JENDL-2
1688.0	0	0.5	57.138	32.868	23.2	1.07	JENDL-2
1724.0	0	0.5	108.817	83.457	23.2	2.16	JENDL-2
1741.6	0	0.5	49.072	25.042	23.2	0.83	JENDL-2
1764.0	0	0.5	75.51	51.66	23.2	0.65	JENDL-2
1771.4	0	0.5	39.52	9.8	29.5	0.22	JENDL-2
1779.0	0	0.5	520.72	491.0	29.5	0.22	JENDL-2
1841.0	0	0.5	159.617	125.717	23.2	10.7	JENDL-2
1853.0	0	0.5	61.787	34.437	23.2	4.15	JENDL-2
1873.0	0	0.5	105.578	77.468	23.2	4.91	JENDL-2
1901.0	0	0.5	235.482	209.282	23.2	3.0	JENDL-2
1916.6	0	0.5	129.103	35.903	23.2	70.0	JENDL-2
1936.0	0	0.5	2225.18	1.98	23.2	2200.0	JENDL-2
1943.3	0	0.5	37.82	8.1	29.5	0.22	JENDL-2
1944.0	0	0.5	32.936	7.936	23.2	1.8	JENDL-2
1949.1	0	0.5	112.077	82.577	23.2	6.3	JENDL-2
1956.2	0	0.5	309.204	261.004	23.2	25.0	JENDL-2
1973.0	0	0.5	92.96	67.96	23.2	1.8	JENDL-2
1991.5	0	0.5	144.22	114.5	29.5	0.22	JENDL-2
1998.3	0	0.5	35.32	5.6	29.5	0.22	JENDL-2
2016.7	0	0.5	78.363	52.523	23.2	2.64	JENDL-2
2022.9	0	0.5	85.22	55.5	29.5	0.22	JENDL-2
2033.4	0	0.5	134.465	101.475	23.2	9.79	JENDL-2
2056.0	0	0.5	97.398	68.468	23.2	5.73	JENDL-2
2082.8	0	0.5	128.52	98.8	29.5	0.22	JENDL-2
2110.7	0	0.5	43.42	13.7	29.5	0.22	JENDL-2
2154.0	0	0.5	39.867	14.387	23.2	2.28	JENDL-2
2182.0	0	0.5	115.32	85.6	29.5	0.22	JENDL-2
2198.2	0	0.5	159.72	130.0	29.5	0.22	JENDL-2
2240.6	0	0.5	63.82	34.1	29.5	0.22	JENDL-2
2256.6	0	0.5	164.22	134.5	29.5	0.22	JENDL-2
2277.9	0	0.5	456.72	427.0	29.5	0.22	JENDL-2
2290.7	0	0.5	238.22	208.5	29.5	0.22	JENDL-2
2303.3	0	0.5	46.92	17.2	29.5	0.22	JENDL-2
2334.4	0	0.5	66.32	36.6	29.5	0.22	JENDL-2
2350.9	0	0.5	61.32	31.6	29.5	0.22	JENDL-2
2365.8	0	0.5	270.72	241.0	29.5	0.22	JENDL-2
2373.4	0	0.5	39.44	9.74	29.5	0.2	JENDL-2
2386.1	0	0.5	48.42	18.7	29.5	0.22	JENDL-2
2405.0	0	0.5	54.82	25.1	29.5	0.22	JENDL-2
2416.0	0	0.5	94.62	64.9	29.5	0.22	JENDL-2
2434.3	0	0.5	234.72	205.0	29.5	0.22	JENDL-2
2459.4	0	0.5	55.32	25.6	29.5	0.22	JENDL-2
2470.8	0	0.5	75.22	45.5	29.5	0.22	JENDL-2
2485.3	0	0.5	50.92	21.2	29.5	0.22	JENDL-2
2521.0	0	0.5	139.22	109.5	29.5	0.22	JENDL-2
2538.6	0	0.5	317.22	287.5	29.5	0.22	JENDL-2
2549.2	0	0.5	109.42	79.7	29.5	0.22	JENDL-2
2575.3	0	0.5	71.398	47.718	23.2	0.48	JENDL-2
2639.5	0	0.5	460.587	425.867	29.5	5.22	JENDL-2
2652.0	0	0.5	74.223	36.563	23.2	14.46	JENDL-2
2692.8	0	0.5	531.905	344.705	23.2	164.0	JENDL-2
2717.0	0	0.5	69.162	40.672	23.2	5.29	JENDL-2
2739.2	0	0.5	208.24	177.0	29.5	1.74	JENDL-2
2748.4	0	0.5	136.629	102.259	23.2	11.17	JENDL-2
2817.6	0	0.5	66.594	41.414	23.2	1.98	JENDL-2
2843.5	0	0.5	180.705	156.815	23.2	0.69	JENDL-2
2860.0	0	0.5	53.284	27.274	23.2	2.81	JENDL-2
2882.0	0	0.5	59.72	30.0	29.5	0.22	JENDL-2
2895.6	0	0.5	89.72	60.0	29.5	0.22	JENDL-2
2905.0	0	0.5	144.72	115.0	29.5	0.22	JENDL-2
2938.0	0	0.5	161.72	132.0	29.5	0.22	JENDL-2
2968.6	0	0.5	114.72	85.0	29.5	0.22	JENDL-2
2980.5	0	0.5	137.72	108.0	29.5	0.22	JENDL-2
2986.2	0	0.5	42.22	12.5	29.5	0.22	JENDL-2

ENERGY (EV)	L	J	TOTAL WIDTH (MEV)	NEUTRON WIDTH (MEV)	GAMMA WIDTH (MEV)	FISSION WIDTH (MEV)	REFERENCE
2994.7	0	0.5	85.72	56.0	29.5	0.22	JENDL-2
3004.0	0	0.5	106.22	76.5	29.5	0.22	JENDL-2
3018.0	0	0.5	146.72	117.0	29.5	0.22	JENDL-2
3029.0	0	0.5	50.72	21.0	29.5	0.22	JENDL-2
3054.7	0	0.5	76.72	47.0	29.5	0.22	JENDL-2
3077.4	0	0.5	157.72	128.0	29.5	0.22	JENDL-2
3088.0	0	0.5	64.72	35.0	29.5	0.22	JENDL-2
3112.7	0	0.5	68.22	38.5	29.5	0.22	JENDL-2
3172.5	0	0.5	254.72	225.0	29.5	0.22	JENDL-2
3192.5	0	0.5	378.72	349.0	29.5	0.22	JENDL-2
3237.5	0	0.5	101.72	72.0	29.5	0.22	JENDL-2
3268.5	0	0.5	163.72	134.0	29.5	0.22	JENDL-2
3332.0	0	0.5	44.22	14.5	29.5	0.22	JENDL-2
3423.0	0	0.5	64.22	34.5	29.5	0.22	JENDL-2
3458.0	0	0.5	97.72	68.0	29.5	0.22	JENDL-2
3465.5	0	0.5	373.72	344.0	29.5	0.22	JENDL-2
3493.5	0	0.5	94.72	65.0	29.5	0.22	JENDL-2
3555.0	0	0.5	120.72	91.0	29.5	0.22	JENDL-2
3567.5	0	0.5	191.72	162.0	29.5	0.22	JENDL-2
3595.0	0	0.5	58.22	28.5	29.5	0.22	JENDL-2
3657.0	0	0.5	322.72	293.0	29.5	0.22	JENDL-2
3665.0	0	0.5	84.22	54.5	29.5	0.22	JENDL-2
3702.0	0	0.5	80.72	51.0	29.5	0.22	JENDL-2
3723.0	0	0.5	89.72	60.0	29.5	0.22	JENDL-2
3800.0	0	0.5	130.72	101.0	29.5	0.22	JENDL-2
3844.0	0	0.5	105.72	76.0	29.5	0.22	JENDL-2
3852.0	0	0.5	127.72	98.0	29.5	0.22	JENDL-2
3872.0	0	0.5	75.72	46.0	29.5	0.22	JENDL-2
3900.0	0	0.5	238.72	209.0	29.5	0.22	JENDL-2
3917.0	0	0.5	192.72	163.0	29.5	0.22	JENDL-2
3954.0	0	0.5	121.72	92.0	29.5	0.22	JENDL-2
3975.0	0	0.5	131.72	102.0	29.5	0.22	JENDL-2
3990.0	0	0.5	58.72	29.0	29.5	0.22	JENDL-2
4031.0	0	0.5	138.72	109.0	29.5	0.22	JENDL-2
4084.0	0	0.5	149.72	120.0	29.5	0.22	JENDL-2
4100.0	0	0.5	286.72	257.0	29.5	0.22	JENDL-2
4122.0	0	0.5	526.72	497.0	29.5	0.22	JENDL-2
4134.0	0	0.5	96.72	67.0	29.5	0.22	JENDL-2
4149.0	0	0.5	294.72	265.0	29.5	0.22	JENDL-2
4161.0	0	0.5	118.72	89.0	29.5	0.22	JENDL-2
4203.0	0	0.5	467.72	438.0	29.5	0.22	JENDL-2
4221.0	0	0.5	97.72	68.0	29.5	0.22	JENDL-2
4270.0	0	0.5	188.72	159.0	29.5	0.22	JENDL-2
4288.0	0	0.5	345.72	316.0	29.5	0.22	JENDL-2
4329.0	0	0.5	331.72	302.0	29.5	0.22	JENDL-2
4376.0	0	0.5	111.72	82.0	29.5	0.22	JENDL-2
4386.0	0	0.5	61.72	32.0	29.5	0.22	JENDL-2
4398.0	0	0.5	107.72	78.0	29.5	0.22	JENDL-2
4422.0	0	0.5	90.72	61.0	29.5	0.22	JENDL-2
4433.0	0	0.5	76.72	47.0	29.5	0.22	JENDL-2
4458.0	0	0.5	131.72	102.0	29.5	0.22	JENDL-2
4570.0	0	0.5	249.72	220.0	29.5	0.22	JENDL-2
4588.0	0	0.5	555.72	526.0	29.5	0.22	JENDL-2
4599.0	0	0.5	104.72	75.0	29.5	0.22	JENDL-2
4615.0	0	0.5	291.72	262.0	29.5	0.22	JENDL-2
4646.0	0	0.5	178.72	149.0	29.5	0.22	JENDL-2
4721.0	0	0.5	539.72	510.0	29.5	0.22	JENDL-2
4745.0	0	0.5	274.72	245.0	29.5	0.22	JENDL-2
4755.0	0	0.5	85.72	56.0	29.5	0.22	JENDL-2
4766.0	0	0.5	44.72	15.0	29.5	0.22	JENDL-2
4771.0	0	0.5	51.72	22.0	29.5	0.22	JENDL-2
4779.0	0	0.5	63.72	34.0	29.5	0.22	JENDL-2
4792.0	0	0.5	162.72	133.0	29.5	0.22	JENDL-2
4812.0	0	0.5	201.72	172.0	29.5	0.22	JENDL-2
4823.0	0	0.5	92.72	63.0	29.5	0.22	JENDL-2
4894.0	0	0.5	88.72	59.0	29.5	0.22	JENDL-2
4958.0	0	0.5	320.72	291.0	29.5	0.22	JENDL-2
4969.0	0	0.5	187.72	158.0	29.5	0.22	JENDL-2
4993.0	0	0.5	121.72	92.0	29.5	0.22	JENDL-2
5072.0	0	0.5	538.72	509.0	29.5	0.22	JENDL-2
5113.0	0	0.5	122.72	93.0	29.5	0.22	JENDL-2
5134.0	0	0.5	71.72	42.0	29.5	0.22	JENDL-2
5148.0	0	0.5	79.72	50.0	29.5	0.22	JENDL-2
5162.0	0	0.5	69.72	40.0	29.5	0.22	JENDL-2
5194.0	0	0.5	342.72	313.0	29.5	0.22	JENDL-2
5215.0	0	0.5	192.72	163.0	29.5	0.22	JENDL-2
5249.0	0	0.5	553.72	524.0	29.5	0.22	JENDL-2
5279.0	0	0.5	169.72	140.0	29.5	0.22	JENDL-2
5299.0	0	0.5	299.72	270.0	29.5	0.22	JENDL-2
5334.0	0	0.5	232.72	203.0	29.5	0.22	JENDL-2
5350.0	0	0.5	182.72	153.0	29.5	0.22	JENDL-2
5367.0	0	0.5	99.72	70.0	29.5	0.22	JENDL-2
5393.0	0	0.5	113.72	84.0	29.5	0.22	JENDL-2
5417.0	0	0.5	284.72	255.0	29.5	0.22	JENDL-2
5489.0	0	0.5	79.72	50.0	29.5	0.22	JENDL-2
5499.0	0	0.5	116.72	87.0	29.5	0.22	JENDL-2
5510.0	0	0.5	384.72	355.0	29.5	0.22	JENDL-2

ENERGY (EV)	L	J	TOTAL WIDTH (MEV)	NEUTRON WIDTH (MEV)	GAMMA WIDTH (MEV)	FISSION WIDTH (MEV)	REFERENCE
5522.0	0	0.5	201.72	172.0	29.5	0.22	JENDL-2
5544.0	0	0.5	611.72	582.0	29.5	0.22	JENDL-2
5574.0	0	0.5	787.72	758.0	29.5	0.22	JENDL-2
5592.0	0	0.5	236.72	207.0	29.5	0.22	JENDL-2
5615.0	0	0.5	91.72	62.0	29.5	0.22	JENDL-2
5681.0	0	0.5	135.72	106.0	29.5	0.22	JENDL-2
5692.0	0	0.5	120.72	91.0	29.5	0.22	JENDL-2

ENERGY (EV)	L	J	TOTAL WIDTH (MEV)	NEUTRON WIDTH (MEV)	GAMMA WIDTH (MEV)	FISSION WIDTH (MEV)	REFERENCE
2.67	0	0.5	27.387	1.97	25.4	0.017	JENDL-2
14.6	0	0.5	24.311	0.061	24.2	0.05	JENDL-2
22.57	0	0.5	20.336	0.286	20.0	0.05	JENDL-2
40.95	0	0.5	29.501	0.451	29.0	0.05	JENDL-2
53.46	0	0.5	75.8949	51.95	23.9	0.045	JENDL-2
67.6	0	0.5	27.1225	4.578	22.5	0.0445	JENDL-2
88.45	0	0.5	24.8782	0.64	24.2	0.0382	JENDL-2
107.32	0	0.5	38.5394	16.99	21.5	0.0494	JENDL-2
131.4	0	0.5	37.0335	6.17	30.8	0.0635	JENDL-2
141.43	0	0.5	24.369	0.119	24.2	0.05	JENDL-2
149.7	0	0.5	39.2954	14.24	25.0	0.0554	JENDL-2
163.5	0	0.5	24.787	0.537	24.2	0.05	JENDL-2
204.8	0	0.5	73.5847	52.73	20.8	0.0548	JENDL-2
210.0	0	0.5	24.74	0.424	24.2	0.116	JENDL-2
215.3	0	0.5	41.384	5.2	36.0	0.184	JENDL-2
219.3	0	0.5	24.606	0.29	24.2	0.116	JENDL-2
232.7	0	0.5	33.071	4.94	28.0	0.131	JENDL-2
264.5	0	0.5	24.697	0.381	24.2	0.116	JENDL-2
271.95	0	0.5	24.481	0.165	24.2	0.116	JENDL-2
273.8	0	0.5	39.332	15.43	23.8	0.102	JENDL-2
274.75	0	0.5	24.486	0.17	24.2	0.116	JENDL-2
281.05	0	0.5	24.446	0.13	24.2	0.116	JENDL-2
298.7	0	0.5	34.426	8.31	26.0	0.116	JENDL-2
303.6	0	0.5	39.987	17.42	22.5	0.067	JENDL-2
319.9	0	0.5	256.478	232.9	23.5	0.0783	JENDL-2
327.6	0	0.5	24.816	0.5	24.2	0.116	JENDL-2
332.4	0	0.5	107.822	77.21	30.5	0.112	JENDL-2
374.3	0	0.5	30.696	6.38	24.2	0.116	JENDL-2
379.63	0	0.5	24.586	0.27	24.2	0.116	JENDL-2
382.2	0	0.5	68.0247	44.68	23.26	0.0847	JENDL-2
396.1	0	0.5	26.816	2.5	24.2	0.116	JENDL-2
399.9	0	0.5	25.936	1.62	24.2	0.116	JENDL-2
410.6	0	0.5	31.646	7.33	24.2	0.116	JENDL-2
424.1	0	0.5	28.546	4.23	24.2	0.116	JENDL-2
425.15	0	0.5	24.596	0.28	24.2	0.116	JENDL-2
473.7	0	0.5	25.106	0.79	24.2	0.116	JENDL-2
482.5	0	0.5	44.502	20.27	23.5	0.732	JENDL-2
494.75	0	0.5	24.586	0.27	24.2	0.116	JENDL-2
503.9	0	0.5	174.386	150.0	24.2	0.186	JENDL-2
536.6	0	0.5	121.177	100.0	21.0	0.177	JENDL-2
548.6	0	0.5	99.1939	74.0	25.0	0.194	JENDL-2
576.1	0	0.5	54.316	30.0	24.2	0.116	JENDL-2
595.0	0	0.5	53.0611	32.04	21.0	0.0211	JENDL-2
599.8	0	0.5	33.412	9.11	24.2	0.102	JENDL-2
610.8	0	0.5	36.214	11.95	24.2	6.399-2	JENDL-2
638.5	0	0.5	28.65	4.41	24.2	0.04	JENDL-2
665.0	0	0.5	26.966	2.7	24.2	0.066	JENDL-2
669.3	0	0.5	37.432	13.14	24.2	9.199-2	JENDL-2
693.2	0	0.5	61.052	36.65	22.0	0.402	JENDL-2
711.6	0	0.5	141.233	121.57	19.5	0.163	JENDL-2
727.6	0	0.5	27.42	3.17	24.2	0.05	JENDL-2
736.7	0	0.5	126.566	101.59	24.2	0.776	JENDL-2
755.1	0	0.5	159.623	135.4	21.5	2.723	JENDL-2
761.2	0	0.5	208.24	4.14	24.2	179.9	JENDL-2
788.5	0	0.5	87.274	61.4	24.2	1.674	JENDL-2
794.0	0	0.5	230.843	206.6	24.2	0.043	JENDL-2
824.5	0	0.5	29.057	4.65	24.2	0.207	JENDL-2
837.7	0	0.5	57.491	37.45	20.0	0.041	JENDL-2
856.6	0	0.5	57.441	35.3	22.0	0.141	JENDL-2
865.6	0	0.5	34.553	10.31	24.2	0.043	JENDL-2
878.1	0	0.5	83.0469	58.82	24.2	0.027	JENDL-2
886.5	0	0.5	51.7555	22.74	29.0	0.0155	JENDL-2
923.2	0	0.5	77.4789	59.45	18.0	0.029	JENDL-2
935.4	0	0.5	35.25	11.0	24.2	0.05	JENDL-2
939.6	0	0.5	34.25	10.0	24.2	0.05	JENDL-2
949.1	0	0.5	40.05	14.0	26.0	0.05	JENDL-2
977.9	0	0.5	38.75	14.5	24.2	0.05	JENDL-2
1004.0	0	0.5	67.2499	43.0	24.2	0.05	JENDL-2
1030.0	0	0.5	70.2499	46.0	24.2	0.05	JENDL-2
1045.0	0	0.5	142.25	118.0	24.2	0.05	JENDL-2
1062.5	0	0.5	57.25	33.0	24.2	0.05	JENDL-2
1087.5	0	0.5	224.25	200.0	24.2	0.05	JENDL-2
1117.0	0	0.5	29.25	5.0	24.2	0.05	JENDL-2
1129.5	0	0.5	34.25	10.0	24.2	0.05	JENDL-2
1148.0	0	0.5	324.25	300.0	24.2	0.05	JENDL-2
1182.5	0	0.5	37.25	13.0	24.2	0.05	JENDL-2
1197.0	0	0.5	119.25	95.0	24.2	0.05	JENDL-2
1207.0	0	0.5	64.2499	40.0	24.2	0.05	JENDL-2
1248.0	0	0.5	33.25	9.0	24.2	0.05	JENDL-2
1267.0	0	0.5	51.25	27.0	24.2	0.05	JENDL-2
1286.0	0	0.5	83.2499	59.0	24.2	0.05	JENDL-2
1696.0	0	0.5	63.3609	39.1	24.2	0.061	JENDL-2
1708.0	0	0.5	117.401	93.2	24.2	0.001	JENDL-2
1737.0	0	0.5	33.385	9.1	24.2	0.085	JENDL-2
1739.0	0	0.5	45.789	21.5	24.2	0.089	JENDL-2
1751.0	0	0.5	33.685	9.4	24.2	0.085	JENDL-2
1762.0	0	0.5	109.616	85.4	24.2	0.016	JENDL-2

ENERGY (EV)	L	J	TOTAL WIDTH (MEV)	NEUTRON WIDTH (MEV)	GAMMA WIDTH (MEV)	FISSION WIDTH (MEV)	REFERENCE
1783.0	0	0.5	24.367	0.022	24.2	0.145	JENDL-2
1789.0	0	0.5	25.13	0.13	24.2	0.8	JENDL-2
1806.0	0	0.5	37.212	12.9	24.2	0.112	JENDL-2
1820.0	0	0.5	28.615	4.1	24.2	0.315	JENDL-2
1836.0	0	0.5	117.8	3.0	24.2	90.6	JENDL-2
1862.0	0	0.5	29.508	4.9	24.2	0.408	JENDL-2
1881.0	0	0.5	108.553	84.3	24.2	0.053	JENDL-2
1891.0	0	0.5	29.1	4.1	24.2	0.8	JENDL-2

Evaluation of Resonance Parameters of ^{233}U, ^{235}U, ^{239}Pu and ^{241}Pu

Yasuyuki KIKUCHI*, Akira ASAMI** and Tadashi YOSHIDA***
Japanese Nuclear Data Committee, Japan Atomic Energy Research Institute

Abstract

The resonance parameters of ^{233}U, ^{235}U, ^{239}Pu and ^{241}Pu were evaluated for Japanese Evaluated Nuclear Data Library Version 2 (JENDL-2). The evaluation was made by two steps. At first, the parameters were evaluated on the basis of the reported measured data with a suitable method which depends on the status of measured data. The most reliable parameter set could be found after some simple examinations for ^{233}U, ^{239}Pu and ^{241}Pu, since total number of measured parameter sets is limited for these nuclides. On the other hand, numerous measurements exist for ^{235}U, and the evaluation was made by taking a suitable average, considering the fission and capture areas. Secondly, the cross sections were calculated with the parameters thus obtained, and were compared with the measured cross sections. Then the parameters were so modified that the calculated cross sections well reproduced the measured data. After modifying the resonance parameters, the remaining discrepancies between the calculated and measured cross sections, which are mainly caused by the interference among levels and are inevitable with the single-level Breit-Wigner formula, were corrected by applying slight background cross sections. The resonance integrals calculated from the presently evaluated parameters agree well with the measured data.

* Japan Atomic Energy Research Institute
** National Laboratory for High Energy Physics
*** Nippon Atomic Industry Group, Ltd.

1. Introduction

Evaluation of resonance parameters for main fissile and fertile materials has been made for several years by a working group of Japanese Nuclear Data Committee in order to provide the evaluataed resonance parameters to Japanese Evaluated Nuclear Data Library (JENDL). The evaluation of resonance parameters is a very complicated problem, and the working group recommended some existing evaluated data such as those of ENDF/B-IV for the first version of JENDL (JENDL-1)[1] in 1975.

After that the evaluation was continued and finished in 1979, and the presently evaluated resonance parameters were adopted in the second version of JENDL (JENDL-2). The present paper describes the evaluation for the fissile materials, while the evaluation for the fertile materials is reported in another paper[2] presented in this meeting. The general evaluation method is described in Chapter 2. The detailed evaluation procedure is given in Chapter 3 for each nuclide. The presently evaluated resonance parameters are tabulated in Appendix.

2. Evaluation Method

Experimental data of resonance parameters were surveyed through CINDA[3] up to CINDA 78. The collected resonance parameters were stored in the resonance parameter storage system REPSTOR[4]. In this system many types of resonance parameters including complicated forms such as $g\Gamma_n\Gamma_\gamma/\Gamma$ or $\sigma_0\Gamma$ can be stored and can be compared with one another in simple tabulation forms.

Experimental cross section data were also surveyed through CINDA. Most of numerical data were obtained from NEA Data Bank, and were stored in the neutron data storage and retrieval system NESTOR[4].

In evaluating nuclear cross sections, a common procedure is to plot at first all the experimental data as a function of neutron energy, and then deduce the most reasonable curve by carefully comparing the different sets of data and studying the accuracy and errors of the data. In the resonance region, however, this procedure is not always adequate, because a resonance shape usually depends on the resolution function of the spectrometer used for the measurement but this function is not well

known in many cases. Furthermore, it is not practical to apply this procedure in the case where many resonances exist in a limited region.

In the present evaluation, therefore, two steps were taken. Firstly, the resonance parameters were evaluated on the basis of the reported measured parameters with a suitable method which depends on the status of measured data. As total number of measured parameter sets is limited for ^{233}U, ^{239}Pu and ^{241}Pu, the most reliable set could be found after some simple examinations for these nuclides. On the other hand, numerous measurements exist for ^{235}U, and the evaluation was made by taking a suitable average of the measured parameters.

Secondly, the cross sections were calculated with the parameters thus obtained, and were compared with the measured cross sections. Then the parameters were so modified that the calculated cross sections well reproduced the measured data. This process was made by using NDES[5] (Neutron Data Evaluation System) in which conversation with the computer is made from a terminal having a cathode ray tube. The calculated cross sections are displayed on the cathode ray tube with the experimental data, and the cross sections calculated with the modified parameters can be also displayed and compared. At present NDES has no function of automatic search for the resonance parameters, and the fitting procedure above mentioned was done by trial and error.

Even after modifying the resonance parameters, the calculated fission cross section failed to reproduce the measured data in limited energy ranges particularly in valleys between resonances. This is caused by the interference among resonances. The multi-level formula is essentially required for fissile nuclides. In the present work, however, the discrepancy was corrected by applying a positive or negative background cross section to the fission cross section. This work was made also by using NDES which has a function to record the X-Y coodinates of any point in the graph displayed on the cathode ray tube into computer memory by using a cross hair cursor.

The thermal cross sections below 1 eV cannot be well reproduced with the resonance parameters for the fissile nuclides because of the interference among levels. Hence the cross sections were given as point-wise data below 1 eV for these 4 nuclides.

3. Evaluation and Discussion

3.1 Uranium-233

This nuclide was not contained in JENDL-1. The resolved resonance region is defined between 1 and 100 eV. Details of the evaluation were described in Ref. (6).

A total of six parameter sets have so far been reported. After examing their experimental conditions and comparing the calculated areas and cross sections, it was concluded that the parameter set deduced by Nizamuddin and Blons[7] was the most reliable. Their parameters were deduced from both the high resolution measurements of fission cross section by Blons[8] and the transmission measurements by Kolar et al.[9] Nizamuddin and Blons gave the parameters for 169 levels, 33 of which are artificial levels added to partially compensate the interference effects among levels. In the energy range below 6 eV, where Nizamuddin and Blons did not give the parameters, the recommended data in BNL-325, 3rd edition[10] were adopted as the initial guess.

The cross sections were calculated from the parameters by assuming the effective scattering radius of 9.93 fm. The calculated total and fission cross sections agree well with the measured data within their scatters in most of energy ranges. It should be noted that the calculated capture cross section agreed well with the measured data by Weston et al.[11], though the resonance parameters were deduced by Nizamuddin and Blons without considering the capture data. This suggests reliability of the parameters of Nizamuddin and Blons. In some energy ranges, however, agreement was not satisfactory between the calculated and measured cross sections. The resonance parameters were modified to improve the agreement in such energy ranges by using NDES[5].

After modifying the parameters, the remaining discrepancies between the calculated and measured fission cross sections were corrected by applying positive or negative background cross sections. Figure 1 shows the fission cross sections calculated with and without the background cross section as well as the measured data in the energy range between 13 and 16 eV. No background correction was applied to the capture and elastic scattering cross sections.

As shown in Table 1 the fission and capture resonance integrals calculated from the present parameters agree with the recommended values in BNL-325, 3rd edition[10] within the quoted errors. They also agree with those calculated from the ENDF/B-IV parameters.

3.2 Uranium-235

The parameters of ENDF/B-IV were recommended in JENDL-1. In JENDL-2, the presently evaluated parameters were applied in the energy region between 1 and 100 eV.

Tremendous number of measurements were made for the resonance parameters of ^{235}U, since this nuclide is one of the most important nuclide in nuclear reactor development. In the present evaluation only the data reported in the last twenty years were collected and stored in REPSTOR.

The evaluation of the resonance parameters at the first step was made in the following way. Since $2g\Gamma_n$ values do not differ appreciably among those of different experiments, a simple average was taken over them to give the evaluated values. In determining Γ_γ values, a weighted average was taken, where a weight of a half was given to those data which were obtained indirectly by analyzing the fission and total cross sections. The evaluation of Γ_f values seems to require a special care, as the reported values are considerably discrepant with one another. Hence the fission area $A_f = g\Gamma_n\Gamma_f/\Gamma$ was first calculated in this case. In the case where only Γ_f values were given, A_f is calculated using the Γ_f and evaluated $g\Gamma_n$ and Γ_γ values. Discrepancy of A_f is usually less than that of Γ_f. A resonance area is, as is well known, independent of the resolution of the spectrometer, and therefore is one of the most suitable quantities to be used in the resonance parameter evaluation. The value of fission width was calculated from the average of fission areas.

The fission, capture and total cross sections were calculated from these parameters thus obtained and were compared with the experimental data. As to the experimental data, we mainly relied on the data of Michaudon et al.[12], Cao et al.[13] and Blons et al.[14] for fission, those of de Saussure et al.[15] and Perez et al.[16] for capture and those of Garg et al.[17] and Michaudon et al.[12] for the total cross section.

In the region where the difference is appreciable between the two, correction of the parameters was made for resonances responsible for this difference. If the magnitudes of the total and either of fission or capture areas were considered to deviate from the experimental values, the $g\Gamma_n$ value was varied. If only the capture area was unsuitable, small corrections $\Delta\Gamma_\gamma$ and $\Delta\Gamma_f$ were obtained by

$$\Delta\Gamma_\gamma = \frac{\Delta A_\gamma}{A_\gamma} \frac{1 + r_1}{1 - r_1 - 2r_1/r_2}, \qquad (1)$$

$$\Delta\Gamma_f = \Delta\Gamma_\gamma / r_2,$$

where

$$r_1 = \frac{\Gamma_\gamma}{\Gamma_f}, \quad \text{and} \quad r_2 = \frac{1}{2}(r_1 - 1). \qquad (2)$$

If the fission cross section is to be varied, similar corrections are obtained by exchanging suffix γ and f. With these corrected parameters, the cross sections were calculated and compared again with the experimental values.

Figure 2 shows an example of the results thus obtained. All the experimental data of the capture and total cross sections available are shown, whereas only some typical data are shown for the fission cross sections. As is seen in the figure, there is a good agreement. In the calculation the Doppler broadening effect is included, which is essential to obtain good fit to the experimental data for most of the resonances in this nuclide. At some energies, particularly at the valleys of resonances, discrepancies still remain. The difference was corrected by the background cross sections. Table 2 compares the fission and capture resonance integrals with the recommended values in BNL-325, 3rd edition[10]. The calculated integrals agree well with the recommended values.

3.3 Plutonium-239

In the compilation of JENDL-1, a set of resonance parameters evaluated by Ribon[18] was adopted, for it is a complete set of parameters which reproduces experimental data fairly well. This parameter set covers the energy range between 1 and 600 eV. Since then, no

complete set of resonance parameters has been evaluated on the basis of new extensive cross section measurements.

For JENDL-2, Ribon's set was adopted again as the initial guess values. Modification of parameters was limited to several resonances, since his parameter set well reproduces the measured cross sections as a whole. Background cross sections were also added to improve agreement between the calculated and measured cross sections. We fitted the calculated data mainly to the fission cross section measured by Derrien et al.[19] and the capture cross section by Gwin et al.[20,21] by using NDES.

Figure 3 shows the fission cross section of JENDL-2 with those of JENDL-1 and ENDF/B-IV as well as the experimental data. The difference between JENDL-2 and JENDL-1 was mainly caused by the background cross section.

Table 3 compares the averaged values of the fission cross section and the capture to fission ratio (α-value) between the evaluated and the measured data. The fission cross section of JENDL-2 seems to be too small in the interval between 200 and 300 eV and too large between 300 and 400 eV. This is reflected on overestimate of the α-value between 200 and 300 eV. The present background correction was made by comparing the resonance cross sections without considering the average cross sections. This drawback on the average cross sections is left for future improvement. Table 3 also compares the fission and capture resonance integrals with those recommended in BNL-325, 3rd edition[10]. Satisfactory agreement is observed for both the integrals.

3.4 Plutonium-241

In JENDL-1, the resonance parameters recommended in BNL-325, 3rd edition[10] were adopted[24] in the energy range from 1 eV to 100 eV. These parameters were mainly taken from analyses by Blons et al.[25] and by Kolar et al.[26] These paremeters satisfactorily reproduce the total and fission cross sections but a little underestimate the capture cross section[24].

In the evaluation of JENDL-2, the same parameters were adopted as the initial guess values, since no extensive measurements have so far been reported on the resonance parameters of ^{241}Pu after JENDL-1.

The cross sections were calculated by assuming the effective scattering radius of 10.0 fm. The resonance parameters were modified so that the calculated total, fission and capture cross sections might reproduce the measured data by Kolar and Carraro[27], by Blons[8] and by Weston and Todd[28], respectively. As the numerical data of Weston and Todd were not available at the time of the present evaluation, the fitting to the capture cross section was made to the resonances below 20 eV for which the peak values of Weston and Todd were read from graphs in Ref. (28).

The background cross sections were applied to both the fission and capture cross sections. The background fission cross section was determined by NDES so as to compensate the remaining discrepancies between the calculated and measured data due to the interference among levels.

As was pointed out previously, the present resonance parameters a little underestimate the capture cross section and the discrepancy was corrected by the smooth background cross section. Table 4 shows the average fission and capture cross sections calculated with and without the background cross sections as well as the average values of measured data. Figure 4 shows the calculated fission and capture cross sections with the measured data as an example.

Table 4 also compares the calculated resonance integrals with the measured data by Eiland et al.[31] The present parameters slightly overestimate the capture integral and underestimate the fission integral, but give better results than JENDL-1 and ENDF/B-IV. Further inprovement is required for the lowest few resonances taking account of the numerical cross section data of Weston and Todd.

4. Concluding Remarks

The resonance parameters were evaluated for ^{233}U, ^{235}U, ^{239}Pu and ^{241}Pu, and were adopted in JENDL-2. In the present work, the resonance parameters were first evaluated on the basis of the measured parameter data, and then were adjusted by fitting the calculated cross sections to

the measured ones. Hence the presently evaluated parameters can reproduce the measured total, fission and capture cross sections very well. The agreement was further improved by applying slight background corrections. Moreover the calculated resonance integrals agree well with the measured ones. Hence the data of JENDL-2 are expected to well predict the thermal reactor characteristics.

The authors wish to thank to members of Working Group on Heavy-Nuclide Nuclear Data of JNDC for their helpful discussion. They particularly acknowledge T. Nakagawa for his advice in using NDES and for his aid in treating the evaluated data files. One of the authors (A.A.) would like to express his sincere thanks to M. Sugimoto for his assistance in the evaluation.

References

1) IGARASI, S., NAKAGAWA, T., KIKUCHI, Y., ASAMI, T. and NARITA, T.: "Japanese Evaluated Nuclear Data Library, Version-1 — JENDL-1 —", JAERI-1261 (1979), NEANDC(J)-59/L, INDC(JAP)-45/L.
2) NAKAGAWA, T., ZUKERAN, A. and KAWAI, M.: "Evaluation of Resonance Parameters of ^{238}U, ^{240}Pu and ^{242}Pu", Contributed paper to IAEA Consultants Meeting on Uranium and Plutonium Isotope Resonance Parameters, 28 Sept. - 2 Oct., 1981, Vienna.
3) IAEA: An Index to the Literature on Microscopic Neutron Data.
4) NAKAGAWA, T.: Proc. 1978 Seminar on Nuclear Data, Dec. 20 - 21, 1978, Tokai, p.51, JAERI-M 8163 (1979) [in Japanese].
5) NAKAGAWA, T.: J. At. Energy Soc. Jpn., 22, 559 (1980) [in Japanese].
6) KIKUCHI, Y.: "Evaluation of Neutron Nuclear Data for ^{233}U in Thermal and Resonance Regions", JAERI-M 9318 (1981), NEANDC(J)-69/U, INDC(JAP)-56/L.
7) NIZAMUDDIN, S. and BLONS, J.: Nucl. Sci. Eng., 54, 116 (1974).
8) BLONS, J.: Nucl. Sci. Eng., 51, 130 (1973).
9) KOLAR, W., CARRARO, G., NASTRI, G.: "Nuclear Data for Reactors", Conf. Proc., Helsinki, 15 - 19 June 1970, Vol. 1, p. 387 (1970), IAEA.
10) MUGHABGAB, S. F. and GARBER, D. I.: "Neutron Cross Sections, Vol. 1, Resonance Parameters", BNL-325, 3rd Edition (1973).
11) WESTON, L. W., GWIN, R., DE SAUSSURE, G., FULLWOOD, R. R. and HOCKENBURY, R. W.: Nucl. Sci. Eng., 34, 1 (1968).
12) MICHAUDON, A., DERRIEN, H., RIBON, P. and SANCHE, M.: Nucl. Phys., 69, 545 (1965).
13) CAO, M. G., MIGNECO, E., THEOBALD, J. P., WARTENA, J. A. and WINTER, J.: J. Nucl. Energy, 22, 211 (1968).
14) BLONS, J., DERRIEN, H. and MICHAUDON, A.: "Neutron Cross Sections and Technology", Proc. Conf., Knoxville, Mar. 15 - 19, 1971, CONF-710301, p. 829 (1971).
15) DE SAUSSURE, G., WESTON, L. W., GWIN, R., INGLE, R. W., TODD, J. H., HOCKENBURY, R. W., FULLWOOD, R. R. and LOTTIN, A.: "Nuclear Data for Reactors", Conf. Proc. Paris, 17 - 21 Oct. 1966, Vol. II, p. 233 (1967), IAEA.
16) PEREZ, R. B., DE SAUSSURE, G., SILVER, E. G., INGLE, R. W. and WEAVER, H.: Nucl. Sci. Eng., 52, 46 (1973).
17) GARG, J. B., HAVENS, W. W., Jr. and RAINWATER, J.: Taken from SCISRS Data (1964).
18) RIBON, P. and LE COQ, G.: "Evaluation des Données Neutroniques de ^{239}Pu", CEA — N — 1484 (1971).
19) DERRIEN, H., BLONS, J. and MICHAUDON, A.: "Nuclear Data for Reactors", Conf. Proc., Helsinki, 15 - 19 June 1970, Vol. 1, p. 481 (1970), IAEA.
20) GWIN, R., WESTON, L. W., DE SAUSSURE, G., INGLE, R. W., TODD, J. H., GILLESPIE, F. E., HOCKENBURY, R. W. and BLOCK, R. C.: Nucl. Sci. Eng., 45, 25 (1971).
21) GWIN, R., SILVER, E. G., INGLE, R. W. and WEAVER, H.: Nucl. Sci. Eng., 59, 79 (1976).
22) WESTON, L. W. and TODD, J. H.: Private Communication to Chrien (1972). Data Taken from Table III of Ref. (20).
23) SOWERBY, M. G. and KONSHIN, V. A.: At. Energy Rev., 10, 453 (1972).
24) KIKUCHI, Y.: J. Nucl. Sci. Technol., 14, 467 (1977).
25) BLONS, J., DERRIEN, H. and MICHAUDON, A.: "Neutron Cross Sections and Technology", Proc. Conf. Knoxville, Mar. 15 - 17, 1971, CONF-710301, p. 836 (1971).
26) KOLAR, W., THEOBALD, J. P. and WARTENA, J. A.: ibid., p. 823.
27) KOLAR, W. and CARRARO, G.: ibid., p. 707.
28) WESTON, L. W. and TODD, J. H.: Nucl. Sci. Eng., 65, 454 (1978).
29) MIGNECO, E., THEOBALD, J. P. and WARTENA, J. A.: "Nuclear Data for Reactors", Conf. Proc., Helsinki, 15 - 19 June 1970, Vol. 1, p. 437 (1970), IAEA.
30) JAMES, G. D.: ibid., Vol. 1, p. 267.
31) EILAND, H. M., ESCH, L. J., FEINER, F. and MEWHERTER, J. L.: Nucl. Sci. Eng., 44, 180 (1971).

Table 1. Resonance Intgrals of ^{233}U.

(barns)

	JENDL-2	ENDF/B-IV	BNL-325[10]
fission	771	763	764 ± 13
capture	138	135	140 ± 6

Table 2. Resonance integrals of ^{235}U.

(barns)

	JENDL-2	ENDF/B-IV (JENDL-1)	BNL-325[10]
fission	279	284	275 ± 5
capture	146	139	144 ± 6

Table 3. Average cross sections and resonance integrals of ^{239}Pu.

(barns)

	Energy (keV)	JENDL-2	JENDL-1	ENDF/B-IV	Gwin 76[21]	Weston 72[22]
σ_f	0.05 ∿ 0.1	60.17	60.30	56.94	56.96	58.76
	0.1 ∿ 0.2	18.67	18.42	18.38	17.96 ± 0.04	18.41
	0.2 ∿ 0.3	17.21	17.49	17.64	17.90 ± 0.05	17.77
	0.3 ∿ 0.4	9.09	9.50	8.35	8.48 ± 0.03	8.43
	0.4 ∿ 0.5	9.64	9.66	9.55	9.40 ± 0.05	9.47
	0.5 ∿ 0.6	15.70	16.20	15.44	15.46 ± 0.09	15.64

	Energy (keV)	JENDL-2	JENDL-1	ENDF/B-IV	Gwin 76[21]	Sowerby 72[23]	Weston 72[22]
α	0.05 ∿ 0.1	0.62	0.61	0.64	0.63	-	0.64
	0.1 ∿ 0.2	0.92	0.82	0.93	0.87 ± 0.015	0.845 ± 0.077	0.87
	0.2 ∿ 0.3	0.98	0.89	0.99	0.94 ± 0.010	0.912 ± 0.094	0.92
	0.3 ∿ 0.4	1.11	0.91	1.13	1.16 ± 0.014	1.15 ± 0.099	1.15
	0.4 ∿ 0.5	0.51	0.40	0.46	0.44 ± 0.013	0.483 ± 0.058	0.42
	0.5 ∿ 0.6	0.69	0.57	0.73	0.72 ± 0.040	0.704 ± 0.069	0.72

		JENDL-2	JENDL-1	ENDF/B-IV	BNL-325[10]
R.I.	fission	302	302	304	301 ± 10
	capture	195	193	194	200 ± 20

Table 4. Average cross sections and resonance integrals of ^{241}Pu.

Fission cross section (barns)

E_{min} (ev)	E_{max} (eV)	Calculated		Experimental			
		with B.C.S.	wihout B.C.S.	Blons[8]*	Migneco[29]	James[30]	Weston[28]
10	20	149.1	147.2	145.9	146.8	—	151.7
20	30	83.9	86.3	81.5	82.9	74.9	86.2
30	40	49.1	50.1	46.6	46.5	45.0	49.3
40	50	40.6	41.5	38.9	36.5	41.0	43.7
50	60	16.7	17.3	15.9	16.8	20.3	17.5
60	70	56.7	59.1	53.8	56.5	59.0	58.7
70	80	22.6	21.6	24.8	28.9	28.7	25.7
80	90	68.9	68.3	65.6	68.6	64.5	73.7
90	100	25.4	25.4	24.9	27.7	31.3	27.2

* Average value of the results with 11 and 50 m flight paths.

Capture cross section (barns)

E_{min} (eV)	E_{max} (eV)	Calculated		Experimental (Weston and Todd[28])	
		with B.C.S.	without B.C.S.	α	σ_c*
10	20	81.1	69.7	0.559	83.3 ± 5.0
20	30	18.7	16.7	0.213	17.9 ± 1.1
30	40	10.7	10.7	0.216	10.6 ± 0.6
40	50	7.38	4.49	0.184	7.47 ± 0.44
50	60	3.01	1.35	0.198	3.31 ± 0.20
60	70	14.2	7.49	0.279	15.8 ± 0.9
70	80	15.2	15.2	0.572	12.9 ± 0.8
80	90	22.7	20.6	0.337	23.2 ± 1.4
90	100	5.42	4.92	0.207	5.26 ± 0.32

* Deduced from α-values using the present evaluated fission cross section. Errors are quoted 6 % errors in α-values.

Resonance integral with cut-off energy of 3 eV (barns)

Quantity	JENDL-2	JENDL-1	ENDF/B-IV	Eiland et al.[31]
fission	531	524	527	569 ± 37
capture	172	138	115	162 ± 8

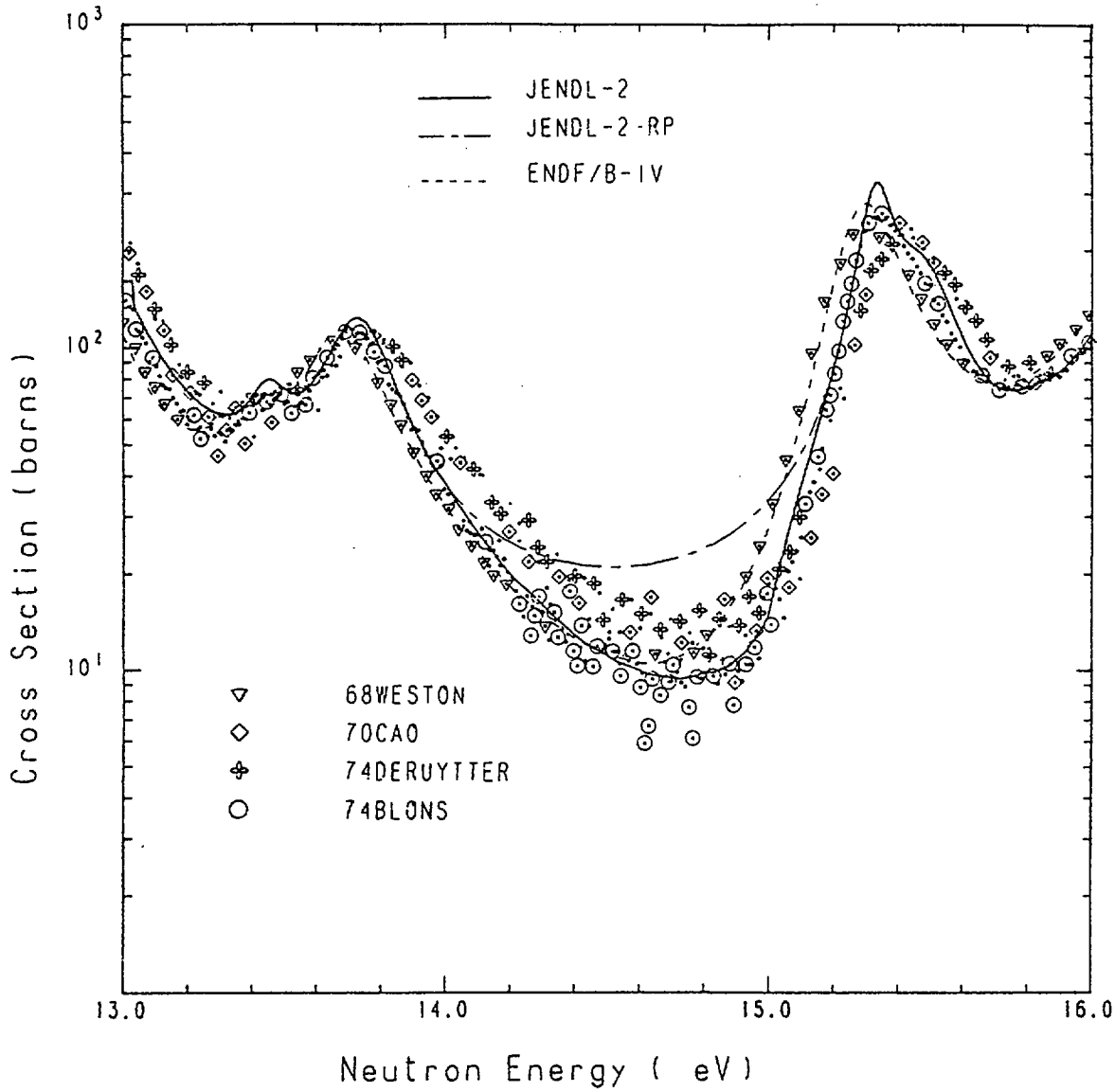

Fig. 1. Fission cross sections of ^{233}U in the energy range between 13 and 16 eV. The solid and dash-dotted lines are calculated from the present resonance parameters with and without the background cross section, respectively. The dotted line represents the value of ENDF/B-IV.

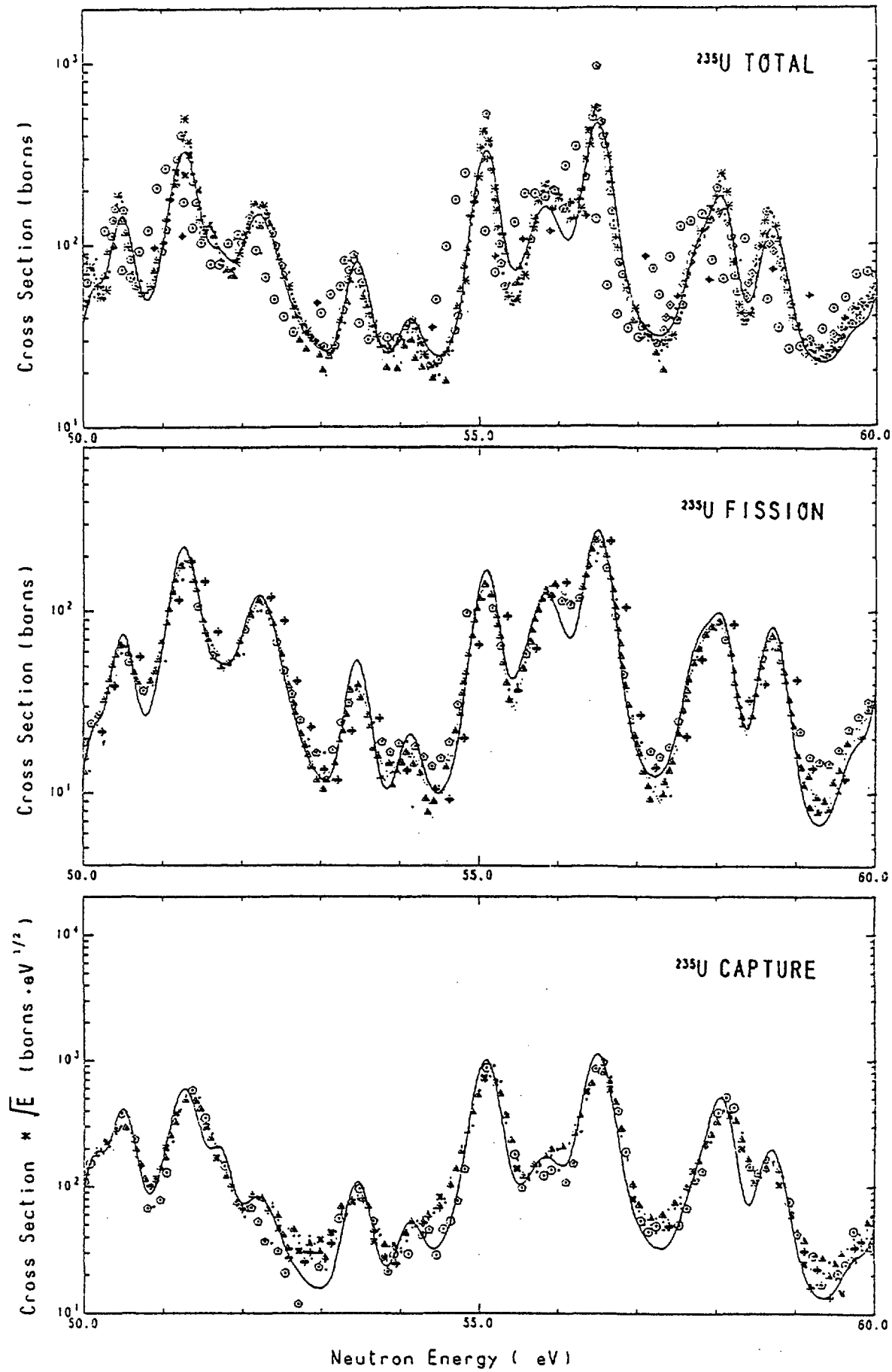

Fig. 2. Total, fission and capture cross sections of ^{235}U in the energy range between 50 and 60 eV. Note that the capture cross section is multiplied by the square root of neutron energy ($\sigma_c \sqrt{E}$ in barn $eV^{1/2}$ unit)

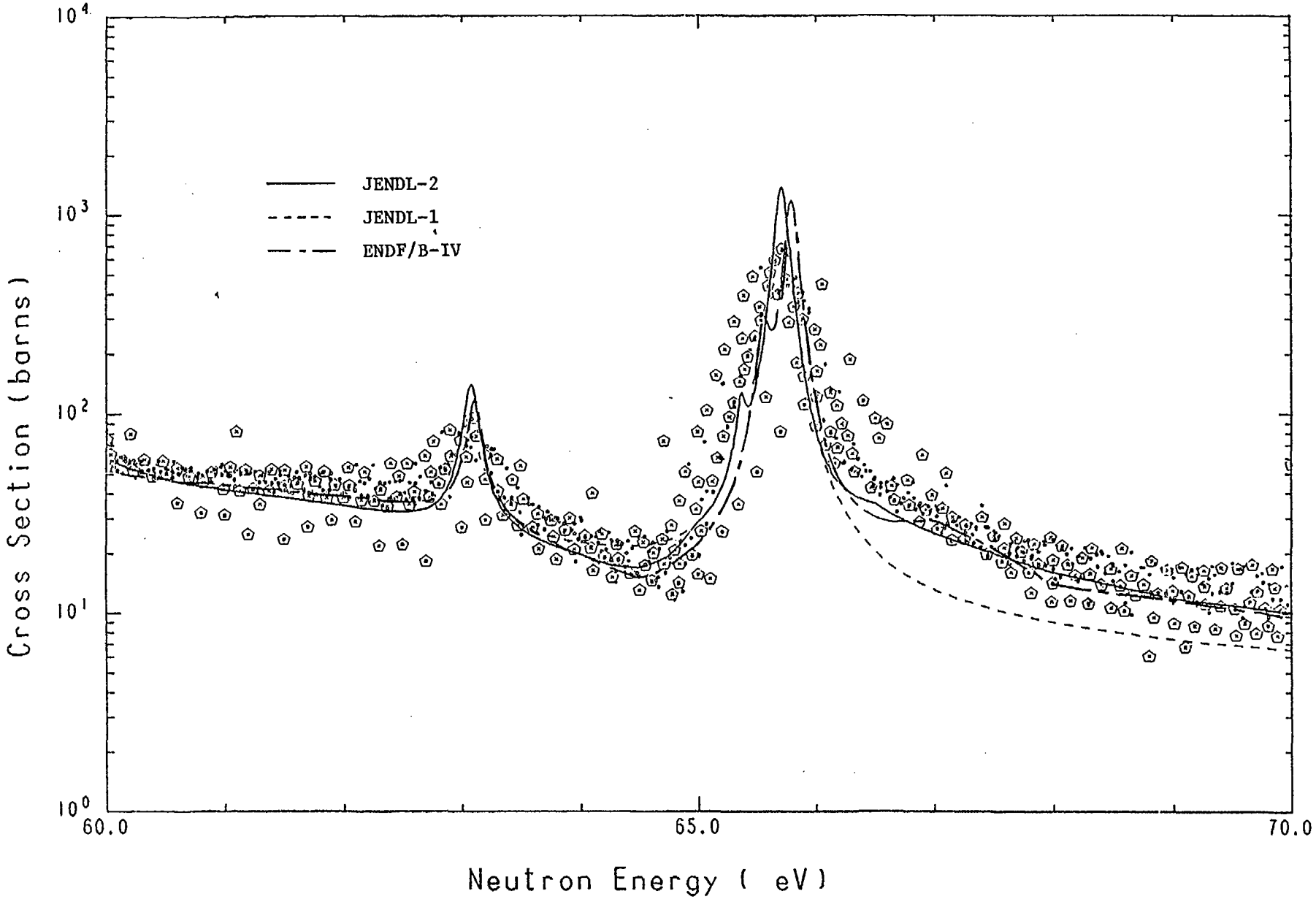

Fig. 3. Fission cross sections of ^{239}Pu in the energy range between 60 and 70 eV. The solid line represents the value of JENDL-2, the dotted line JENDL-1 and the dot-dashed line ENDF/B-IV.

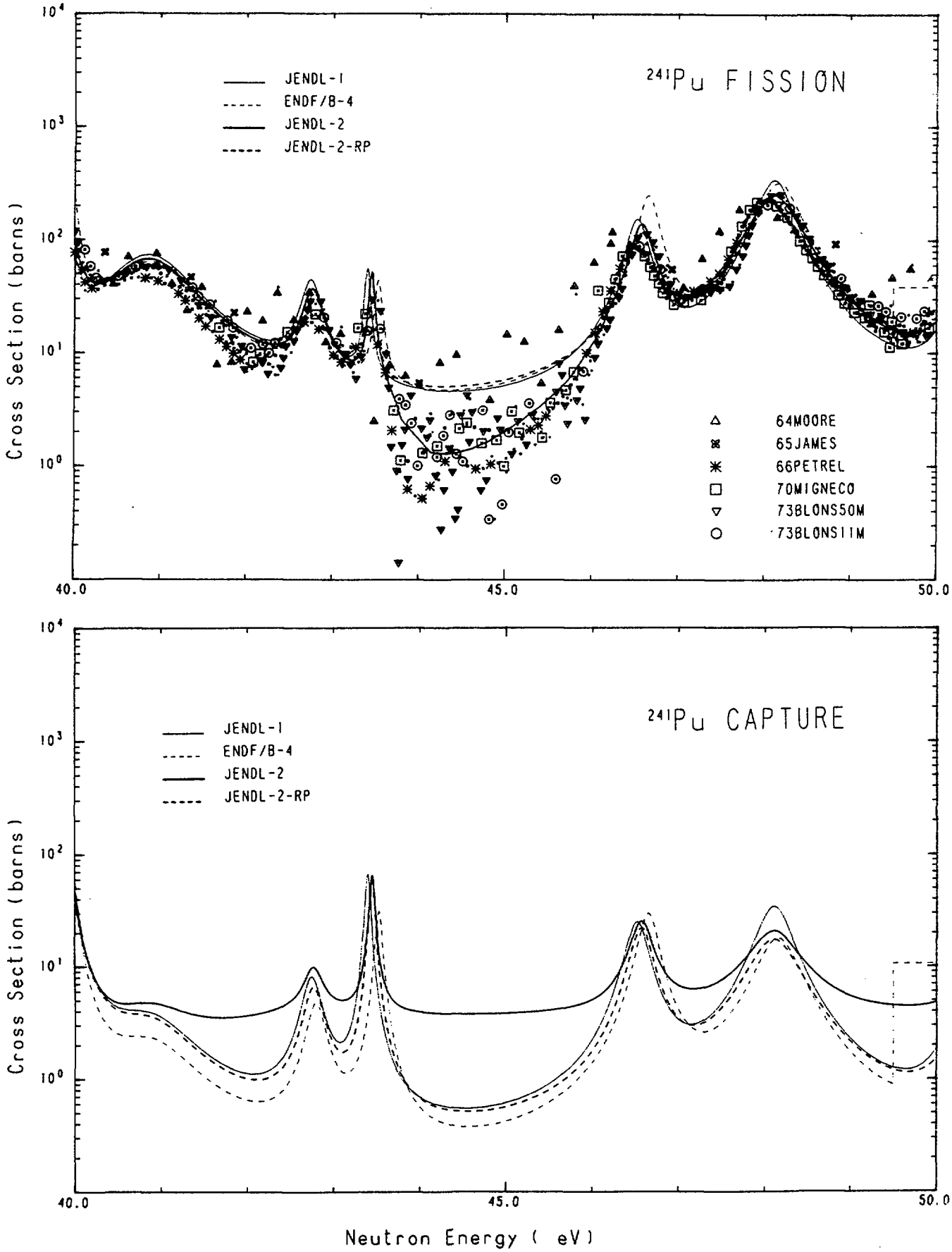

Fig. 4. Fission and capture cross sections of ^{241}Pu in the energy range between 40 and 50 eV. The thick solid and dotted lines are calculated from the present parameters with and without the background cross sections, respectively. The thin solid and dotted lines represent the values of JENDL-1 and ENDF/B-IV, respectively.

U-233 1

ENERGY (EV)	L	J	TOTAL WIDTH (MEV)	NEUTRON WIDTH (MEV)	GAMMA WIDTH (MEV)	FISSION WIDTH (MEV)	REFERENCE
-2.81	0	2.5	754.5	4.5	30.0	720.0	JENDL-2
0.17	0	2.5	100.0	0.0002	40.0	60.0	JENDL-2
1.45	0	2.5	530.11	0.11	30.0	500.0	JENDL-2
1.78	0	2.5	260.334	0.334	50.0	210.0	JENDL-2
2.17	0	2.5	125.03	0.03	10.0	115.0	JENDL-2
2.29	0	2.5	110.17	0.17	50.0	60.0	JENDL-2
3.49	0	2.5	500.07	0.07	45.0	455.0	JENDL-2
3.62	0	2.5	185.1	0.1	50.0	135.0	JENDL-2
4.76	0	2.5	900.31	0.31	45.0	855.0	JENDL-2
5.89	0	2.5	320.133	0.13282	39.0	281.0	JENDL-2
6.27	0	2.5	538.062	6.178-2	39.0	499.0	JENDL-2
6.64	0	2.5	500.313	0.31264	39.0	461.0	JENDL-2
6.82	0	2.5	138.796	0.79645	39.0	99.0	JENDL-2
7.5	0	2.5	200.028	0.028	39.0	161.0	JENDL-2
8.0	0	2.5	2039.08	0.08	39.0	2000.0	JENDL-2
8.64	0	2.5	339.05	0.05	39.0	300.0	JENDL-2
9.26	0	2.5	298.12	0.12	39.0	259.0	JENDL-2
9.71	0	2.5	500.06	0.06	39.0	461.0	JENDL-2
10.39	0	2.5	316.662	1.6618	57.0	258.0	JENDL-2
10.86	0	2.5	1000.01	8.606-3	39.0	961.0	JENDL-2
11.31	0	2.5	439.2	0.2	39.0	400.0	JENDL-2
11.89	0	2.5	2000.5	0.5	39.0	1961.0	JENDL-2
12.79	0	2.5	310.446	1.4457	55.0	254.0	JENDL-2
13.45	0	2.5	144.056	5.619-2	39.0	105.0	JENDL-2
13.73	0	2.5	255.309	0.30863	39.0	216.0	JENDL-2
15.33	0	2.5	122.464	0.46448	30.0	92.0	JENDL-2
15.47	0	2.5	255.473	0.47292	39.0	216.0	JENDL-2
15.82	0	2.5	200.02	0.02	39.0	161.0	JENDL-2
16.2	0	2.5	426.896	0.89638	39.0	387.0	JENDL-2
16.56	0	2.5	219.706	0.70587	39.0	180.0	JENDL-2
17.97	0	2.5	208.32	0.32005	39.0	169.0	JENDL-2
18.28	0	2.5	379.015	0.015	39.0	340.0	JENDL-2
18.48	0	2.5	135.158	0.15834	39.0	96.0	JENDL-2
18.96	0	2.5	317.754	1.7538	22.0	294.0	JENDL-2
19.63	0	2.5	2500.39	0.39487	39.0	2461.0	JENDL-2
20.59	0	2.5	364.773	0.77279	39.0	325.0	JENDL-2
21.58	0	2.5	2000.59	0.58669	39.0	1961.0	JENDL-2
21.86	0	2.5	255.062	1.0621	39.0	215.0	JENDL-2
22.34	0	2.5	415.332	3.3317	48.0	364.0	JENDL-2
22.9	0	2.5	692.554	0.55448	39.0	653.0	JENDL-2
23.75	0	2.5	453.554	0.55419	39.0	414.0	JENDL-2
24.3	0	2.5	1000.52	0.51997	39.0	961.0	JENDL-2
25.25	0	2.5	274.74	0.73993	39.0	235.0	JENDL-2
25.78	0	2.5	660.522	0.52169	39.0	621.0	JENDL-2
26.25	0	2.5	495.239	0.23872	39.0	456.0	JENDL-2
26.62	0	2.5	260.358	0.35778	39.0	221.0	JENDL-2
26.98	0	2.5	592.154	0.15398	39.0	553.0	JENDL-2
27.76	0	2.5	900.508	0.5083	39.0	861.0	JENDL-2
28.07	0	2.5	168.028	2.784-2	39.0	129.0	JENDL-2
28.28	0	2.5	230.233	0.23343	39.0	191.0	JENDL-2
29.04	0	2.5	541.764	1.7641	39.0	501.0	JENDL-2
29.58	0	2.5	112.138	0.13826	39.0	73.0	JENDL-2
30.35	0	2.5	396.154	0.15384	39.0	357.0	JENDL-2
30.72	0	2.5	261.627	0.62701	37.0	224.0	JENDL-2
31.33	0	2.5	325.298	0.29827	39.0	286.0	JENDL-2
31.69	0	2.5	600.465	0.46464	39.0	561.0	JENDL-2
32.01	0	2.5	217.951	0.95107	39.0	178.0	JENDL-2
33.14	0	2.5	740.719	0.71939	39.0	701.0	JENDL-2
33.95	0	2.5	1301.79	1.786	39.0	1261.0	JENDL-2
34.51	0	2.5	648.192	1.1924	48.0	599.0	JENDL-2
35.25	0	2.5	395.238	0.2383	39.0	356.0	JENDL-2
35.75	0	2.5	900.683	0.68306	39.0	861.0	JENDL-2
36.53	0	2.5	197.798	0.79785	39.0	158.0	JENDL-2
37.2	0	2.5	420.094	9.369-2	39.0	381.0	JENDL-2
37.48	0	2.5	395.697	0.69679	39.0	356.0	JENDL-2
39.33	0	2.5	686.794	0.794	39.0	647.0	JENDL-2
39.83	0	2.5	445.266	0.26599	39.0	406.0	JENDL-2
40.41	0	2.5	901.062	1.0616	39.0	861.0	JENDL-2
41.03	0	2.5	175.34	0.34	39.0	136.0	JENDL-2
41.79	0	2.5	392.035	3.534-2	39.0	353.0	JENDL-2
42.09	0	2.5	592.137	0.13727	39.0	553.0	JENDL-2
42.62	0	2.5	209.77	0.77	57.0	152.0	JENDL-2
43.5	0	2.5	341.4	0.4	20.0	321.0	JENDL-2
44.52	0	2.5	519.3	0.3	19.0	500.0	JENDL-2
45.25	0	2.5	138.025	0.025	39.0	99.0	JENDL-2
45.45	0	2.5	150.025	0.025	39.0	111.0	JENDL-2
46.1	0	2.5	192.39	0.39	39.0	153.0	JENDL-2
46.53	0	2.5	245.08	0.08	39.0	206.0	JENDL-2
47.22	0	2.5	507.88	0.88	39.0	468.0	JENDL-2
48.68	0	2.5	172.6	1.6	40.0	131.0	JENDL-2
49.1	0	2.5	516.5	0.5	39.0	477.0	JENDL-2
50.4	0	2.5	1100.84	0.84	39.0	1061.0	JENDL-2
51.0	0	2.5	500.114	0.114	39.0	461.0	JENDL-2
51.85	0	2.5	150.021	0.021	39.0	111.0	JENDL-2
52.1	0	2.5	280.055	0.055	39.0	241.0	JENDL-2
53.03	0	2.5	240.47	0.47	39.0	201.0	JENDL-2
53.32	0	2.5	360.44	0.44	39.0	321.0	JENDL-2

ENERGY (EV)	L	J	TOTAL WIDTH (MEV)	NEUTRON WIDTH (MEV)	GAMMA WIDTH (MEV)	FISSION WIDTH (MEV)	REFERENCE
53.94	0	2.5	230.198	0.19788	39.0	191.0	JENDL-2
54.05	0	2.5	501.3	1.3	39.0	461.0	JENDL-2
54.41	0	2.5	295.095	9.550-2	39.0	256.0	JENDL-2
54.78	0	2.5	264.1	1.1	39.0	224.0	JENDL-2
55.2	0	2.5	490.137	0.13703	39.0	451.0	JENDL-2
55.35	0	2.5	862.678	2.6782	39.0	821.0	JENDL-2
56.44	0	2.5	374.04	1.04	42.0	331.0	JENDL-2
56.88	0	2.5	1501.25	1.2454	39.0	1461.0	JENDL-2
57.48	0	2.5	782.36	2.36	49.0	731.0	JENDL-2
58.18	0	2.5	1301.51	1.5075	39.0	1261.0	JENDL-2
58.52	0	2.5	225.56	0.56	39.0	186.0	JENDL-2
60.95	0	2.5	940.87	0.87	39.0	901.0	JENDL-2
61.38	0	2.5	401.45	1.45	39.0	361.0	JENDL-2
62.59	0	2.5	213.5	1.5	52.0	160.0	JENDL-2
63.49	0	2.5	1000.2	0.2	39.0	961.0	JENDL-2
64.03	0	2.5	370.763	0.76317	39.0	331.0	JENDL-2
64.44	0	2.5	240.466	1.4662	39.0	200.0	JENDL-2
65.09	0	2.5	238.593	0.59289	39.0	199.0	JENDL-2
65.49	0	2.5	630.478	0.47853	39.0	591.0	JENDL-2
66.56	0	2.5	770.641	0.64077	39.0	731.0	JENDL-2
67.3	0	2.5	940.396	0.39572	39.0	901.0	JENDL-2
67.98	0	2.5	333.469	0.46914	39.0	294.0	JENDL-2
69.23	0	2.5	1002.3	2.3044	39.0	961.0	JENDL-2
70.19	0	2.5	534.989	1.9892	46.0	487.0	JENDL-2
71.75	0	2.5	349.246	0.24608	39.0	310.0	JENDL-2
72.22	0	2.5	800.52	0.5204	39.0	761.0	JENDL-2
73.43	0	2.5	126.707	1.707	39.0	86.0	JENDL-2
74.03	0	2.5	514.762	4.762	39.0	471.0	JENDL-2
75.0	0	2.5	258.673	0.67293	39.0	219.0	JENDL-2
75.49	0	2.5	293.255	3.255	39.0	251.0	JENDL-2
76.77	0	2.5	872.551	0.55086	39.0	833.0	JENDL-2
78.18	0	2.5	571.981	1.9814	39.0	531.0	JENDL-2
78.46	0	2.5	900.375	0.37478	39.0	861.0	JENDL-2
79.0	0	2.5	1200.68	0.68408	39.0	1161.0	JENDL-2
79.78	0	2.5	598.536	2.5356	39.0	557.0	JENDL-2
81.47	0	2.5	1301.6	1.5992	39.0	1261.0	JENDL-2
82.35	0	2.5	741.721	1.7214	39.0	701.0	JENDL-2
82.78	0	2.5	137.128	2.1278	39.0	96.0	JENDL-2
84.75	0	2.5	815.475	0.47454	39.0	776.0	JENDL-2
85.22	0	2.5	400.791	0.79108	39.0	361.0	JENDL-2
85.73	0	2.5	590.349	0.34957	39.0	551.0	JENDL-2
86.78	0	2.5	295.076	7.616-2	39.0	256.0	JENDL-2
87.13	0	2.5	150.359	0.3587	39.0	111.0	JENDL-2
87.7	0	2.5	88.012	1.199-2	39.0	49.0	JENDL-2
88.89	0	2.5	344.139	2.1396	39.0	303.0	JENDL-2
89.76	0	2.5	558.588	0.588	39.0	519.0	JENDL-2
90.55	0	2.5	260.256	7.2564	39.0	214.0	JENDL-2
91.72	0	2.5	740.59	0.58993	39.0	701.0	JENDL-2
92.67	0	2.5	518.298	1.2977	39.0	478.0	JENDL-2
93.25	0	2.5	590.38	0.38024	39.0	551.0	JENDL-2
93.77	0	2.5	105.6	1.5997	39.0	65.0	JENDL-2
95.22	0	2.5	102.654	1.6539	39.0	62.0	JENDL-2
96.42	0	2.5	1603.31	3.3119	39.0	1561.0	JENDL-2
97.81	0	2.5	233.759	4.7586	39.0	190.0	JENDL-2
98.58	0	2.5	316.971	1.9708	39.0	276.0	JENDL-2
99.3	0	2.5	541.386	1.3858	39.0	501.0	JENDL-2
99.95	0	2.5	542.626	2.6256	39.0	501.0	JENDL-2
101.29	0	2.5	1000.24	0.24082	39.0	961.0	JENDL-2
102.89	0	2.5	226.517	1.5167	39.0	186.0	JENDL-2
104.79	0	2.5	46140.6	1.5581	39.0	46100.0	JENDL-2
105.23	0	2.5	430.088	8.813-2	39.0	391.0	JENDL-2
105.95	0	2.5	192.437	2.4368	39.0	151.0	JENDL-2
106.51	0	2.5	273.034	3.0341	39.0	231.0	JENDL-2
106.95	0	2.5	327.869	2.8694	39.0	286.0	JENDL-2
107.83	0	2.5	351.479	1.4788	39.0	311.0	JENDL-2
108.2	0	2.5	400.822	0.82178	39.0	361.0	JENDL-2
108.64	0	2.5	220.402	0.40228	39.0	181.0	JENDL-2
109.36	0	2.5	419.045	4.0449	39.0	376.0	JENDL-2
109.98	0	2.5	520.815	0.81499	39.0	481.0	JENDL-2
110.88	0	2.5	409.234	5.2344	39.0	365.0	JENDL-2
112.53	0	2.5	1203.37	3.3662	39.0	1161.0	JENDL-2
113.55	0	2.5	1003.78	3.7796	39.0	961.0	JENDL-2

ENERGY (EV)	L	J	TOTAL WIDTH (MEV)	NEUTRON WIDTH (MEV)	GAMMA WIDTH (MEV)	FISSION WIDTH (MEV)	REFERENCE
-1.49	0	3.5	245.881	3.68	35.2015	207.0	JENDL-2
0.273	0	3.5	135.003	0.0032	36.0	99.0	JENDL-2
1.14	0	3.5	162.015	0.0154	41.0	121.0	JENDL-2
2.035	0	3.5	48.0081	0.0081	37.0	11.0	JENDL-2
2.84	0	3.5	191.005	0.0048	40.0	151.0	JENDL-2
3.14	0	3.5	131.021	0.021	36.0	95.0	JENDL-2
3.61	0	3.5	90.0469	0.047	36.0	54.0	JENDL-2
4.85	0	3.5	39.462	0.062	36.0	3.4	JENDL-2
5.45	0	3.5	90.0029	0.003	60.0	30.0	JENDL-2
5.6	0	3.5	620.033	0.033	20.0	600.0	JENDL-2
6.21	0	3.5	269.056	0.056	42.0	227.0	JENDL-2
6.39	0	3.5	49.27	0.27	38.0	11.0	JENDL-2
7.08	0	3.5	61.125	0.125	35.0	26.0	JENDL-2
8.79	0	3.5	131.15	1.15	33.0	97.0	JENDL-2
9.29	0	3.5	137.182	0.182	42.0	95.0	JENDL-2
9.73	0	3.5	245.046	0.046	45.0	200.0	JENDL-2
10.2	0	3.5	95.063	0.063	41.0	54.0	JENDL-2
10.8	0	3.5	927.093	0.093	67.0	860.0	JENDL-2
11.65	0	3.5	48.103	0.603	42.0	5.5	JENDL-2
12.4	0	3.5	69.28	1.28	43.0	25.0	JENDL-2
12.86	0	3.5	79.0448	0.0448	31.0	48.0	JENDL-2
13.28	0	3.5	98.047	0.047	36.0	62.0	JENDL-2
13.69	0	3.5	115.046	0.046	34.0	81.0	JENDL-2
14.0	0	3.5	469.48	0.48	36.0	433.0	JENDL-2
14.51	0	3.5	63.135	0.135	40.0	23.0	JENDL-2
15.4	0	3.5	85.245	0.245	43.0	42.0	JENDL-2
16.08	0	3.5	51.36	0.36	35.0	16.0	JENDL-2
16.69	0	3.5	124.283	0.283	34.0	90.0	JENDL-2
18.07	0	3.5	169.37	0.37	40.0	129.0	JENDL-2
18.96	0	3.5	91.095	0.095	48.0	43.0	JENDL-2
19.31	0	3.5	104.14	3.14	42.0	59.0	JENDL-2
20.13	0	3.5	260.12	0.12	31.0	229.0	JENDL-2
20.61	0	3.5	92.2	0.2	44.0	48.0	JENDL-2
21.08	0	3.5	67.49	1.49	42.0	24.0	JENDL-2
22.94	0	3.5	84.47	0.47	40.0	44.0	JENDL-2
23.42	0	3.5	37.66	0.66	30.0	7.0	JENDL-2
23.63	0	3.5	185.77	0.77	45.0	140.0	JENDL-2
24.25	0	3.5	70.322	0.322	37.0	33.0	JENDL-2
24.37	0	3.5	88.1399	0.14	35.0	53.0	JENDL-2
25.2	0	3.5	770.5	0.5	40.0	730.0	JENDL-2
25.59	0	3.5	414.66	0.66	24.0	390.0	JENDL-2
26.48	0	3.5	192.48	0.48	32.0	160.0	JENDL-2
27.15	0	3.5	115.12	0.12	40.0	75.0	JENDL-2
27.82	0	3.5	129.68	0.68	44.0	85.0	JENDL-2
28.38	0	3.5	146.17	0.17	35.0	111.0	JENDL-2
28.71	0	3.5	202.055	0.055	50.0	152.0	JENDL-2
29.64	0	3.5	68.18	0.18	40.0	28.0	JENDL-2
30.59	0	3.5	149.21	0.21	50.0	99.0	JENDL-2
30.86	0	3.5	60.5	0.5	39.0	21.0	JENDL-2
32.07	0	3.5	114.04	2.04	46.0	66.0	JENDL-2
33.53	0	3.5	59.82	1.82	36.0	22.0	JENDL-2
34.39	0	3.5	83.2199	2.22	44.0	37.0	JENDL-2
34.83	0	3.5	118.95	0.95	40.0	78.0	JENDL-2
35.2	0	3.5	134.6	3.6	43.0	88.0	JENDL-2
35.3	0	3.5	691.57	1.57	40.0	650.0	JENDL-2
36.4	0	3.5	1540.12	0.12	40.0	1500.0	JENDL-2
37.5	0	3.5	1540.17	0.17	40.0	1500.0	JENDL-2
38.3	0	3.5	308.34	0.34	42.0	266.0	JENDL-2
39.41	0	3.5	94.4999	2.5	38.0	54.0	JENDL-2
39.9	0	3.5	112.29	0.29	28.0	84.0	JENDL-2
40.54	0	3.5	222.43	0.43	36.0	186.0	JENDL-2
41.35	0	3.5	347.38	0.38	37.0	310.0	JENDL-2
41.59	0	3.5	165.224	0.224	31.0	134.0	JENDL-2
41.88	0	3.5	72.4	1.4	47.0	24.0	JENDL-2
42.23	0	3.5	139.3	0.3	53.0	86.0	JENDL-2
42.7	0	3.5	62.3	0.3	47.0	15.0	JENDL-2
43.39	0	3.5	68.7	0.7	44.0	24.0	JENDL-2
43.9	0	3.5	103.17	0.17	28.0	75.0	JENDL-2
43.97	0	3.5	250.34	0.34	20.0	230.0	JENDL-2
44.6	0	3.5	186.93	0.93	40.0	146.0	JENDL-2
45.0	0	3.5	535.76	0.76	31.0	504.0	JENDL-2
45.79	0	3.5	105.188	0.188	26.0	79.0	JENDL-2
46.79	0	3.5	152.65	0.65	34.0	118.0	JENDL-2
47.01	0	3.5	140.96	0.96	39.0	101.0	JENDL-2
47.95	0	3.5	78.8799	0.88	41.0	37.0	JENDL-2
48.3	0	3.5	165.771	0.771	25.0	140.0	JENDL-2
48.8	0	3.5	79.87	0.87	29.0	50.0	JENDL-2
49.0	0	3.5	240.177	0.177	20.0	220.0	JENDL-2
49.43	0	3.5	60.82	0.82	40.0	20.0	JENDL-2
50.14	0	3.5	53.27	0.27	32.0	21.0	JENDL-2
50.49	0	3.5	96.09	1.09	43.0	52.0	JENDL-2
51.27	0	3.5	190.67	3.67	51.0	136.0	JENDL-2
51.72	0	3.5	62.29	0.29	36.0	26.0	JENDL-2
52.22	0	3.5	353.25	2.25	26.0	325.0	JENDL-2
53.46	0	3.5	100.61	0.61	22.0	78.0	JENDL-2
54.13	0	3.5	142.23	0.23	36.0	106.0	JENDL-2
55.08	0	3.5	107.16	3.16	48.0	56.0	JENDL-2

ENERGY (EV)	L	J	TOTAL WIDTH (MEV)	NEUTRON WIDTH (MEV)	GAMMA WIDTH (MEV)	FISSION WIDTH (MEV)	REFERENCE
55.84	0	3.5	335.5	2.5	45.0	288.0	JENDL-2
56.5	0	3.5	125.92	4.92	43.0	78.0	JENDL-2
57.8	0	3.5	221.13	1.13	35.0	185.0	JENDL-2
58.06	0	3.5	69.36	1.36	32.0	36.0	JENDL-2
58.7	0	3.5	127.25	1.25	30.0	96.0	JENDL-2
59.76	0	3.5	267.245	0.245	41.0	226.0	JENDL-2
60.19	0	3.5	129.9	0.9	18.0	111.0	JENDL-2
60.85	0	3.5	148.51	0.51	25.0	123.0	JENDL-2
61.18	0	3.5	100.35	0.35	30.0	70.0	JENDL-2
61.57	0	3.5	540.23	0.23	40.0	500.0	JENDL-2
61.9	0	3.5	540.17	0.17	40.0	500.0	JENDL-2
62.4	0	3.5	460.26	0.26	60.0	400.0	JENDL-2
63.02	0	3.5	240.091	0.091	40.0	200.0	JENDL-2
63.32	0	3.5	250.102	0.102	50.0	200.0	JENDL-2
63.69	0	3.5	592.8	0.8	16.0	576.0	JENDL-2
64.31	0	3.5	54.25	1.25	45.0	8.0	JENDL-2
65.82	0	3.5	83.42	0.42	40.0	43.0	JENDL-2
66.38	0	3.5	81.4699	0.47	39.0	42.0	JENDL-2
67.25	0	3.5	97.0809	0.0809	48.0	49.0	JENDL-2
68.53	0	3.5	150.12	0.12	60.0	90.0	JENDL-2
69.29	0	3.5	200.72	0.72	40.0	160.0	JENDL-2
70.4	0	3.5	182.8	2.8	50.0	130.0	JENDL-2
70.75	0	3.5	229.3	2.3	36.0	191.0	JENDL-2
71.61	0	3.5	110.25	0.25	15.0	95.0	JENDL-2
72.4	0	3.5	141.7	2.7	31.0	108.0	JENDL-2
72.91	0	3.5	571.33	0.33	40.0	531.0	JENDL-2
74.57	0	3.5	103.9	2.9	46.0	55.0	JENDL-2
75.17	0	3.5	258.9	0.9	45.0	213.0	JENDL-2
75.54	0	3.5	237.27	1.27	28.0	208.0	JENDL-2
76.75	0	3.5	110.081	0.081	36.0	74.0	JENDL-2
77.53	0	3.5	147.01	1.01	39.0	107.0	JENDL-2
78.11	0	3.5	162.23	1.23	45.0	116.0	JENDL-2
78.7	0	3.5	86.13	0.13	48.0	38.0	JENDL-2
79.69	0	3.5	137.78	0.78	46.0	91.0	JENDL-2
80.37	0	3.5	203.8	0.8	35.0	168.0	JENDL-2
81.46	0	3.5	128.93	0.93	36.0	92.0	JENDL-2
82.06	0	3.5	64.05	0.05	40.0	24.0	JENDL-2
82.76	0	3.5	82.9	1.9	56.0	25.0	JENDL-2
83.59	0	3.5	111.17	1.17	55.0	55.0	JENDL-2
84.05	0	3.5	285.65	1.65	36.0	248.0	JENDL-2
84.37	0	3.5	234.1	2.1	29.0	203.0	JENDL-2
85.04	0	3.5	403.66	1.66	35.0	367.0	JENDL-2
85.57	0	3.5	390.6	0.6	40.0	350.0	JENDL-2
86.14	0	3.5	118.05	0.05	40.0	78.0	JENDL-2
86.88	0	3.5	127.58	0.58	41.0	86.0	JENDL-2
87.54	0	3.5	208.47	0.47	43.0	165.0	JENDL-2
88.75	0	3.5	340.28	2.28	18.0	320.0	JENDL-2
89.11	0	3.5	135.18	0.18	50.0	85.0	JENDL-2
89.85	0	3.5	134.79	0.79	45.0	89.0	JENDL-2
90.44	0	3.5	60.23	4.83	46.0	9.4	JENDL-2
91.28	0	3.5	286.96	2.96	33.0	251.0	JENDL-2
92.08	0	3.5	119.72	0.72	44.0	75.0	JENDL-2
92.6	0	3.5	94.53	2.53	48.0	44.0	JENDL-2
93.23	0	3.5	83.33	0.33	26.0	57.0	JENDL-2
94.12	0	3.5	75.4999	4.0	62.0	9.5	JENDL-2
94.76	0	3.5	107.5	0.5	41.0	66.0	JENDL-2
95.58	0	3.5	481.96	0.96	34.0	447.0	JENDL-2
96.5	0	3.5	255.59	0.59	18.0	237.0	JENDL-2
98.13	0	3.5	219.5	2.5	34.0	183.0	JENDL-2
99.6	0	3.5	145.53	0.53	35.0	110.0	JENDL-2
100.4	0	3.5	133.66	0.66	60.0	73.0	JENDL-2

ENERGY (EV)	L	J	TOTAL WIDTH (MEV)	NEUTRON WIDTH (MEV)	GAMMA WIDTH (MEV)	FISSION WIDTH (MEV)	REFERENCE
-0.22	0	0	504.644	0.0437	46.6	458.0	JENDL-2
0.297	0	0	98.84	0.24	38.2	60.4	JENDL-2
7.82	0	1.0	88.3997	0.7997	40.0	47.6	JENDL-2
10.93	0	1.0	199.877	1.8769	55.0	143.0	JENDL-2
11.89	0	1.0	67.0179	1.0179	42.0	24.0	JENDL-2
14.31	0	1.0	101.601	0.6015	34.0	67.0	JENDL-2
14.68	0	1.0	69.8903	1.8903	38.0	30.0	JENDL-2
15.46	0	0	994.4	2.4	42.0	950.0	JENDL-2
17.66	0	1.0	74.8109	1.8109	39.0	34.0	JENDL-2
22.29	0	1.0	108.644	2.6437	44.0	62.0	JENDL-2
23.94	0	0.5	70.1288	0.1288	32.0	38.0	JENDL-2
26.24	0	1.0	83.454	1.454	38.0	44.0	JENDL-2
27.24	0	0.5	42.2082	0.2082	37.0	5.0	JENDL-2
32.31	0	0	151.833	0.8328	41.0	110.0	JENDL-2
34.6	0	0.5	91.5198	0.0198	41.5	50.0	JENDL-2
35.5	0	1.0	47.2841	0.2841	43.0	4.0	JENDL-2
41.42	0	1.0	52.0977	4.0977	44.0	4.0	JENDL-2
41.66	0	0.5	106.003	2.0026	58.0	46.0	JENDL-2
44.48	0	1.0	58.5895	6.5895	47.0	5.0	JENDL-2
47.6	0	0	311.671	5.6708	58.0	248.0	JENDL-2
49.71	0	0	800.362	4.362	50.0	746.0	JENDL-2
50.08	0	1.0	57.0072	3.0072	41.0	13.0	JENDL-2
52.6	0	1.0	68.3765	10.3765	49.0	9.0	JENDL-2
55.63	0	1.0	58.454	1.454	36.0	21.0	JENDL-2
57.44	0	0	499.888	12.888	42.0	445.0	JENDL-2
58.84	0	0	1099.91	10.9052	42.0	1047.0	JENDL-2
59.22	0	1.0	180.42	5.4196	52.0	123.0	JENDL-2
60.94	0	0	6797.83	19.828	42.0	6736.0	JENDL-2
63.08	0	0.5	155.19	1.1896	43.0	111.0	JENDL-2
65.36	0	0.5	92.0354	0.5354	41.5	50.0	JENDL-2
65.71	0	1.0	137.042	12.0421	54.0	71.0	JENDL-2
74.05	0	1.0	71.1393	3.1393	36.0	32.0	JENDL-2
74.95	0	1.0	146.943	21.9427	41.0	84.0	JENDL-2
78.95	0	0.5	91.66	0.16	41.5	50.0	JENDL-2
81.76	0	0	2047.91	9.914	42.0	1996.0	JENDL-2
82.68	0	0.5	70.7436	0.7436	40.0	30.0	JENDL-2
83.52	0	0	1750.38	2.3792	42.0	1706.0	JENDL-2
85.32	0	0	2096.0	52.0	42.0	2002.0	JENDL-2
85.48	0	1.0	74.7989	7.7989	51.0	16.0	JENDL-2
90.75	0	1.0	59.7941	12.1941	39.0	8.6	JENDL-2
92.97	0	0.5	57.041	1.041	47.0	9.0	JENDL-2
95.36	0	1.0	98.0819	2.0819	66.0	30.0	JENDL-2
96.491	0	0	1700.24	13.2448	42.0	1645.0	JENDL-2
100.25	0	0	6000.1	11.1036	42.0	5947.0	JENDL-2
102.99	0	1.0	47.5993	1.5993	36.0	10.0	JENDL-2
105.3	0	1.0	48.0	4.6	38.0	5.4	JENDL-2
106.67	0	1.0	75.6265	9.2265	40.0	26.4	JENDL-2
110.38	0	0.5	43.6542	0.6542	30.0	13.0	JENDL-2
114.44	0	0	1499.39	1.388	42.0	1456.0	JENDL-2
115.1	0	0.5	205.317	0.3172	40.0	165.0	JENDL-2
116.303	0	0	267.727	10.7268	39.0	218.0	JENDL-2
118.83	0	1.0	102.831	17.8307	43.0	42.0	JENDL-2
120.99	0	0	78.336	7.336	32.0	39.0	JENDL-2
123.44	0	0.5	63.694	0.694	24.0	39.0	JENDL-2
126.22	0	0	95.8688	5.8688	70.0	20.0	JENDL-2
127.51	0	0.5	64.7634	0.7634	40.0	24.0	JENDL-2
131.75	0	0	3799.69	35.6904	42.0	3722.0	JENDL-2
133.78	0	1.0	55.5385	5.5385	44.0	6.0	JENDL-2
136.75	0	0	70.1516	10.1516	32.0	28.0	JENDL-2
139.28	0	0.5	321.678	0.1784	41.5	280.0	JENDL-2
142.92	0	1.0	137.212	3.2121	52.0	82.0	JENDL-2
143.47	0	1.0	83.0448	4.0448	48.0	31.0	JENDL-2
146.25	0	1.0	69.9927	6.9927	50.5	12.5	JENDL-2
147.44	0	0	1000.38	2.3792	42.0	956.0	JENDL-2
148.21	0	0.5	149.694	0.694	47.0	102.0	JENDL-2
149.42	0	0.5	119.597	2.5974	67.0	50.0	JENDL-2
157.08	0	0	621.6	33.6	48.0	540.0	JENDL-2
160.8	0	0.5	141.208	0.2081	41.0	100.0	JENDL-2
161.96	0	0.5	150.208	0.2081	40.0	110.0	JENDL-2
164.54	0	1.0	78.7587	27.7587	43.0	8.0	JENDL-2
167.1	0	1.0	111.783	5.7831	37.0	69.0	JENDL-2
170.49	0	0.5	158.653	0.8526	38.0	120.0	JENDL-2
171.08	0	0	999.765	1.7648	42.0	956.0	JENDL-2
174.56	0	0.5	241.559	0.0594	41.5	200.0	JENDL-2
175.98	0	0.5	73.1128	3.1128	39.0	31.0	JENDL-2
177.22	0	1.0	51.5425	3.5425	41.5	6.5	JENDL-2
178.9	0	1.0	58.2095	1.2095	43.0	14.0	JENDL-2
183.64	0	0.5	72.2702	2.2702	42.0	28.0	JENDL-2
184.87	0	0	2098.64	18.638	42.0	2038.0	JENDL-2
188.27	0	0.5	52.912	0.912	43.0	9.0	JENDL-2
190.64	0	0	66.9768	4.9768	49.0	13.0	JENDL-2
195.36	0	0	446.484	59.484	52.0	335.0	JENDL-2
196.69	0	1.0	111.653	4.6529	53.0	54.0	JENDL-2
199.39	0	1.0	132.577	9.5768	43.0	80.0	JENDL-2
203.46	0	0.5	72.4484	5.9484	41.5	25.0	JENDL-2
203.93	0	0	440.6	53.6	42.0	345.0	JENDL-2
207.37	0	1.0	56.9397	6.9397	44.0	6.0	JENDL-2

ENERGY (EV)	L	J	TOTAL WIDTH (MEV)	NEUTRON WIDTH (MEV)	GAMMA WIDTH (MEV)	FISSION WIDTH (MEV)	REFERENCE
211.09	0	0	789.776	2.776	42.0	745.0	JENDL-2
212.02	0	0	1500.38	2.3792	42.0	1456.0	JENDL-2
213.28	0	0.5	199.694	0.694	42.0	157.0	JENDL-2
216.35	0	1.0	67.2127	6.2127	50.0	11.0	JENDL-2
219.49	0	1.0	70.5425	3.5425	41.0	26.0	JENDL-2
220.22	0	1.0	52.3627	7.3627	34.0	11.0	JENDL-2
223.16	0	1.0	59.3839	3.3839	47.0	9.0	JENDL-2
224.89	0	0.5	85.5378	2.5378	58.0	25.0	JENDL-2
227.77	0	0	8096.03	30.5348	41.5	8024.0	JENDL-2
227.89	0	1.0	66.6787	1.6787	33.0	32.0	JENDL-2
231.4	0	1.0	53.7645	11.7645	37.0	5.0	JENDL-2
232.63	0	0.5	120.654	0.6544	40.0	80.0	JENDL-2
234.32	0	1.0	74.1452	10.1452	49.0	15.0	JENDL-2
239.04	0	1.0	72.3865	5.3865	51.0	16.0	JENDL-2
240.6	0	0.5	241.55	0.0496	41.5	200.0	JENDL-2
242.88	0	1.0	96.5564	6.5564	34.0	56.0	JENDL-2
247.5	0	0.5	280.348	1.3482	45.0	234.0	JENDL-2
248.86	0	1.0	61.6253	14.6253	42.0	5.0	JENDL-2
251.23	0	1.0	82.2293	27.2293	43.0	12.0	JENDL-2
254.5	0	1.0	54.7759	2.7759	27.0	25.0	JENDL-2
256.11	0	1.0	91.2788	6.2788	53.0	32.0	JENDL-2
259.0	0	0.5	241.897	0.3966	41.5	200.0	JENDL-2
262.73	0	0	6299.14	99.14	42.0	6158.0	JENDL-2
262.74	0	0.5	59.6086	3.6086	46.0	10.0	JENDL-2
264.23	0	0.5	341.748	0.2478	41.5	300.0	JENDL-2
269.11	0	0.5	130.082	2.0818	42.0	86.0	JENDL-2
269.54	0	1.0	71.8333	3.8333	40.0	28.0	JENDL-2
272.62	0	1.0	91.626	27.626	33.0	31.0	JENDL-2
274.8	0	0.5	791.88	13.8796	42.0	736.0	JENDL-2
275.57	0	1.0	149.199	23.1987	54.0	72.0	JENDL-2
277.23	0	0	5299.85	17.8452	42.0	5240.0	JENDL-2
279.59	0	0	111.097	21.0968	34.0	56.0	JENDL-2
282.92	0	1.0	84.983	24.983	49.0	11.0	JENDL-2
285.73	0	0.5	341.599	9.919-2	41.5	300.0	JENDL-2
288.0	0	0	6498.55	28.552	42.0	6428.0	JENDL-2
288.3	0	0.5	341.579	7.939-2	41.5	300.0	JENDL-2
292.33	0	0	114.54	11.5396	31.0	72.0	JENDL-2
296.46	0	1.0	81.2319	3.2319	48.0	30.0	JENDL-2
298.59	0	1.0	73.4427	10.4427	43.0	20.0	JENDL-2
301.81	0	1.0	108.043	18.043	42.0	48.0	JENDL-2
308.2	0	0.5	150.362	4.362	48.0	98.0	JENDL-2
309.01	0	1.0	84.945	13.945	47.0	24.0	JENDL-2
311.12	0	0.5	82.2238	0.7238	41.5	40.0	JENDL-2
313.62	0	1.0	61.483	13.483	38.0	10.0	JENDL-2
316.6	0	1.0	73.1221	5.1221	43.0	25.0	JENDL-2
320.0	0	0.5	5061.5	20.0	41.5	5000.0	JENDL-2
321.75	0	0.5	341.698	0.1982	41.5	300.0	JENDL-2
323.36	0	0	159.88	59.88	53.0	47.0	JENDL-2
325.3	0	1.0	104.46	8.4599	50.0	46.0	JENDL-2
329.65	0	0	1999.71	10.7068	42.0	1947.0	JENDL-2
333.91	0	1.0	67.446	5.446	52.0	10.0	JENDL-2
335.93	0	1.0	82.58	17.58	47.0	18.0	JENDL-2
337.95	0	1.0	73.991	7.991	55.0	11.0	JENDL-2
339.24	0	0	80.7552	9.7552	37.0	34.0	JENDL-2
343.18	0	1.0	74.657	15.657	41.0	18.0	JENDL-2
346.56	0	0	1200.31	10.3104	42.0	1148.0	JENDL-2
350.3	0	1.0	97.315	21.315	41.0	35.0	JENDL-2
352.82	0	1.0	68.8597	3.8597	48.0	17.0	JENDL-2
354.89	0	0.5	79.0948	0.5948	41.5	37.0	JENDL-2
357.87	0	0	5999.92	8.9224	42.0	5949.0	JENDL-2
359.99	0	0.5	113.646	1.6458	32.0	80.0	JENDL-2
361.28	0	0.5	341.827	0.3272	41.5	300.0	JENDL-2
364.0	0	0.5	3051.5	10.0	41.5	3000.0	JENDL-2
366.0	0	0	4999.71	10.7068	42.0	4947.0	JENDL-2
368.33	0	0.5	162.095	0.5948	41.5	120.0	JENDL-2
370.31	0	0.5	89.8664	3.8664	57.0	29.0	JENDL-2
371.72	0	0	3399.8	22.802	42.0	3335.0	JENDL-2
375.02	0	0	42.9312	7.9312	29.0	6.0	JENDL-2
377.1	0	0.5	99.9542	2.9542	58.0	39.0	JENDL-2
378.04	0	0.5	224.364	1.8638	41.5	181.0	JENDL-2
382.43	0	0.5	129.625	0.6246	43.0	86.0	JENDL-2
384.26	0	1.0	108.651	5.6509	28.0	75.0	JENDL-2
385.9	0	0	999.776	2.776	42.0	955.0	JENDL-2
389.51	0	0.5	74.072	2.072	51.0	21.0	JENDL-2
391.52	0	0.5	124.874	1.8738	55.0	68.0	JENDL-2
394.43	0	1.0	106.464	6.4639	48.0	52.0	JENDL-2
396.91	0	0.5	108.143	3.1426	44.0	61.0	JENDL-2
401.56	0	1.0	219.232	19.232	46.0	154.0	JENDL-2
404.24	0	1.0	155.0	23.0	56.0	76.0	JENDL-2
406.03	0	0.5	321.206	2.7064	41.5	277.0	JENDL-2
406.95	0	0.5	331.447	1.4474	30.0	300.0	JENDL-2
408.71	0	0.5	114.924	1.9238	55.0	58.0	JENDL-2
412.31	0	1.0	144.863	8.8631	56.0	70.0	JENDL-2
415.66	0	0.5	61.8478	4.8478	50.0	7.0	JENDL-2
417.6	0	0.5	230.399	2.3992	50.0	178.0	JENDL-2
419.85	0	1.0	139.021	6.0211	59.0	74.0	JENDL-2
425.67	0	0.5	341.897	0.3966	41.5	300.0	JENDL-2

ENERGY (EV)	L	J	TOTAL WIDTH (MEV)	NEUTRON WIDTH (MEV)	GAMMA WIDTH (MEV)	FISSION WIDTH (MEV)	REFERENCE
426.37	0	0	6996.35	29.3452	42.0	6925.0	JENDL-2
429.64	0	0.5	779.411	5.4112	42.0	732.0	JENDL-2
431.29	0	0.5	3491.44	6.9398	41.5	3443.0	JENDL-2
432.73	0	0.5	341.027	1.5268	41.5	298.0	JENDL-2
437.76	0	1.0	61.6701	2.6701	49.0	10.0	JENDL-2
438.72	0	1.0	60.8835	2.8835	55.0	3.0	JENDL-2
440.07	0	0.5	341.916	0.4164	41.5	300.0	JENDL-2
442.41	0	0	411.819	20.819	44.0	347.0	JENDL-2
449.75	0	0.5	133.483	1.9828	41.5	90.0	JENDL-2
451.35	0	1.0	59.145	13.945	41.5	3.7	JENDL-2
454.45	0	0.5	402.194	0.694	41.5	360.0	JENDL-2
455.73	0	0	615.216	78.716	41.5	495.0	JENDL-2
457.33	0	0.5	170.504	11.0044	41.5	118.0	JENDL-2
458.8	0	1.0	79.0604	4.5604	41.5	33.0	JENDL-2
461.26	0	0.5	97.3698	3.4698	41.5	52.4	JENDL-2
462.64	0	0.5	128.293	0.7932	41.5	86.0	JENDL-2
468.2	0	0.5	2092.94	6.444	41.5	2045.0	JENDL-2
470.0	0	0.5	5086.37	14.871	41.5	5030.0	JENDL-2
473.1	0	1.0	55.5977	4.0977	41.5	10.0	JENDL-2
475.31	0	0.5	582.052	5.5518	41.5	535.0	JENDL-2
476.9	0	0.5	1994.18	2.6766	41.5	1950.0	JENDL-2
479.24	0	0.5	201.698	0.1982	41.5	160.0	JENDL-2
484.15	0	0.5	59.8664	3.8664	41.5	14.5	JENDL-2
487.29	0	0.5	224.772	3.2716	41.5	180.0	JENDL-2
487.81	0	0.5	226.655	5.1552	41.5	180.0	JENDL-2
490.65	0	0.5	2281.33	19.828	41.5	2220.0	JENDL-2
494.1	0	1.0	116.06	4.5604	41.5	70.0	JENDL-2
495.63	0	0.5	202.69	1.1899	41.5	160.0	JENDL-2
500.5	0	1.0	76.8707	3.3707	41.5	32.0	JENDL-2
502.86	0	1.0	85.2645	11.7645	41.5	32.0	JENDL-2
505.78	0	0.5	442.392	0.8922	41.5	400.0	JENDL-2
508.22	0	0.5	692.194	0.694	41.5	650.0	JENDL-2
509.74	0	1.0	260.184	51.684	41.5	167.0	JENDL-2
511.52	0	0.5	3354.29	12.789	41.5	3300.0	JENDL-2
515.16	0	0.5	482.491	0.9914	41.5	440.0	JENDL-2
516.57	0	0.5	321.797	0.2974	41.5	280.0	JENDL-2
517.98	0	0.5	362.194	0.694	41.5	320.0	JENDL-2
520.22	0	1.0	99.304	14.804	41.5	43.0	JENDL-2
524.21	0	1.0	91.836	30.336	41.5	20.0	JENDL-2
525.4	0	0.5	10661.4	119.898	41.5	10500.0	JENDL-2
526.0	0	0.5	92.987	1.487	41.5	50.0	JENDL-2
527.38	0	0.5	58.987	1.487	41.5	16.0	JENDL-2
530.52	0	0	243.0	126.5	41.5	75.0	JENDL-2
539.17	0	1.0	55.2019	11.3019	41.5	2.4	JENDL-2
540.71	0	0.5	85.4656	3.9656	41.5	40.0	JENDL-2
541.65	0	0.5	89.431	7.931	41.5	40.0	JENDL-2
543.08	0	1.0	58.1324	11.6324	41.5	5.0	JENDL-2
545.85	0	0.5	1178.85	17.3494	41.5	1120.0	JENDL-2
547.14	0	0.5	843.285	1.7846	41.5	800.0	JENDL-2
549.67	0	1.0	60.1984	11.6984	41.5	7.0	JENDL-2
550.5	0	0.5	61.3538	16.8538	41.5	3.0	JENDL-2
554.13	0	0.5	1233.25	51.75	41.5	1140.0	JENDL-2
555.72	0	0.5	446.358	4.8578	41.5	400.0	JENDL-2
559.16	0	1.0	89.4653	26.9653	41.5	21.0	JENDL-2
562.84	0	0.5	274.638	53.138	41.5	180.0	JENDL-2
564.03	0	0.5	53.2156	9.7156	41.5	2.0	JENDL-2
565.81	0	0.5	60.5778	14.0778	41.5	5.0	JENDL-2
571.11	0	1.0	83.026	8.526	41.5	33.0	JENDL-2
574.0	0	0	419.132	157.632	41.5	220.0	JENDL-2
575.77	0	1.0	88.957	39.457	41.5	8.0	JENDL-2
578.0	0	0.5	79.9784	2.4784	41.5	36.0	JENDL-2
579.04	0	1.0	55.3076	6.8076	41.5	7.0	JENDL-2
584.81	0	0.5	322.194	0.694	41.5	280.0	JENDL-2
588.09	0	1.0	62.6697	11.1697	41.5	10.0	JENDL-2
589.94	0	0.5	441.996	0.4956	41.5	400.0	JENDL-2
593.52	0	0.5	48.6724	3.1724	41.5	4.0	JENDL-2
597.35	0	1.0	55.026	8.526	41.5	5.0	JENDL-2
598.04	0	0.5	5977.32	20.818	41.5	5915.0	JENDL-2
604.01	0	1.0	69.8506	24.8506	41.5	3.5	JENDL-2
607.64	0	1.0	58.8496	9.6496	41.5	7.7	JENDL-2
609.29	0	1.0	63.6973	15.5973	41.5	6.6	JENDL-2
612.8	0	0.5	64.2242	8.7242	41.5	14.0	JENDL-2
620.48	0	1.0	58.6645	11.7645	41.5	5.4	JENDL-2
622.59	0	1.0	61.0156	9.7156	41.5	9.8	JENDL-2
625.17	0	1.0	56.7989	7.7989	41.5	7.5	JENDL-2
628.21	0	0.5	52.681	2.181	41.5	9.0	JENDL-2
632.97	0	0.5	3875.21	33.706	41.5	3800.0	JENDL-2
636.47	0	0.5	65.431	7.931	41.5	16.0	JENDL-2
639.28	0	1.0	56.6869	9.1869	41.5	6.0	JENDL-2
641.42	0	0.5	522.194	0.694	41.5	480.0	JENDL-2
644.94	0	1.0	50.3161	5.8161	41.5	3.0	JENDL-2
646.65	0	0.5	242.987	1.487	41.5	200.0	JENDL-2
658.29	0	1.0	141.133	80.633	41.5	19.0	JENDL-2

ENERGY (EV)	L	J	TOTAL WIDTH (MEV)	NEUTRON WIDTH (MEV)	GAMMA WIDTH (MEV)	FISSION WIDTH (MEV)	REFERENCE
-0.209	0	3.0	132.063	0.063	35.0	97.0	JENDL-2
0.257	0	3.0	132.051	0.05143	35.0	97.0	JENDL-2
4.28	0	3.0	95.69	0.69	50.0	45.0	JENDL-2
4.58	0	2.0	184.42	0.42	49.0	135.0	JENDL-2
6.11	0	2.0	1338.24	3.24	35.0	1300.0	JENDL-2
6.93	0	3.0	155.72	0.72	35.0	120.0	JENDL-2
8.62	0	3.0	141.94	0.94	41.0	100.0	JENDL-2
9.57	0	2.0	385.528	0.528	35.0	350.0	JENDL-2
10.06	0	2.0	636.32	1.32	35.0	600.0	JENDL-2
12.79	0	3.0	280.677	0.67714	50.0	230.0	JENDL-2
13.42	0	2.0	123.55	3.55	60.0	60.0	JENDL-2
14.75	0	3.0	183.4	5.4	48.0	130.0	JENDL-2
15.97	0	3.0	556.42	1.42	35.0	520.0	JENDL-2
16.67	0	2.0	227.28	1.28	42.0	184.0	JENDL-2
17.85	0	2.0	64.98	2.98	39.0	23.0	JENDL-2
18.22	0	2.5	75.15	0.15	35.0	40.0	JENDL-2
20.69	0	3.0	105.309	0.30857	43.0	62.0	JENDL-2
21.05	0	2.5	335.01	0.01	35.0	300.0	JENDL-2
21.91	0	2.5	70.17	0.17	50.0	20.0	JENDL-2
23.0	0	3.0	370.986	0.98571	35.0	335.0	JENDL-2
23.7	0	2.5	380.39	0.39	55.0	325.0	JENDL-2
24.04	0	3.0	127.183	1.18286	46.0	80.0	JENDL-2
24.61	0	2.5	549.15	0.15	40.0	509.0	JENDL-2
26.39	0	3.0	313.857	3.85714	45.0	265.0	JENDL-2
28.89	0	2.0	700.76	5.76	40.0	655.0	JENDL-2
29.42	0	3.0	125.471	0.47143	40.0	85.0	JENDL-2
31.03	0	3.0	299.203	2.20286	56.0	241.0	JENDL-2
32.5	0	2.5	2541.0	1.0	40.0	2500.0	JENDL-2
33.3	0	2.5	160.17	0.17	40.0	120.0	JENDL-2
33.77	0	2.5	140.3	0.3	40.0	100.0	JENDL-2
34.9	0	2.5	1142.07	2.07	40.0	1100.0	JENDL-2
34.98	0	2.5	55.41	0.41	40.0	15.0	JENDL-2
37.5	0	2.5	640.15	0.15	40.0	600.0	JENDL-2
38.17	0	2.5	240.5	0.5	40.0	200.0	JENDL-2
39.35	0	2.5	201.49	1.49	40.0	160.0	JENDL-2
39.89	0	2.5	154.59	1.59	53.0	100.0	JENDL-2
40.87	0	2.5	1042.12	2.12	40.0	1000.0	JENDL-2
42.77	0	2.5	240.28	0.28	40.0	200.0	JENDL-2
43.45	0	2.5	70.25	0.25	40.0	30.0	JENDL-2
46.57	0	2.5	281.5	1.5	40.0	240.0	JENDL-2
48.11	0	2.5	626.2	6.2	40.0	580.0	JENDL-2
50.35	0	2.5	540.69	0.69	40.0	500.0	JENDL-2
52.07	0	2.5	140.04	0.04	40.0	100.0	JENDL-2
58.37	0	2.5	621.75	1.75	40.0	580.0	JENDL-2
59.28	0	2.5	582.2	2.2	40.0	540.0	JENDL-2
60.53	0	2.5	281.3	4.3	27.0	250.0	JENDL-2
62.25	0	2.5	644.62	4.62	40.0	600.0	JENDL-2
63.0	0	2.5	1242.0	2.0	40.0	1200.0	JENDL-2
64.52	0	2.5	316.25	0.25	40.0	276.0	JENDL-2
65.68	0	2.5	344.26	5.26	39.0	300.0	JENDL-2
66.55	0	2.5	243.04	3.04	40.0	200.0	JENDL-2
68.22	0	2.5	141.18	1.18	40.0	100.0	JENDL-2
69.18	0	2.5	160.7	0.7	40.0	120.0	JENDL-2
71.77	0	2.5	100.07	0.07	53.0	47.0	JENDL-2
72.17	0	2.5	411.53	1.53	40.0	370.0	JENDL-2
73.8	0	2.5	53.5	0.5	40.0	13.0	JENDL-2
75.94	0	2.5	159.76	4.76	52.0	103.0	JENDL-2
77.06	0	2.5	80.45	4.45	58.0	18.0	JENDL-2
77.73	0	2.5	1698.7	1.7	60.0	1637.0	JENDL-2
80.14	0	2.5	124.87	4.87	40.0	80.0	JENDL-2
81.36	0	2.5	261.9	6.9	40.0	215.0	JENDL-2
81.98	0	2.5	1017.9	2.9	40.0	975.0	JENDL-2
83.12	0	2.5	118.02	5.02	40.0	73.0	JENDL-2
85.35	0	2.5	200.5	3.5	52.0	145.0	JENDL-2
85.67	0	2.5	272.8	2.8	40.0	230.0	JENDL-2
86.0	0	2.5	350.72	0.72	40.0	310.0	JENDL-2
86.93	0	2.5	130.4	7.4	43.0	80.0	JENDL-2
87.8	0	2.5	322.35	2.35	40.0	280.0	JENDL-2
89.12	0	2.5	792.23	2.23	40.0	750.0	JENDL-2
90.6	0	2.5	216.7	1.7	40.0	175.0	JENDL-2
91.4	0	2.5	60.1	0.1	39.0	21.0	JENDL-2
91.88	0	2.5	60.12	0.12	35.0	25.0	JENDL-2
93.77	0	2.5	296.4	0.4	46.0	250.0	JENDL-2
95.24	0	2.5	683.6	0.6	40.0	643.0	JENDL-2
96.18	0	2.5	1041.5	1.5	40.0	1000.0	JENDL-2
97.53	0	2.5	499.85	0.85	40.0	459.0	JENDL-2
98.28	0	2.5	193.28	7.28	40.0	146.0	JENDL-2
99.74	0	2.5	350.16	2.16	18.0	330.0	JENDL-2
100.5	0	2.5	55.6	1.3	40.0	14.3	JENDL-2
101.42	0	2.5	147.61	1.61	72.0	74.0	JENDL-2
102.33	0	2.5	58.7	1.4	40.0	17.3	JENDL-2
103.52	0	2.5	48.73	1.53	40.0	7.2	JENDL-2
107.54	0	2.5	41.2	0.5	40.0	0.7	JENDL-2
107.85	0	2.5	92.2	1.2	40.0	51.0	JENDL-2
109.05	0	2.5	491.92	1.92	40.0	450.0	JENDL-2
110.2	0	2.5	791.45	0.45	40.0	751.0	JENDL-2
113.13	0	2.5	86.75	0.75	40.0	46.0	JENDL-2

ENERGY (EV)	L	J	TOTAL WIDTH (MEV)	NEUTRON WIDTH (MEV)	GAMMA WIDTH (MEV)	FISSION WIDTH (MEV)	REFERENCE
115.4	0	2.5	1581.7	1.7	40.0	1540.0	JENDL-2
117.23	0	2.5	357.48	3.48	40.0	314.0	JENDL-2
120.33	0	2.5	545.8	0.8	40.0	505.0	JENDL-2
122.11	0	2.5	465.95	6.95	40.0	419.0	JENDL-2
123.24	0	2.5	101.35	2.35	40.0	59.0	JENDL-2

PARAMETRIZATION OF THE DATA ON NEUTRON RESONANCE DENSITY AND DISCRETE SPECTRUM FOR TRANSACTINIDES

V.M. Maslov, G.V. Antsipov and V.A. Konshin
Heat and Mass Transfer Institute of the BSSR Academy of Sciences, Minsk, U S S R

ABSTRACT

Using the data on $\langle D \rangle_{obs}$, the level density parameters in the superfluid nucleus model involving the collective effects are obtained. In the low energy region this model is matched with the constant temperature one whose parameters are determined from the description of the discrete level spectrum of ^{225}Th to $^{254}C_f$. The systematics of the main parameters are given.

1. INTRODUCTION

Solution of many problems in nuclear engineering needs information on neutron cross sections for a wide class of transactinide nuclei. The absence of the experimental data in many cases regards the theoretical calculations as of paramount importance for nuclear data evaluation. The great majority of calculations is connected to this or another extent with the knowledge of excited nucleus level spectra. The nuclear data evaluation makes especially high demands of the level spectra knowledge due to a high accuracy of the neutron cross sections predicted. Therefore, the individual input information for each nucleus has to be used, and only if no such information available the systematics must be applied to.

The range of discrete spectrum for transactinides known from different experiments is usually limited to 0.5 and 1.5 MeV. In the higher energy region the nuclear level models have to be used. As the neutron cross sections calculated are very sensitive to the level density models, and their parameters, in particular, the radiative capture cross section [1]. They can be used provided the all available experimental data are uncontradictorily described. The discrete spectrum in the low excitation energy region and neutron resonance density near the neutron binding energy are most direct of them.

Using the data available on $\langle D \rangle_{obs}$ for ^{225}Th to $^{254}C_f$, the level density parameters in the superfluid nucleus model involving the collective effects are obtained. In the low energy region this model is matched with the constant temperature one. The parameters of the latter model are determined from the description of discrete level spectra. The calculation results fit into rather simple systematics which suggests their successful application in further calculations. This holds, first of all, for the region where the constant temperature model is applied. In the present analysis, as compared to [2,3], we are using the superfluid nucleus model involving the contribution of the rotational and vibrational degrees of freedom. Besides, by the time, Ref. [2] has been published, there were scanty data on $\langle D \rangle_{obs}$ for

transactinides, while in [3] this nucleus region was not considered at all.

2. NEUTRON RESONANCE DENSITY DATA FOR TRANSACTINIDES

When using data on neutron resonance density ρ_{obs} obtained from neutron cross section measurements in the region of resolved resonances, the account must be taken of the effects which may be exerted on the final value. These are: (i) omission of resonances due to their grouping or smallness of neutron widths and (ii) presence of p-resonances. The latter refers to odd--odd nucleus-targets.

Of all available resonance parameter data and evaluations, in the first turn, we give preference to $\langle D \rangle_{obs}$ from Table 1. Up to date there are data on $\langle D \rangle_{obs}$ for 32 transactinide nuclei. Note that in [4] $\langle D \rangle_{obs} = 0.55 \pm 0.04$ eV is given for ^{234}Th (compound nucleus) with reference to the ENDF/B-IV library. However, the study of versions IV [5] and V of the ENDF/B-library indicated no resonance parameters for the given nucleus. This value is not used in what follows.

Table 1 also contains spins and parities for the ground states of nucleus-targets and neutron separation energies [6].

3. DISCRETE LEVEL SPECTRUM DATA FOR TRANSACTINIDES

In order to obtain the parameters for the level density model used , the level scheme data have been used as from the Nuclear Data Sheets, 1976-1978, that have been sent to us by the Centre on Atomic Nuclear Structure and Nucleus Reactions Data of the USSR State Committee on the Utilization of Atomic Energy. These data include about 100 isotopes of ^{225}Th to ^{254}Cf.

4. LEVEL DENSITY MODEL

The level density of deformed axial-symmetric nuclei involving transactinides under equilibrium deformations is governed by the following expression from [7] allowing for the contribution of rotational freedom degrees:

$$\rho_{in+rot}(U,J)=\frac{\omega(U)}{2\sqrt{2\pi}\sigma_{\parallel}}\sum_{K=-J}^{J}\exp\left[-\frac{J(J+1)}{2\sigma_{\perp}^{2}}-K^{2}\left(\frac{1}{2\sigma_{\parallel}^{2}}-\frac{1}{2\sigma_{\perp}^{2}}\right)\right], \quad (1)$$

where $\omega(U)$ is the density of inner excited states; $\sigma_{\perp}^{2}=F_{\perp}t$ and $\sigma_{\parallel}^{2}=F_{\parallel}t$ are the spin-dependence parameters associated with normal $F_{\perp}$ and parallel $F_{\parallel}$ nucleus inertia moments; K is the angular momentum projection to the symmetry axis; t is the excited nucleus temperature.

The deformation values representative of transactinides allow equation (1) to be simplified as:

$$\rho_{in+rot}(U,J)=\frac{(2J+1)\,\omega(U)}{2\sqrt{2\pi}\,\sigma_{\parallel}}\exp\left[-\frac{J(J+1)}{2\sigma_{\perp}^{2}}\right]. \quad (2)$$

The contribution of vibrational freedom degrees to the level density may be allowed for by introducing the coefficient K_{vib} [8] in-

to (1) or (2):

$$\rho(U,J)=\rho_{in+rot+vib}(U,J)=K_{vib}\,\rho_{in+rot}(U,J), \quad (3)$$

where

$$K_{vib}=\exp\left[1{,}7\left(\frac{3m_0A}{4\pi\sigma_{LDM}}\cdot\frac{C_{LDM}}{C}\right)^{2/3}t^{4/3}\right]. \quad (4)$$

Here σ_{LDM} is the surface tension coefficient in the liquid drop model; the ratio $\frac{C}{C_{LDM}}$ characterizes the difference between the rigidity coefficients for an excited nucleus and liquid drop.

The values necessary for level density prediction are calculated by the modification formulae [9] for the superfluid nucleus model. Shell effects are allowed for in terms of the dependence of the main level density parameter a vs the excitation energy and the shell correction δW in the nucleus binding energy in the region above the phase transition point as follows [10];

$$a=\tilde{a}\left\{1+\left[1-\exp\left[-\gamma(U-E_{cond})\right]\frac{\delta W}{U-E_{cond}}\right\}, \quad (5)$$

where $\tilde{a}$ is the asymptotic value of the parameter a at $U\to\infty$ determined here from the neutron resonance density; γ is the energy dependence parameter; E_{cond} is the condensation energy. The Myers-Swiatecki parameters [11] are used to calculate the shell correction δW. The δW-values for the nuclei where the data on $\langle D\rangle_{obs}$ are available are given in Table 1. The necessary parameters are taken from [8]. Note that the correlation functions for protons and neutrons are determined from the systematics:

$$\Delta_{0Z}=\Delta_{0N}=\frac{12}{\sqrt{A}} \quad (6)$$

The description of the discrete level spectrum would be a highly severe requirement to any density level model; whose main parameter is determined from the neutron resonance density. The model adopted in the present work is not an exception. It seems therefore natural to use, for the low excitation energy, an alternative model whose parameters would be determined from the condition of discrete spectrum description and which would provide matching with the model adopted for the region around the neutron binding energy. To this purpose, the constant temperature model widely used to date has been employed. In terms of this model, the increasing sum of levels is represented by a straight line in the semi-logarithmic scale

$$N(E)=\exp\left[(E-E_0)/T\right], \quad (7)$$

while the total level density is

$$\rho(E)=\frac{dN(E)}{dE}=\frac{1}{T}\exp\left[(E-E_0)/T\right] \quad (8)$$

Temperature T is defined as an inverse logarithmic derivative $\rho(E)$; E_0 is the calculation parameter.

The analysis of the level schemes for the even-even transactinide nuclei gives the linear N(E) dependence in the semi-loga-

rithmic scale (Figs. 1,2). The deviation from this dependence with increasing energy is attributed to the omission of levels. No such a dependence is observed for odd and odd-odd nuclei (Figs. 3,4), but it must be borne in mind that their level density is much higher than that of even-even nuclei. Hence, the omission of levels here will be more essential.

Usually the physical grounds of the constant temperature model have been criticized. Its success becomes understandable due to calculations in terms of the superfluid nucleus model which displays a weaker fall $\rho(U)$ to zero excitation energy than *the Fermi-gas model*. At low energies, $\rho(U)$ calculation using the superfluid nucleus model gives a practically straight line in the semi-logarithmic scale.

Matching of the level density models is determined by the following conditions [2,3]:

(i) Description of the increasing sum of discrete spectrum levels.

(ii) Equality of the densities at the matching point

$$\rho_1(E_x) = \rho_2(E_x), \tag{9}$$

whence

$$E_0 = E_x - T\ln\left[\rho_2(E_x)\,T\right]. \tag{10}$$

(iii) Equality of the logarithmic derivatives for level densities at the point E_x.

$$\left.\frac{d\ln\rho_1(E)}{dE}\right|_{E_x} = \left.\frac{d\ln\rho_2(E)}{dE}\right|_{E_x}, \tag{11}$$

whence

$$T = \left[\left.\frac{d\ln\rho_2(E)}{dE}\right|_{E_x}\right]^{-1} \tag{12}$$

5. PARAMETRIZATION OF DATA ON NEUTRON RESONANCE DENSITY AND DISCRETE SPECTRUM FOR TRANSACTINIDES

The neutron resonance density data cited in Table 1 have been used to obtain the asymptotic value of $\tilde{a}$ of the main level density parameter a. They are given in Fig. 5 as the ratio $\tilde{a}/A$ In the same figure the solid line plots the dependence

$$\frac{\tilde{a}}{A} = \alpha - \beta A^{-1/3}; \quad \alpha = 0{,}073; \ \beta = 0{,}1147; \tag{13}$$

obtained in [8] for nuclei at A=150-250. The dependence is seen to fit the data but the tendency of more rapid $\tilde{a}/A$ decrease with increasing A is observed (dashed line). The parameter systematics has been made in [8] with the experimental data on $\langle D\rangle_{obs}$ which both in reliability and number yield to the data used here.

Note that appreciable deviations for ^{245}Pu and ^{253}Cf from the mean dependence in Fig. 5 can be attributed to the nonreliable $\langle D\rangle_{obs}$ determination. Besides, a certain value of $\tilde{a}/A$ fluctuations is perhaps due to the use of systematics (6) which does not present the individual properties of particular nuclei. The values of the parameters T, E_0 in the constant tempe-

rature model and the matching points E_x for even-even and odd nuclei, for which the neutron resonance data and descrete level spectrum are available, are presented in Figs. 6 through 10. The quality of describing the increasing sum of discrete spectrum levels for individual nuclei is demonstrated in Figs. 1 through 4. As seen from Fig. 6, the temperature T for even-even nuclei displays rather weak fluctuations about the average value T= 0.385 MeV. For odd nuclei, T fluctuations are noticeably greater (Fig. 7). Besides, the values of T for them are, on the average, somewhat lower than for even-even nuclei. But this stems from less reliable determination of the discrete spectrum for odd nuclei rather than points to T dependence on nucleus parity. This is supported by the fact that for the nuclei whose discrete spectra are more thoroughly studied (for example, ^{235}U), T parameters are close to the average value for even-even nuclei. Note that the low value of T for ^{245}Pu is attributed to lower density of the known levels compared to the well-studied neighbouring odd nuclei and real density can be expected to be higher.

It follows from the aforesaid that for the nuclei with no data on the discrete spectrum available the value of $\overline{T}$ = 0.385 MeV average for even-even nuclei can be recommended.

The analysis of the parameter E_0 shows that for even-even nuclei its values are very densely grouped arround zero (Fig. 8). For odd nuclei, the parameter E_0 is, on the average, by 0.6 MeV lower than for even-even nuclei. This suggests an idea to relate the parameter E_0 for odd nuclei to the values of the correlation function $\Delta_{o\_}$ in the ground state. Really, it is seen from Fig. 9 that for the nuclei with the most studied discrete spectra the values of $E_0 + \Delta_0$ are grouped around zero. $E_0 + \Delta_0$ fluctuations and their considerable difference from zero for a number of nuclei can be attributed to the same reasons as for the parameter T. Similar nature of T and $E_0 + \Delta_0$ fluctuations for odd nuclei is seen from their correlation in Figs. 7 and 9.

The aforesaid demonstrates the possibility of applying the average parameters E_0=0 and E_0=-Δ_0 for even-even and odd nuclei in the case of the nuclei having no data available on resonance discrete spectra and density of neutron resonances. This is also supported by the description of the increasing level sums- for the nuclei with comparatively well-studied discrete spectra but having no data on $\langle D \rangle_{obs}$ using average parameters T and E_0 (Figs. 11 and 12).

The point is different with odd-odd nuclei. The analysis shows that in their case the application of the superfluid model gives satisfactory description of the increasing discrete spectrum levels. However, this can be explained by in - sufficient study of the discrete spectrum rather than by the success of the model. Following the systematics, the level sums for them must increase more rapidly than for odd nuclei for even-even nuclei. At the same time, the up-to-date level schemes give the same N(E) behaviour as for odd nuclei. It can be therefore suggested that for odd-odd nuclei the desc-

ription of the true discrete spectrum will be ensured by the parameters T=0.385 MeV (average over even-even nuclei) and $E_0=-2\Delta_0$. This will be confirmed below.

Evidently, the recovery of the observed neutron resonance density can support the validity of the systematics obtained for T and E_0 in the constant temperature model. To this end, equations (3) and (10) should be used to give the parameters E_x and $\tilde{a}$. The calculation results as $\langle D\rangle_{theor}/\langle D\rangle_{exp}$ are given in Fig.13. It is easily seen that the bulk of the values lie within $\pm$ 50% which is a fair result for the approximations used in the present work. The nuclei ^{238}Np, ^{245}Pu, ^{243}Cm and ^{253}Cf are an exception, and among them ^{245}Pu and ^{253}Cf have nonreliable $\langle D\rangle_{obs}$ data.

It should be also supposed that T, E_0 and $\tilde{a}$ as well as $\langle D\rangle_{theor}/\langle D\rangle_{exp}$ fluctuations are to a certain degree attributed to $\Delta_0 = 12/\sqrt{A}$, which does not allow for the individual properties of particular nuclei. Note that this estimate is highly overestimated for neutron pair energies for transactinides being satisfactory for the whole range of mass numbers. One can hope that the use of experimental pair energies will appreciably improve the parameter systematics.

6. CONCLUSION

The main results of the present work are as follows:

1. The analysis is made and the data are given on the average distances between neutron resonances for transactinides.
2. The parameters of the superfluid nucleus and constant temperature model for level densities are obtained and systematized.
3. It is shown that for the nuclei with no data on discrete spectrum at low energies a good approximation can be obtained through the use of the average T=0.385 MeV and $E_0=0$ for even-even $E_0=-\Delta_0$ for odd and $E_0=-2\Delta_0$ for odd-odd nuclei. These parameters provide agreement between theoretical and experimental $\langle D\rangle$ within $\pm$ 50%, on the average.
4. The superfluid nucleus model including the contribution of collective modes to the level density ensures the model matching at rather low temperatures and matching points E_x of about 4, 3 and 2 MeV for even-even, odd and odd-odd nuclei, respectively.

Table 1

Data on Mean Distances Between Neutron Resonances and Shell Corrections

Compound nucleus	I^{π} nucleus-targets	S_n, MeV	$\langle D \rangle_{obs}$, eV	Ref.	δW, MeV
1	2	3	4	5	6
^{230}Th	5/2+	6,790	0,40	I2	-I,008
^{23I}Th	0+	5.I28	9,8 ± I.6	I3	-I,024
^{233}Th	0+	4,787	I6,6 ± 0,9	I4	-0,9I7
^{232}Pa	(3/2-)	5,550	0,37*	I5	-I,3I5
^{234}Pa	3/2-	5,I97	0,69	I6	-I,272
^{233}U	0+	5,744	4,I**	I7	-I,733
^{234}U	5/2+	6,84I	0,6I± 0,07	I8	-I,704
^{235}U	0+	5,305	I0,5± 0,5	I9	-I,700
^{236}U	7/2-	6,546	0,438± 0,038	20	-I,624
^{237}U	0+	5,I25	I6,2± 0,8	2I	-I,680
^{238}U	I/2+	6,I43	3,5± 0,8	22	-I,447
^{239}U	0+	4,804	24,8± 2	23	-I,4I8
^{238}Np	5/2+	6,480	0,740± 0,06I	24	-2,04I
^{239}Pu	0+	6,655	9,2 ± 0,7	25	-2,365
^{240}Pu	I/2+	6,534	2,38 ± 0,06	26	-2,II6
^{24I}Pu	0+	5,24I	I3,5 ± 0,5	***	-2,II8
^{242}Pu	5/2+	6,30I	I,34 ± 0,I0	27	-I,883
^{243}Pu	0+	5,037	I4,23± 0,54	28	-I,9I7
^{245}Pu	0+	4,720	II,4 ± 4	29	-I,59I
^{242}Am	5/2-	5,529	0,58 ± 0,04	30	-2,487
^{243}Am	5-	6,425	0,45	3I	-2,I28
^{244}Am	5/2-	5,364	0,68 ± 0,06	32	-2,287
^{243}Cm	0+	5,70I	I7,6 ± 3,3	33	-2,692
^{244}Cm	5/2+	6,799	0,50 ± 0,20	4	-2,559
^{245}Cm	0+	5,5I9	II,8 ± I,2	4	-2,676
^{246}Cm	7/2+	6,45I	I,I4 ± 0,I4	34	-2,439
^{247}Cm	0+	5,I57	2I,3 ± 5,3	35	-2,430
^{248}Cm	9/2-	6,2I0	I,2	36	-2,I93
^{249}Cm	0+	4,7I3	40 ± 5	37	-I,97I
^{250}Bk	7/2+	4,969	I,I	38	-2,335
^{250}Cf	9/2-	6,6I8	I,07 ± 0,I4	39	-2,955
^{253}Cf	0+	4,792	I6	40	-2,0I3

* Corrected for level omission

** The authors of [17] do not cite this value. It is given in [41] with reference to [17]

*** Estimate obtained by V.A. Konshin et al. in compiling a new file of ^{240}Pu data

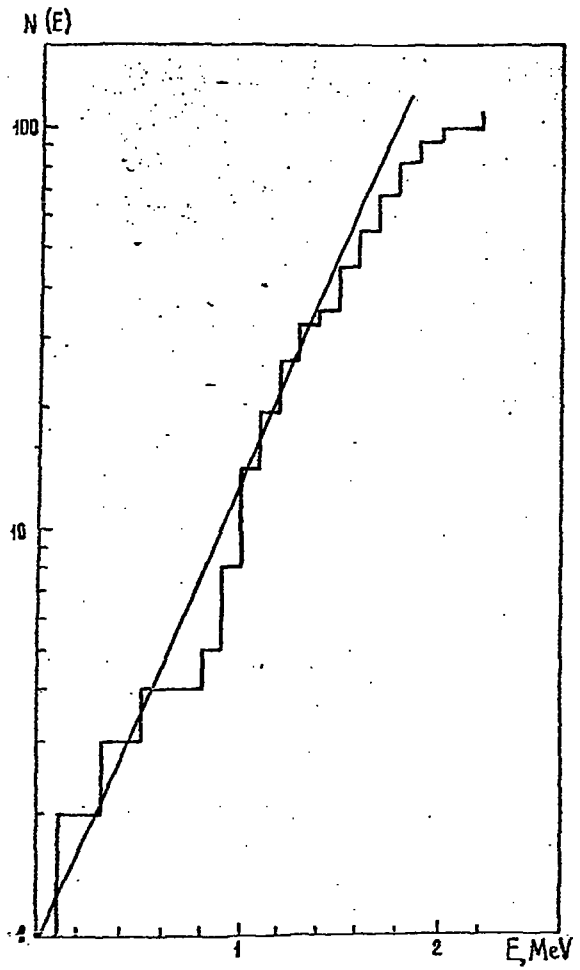

Fig. 1. Description of the increasing sum of ^{234}U levels using the constant temperature model with T=0.392 MeV and E_o=0.014 MeV.

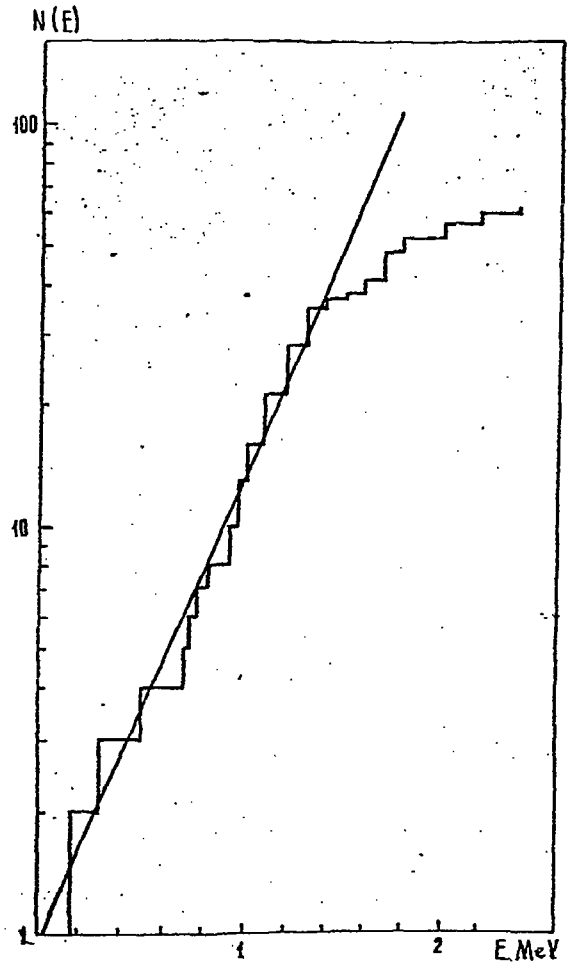

Fig. 2. Description of the increasing sum of ^{238}U levels using the constant temperature model with T=0.383 MeV and E_o=0.010 MeV.

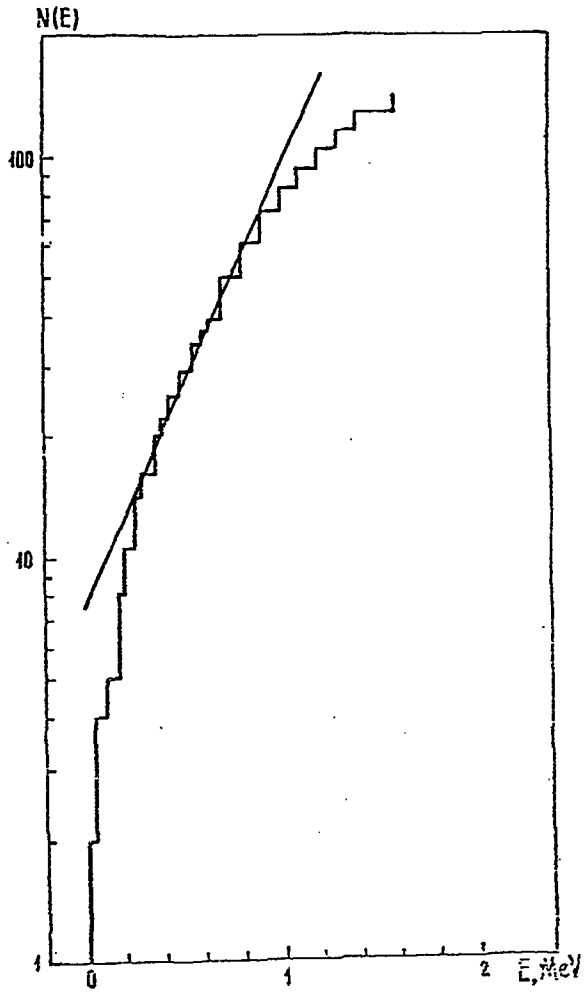

Fig. 3. Description of the increasing sum of ^{235}U levels using the constant temperature model with T=0.385 MeV and E_0=-0.742 MeV ($E_0 + \Delta_0$ = 0.041 MeV).

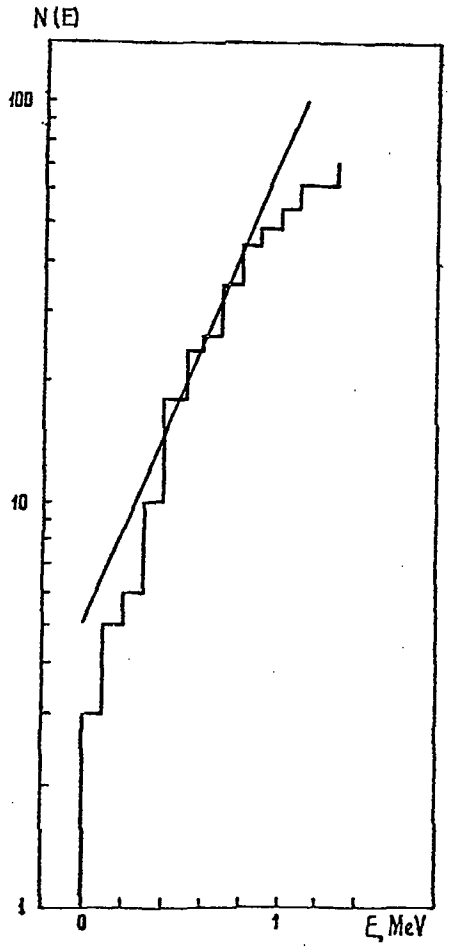

Fig. 4. Description of the increasing sum of ^{239}Pu levels using the constant temperature model with T=0.377 and E_0=-0.608 MeV ($E_0 + \Delta_0$ = 0.168 MeV).

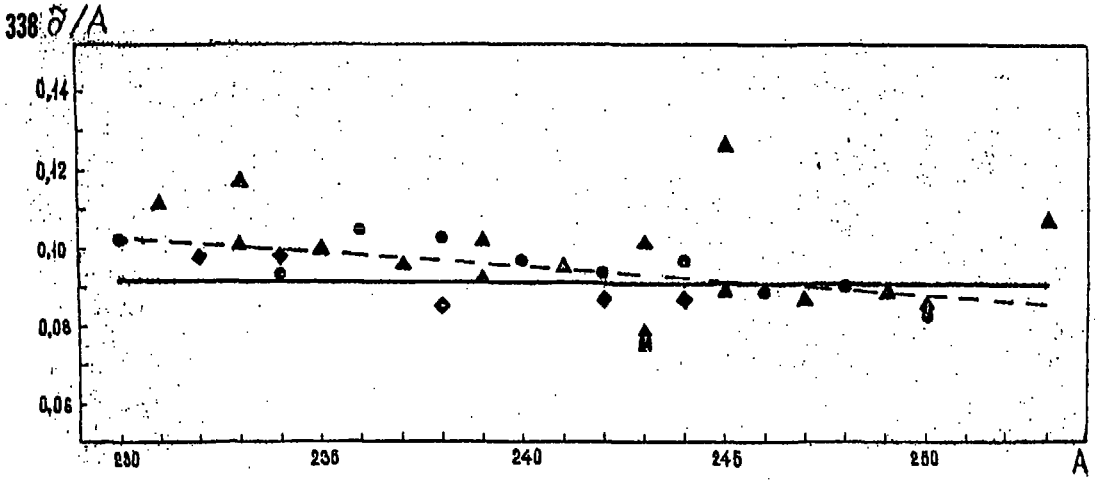

Fig. 5. $\tilde{a}/A$ vs mass number A. Solid line, relation (13). ●, even-even nuclei; ▲, even-odd nuclei; ■, odd-even nuclei; ◆, odd-odd nuclei.

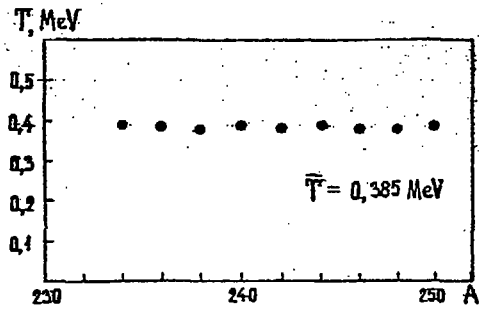

Fig. 6. Parameter T in the constant temperature model for even-even nuclei vs mass number.

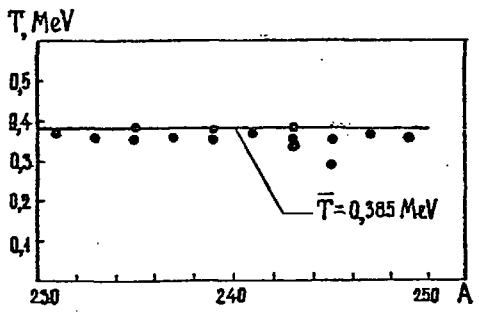

Fig. 7. Parameter T in the constant temperature model for odd nuclei vs mass number.

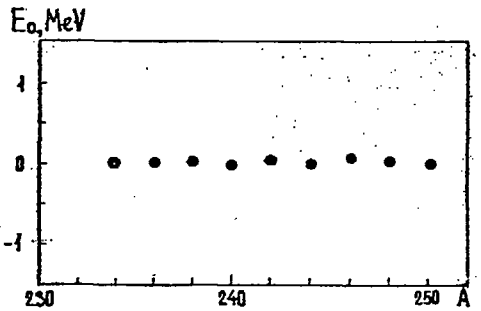

Fig. 8. Parameter E_0 in the constant temperature model for even-even nuclei vs mass number.

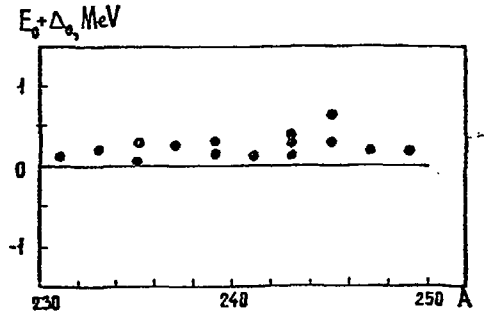

Fig. 9. $E_0 + \Delta_0$ for odd nuclei vs mass number.

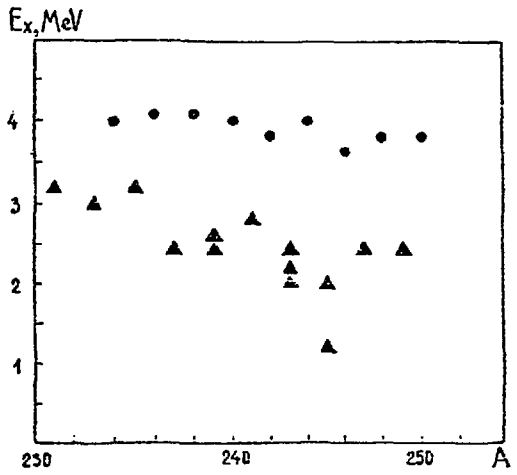

Fig. 10. Energy E_x of level density model matching for even-even (●) and odd (▲) nuclei vs mass number.

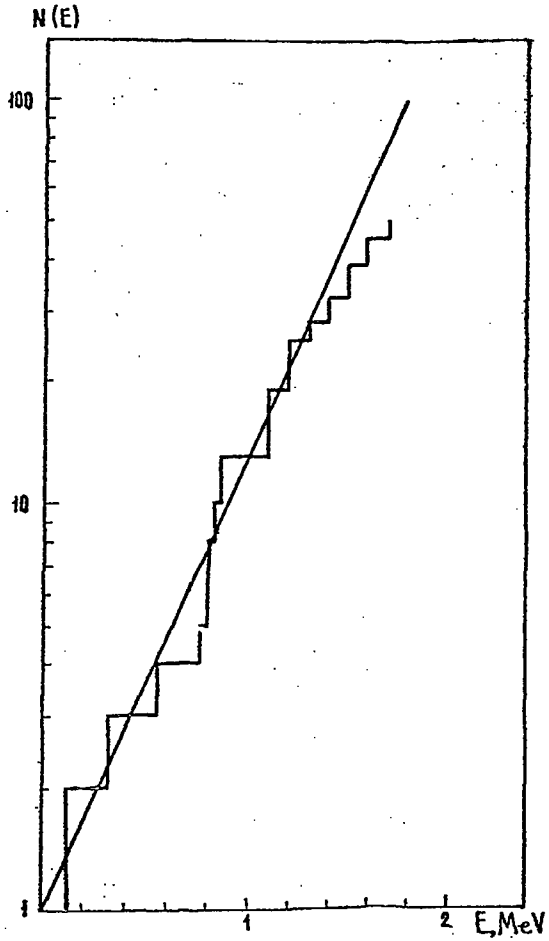

Fig. 11. Description of the increasing sum of ^{232}Th levels using the constant temperature model with T=0.385 MeV and E_0=0.

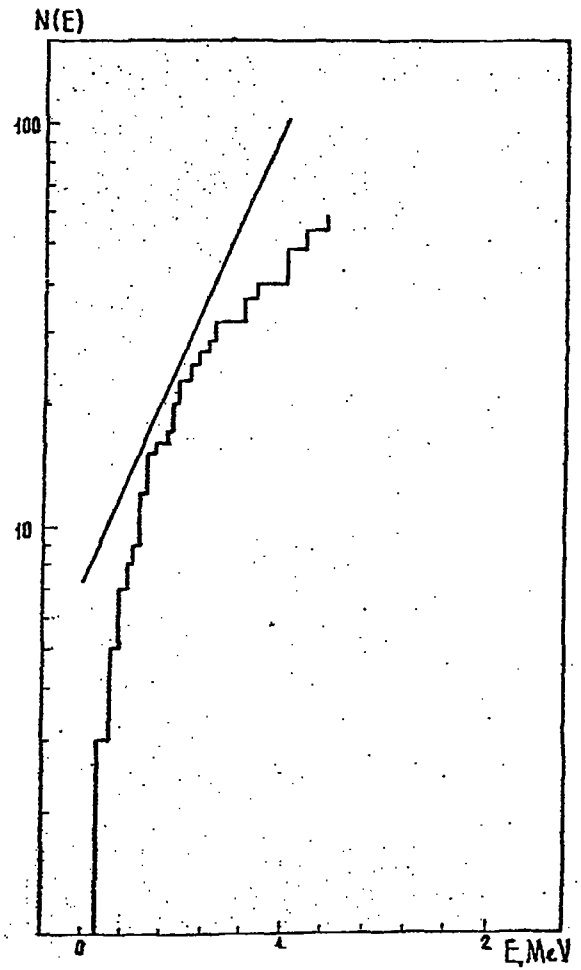

Fig. 12. Description of the increasing sum of ^{239}Np levels using the constant temperature model with T=0.385 MeV and $E_0=-\Delta_0$.

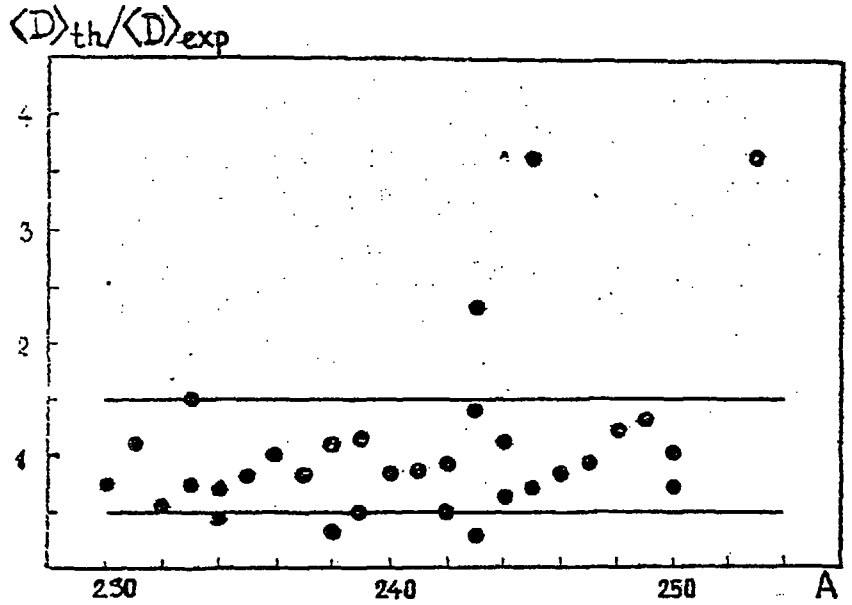

Fig. 13. Ratio of $\langle D \rangle$ calculated by the constant temperature model parameter to experimental one for Th-Cf.

REFERENCES

1. Antsipov G.V., Zenevich V.A., Klepatskii A.B., Konshin V.A., Sukhovitsky E.Sh., Proc. of the IXth Intern. Symposium on Fast Neutron Interactions with Nuclei, Dresden, GDR, 26-30 Nov., 1979, TFK-410, pp. 141-146.
2. Cameron A.G.W., Gilbert G., Can. J. Phys., v. 43, 1965, p. 1446.
3. Reffo G., Parameter Systematics for Statistical Theory Calculations of Neutron Reactions Cross Sections, RT/FI(78) 11, 1978.
4. Fröhner F.H., Fischer U., John H., NEANDC(E)-202 U, v.5, INDC(Ger.)-21L, 1979, p. 31.
5. ENDF-102 Data Formats and Procedures for the Evaluated Nuclear Data File, ENDF revised by Garber D., Dunford C., Pearlstein S., BNL-NCS-50496, 1975.
6. Kravtsov V.A. Atom masses and binding energies of nuclei, M., Atomizdat, 1974.
7. Bohr O., Mottelson B., Structure of Atomic Nucleus, v. 2, M., Mir, 1977.
8. Ignatyuk A.V., Istekov K.K., Smirenkin G.N., Nuclear Physics, v. 29, 1979, p. 875.
9. Ignatyuk A.V., Shubin Yu.N., Izv. AN SSSR, Ser. Fiz., v. 37, 1973, p. 1947.
10. Ignatyuk A.V., Smirenkin G.N., Tishin A.S., Nuclear Physics, v. 21, 1975, p. 485.
11. Myers W.D., Swiatecki W.S., Ark. Fysik, v. 36, 1967, p. 593.
12. Luers B.R., Felvinci J.P., Melkonian E., Havens W.W., BNL-NCS-2473, DOEINDC-12/U, NEANDC(US)-203/U, INDC(USA)-79/U, 1978, p. 43.
13. Kalebin S.M., Palei P.N., Ivanov R.N., Karalova Z.K., Kukavadze G.M., Pyzhova Z.I., Rukolaine G.V., Atom. Energ., v. 26, 1969, p. 507.
14. Vasiliev G., Mateescu S. et al., Nuclear Data Evaluation for ^{232}Th, INPR, Pitesti-Romania, 1979.
15. Simpson F.B., Burgus W.H., Evans J.E., Kirby H.W., Nucl. Sci. Eng., v. 12, 1962, p. 243.
16. Simpson F.B., Codding J.W., Nucl. Sci. Eng., v. 28, 1967, p. 133.
17. Auchampaugh G.F., Bowman C.D., Evans J.E., Nucl. Phys., v. A112, 1968, p. 329.
18. Kolar W., Carraro G., Nastri G., Proc. IAEA Conf. on Nuclear Data for Reactors, Helsinki, 1970, v. 1, p. 387.
19. James G.D., Dabbs J.W.T., Harwey J.A., Hill N.W., Schindler R.H., Phys. Rev. C., v. 15, 1977, p. 2083.
20. Moore M.S., Moses J.D., Keyworth G.A., Dabbs J.W.T., Hill N.W., Phys. Rev. C, v.18, 1978, p. 1328.
21. Carraro G., Brusegan A., Nucl. Phys., v. A257, 1976, p. 333.
22. McNally J.H., Barnes J.W., Drpesky B.J., Seeger P.A., Wolfsberg K., Phys. Rev. C, v. 9, 1974, p. 717.
23. De Saussure G., Olsen D.K., Perez R.B., Oifilippo F.C., Progress in Nucl. Energy, v. 3, 1979, p. 87.

24. Mewissen L., Rortmans F., Cornelis E., Vanpraet G., Angeletti A., Rohr G., Weigman H., Nucl. Sci. Eng., v. 70, 1979, p. 155.

25. Caner M., Yiftah S., Neutron Cross Sections for Plutonium-238, IA-1301, INDC(ISL)-2/L, 1976.

26. Konshin V.A., Morogovsky G.B., Sukhovitsky E.Sh., Izv. AN BSSR, Ser. Fiz-Energ. Nauk, No. 2, 1974, p. 21.

27. Konshin V.A., Antsipov G.V., Sukhovitsky E.Sh., Bakhanovich L.A., Klepatsky A.B., Morogovsky G.B., Porodzinsky Yu.V., Evaluation of Nuclear Data for Pu-241 in Neutron Energy Range from 10^{-3} eV to 15 MeV, INDC(CCP)-142/GJ,1980.

28. Antsipov G.V., Bakhanovich L.A., Bendersky A.R., Zenevich V.A., Klepatsky A.B., Konshin V.A., Sukhovitsky E.Sh., Evaluation of Nuclear Data for ^{242}Pu in the 10^{-5} eV-15 MeV Neutron Energy Region, INDC(CCP)-150, LJH, 1980.

29. Auchampaugh G.F., Farrel J.A., Bergen D.W., Nucl. Phys., v. A171, 1971, p. 31.

30. Maino G., Menapace E., Motta M., Ventura A., ^{241} Am Neutron Cross Sections in the Resonance Region, 1979.

31. Browne J.C., Howe R.E., Dougan R.J., Dupsyk R.J., Landrum J.H., Proc. Intern. Conf. on Neutron Physics and Nuclear Data for Reactors and other Applied Purposes, Harwell, 1978, p. 887.

32. Simpson O.D., Simpson F.B., Harkey J.A., Slaughter G.G., Benjamin R.W., Ahlfeld C.E., Nucl. Sci. Eng., v. 55, 1974, p. 273.

33. Artamonov V.S., Ivanov R.N., Kalebin S.M., Rukolaine G.V., Anufriev V.A., Babich S.I., Belanova T.S., Kocherygin N.G., Kolesov A.G., Nikolsky S.N., Nefedov V.N., Poruchikov V.A., Safonov V.A., Tikhomirov V.V., Proc. 4th All-Union Conference on Neutron Physics, Kiev, 1977, pt. 2, p. 257.

34. Browne J.C., Benjamin R.W., Karraker D.G., Nucl. Sci. Eng., v. 65, 1979, p. 166.

35. Martinelli T., Menapace E., Motta M., Kaccari M., Ventura A., Evaluation of ^{246}Cm Neutron Cross Sections in the Resonance Region, RT/FI(80), 1980.

36. Martinelli T., Menapace E., Motta M., Vaccoci M., Evaluation of Cm-247 Neutron Cross Sections in the Resonance Region, 1980.

37. Benjamin R.W., Ahlfeld C.E., Harvey J.A., Hill N.W., Nucl. Sci. Eng., v. 55, 1974, p. 440.

38. Harvey J.A., Benjamin R.W., Hill N.W., Raman S., The Neutron Total Cross Section and Resonance Parameters of ^{249}Bk, BNL-NCS-21501, ERDA/NDC-3/U, 1976, p. 198.

39. Silber M.G., Nucl. Sci. Eng., v. 51, 1973, p. 376.

40. Moore M.S., McNally J.H., Phys. Rev. C, v. 4, 1971, p.273.

41. Lynn J.E., Systematics for Neutron Reactions of the Actinide Nuclei, AERE-R7468, 1974.

DEPENDENCE OF TRANSACTINIDE LEVEL DENSITY ON PARITY AND ANGULAR MOMENTUM

G.V. Antsipov, V.A. Konshin and V.M. Maslov

Heat & Mass Transfer Institute, BSSR Academy of Sciences, Minsk, U.S.S.R.

ABSTRACT. The dependence of level density on the parity and angular momentum is considered based on the discrete spectrum analysis.

1. INTRODUCTION

In authors' another contribution to this Meeting considered are the problems of transactinide nuclear level density parametrization using the superfluidity nucleus model involving collective (vibrational and rotational) degrees of freedom.However, only the dependence of the level density on excitation energy was discussed. The problems of level density dependence on parity and angular momentum were not dealt with. To discuss the $\rho(J,\pi)$-dependence all nuclear level schemes for transactinides from ^{225}U to ^{254}Cf recommended by Nuclear Data Sheets (1976-1978) were used.

2. PARITY DEPENDENCE OF LEVEL DENSITY

As a rule, nuclear level density models suppose equally probable parity distribution. The combinatorial /1,2/ and statistical /3/ calculations show that in a number of cases at low energies this assumption does not hold. At the same time, it is emphasized in /3/ that for deformed nuclei the deviations from the equality $\rho_+ = \rho_-$ are presumably negligible. It is reasonable, therefore, to verify the assumption on the equally probable parity distribution for the nuclei being essentially deformed. This can be done in principle by analysing average radiative widths $\langle \Gamma_\gamma \rangle$ for different parity resonances, average distances between different parity resonances or spectroscopic information on the discrete spectrum.

Unfortunately, the value of $\langle \Gamma_\gamma \rangle$ for p-resonances is unknown even for the ^{238}U which is most comprehensively studied. The existing evaluations of the average distances between s- and p-resonances indicate the validity of the condition $\rho_+ = \rho_-$ at the excitation energy near the neutron binding energy.Thus, for ^{238}U $\langle D \rangle_{\ell=0} = 24.8 \pm 2.0$ eV and $\langle D \rangle_{\ell=1} = 8.91 \pm 0.10$eV /4/ which consists with the law $(2J+1)$ within the errors. The analysis of level parity for the discrete spectrum for Th - Cf has shown that $\rho_+ = \rho_-$ holds within $\pm$ 50% for 69% nuclei out of 51 nuclei (Fig.1). With view of insufficiently reliable information on the level parity and poor statistics, such an agreement seems to be adequate to think the assumption $\rho_+ = \rho_-$ does not contradict to the data available at low excitation energies, i.e. above the known discrete spectrum. The ratio N_-/N_+ being, on the average, somewhat below unity (Fig.1). It can be partly due to the fact that the bulk of the

nuclei studied have positive parity of the ground state. In other words, this may demonstrate the effect of the ground state bound levels.

3. LEVEL DENSITY DEPENDENCE ON ANGULAR MOMENTUM

In the previous work we used the following expression for $\rho(U, J)$:

$$\rho(U,J) = K_{vib}(U)\frac{\omega(U)}{2\sqrt{2\pi}\,\sigma_{11}}\sum_{K=-J}^{J} \exp\left[\frac{J(J+1)}{2\sigma_{\perp}^2} + \frac{1}{2}K^2\left(\frac{1}{\sigma_{\perp}^2} - \frac{1}{\sigma_{11}^2}\right)\right] \qquad (1)$$

where $K_{vib}(U)$ is the coefficient allowing for the contribution of vibrational degrees of freedom; $\omega(U)$ is the total density of internal excited states; σ_{11}^2 and $\sigma_{\perp}^2$ are the spin dependence parameters associated with parallel and perpendicular nucleus inertia moments, K is the angular moment projection to the symmetry axis. Due to the essential deformation of transactinide nuclei ($\varepsilon \approx 0.24$), expression (1) can be given as

$$\rho(U,J) = K_{vib}(U)\,K_{rot}(U)\frac{(2J+1)\,\omega(U)}{2\sqrt{2\pi}\,\sigma_{11}\,\sigma_{\perp}^2}\exp\left[-\frac{J(J+1)}{2\sigma_{\perp}^2}\right], \qquad (2)$$

where

$$K_{rot}(U) = \sigma_{\perp}^2 \qquad (3)$$

is the coefficient allowing for the level density increase due to the contribution of rotational degrees of freedom.

Represent (2) in terms of the total level density $\rho(U)$:

$$\rho(U,J) = \rho(U)\,f(U,J), \qquad (4)$$

where

$$\rho(U) = \frac{K_{vib}(U)\,K_{rot}(U)\,\omega(U)}{\sqrt{2\pi}\,\sigma_{11}}, \qquad (5)$$

$$f(U,J) = \frac{(2J+1)\exp\left[-J(J+1)/2\sigma_{\perp}^2\right]}{2\sigma_{\perp}^2}. \qquad (6)$$

Expression (6) is none other than the well-known angular moment level density distribution in the Fermi-gas level density model with the parameter $\sigma_{\perp}^2$ for σ^2. That is, under the conditions which enable one to proceed from (1) to (2) the inclusion of the collective degrees of freedom does not change qualitatively the angular moment distribution law.

The applicability of the law of type (6) in the spin region being important for the neutron cross-section evaluation would not usually call any doubts. It is natural to try to extent law (6) to the low energy region where the total level density is represented by the constant temperature law. Similar problem is considered in /5/ which, however, does not deal with transactinides. Analysis of discrete spectra for nuclei considered shows that the level spin assignment is not made, as a rule, with great confidence, for the exception of low bands. Nevertheless even from such information it is possible to make some conclusions.

For law (6), the maximum probability method can yield the following estimation of the parameter $\sigma_\perp^2$:

$$\sigma_{\perp\,exp}^2 = \frac{1}{2N}\sum_i^N J_i(J_i+1), \qquad (7)$$

where N is the number of levels identified over the spin. Despite that the estimation (7) is weak-sensitive to the level omission, we have used for $\sigma_{\perp\,exp}^2$ determination only the data in the energy region with relatively low level omission. This was checked by describing the increasing level sum using the constant temperature model. Parameters $\sigma_{\perp\,exp}^2$ for 41 nuclei having fairly studied discrete spectra are given in Fig.2. It is easily seen that $\sigma_{\perp\,exp}^2$ for even-even nuclei is much higher. But there are only two of them. No difference is observed in $\sigma_{\perp\,exp}^2$ for odd-odd and even nuclei. That is, it is difficult to say something on the existence of $\sigma_{\perp\,exp}^2$ dependence on parity. Despite the difference between the spins in the ground state and the states considered it is seen that the values of $\sigma_{\perp\,exp}^2$ can be fairly described on the average by the linear dependence on the mass number A . The least square method gives the following parametrization for $\sigma_{\perp\,exp}^2$:

$$\sigma_{\perp\,exp}^2 = 0{,}15624\,A - 26{,}76\,. \qquad (8)$$

The data available on spin distribution of transactinide discrete spectrum levels are satisfactorily described by (6) with $\sigma_\perp^2 = \sigma_{\perp\,exp}^2$. This is supported by Figs.3a- 3u giving distributions for all nuclei with relatively large number of spin-identified levels. The values of $\sigma_{\perp\,exp}^2$ allow the constant-temperature law to be used fatisfactorily to describe the increasing sum of $N(U, J)$ levels for ^{234}U , ^{235}U, ^{239}Pu, ^{240}Pu, ^{245}Cm and ^{246}Cm nuclei for which a comparatively large number of levels exists with identified J (Fig.4a- f).

All this points to the possibility of substituting, if necessary, the discrete spectrum by the continuous one using the constant temperature model and the law (6) including the parameter $\sigma_{\perp\,exp}^2$ and of extending the law (6) to the energy region above the known discrete spectrum with the appropriate choice of the parameter $\sigma_\perp^2$

It seems not quite correct to use the results of $\sigma_\perp^2$ calculation by the superfluid nucleus as well as by any other statistic model, since the main parameter a which can be determined from the observed neutron resonance density or from the systematics hardly displays the structure of levels at rather low excitations. Therefore, the approach similar to /5/ seems to be more natural. It implies that the use of $\sigma_\perp^2 = \sigma^2_{\,exp}$ up to the energies where the discrete spectrum can be regarded identified rather reliably ($E_{bound.}$) , then σ^2 , from $E_{bound.}$ to the point, E_x, (the matching point for the superfluid nucleus model and the constant temperature model), is determined by the linear interpolation between $\sigma_{\perp\,exp}^2$ and $\sigma_\perp^2(E_x)$ calculated by the superfluid nucleus model. Above E_x the calculations using the same model are made.

For the nuclei, whose discrete spectra are insufficiently identified, $\sigma_\perp^2$ can be calculated using the equation (8) and

the following values of E_{bound}:

$$E_{bound} = 1.2 \text{ MeV for odd-odd nuclei}$$

$$E_{bound} = 0.6 \text{ MeV for even nuclei}$$

$$E_{bound} = 0.3 \text{ MeV for even-even nuclei}$$

being the average for the respective groups of nuclei.

4. CONCLUSION

The main results are as follows:

(i) The analysis of discrete transactinide spectrum suggests the independence of nuclear level density parity at rather low excitation energies.

(ii) Parametrization of the parameter $\sigma_{\perp}^{2}{}_{exp}$ is made and its dependence on mass number is obtained.

(iii) It is shown that the law (6) of level density distribution on angular moment is applicable not only near the neutron binding energy and above, but describes the data available on the discrete spectrum fairly well, i.e. can be used for low excitation energies with the appropriate choice of $\sigma_{\perp}^{2}$.

REFERENCES

1. Hillman M., Grover J., Phys.Rev., v.185, 1969, p.1303.
2. Soloviev V.G., Stoyanov Ch., Vdovin A.I., Nucl. Phys., v.A224, 1974, p.411.
3. Blokhin A.I., Ignatyuk A.V., The proceedings of the3rd All-Union Conference on Neutron Physics, Kiev, 1975, Part 3,p.3.
4. De Saussure G., Olsen D.K., Perez R.B., Difilippo F.C., Progress in Nucl. Energy, v.3, 1979, p.87.
5. Reffo G., Parameter Systematics for Statistical Theory Calculations of Neutron Reaction Cross Sections. Proc. of the Course on Nuclear Theory for Applications, Trieste,1978. ICTP , Trieste, IAEA-SMR-43, p.205-230.

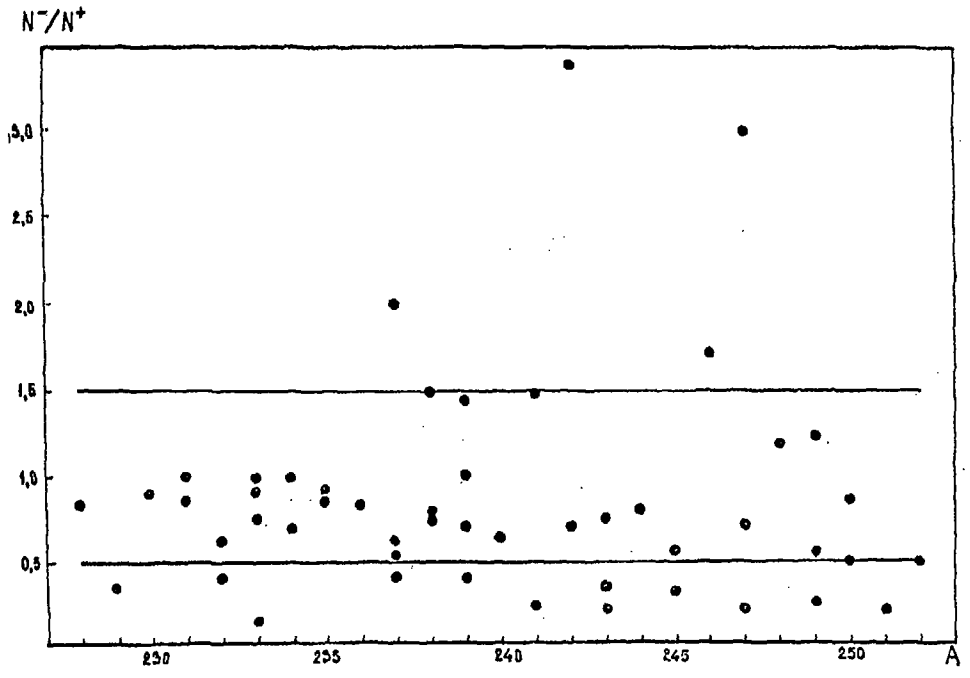

Fig.1. Ratio of the number of different parity levels for discrete Th - Cf transactinide spectrum.

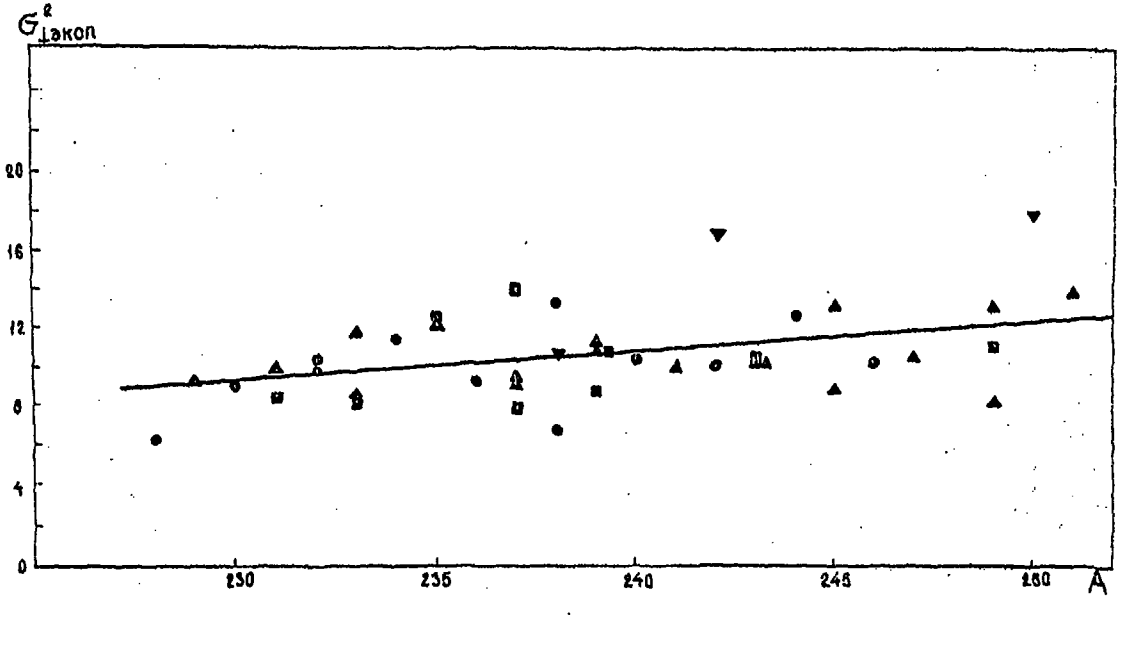

Fig.2. Parameter $\sigma^2_{\perp exp}$ vs mass number A: ● , even-even nuclei; ▲ , even-odd nuclei; ■ , odd-even nuclei; ▼ , odd-odd nuclei. Straight line, relationship (8).

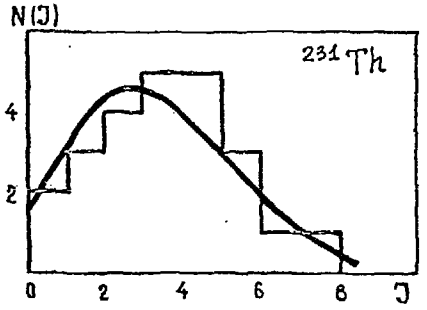

Fig.3a

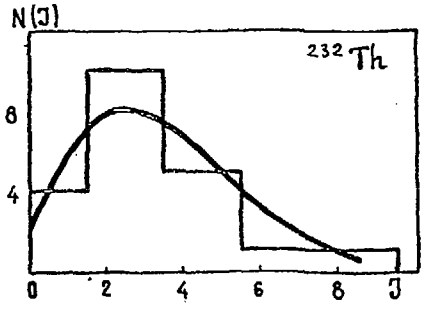

Fig.3b

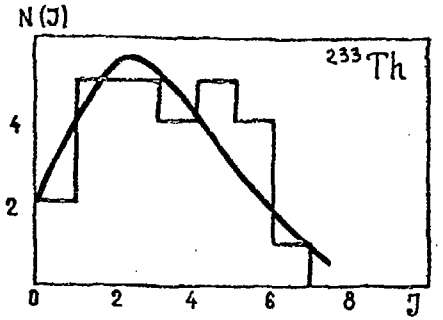

Fig.3c

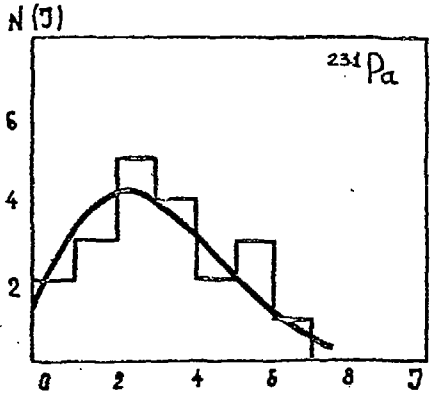

Fig.3d

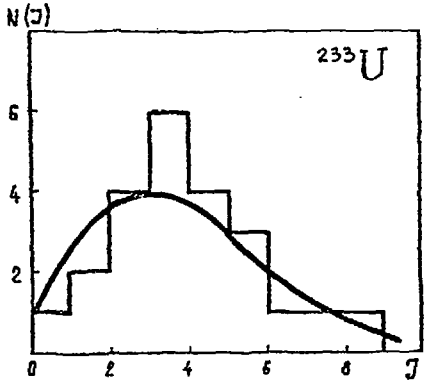

Fig.3e

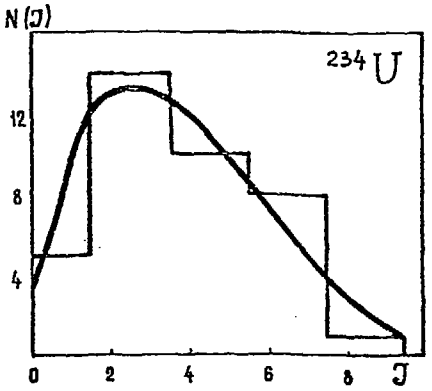

Fig.3f

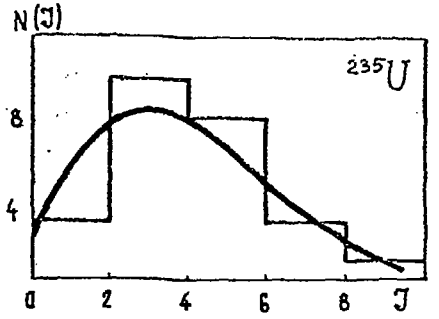

Fig.3g

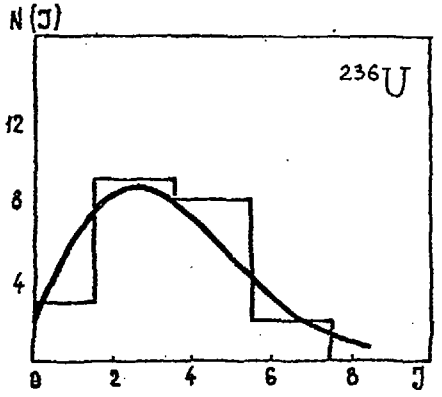

Fig.3h

Fig.3. Description of the experimental spin distributions of discrete nuclei spectra levels in terms of the parameter $\sigma^2_{\perp\,exp}$: a, ^{231}Th; b, ^{232}Th; c, ^{233}Th; d, ^{231}Pa; e, ^{233}U; f, ^{234}U; g, ^{235}U; h, ^{236}U; i, ^{238}U; j, ^{239}Np; k, ^{239}Pu; l, ^{240}Pu; m, ^{241}Pu; n, ^{242}Pu; o, ^{242}Am; p, ^{243}Am; q, ^{245}Cm; r, ^{246}Cm; s, ^{247}Cm; t, ^{249}Cm; u, ^{250}Bk.

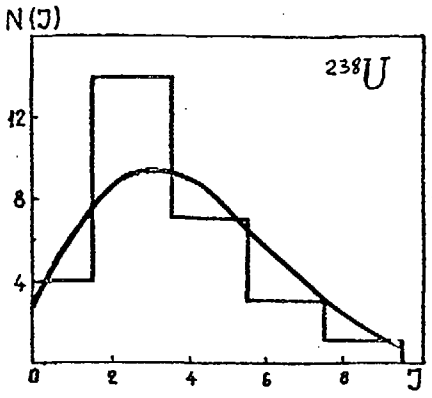

Fig.3i

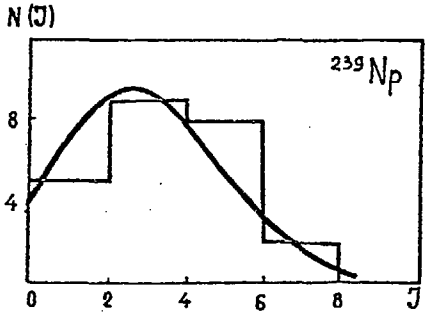

Fig.3j

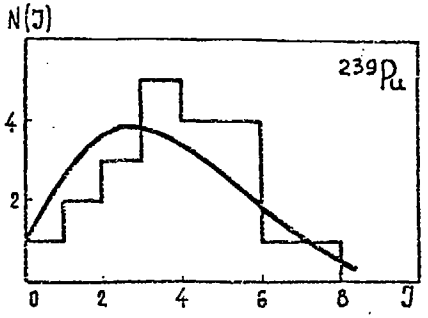

Fig.3k

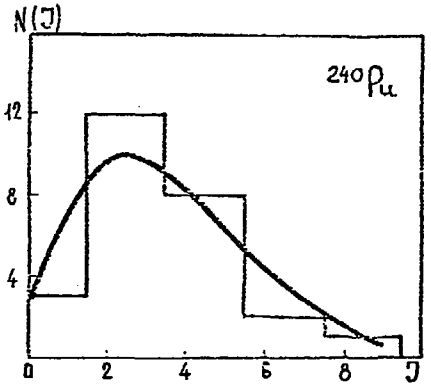

Fig.3l

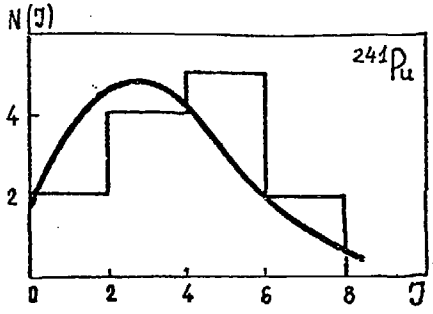

Fig.3m

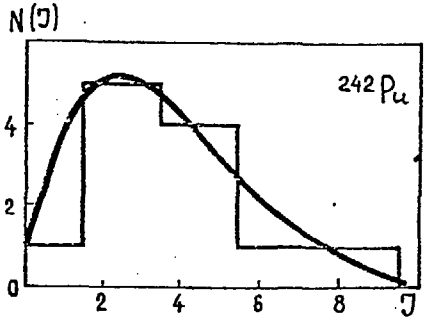

Fig.3n

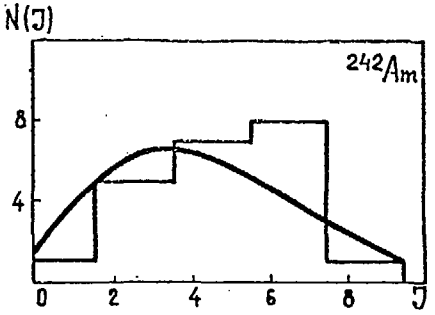

Fig.3o

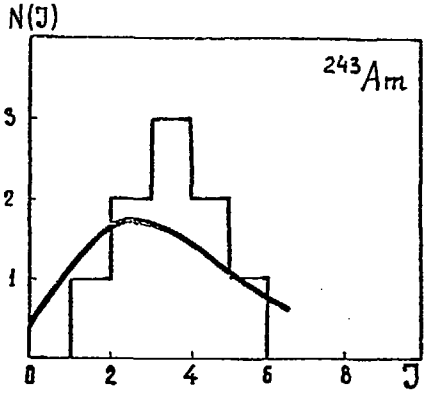

Fig.3p

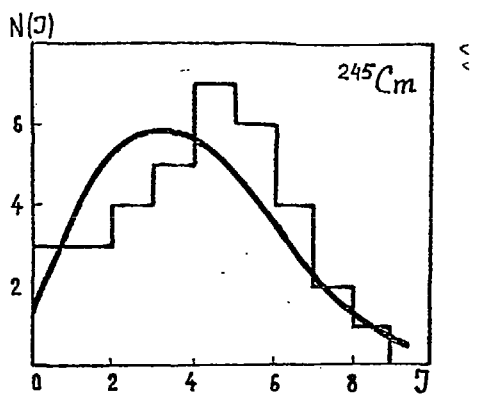

Fig.3q

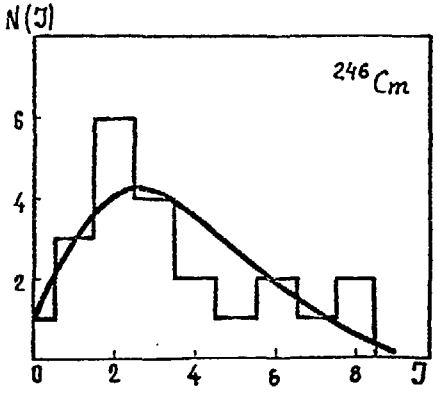

Fig.3r

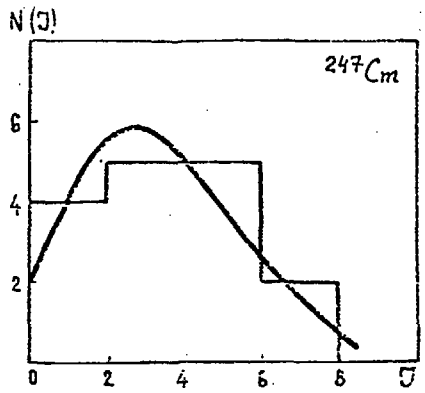

Fig.3s

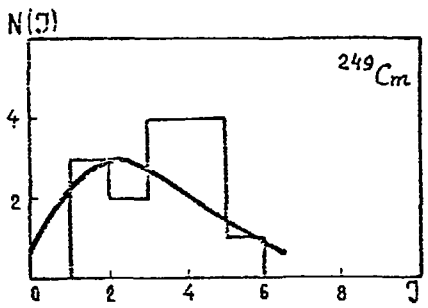

Fig.3t

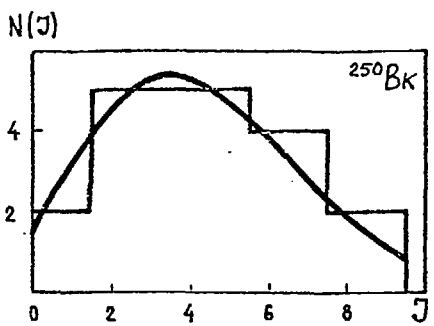

Fig.3u

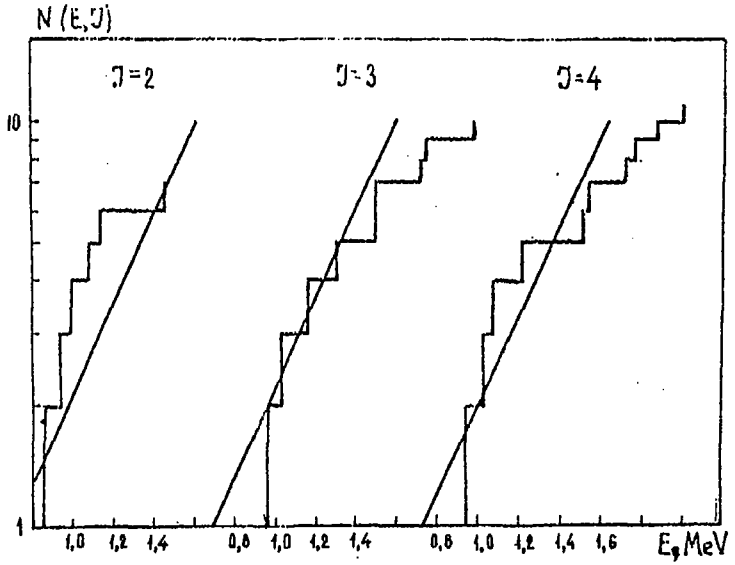

Fig.4a

Fig.4. Description of increasing level sums including J data in terms of the constant temperature model and law (6) with $\sigma^2_{\perp\,exp} = \sigma^2_{\perp}$: a, ^{234}U; b, ^{240}Pu; c, ^{235}U; d, ^{239}Pu; e, ^{245}Cm; f, ^{246}Cm.

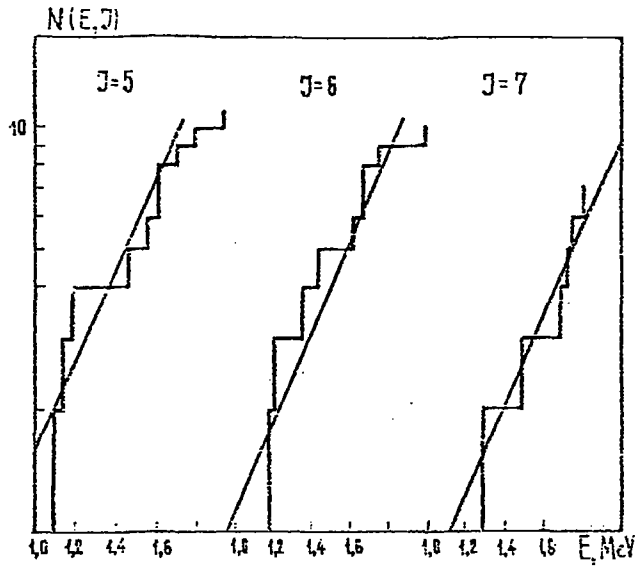

Fig.4a

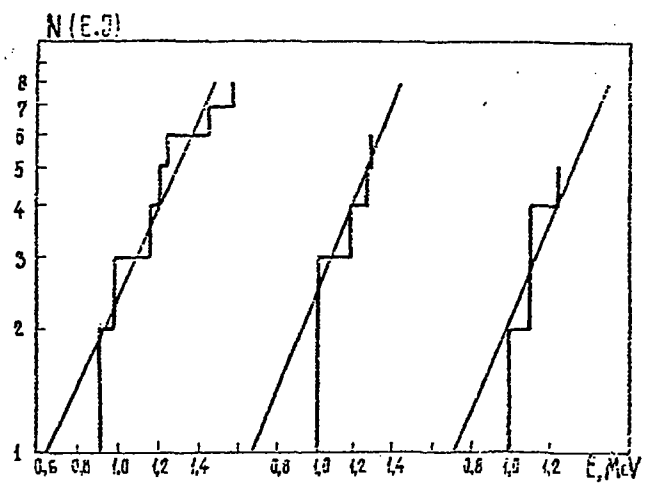

Fig.4b

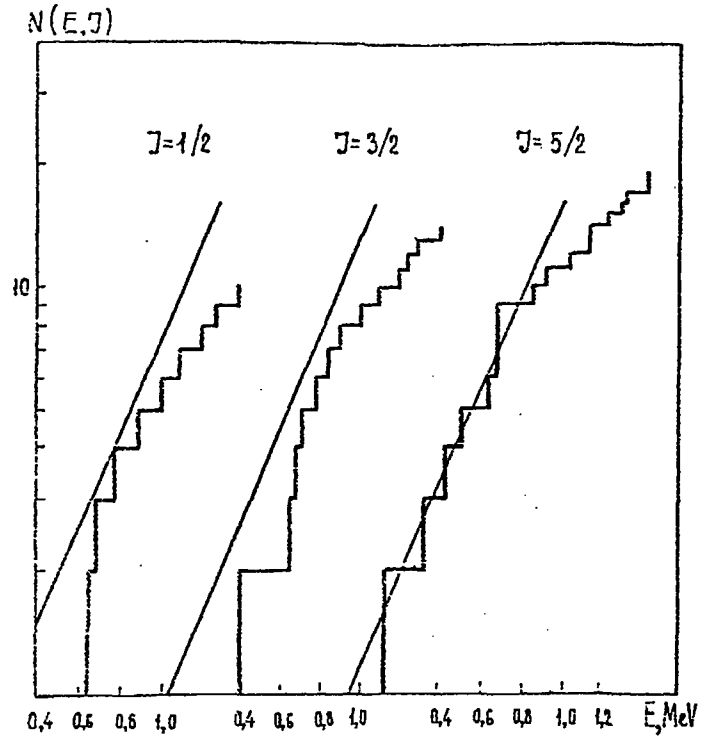

Fig.4c

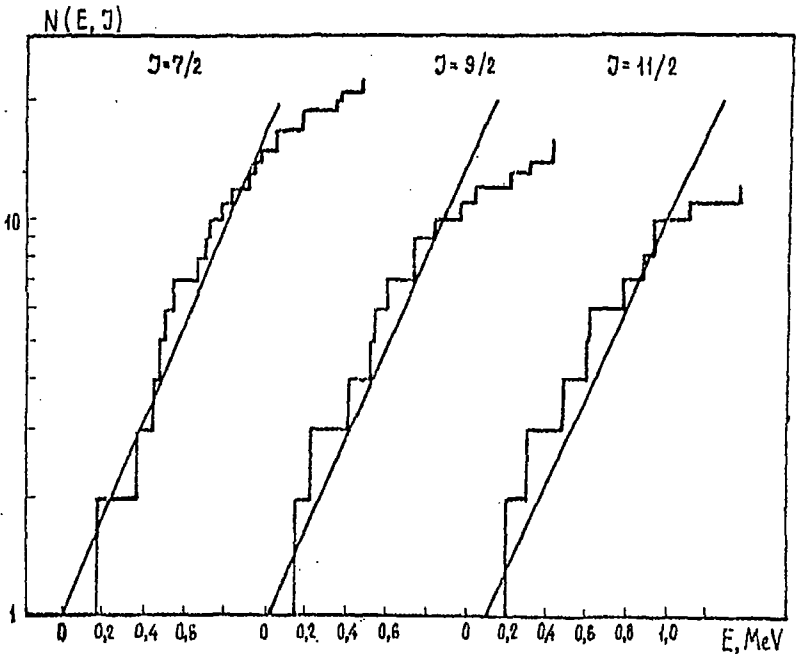

Fig.4c

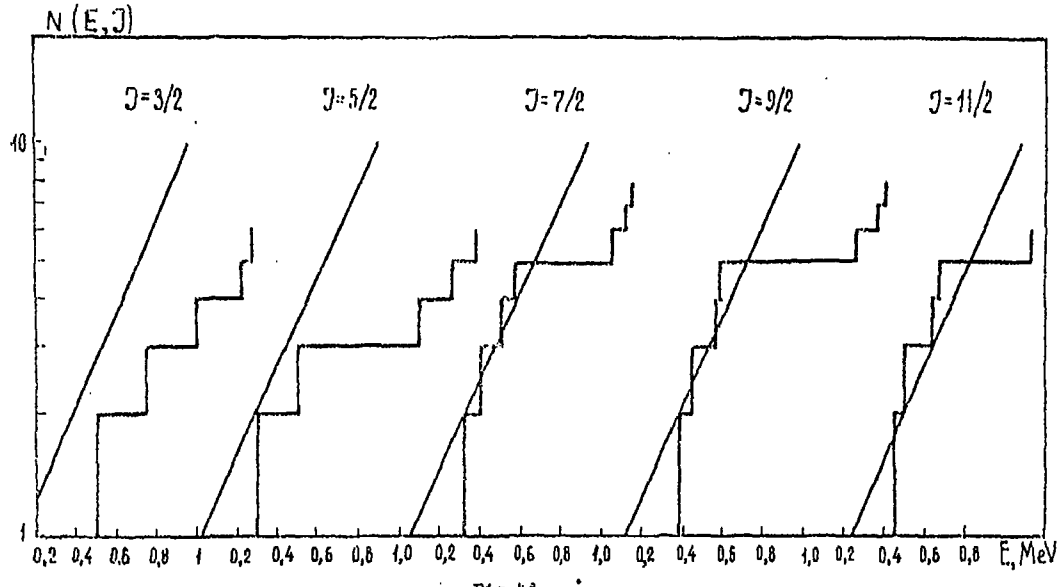

Fig.4d

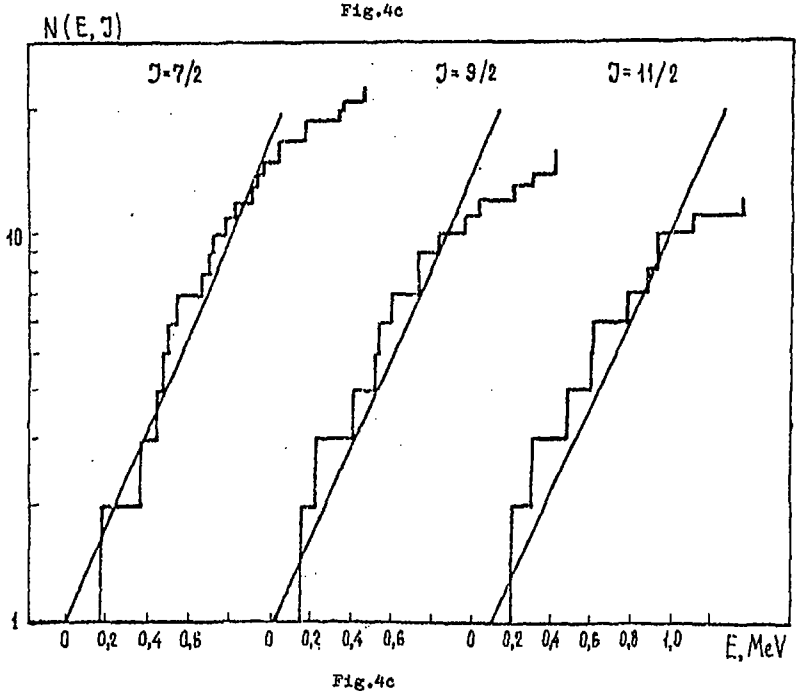

Fig.4c

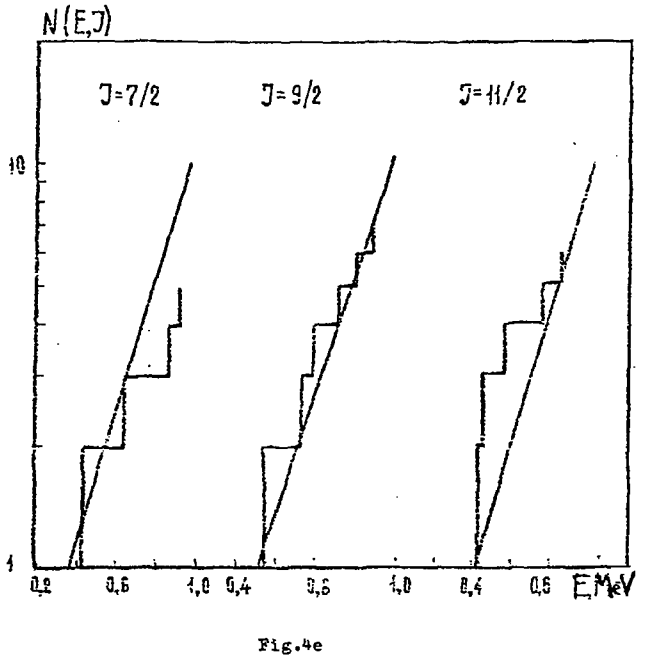

Fig.4e

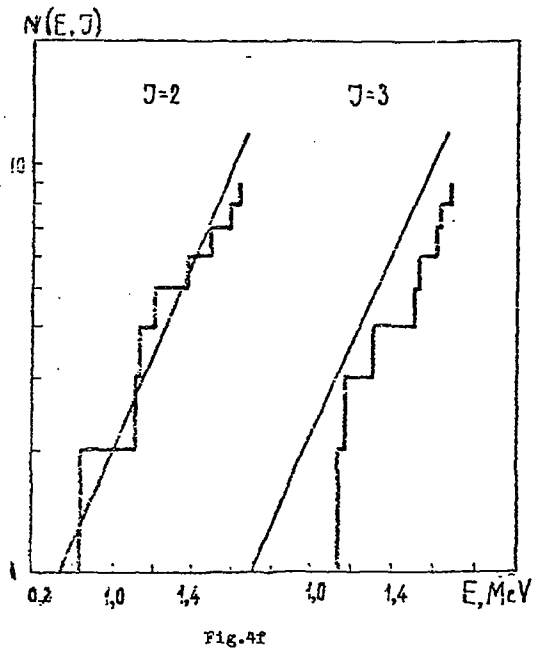

Fig.4f

EFFECT OF DIFFERENT NUCLEAR LEVEL DENSITY MODELS ON ACTINIDE NEUTRON CROSS SECTION CALCULATIONS

V.A. Konshin
Heat and Mass Transfer Institute, BSSR
Academy of Sciences, Minsk, U S S R

ABSTRACT

The nonspherical optical potential, spectral Lorentz factor and the Fermi-gas level density model involving the collective modes give a self-consistent description of all kinds of neutron cross sections, including $\sigma_{n\gamma}$, for actinides.

The application of the traditional Fermi-gas level density model results in an appreciable difference between experimental and calculated $\sigma_{n\gamma}$ for both kinds of spectral factors that cannot be attributed to the uncertainties of the parameters used.

The relationships of the Fermi-gas model widely used in statistical calculations rely on the idea of a complete mixing of collective degrees of freedom in an excited nucleus and, hence, neglect collective effects. The semi-microscopic method of the level density calculation suggested by Soloviev et al [1,2] enables one to allow for the vibrational and rotational contributions. But these methods being rather tedious, especially when used for high energies, find a limited use in the nuclear data evaluation.

In neutron cross-section calculations the collective effects can be taken into account in the framework of the statistical method developed by Ignatyuk et al. [3]. The method allows for the shell nonuniformities in the single-particle level spectra, correlation effects of a superconductive type and coherent collective effects.

The Fermi-gas model considers the shell effects vs the dependence of the parameter a on the excitation energy and shell correction δW. The effect of the energy dependence of the parameter a is most essential for nuclei around closed shells. The shell correction for actinides is relatively small, and its effect is negligible.

The level density equations for the superfluid nucleus model are given in [3]. These formulae hold not only for odd-odd but also for even and even-even nuclei provided the excitation is somewhat renormalized.

Considering the collective effects, the level density formula takes the form:

$$\rho(U,J) = K_{rot} K_{vib} \rho_{F.-g.}(U,J).$$

The adiabatic estimation of the level density increase coefficients K_{rot} and K_{vib} due to rotational and vibrational modes as well as of the factor σ^2 gives the following expressions [3]

$$K_{rot} = F_{\perp} t,$$

$$K_{vib} = \exp(0.25\, U^{2/3}),$$

$$\sigma^2 = F_{\perp}^{2/3} F_{\parallel}^{1/3} t \quad ,$$

where $F_{\perp}$ and $F_{\parallel}$ are the normal and parallel inertia moments; t is the excited nucleus temperature.

Different level density models yield different energy dependence of the level density, thus affecting the value of the neutron cross sections calculated using the statistical model. As the calculated fission cross sections for the energies above 1 MeV are usually fitted to the experimental data, the radiative capture cross section $\sigma_{n\gamma}$ in statistical calculations is most sensitive to the choice of this or another level density model. Our calculations [4,5] show that the conventional level density Fermi-gas model gives an appreciable discrepancy between the experimental and calculated $\sigma_{n\gamma}$ for both kinds of the spectral factor that cannot be attributed to the uncertainties of the parameters used (Figs. 1 and 2).

The best agreement with the experimental data in the whole energy region considered is achieved with the Fermi-gas level density model allowing for the collective modes. The use of the Weisskopf spectral factor (curve 4, Figs. 1 and 2) does not result in better agreement of $\sigma_{n\gamma}$ with the experimental data than the one achieved through the use of the Lorentz spectral factor and the Fermi-gas model involving the collective modes. Therefore, due to the more comprehensive physical grounds for the Lorentz factor supported by the agreement between the calculated and experimental data for the radiative strength functions [6] and the experimental data on the widths of the $(n,\gamma f)$-process (see Table 1) it seems reasonable to use this very spectral factor in calculations by the statistical model.

The coupled-channel method is the most correct one for calculating neutron transmission coefficients. The difference in the neutron transmission coefficients T_n calculated using the spectral model and coupled-channel model is becoming more essential when the orbital momentum ℓ increases and the coefficients T_n decrease. This affects mostly the radiative capture cross-section calculation, as $\sigma_{n\gamma}$ is mostly determined by the contributions of the channels with small neutron transmissions which compete weakly with the (n,γ)-process. Therefore, using of the neutron transmission coefficients calculated by the coupled-channel method leads to better agreement between the experimental and theoretical data for $\sigma_{n\gamma}$ for actinides.

The correct calculation of neutron transmission coefficients affects, in the first turn, the value of the compound nucleus cross section and, hence, the radiative capture and inelastic scattering cross sections. The difference in $\sigma_{n\gamma}$ calculated by the spherical and nonspherical optical models is energy dependent and ranges from 5 to 20%.

In our self-consistent evaluation of all types of neutron cross sections, neutron transmission coefficients for inlet channels are calculated by the coupled-channel method with the careful optimization of the nonspherical pot ntial parameters by the SPRT-method [11] using the χ^2-criterion [10].

In the calculation of outlet neutron transmission coefficients the use of the spherical potential seems to be justified since even for the main rotation band the channel coupling is hardly preserved when a neutron is in interaction with an excited nucleus.

The use of neutron transmission coefficients of the generalized optical model and regard for direct excitation of lower levels result in fair agreement between experimental and theoretical excitation cross sections both for the lower levels and for those, whose excitation levels are completely determined by the compound nucleus decay.

The choice of the level density model does not practically affect the total inelastic scattering cross section. The difference in different nuclear level density models for a target-nucleus causes changes in the relationship between scattering cross sections for discrete and continuous level spectra and in discrete level excitation cross sections.

It is seen from Fig. 3 that the best agreement between calculated and experimental data for the ^{239}Pu level excitation cross sections is achieved through the use of the Fermi-gas level density model involving the collective modes.

Thus, the nonspherical optical potential, the Lorentz spectral factor and the Fermi-gas level density model with allowance for the collective modes permit a self-consistent description of all types of the neutron cross sections, including $\sigma_{n\gamma}$, for odd-odd ^{238}U-type nucleus targets in a wide energy range. Since for even nucleus-targets the correct allowance for fission competition is most important the choice of different level density models has a less pronounced effect on the calculated cross sections.

Hence, the application of the traditional Fermi-gas nuclear level density model leads to a considerable discrepancy between experimental and calculated $\sigma_{n\gamma}$ for both kinds of spectral factors that cannot be attributed to the uncertainties of the parameters used.

The neutron transmission coefficients, T_n, used are in fact the ones for the excited nucleus states but sometimes these are identified with T_n for the ground state. This was remarked by Ignatyuk et al. [14] and investigated thoroughly by Klepatskii and Sukhovitsky E. in our laboratory using the coupled-channel method. They investigated the difference between the strength functions and transmission coefficients for the ground and excited states. Table 2 shows that the strength functions and, hence, the transmission coefficients for different states differ greatly in the low energy region, but with energy increasing this difference decreases. The difference in the transmission coefficients affects the radiative capture cross section. Our calculations of $\sigma_{n\gamma}$ (^{238}U) show that taking into account this effect allows a better agreement with the experimental data below 1 MeV to be reached (Curve 4, Fig. 4). Note that Curve 1 is for T_n obtained for nonspherical optical model inlet and spherical outlet channels, and Curve 4 is for T_n obtained for nonspherical inlet and outlet channels.

REFERENCES

1. Soloviev V.G., Stoyanov Ch., Vdovin A.I., Nucl. Phys., 1974, v. A224, p. 411.
2. Voronov V.V., Komov A.L., Malov L.A., Soloviev V.G., Nuclear Physics, 1976, v. 24, p. 504.
3. Ignatyuk A.V., Istekov K.K., Smirenkin G.N., Nuclear Physics, 1979, v. 29, p. 875.
4. Zenevich V.A., Klepatskii A.B, Konshin V.A., Sukhovitsky E.Sh., Neutron Physics (Proc. 5th All-Union Conference on Neutron Physics, Kiev, 1980). M., TsNIIATOMINFORM, 1980, pt. 3, p. 245-249, see translation by MAGATE INDC (CCP)-161/L, p. 27.
5. Zenevich V.A., Klepatskii A.B., Konshin V.A., Sukhovitsky E.Sh., Neutron Physics (Proc. 5th All-Union Conference on Neutron Physics, Kiev, 1980). M., TsNIIATOMINFORM, 1980, pt. 3, p. 250-255, see translation by MAGATE INDC (CCP)--161/L, p. 19.
6. Bartolomeew G.A. et al., Advances in Nucl. Physics, 1974, v. 7, p. 232.
7. Zen Chan Bom, Panteleev I., Tyan San Khak, Izv. AN SSSR, Ser. Fiz., 1973, v. 37, p. 82.
8. Raybov Yu., Trochon J., Shackleton D., Frehaut J., Nucl. Phys., 1973, v. A216, p. 395.
9. Borukhovich G.Z., Zvezdkina T.K., Ivanov K.N. et al., Preprint of Leningrad Institute of Nuclear Physics, Leningrad, 1978, No. 452.
10. Klepatskii A.B., Konshin V.A., Sukhovitsky E.Sh., The optical potential for heavy nuclei, Proc. 5th All-Union Conference on Neutron Physics, Kiev, 1980, Translation in INDC(CCP)-161/L, p. 9.
11. Lagrange Ch., Proc. of the EANDC Topical Discussion on Critique of Nuclear Models and Their Validity in the Evaluation of Nuclear Data, 1975, p. 58.
12. De Saussure G., Olsen D.K., Perez R.D. et al., Progress in Nuclear Energy, 1979, v. 3, p. 87.
13. Sukhovitsky E.Sh., Klepatskii A.B., Konshin V.A., Antsipov G.V., Neutron Physics (Proc. 4th All-Union Conference on Neutron Physics, Kiev, 1977). M., TsNIIATOMINFORM, 1977, pt. 4, p. 68.
14. Ignatyuk A.V., Lunev V.P., Proc. 5th All-Union Conference on Neutron Physics, Kiev, 1980, pt. 1, 1980, p. 77.

Table 1

Comparison of theoretical and experimental $\Gamma_{\gamma f}$ widths for ^{239}Pu

Level density models and spectral factor used	$\langle\Gamma_{\gamma f}\rangle^{0+} - \langle\Gamma_{\gamma f}\rangle^{1+}$, meV	$\langle\Gamma_{\gamma f}\rangle^{1+}$, meV
Fermi-gas model, Lorentz spectral factor	5.94	5.46
Fermi-gas model, Weisskopf spectral factor	10.59	11.55
Fermi-gas model involving the collective modes, Lorentz spectral factor	3.62	3.11
Fermi-gas model involving the collective modes, Weisskopf spectral factor	7.25	7.28
Superfluid nuclear model involving the collective modes, Lorentz spectral factor	5.80	5.24
Superfluid nuclear model involving the collective modes, Weisskopf spectral factor	11.42	13.37
Experiment -[7]	< 4	
[8]	-	4.1 ± 0.9
[9]	-	6.1 ± 2.9

Table 2

s-and p-strength functions(^{238}U) for the ground and excited states

Neutron, energy MeV	S_0, 10^{-4}			S_1, 10^{-4}		
	Ground state	State 2^+	State 4^+	Ground state	State 2^+	State 4^+
$0.5 \cdot 10^{-3}$	1.163	1.032	0.790	1.947	1.893	3.745
0.005	1.133	1.016	0.780	1.941	1.717	2.997
0.01	1.121	1.006	0.774	1.944	1.721	3.003
0.03	1.091	0.981	0.757	1.952	1.731	3.010
0.10	1.034	1.003	0.736	1.916	1.731	3.407
0.20	0.990	0.920	0.717	2.109	1.828	3.068
0.40	0.945	0.912	0.712	1.801	1.462	2.463
1.0	0.820	0.790	0.695	1.428	1.151	1.183

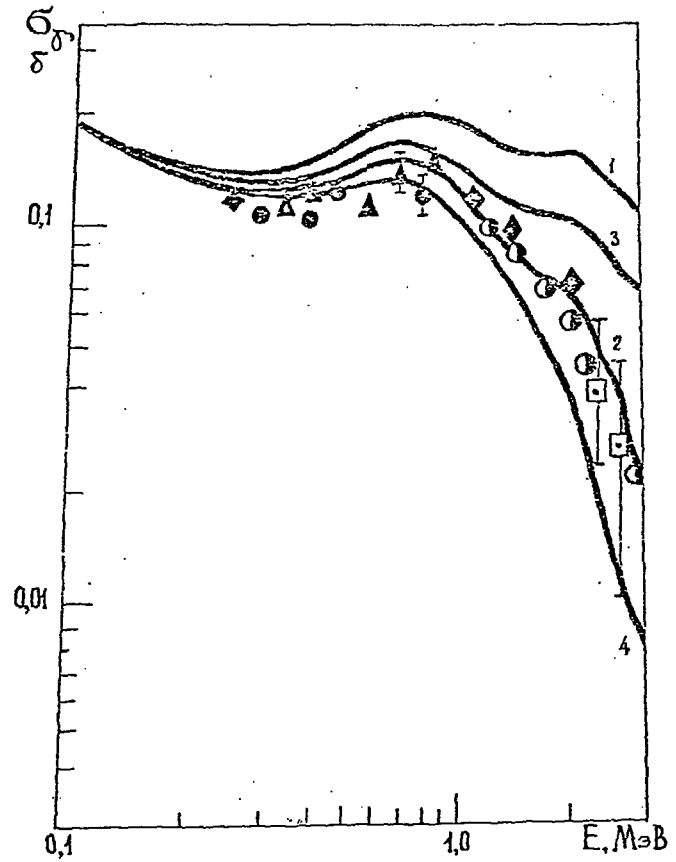

Fig. 1. Comparison of the experimental data for $\sigma_{n\gamma}$ (^{238}U) and theoretical ones obtained using different level density models: 1, Fermi-gas model, Lorentz spectral factor; 2, Fermi-gas model involving the collective effects, Lorentz spectral factor; 3, superfluid nuclear model involving the collective effects, Lorentz spectral factor; 4, Fermi-gas model involving the collective effects, Weisskopf spectral factor ($\langle D \rangle_{obs}$ = 24.8 eV [12], $\langle \Gamma_\gamma \rangle_{obs}$ = 23.5 meV).

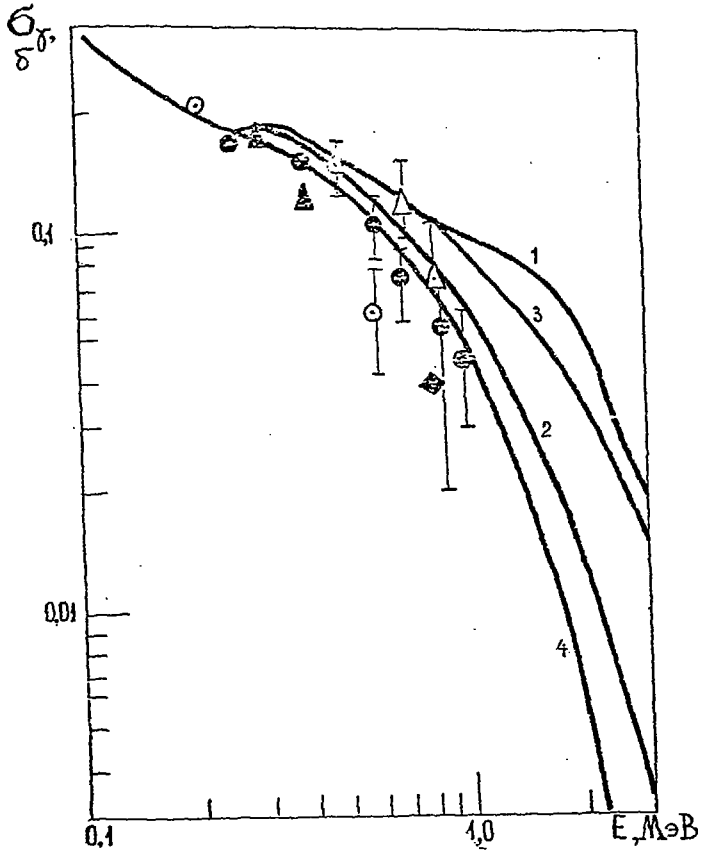

Fig. 2. Comparison of the experimental data for $\sigma_{n\gamma}$ (^{239}Pu) and theoretical ones obtained using different level density models: 1, Fermi-gas model, Lorentz spectral factor; 2, Fermi-gas model involving the collective effects; 3, superfluid nuclear model involving the collective effects, spectral Lorentz factor; 4, Fermi-gas model involving the collective effects, Weisskopf spectral factor ($\langle D \rangle_{obs}$ = 2.38 eV and $\langle \Gamma_\gamma \rangle_{obs}$ = 43.3 meV [13]).

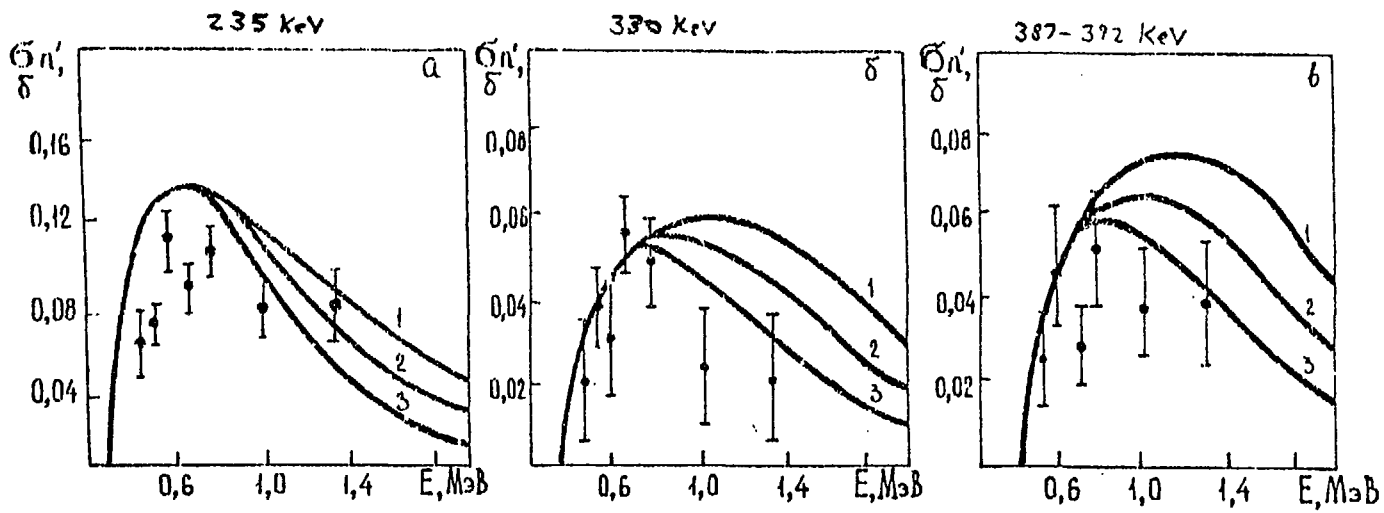

Fig. 3. ^{239}Pu level excitation cross sections for different level density models: a, E_q=235 keV; b, E_q=330 keV; c, 387 keV $\leq E_q \leq$ 392 keV. Curve 1, Fermi-gas model; 2, superfluid nuclear model; 3, Fermi-gas model involving the collective modes.

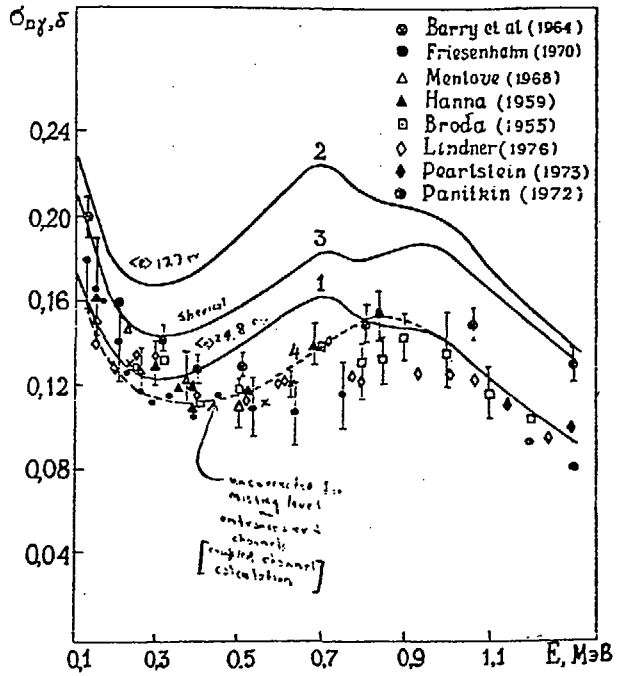

Fig. 4.

Dependence of $\sigma_{n\gamma}$ (^{238}U) on $\langle D\rangle_{obs}$ and neutron transmission coefficients T_n (calculations were made using the Fermi-gas model involving the collective effects, Lorentz spectral factor and $\langle\Gamma_\gamma\rangle_{obs}$ = 23.5 meV). Curve 1, $\langle D\rangle_{obs}$ = 24.8 eV [12], the coeffcients T_n were calculated by the coupled-channel method; curve 2, $\langle D\rangle_{obs}$ = 17.7 eV, the coupled-channel method is used for T_n calculation; curve 3, $\langle D\rangle_{obs}$ = 17.7 eV, the coefficients T_n were calculated by the spherical optical method; curve 4, the same as 1 but with using T_n for excited and ground states.

^{239}PU RESONANCE PARAMETER TESTING BY THE NEUTRON TRANSMISSION FUNCTION MEASUREMENTS

V.A. Konshin and G.B. Morogovsky

Heat & Mass Transfer Institute, BSSR Academy of Sciences,
Minsk, USSR

ABSTRACT. The results are reported on testing ^{239}Pu resonance parameters by measuring neutron transmission functions for samples of different thicknesses. Corrected resonance parameters are obtained. The experimental data used in the study and the requirements to experiments are discussed.

Recent detailed measurements of the neutron transmission functions for a number of ^{239}Pu sample thicknesses [1] permit testing ^{239}resonance parameters. The transmission functions were measured [1] using a time-of-flight spectrometer of the reactor IBR-30 with a 1000 m path length (a resolution time is 100 ns/m). The sample-to-detector distance being 500 m, this allowed neglecting of neutron scattering to the detector. Measurements were made for five samples with thicknesses from 0.00862 nucl./barn to 0.1294 nucl./barn at room temperature. ^{240}Pu admixture in the samples amounted to ~ 4.7 %.

In the present analysis the neutron energies at experimental points are estimated by the expression

$$E = \left[\frac{72{,}3\,B}{32(n-n_0)}\right]^2 ,$$

where B is the path length in m, n is the number of the analyser channel, n_0 is the delay. The average B value is equal to 1005 ± 5 m, particular values of B and n_0 for each sample are calculated using the energy scale adopted with the certain resonances normalization. The energy resonance scale for ^{239}Pu seems to be determined most reliably in the Saclay experiments [2] . The energy scale determined by Gwin et al [3] practically coincides with it.

The resolution function in the transmission experiments is of the form

$$R(E,E') = \frac{1}{\sqrt{2\pi\sigma^2}}\, e^{-\frac{(E'-E)^2}{2\sigma^2 W^2}} \cdot \frac{1}{W} ,$$

where

$$\sigma = 29{,}72, \quad W = \frac{2E^{3/2}}{72{,}3\,B} .$$

For each energy point, the integration of calculated transmission over the resolution function was made within $\pm 2\sigma W$. The Doppler resonance broadening was taken into account as usually in terms of ψ and χ-functions being adequate for ^{239}Pu with its wide and closely placed levels.

Experimental values of the transmission function errors (the error of background subtraction due to its approximation, statistic error, corrections for admixtures in a sample) were taken as

$$\Delta T_t = \sqrt{\frac{T_t}{\frac{N_0^\circ}{T_0} + K(n-N_0)}} + \frac{T_t}{\sqrt{N_n^\circ + K(n-N_0)}} + 0{,}02\,\log_2\left(\frac{\rho}{0{,}0862}\right),$$

where n is the number of the analyser channel. The values of K, T_o, N_o^o, N_o, N_n^o, ρ, are given in Table 1.

The above experimental data on the transmission functions for ^{239}Pu can be applied to testing resonance parameters for energies not more than 50 eV since even at this energy the distance between the experimental energy points becomes ~ 0.3 eV.

The experimental data for five transmission values between 4.3 and 50.0 eV were simultaneously analysed by the least-square method using the Breight-Wigner formalism. The contribution of 25 resonances on each side of the tested one was taken into account. This allowed contribution to the last of the tested resonances at 49.7 eV made by wide resonances with large Γ_f at 96.46 eV and 100.25 eV. The contribution of the 100.25 eV resonance to the tested one was equal to 0.07 barn.

Our evaluated ^{239}Pu resonance parameters [4] were taken as the input ones. The parameters of two negative levels at - 1.8 eV and - 0.07 eV were also taken from [4] to describe the experimental data in the thermal energy region within their accuracy. The potential cross section scattering σ_p was obtained from a simultaneous analysis of the experimental data in the thermal and keV-energy regions to give 10.35 ± 0.45 barn. This consists with Uttley's data [5] (10.30 ± 0.15 barn), data of [6] and allows agreement to be achieved between the scattering cross section at the thermal point (7.4 b) and the evaluation of [7] (7.2 ± 1.4 b) for the neutron cross section parametrisation in the thermal region.

The ^{240}Pu admixture in samples (~4.7%) was allowed for in the calculations. Most appreciable contribution to the energy region considered is due to 13 ^{240}Pu resonances. The evaluated ^{240}Pu resonance parameters were taken from [8].

The calculation results are presented in Figs 1 through 20 and in Table 2. The solid line gives the calculations for the transmission function with the input resonance parameters. Dashed line gives the results of optimization calculations with Γ_n^o and $\Gamma_a = \Gamma_f + \Gamma_\gamma$, varying to give the best simultaneous description of the transmission functions for all of the five samples.

It is seen from the figures that the calculated transmission values for the first two sample thicknesses fairly reproduce the behaviour of the curve in the interresonance region and on the resonance slopes, but lieing much below the experimental data at the resonance peaks. Evidently, the resonance peaks were measured inaccurately and, hence, the transmissions below 10^{-3} were neglected. It is also seen that the calculated transmissions for the sample No. 3 are systematically above while for Nos 4 and 5 systematically below the experimental values for the whole energy range considered. It can be understood assuming that sample thicknesses differ from those indicated in [1]. In particular, sample No. 3 may have the greater, and samples Nos 4 and 5 smaller thicknesses than it is shown in Table 1. Besides,

in the experiments with a cladding material model its thickness might been inaccurately accounted for. Recent discussions with the authors [1] confirmed these conclusions and respective calculations with correct thicknesses will be made.

These errors nevertheless did not exert a remarkable effect on resonance parameter testing. The point is, that the deviations of the calculation curves for sample No. 3 and samples Nos 4 and 5 almost compensate one another and do not need any changes in the parameters made. Besides, in the case of samples Nos 3 - 5 for the resonance of 7.82 eV a remarkable distortion of the resonance sides is observed The reason for it is not clear yet.

Table 2 shows that in general the final set of resonance parameters differs from the initial one not more than by 16 % except the cases of duplets 14.31 - 14.68 eV, 26.24 - 27.24 eV, 41.42 - 41.66 eV which are inaccurately measured, and the region above 44 eV where insufficient experimental resolution displaies itself.

CONCLUSIONS.

1. The results show that resonance parameters have to be preferably tested by the shape analysis method since in this case the effect of inaccurate measuring of transmission function in the resonance peaks is less pronounced.

2. Further testing researches need the experimental data on ^{239}Pu fission self-indication for different thickness samples, and these testings are planned.

3. It is desirable to measure the transmission functions and fission self-indications for the samples of ^{235}U and ^{239}Pu of different thickness with cooling.

REFERENCES

1. Vankov A.A., Grigoriev Yu.V., Ukraintsev V.F., Bakalov T., Ilchev G., Toshkov S., Chan Khan Mai. Experimental Investigation of Resonance Self-Shielding for σ_t and σ_f ^{239}Pu, In col. of papers "Problems of Atomic Science and Engineering", Series: "Nuclear Constants", 1980, v. 2(37), p. 44 - 50.
2. Ribon P., Le Coq. G., Evaluation des Donnees Neutroniques de ^{239}Pu, CEA-N-1484.
3. Gwin R., Weston L.W., de Saussure G., Ingle R.W., Todd J.H., Gillespie F.E.. Simultaneous Measurement of the Neutron Fission and Absorbtion Cross Sections of ^{239}Pu Over the Energy Region 0.02 eV to 30 keV, Nucl. Sci. Eng., 1971, v. 45, p. 25 - 36.
4. Antsipov G.V., Bakhanovich L.A., Zharkov V.F., Zenevich V.A. Klepatskii A.B., Konshin V.A., Maslov V.M., Morogovskii G.B. Porodzinskii Yu.V., Sukhovitskii E.Sh., Nuclear Data Evaluation for ^{239}Pu in the Energy Region 10^{-5} eV to 15 Mev., IAEA Report on the Research Agreement N2328/CF, 1981.
5. Uttley C.A., Report AERE-PR/N, 1967, p. 11, EANDC (UK)-35B, 1964; EANDC(UK) - 40 "L", 1964.

6. Derrien H., Private Communication in ref.2.

7. Lemmel H.D.. The Third IAEA Evaluation of the 2200 m/s and 20°C Maxwellian Neutron Data for ^{233}U, ^{235}U, ^{239}Pu, ^{241}Pu, Proc. of a Conf. on Nuclear Cross Sections and Technology, Washington, 1975,NBS Spec.Publ. 425, v.1, p.286 - 292.

8. Antsipov G.V., Konshin V.A., Sukhovitskii E.Sh. Nuclear constants for Plutonium Isotopes, "Nauka i Tekhnika", Minsk, 1981.

Table 1

Thicknesses of samples and coefficients K, T_o, N_o^o, N_o, N_n^o for calculation of experimental errors of transmissions functions

No. of samples	ρ $\frac{\text{nuclei}}{b}$	K	T_o	N_o^o	N_o	N_n^o
I	0,00862		0,90	950	870	
2	0,0I725		0,80	3200	2000	
3	0,03449	-I,I7	0,55	5000	800	5I2
4	0,0689		0,45	4500	850	
5	0,I294		0,20	3400	II00	

Resonance parameters of ^{239}Pu

N	E_r, eV	J	$g\Gamma_n^{input}$, eV	$g\Gamma_n^{final}$, eV	$\frac{g\Gamma_n^{input} - g\Gamma_n^{final}}{g\Gamma_n^{input}}$, %	Γ_a^{input}, eV	Γ_a^{final}, eV	$\frac{\Gamma_a^{input} - \Gamma_a^{final}}{\Gamma_a^{input}}$, %
1	2	3	4	5	6	7	8	9
1	5.90	0	4.7000-03	4.7000-03	0	3.3023+00	3.3023+00	0
2	7.82	1	5.7351-04	5.4623-04	4,76	8.7000-02	8.4097-02	3.34
3	10.93	1	1.3239-03	1.1969-03	9.59	1.9880-01	1.6683-01	16.08
4	11.50	1	4.2527-05	5.8980-05	-38.69	5.1600-02	1.5693-01	-204.13
5	11.89	1	6.6947-04	5.6876-04	15.04	7.6000-02	6.4517-02	15.11
6	14.31	1	4.3221-04	7.1860-04	66.26	1.0100-01	1.0128-01	- 0.28
7	14.68	1	1.4198-03	1.4235-03	-0.26	6.8000-02	6.5050-02	4.34
8	15.46	0	4.6707-04	4.6707-04	0	6.9890-01	6.9890-01	0
9	17.66	1	1.2249-03	1.2249-03	0	7.3000-02	7.3000-02	0
10	22.29	1	1.8573-03	2.0290-03	-9.24	1.0600-01	9.5687-02	9.73
11	23.94	1	6.3860-05	6.9512-04	-8.85	7.0000-02	6.3603-02	9.14
12	26.24	1	8.9929-04	1.1273-03	-25.35	8.2002-02	8.5466-02	-4.23
13	27.24	1	1.0735-04	1.0198-04	5.0	4.2000-02	3.6053-02	14.16
14	32.31	0	1.8747-04	1.8747-04	0	1.5100-01	1.5100-01	0
15	34.60	1	9.1600-06	9.1600-06	0	9.1000-02	9.1000-02	0
16	35.50	1	2.0441-04	2.0441-04	0	4.7000-02	4.7000-02	0
17	41.42	1	3.1786-03	3.2534-03	-2.35	4.8000-02	5.3453-02	-11.36
18	41.66	1	1.1150-03	9.3824-04	-15.85	1.0400-01	8.7968-02	15.42
19	44.48	1	4.7088-03	4.0003-03	15.05	5.2000-02	3.9964-02	23.15
20	47.60	0	1.4101-03	1.2060-03	14.47	3.0600-01	2.3284-01	23.91
21	49.71	0	1.0143-03	9.1581-04	9,71	7.9800-01	8.9692-01	12.40

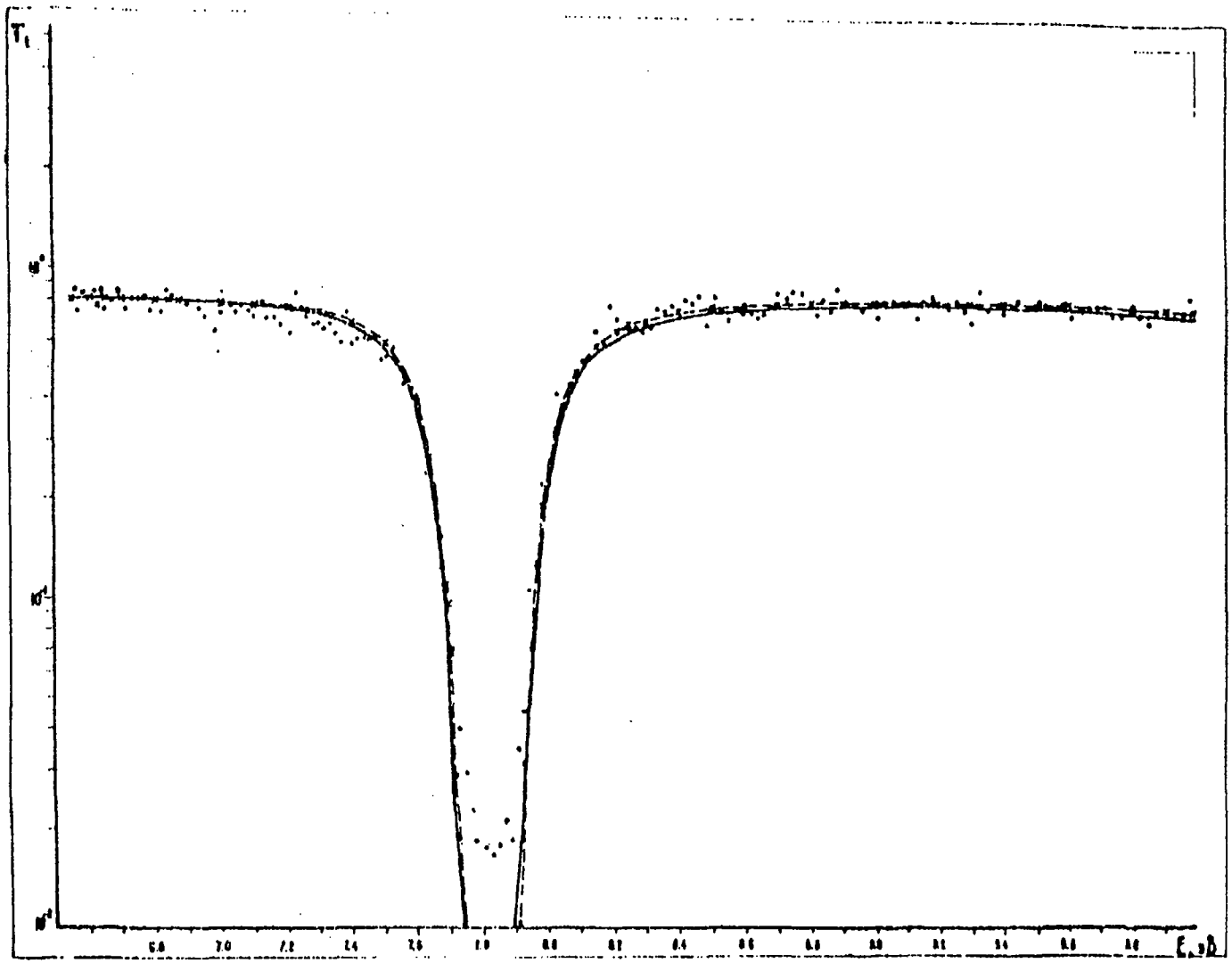

Fig. 1

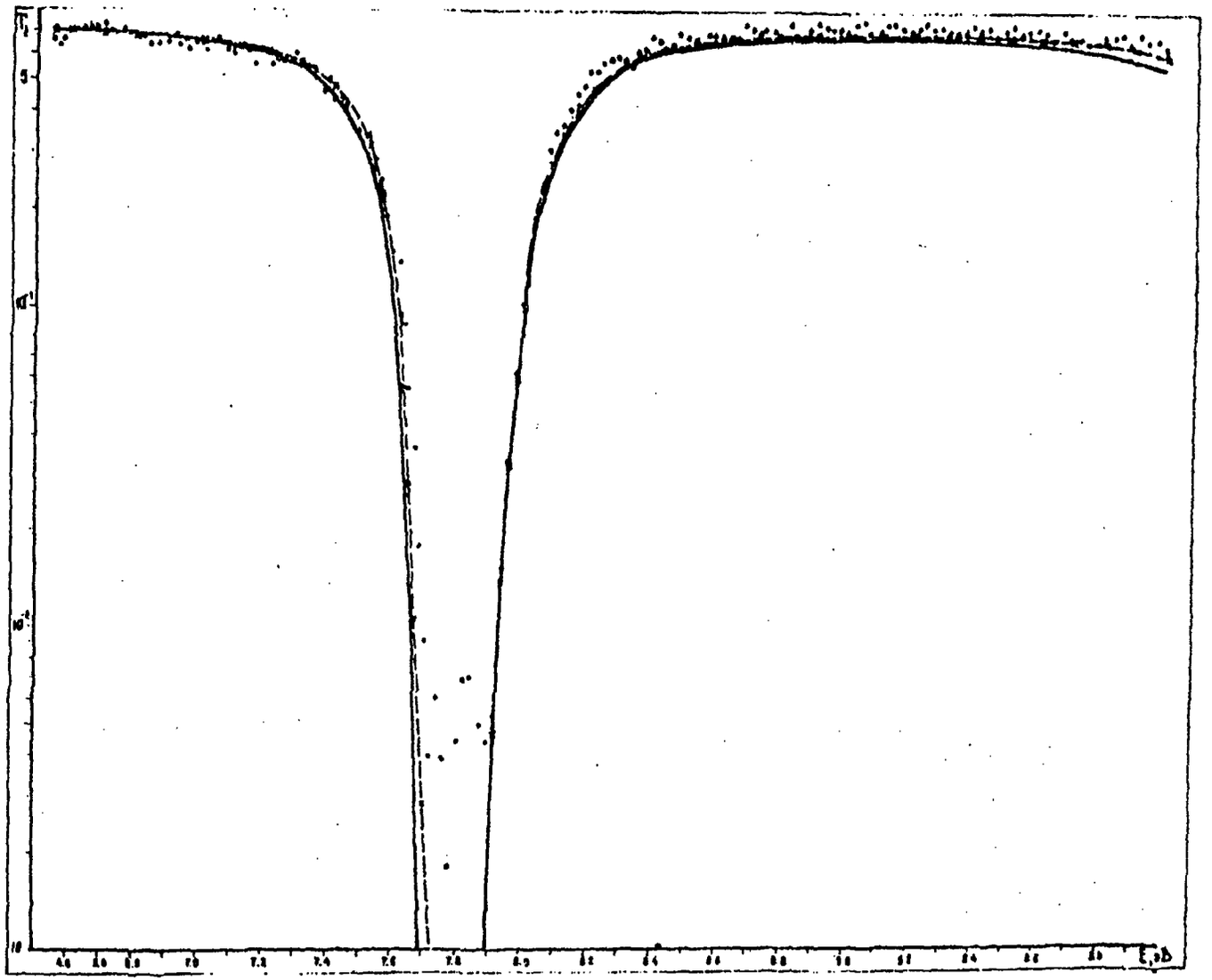

Fig. 2

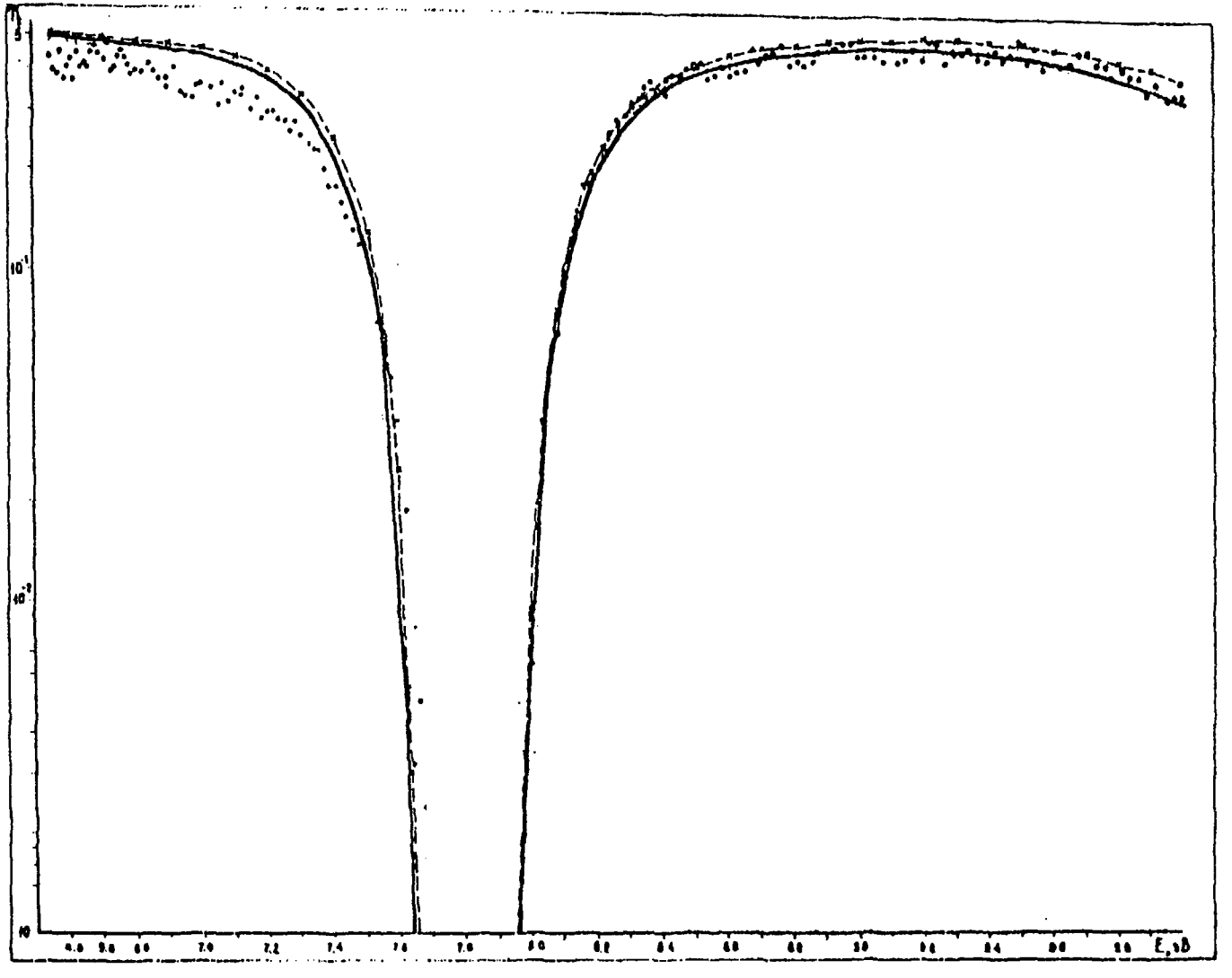

Fig. 3

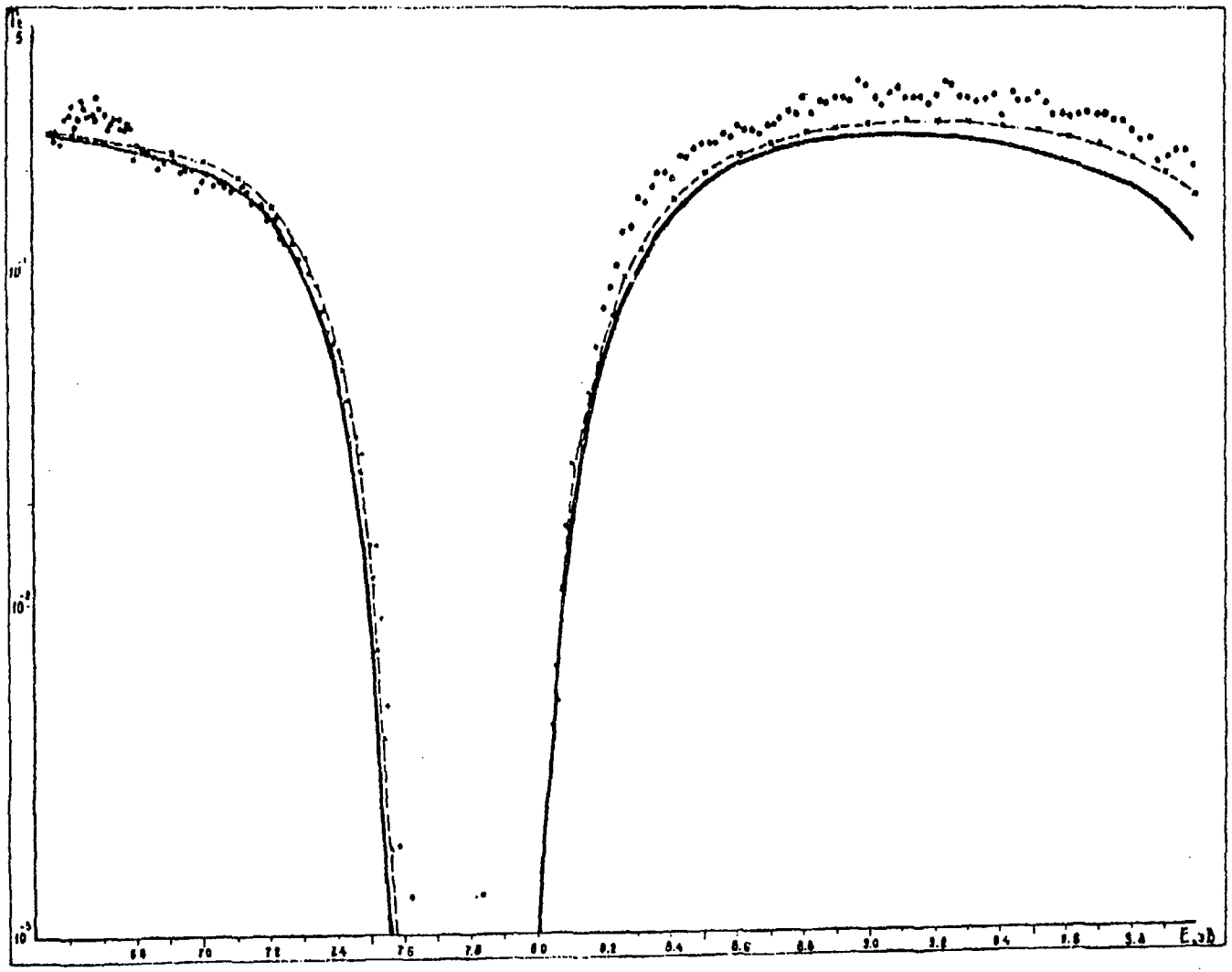

Fig. 4

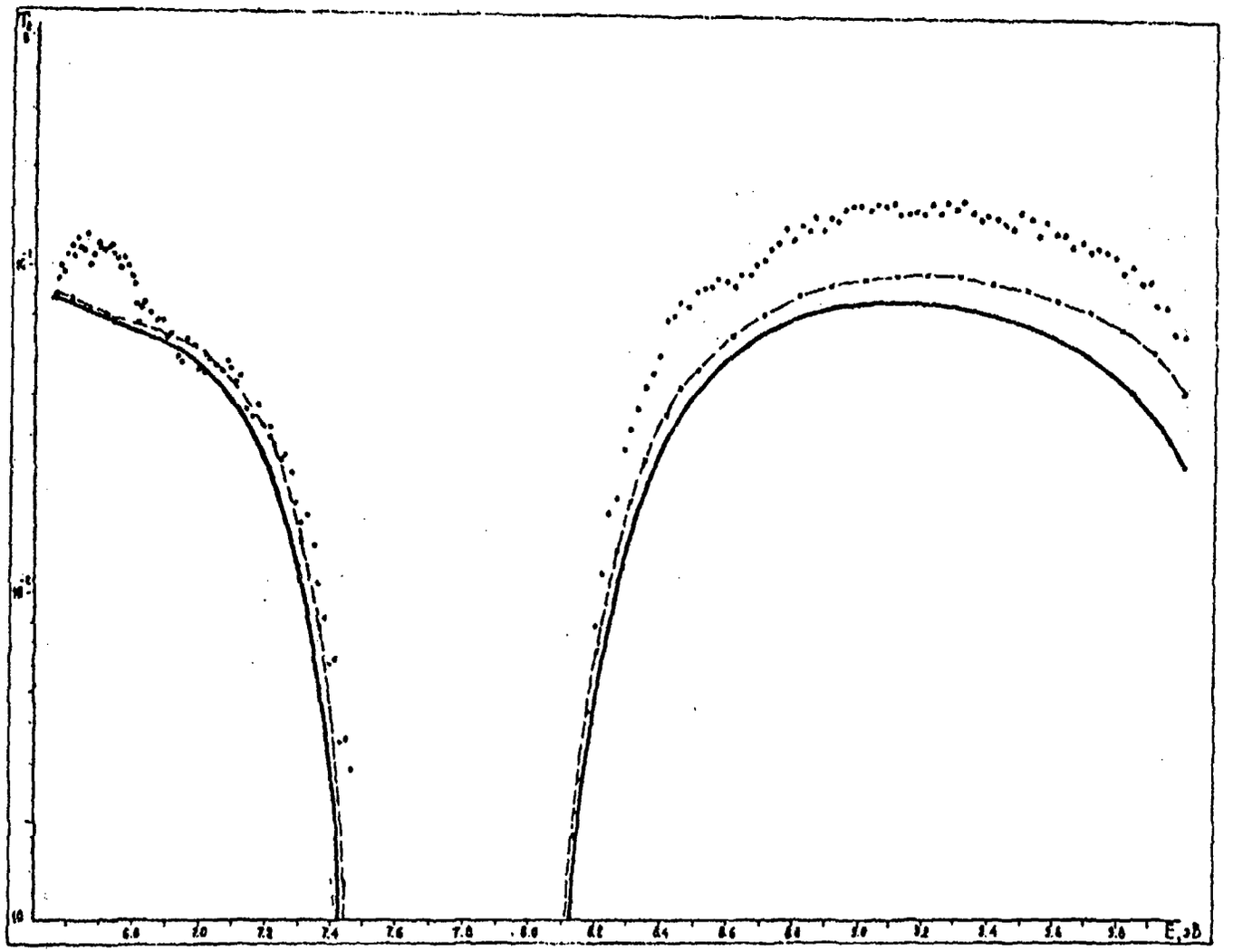

Fig. 5

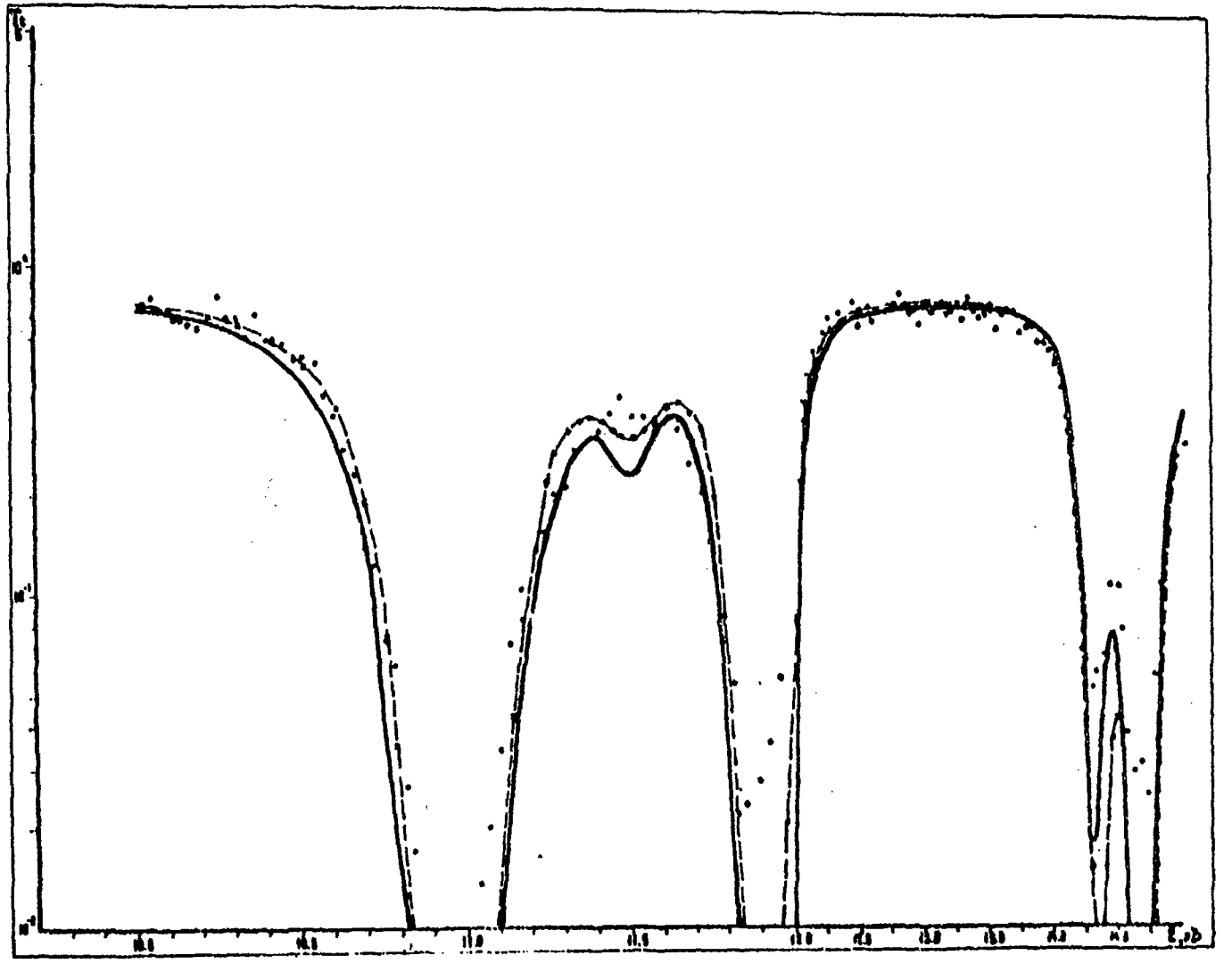

Fig. 6

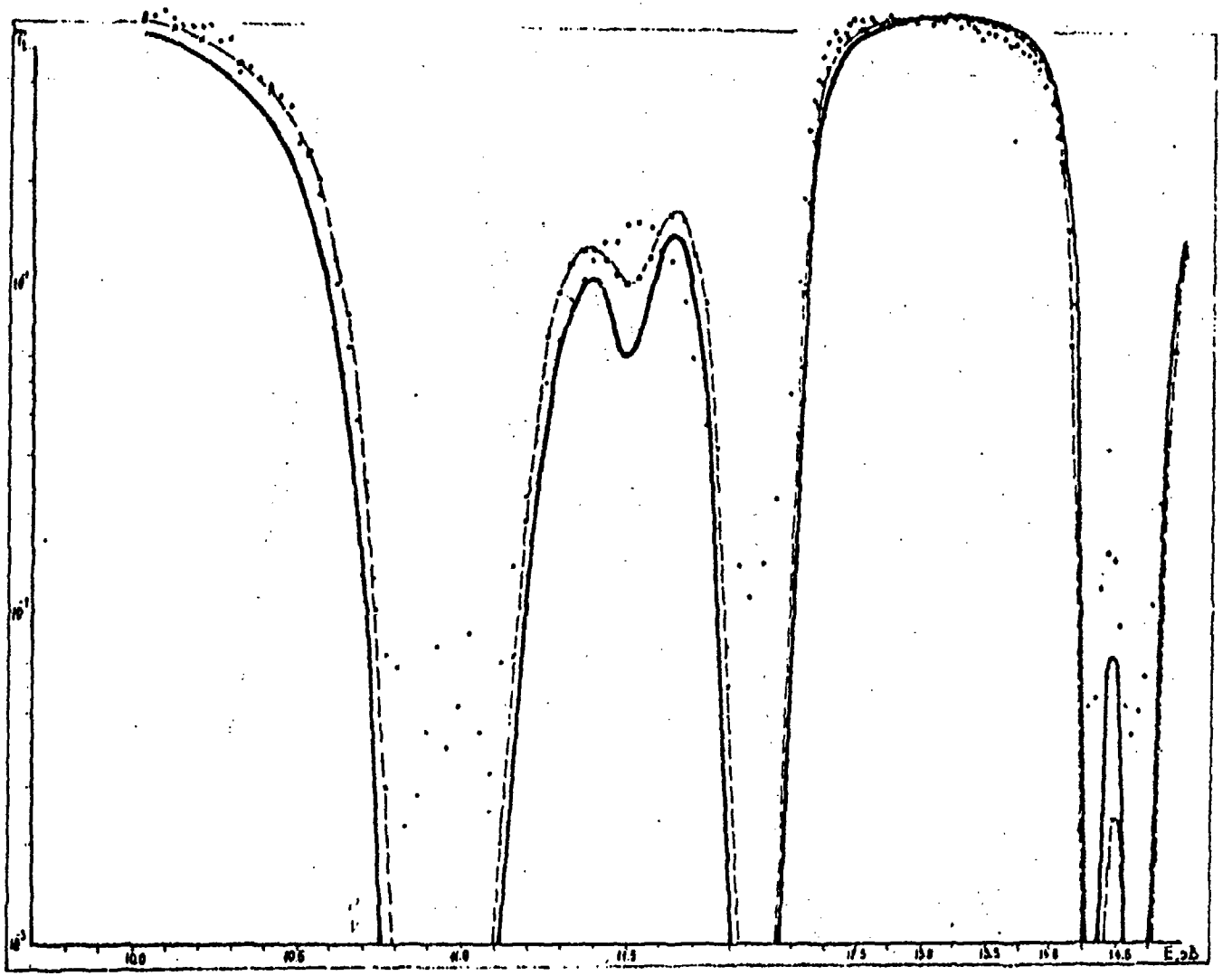

Fig. 7

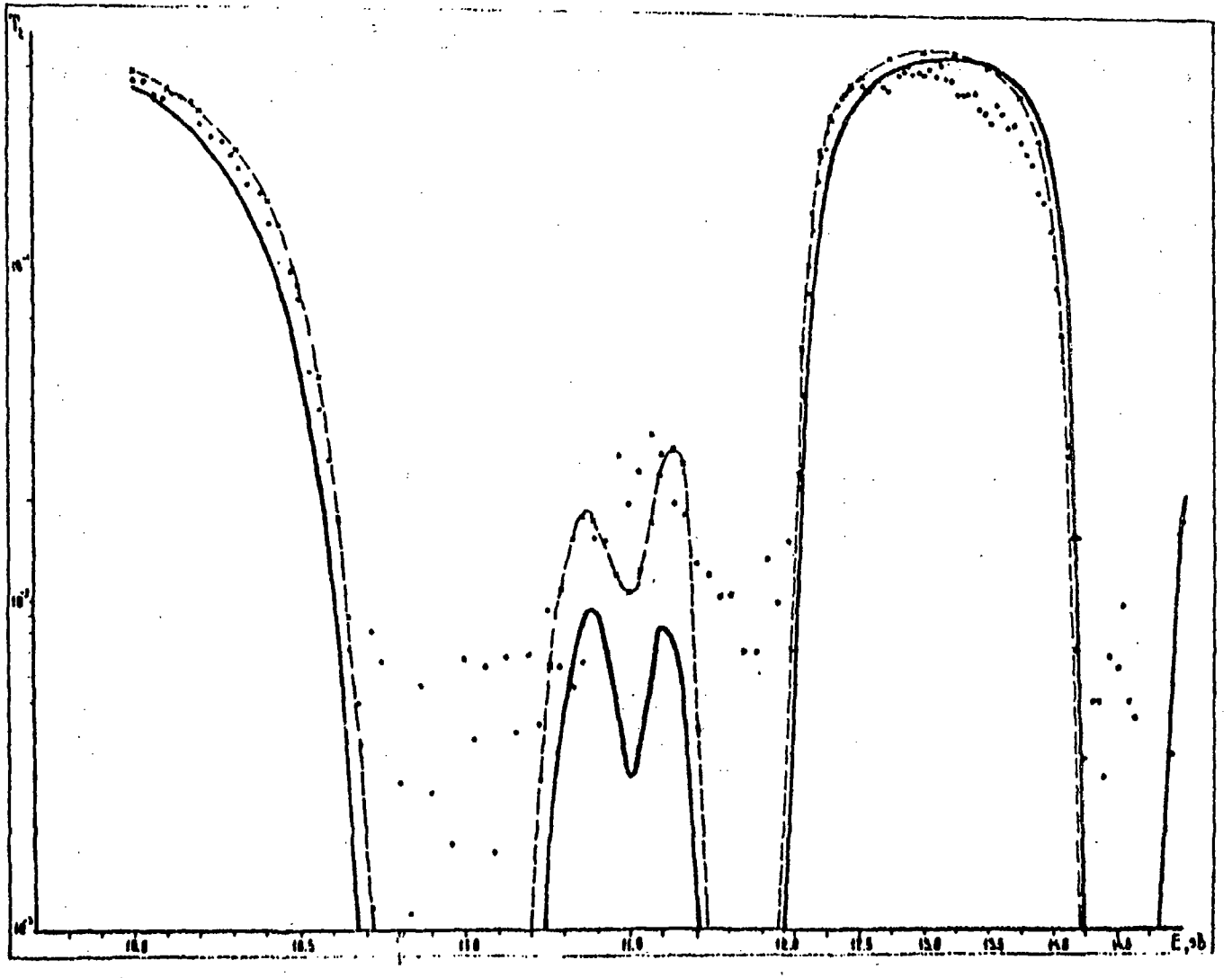

Fig. 8

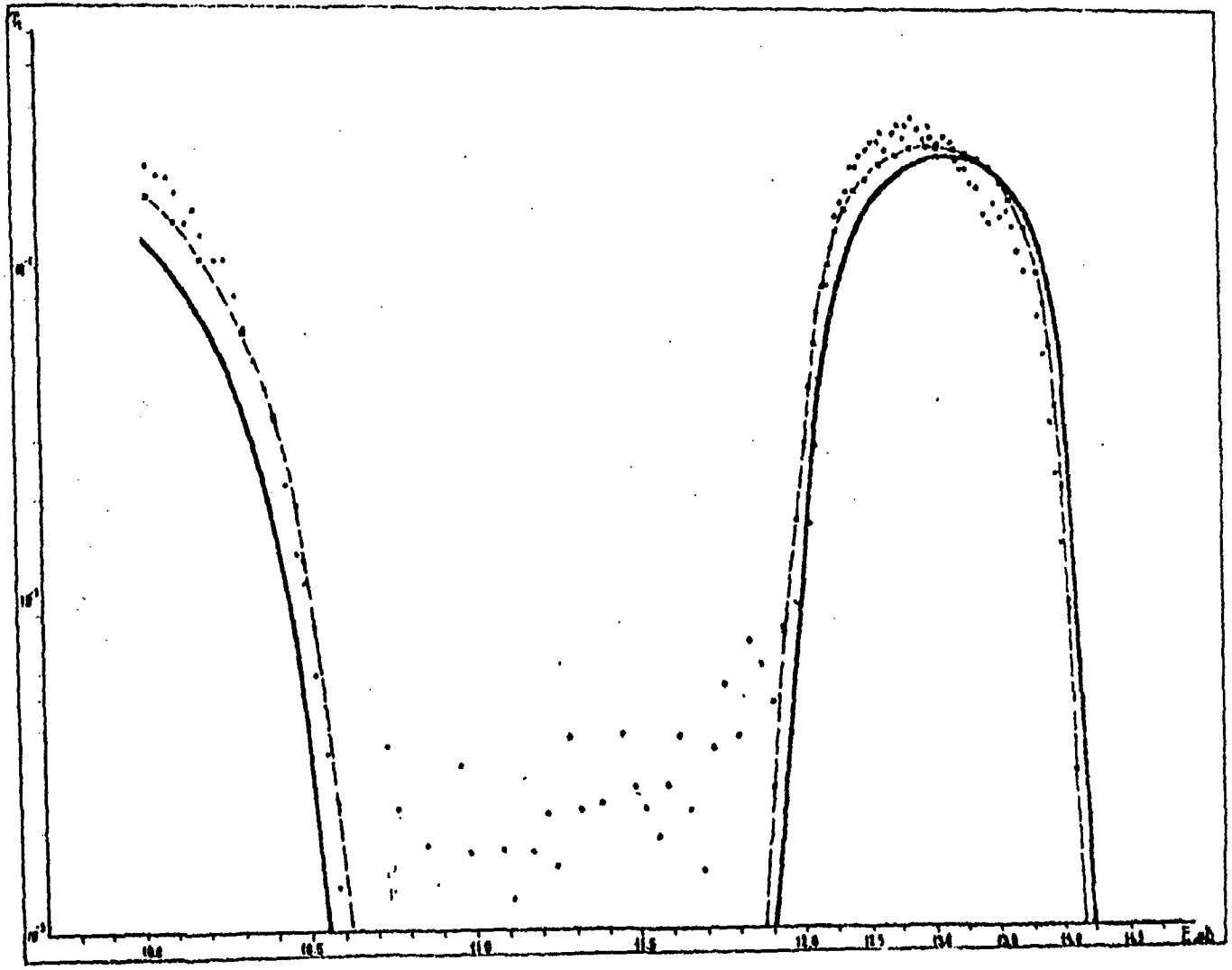

Fig. 9

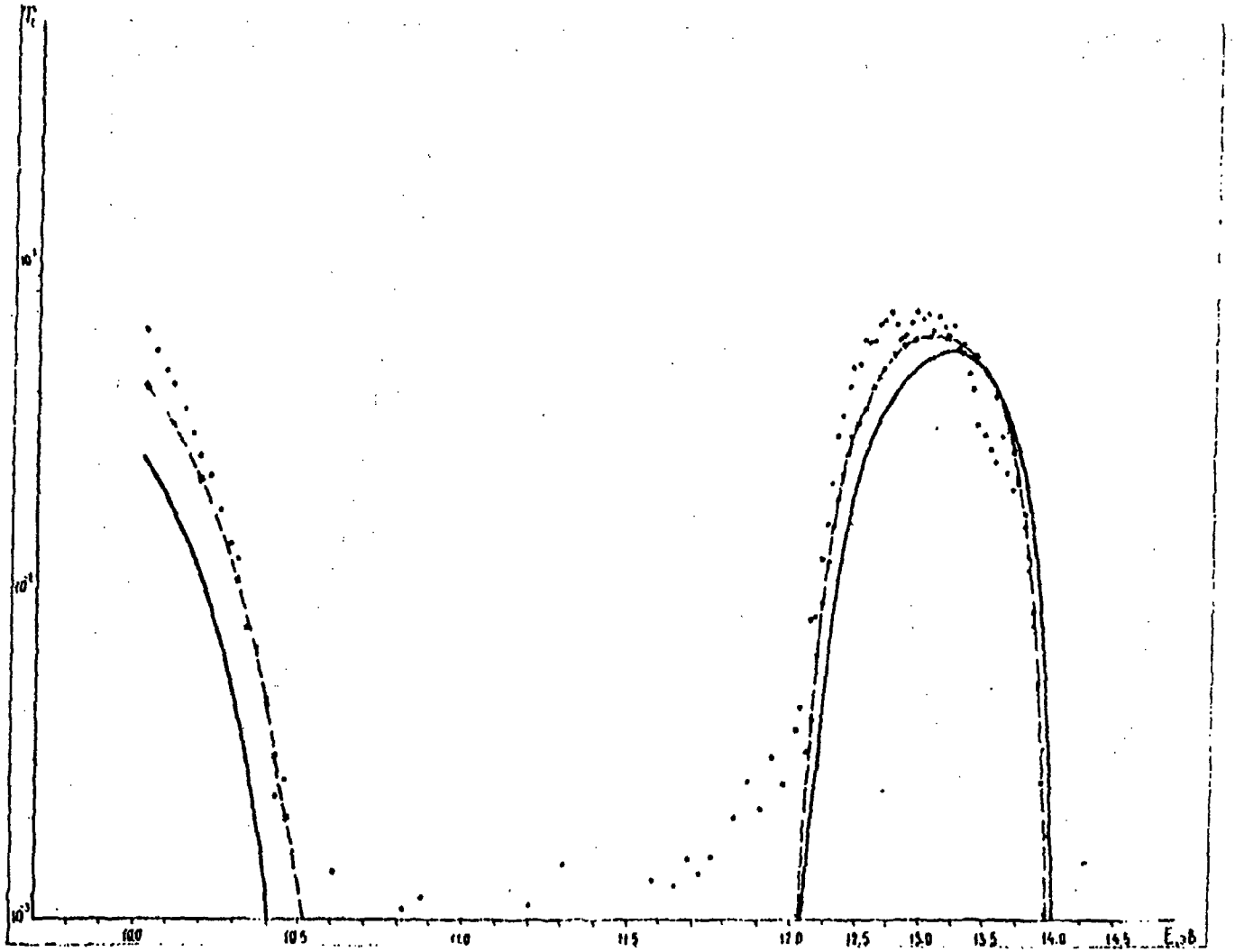

Fig. 10

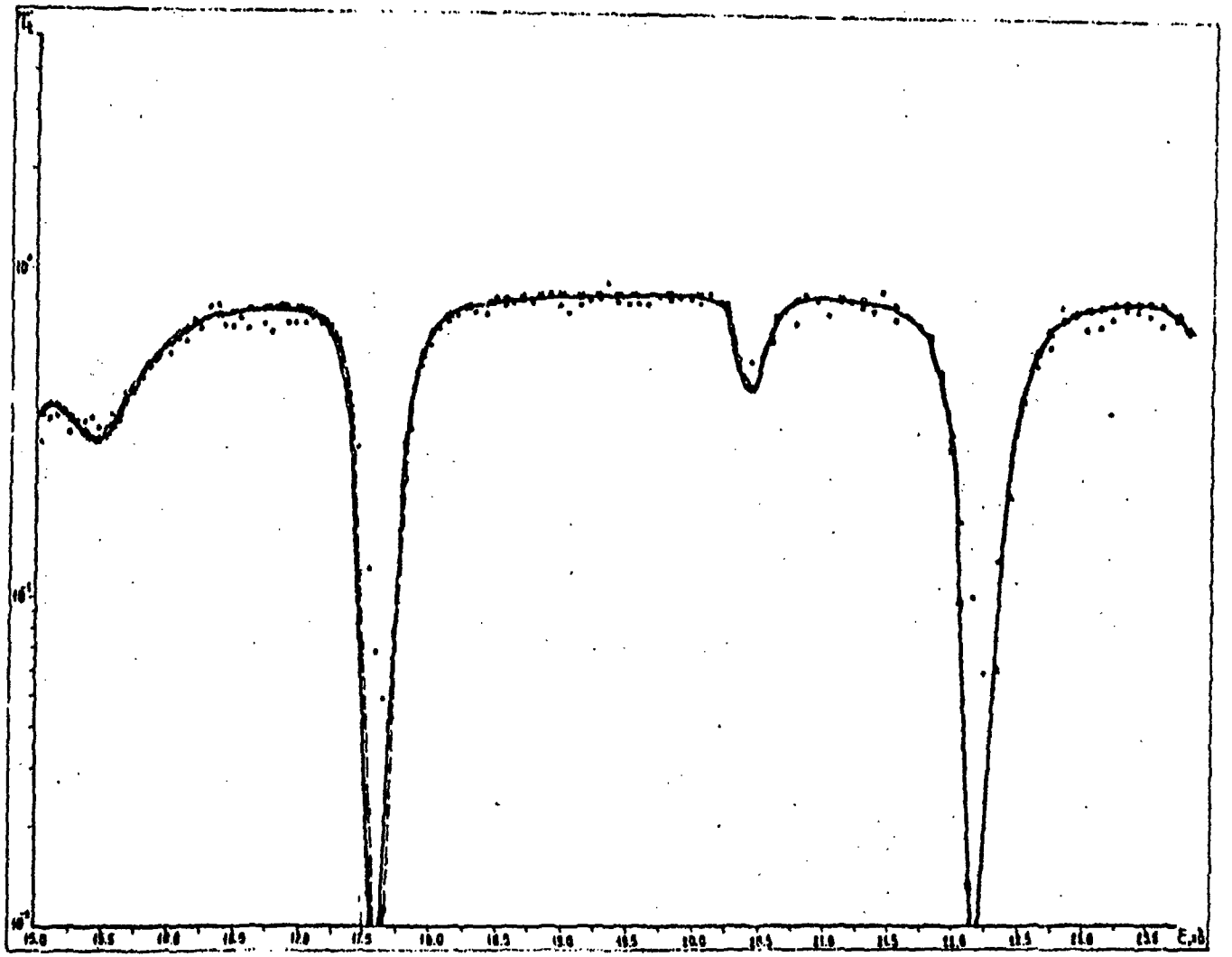

Fig. 11

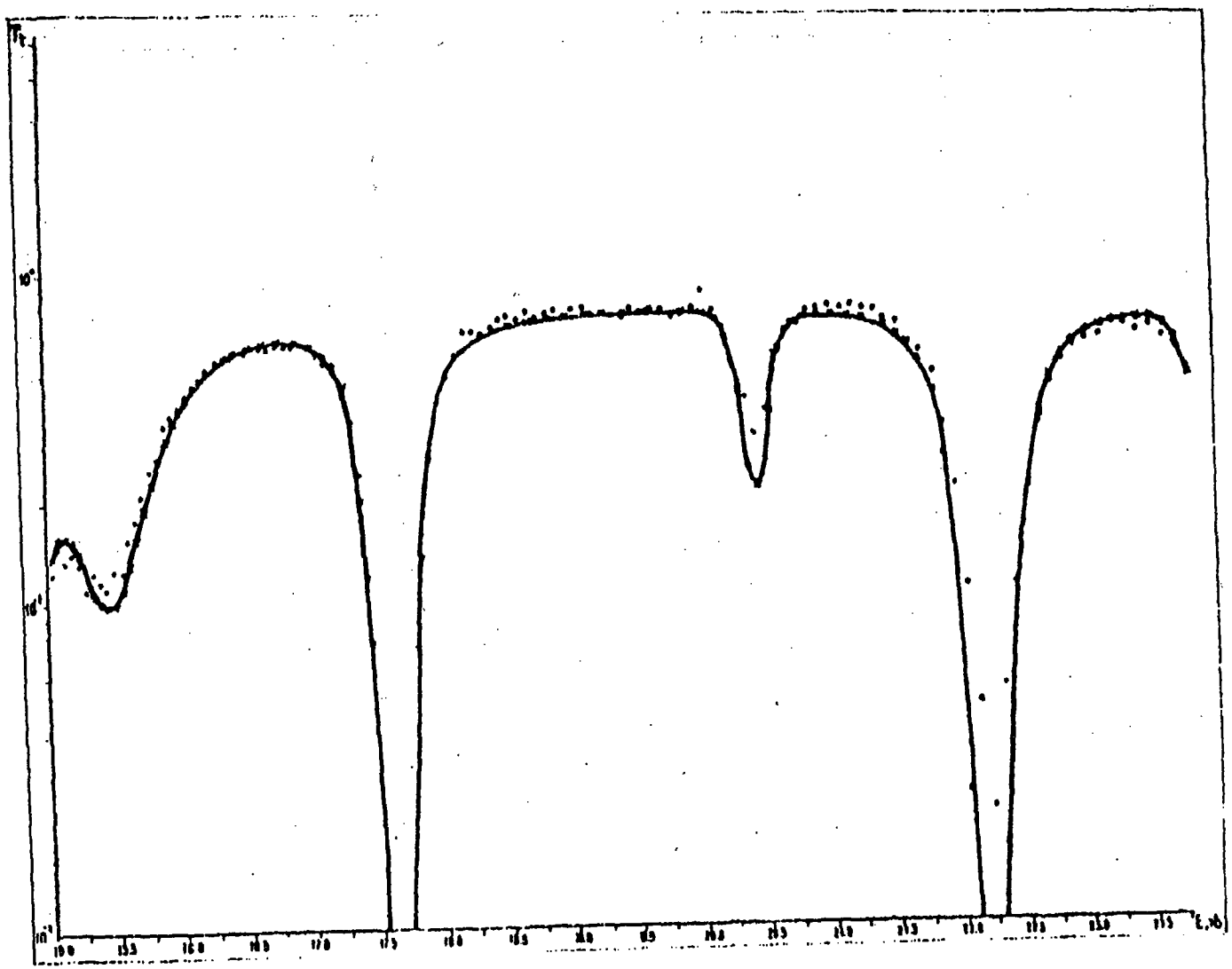

Fig. 12

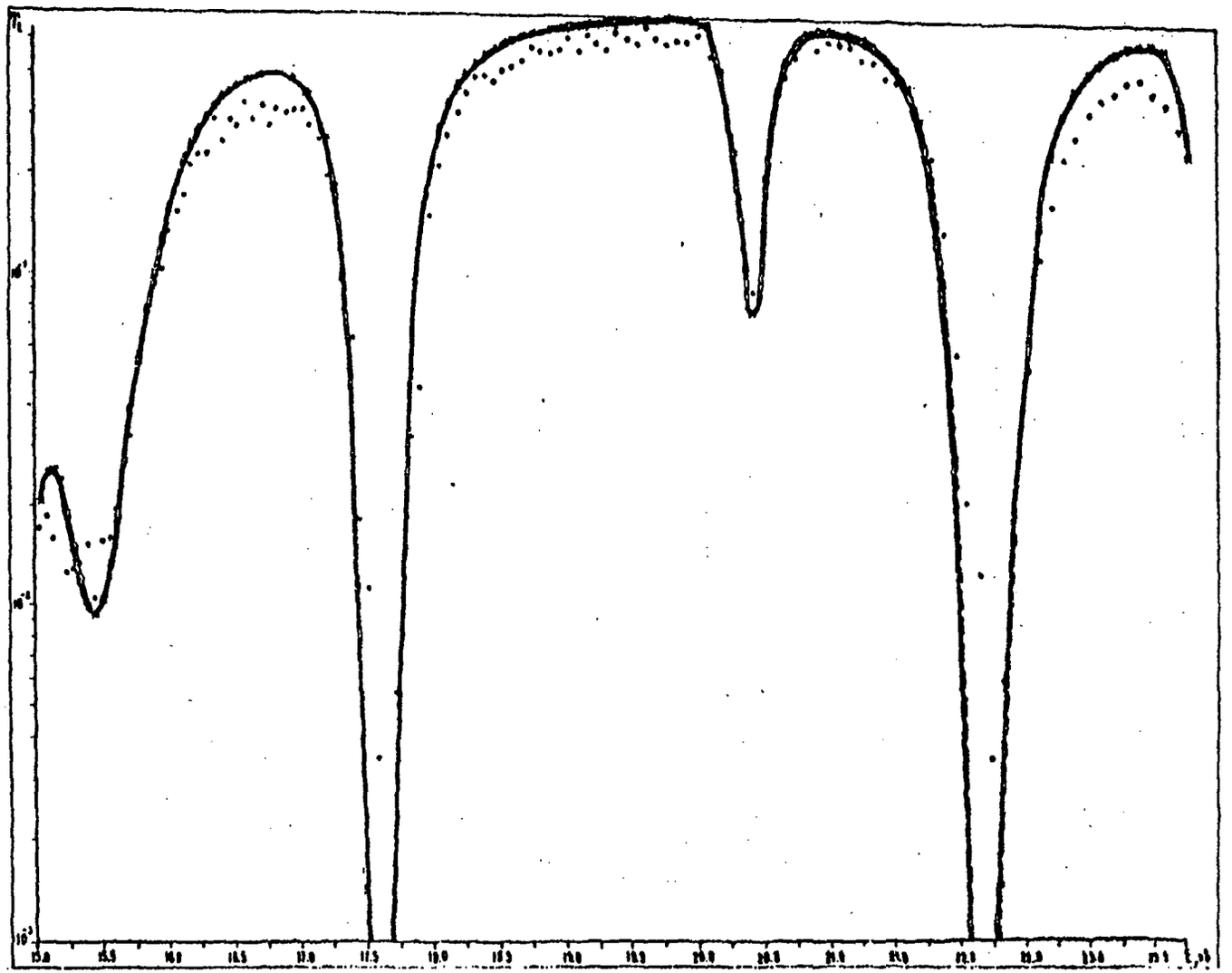

Fig. 13

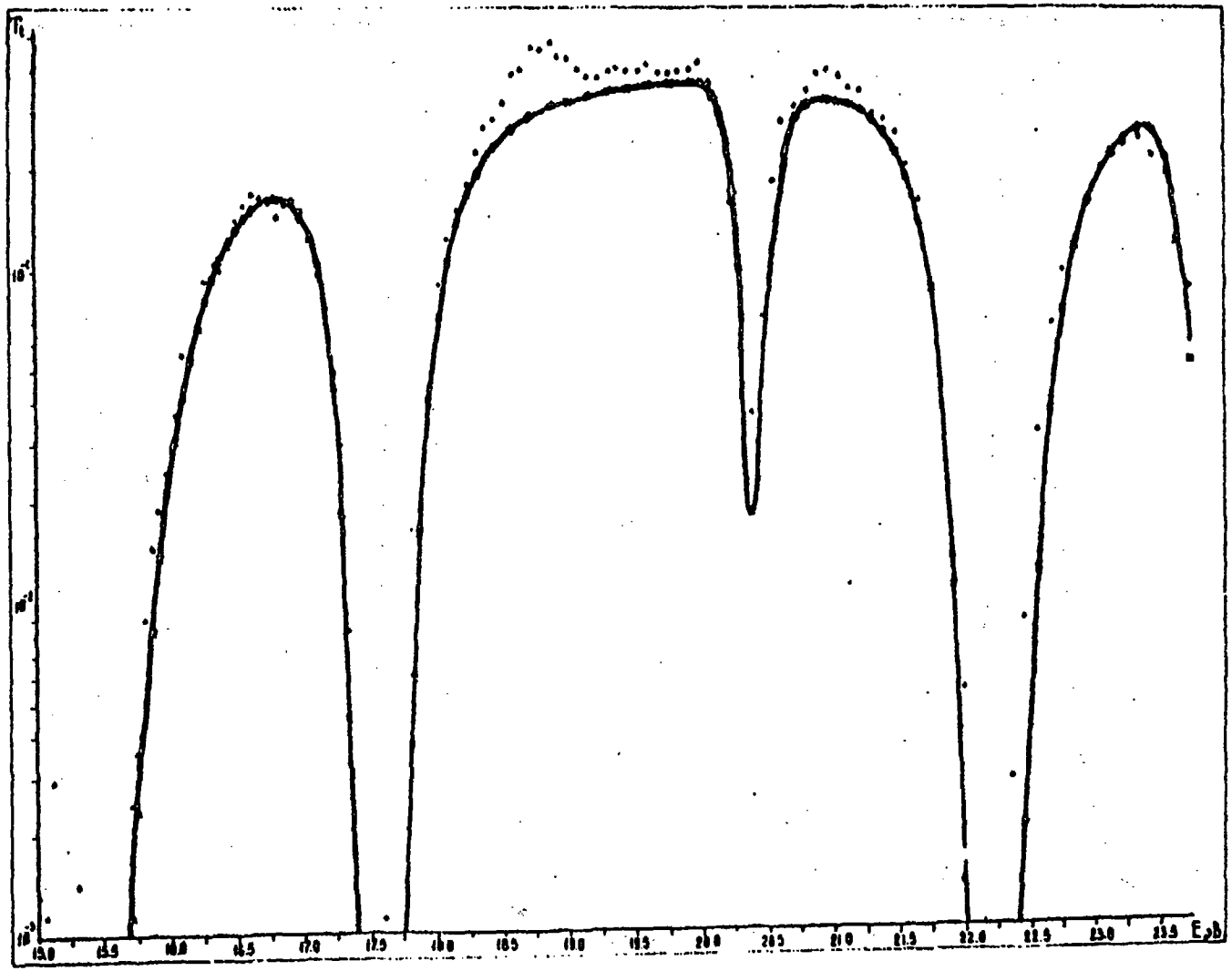

Fig. 14

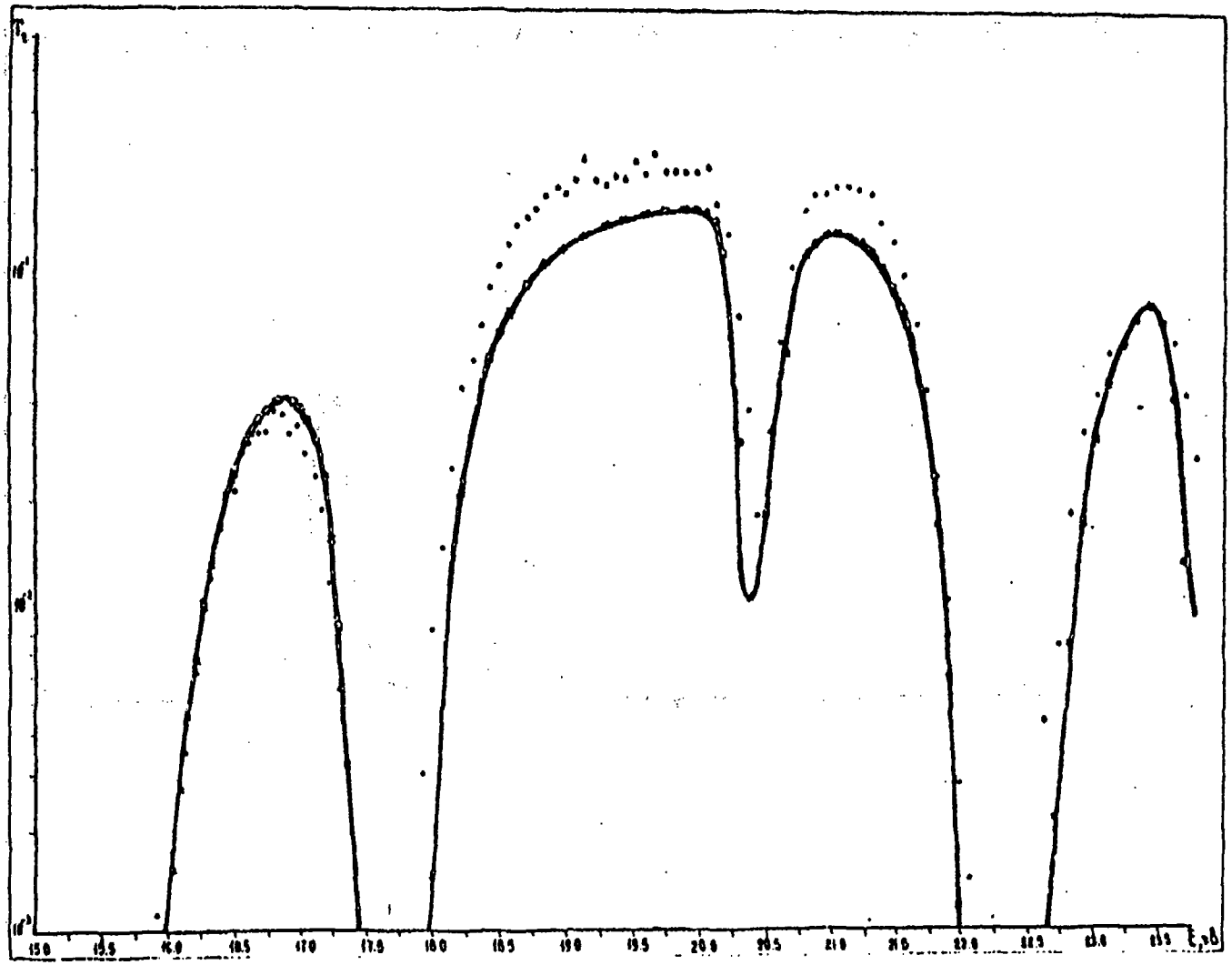

Fig. 15

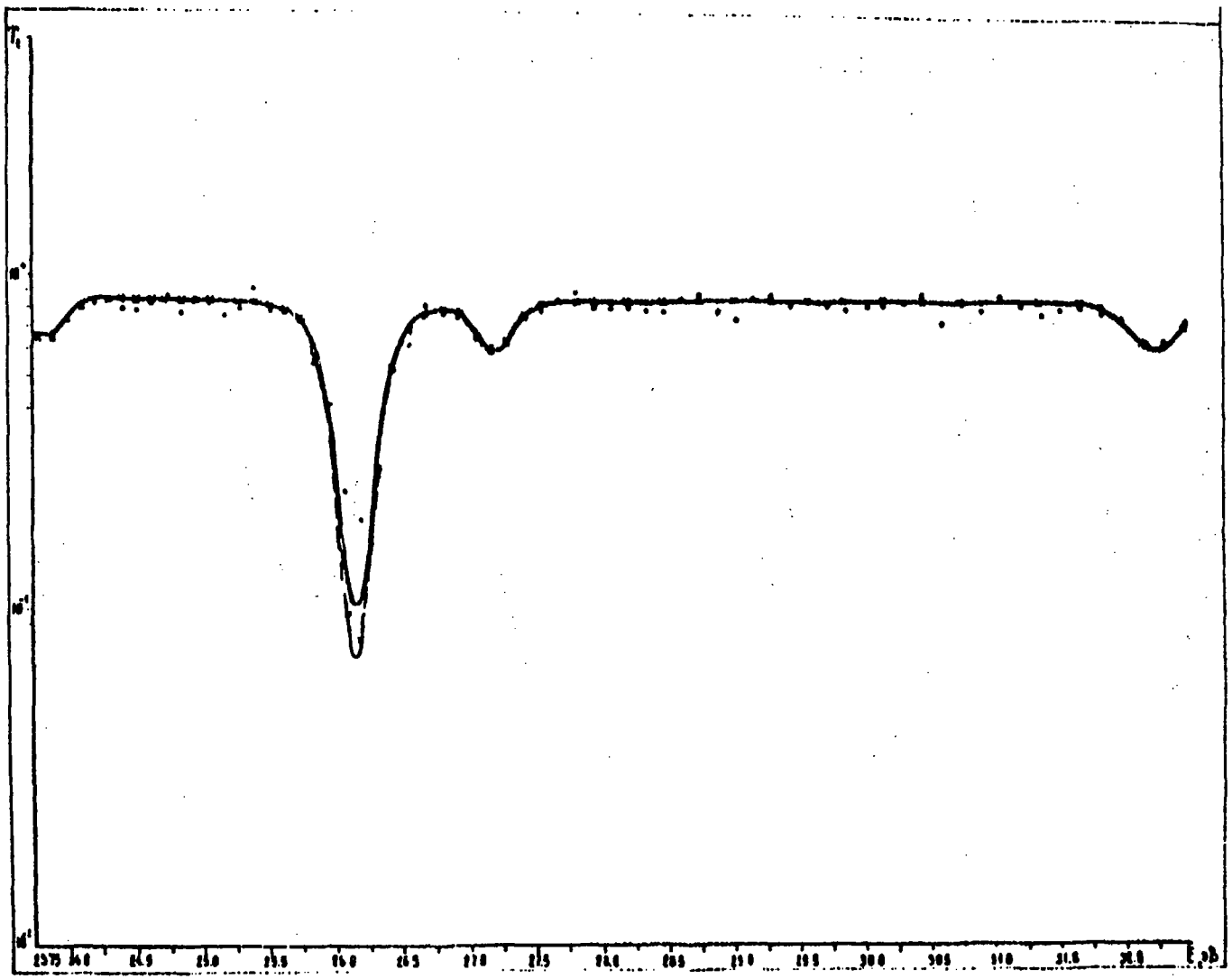

Fig. 16

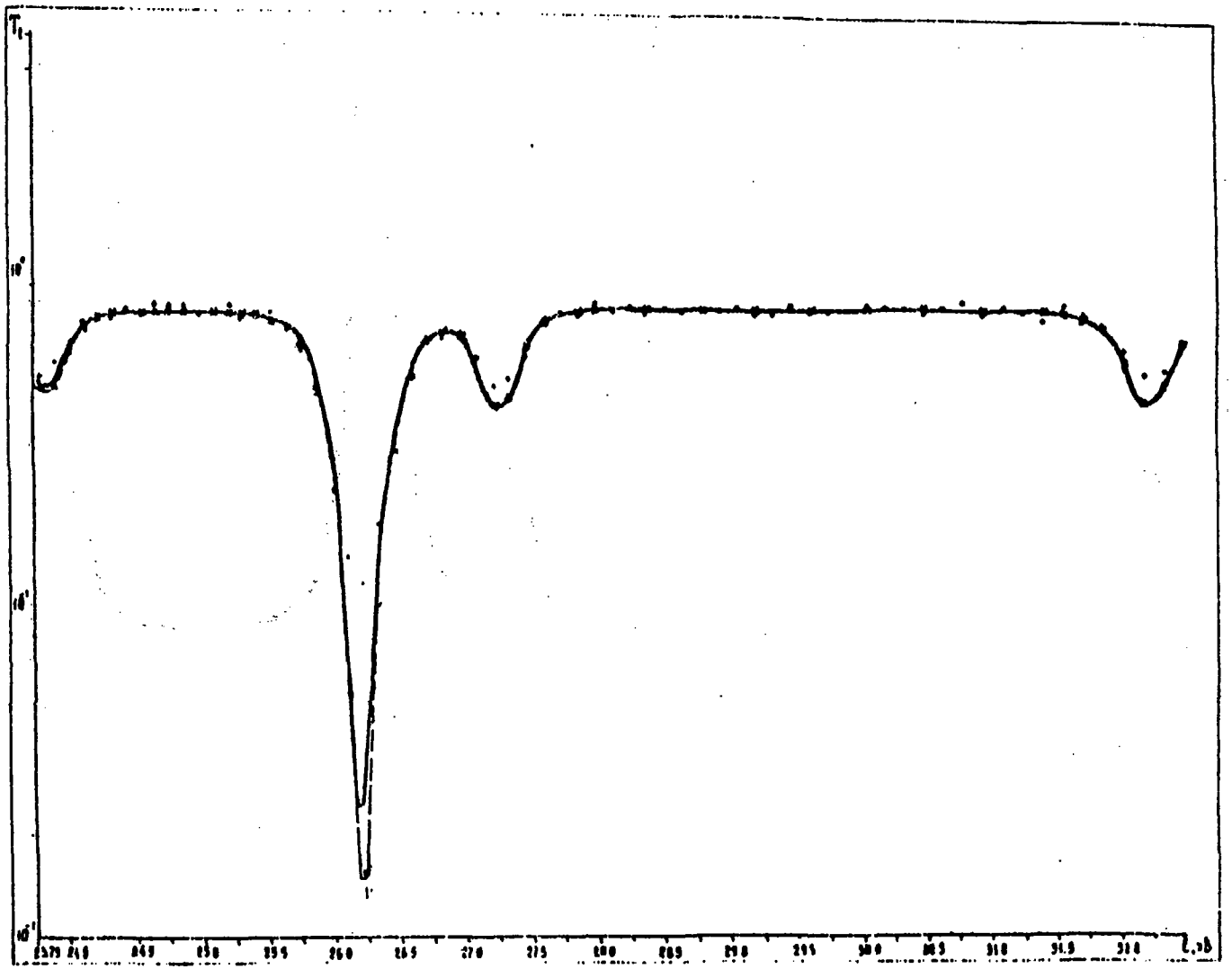

Fig. 17

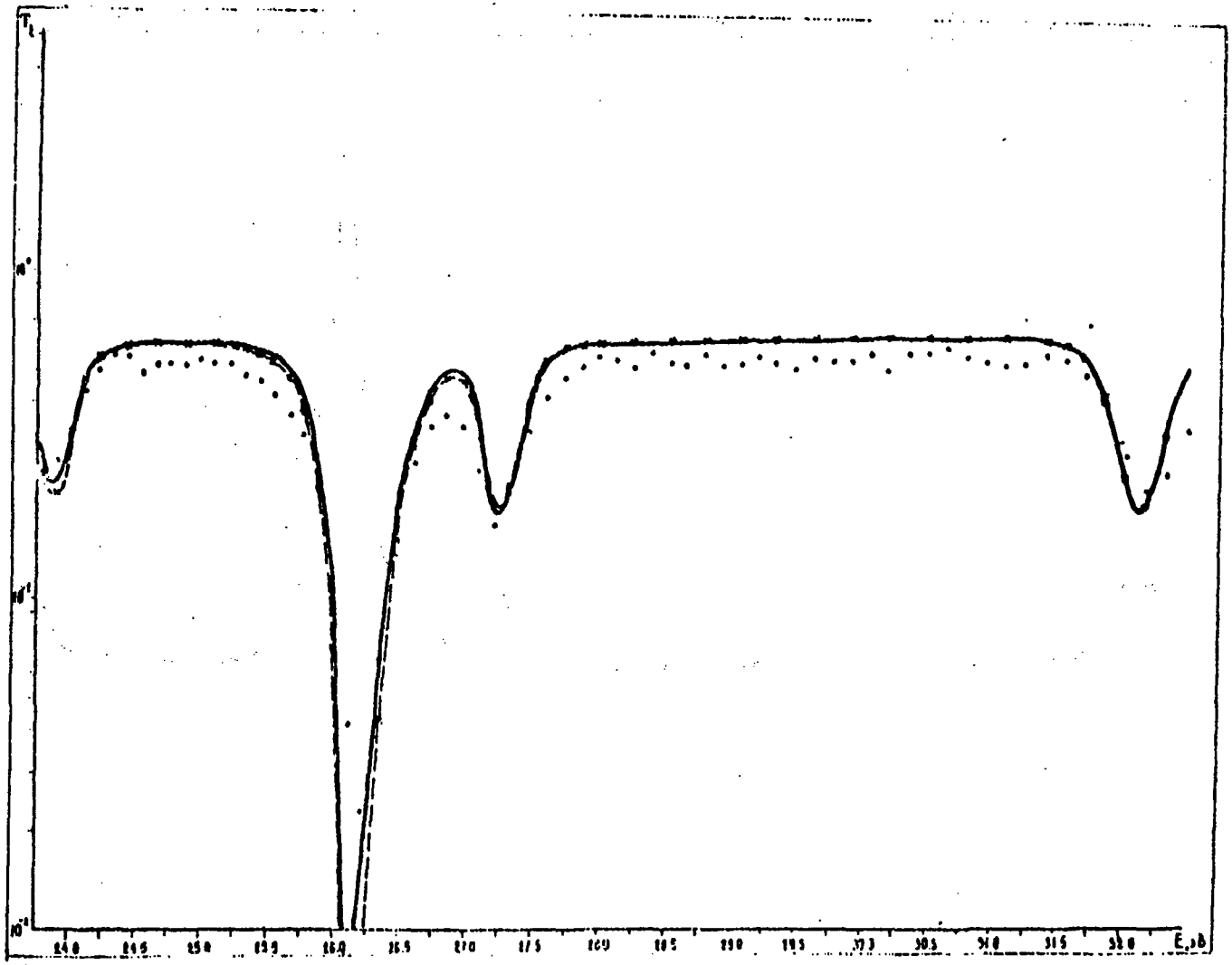

Fig. 18

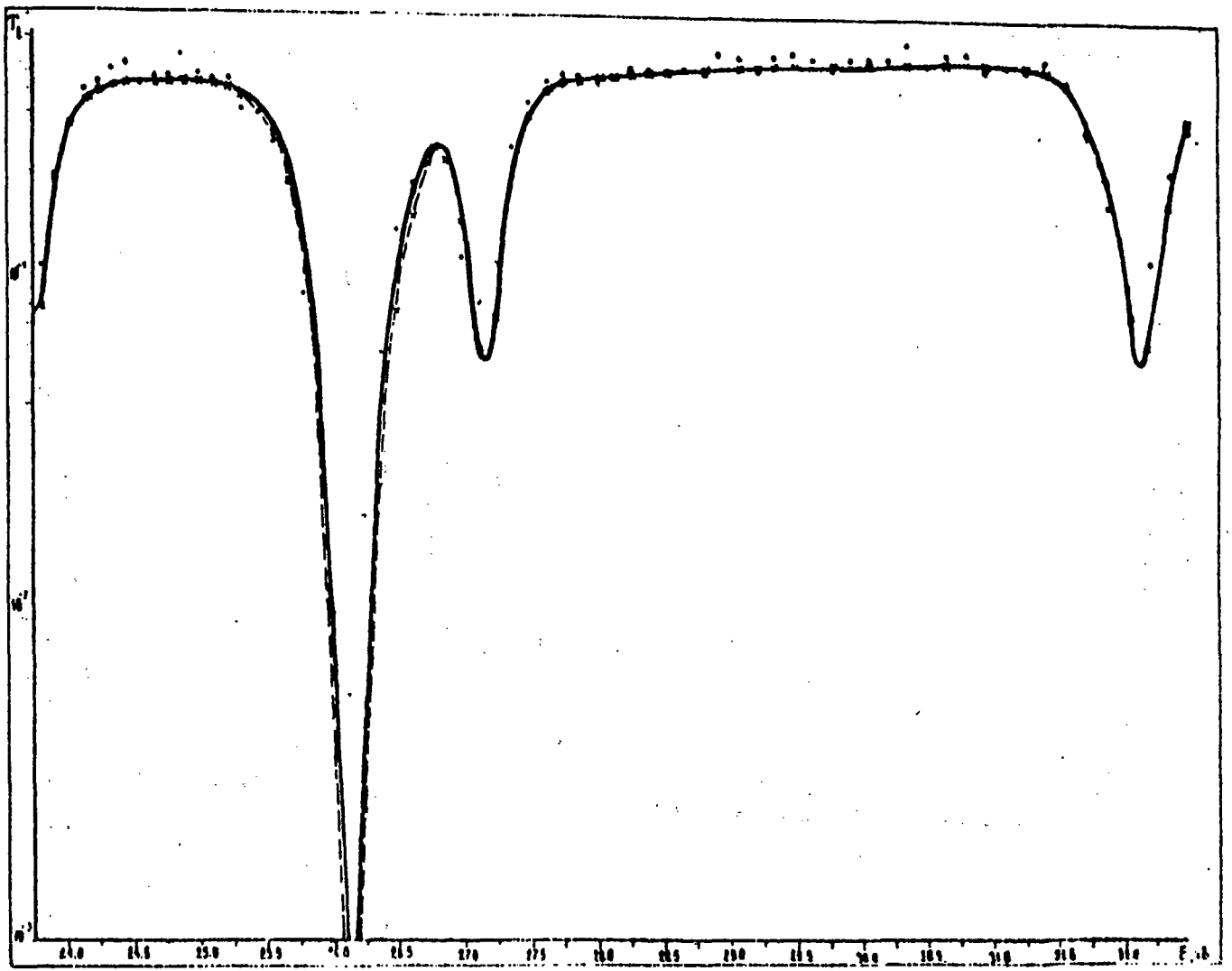

Fig. 19

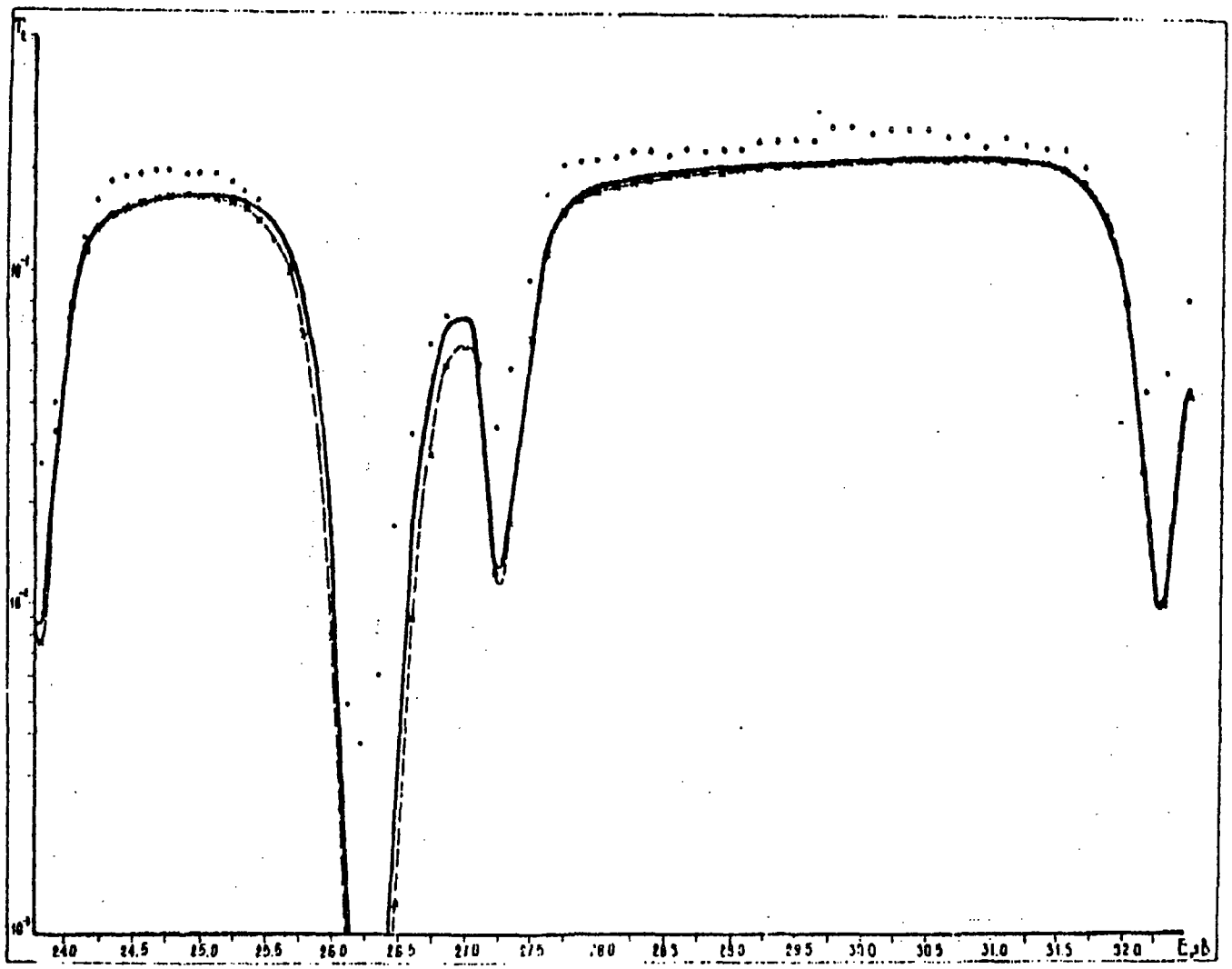
24.0
24.5
25.0
25.5
26.0
26.5
27.0
27.5
28.0
28.5
29.0
29.5
30.0
30.5
31.0
31.5
32.0
E,ab

Fig. 20

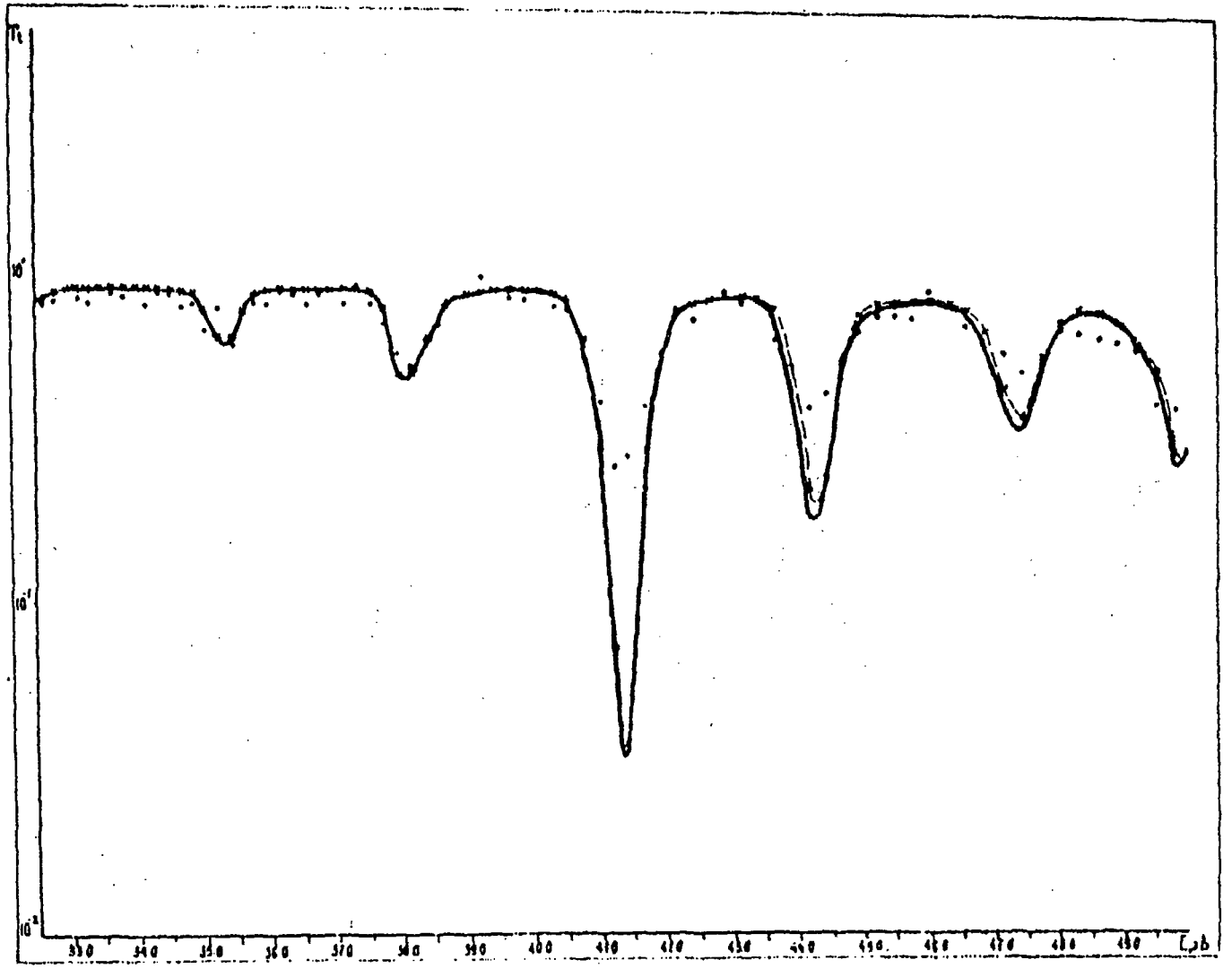

Fig. 21

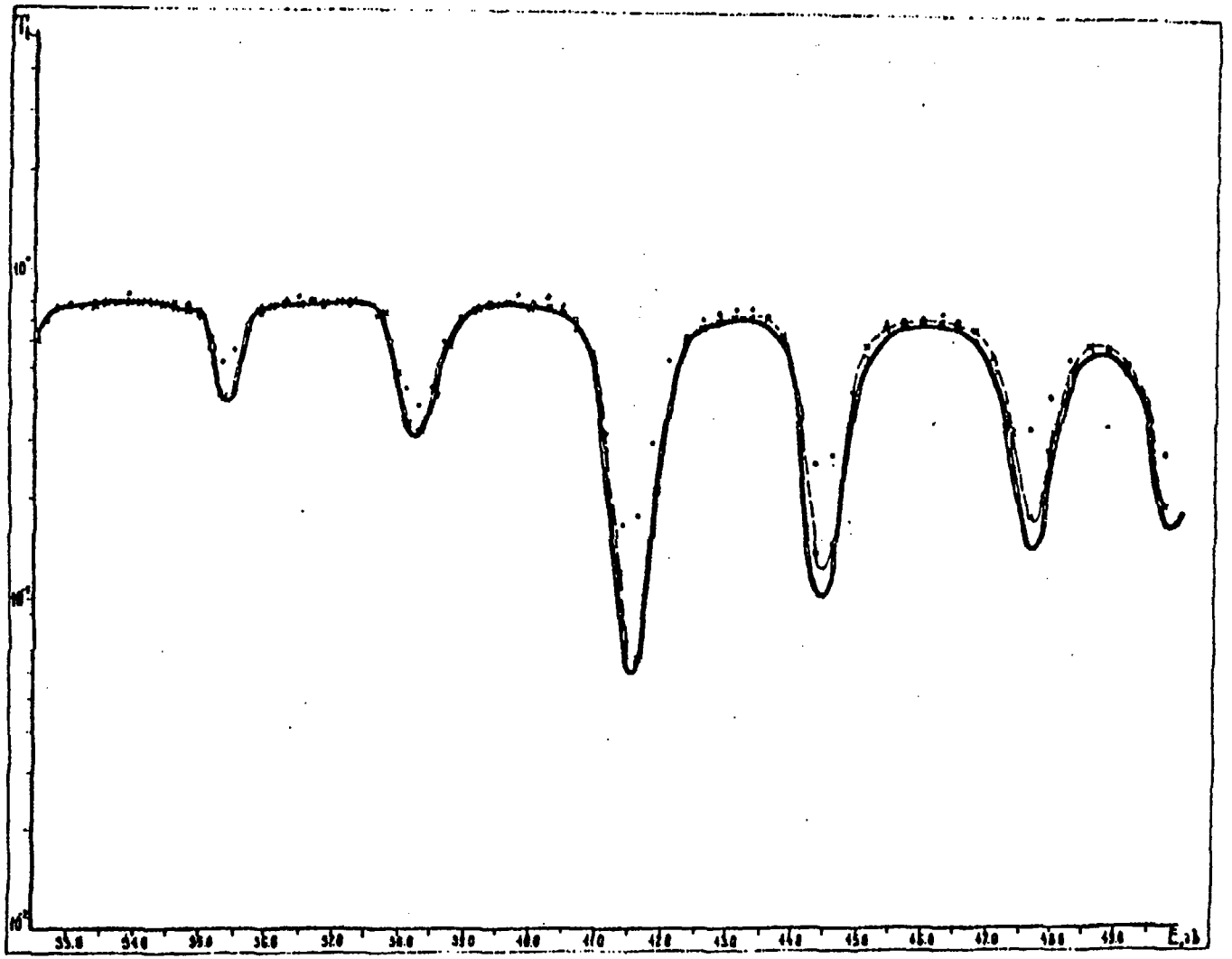

Fig. 22

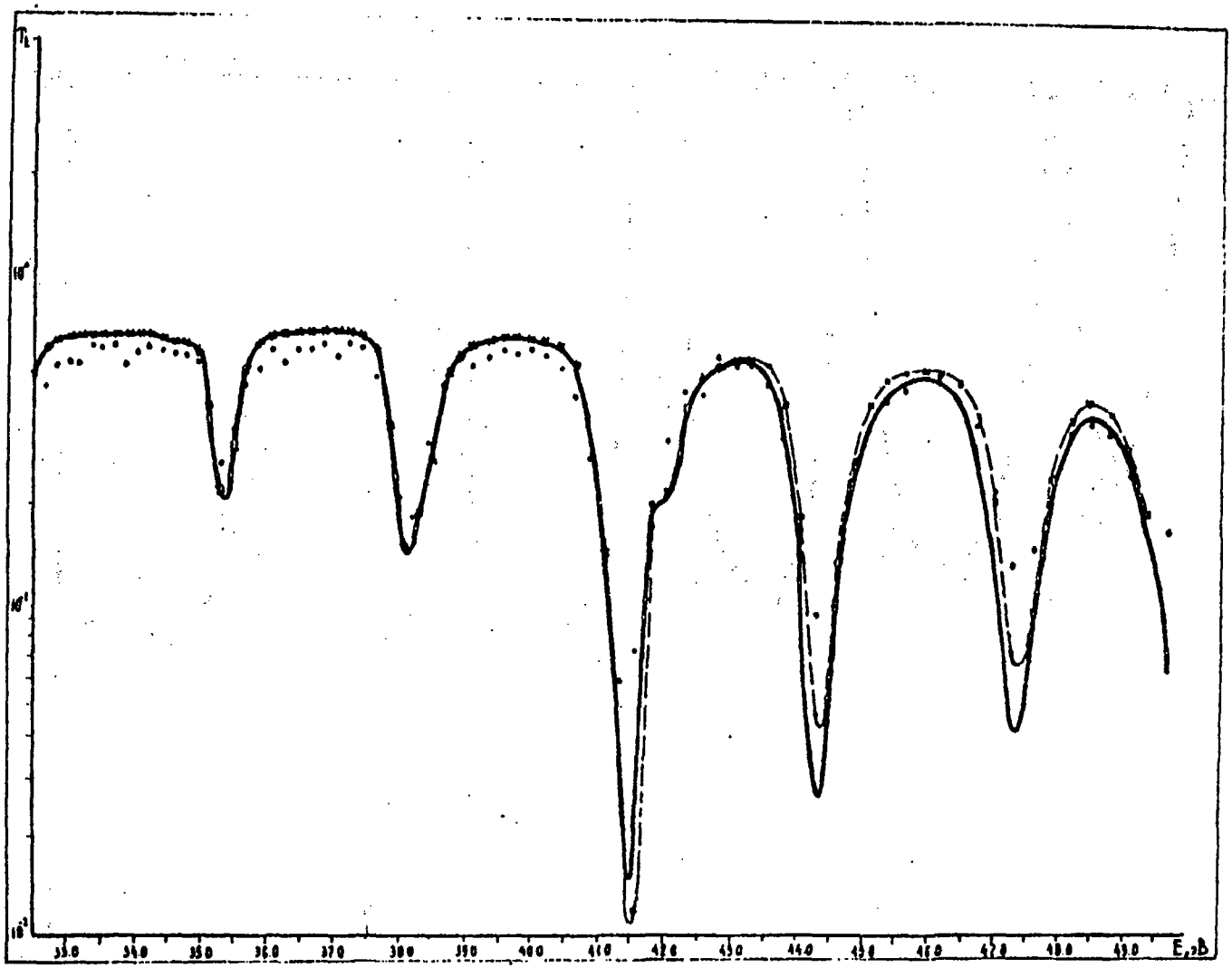
T_L
10^0
10^{-1}
10^{-2}
33.0
34.0
35.0
36.0
37.0
38.0
39.0
40.0
41.0
42.0
43.0
44.0
45.0
46.0
47.0
48.0
49.0
E_{γ},B

Fig. 23

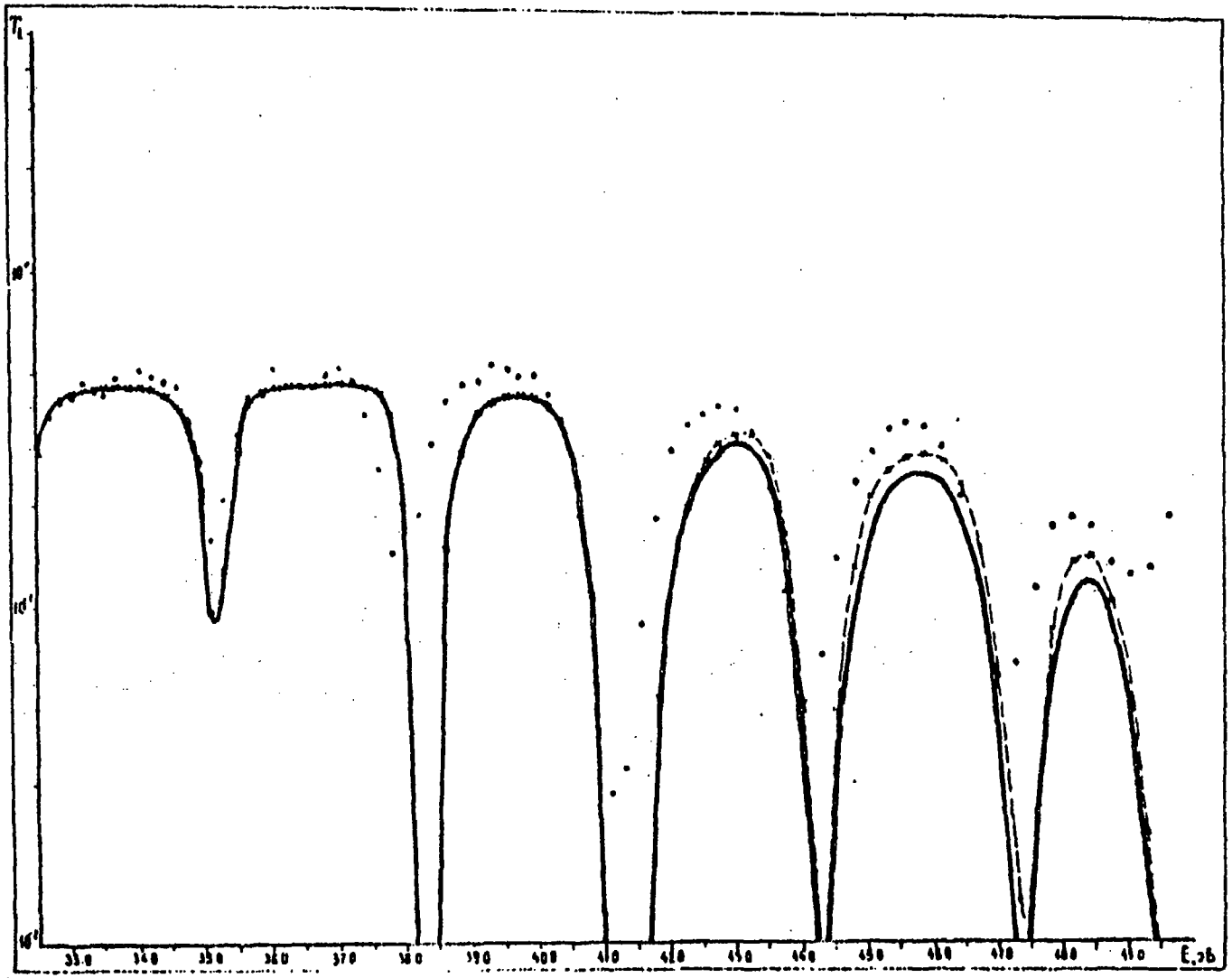

Fig. 24

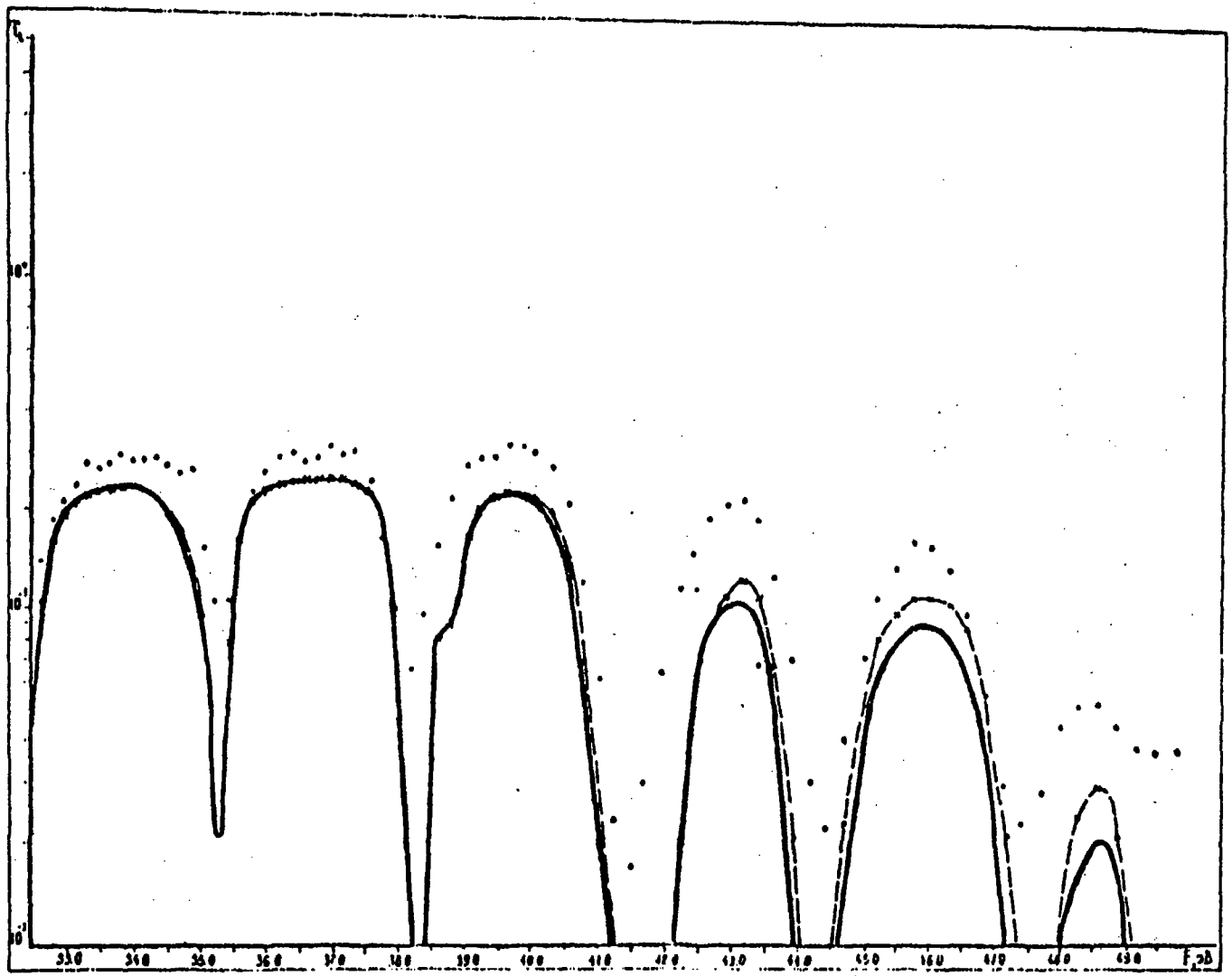

Fig. 25

REICH-MOORE FORMALISM AS APPLIED FOR SEARCHING RESONANCE PARAMETERS FROM EXPERIMENTAL DATA

V.F. Zharkov

A.V.Luikov Heat & Mass Transfer Institute,
BSSR Academy of Sciences, Minsk, U.S.S.R.

ABSTRACT

Consideration is made of the resonance fission width sign effect on the resonance interference allowed for using the Reich-Moore formalism. Reconstruction of ^{235}U cross sections from the experimental data on the Reich-Moore parameters is illustrated.

Among the majority of problems dealing with nuclear reactor design the one is encountered which considers the reconstruction of energy-dependent neutron cross sections from different parameters including resonance ones. With this in view, different evaluated nuclear data libraries, for example ENDF, are compiled which are permanently supplied with new experimental data, new evaluated data and parameters obtained through the use of new models analysing the neutron-nucleus interaction. These libraries are catered for by a great number of various programs which allow processing of the available information.

R E C E N T /1/ is one of such programs. It ensures reconstruction of the energy-dependent neutron total, elastic, capture and fission cross sections from the combination of resonance parameters and tabulated background cross-sections. In the resolved-resonance region, the program allows resonance parameters from four different formalisms:

1. Breit-Wigner single-level parameters
2. Breit-Wigner multy-level parameters
3. Reich-Moore parameters
4. Adler-Adler parameters

Unfortunately, the parametrization of the third type has not been realized in the RECENT program since for the moment there are no available Reich-Moore resonance parameters to describe simultaneously all types of heavy fission nucleus cross sections. This displays the complexity and tediousness of the problem of searching resonance parameters from experimental data.

The essence of the R-matrix Reich-Moore formalism is considered in detail in /2/. This method is one of the versions of the general R-matrix formalism in the approximation of a single neutron channel, several fission channels and a great number of radiation channels. It is assumed that there is no

intraresonance interference in the latter channels due to their large number. Such an approach makes it possible to construct a low-order matrix, invert it and compute any type of cross sections for a real time. The method is advantageous for possible account of the contribution of each resonance level to the cross sectional structure. But its calculations, especially those including the Doppler resonance broadening, are tedious and require rigorous spin separation of resonances. In general, the latter imposes the most severe restrictions to the application of this formalism since there is no information on resonance spins for the majority of fission nuclei.

Just recently, the results of evaluating resonance structure in (^{235}U + n) have appeared. This has permitted more particular approach to resonance parameter searching from the experimental data based on the Reich-Moore formalism using the program for ^{235}U derived by that time at the Heat and Mass Transfer Institute of the BSSR Academy of Sciences. The main scope of the present paper is to formulate the most difficult problems encountered at the first stage of researching which have to be solved.

In the program developed at the Institute the Reich-Moore formalism is realized with one neutron channel (for resolved resonances $\ell = 0$), one radiation channel (allowing for the contribution of all possible radiation channels) and two fission channels with the account taken of the signs of each channel. It is regarded that the signs influence upon the phases of the wave functions in output channels.

This being the situation, in addition to conventional interference determined by the distance between resonances some "sign" interference must exist being determined by a combination of signs in different channels. To make the problem clear, calculations for two resonances with equal parameters are performed, fission widths being divided equally for two channels. Initial resonances have the following parameters $E_{r_1} = 1$eV, $E_{r_2} = 2$eV, $\Gamma_{\gamma_1} = \Gamma_{\gamma_2} = 0.04$eV, $\Gamma_{n_1} = \Gamma_{n_2} = 0.2 \cdot 10^{-4}$ eV; $\Gamma_{f_{11}} = \Gamma_{f_{21}} = 0.02$eV and $\Gamma_{f_{12}} = \Gamma_{f_{22}} = 0$. First, the cross sections of all types are estimated by the Breit-Wigner formula for $J = 3$. All the subsequent results are compared with the obtained ones. If with some combination of signs in the fission channels of two resonances the cross sections coincide with the Breit-Wigner parameters, it is regarded that sign interference is absent (N.I. -No Interference). C.D.C. means that the cross section has increased to the left of the first resonance and to the right of the second (constructive interference) while it has decreased between the resonances (Destructive interference). D.C.D means the reverse. C.D.C. + D.C.D. implies that mainly interference remains to be destructive though not so obvious. D.C.D. + C.D.C. refers to the case of weaker constructive interference between resonances.

It must be noted that if some combinations of signs are in one group, for example C.D.C. + D.C.D., then the values

of cross sections are the same for all cases. The results of the analysis are cited in Table 1.

Figures 1 through 4 give neutron total, fission and capture cross sections for four cases of sign interference between two resonances. At E =1.5 eV for the N.I. case, σ_t = 15.847 barn, σ_f = 7.787 barn and σ_γ =1.557 barn. For the C.D.C. case, σ_t =8.243 barn, σ_f =0.143 barn and σ_γ =1.595 barn. For C.D.C. + D.C.D., σ_t =10.499 barn, σ_f = 2.449 barn and σ_γ =1.546 barn. For D.C.D., σ_t=24.188 barn, σ_f =15.788 barn and σ_γ =1.896 barn. In all the cases, the total cross section is underestimated by about 5 barns since potential scattering is computed by the program for each series of spins individually. It is evident from the figures 1–4 and cited cross sectional values that the combination of signs essentially affects the interference. Also, if fission widths are asymmetric, then one kind of the interference is developing into another.

Searching for resonance parameters relies upon the least square method. The program searches for a set of resonance parameters minimizing the functional $\sum_i \sum_j |\sigma_{ij}^{exp} - \sigma_{ij}^{calc}|^2$ where i=1,2,3 for three types of cross sections; j is the number of experimental points. Correct evaluation of the above functional requires the consideration of the thermal motion of atoms and experimental resolution of the apparatuses for the energy dependence of the cross sections in the region of resolved resonances. This is often achieved through averaging the cross sections over the Gaussian function

$$\overline{\sigma}(E) = \int_{-\infty}^{\infty} \sigma(E') e^{-\frac{(E-E')^2}{\Delta^2}} dE' \qquad (1)$$

As has been recently found the algorithm of averaging the tabulated cross sections which has been developed by the present authors independently differes only in some detail from the one described in /3/. This is, in particular, the mode of calculating the tabulated cross sections. Thus, in the range between 0.2 and 7eV, the table contains 2384 points in the ^{235}U case for each cross section. This constitutes, on the average, about 198 points per a resonance with a relative error due to linear approximation of 0.1%.

The contribution to dispersion Δ^2 includes thermal motion of atoms Δ_{th}^2 and experimental resolution Δ_r^2, i.e. $\Delta^2 = \Delta_{th}^2 + \Delta_r^2$. The temperature term is calculated rather simply (see, for example (3)). It is more difficult to allow for experimental resolution. If the resolution function is not determined experimentally, in the authors' program the resolution is included in the formula

$$\Delta_r^2 = 7.7284 \cdot 10^{-4} \cdot \Delta t \cdot E^3 \qquad (2)$$

where Δt is resolution in μs/m.

In its turn, Δt is determined as

$$\Delta t = (SNB + SCA + 1.8/\sqrt{E})/BTF \qquad (3)$$

where SNB is the accelerator beam width (μs),

SCA is the analyser channel width (μs),

$1.8/\sqrt{E}$ (Ein eV) is the time uncertainty (μs) due to fluctuations of the time of neutron moderation to the energy E. This assumption holds for water and plastics.

BTF is the flight path (m).

It is evident from (3) what requirements are made of the experimental data used for searching resonance parameters. Besides, it is desirable to know the exact experimental procedure, corrections for the energy scale, if these are available at all. As the effective temperature is needed to take account of the temperature broadening, it should be given for the target material. The statistic errors cited by the authors do not participate in computations since the difference between experimental and theoretical cross sections (discrepancies) is taken with a unit weight. This is because all types of the cross sections are optimized simultaneously differing in value, for example, due to different experimental temperatures.

Resonance parameters of ^{235}U are sought from the experiments by: Shore, Sailor /4/, Michaudon et al /5/ for σ_t; Deruytter et al /6/, Gwin et al /7/, Moore et al /8/, for σ_f, De Saussure /9/ and mean values of $(\sigma_a - \sigma_f)$ from /7/ for σ_γ. The data of /4/ are used without renormalization with the resolution $\Delta t = 0.17\mu s/m$ above 0.3eV and $\Delta t = 0.26\mu s/m$ below 0.3eV. There is no more detailed information for Δt calculation. Neither the data of /5/ are renormalized. Rather complete information on Δt is available. But the experimental data obtained from two experimental series have no indications on a particular series. Data of /6/ are not renormalized. There is no information on resolution. The analyser channel width is chosen from the data listing equal to 1.6μs (from 1 to 11 eV). The value of 1 μs is taken for the accelerator beam width. The data of /7/ and /8/ are not renormalized. No information is available on resolution. Therefore even such data as /8/ with the indication of resonance spins cannot be correctly used for evaluating resonance parameters. Data of /9/ and σ_γ of /7/ are renormalized to $\bar{d}_m$ between 0.1 and 1 eV obtained in /10/. In /9/ the resolution function and data on energy scale shift are given. For mean values used for estimation of σ_γ from /7/ and 15 σ_t points between 0.02 and 0.08 eV from /11/, Δ_r^2 is assumed to be zero.

Figs. 5 through 39 give several versions of theoretical σ_t, σ_f and σ_γ calculated by the Reich-Moore parameters (see Table 2) evaluated from the above experimental data. Resonance parameters of /8/ neglecting interference are used in Table 2 as reference data. Preliminary adjustment of parameters has been done up to 10 eV. The negative resonance is required to describe low energy regions. The signs of the fission widths for this resonance can be different from those in this Table (see Table 3). It is easily seen from the figures, that the resonance parameters being the same, the com-

bination of signs for other resonances can be found to satisfactorily describe experiments.

Now, consider the description of resonance cross sections for different energy regions. Between 0 and 0.75eV (fig.5-7), the energy dependence of the total, fission and capture cross sections are fairly described for all the fission width sign combinations considered. The negative resonance is most important here. Individual inspection of the negative and $J = 4$ resonances at $E_r = 1.143$ eV shows that in all three cases the fission widths signs are distributed in such a way that these resonances would not interfere if the fission widths were equally distributed over the channels (see Table 1). Any other combination of signs different from the N.I. case for these two resonances drastically distorts the agreement between calculation and experiment.

For 0.75 ÷ 2.25 eV (Figs. 9 and 10), the experimental data are fairly plotted by the theoretical curve with different combinations of fission widths signs. Thus, it may be stated that the kind of the interference is chosen correctly and subsequent optimization may improve the agreement between theory and experiment at the expense of redistribution of all the widths and fission ones, in the first turn. However, it works well only with appropriate mode of interference in more distant resonances because their contribution is essential. Thus, in the case of a random scatter of the fission widths signs in the resonances from 10 eV to 24 eV (parameters from Table 2), the sum of squared discrepancies for 0 - 4 eV region has changed by more than 20%, while the theoretical curves between 0 - 2.25 eV have ascended or descended. The optimum combination of fission width signs in the resonances above 10 eV found for the region between 4 and 10 eV and it is neglected.

The cross-sections in the region between 4.25 and 5.75 eV (figs. 16 through 22) are strongly dependent on the signs of fission widths of neighbouring resonances. It is easily seen from Figs. 16 through 18 how strong is the effect of sign interference with a resonance at $E_r = 5.5$ eV. Figs. 19 through 22 show the effect of the resonance fission width sign at $E_r = 4.2$ eV. The latter effect is stronger due to large fission widths. The case is somewhat different with the resonance with $E_r = 4.2$ eV. It is stronger and its effect on other resonances is more pronounced. Presumably, negative resonance with $J = 3$ may "tame" it a little bit. The resonance with $E_r = 2.762$ eV displays similar "character". But in the version 045 the experiment has been correctly described at the expense of negative resonance (Fig.11). It seems that one more negative resonance of another spin may help in eliminating the "swings" around the resonance $E_r = 4.2$ eV with a random sign scattering in the resonances above 10 eV.

The region between 5.75 and 6.75 eV (Figs. 23-25) is not greatly affected by the resonances below 5 eV. It is seen from comparing versions 45-2 and 047 in Figs. 23 and 24. However, in version 47-4 this effect is almost insufficient

(compare Figs. 23 and 25). For the resonance E_r = 6.17 eV no alternative sign version has been chosen.

Within 6.75 ÷ 8.25 eV (Figs. 26 through 29) the most pronounced effect is exerted by the resonance with E_r =7.07 eV and with E_r = 8.97 interfering with the resonance E_r= 7.7 eV. The version 47-2 seems to be most appropriate. Perhaps the parameters of the resonance with E_r = 7.7 eV must be first corrected by the value and then the interference considered.

The region of 8.25 eV to 9.25 eV (Figs. 30 through 33) is not essentially affected by any sign interchanges. Evidently the main contribution here is made by the resonance with E_r = 8.781 eV. No interchanges of fission width signs have been made for this resonance yet.

The region between 9.25 eV and 11 eV (Figs. 34 through 38) seems to demonstrate more vividly the effect of "sign" interference on the cross sectional structure. The total cross section is not given in the Figures. All the events due to sign interchanges in this region in resonances with E_r = 9.28 eV, 9.76 eV and 10.9 eV do not exert very strong effects on the section up to 9 eV. This gives hope that this region can be put in order. The energy dependence of the cross sections seems to be most correctly described in the version 047. The latter presumably may be taken as a basis for parameter optimization.

Finally, Fig.39 presents the fission and capture cross sections between 11 and 13 eV for the version 047. The correct behaviour of cross sections in this region supports fission width sign distribution for the resonances between 9.25 and 11 eV given in the version 047.

Thus, it is shown through a great number of figures that due to the Reich-Moore formalism and with the knowledge of the effect of fission width signs exerted on the interference of two neighbour resonances, a success can be achieved in searching for resonance parameters of ^{235}U. Unfortunately, this procedure is rather tedious and requires large computer time. Since, to the authors' mind, visual control of the discrepancies between theory and experiment is the only test in optimization, a great number of graphs have to be plotted for each version and almost for all regions. The attempt to use the sum of squared discrepancies in this case has failed. As its minimization may be performed, for example, due to curve levelling as in Fig.13 at E_r = 2.76 eV. This means that the curve describes experiment " on the average" and the sum of squared discrepancies has decreased, the parameters being rearranged to change the kind of information.

In this ideal case it is desirable to optimize simultaneously the parameters of all the resonances from the region of resolved resonances. However, the computer resources do not allow simultaneous input of all the experimental data and the use of external devices essentially prolongs optimization. Besides, there is no software allowing simultaneous optimization of 1000 parameters. Hence, it is necessary to optimize

small regions. In this case one faces "redistribution" when the improvement of the discrepancy sum in one region causes its deterioration of another. The experience has shown that it is inadvisable to fit the parameters of one resonance. Their number must constitute 5 to 10 in any energy region under consideration corresponding to 25-30 variable parameters. Optimization with such a number of parameters is very slow. This gives rise to the urgent problem of deriving the optimization program for exactly searching the Reich-Moore parameters.

At present, the work is in progress on searching the Reich-Moore parameters for ^{235}U. Therefore, the parameters cited in the present study must be considered as preliminary ones. The results and figures given in the work make the solution of the problem promising.

REFERENCES

1. D.E. Cullen, Program RECENT (version 79-1): reconstruction of energy-dependent neutron cross sections from resonance parameters in the ENDF/B format, UCRL-50400, vol. 17, 1979, part C.
2. C.W.Reich, M.S.Moore, Multilevel formula for the fission process, Phys. Rev., v.111, No.3, 1958, pp.929-933.
3. D.E.Cullen, C.R.Weisbin, Exact Doppler broadening of tabulated cross sections, Nucl.Sci. and Engng v.60, 1976, pp. 199-229.
4. F.J.Shore, V.L.Sailor, Slow neutron resonances in ^{235}U, Phys.Rev., v.112, No.1, 1958, pp. 191-202.
5. A.Michaudon, H.Derrien, P.Ribon, M.Sanche, Propitietes Statisfiques des Niveaux de $l'U^{236}$ Induits Dans $l'U^{235}$ Par Les Neutrons Lents, Nucl. Phys., v.69, 1969, pp. 545-572.
6. A.I.Deruytter, C.Wagemans, Measurements and Normalization of the Relative ^{235}U Fission Cross Section in the Low Resonance Region, J.Nucl. Engng v.25, 1971, pp. 263-272.
7. R.Gwin, E. G. Silver, R.W.Ingle, H.Weaver, Measurement of the Neutron Capture and Fission Cross Sections of ^{239}Pu and ^{235}U, 0.02 eV to 200 keV, the Neutron Capture Cross Sections of ^{197}Au, 10 to 50 KeV, and Neutron Fission Cross Sections of ^{233}U, 5 to 200 KeV, Nucl.Sci and Engng v. 59, No.2, 1976, pp. 79-105.
8. M.S.Moore, J.D.Moses, G.A.Keyworth, Spin Determination of Resonance Structure in (^{235}U + n) below 25 KeV, Phys. Rev., v.18, No.3, 1978, pp. 1328-1348.
9. G.De Saussure, ORNL-TM-1804, Simultaneous Measurements of the Neutron Fission and Capture Cross Sections for ^{235}U for Incident Neutron Energies from 0.4 eV to 3 KeV.
10. G.V.Muradyan, Yu.G.Shchepkin et al. Measurement of the absolute value of the alpha ^{235}U in the neutron energy region from 0.1 to 30 KeV, Neutron Physics,

Proc. 5th All-Union Conference on Neutron Physics, Kiev, 1980, M., TsNIIATOMINFORM, 1980, pt.2, pp.119-125.

11. V.A.Konshin et al, Proc. 3rd All-Union Conference on Neutron Physics, Kiev, 9-13 June, Evaluation of Nuclear Constants for ^{235}U in the Neutron Energy Region from 10^{-4} eV to 15 MeV, 1976, pt.2, p.43.

Table 1

Interference variation at different combinations of signs in two fission channels of two resonances with the same parameters

S_{ij}-sign.I. E_{r_1} = 1eV, Γ_{γ_1} = 0.04 eV, Γ_{n_1} = $0.2 \cdot 10^{-4}$ eV, $\Gamma_{f_{11}} = S_{11} \cdot 0.01$ eV, $\Gamma_{f_{12}} = S_{12} \cdot 0.01$ eV
E_{r_2} = 2 eV, Γ_{γ_2} = 0.04 eV, Γ_{n_2} = $0.2 \cdot 10^{-4}$ eV, $\Gamma_{f_{21}} = S_{21} \cdot 0.01$ eV, $\Gamma_{f_{22}} = S_{22} \cdot 0.01$ eV

N.I.		C.D.C.	D.C.D.	C.D.C. + D.C.D.		D.C.D. + C.D.C.	
$S_{11}\ S_{12}\ S_{21}\ S_{22}$	$S_{11}\ S_{12}\ S_{21}\ S_{22}$	$S_{11}\ S_{12}\ S_{21}\ S_{22}$	$S_{11}\ S_{12}\ S_{21}\ S_{22}$	$S_{11}\ S_{12}\ S_{21}\ S_{22}$	$S_{11}\ S_{12}\ S_{21}\ S_{22}$	$S_{11}\ S_{12}\ S_{21}\ S_{22}$	$S_{11}\ S_{12}\ S_{21}\ S_{22}$
+ 0 0 +	+ + + −	+ 0 + 0	+ 0 − 0	+ 0 + +	+ + + 0	+ 0 − +	+ + − 0
+ 0 0 −	+ + − +	0 + 0 +	0 + 0 −	+ 0 + −	+ + 0 +	+ 0 − −	+ + 0 −
0 + + 0	+ − + +	− 0 − 0	− 0 + 0	0 + + +	+ − + 0	0 + + −	+ − 0 +
0 + − 0	+ − − −	0 − 0 −	0 − 0 +	0 + − +	+ − 0 −	0 + − −	+ − − 0
− 0 0 +	− + + +	+ + + +	+ + − −	− 0 − +	− + 0 +	− 0 + +	− + + 0
− 0 0 −	− + − −	+ − + −	+ − − +	− 0 − −	− + − 0	− 0 + −	− + 0 −
0 − + 0	− − + −	− + − +	− + + −	0 − + −	− − − 0	0 − + +	− − + 0
0 − − 0	− − − +	− − − −	− − + +	0 − − −	− − 0 −	0 − − +	− − 0 +

Table 2

Resonance parameters for ^{235}U obtained using the Reich-Moore formalism

J	E_r, eV	Γ_γ, eV	Γ_n, eV	Γ_{f1}, eV	Γ_{f2}, eV
I	2	3	4	5	6
4	-I.5894	$2.8546 \cdot 10^{-2}$	$2.955142 \cdot 10^{-3}$	$2.113000 \cdot 10^{-1}$	$4.516611 \cdot 10^{-2}$
3	0.286	$3.8089 \cdot 10^{-2}$	$3.042652 \cdot 10^{-6}$	$3.481131 \cdot 10^{-2}$	$-4.506648 \cdot 10^{-2}$
4	I.I430	$3.7632 \cdot 10^{-2}$	$1.242933 \cdot 10^{-5}$	$-7.040837 \cdot 10^{-2}$	$4,818616 \cdot 10^{-2}$
3	2.0330	$4.2573 \cdot 10^{-2}$	$9.008880 \cdot 10^{-6}$	$-2.612829 \cdot 10^{-4}$	$1.198785 \cdot 10^{-2}$
4	2.7620	$3.9613 \cdot 10^{-2}$	$1.320712 \cdot 10^{-6}$	$4.294973 \cdot 10^{-2}$	$7.570420 \cdot 10^{-2}$
3	3.1360	$3.7419 \cdot 10^{-2}$	$2.733245 \cdot 10^{-5}$	$-7.260642 \cdot 10^{-3}$	$-1.204470 \cdot 10^{-1}$
4	3.6115	$3.9447 \cdot 10^{-2}$	$4.185623 \cdot 10^{-5}$	$1.852562 \cdot 10^{-2}$	$-4.782280 \cdot 10^{-2}$
3	4.2000	$3.0367 \cdot 10^{-2}$	$2.129526 \cdot 10^{-6}$	$8.970278 \cdot 10^{-2}$	$-1.063077 \cdot 10^{-1}$
4	4.8480	$3.4873 \cdot 10^{-2}$	$4.850763 \cdot 10^{-5}$	$-7.727471 \cdot 10^{-5}$	$-2.908714 \cdot 10^{-3}$
4	5.5000	$3.5948 \cdot 10^{-2}$	$2.672297 \cdot 10^{-5}$	$1.027504 \cdot 10^{-1}$	$-1.599342 \cdot 10^{-1}$
3	6.1700	$4.1448 \cdot 10^{-2}$	$6.176259 \cdot 10^{-5}$	$6.675533 \cdot 10^{-3}$	$-1.561816 \cdot 10^{-1}$
4	6.3800	$2.2454 \cdot 10^{-2}$	$2.225588 \cdot 10^{-4}$	$5.266091 \cdot 10^{-4}$	$8.733674 \cdot 10^{-3}$
3	6.9500	$3.3884 \cdot 10^{-2}$	$5.768120 \cdot 10^{-6}$	$3.199524 \cdot 10^{-1}$	$6.963777 \cdot 10^{-2}$
4	7.0700	$3.2246 \cdot 10^{-2}$	$1.057311 \cdot 10^{-4}$	$7.850464 \cdot 10^{-3}$	$2.128596 \cdot 10^{-2}$
4	7.5500	$3.3844 \cdot 10^{-2}$	$3.086844 \cdot 10^{-6}$	$3.393382 \cdot 10^{-2}$	$-9.285930 \cdot 10^{-4}$
3	7.7000	$3.3104 \cdot 10^{-2}$	$3.897648 \cdot 10^{-6}$	$-9.444194 \cdot 10^{-2}$	$-9.444203 \cdot 10^{-2}$
4	8.7814	$2.9538 \cdot 10^{-2}$	$9.663202 \cdot 10^{-4}$	$9.450023 \cdot 10^{-4}$	$-8.502753 \cdot 10^{-2}$
3	8.9700	$3.3094 \cdot 10^{-2}$	$8.410074 \cdot 10^{-5}$	$6.143662 \cdot 10^{-1}$	$2.903010 \cdot 10^{-3}$

Table 2 (continued)

I	2	3	4	5	6
4	9.2790	$3.3094 \cdot 10^{-2}$	$1.306350 \cdot 10^{-4}$	$-5.666210 \cdot 10^{-2}$	$2.175175 \cdot 10^{-2}$
3	9.7600	$3.5 \cdot 10^{-2}$	$3.820327 \cdot 10^{-5}$	$1.6 \cdot 10^{-1}$	$-1.6 \cdot 10^{-1}$
4	10.1770	$3.5 \cdot 10^{-2}$	$5.728075 \cdot 10^{-3}$	$-2.0 \cdot 10^{-3}$	$-6.0 \cdot 10^{-2}$
3	10.9000	$3.5 \cdot 10^{-2}$	$6.792687 \cdot 10^{-6}$	$1.1 \cdot 10^{-1}$	$-1.0 \cdot 10^{-1}$
4	11.6690	$3.5 \cdot 10^{-2}$	$5.283400 \cdot 10^{-4}$	$-3.0 \cdot 10^{-3}$	$-2.8 \cdot 10^{-3}$
3	12.3960	$3.5 \cdot 10^{-2}$	$1.472698 \cdot 10^{-3}$	$-7.0 \cdot 10^{-3}$	$-2.2 \cdot 10^{-2}$
4	12.4300	$3.5 \cdot 10^{-2}$	$5.390281 \cdot 10^{-5}$	$-5.0 \cdot 10^{-3}$	$-1.2 \cdot 10^{-1}$
4	12.8620	$3.5 \cdot 10^{-2}$	$6.790180 \cdot 10^{-5}$	$1.0 \cdot 10^{-1}$	$9.0 \cdot 10^{-3}$
4	13.2700	$3.5 \cdot 10^{-2}$	$4.759926 \cdot 10^{-5}$	$-7.0 \cdot 10^{-2}$	$-6.4 \cdot 10^{-2}$
4	13.6960	$3.5 \cdot 10^{-2}$	$5.263375 \cdot 10^{-5}$	0.0	$-5.7 \cdot 10^{-2}$
3	13.9960	$3.5 \cdot 10^{-2}$	$5.472728 \cdot 10^{-4}$	$6.0 \cdot 10^{-2}$	$-5.0 \cdot 10^{-1}$
3	14.5520	$3.5 \cdot 10^{-2}$	$1.216346 \cdot 10^{-4}$	0.0	$1.84 \cdot 10^{-2}$
4	15.4080	$3.5 \cdot 10^{-2}$	$2.149321 \cdot 10^{-4}$	$-3.0 \cdot 10^{-2}$	$1.28 \cdot 10^{-2}$
3	15.5100	$3.5 \cdot 10^{-2}$	$1.620318 \cdot 10^{-5}$	$-1.0 \cdot 10^{-1}$	$7.5 \cdot 10^{-2}$
4	16.0900	$3.5 \cdot 10^{-2}$	$3.351608 \cdot 10^{-4}$	$1.0 \cdot 10^{-2}$	$1.05 \cdot 10^{-2}$
4	16.6640	$3.5 \cdot 10^{-2}$	$2.536379 \cdot 10^{-4}$	$9.6 \cdot 10^{-2}$	$-1.0 \cdot 10^{-3}$
3	17.2200	$3.5 \cdot 10^{-2}$	$1.185628 \cdot 10^{-5}$	$-5.0 \cdot 10^{-3}$	$1.0 \cdot 10^{-1}$
3	18.0500	$3.5 \cdot 10^{-2}$	$3.058940 \cdot 10^{-4}$	$4.9 \cdot 10^{-2}$	$4.0 \cdot 10^{-2}$
4	18.1200	$3.5 \cdot 10^{-2}$	$9.081086 \cdot 10^{-5}$	$1.3 \cdot 10^{-1}$	$1.3 \cdot 10^{-1}$
4	18.9720	$3.5 \cdot 10^{-2}$	$9.098543 \cdot 10^{-5}$	$8.0 \cdot 10^{-3}$	$2.4 \cdot 10^{-2}$
4	19.2970	$3.5 \cdot 10^{-2}$	$2.604463 \cdot 10^{-3}$	$-1.5 \cdot 10^{-1}$	$7.0 \cdot 10^{-2}$
3	19.3200	$3.5 \cdot 10^{-2}$	$2.712621 \cdot 10^{-4}$	$-1.5 \cdot 10^{-1}$	$7.0 \cdot 10^{-2}$

Table 2 (continued)

1	2	3	4	5	6
4	20.0600	$3.5 \cdot 10^{-2}$	$3.983174 \cdot 10^{-5}$	$1.5 \cdot 10^{-2}$	$1.0 \cdot 10^{-2}$
3	20.1700	$3.5 \cdot 10^{-2}$	$4.619419 \cdot 10^{-5}$	$6.2 \cdot 10^{-2}$	$6.3 \cdot 10^{-2}$
4	20.6300	$3.5 \cdot 10^{-2}$	$1.618979 \cdot 10^{-4}$	$4.17 \cdot 10^{-2}$	0.0
3	20.9100	$3.5 \cdot 10^{-2}$	$1.620058 \cdot 10^{-5}$	$2.8 \cdot 10^{-1}$	0.0
4	21.0680	$3.5 \cdot 10^{-2}$	$1.362716 \cdot 10^{-3}$	$2.0 \cdot 10^{-3}$	$-2.2 \cdot 10^{-2}$
3	22.0500	$3.5 \cdot 10^{-2}$	$1.931962 \cdot 10^{-5}$	$1.3 \cdot 10^{-1}$	$1.3 \cdot 10^{-1}$
4	22.9340	$3.5 \cdot 10^{-2}$	$4.095080 \cdot 10^{-4}$	$2.0 \cdot 10^{-2}$	$2.45 \cdot 10^{-2}$
4	23.4110	$3.5 \cdot 10^{-2}$	$7.053445 \cdot 10^{-4}$	0.0	$1.18 \cdot 10^{-2}$
3	23.6120	$3.5 \cdot 10^{-2}$	$9.052028 \cdot 10^{-4}$	$-6.3 \cdot 10^{-2}$	$6.3 \cdot 10^{-2}$
3	24.2300	$3.5 \cdot 10^{-2}$	$3.881662 \cdot 10^{-4}$	$-2.9 \cdot 10^{-2}$	$1.7 \cdot 10^{-3}$

Table 3

Different combinations of fission width signs for the parameters given in Table 2

E_r	Number of versions						
	045	45-I	45-2	0-47	47-2	47-3	47-4
I	2	3	4	5	6	7	8
-I.5894	+ +			+ −		+ +	+ −
0.286616	+ −			− +		+ +	− +
I.I43	− +			− −		− +	− −
2.033	− +			+ +		− +	+ +
2.762	+ +			+ +		− +	+ +
3.I36	− −			+ −		− −	+ −
3.6II5	+ −			− +		− −	− +
4.2	+ −			− +	+ +	+ +	− +
4.848	− −	− −	− −	− −	− +	− +	
5.5	− −	− +	+ −	+ −	+ +	+ +	
6.I7	+ −			+ −			
6.38	+ +			+ +			
6.95	+ +			− +			+ −
7.07	+ +			+ +	− +	− +	
7.55	+ −			+ −			
7.70	− −			− +	+ −	+ −	+ +
8.78I4	+ −			+ −			
8.97	+ +			+ +	− −	− −	− +
9.279	− +			− +	+ +	+ +	− +
9.76	+ −			− −	− +	− +	− +
I0.I77	− −			− −			
I0.9	+ −			+ −	− −	− −	+ −

I	2	3	4	5	6	7	8
II.669	− −			− −			
I2.396	− −			− −			
I2.43	− −			− −			
I2.862	+ +			+ +			
I3.27	− −			− −			
I3.696	0 −			0 −			
I3.996	+ −			+ −			
I4.552	0 +			0 +			
I5.408	− +			− +			
I5.5I	− +			− +			
I6.09	+ +			+ +			
I6.664	+ −			+ −			
I7.22	− +			− +			
I8.05	+ +			+ +			
I8.I2	+ +			+ +			
I8.972	+ +			+ +			
I9.32	− +			− +			
20.08	+ +			+ +			
20.I7	+ +			+ +			
20.63	+ 0			+ 0			
20.9I	+ 0			+ 0			
2I.068	+ −			+ −			
22.050	+ +			+ +			
22.934	+ +			+ +			
23.6I2	− +			− +			
24.23	− +			− +			

Note: It is assumed that in places where the signs are not typed these are the same as in the previous version.

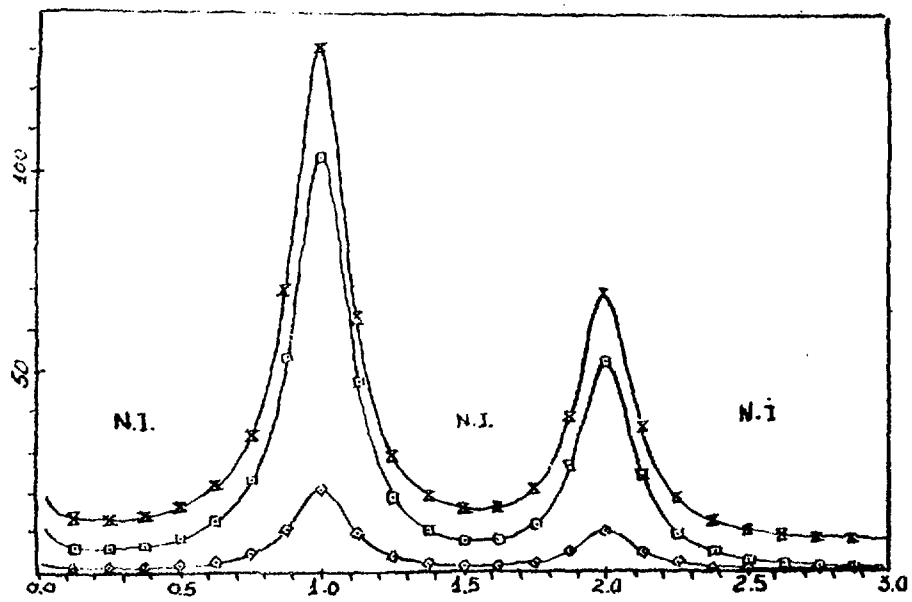

Fig.1 Interference between two resonances with the same parameters (non-interference case).

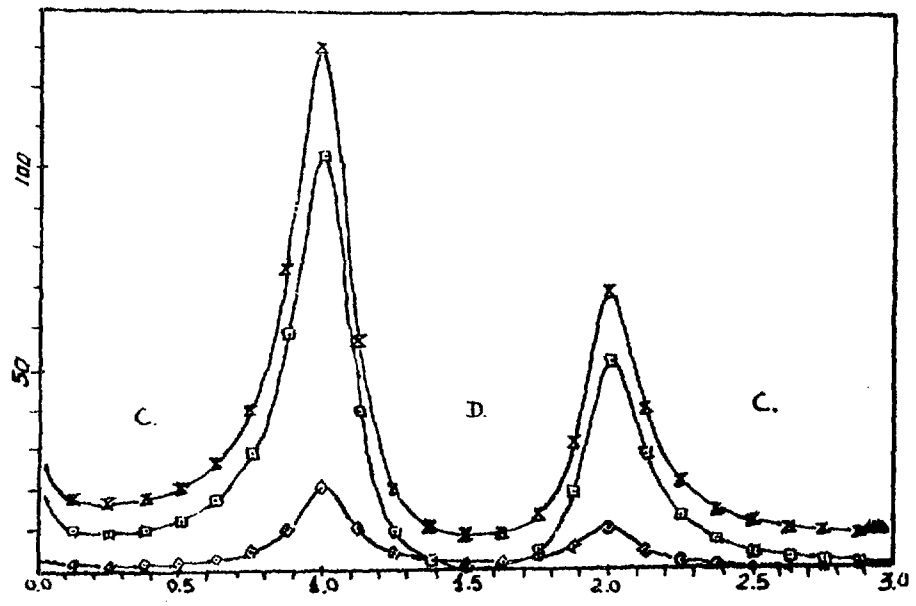

Fig.2 Interference between two resonances with the same parameters (C.D.C. case).

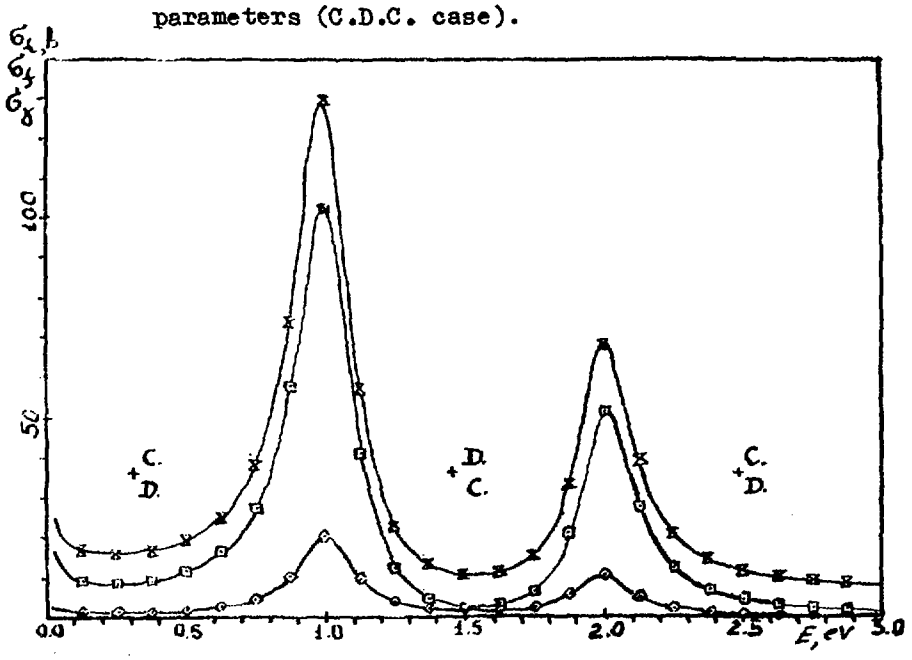

Fig.3 Interference between two resonances with the same parameters (C.D.C. + D.C.D. case).

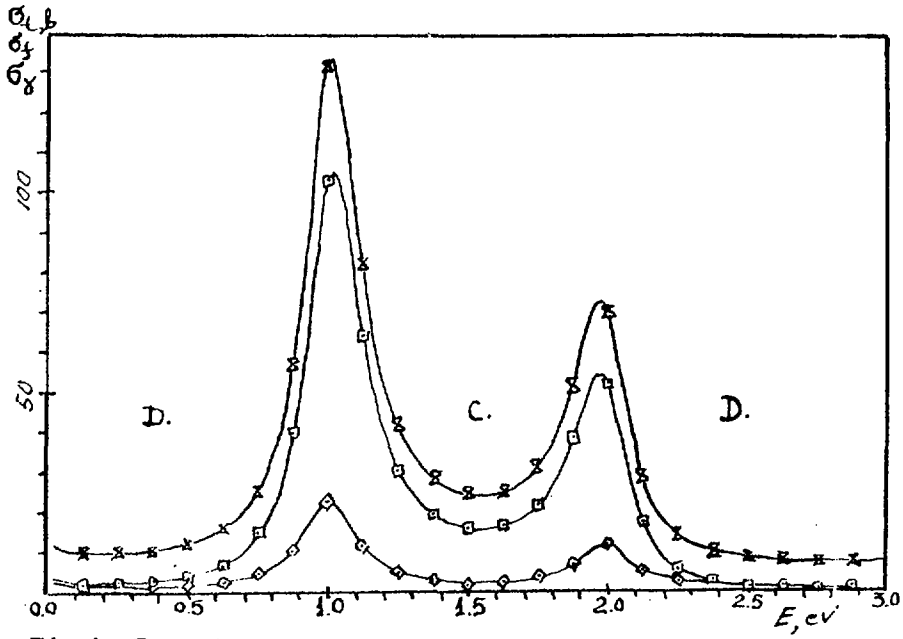

Fig.4 Interference between two resonances with the same parameters (D.C.D. case).

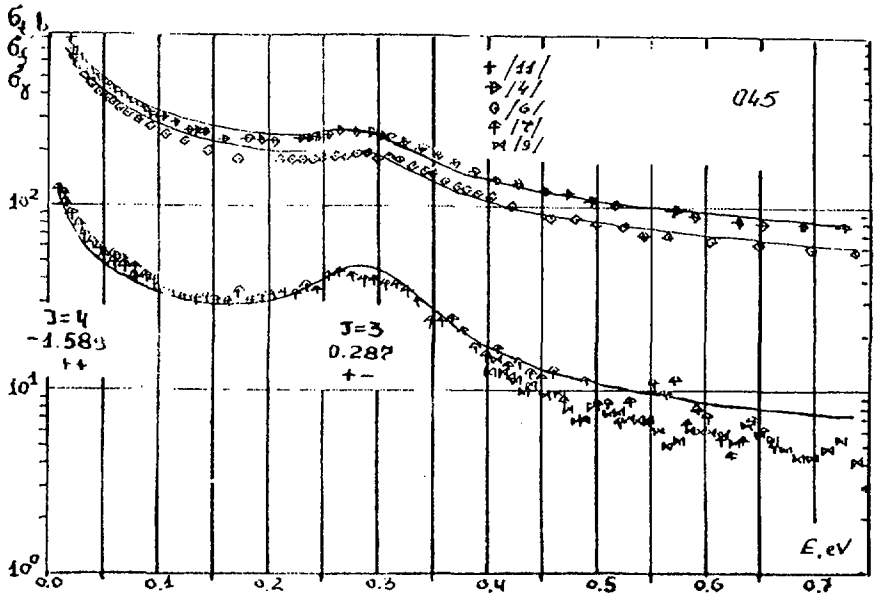

Fig.5 Resonance cross section in the 0 + 0.75 eV region (version 45-2).

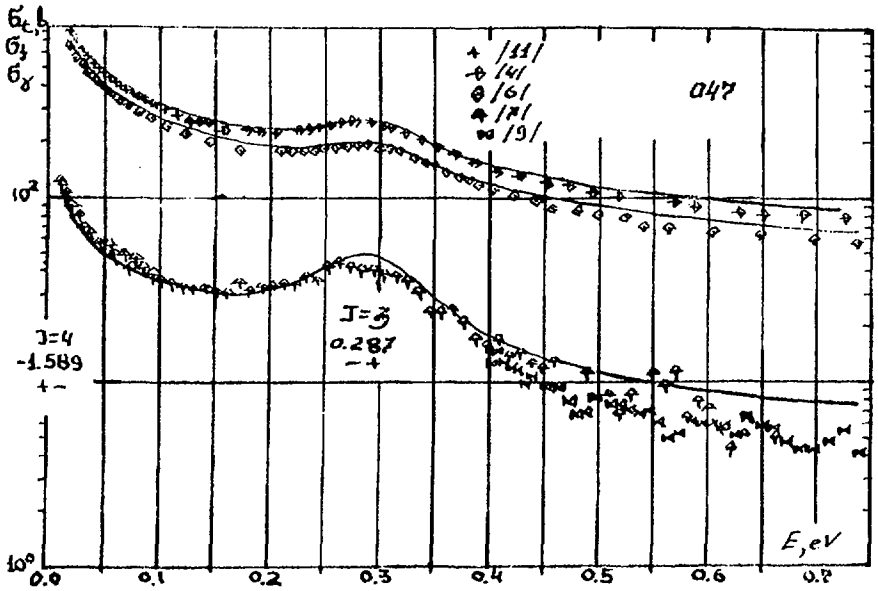

Fig.6 Resonance cross section structure in the 0 + 75 eV region (version 047).

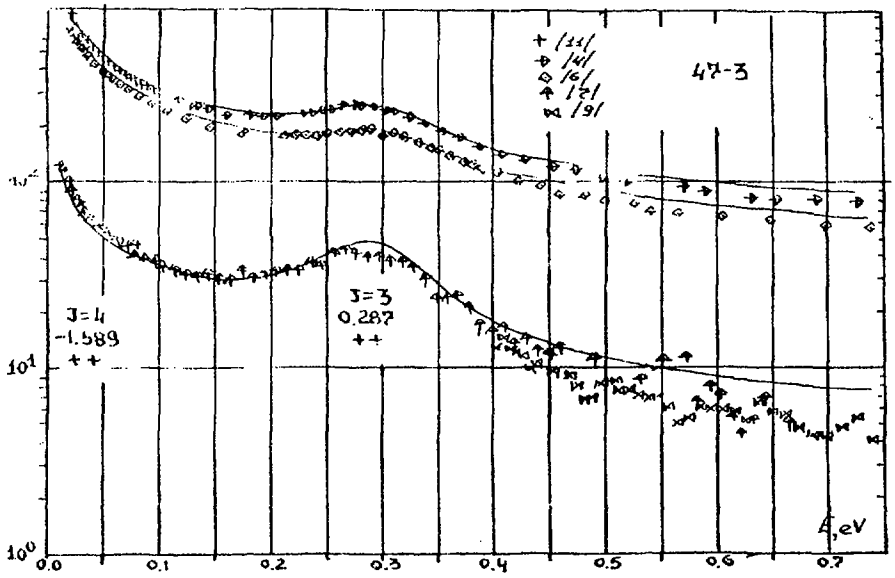

Fig.7 Resonance cross section structure in the 0 ÷ 75 eV region (version 47-3).

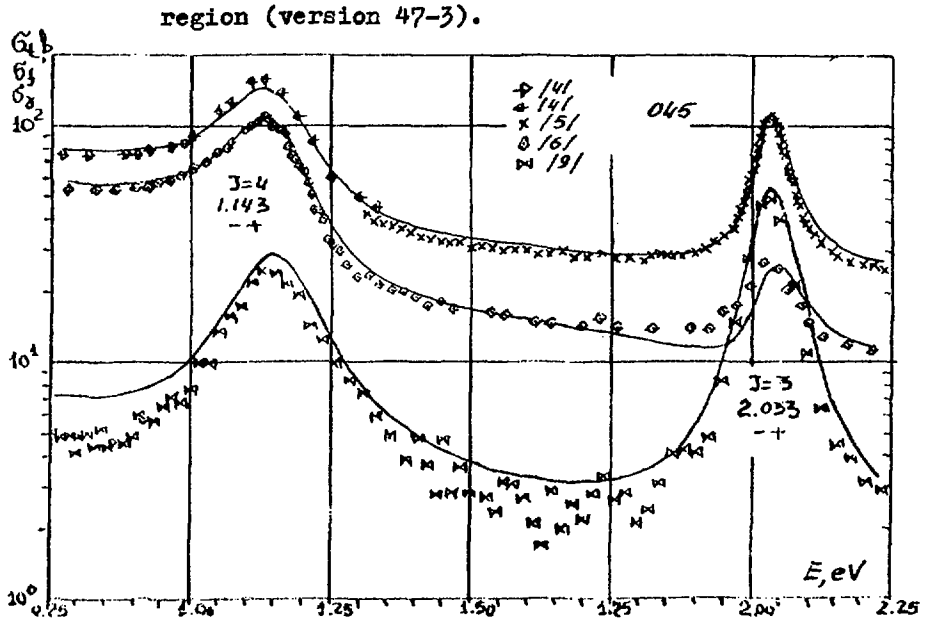

Fig.8 Resonance cross section structure in the 0.75 ÷ 2.25 eV region (version 45-2).

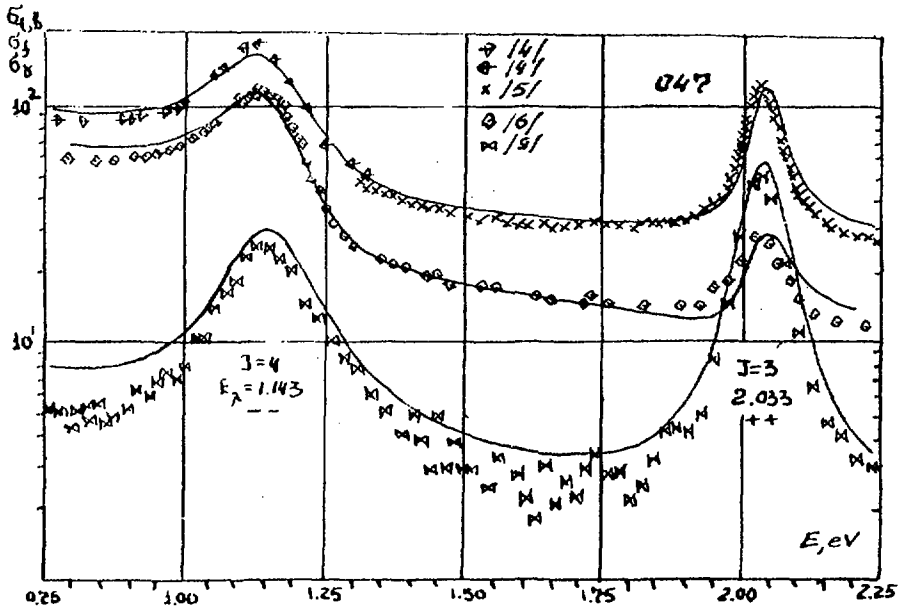

Fig.9 Resonance cross section structure in the 0.75 ÷ 2.25 eV region (version 047).

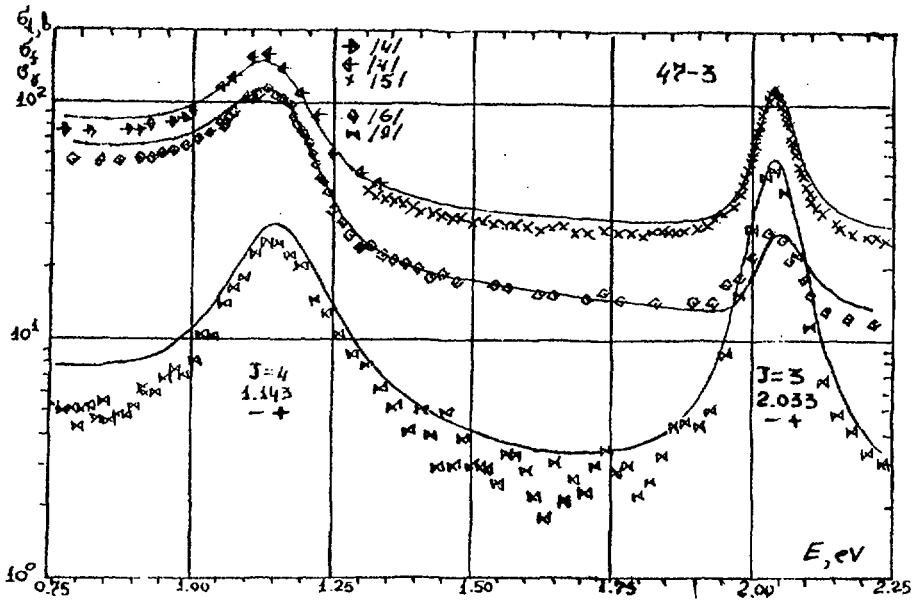

Fig.10 Resonance cross section structure in the 0.75 ÷ 2.25 eV region (version 47-3).

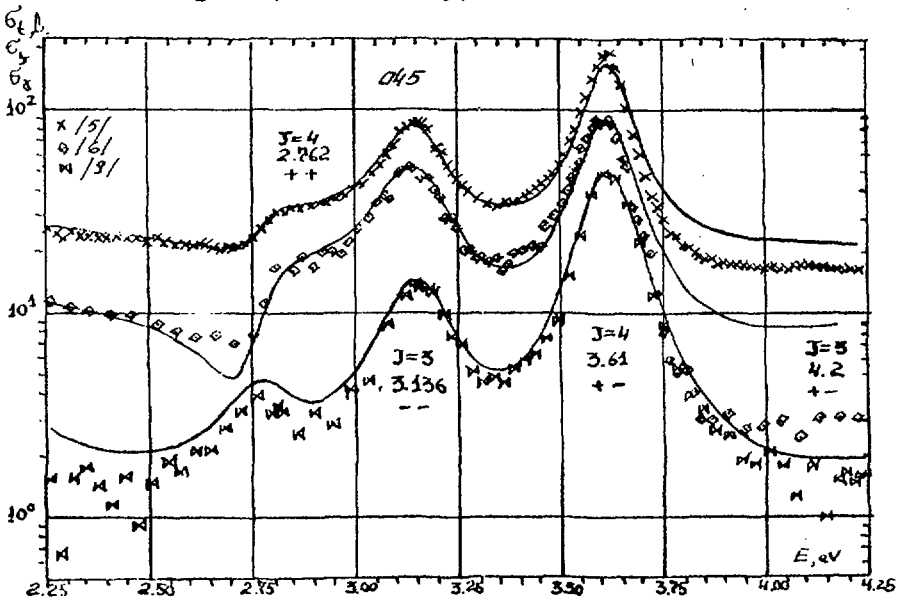

Fig.11 Resonance cross section structure in the 2.25 ÷ 4.25 eV region (version 045).

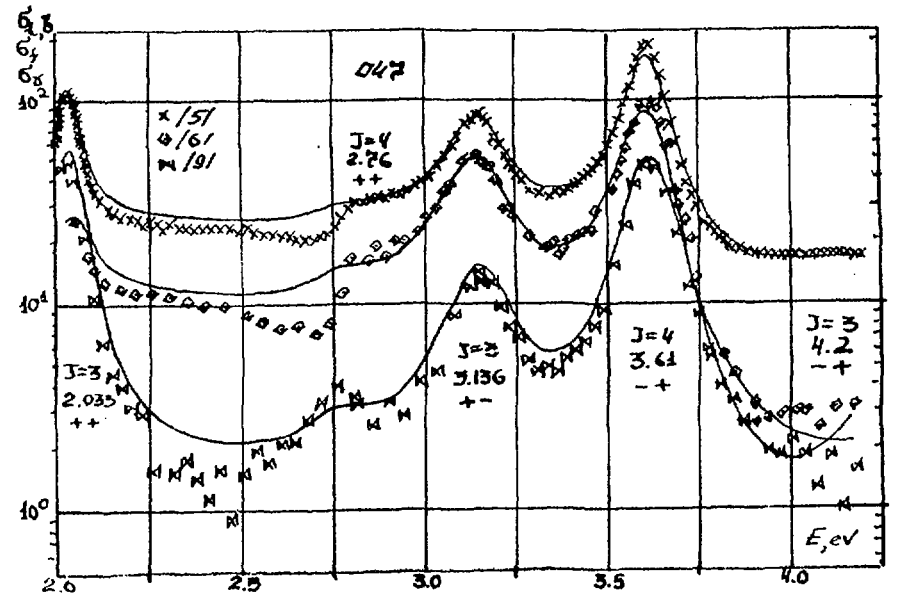

Fig.12.Resonance cross section structure in the 2.25 ÷ 4.25 eV region (version 047).

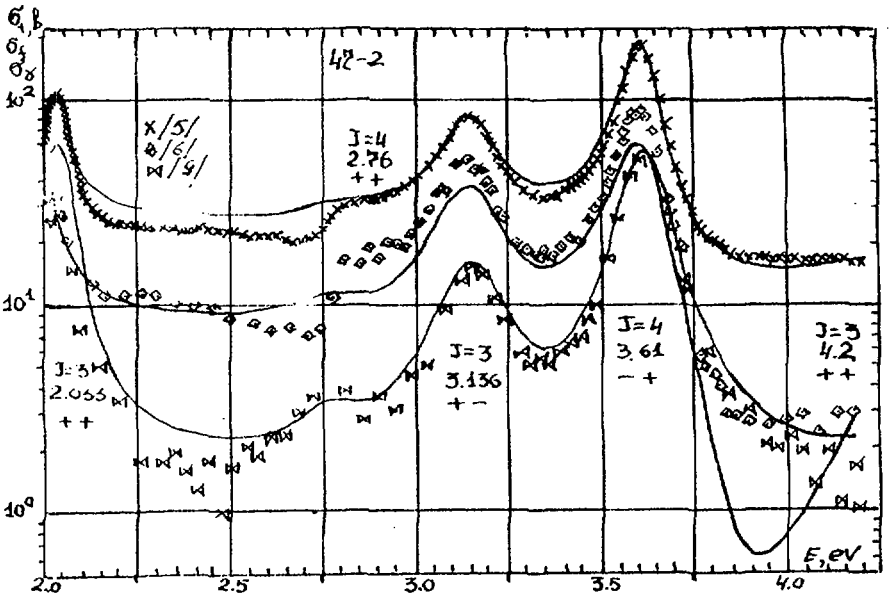

Fig.13 Resonance cross section structure in the 2.00 ÷ 4.25 eV region (version 47-2).

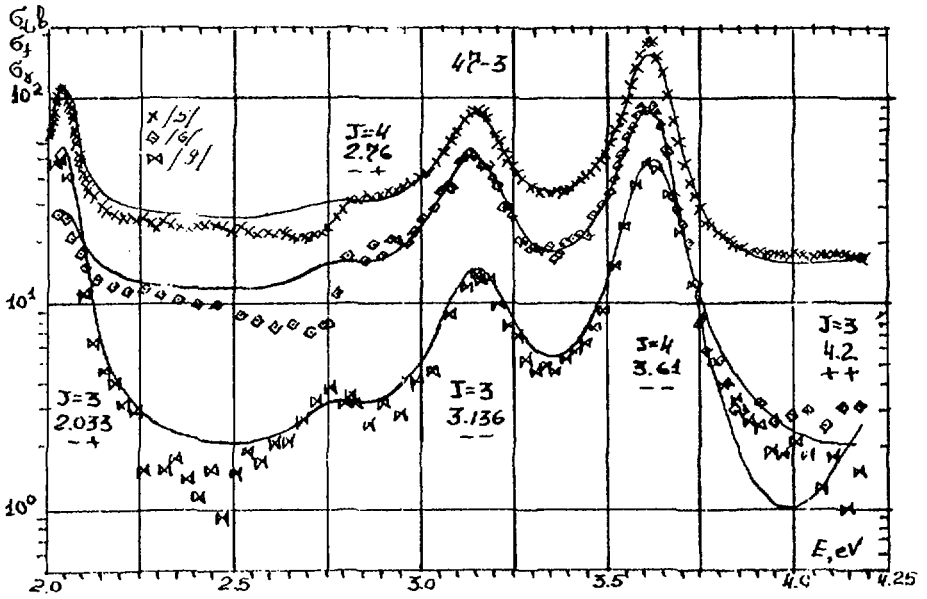

Fig.14 Resonance cross section structure in the 2.00 ÷ 4.25 eV region (version 47-3).

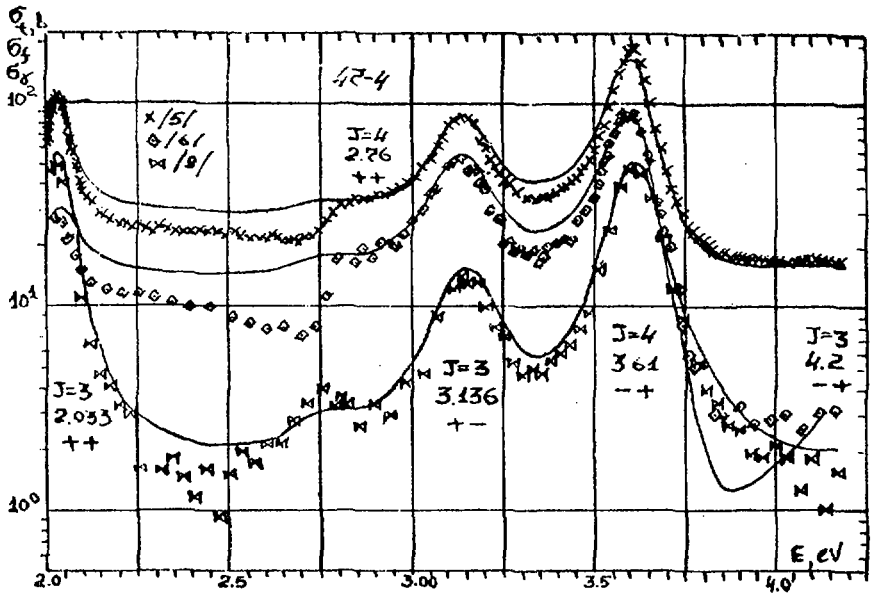

Fig.15 Resonance cross section structure in the 2.00 ÷ 4.25 eV region (version 47-4).

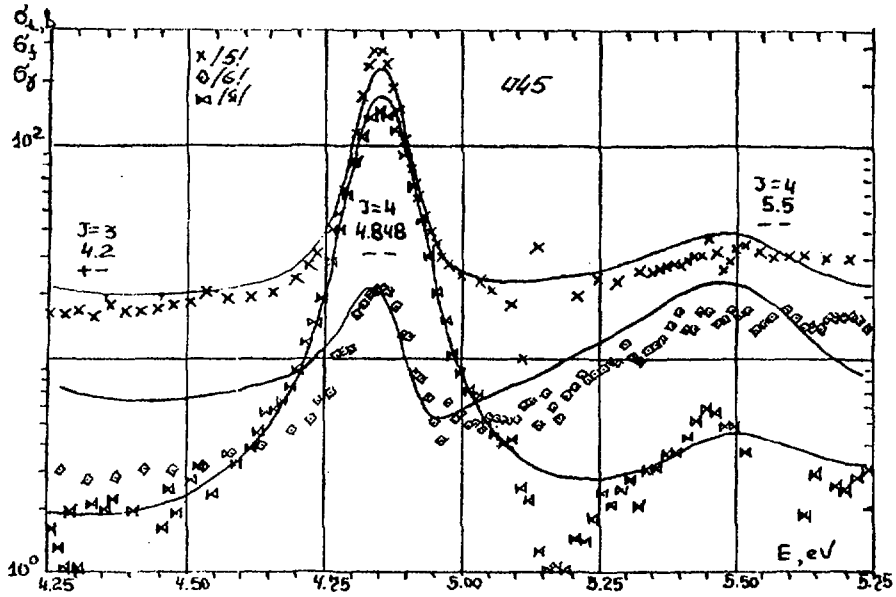

Fig.16 Resonance cross section structure in the 4.25 ÷ 5.75 eV region (version 045).

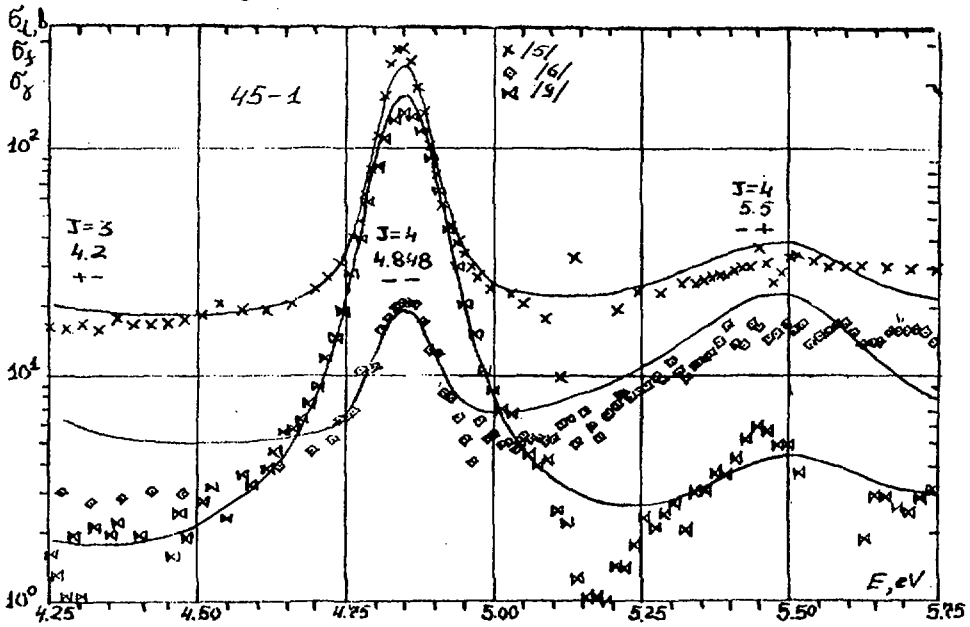

Fig.17 Resonance cross section structure in the 4.25 ÷ 5.75 eV region (version 45-1).

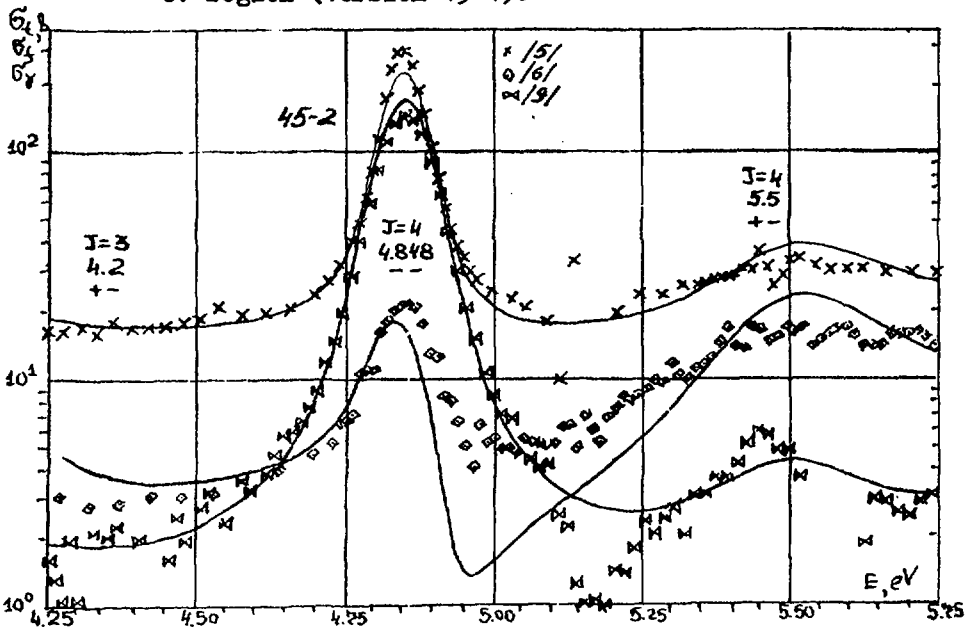

Fig.18 Resonance cross section structure in the 4.25 ÷ 5.75 eV region (version 45-2).

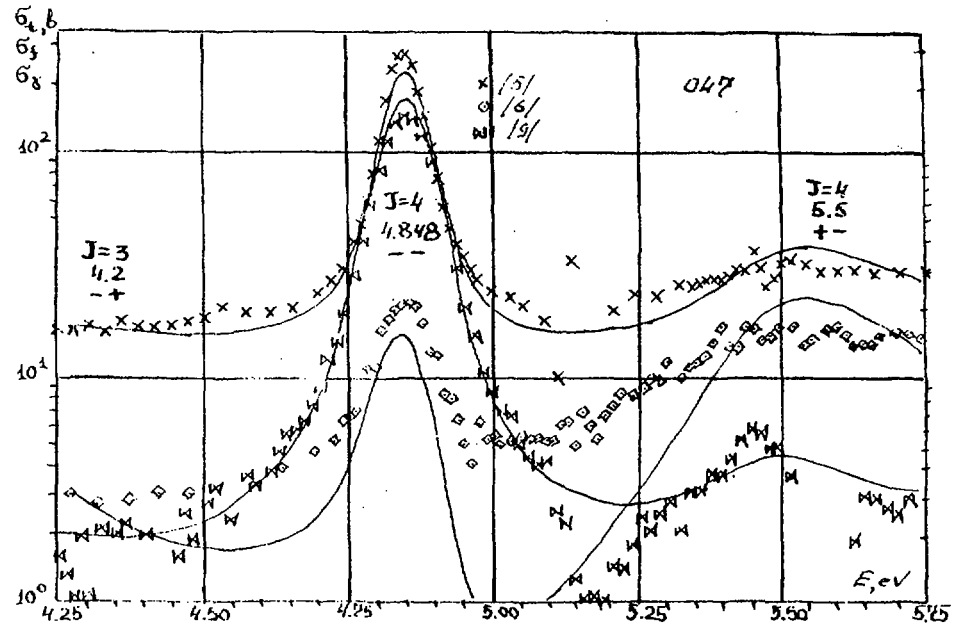

Fig.19 Resonance cross section structure in the 4.25 ÷ 5.75 eV region (version 047).

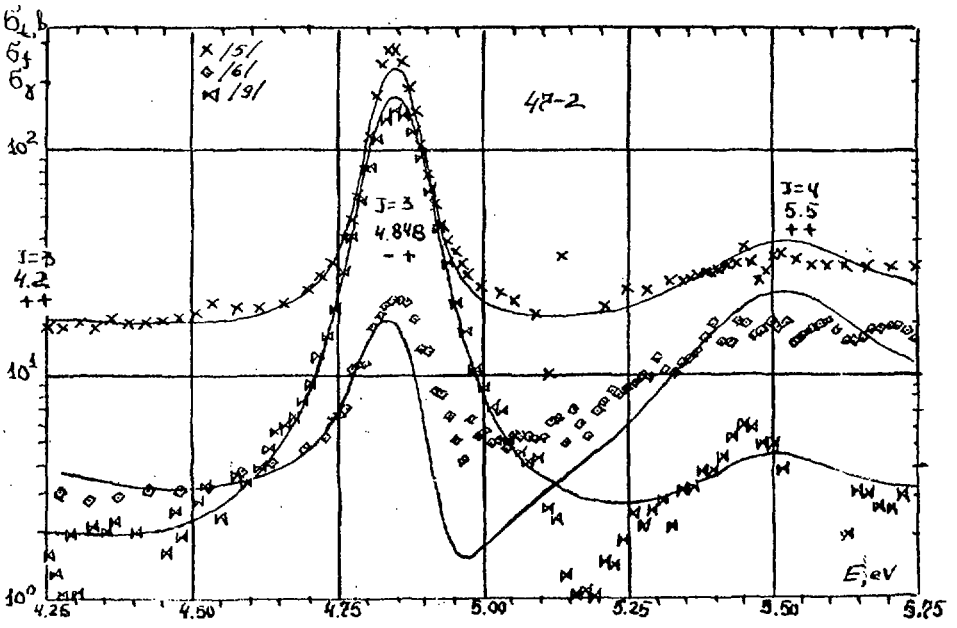

Fig.20 Resonance cross section structure in the 4.25 ÷ 5.57 eV region (version 47-2).

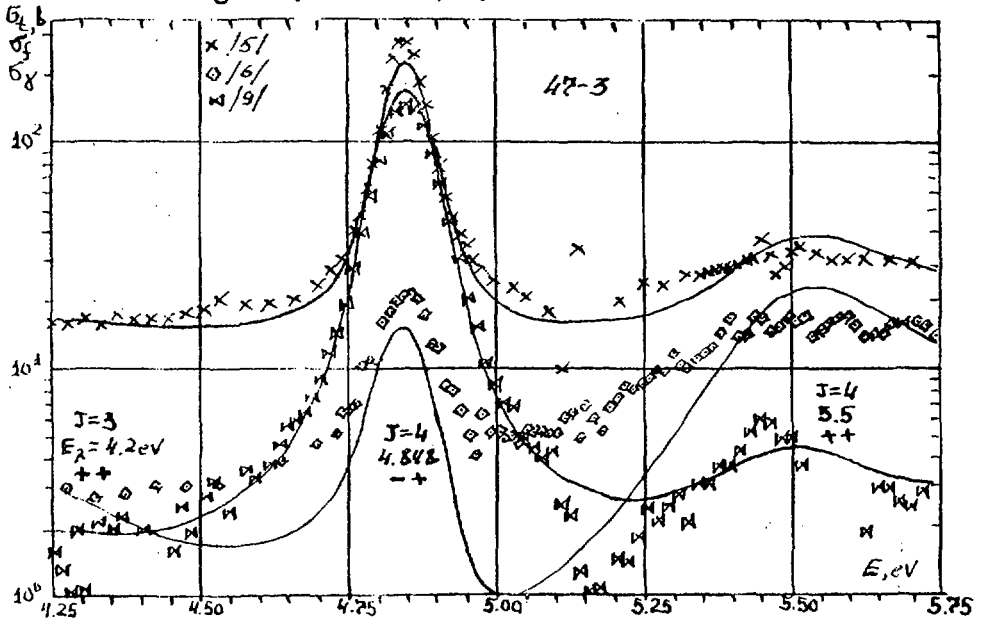

Fig.21 Resonance cross section structure in the 4.25 ÷ 5.75 eV region (version 47-3).

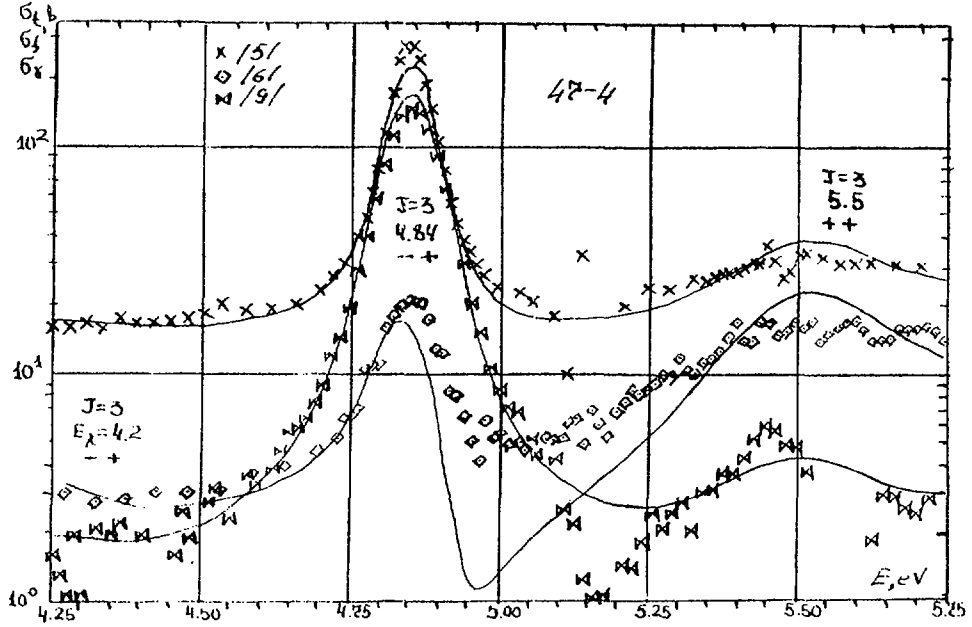

Fig.22 Resonance cross section structure in the 4.25 ÷ 5.75 eV region (version 47-4).

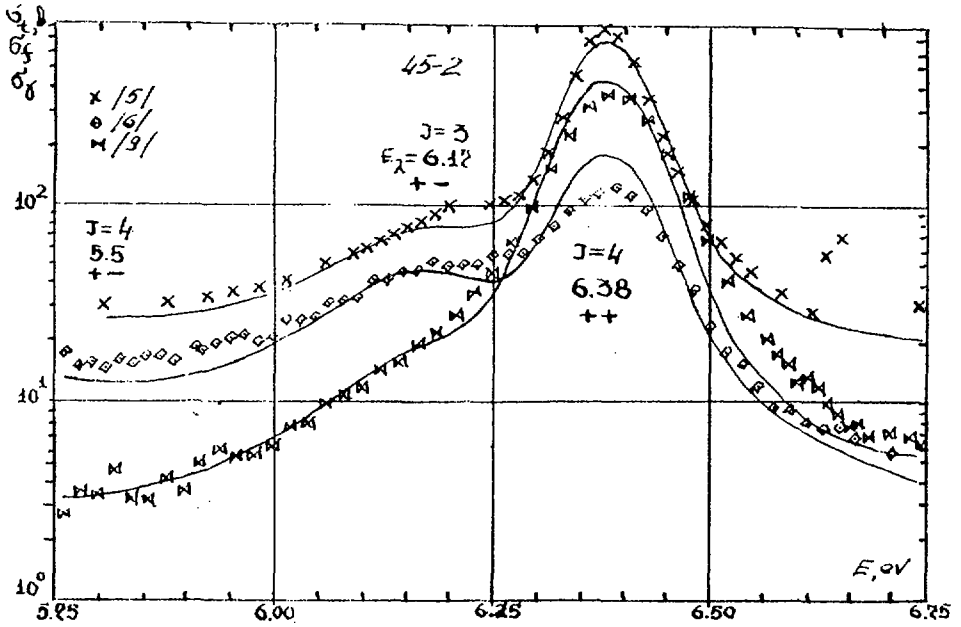

Fig.23 Resonance cross section structure in the 5.75 ÷ 6.75 eV region (version 45-2).

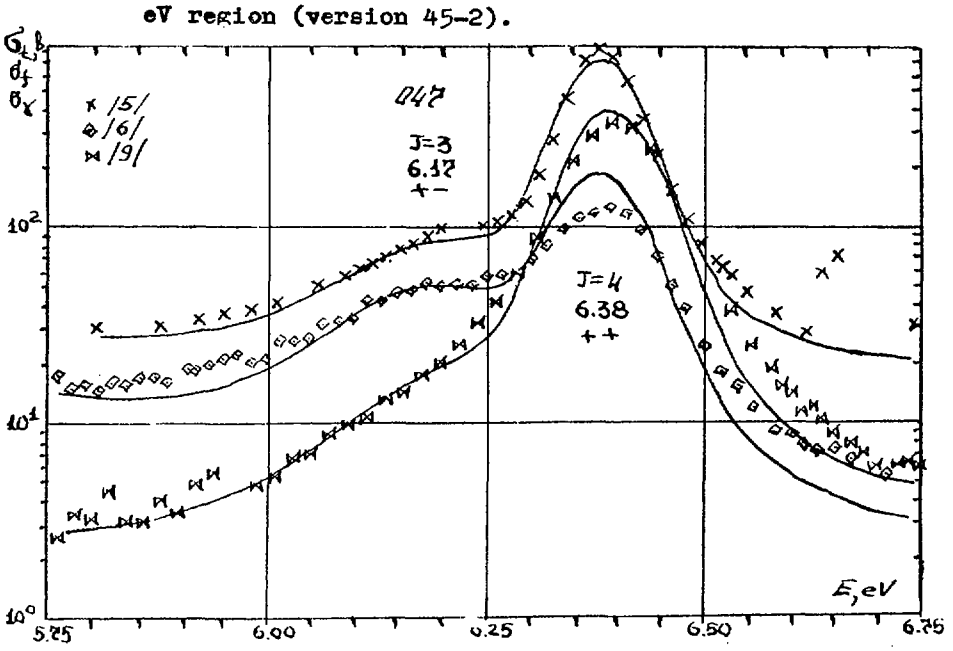

Fig.24 Resonance cross section structure in the 5.75 ÷ 6.75 eV region (version 047).

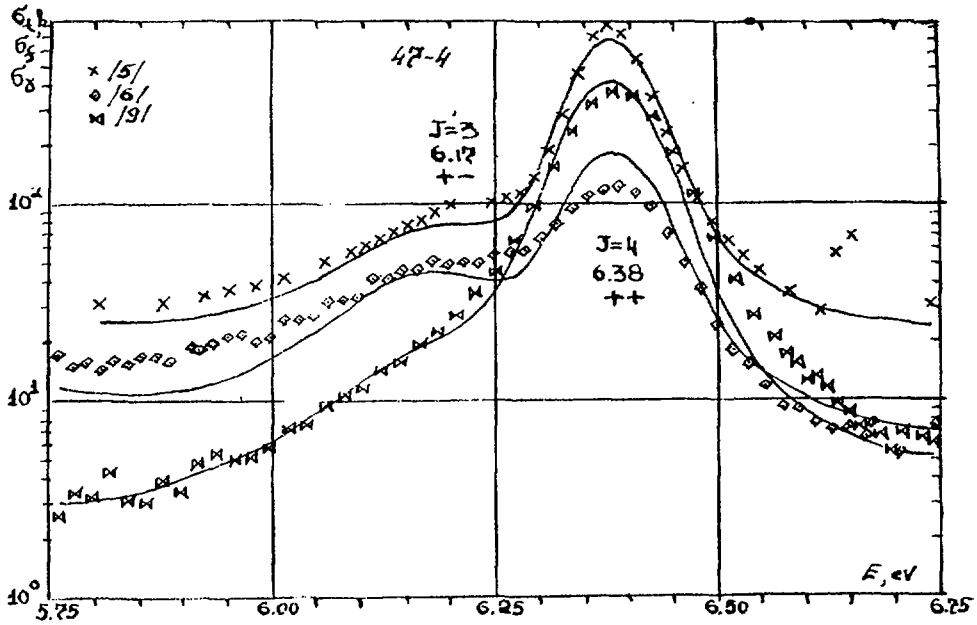

Fig.25 Resonance cross section structure in the 5.75 ÷ 6.75 eV region (version 47-4).

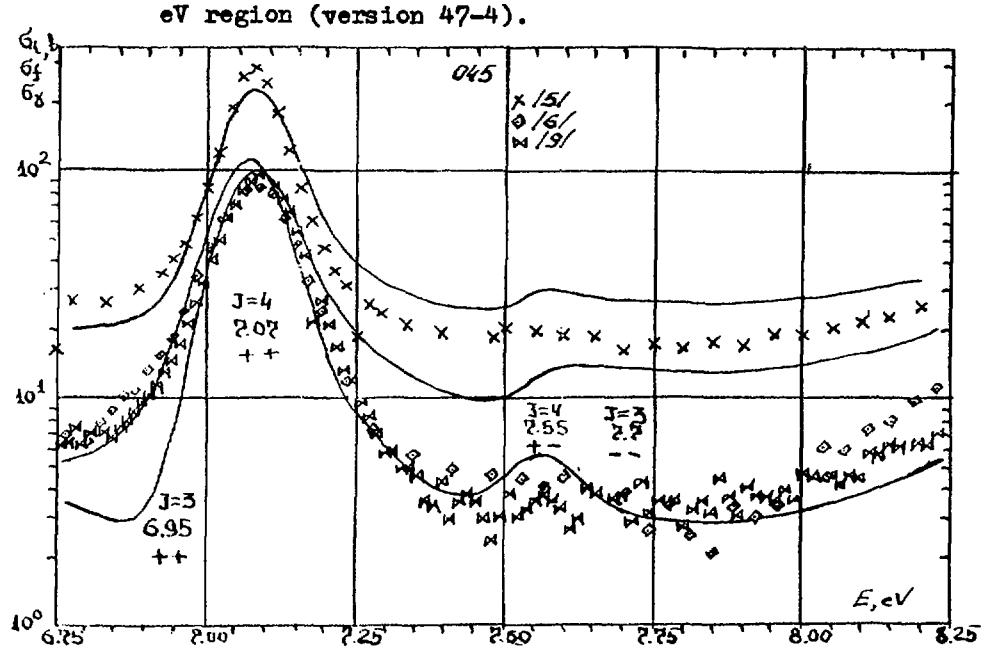

Fig.26 Resonance cross section structure in the 6.75 ÷ 8.25 eV region (version 045).

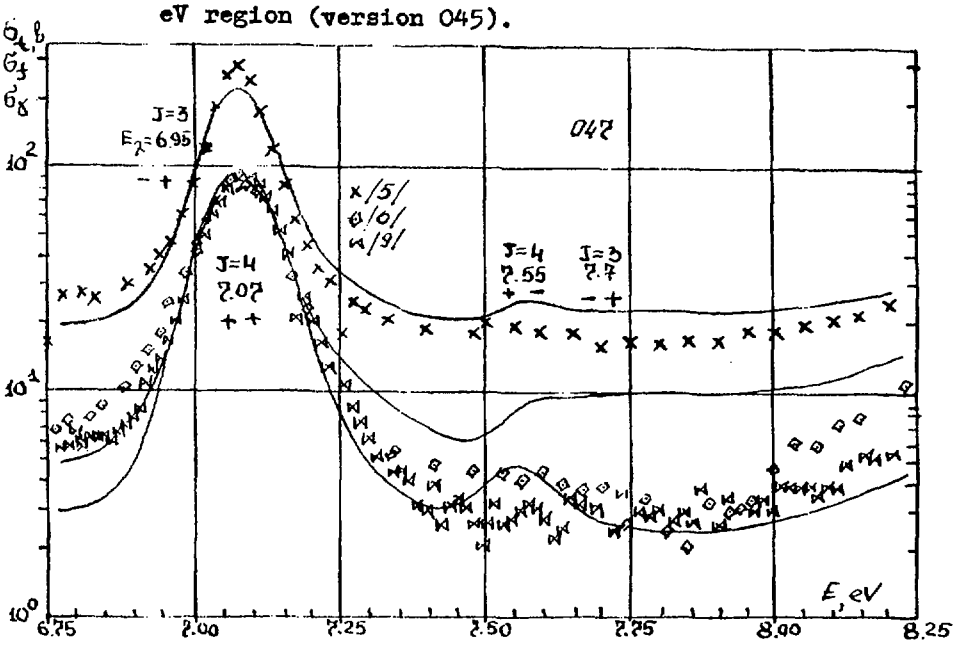

Fig.27 Resonance cross section structure in the 6.75 ÷ 8.25 eV region (version 047).

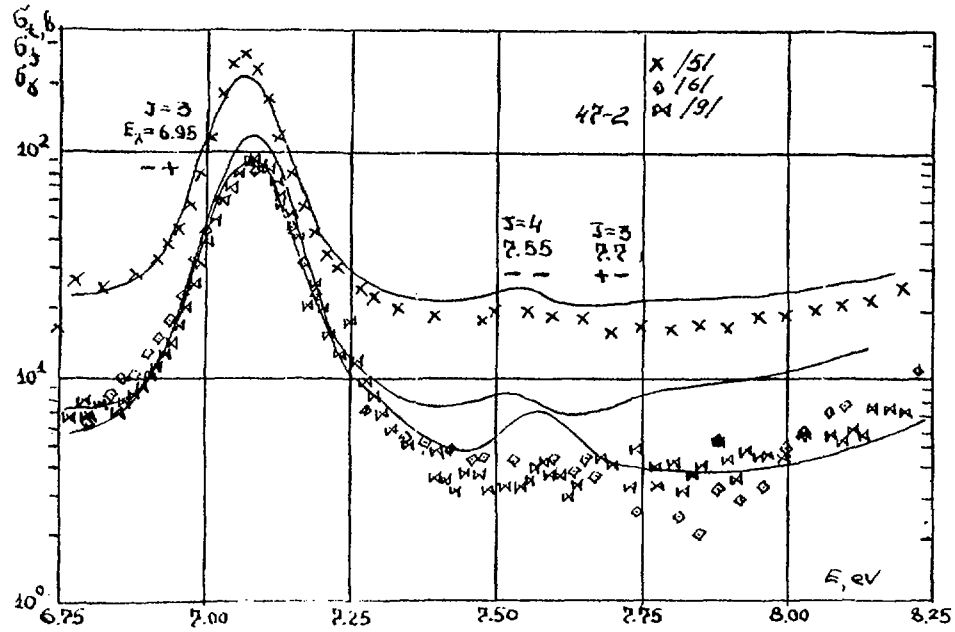

Fig.28 Resonance cross section structure in the 6.75 ÷ 8.25 eV region (version 47-2).

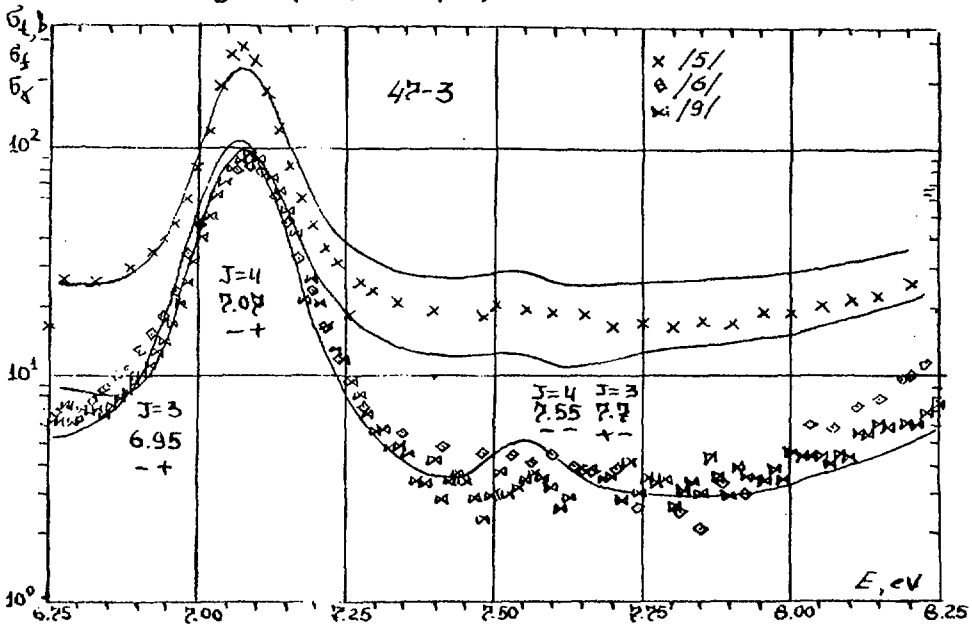

Fig.29 Resonance cross section structure in the 6.75 ÷ 8.25 eV region (version 47-3).

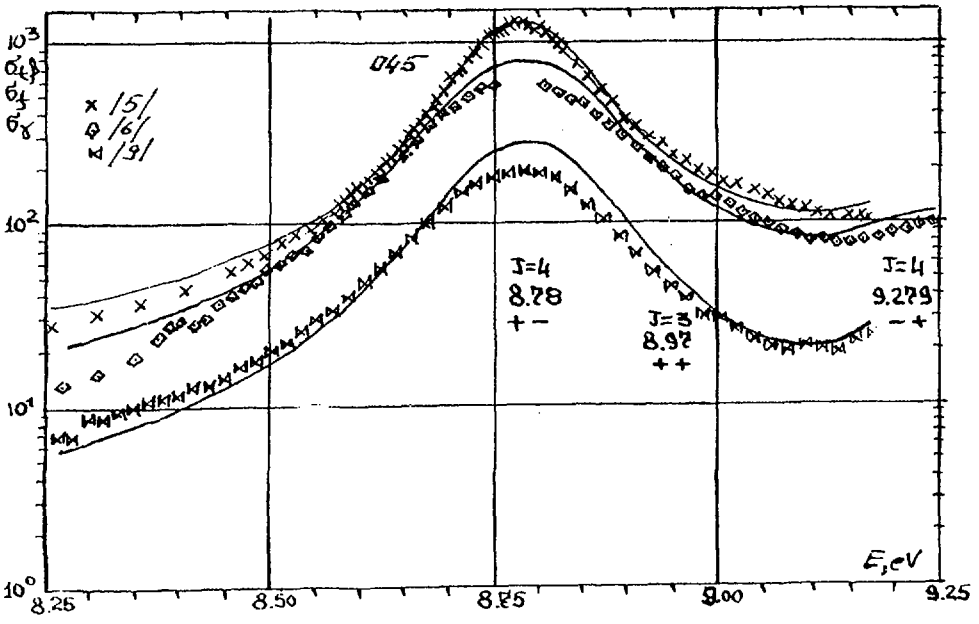

Fig.30 Resonance cross section structure in the 8.25 ÷ 9.25 eV region (version 045).

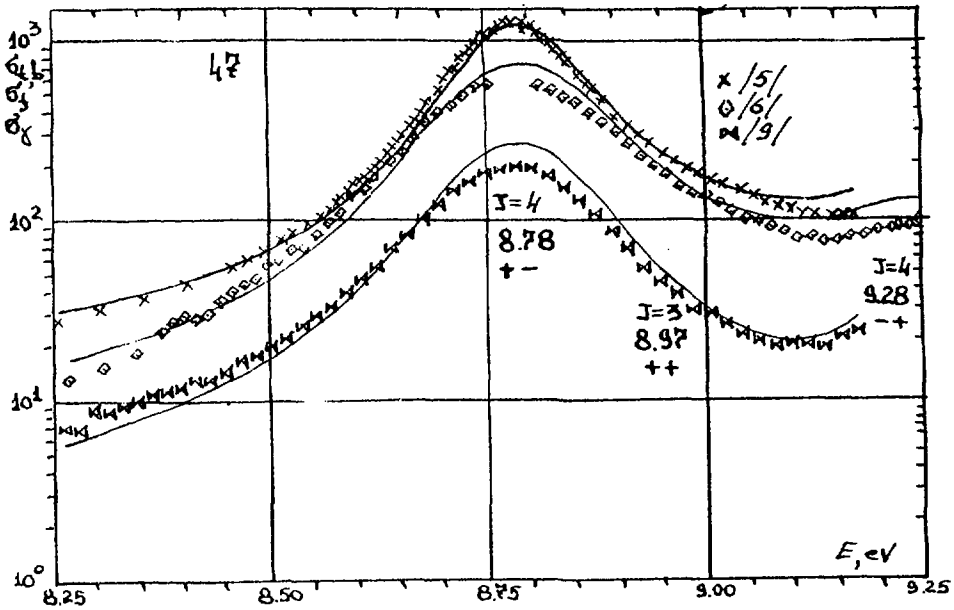

Fig.31 Resonance cross section structure in the 8.25 ÷ 9.25 eV region (version 047).

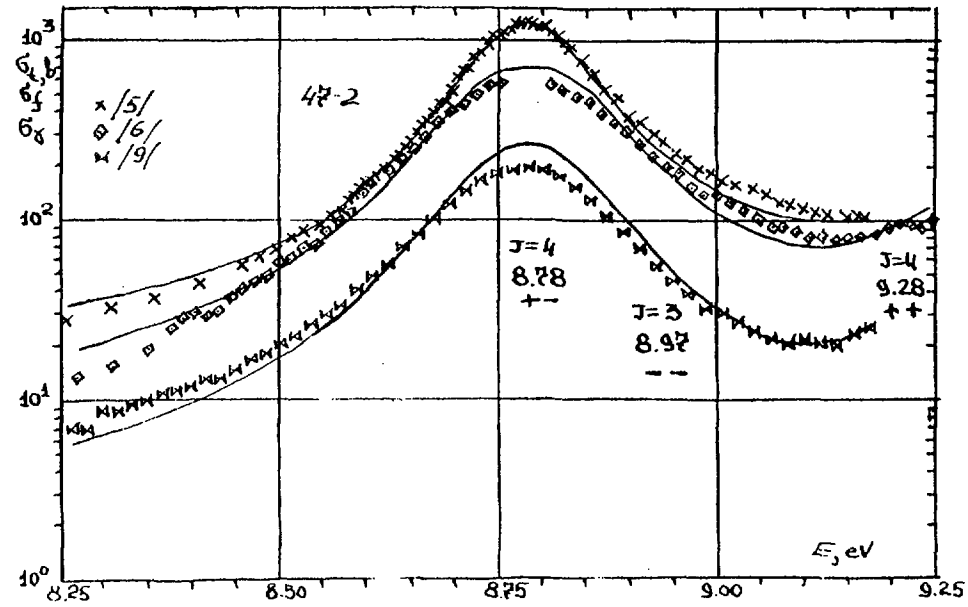

Fig.32 Resonance cross section structure in the 8.25 ÷ 9.25 eV region (version 47-2).

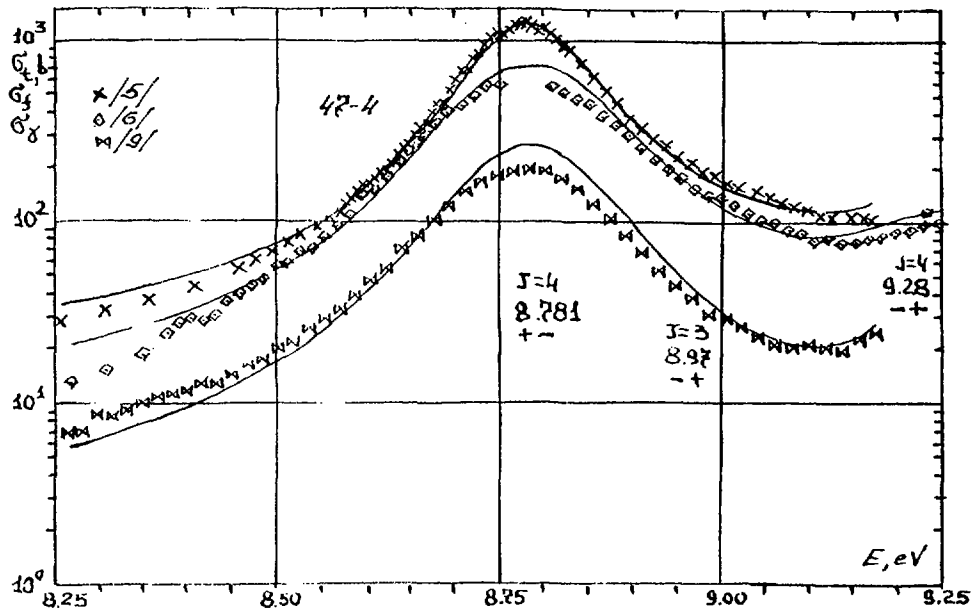

Fig.33 Resonance cross section structure in the 8.25 ÷ 9.25 eV region (version 47-4).

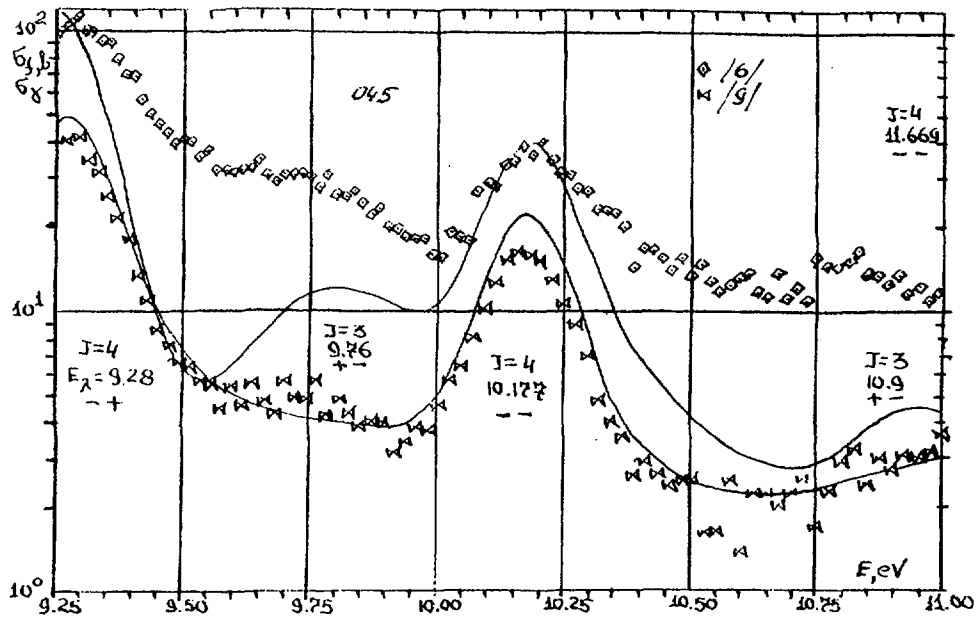

Fig.34 Resonance cross section structure in the 9.25 ÷ 11 eV region (version 045).

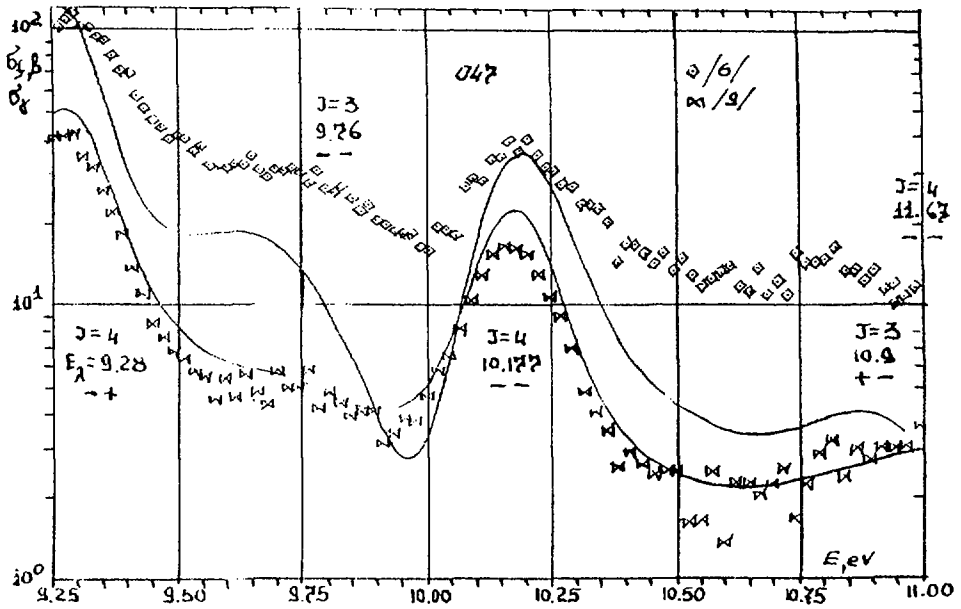

Fig.35 Resonance cross section structure in the 9.25 ÷ 11 eV region (version 047).

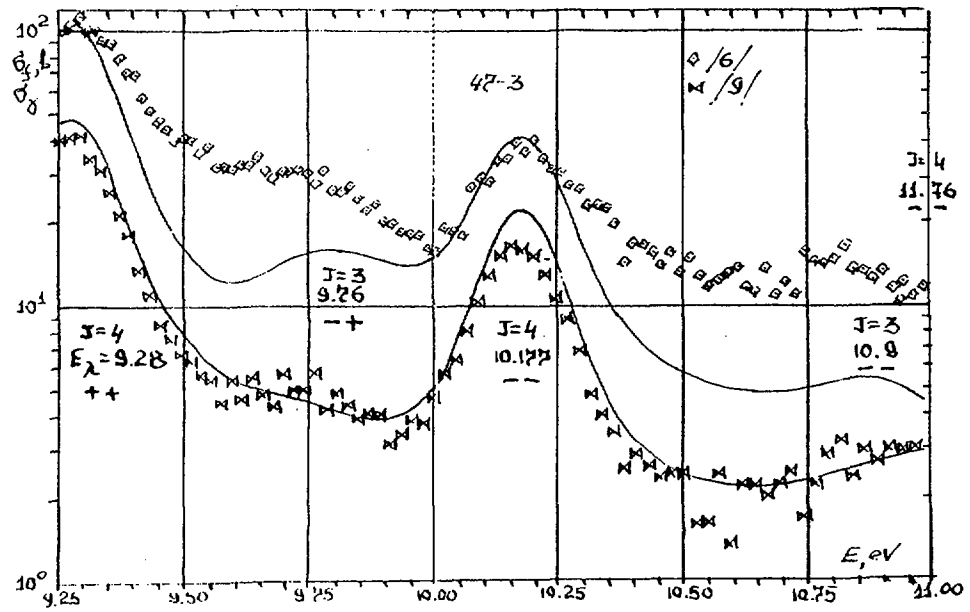

Fig.36 Resonance cross section structure in the 9.25 ÷ 11 eV region (vesrion 47-3).

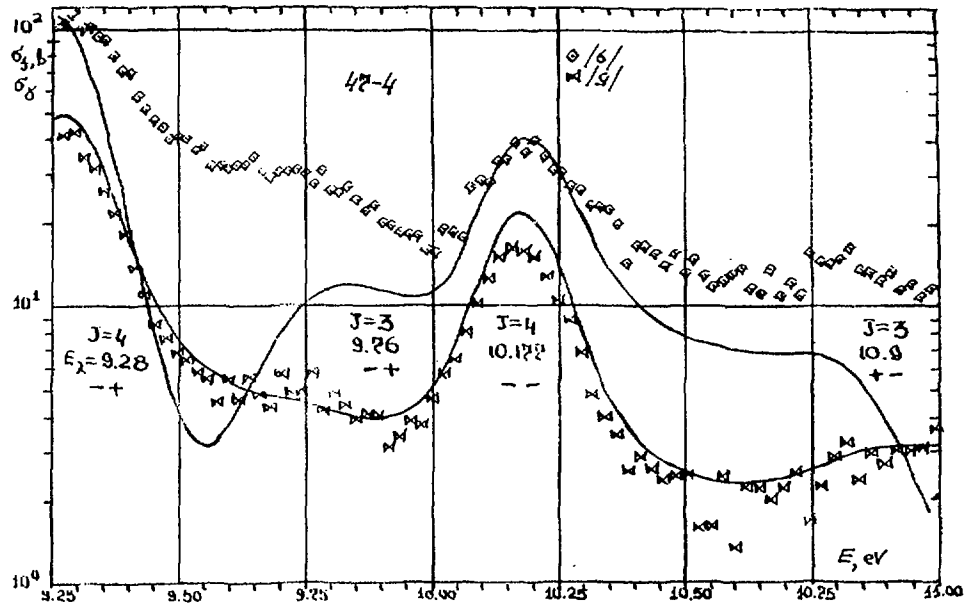

Fig.37 Resonance cross section structure in the 9.25 ÷ 11 eV region (version 47-4).

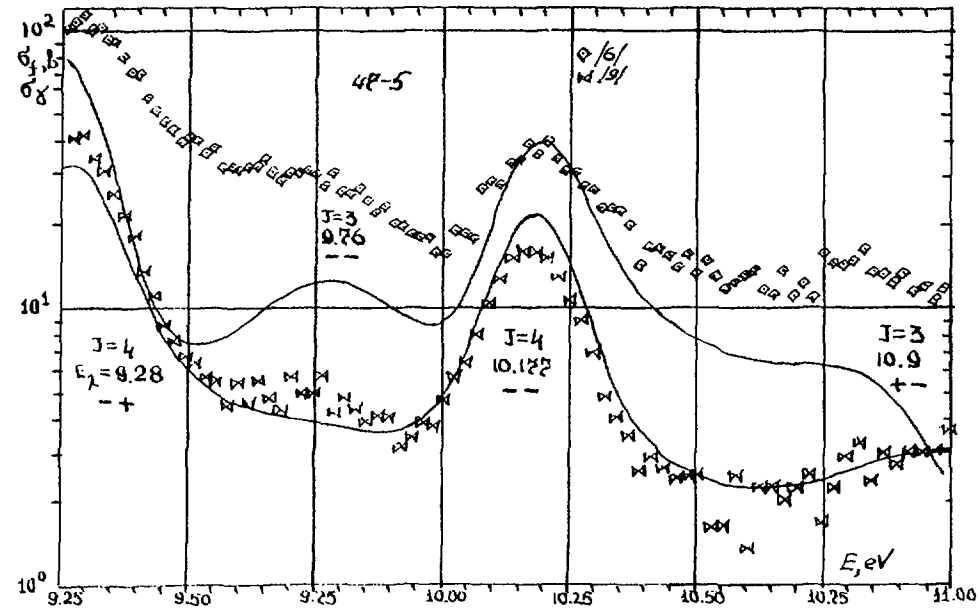

Fig.38 Resonance cross section structure in the 9.25 ÷ 11 eV region (version 47-5). Version 47-5 is obtained from 047 after subsequent optimization in the regions 4-7 eV and 7-10 eV.

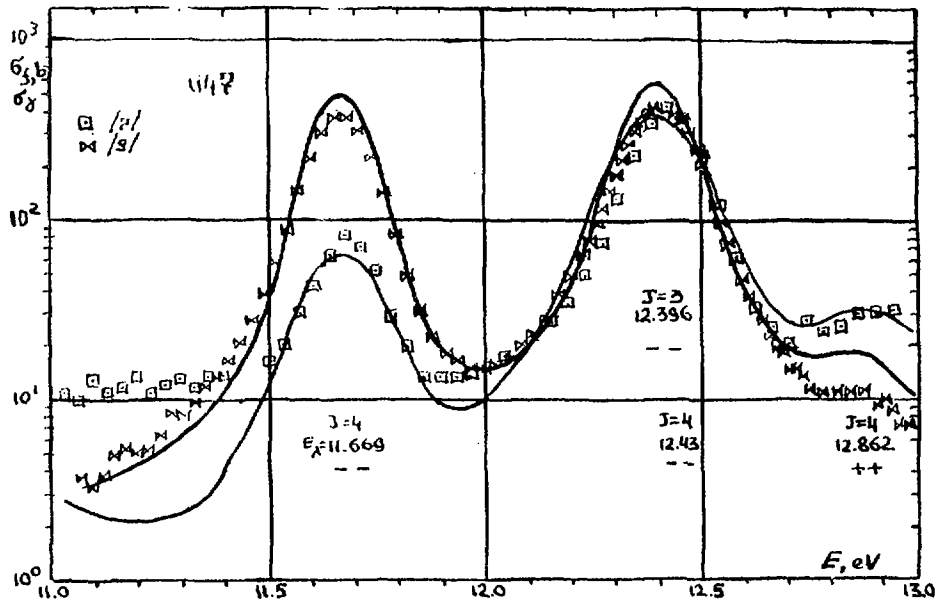

Fig.39 Resonance cross section structure in the 11-13 eV region (version 047).

ON THE NEED FOR CHANGING ENDF/B CONVENTION IN THE REPRESENTATION OF CROSS SECTIONS IN THE UNRESOLVED RESONANCE REGION FOR FERTILE AND FISSILE NUCLEI

S.Ganesan
Reactor Research Centre
Kalpakkam
Tamil Nadu 603 102
INDIA

ABSTRACT

A more fundamental scientific basis for the prediction of Doppler effect in fast reactor systems demands that the usual ENDF/B and KEDAK conventions for the representation of cross sections in the unresolved resonance region should be changed. This conclusion is based upon the experiences in evaluations of statistical mean resonance parameter sets performed at RRC Kalpakkam for use in neutronic calculations of fast reactors in the recent past for ^{235}U, ^{239}Pu, ^{232}Th, ^{233}U and ^{238}U. This paper gives a brief account of several sensitivity studies and neutronic calculations performed using these mean resonance data sets. The existence of non-uniqueness of mean resonance data set has been clearly established and an uncertainty due to the choice of the mean resonance data set is found to be associated with the theoretical calculations of neutronic parameters of reactor systems. This uncertainty identified at Kalpakkam has not received attention in the past and is found to be significant in the case of calculation of Doppler coefficient in fast power reactors. It should have been taken into account in the interpretation of Doppler effect experiments performed in fast critical facilities for both fissile and fertile samples.

The present method of statistical representation of cross sections leads to higher statistical uncertainty as compared to the normal core case in the prediction of Doppler reactivity effect under coolant voided conditions in fast power reactors. Also the effect of inclusion of intermediate structure in the fission cross section for ^{239}Pu on the temperature derivative of self shielding factors is significant and cannot be modelled satisfactorily at present.

If the high resolution cross section measurements on suggested by de Saussure and Perez are made available for main fissile and fertile isotopes, thinning and direct Doppler broadening of the cross section data by preprocessing methods developed by Cullen and his coworkers appear to be a promising approach. Until such time the evaluated nuclear data files should attempt to contain self shielding factors directly evaluated with the support of self indication and transmission measurements instead of the present convention of having mean resonance data sets in the unresolved resonance region.

INTRODUCTION

This paper addresses the effects due to the present methods of representing cross sections and their processing in the unresolved resonance region as followed by American ENDF/B[1,2] and German

KEDAK[3,4] conventions. The author has high regards for and greatly appreciates the pioneering efforts made by ENDF/B and KEDAK evaluators and sincerely has no intention of making a criticism of these voluminous evaluations. Rather, the author sincerely hopes that comments made in this paper based on author's own experiences in the evaluations of mean resonance data sets in the unresolved resonance region may generate valuable discussions and thereby possibly lead, in future, to improved versions of these evaluated nuclear data files to guarantee on adequate and appropriate treatment of the unresolved resonance range with a satisfying fundamental scientific basis.

REMARKS ON PRESENT ENDF/B AND KEDAK CONVENTIONS

We recall briefly that in the unresolved resonance range the evaluated nuclear data file (ENDF/B OR KEDAK) contains as functions of energy, average values for the statistical resonance parameters such as $\overline{\Gamma}_x^{(\ell,J)}(\bar{E})$, $\langle D \rangle^{(\ell,J)}(\bar{E})$ etc. The representation of mean cross sections by these parameters and their distribution functions has provided a convenient method for calculations of self shielded cross sections as functions of background dilutions and temperatures[2,4].

Using well known notations, we recall for convenience here that the mean partial cross sections are calculated from the expressions

$$\langle \sigma_{nx} \rangle (\bar{E}) = 2\pi^2 \lambda^2 \sum_{(\ell,J)} \frac{g_J \overline{\Gamma}_n^{(\ell,J)}(\bar{E}) \overline{\Gamma}_x^{(\ell,J)}(\bar{E})}{\overline{\Gamma}^{(\ell,J)}(\bar{E}) \langle D \rangle^{(\ell,J)}(\bar{E})} S_{x,\ell,J,\bar{E}}$$

$$S_{x,\ell,J,\bar{E}} = \left\langle \frac{\Gamma_n \Gamma_x}{\Gamma} \right\rangle_{(\ell,J)} \cdot \frac{\overline{\Gamma}^{(\ell,J)}(\bar{E})}{\overline{\Gamma}_n^{(\ell,J)}(\bar{E}) \overline{\Gamma}_x^{(\ell,J)}(\bar{E})}$$

The expectation values $\langle \sigma_{nx} \rangle (\bar{E})$ represent the values of mean cross sections for an energy region for which the mean resonance parameters are to be specified. Thus from fundamental physics point of view the mean resonance data set in the unresolved resonance region stand for the representation of the cross section structure in an energy region. However we note that in ENDF/B file and in the KEDAK file the mean resonance data is stored as a function of energy point and not as a function of energy region. This contradicts the physics, if one does not assume that the energy region is to be taken to be roughly equal to the interval between successive energy points at which mean resonance parameters are specified in the file. There is an additional assumption implicit in this method of representation, namely that the energy region should be broad enough to include a number of resonances so as to make the application of statistics precise and at the same time the energy region should be narrow enough so that the mean resonance parameters can be treated as constants within the region. There are no standard procedures for selection of width of energy to specify statistically meaningful representations. These approximations lack a firm theoretical foundation and do not guarantee the generation of correct self shielded cross sections. There is strictly no scientific basis for the present convention of fitting a particular or a subset of the mean resonance data set (such as s or p wave strength functions or a combination of both along with some partial reaction widths such as fission widths, etc.) as a function of energy to reproduce the evaluated total and partial cross sections locally in energy space.

COMMENTS ON ENDF/B AND KEDAK METHODS OF PROCESSING DATA IN UNRESOLVED RESONANCE REGION

A brief comparison of ENDF/B procedure[2] and KEDAK procedure[4] for the processing of unresolved resonance data further supports our case for changing the presently used convention in unresolved resonance range.

In ENDF/B processing code, the mean partial cross sections at an intermediate energy point in the unresolved resonance range are calculated as follows. First, the self shielded cross sections at the end points of an energy interval are calculated using the mean resonance data set specified at the end points of the interval in the data file. The self shielded cross section at the intermediate energy point is then calculated by interpolation of the self shielded cross section values calculated at the end points.

In MILOS-3, the processing code for KEDAK, the mean resonance data itself is first obtained at the intermediate energy point by interpolation of the mean resonance data provided at the end points. The self shielded cross section is then calculated using the mean resonance data set thus obtained at the intermediate energy point. The additional assumption that is implicit in the procedure followed by KEDAK and MILOS is that the mean resonance parameters vary smoothly in the entire unresolved resonance region. There is no physical basis in these procedures followed by ENDF/B and KEDAK conventions though an unfounded argument may be forwarded that these approximations make little difference in the results of neutronic calculations for fast reactor systems. There is no guarantee that the use of such approximations in the processing of mean resonance data in the unresolved resonance region lead to correct calculations of self shielded cross sections and their temperature derivaties.

EXISTENCE OF NON-UNIQUENESS IN THE CHOICE OF MEAN RESONANCE DATA SET AND ITS INFLUENCE ON DOPPLER EFFECT PREDICTIONS

It was demonstrated several years ago by the author[5,6] that there exists different sets of consistent mean resonance data for a given energy region in the unresolved resonance range all such sets leading to the same values of mean partial and total cross sections (within their uncertainties). These consistent mean resonance data sets however lead to different values for self shielding factors and their temperature derivatives. We recall here some results for ^{239}U in Table I where the numbers indicate that the temperature derivative of self shielding factors can have an unacceptable spread of 20%, corresponding to the use of different mean resonance data sets. This spread reduces to about 10% when a good knowledge of $\langle \sigma_t \rangle$ is available. These conclusions are also supported by independent and recent study reported by de Saussure and Perez[7]. As an illustration of non uniqueness of mean resonance data sets we give in Fig.1 histograms of adjusted p wave strength function corresponding to different values of other mean resonance parameters. Though the data used in these calculations correspond to those that were available to the author at that time, the physical conclusions remain valid as confirmed by the recent systematic study of de Saussure and Perez[7]. The values of self shielding factors (SSF) themselves had a spread of 4 to 5% but the temperature derivative of SSFs showed a

TABLE I

Different Sets of Mean Resonance Data Sets Leading to the Same Infinite Dilution Cross Sections But Different Values of Temperature Derivative of Self Shielding Factors (SSF) T : Temperature σ_p : Back ground Dilution (After Ref.6)

Mean resonance Data Set No.	$S_0 \times 10^4$	$S_1 \times 10^4$	$\bar{E}$ (ev)	$10^5 \times \frac{\Delta SSF}{\Delta T}$ for $\Delta T \rightarrow 300$ to $900^\circ K$, σ_p = 100 barns
1	1.18	1.57	0.02355	6.03
2	1.18	1.40	0.02470*	6.18
3	1.18	1.36*	0.02560	5.63
4	0.9	1.68*	0.02355	5.54
5	0.9	2.5	0.01790*	5.21
6	0.9	1.47*	0.02560	5.04

$\bar{E}$ = 7500 eV E_L = 7000 eV E_U = 8000 eV (E_L, E_U define the width of the region)

* Values obtained by adjustment using ADDJA code[5,6].

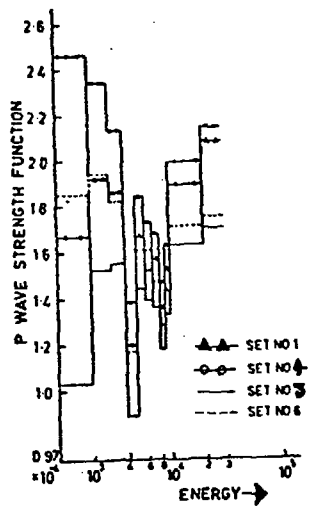

Fig.1 The histograms of the adjusted ℓ wave strength functions corresponding to different correlated values of other mean resonance parameters (After Ref.6)

much larger spread corresponding to the use of different consistent mean resonance data sets.

For a fissile isotope such as ^{235}U or ^{239}Pu the net Doppler effect is the difference between a positive fission source term and a negative absorption term. It was demonstrated[8,9] that the choice of the mean resonance data set in the case ^{235}U can lead easily to a spread of 12% in the calculated value of Doppler reactivity effect of this isotope. The histogram in Fig.2 plotted using results obtained by running ADDJA code[6] illustrates again the existence of non-uniqueness in the choice of mean resonance data set for the isotope ^{235}U. Figure 2 also illustrates that for ^{235}U, the adjusted mean fission width is very sensitive to the assumed value of s wave strength function. In Table II we reproduced our results[9] to illustrate the uncertainty in the calculation of Doppler constant because of parametrization of unresolved resonance range. Because the Doppler coefficient of a fissile isotope ^{235}U entirely depends on unresolved resonance region (which starts from 100 ev onwards) the central Doppler worth calculated for ^{235}U-Enriched uranium sample in ZPR-6-7 assembly is quite sensitive to the choice of the mean resonance data set. We infer from Table II that keeping the spread in S_o to be 4% corresponding to a spread of 2% in $\langle \sigma_f \rangle$ result in a spread of 12% for the calculated Doppler coefficient for ^{235}U in this assembly.

On the other hand in the case of fertile isotopes such as ^{238}U, ^{232}Th etc. the Doppler effect is determined by the negative absorption term. Furthermore, in the case of a fertile isotope such as ^{238}U, the resolved resonance region extends to a few kev thereby

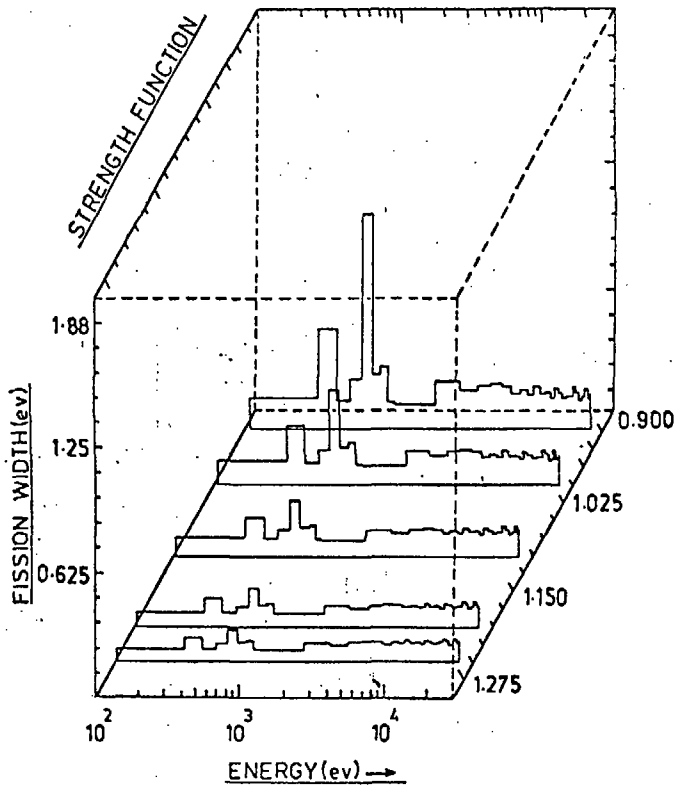

Fig.2 Illustration of existence of non-uniqueness in the choice of mean resonance data set for ^{235}U. Adjusted mean fission width is plotted against s wave strength function as a function of energy to reproduce evaluated mean fission cross sections (After Ref.8, p.131) See Text. In the sensitivity study the variation in S_o is limited.

reducing the contribution of unresolved resonance region contributed by this isotope (in Liquid Metal Cooled Fast Reactors (LMFBRs) fuelled with PuO_2-UO_2 fuel). The breakup of the contributions to Doppler effect arising from unresolved and resolved resonance ranges indicate that the uncertainty in the net Doppler coefficient of ^{238}U is expected to be about 5% due to non-uniqueness in the mean resonance data sets in the normal sodium-in case in LMFBRs and will be more (by about 8%) in the coolant voided i.e. sodium-out condition of the power plant. This conclusion is reached by assuming that ~ 12% spread exists in the temperature derivative of self shielding factors because of non-uniqueness in the choice of mean resonance data sets in the unresolved resonance range. Since the Doppler effect under coolant voided conditions is important from safety considerations in LMFBRs, we focus our attention in the next section on this aspect.

TABLE II

Dependence of Central Doppler Worth Calculated for the ^{235}U - Enriched Uranium Sample in ZPR-6-7 Assembly on the Choice of the Mean Resonance Data Set (After Ref.8)

Mean Resonance Data Set with the Strength Function S_o and the corresponding correlated Mean Fission Widths	Calculated Values (In hour/kg)		
	Central Worth at 1057°K	Central Worth at 300°K	Central Doppler Worth
1.10×10^{-4}	134.232	133.212	1.020
1.25×10^{-4}	130.125	128.717	1.408

RELIABILITY OF CALCULATED DOPPLER CONSTANT AS A FUNCTION OF SODIUM VOIDING IN LMFBRs.

The contributions of ^{238}U, ^{239}Pu and ^{235}U to whole core Doppler effect is typically in the ratio +134: -20: -0.5 for a PuO_2-UO_2 fuelled fast reactor of 500 mwe size. The whole core Doppler effect is dictated both in sign and in magnitude by ^{238}U isotope and is negative. The ^{239}Pu contribution is found to be positive and is typically about 15 to 20% of the magnitude of ^{238}U Doppler effect. The Doppler effect of ^{235}U is positive but however negligible in PuO_2-UO_2 fuelled systems as the number of ^{235}U atoms in such systems are relatively small.

Calculations of the distribution of Doppler effect in energy for the whole core of ZPR-6-7 assembly were performed corresponding to a temperature rise from 300°K to 2100°K, using DOP code[10] and the results are briefly shown in Table 3 for both sodium-in and sodium voided conditions. When there is voiding of sodium in the core of LMFBR the resultant hardening of the neutron spectrum leads to a lower value for the magnitude of the negative Doppler coefficient thus lowering the plant safety factor for LMFBRs. The unresolved resonance region contributes more to the Doppler

Table III

Relative Contributions to Doppler Effect From Resolved and Unresolved Resonance Regions (R.R and U.R.R). The values have been normalized to the contributions to Doppler change from the respective nuclides (After Ref.11)

Nuclide	R.R. (kev)	U.R.R. (kev)	Relative contributions to Doppler change in Percentage			
			Sodium-in		Sodium-out (full core)	
			R.R.	U.R.R.	R.R.	U.R.R.
^{238}U	0-3.36	3.36-100.0	59.72	40.28	36.14	63.86
^{239}Pu	0-0.455	0.455-100.0	22.57	77.43	10.43	89.57
^{235}U	0-0.101	0.101-100.00	4.36	95.64	1.03	98.97

Calculated whole-core Doppler change for ZPR-6-7; 300°K to 2100°K

$\left\{ \frac{\Delta k}{k} \right\}$ Sodium-in : 0.015371

$\left\{ \frac{\Delta k}{k} \right\}$ Sodium-out : 0.009676

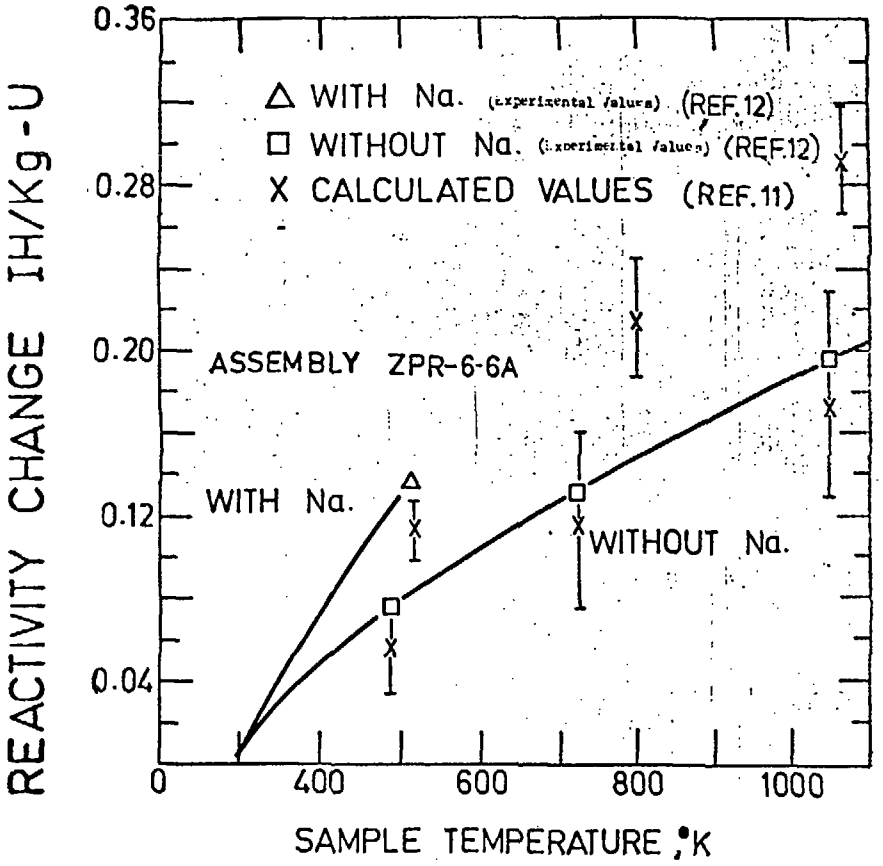

Fig.3 Comparison of Calculated Doppler effect with measured values of Doppler effect for natural UO_2 sample in normal (sodium-in) and sodium-out conditions. The calculated values of Doppler effect in the sodium-voided case is shown to have higher uncertainty as a result of statistical representation of cross sections. The error bars are not quantitative but illustrate the effects relative to normal core case. (after Ref.11).

effect in the sodium voided case and thus the reliability of the Doppler constant reduces as a function of sodium voiding in LMFBRs because of statistical representation of cross sections in the unresolved resonance range[11].

Though a calculation of Doppler effects of natural UO_2 Doppler measurements performed in ZPR-6-6A assembly shows an unalarming underprediction of around 15 to 20% we emphasize that in the case of voided core the uncertainty in the calculated magnitude of Doppler effect is more in sodium-out case than sodium-in case. This uncertainty bar is qualitatively shown to be higher in our interpretations of natural UO_2 Doppler measurements performed[12] in ZPR-6-7 assembly in Fig.3 for the sodium-out case. From safety considerations in LMFBRs the Doppler coefficient under sodium voided conditions is to be known relatively with a higher accuracy. Unfortunately the present method of representation of cross sections by BNAK/B convention makes the calculated value of Doppler coefficient under voided conditions to have higher uncertainties.

EFFECT OF INTERMEDIATE STRUCTURE IN $\langle \sigma_f \rangle$ OF ^{239}Pu ON DOPPLER EFFECT

The effect of inclusion of intermediate structure in $\langle \sigma_f \rangle$ of ^{239}Pu on Doppler effect by using 'ladder approach' has been studied by several workers[13-15]. In one case the ladder of resonances is generated using constant mean fission width and in another case the mean fission width is modulated using intermediate structure. The technical details of this statistical method have been described elsewhere[14,15].

Table IV gives the results. The temperature derivative of the self shielding factor for the fission process changes significantly for low dilutions i.e. higher self shielded conditions as a result of inclusion of intermediate structure. As expected, for larger dilutions the self shielding factors and their temperature derivatives are less sensitive to the inclusion of intermediate structure. This method of assessing the effect of intermediate structure is incomplete as it covers a small energy region and merely demonstrates qualitatively that the effect is significant. Also the models used in the study are subject to many questionable assumptions. (See References 13 to 15 for the details) apart from the inherent statistical error associated with sampling. The method itself is laborious and demands a large memory on the computer.

CONCLUSIONS AND REMARKS

1. The present convention of representation of cross sections in the unresolved resonance region and the processing of these data by ENDF/B and KEDAK conventions lack any scientific foundation and do not guarantee correct generation of self shielded cross sections and their temperature derivatives.

2. The analysis of Doppler effect measurements has ignored the existence of an uncertainty in the calculated value of Doppler constant arising due to the nonuniqueness in the choice of mean resonance data set used to represent cross sections in the unresolved resonance region. This uncertainty is significant in the case of fissile isotopes such as ^{239}Pu and ^{235}U in the case of normal core of LMFBR. In the case of sodium

Table IV

Effect of Intermediate Structure (IS) on Self Shielding Factors (SSF) of Fission Process, Energy Region 600 - 700 eV (After Ref.15)

$\overline{\Gamma_f}^{1/4} = 0.006$ eV ; $\langle \sigma_f \rangle = 4.494$ barns

Case	σ_p = 100 barns			σ_p = 1000 barns		
	T = 300°K	T = 900°K	$\frac{\Delta SSF}{\Delta T}$	T = 300°K	T = 900°K	$\frac{\Delta SSF}{\Delta T}$
With IS	0.7877	0.8061	3.1×10^{-5}	0.9615	0.9700	1.42×10^{-5}
Without IS	0.7318	0.7535	3.6×10^{-5}	0.9481	0.9568	1.45×10^{-5}

voided core, this uncertainty in the Doppler effect of the fertile isotope ^{238}U is also significant.

3. With the present method of representing cross sections in the unresolved resonance range the inclusion of intermediate structure cannot be satisfactorily treated to yield correct self shielding factors and their temperature derivatives.

4. If the high resolution cross section measurements, as suggested by de Saussure and Perez[16] are made available for main fertile and fissile isotopes, thinning and direct Doppler broadening of the cross section data by preprocessing codes developed by Cullen[17] and his coworkers appear to be a promising approach.

Until such time as pointed out elsewhere[11,18], the evaluated nuclear data files should attempt to contain self shielding factors directly evaluated with the support of self-indication and transmission measurements instead of the present convention of having mean resonance data sets in the unresolved resonance region.

As summarized very recently in an excellent review by de Saussure and Perez[7], other methods of treatment of unresolved resonance region suggested by Pearlstein[19], Gur and Yiftah[20] and Cullen[17] should be examined. Till high resolution cross section measurements are made available one of these alternate treatments perhaps can replace the existing ENDF/B convention in the unresolved resonance region.

REFERENCES

1. ENDF-102, Data Formats and Procedures for the Evaluated Nuclear Data File, ENDF; Revised by R.Kinsey, October 1979, BNL-NCS-50496 (1979).

2. H.Henryson II, B.J. Toppel and C.G.Stenberg, MC^2-2: A Code to calculate Fast Neutron Spectra and Multigroup Cross Sections ANL-8144 (ENDF 239) (1976).

3. B.Krieg, 'The KEDAK Program Compendium, Part II KEDAK Basic Management' KfK -2387/II (1977) Kernforschungszentrum, Karlsruhe.

4. I.Broeders et al., 'MIGROS-3 : A Code for the Generation of Group Constants for Reactor Calculations From Neutron Nuclear Data in KEDAK Format', KfK-2388, Kernforschungszentrum, Karlsruhe (1977).

5. S.Ganesan, 'Evaluation of Statistical Resonance Parameters for ^{238}U using ADDJA code in the Energy Range 4 to 25 keV, in Proceedings of the Symposium on Reactor Physics p.559-563, BARC, Bombay (1976).

6. S.Ganesan, Atomkernenergie 29, 14 (1977).

7. G.de Saussure and R.B.Perez, 'Representation of the Neutron Cross Sections of Several Fertile and Fissile Nuclei in the Resonance Regions', CuL-TM/7945 (1981).

8. S.Ganesan, 'Studies on Sodium Void and Doppler Reactivity Effects in Fast Power Reactors' Ph.D. Thesis University of Bombay (1979).

9. S.Ganesan, Nucl. Sci. Eng., 74, 49 (1980).

10. S.Ganesan and K.M.Hamanadhan, 'The Calculation of Isotopic and Groupwise Breakdown of Doppler Constant for Fast Systems, 'Internal Note RRC-FRG/01100/76/RP-103 (1976), Kalpakkam

11. S.Ganesan and K.K.Ramanadhan, 'On the Effect of Using Statistical Approach to the Unresolved Resonance Region on the Reliability of the Calculated Doppler constant As a Function of Sodium Voiding in a Fast Critical Assembly', Internal Note: MRC-PHY/01100/77/IR-118 (1977) Kalpakkam.

12. R.B.Pond and J.W.Daughtry, 'Uranium Doppler Effect Measurements in ZPR-Assembly 6A, in ANL-7910 (1972) p.166.

13. J.P.L.Heriteau and J.Neviere, 'Influence of Intermediate Structure in Subthreshold Fission on Self Shielding Factor and Doppler Effect', Proceedings of Third Conference on Neutron Cross Sections and Technology CONF-710301, Vol.2, p.848 (1971).

14. R.N.Hwang, 'Some Recent Developments in Resonance and Doppler Theory' Proceedings of National Topical Meeting on New Developments in Reactor Physics and Shielding, CONF-720901, Vol.2, p.1166 (1972). See also R.N.Hwang, 'Theoretical consideration Pertinent to the treatment of Unresolved Resonances' in BNL-50387 (1973).

15. S.Ganesan, 'A Study of the Effect of Intermediate Structure in the Fission Cross Section of ^{239}Pu on Self Shielding Factors' Proceedings of the Symposium on Reactor Physics p.564-568, BARC, Bombay (1976).

16. J. de Saussure and P.B.Perez, Nucl. Cross Section Technology I, 371 (1975) NBS-SP 425.

17. D.E.Cullen, UCRL-50400 Series, Vol.20 (1978) Vol.17, Part D (1980); References made in the latter report to the earlier works of D.E.Cullen and his coworkers describe the LINEAR-RECENT-SIGMA1-GROUPIE code system. See also D.E.Cullen, Nucl. Sci. Eng. 55, 387 (1974).

18. S.Ganesan, RRC-42 (1980);

19. Pearlstain, Nucl. Sci. Eng. 58, 354 (1975) and 68, 10 (1978).

20. Y.Gur and Yiftah Nucl. Sci. Eng. 65, 468 (1978).

Some Highlights in the Evaluations of the Thermal Cross Sections and Resonance Parameters of the Actinides*

S. F. Mughabghab and M. Divadeenam
Brookhaven National Laboratory
Upton, New York 11973

ABSTRACT

The resonance parameters and thermal cross sections of $^{235,238}U$ and $^{239-242}Pu$ are reevaluated by considering the measurements carried out since 1973. Capture, scattering, fission cross sections as well as resonance integrals are calculated from the parameters and are compared with experimental values with the objective of achieving consistency between calculations and measurements. The Dyson-Mehta Δ_3 statistical analysis was applied in order to calculate average level spacings. Calculations of average radiative widths based on systamatics are carried out and are compared with experimental values as well as with Moore's and Lynn's estimates.

1. INTRODUCTION

An accurate knowledge of the individual as well as average resonance parameters and thermal neutron cross sections of the actinides is important in the design of thermal and fast reactors, in doppler coefficient studies, and optical model and systematic investigations. Since 1973, several data sets became available in the open literature and via private communications which warranted a new reevaluation of these parameters. The final results will be published shortly.[1]

* Research supported by the U.S. Department of Energy

2. THE EVALUATION PROCEDURE

We briefly describe the steps adopted in the evaluation of the resonance parameters. The evaluation of the thermal cross sections was discussed previously in detail.[2]

(1) The first step in the evaluation of the resonance parameters is compilation of the data. A complete and correct documented data base is imperative. The National Nuclear Data Center CSISRS Library was used for this purpose. A computerized resonance parameter file supplemented by the most recent data which was obtained via private communications was created.

(2) The second step is a reduction of the various data sets to a standard form such as $g\Gamma_n$ values.

(3) This is followed by grouping of the various data sets according to resonance energy and $g\Gamma_n$ values, taking the weighted averages, and calculating the internal and external errors for the parameters of each resonance.

(4) Examination of the results of the previous step and making necessary adjustments.

(5) The computerized recommended resonance parameter file is subsequently transformed into an ENDF-type format. Then physics checking computer codes partially based on ENDF codes operate on this file to calculate capture, fission, scattering (coherent and incoherent amplitudes) cross sections as well as resonance integrals and strength functions.

(6) In addition, staircase plots of the cumulative number of resonances and reduced neutrons widths are produced. Values of the Δ_3 statistics are calculated and are compared with experimental values to check on the possible missing or misassigning of the ℓ and J values of resonances.

(7) Consistentcy checks between differential and integral measurements are made. Possible adjustments in the parameters of the low-lying resonances are made to achieve this objective and/or negative energy resonances are postulated.

It may be necessary that several iterations of these steps are required before a satisfactory recommended set of resonance parameters is obtained.

To estimate reliable average Level spacings tests other than the Porter-Thomas distribution are required for estimating whether any levels have been missed. The Dyson-Mehta Δ_3 statistics[3] can provide an independent test.

Both Dyson's ensemble theory and Wigner's random matrix theory[4] predict high correlation of single population of levels resulting in approximately equal spacings. This means that the levels are highly ordered rather than randomly distributed.

The Δ_3 statistics is sensitive to the position of individual levels and is given by

$$\Delta_3 = \min_{A,B} \frac{1}{\Delta E} \int_o^{\Delta E} [N(E) - AE - B]^2 \, dE$$

$$\langle \Delta_3 \rangle = \frac{1}{\pi^2} [\ln(N) - 0.0687]$$

$$\text{Error } (\langle \Delta_3 \rangle) = 0.11$$

Based on Monte Carlo calculations Georgopulos and Camarda[5] have provided graphs which help in determining the number of missed levels by making use of the Δ_3 statistics calculated for the observed single population sequence. The average level spacings were evaluated by applying the Δ_3 statistics in combination with staircase plots of the cumulative number of resonances versus neutron energy as shown in Fig. 1.

A brief description of the results of the evaluation follows.

3. RESULTS

^{235}U:

^{235}U is an important material in connection with power reactors and related applications. The need for an evaluated set of resonance parameters for this material need not be emphasized.

Some of the problems associated with the ^{235}U resonance parameters have been discussed by Keyworth and Moore[6] and Moore et al.[7] Since 1973, no new measurements of the widths of resonances of ^{235}U have been made.

In addition to Keyworth's[8] polarization measurements Michaudon et al.,[9] and Blons et al.,[10] reported total and fission cross-section measurements which extended up to 150 eV. Also three other data sets by Ryabov et al.,[11], Corvi et al.,[12] and Felvinci[13] were considered to arrive at a recommended resonance parameter set for ^{235}U. Other data sets available at the NNDC (CSISRS Library) were also surveyed for the purpose of ^{235}U resonance parameter evaluation.

In evaluating the resonance parameters an attempt was made to conserve fission areas with proper $2g\Gamma_n$, Γ_f and Γ_γ ($\Gamma \sim \Gamma_f + \Gamma_\gamma$; $\Gamma_n \ll \Gamma$) and these

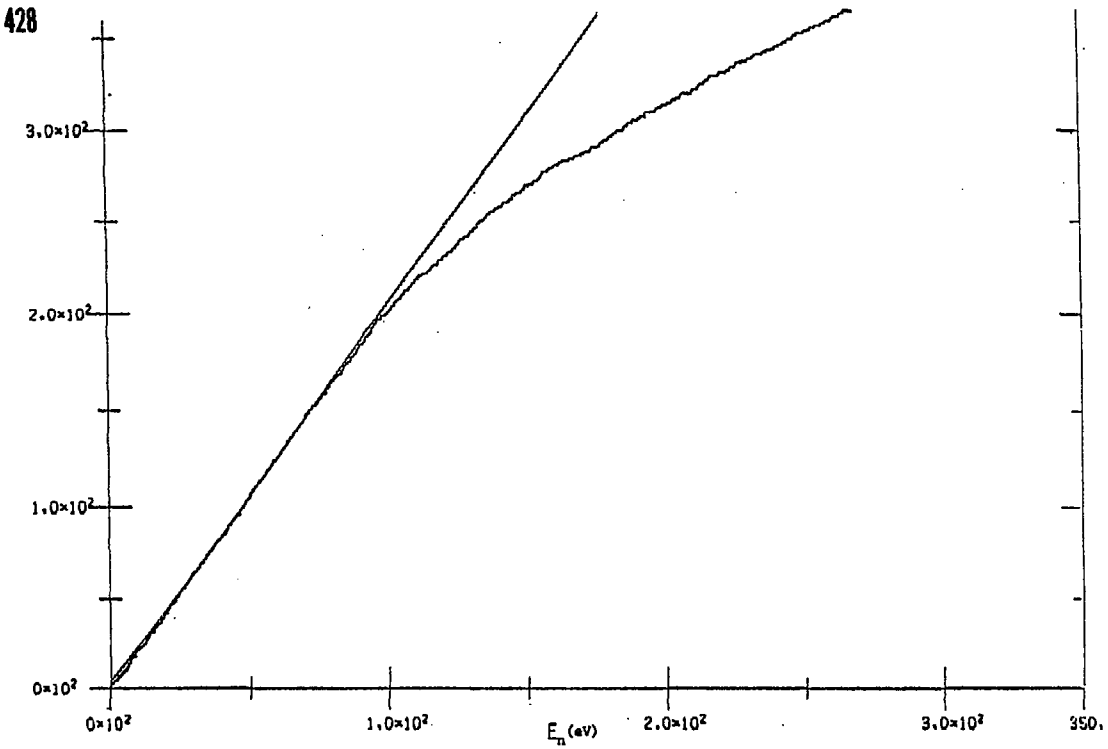

Fig. 1. Staircase plot of ^{235}U resonances.
The average spacing obtained from the straight line least squares fit yields 0.496 eV is consistent with the value of 0.49 derived from Δ_3 statistics.

parameters were mainly derived from Moore et al.,[14], Michaudon et al.,[9] and Blons et al.,[10] combined set, and Ryabov et al.,[11] data set.

The spin assignments made by Keyworth et al.,[8] based on their polarization measurements were adopted up to 300 eV. However, the resonance parameters $2g\Gamma_n$, Γ_f, Γ_γ, and $\sigma_o\Gamma_f$ extend up to about 150 eV, beyond which only the spins are given extending up to 300 eV. More precise capture measurements would reduce the errors on Γ_γ values and would provide a further check on the total widths required to describe resonances. The total widths derived by Michaudon et al.,[9] are not always compatible with the fission widths and areas reported by Moore et al.[14] The recommended parameters reflect the single-level aspect of the Breit-Wigner formalism. These should not be compared with any multi-level parameters for ^{235}U.

A calculation of the thermal capture and fission* cross-sections indicates that bound levels are required to describe these cross-sections and the capture and fission resonance integrals as well. Table I presents the recommended average resonance parameters. For comparison Moore's[15] and Lynn's[16] estimates of average capture widths are included along with our own estimation based on the expression derived by Malecky[17] and which was derived from systematics.

Since the resonance spins are uniquely assigned ($J^\pi=3^-$ and 4^-) for s-wave resonances, ^{235}U provides a very good example for testing the Δ_3 statistics on a target with nonzero spin: Each (ℓ,J) sequence of resonances may be considered as a pure sample for statistical purposes. The Δ_3 values calculated for the observed sequence of levels for J=3 and 4 are listed in Table II at E_n=60 eV, 70 eV and the maximum energy considered for evaluating the average level spacing for each set. The corresponding theoretical (Δ_3) values are also included with 0.11 as uncertainty.

In the case of J=3 resonances the experimental Δ_3 value agrees with the theoretical value up to about 100 eV. Based on the Δ_3 value of 0.366 one could estimate the number of missed levels with the help of probability curves

* A reevaluation of the ^{235}U thermal parameters and resonance integrals is in progress, as such consistency check of the differential and itegral measurements was not undertaken yet.

provided by Georgopulos and Camarda[5]. The number of missed J=3 levels seems to be about 5. Hence the recommended average level spacing for spin 3 resonances is $1.10 \pm \begin{matrix}0.00\\0.06\end{matrix}$ eV.

In the case of J=4 resonances it is estimated that 6 levels are missed in an energy region up to 73 eV. Thus the average level spacing is 0.86 $\pm \begin{matrix}0.00\\0.05\end{matrix}$ eV. The quoted errors reflect only the missed level information.

It is interesting to note the comparison between experimental and theoretical Δ_3 values for J=3 and J=4 resonances. A sudden increase in the experimental Δ_3 value indicates possible missing of levels (Fig. 2) or the presence of spurious levels.

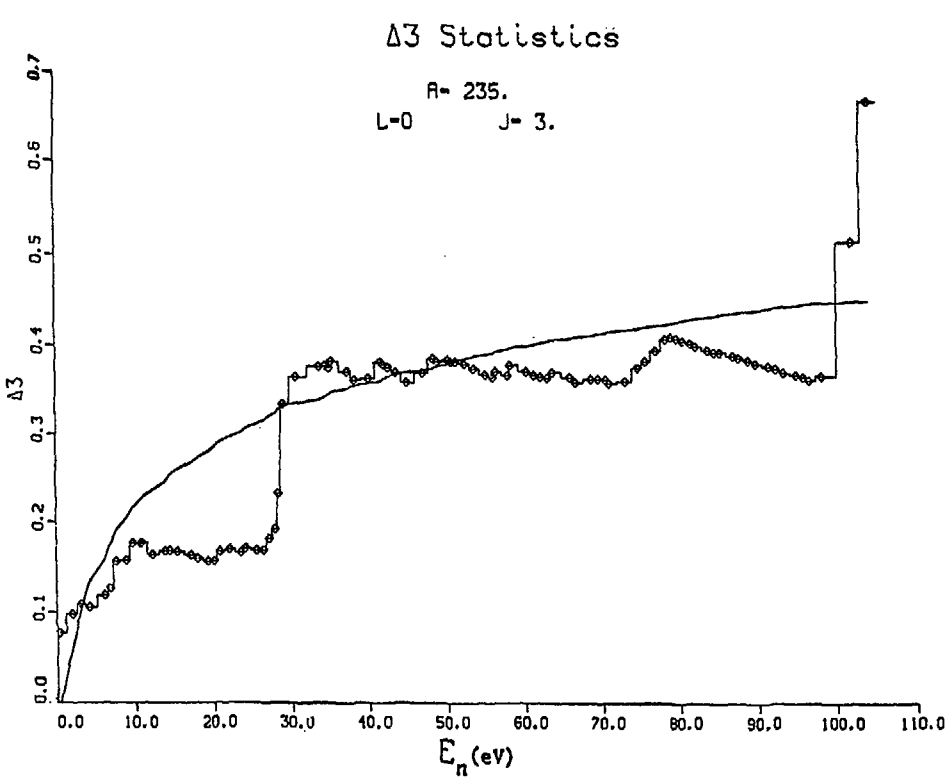

Fig. 2a.

Comparison of experimental and theoretical Δ_3 values for ^{235}U J=3$^-$ resonances.

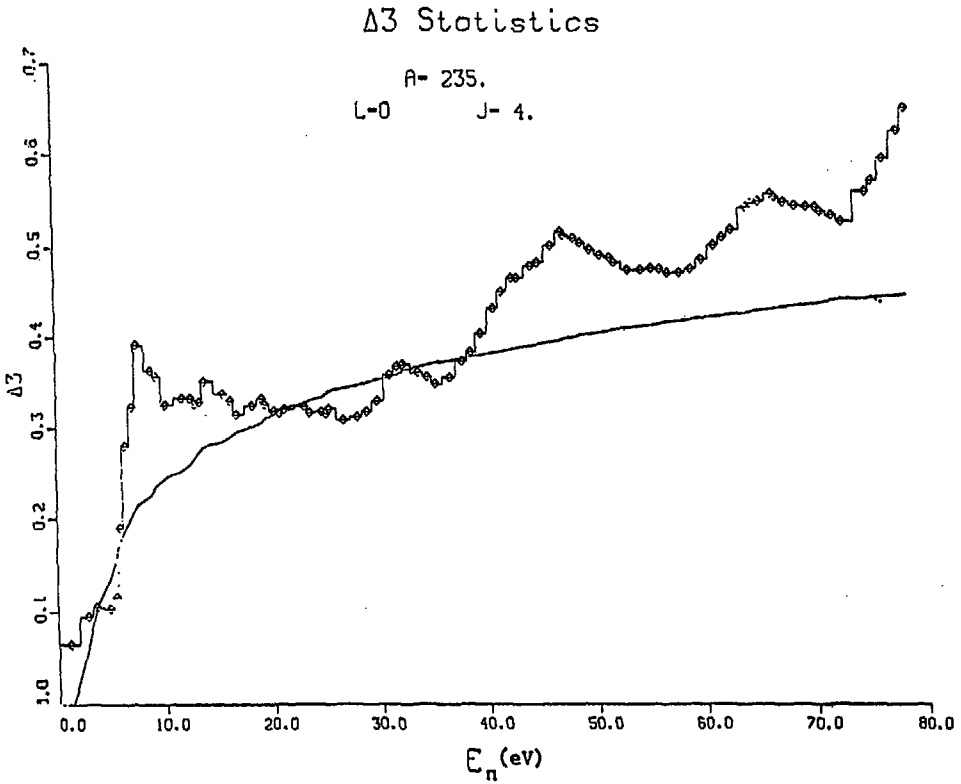

Fig. 2b.

Comparison of experimental and theoretical Δ_3 values for ^{235}U J=4$^-$ resonances.

Table I

Average Resonance Parameters

Target	B_n(KeV)	J^π	D_J(eV)	S_0	S_1	Γ_γ(meV)	Γ_γ(meV)[a]	Γ_γ(meV)[b]	Γ_γ(meV)[c]
^{235}U	6550	3^-	1.10±0.06	1.03±0.10	1.8±0.3	39±3	37	37	35.4±1.9
		4^-	0.88±0.05						34.2±2.0
^{238}U	4806	$1/2^+$	22.5±1.4	1.0±0.1	1.7±0.3	23.2±0.3	34	25	21.5±1.4
^{239}Pu	6534	0^+	7.9±0.8	1.3±0.1		42±3	43	48	36.0±2.4
		1^+	3.4±0.2						35.9±2.5
^{240}Pu	5241	$1/2^+$	11.5±1.9	0.93±0.08		31±2	38	36	29.7±1.5
^{241}Pu	6309	2^+	2.7±0.3	1.5±0.3		38±3	38	33	35.9±1.0
		3^+	2.7±0.3						35.6±1.0
^{242}Pu	5034	$1/2^+$	15.6±1.7	0.90±0.16		27±2	36	26	27.0±1.3

(a) Present calculations based on systematics (ref. 17).
(b) Lynn calculations based on giant dipole resonance model (ref. 16).
(c) Moore calculations based on giant dipole resonance model (ref. 15).

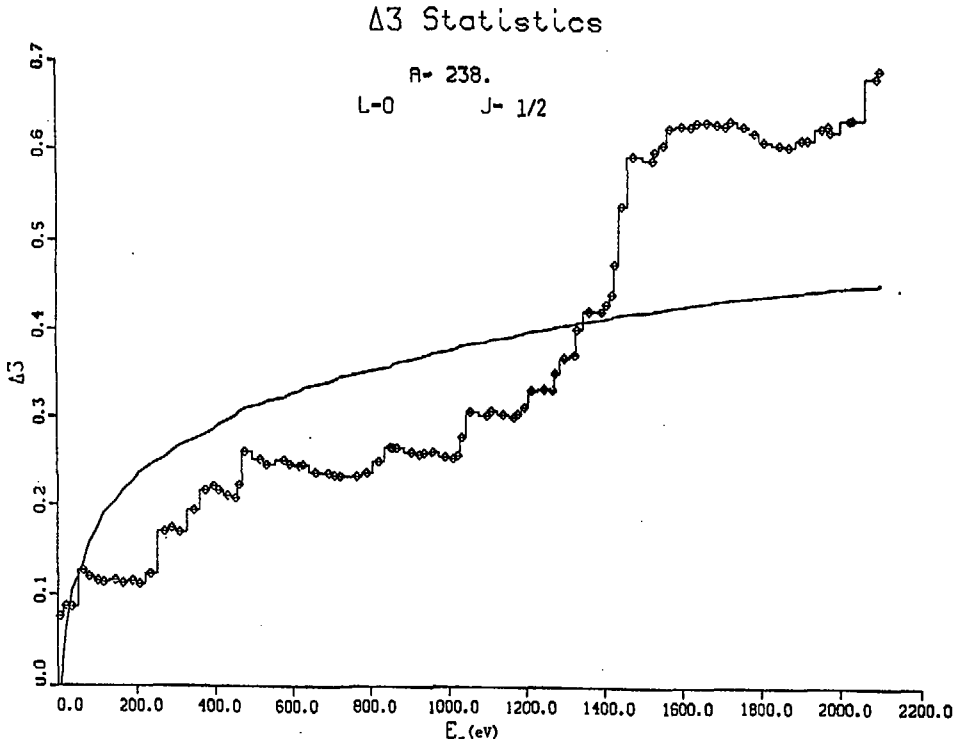

Fig. 3.
Comparison of experimental and theoretical Δ_3 values for ^{238}U s-wave resonances.

^{238}U:

Several measurements[18-24] to determine more accurate values of the resonance parameters of ^{238}U have been carried out. These include transmission, scattering, capture, and self indication measurements. The major emphasis was placed on the determination of the radiative widths of the low energy s-wave resonances. The results of these investigations are the decrease of the value of the radiative width of the 6.67 eV resonance from 26 ± 2 meV to 22.8 ± 0.6 meV and the increase of the scattering width of the 20.9 eV resonance from 8.7 ± 0.5 meV to 10.0 ± 0.2 meV.

In addition, the parity assignments of resonances are at present placed on a firm basis because a new technique to establish the ℓ values of ^{238}U resonances was developed by Corvi et al.[25] This is based on the gamma ray spectra differences between s and p-wave neutron capture.

With the aid of this technique, Corvi et al.,[25] were able to identify the p-wave resonances of ^{238}U in the energy range 63-1548 eV. More recently Moore et al., [26] successfully extended these measurements up to an energy of 3341 eV.

Table II Comparison between Theoretical and Experimental Δ_3 Values

J^π	E_n(eV)	Δ_3 Experimental	Δ_3 Theoretical	No. of Resonances	D_J(eV)
3^-	60	0.370	0.399 ± 0.11	54	1.091 ± 0.077*
	70	0.362	0.413 ± 0.11	63	1.090 ± 0.071
	100	0.366	0.448 ± 0.11	89	1.090 ± 0.060
4^-	60	0.487	0.422 ± 0.11	68	0.854 ± 0.053
	70	0.545	0.437 ± 0.11	79	0.862 ± 0.050
	73	0.523	0.442 ± 0.11	88	0.863 ± 0.049

* The errors are estimated with the help of the equation $\Delta\langle D\rangle = 0.52\langle D\rangle N^{-1/2}$.

The variation of the theoretical and experimental Δ_3 values calculated for the s-wave resonances is illustrated in Fig. 3. As shown, the sudden increase of the experimental Δ_3 value at a neutron energy of 1400 eV indicates that s-wave levels are either missed or possibly misassigned as p-wave levels. Below this energy, the s-wave average level spacing is determined to be 22.5 ± 1.4 eV. The recommeded average resonance parameters of ^{238}U are shown in Table I.

The recommended positive energy s-wave resonances contribute 2.35b to the 2200 m/sec capture cross section. This is to be compared with the recent measurement of Poenitz et al.,[27] who reports σ_γ = 2.68 ± 0.019 b. Calculations of the direct capture component in the framework of the Lane and Lynn[31] theory following the Mughabghab [28] approach indicate that the nonresonant contribution to the thermal capture cross section is ≃ 0.08 b. Therefore, a negative energy resonance is postulated in order to take into account the difference between the calculations and the measurement and to describe the coherent scattering length. The parameters of this resonance are shown in Table III.

^{239}Pu:

No major changes have taken place in the recommended resonance parameters of ^{239}Pu because no new measurements have been carried out as yet.

^{240}Pu:

The importance of the parameters of the 1.056 eV resonance has been recently emphasized by Weston.[29] It was suggested[30] that the parameters of this resonance may provide a solution to the discrepancy between the microscopic differential and integral data. Since this resonance contributes 98% to the 2200 m/sec capture cross section, the highly accurate measurement of the thermal capture cross section by Lounsbury et al.,[31] imposes a constraint on the product $\Gamma_n\Gamma_\gamma$. Recent transmission and capture measurements carried out by Liou and Chrien[32] reveal that the capture width of this resonance is Γ_γ = 32.4 ± 1.0 meV and the scattering width is Γ_n = 2.32 ± 0.06 meV. These are more accurate than, but consistent with, the previously recommended parameters[33] : Γ_n = 2.30 ± 0.15 meV and Γ_γ = 31 ± 3 meV. Other recent measurements on the fission cross section by Auchampaugh and Weston[34] are concerned with the study of the subthreshold fission widths and hence the fission reaction mechanism. Previous similar investigations were made by Migneco and Theobald[35] .

The recommended resonance parameters of ^{240}Pu cover the energy range from thermal to 5.692 keV and are basically based on the measurements of Kolar and Bockoff[36] , Weigmann and Theobald[37] , Weigmann and Schmid[38] , and Hockenbury et al.[39] . The parameters of the 1.056 eV resonance are based on the very recent measurements of Liou and Chrien[32] . The highly accurate values of both the thermal capture cross section (σ_γ^o = 289.5 ± 1.4 b) and the coherent scattering length (b = 3.5 ± 0.1 fm at E_n = 0.08 eV) indicate that a bound level is required to fit the thermal region. The parameters of this negative energy resonance are derived and are included in the evaluation. The position of this resonance is determined to be - 9.8 eV which is comparable with an average level spacing of 11.5 ± 1.9 eV.

The latter is obtained with the aid of the Δ_3 statistics. It is interesting to remark here that a calculation of the average radiative width on the basis of systematics does not reproduce the experimental value $\langle\Gamma_\gamma\rangle$ = 31 ± 2 meV.

Table III. The Recommended Thermal Cross Sections, Average Resonance Parameters and the Low Energy Resonances of ^{238}U.

$^{238}_{92}U$ [4.468 · 10⁹ yr]

THERMAL CROSS SECTIONS

σ_γ^0 = 2.680±0.010 b
σ_s = 9.38±0.09 b
σ_a = 0.0013±0.0008 mb
σ_f^0 = 0.047 mb
ν_{sp} = 1.98±0.03
b_{coh} = 8.55±0.04 fm
R' = 9.6±0.1 fm

RESONANCE PROPERTIES

$\langle\Gamma_{\gamma 0}\rangle$ = 0.0232±0.0003 eV
D_0 = 22.5±1.4 eV
D_1 = 9.7±1.3 eV
S_0 = 1.0±0.1
S_1 = 1.7±0.3
$S_{\gamma 0}$ = 10.3±0.6
I_γ = 277±3 b
I_f^0 = 1.50±0.15 mb

RESONANCE PARAMETERS

$I^\pi = 0^+$
$\sigma_\gamma(+) = 2.35$ b
$\sigma_\gamma(B) = 0.33$ b
S_n = 4806.2±0.4 keV
$\sigma_\gamma(D) = 0.09$ b

E_0 (eV)	J	l	Γ (meV)	$g\Gamma_n$ (meV)	Γ_γ (meV)	$g\Gamma_n^0$ (meV)	$g\Gamma_n^1$ (meV)	Γ_f (meV)
−137					(23.2)	64.4		
4.469±0.004		1		0.00011± 0.00001			3.5 ±0.3	
*6.671±0.002	1/2	0	24.3 ± 0.6	1.50 ± 0.02	22.8±0.6	0.581 ±0.008		0.0000007±0.000001
*10.237±0.003	3/2	1		0.00165± 0.00005			14.0 ±0.5	
11.309±0.006		1		0.00039± 0.00003			3.0 ±0.2	
18.529±0.006		1		0.0013 ± 0.0001			4.5 ±0.3	
*20.872±0.006	1/2	0	33.64± 0.50	10.04 ± 0.20	23.5±0.8	2.196 ±0.044		0.000056 ±0.000001
*36.680±0.011	1/2	0	57.5 ± 0.5	34.0 ± 0.4	23.5±0.3	3.61 ±0.07		0.0000008±0.000001
45.17 ±0.04		1		0.0019 ± 0.0005			1.0 ±0.5	
49.62 ±0.07		1		0.0012 ± 0.0006			1.0 ±0.5	

$^{238}_{92}U$ [4.468 · 10⁹ yr]

Table IV. The Recommended Thermal Cross Sections, Average Resonance Parameters and the Low-Energy Resonances of ^{240}Pu.

THERMAL CROSS SECTIONS

σ_γ^0 = 289.5±1.4 b
σ_a = 1.64±0.09 b
σ_f = 0.058±0.030 b
ν_{sp} = 2.17±0.01
b_{coh} = 3.5±0.1 fm
R' = 9.8±0.2 fm

RESONANCE PROPERTIES

$\langle\Gamma_{\gamma 0}\rangle$ = 0.031±0.002 eV
D_0 = 11.5±1.0 eV
S_0 = 0.03±0.00
$S_{\gamma 0}$ = 27±5
I_γ = 8100±200 b
I_f^0 = 1.0 b

RESONANCE PARAMETERS

$I^\pi = 0^+$
$\sigma_\gamma(+)$ = 286.3 b
$\sigma_\gamma(0)$ = 3.2 b
S_n = 6241.3±0.7 keV

E_0 (eV)	J	l	$g\Gamma_n$ (meV)	Γ_γ (meV)	$g\Gamma_n^0$ (meV)	Γ_f (meV)
-0.84				(32.4)	3.84	
1.057±0.002	1/2	0	2.32± 0.08	32.4±1.0	2.258 ±0.000	0.006
20.45 ±0.01			2.65± 0.07	32.2±2.4	0.586 ±0.015	
36.32 ±0.02	1/2	0	17.3 ± 0.5	29.4±2.8	2.70 ±0.08	
41.84 ±0.02			16.7 ± 0.6		2.50 ±0.09	
66.20 ±0.04			54 ± 1	31.0±1.7	6.6 ±0.1	
72.77 ±0.04			21.4 ± 0.7	28.5±1.5	2.51 ±0.06	
80.78 0.00			12.8 ± 0.3	27.5±3.0	1.34 ±0.03	
82.51 ±0.06			3.1 ± 0.1		0.32 ±0.01	
105.00 ±0.07			44.0 ± 1.5	35.6±2.0	4.20 ±0.15	
121.6 ±0.1			14.2 ± 0.8	31 ±4	1.20 ±0.05	
130.7 ±0.1			0.17± 0.03		0.015 ±0.003	
135.3 ±0.1			18.7 ± 1.5	31.5±2.6	1.41 ±0.13	

$^{240}_{94}$Pu [6.569 · 10³ yr]

The same trend seems to be true for the other even-even target nuclei ^{238}U and ^{242}Pu. The recommended average resonance parameters along with the individual parameters of resonances up to 135.3 eV are shown in Table IV.

^{241}Pu:

Since 1973, only one resonance parameter data set by Blons and Dirrien[40] is reported. The Reich-Moore formalism was applied to the fission cross section measurement which was carried out on a sample cooled down to 77K to reduce the Doppler effect. The neutron energy region covered in their measurements is from 0.26 eV to 103.66 eV. These parameters were adopted in the evaluation.

In addition, the average radiative width is calculated on the basis of the systematics[17] and is determined to be 38 meV. This is to be compared with values of 33 meV and 35.9 ± 1.0 meV ($J^\pi = 2^+$) and 35.6 ± 1.0 meV ($J^\pi = 3^+$) calculated respectively by Lynn[16] and Moore[15] on the basis of the giant dipole resonance model. The average level spacing for both spin states is determined as 1.3 ± 0.1 eV.

^{242}Pu:

The recommended thermal capture cross section at 0.0253 eV is evaluated as $\sigma_\gamma^o = 18.46 \pm 0.49$ b, which is based on the measurements of Young et al.[41] Durham et al.,[42] and Butler et al.[43] The scattering cross section, $\sigma_s = 8.24 \pm 0.20$ b, is determined from the coherent scattering length b = 8.1 ± 0.1 fm. These thermal constants provide constraints on the parameters of a bound level and the first resonance at 2.68 eV.

Recent measurements of the resonance parameters of ^{242}Pu have been carried out by Poortmans et al.,[44] (σ_t, σ_γ, σ_s), Harvey et al.,[45] (σ_t), and Auchampaugh and Weston[46] (σ_f). In addition, fission areas reported by Auchampaugh et al.,[44] were used in deriving subthreshold fission widths for ^{242}Pu. There is general agreement between the various Γ_n values reported by these authors. The average radiative width determined by Poortmans et al.,[44] is 21.9 ± 1.1 meV which is slightly lower than the radiative width[48] of the 2.675 ± 0.002 eV resonance. A coherent scattering length of 8.1 ± 0.1 fm combined with a potential scattering length of 9.6 ± 0.2 fm obtained from the systematics and from neighboring nuclides indicate the presence of a nearby negative energy resonance. To obtain acceptable values for the parameters of this bound level, it was necessary to adopt the lower limit of the capture width (Γ_γ = 25.0 ± 1.5 meV) of the 2.68 eV resonance which was derived by Young and Reeder[48] who used a shape fit analysis adopting the Reich-Moore multilevel formula. It is interesting to point out here that the accurate position of the resonance energy, E_o = 2.676 ± 0.002, as determined by Schrack[49] and Harvey[45] can be used as a neutron energy standard.

The fission cross section at 0.0253 eV is calculated as 0.21 b from the evaluated resonance parameters. In addition, the parameters indicate that the capture and fission resonance integrals are 1107 b and 6.4 b respectively. With the aid of the Δ_3 statistics, the average level spacing is determined as D_o =15.6 ± 1.7 eV.

4. CONCLUSION AND SUMMARY

The current status of the resonance parameters of the actinides $^{235,238}U$ and $^{239-241}Pu$ is briefly described. Average resonance parameters are derived and in particular the Dyson-Mehta Δ_3 statistics was applied in conjunction

with the staircase plots to arrive at average level spacings. Average radiative widths are calculated here on the basis of systematics as derived by Malecky et al.,[17] and are compared with Moore's[15] and Lynn's[16] estimates. It is interesting to point out that the calculations on the basis of systematics are in reasonable agreement with the experimental values for the even-odd target nuclides ^{235}U and $^{239,241}Pu$ but not for the even-even target nuclides ^{238}U and $^{240,242}Pu$. The radiative widths of the low energy neutron resonances of ^{238}U are at present well established thus resolving a previous discrepancy between integral and differential measurements. Additional spin assignments for ^{235}U have been made using polarization measurement. It seems that the (2J+1) law is obeyed in this case. It will be of great interest to apply the same experimental technique to determine the spins of ^{241}Pu resonances. At present these were determined by the method of interference in the fission channel which does not give unambiguous assignments.

The scattering and radiative widths of the ^{240}Pu resonance at 1.057 eV are determined[32] to a higher accuracy. The result of this measurement indicates that a re-examination of the integral measurements for ^{240}Pu is necessary.

The recommended resonance parameters of "BNL-325" which can be presented in an ENDF-type format are available on request from the National Nuclear Data Center.

Acknowledgments

We gratefully acknowledge useful discussions with Dr. H. I. Liou regarding the Δ_3 statistics and Dr. M. S. Moore regarding the ^{235}U resonance parameter analysis.

References

1. S.F. Mughabghab, M. Divadeenam and N.E. Holden, Neutron Resonance Parameters and Thermal Cross Sections. To be published (Academic Press)
2. S.F. Mughabghab, Proceedings of the Conference on Nuclear Data Evaluation Methods and Procedures, BNL-NCS-51363, p. 339, 1981.
3. F.J. Dyson and M.L. Mehta, J. of Math. Phys. 4,7.1 (1963), and references therein.
4. E.P. Wigner, Conference on Neutron Physics by Time of Flight, ORNL-2309, p. 59, 1957.
5. P.D. Georgopulos and H.S. Camarda, Phys. Rev. C 24, 42 (1981).
6. G.A. Keyworth and M.S. Moore, in Neutron Physics and Neclear Data, Harwell, 1978, p. 241.
7. M.S. Moore, G. de Saussure and J.R. Smith, contirbuted paper to the present conference (1981).
8. G.A. Keyworth, C.E. Olsen, F.T., Seibel, J.W.T. Dabbs and N.W. Hill, Phys. Rev. Letters, 31, 1077 (1973).
9. A Michaudon, H. Derrien, P. Ribon, and M. Sanche, Nucl. Phys. 69, 545 (1965).
10. J. Blons, H. Derrien and A. Michaudon, in Neutron Cross Sections and Tehnology, Knoxville, 1971. Vol. 2, p. 829.
11. N.B.R. Ryabov, et.al., Physics and Chemistry of Nuclear Fission, Helsinki, 1970, p. 1, 410 (1971).
12. F. Corvi, M. Stefanon, C. Coceva and P. Giacobbe, Nucl. phys. A203 145 (1973).

13. Felvinci, Private communication to NNDC, CISRS Library. A/N.

14. M.S. Moore, J.D. Moses, G.A. Keyworth, J.W.T. Dabbs, and N.W. Hill, Phys. Rev. C 18, 1328 (1978).

15. M.S. Moore, in Neutron Physics and Neclear Data, Harwell, 1978, p. 313.

16. J.E. Lynn, in Nuclear Fission and Neutron-Induce Fission Cross-Sections (edited by Michaudon et.al., 1981), p. 157, Pergamon Press.

17. H. Malecky, L.B. Pickelner, I.M. Salamatin and E.I. Sharapov, Yad. Phys. 13, 240 (1971).

18. D.K. Olsen, G. de Saussure, R.B. Perez, F.C. Difilippo, R.W. Ingle, and H. Weaver, Nucl. Sci. and Eng. 69, 202, 1979.

19. Y. Nakajima, Annals of Nucl. Eng., 7, 25 (1980).

20. R.C. Block, D.R. Harris, S.H. Kim, and K. Kobayashi, Transactions of Am. Nucl. Soc., 27, 868 (1977). See also EPRI NP-1704.

21. T.J. Haste and M.C. Moxon, Neutron Physics and Nuclear Data for Reactors and other Applied Purposes, 337, 1978

22. P. Stavelos and E. Cornelis, Nucl. Sci. and Eng., 66, 349 (1978).

23. F. Poortmans, E. Cornelis, L. Mewissen, G. Rohr, R. Shelly, T. van der Veen, G. Vanpraet, and H. Weigmann, private communication, 1977.

24. H.I. Liou and R.E. Chrien, Nucl. Sci. and Eng., 62, 463 (1977).

25. F. Corvi, G. Rohr, and H. Weigmann, Nuclear Cross Sections and Technology, Washington, p. 733 (1975).

26. M.S. Moore, F. Corvi, L. Mewissen, and F. Poortmans, this conference and private communication.

27. W. Poenitz, L.R. Fawcett and D.L. Smith, Nucl. Sci. and Eng., 78, 239 (1981).

28. S.F. Mughabghab, Phys. Letters, 81B, 92 (1979).

29. L.W. Weston, Proceedings of the Specialists' Meeting on Nuclear Data of Plutonium and Americium Istopes for Reactor Applications, BNL-50991, Editor, R.E. Chrien, p. 1 (1978).

30. L.W. Weston, private communication (1981).

31. M. Lounsbury, R.W. Durham, and G.C. Hanna, Proc. Conf. on Nuclear Data for Reactors Helsinki, 1970, Vol. 1, p. 287.

32. H.I. Liou and R.E. Chrien, private communication 1981 (to be published).

33. S.F. Mughabghab and D.I. Garber, BNL-325, Neutron Cross Sections, Vol.1, Resonance Parameters, 3rd Edition 1973.

34. G.F. Auchampaugh and L.W. Weston, Phys. Rev., C12, 1850 (1975).

35. E. Migneco and J.P. Theobald, Nucl. Phys., A112, 603 (1968).

36. W. Kolar and K.H. Bockoff, J. of Nucl. Energy, 22, 299 (1968).

37. H. Weigmann and J.P. Theobald, J. of Nucl. Energy, 26, 643 (1972).

38. H. Weigmann and H. Schmid, J. of Nuclear Energy, 22, 317 (1968).

39. R.W. Hockenbury, W.R. Moyer and R.C. Block, Nucl. Sci. and Eng., 49, 153 (1972).

40. J. Blons and H. Derrien, Journal de Physique, 37, 659 (1976).

41. T.E. Young, F.G. Simpson and R.E. Tate, Nucl. Sci. and Eng. 43, 341 (1971).

42. R.W. Durham and F. Modson, Can. J. of Phys. 48, 716 (1970).

43. J.P. Butler, M. Lounsbury and J.S. Herritt, Can. J. Phys. 35, 147 (1957).

44. F. Poortmans, G. Rohr, J.P. Theobald, H. Weigmann and G.J. Vanpraet.

45. J.A. Harvey, N.W. Hill, R.W. Benjamin, C.E. Ahlfeld, F.B. Simpson, O.D. Simpson and H.G. Miller, ORNL-4844, 90 (1973).

46. G.F. Auchampaugh and L.W. Wiston, Phys, Rev. C6, 1850 (1975).

47. G.F. Auchampaugh, J.A. Farrell and D.W. Bergen, Nucl. Phys. A171, 311 (1971).

48. T.E. Young and S.D. Reeder, Nucl. Sci. and Eng., 40, 389 (1970).

49. R. Schrack, private communication, 1981.

Neutron Cross Sections and Doppler Effect of the 1.056 eV Resonance in ^{240}Pu

H. I. Liou and R. E. Chrien
Brookhaven National Laboratory, Department of Physics
Upton, New York, 11973

Abstract

Neutron transmission and capture measurements for the 1.056 eV resonance in ^{240}Pu have been carried out with metallic and oxide targets of high purity at room, liquid N_2 and He temperatures. This work was motivated by the considerable importance of this resonance in reactor design and by the interest in possible influence of molecular binding on the neutron cross section. Consistent results were obtained from different measurements, using least-squares shape-fit analysis. We obtain Γ_n = (2.32 ± .06) meV and Γ_γ = (32.4 ± 1.0) meV, which are 0.9% and 4.5% higher, respectively, than previously recommended values The influence of this resonance on thermal capture and the resonance capture integral is discussed. The effective temperature T' defined by Lamb for weak binding, and consequently the Debye temperature θ_D, were extracted. The result for T', 275 ± 8°K, for ^{240}Pu oxide at T = 294°K can not be explained by Lamb's theory for weak binding. Within statistical uncertainties all measured Debye temperatures are consistent with θ_D = 175°K except the case of metallic ^{240}Pu at liquid N_2 temperature, where the θ_D value is a little higher.

I. Introduction

^{240}Pu possesses a value for the dilute resonance capture integral that is mostly due to the resonance at 1.056 eV. It is important to the neutron economy of a reactor to know the accurate size of the resonance, i.e., Γ_n and Γ_γ. The HFBR fast chopper facility has been used to make a determination of these reson-

ance parameters. In this low energy region the intensity and resolution of the instrument are adequate for precise measurements.

To derive neutron resonance parameters, one needs to correct Doppler broadening effect on measured cross sections. Assuming a Maxwellian velocity distribution of the gas atoms, Bethe and Placzek[1] derived a line shape consisting of the well-known ψ function with Doppler width $\Delta=(4k_BTE/A)^{1/2}$. For a crystalline target Lamb,[2] by considering the lattice binding effect, derived a basic formalism which in principle can be computed if the detailed spectrum of phonon frequencies is known. Particularly in the weak binding limit, $(\Delta+\Gamma)>>2\theta_D$ (θ_D=Debye temperature), the neutron cross section has the same form as it would in a perfect gas except that the crystal temperature T in Δ is replaced by an effective temperature T'. Applying the Debye continuum theory, Lamb obtained a simple relation between T' and θ_D,

$$\frac{T'}{T} = 3\left(\frac{T}{\theta_D}\right)^3 \int_0^{\theta_D/T} \left(\frac{1}{e^t-1} + \frac{1}{2}\right) t^3 dt. \qquad (1)$$

Since the Debye theory is too simple to describe the specific heat data for many materials, in studies of lattice dynamics one usually expresses θ_D as smooth function of temperature.

Lamb also predicted that if an atom is more strongly bound in a lattice, i.e. approaching the medium binding condition $(\Delta+\Gamma)\sim 2\theta_D$, some fine structure may appear in its broadened line shape. A number of attempts[3,4,5] have been made to study the Doppler broadening of resonance line shapes. Generally speaking, the medium binding condition is more likely to be fulfilled, if (1) the resonance is at low energy, (2) the capture width is small, and (3) the target mass number is high. We find that the 1.056 eV resonance in ^{240}Pu is an excellent case to search for possible fine structure due to crystal binding effects, despite the lack of knowledge of its Debye temperature. This is another motivation behind our pursuing a study of this resonance.

We did transmission measurements for ^{240}Pu oxide at room temperature, and capture measurements for both ^{240}Pu metal and oxide at room, liquid N_2 and He temperatures. The resolution of our experiment at 1 eV is nearly an order smaller than the resonance intrinsic width and Doppler width. So the level parameters, Γ_n and Γ_γ, can be properly determined by a systematic study of shape analysis. We also attempt to examine how the lattice binding effect in ^{240}Pu metal and oxide varies with temperature, and whether any fine structure appears at the resonance-broadened line shape.

II. Experiments and Samples

The measurements were carried out at the High Flux Beam Reactor of Brookhaven National Laboratory, using the fast chopper time-of-flight (TOF) spectrometer[6] with its 22 m flight path. The narrow-slitted rotor was operated at a repetition rate of 200 s^{-1}, giving a beam intensity of $\sim 1.5\times10^3$ E^{-1} n/(cm$^2\cdot$s$\cdot$eV) and a burst width of 5 μs. A 0.43 mm Cd filter was inserted in front of the chopper in order to suppress the background due to thermal fission of the ^{239}Pu impurity in the target. For transmission measurements a thin ^{3}He detector was directly set in the beam, and the oxide sample was placed at the exit port of the chopper shielding, ~19 m from the detector. For capture measurements the target sample was clamped in the end cup of a double layered cryostat, directly contacting the cold finger and perpendicularly facing the incident neutron beam. A coaxial Ge(Li) detector with 10% relative efficiency was allowed to view the target in an angle of 45° through a 0.32 cm of lead shielding.

Each datum consists of one TOF parameter, and one pulse height parameter. The γ-ray pulse height spectrum covers an energy range from 150 to ~5240 keV (the neutron separation energy). Immediate on-line event sorting was implemented

with our new data acquisition system[7] and PDP 11/20 computer. The sorted spectra were directly stored on the one megaword extended memory. The dead time correction as a function of TOF was done by injecting a free-running pulse (uncorrelated with the TOF frame) of constant rate into the detector preamplifier and recording the counts in each time channel simultaneously with the data.

The metallic and oxide ($^{240}PuO_2$) samples, each 6.35 cm x 5.72 cm, have n values for ^{240}Pu of 224×10^{-7} and 179×10^{-7} a/b, and are 98.3% and 96.3% pure in ^{240}Pu respectively. The sample thickness was deliberately chosen such that the experimental value of $n\sigma$ at peak of the 1.056 eV resonance is near 2 to give a good sensitivity for shape analysis. The oxide sample, being fine powder, was spread on a thin Al backing using a vacuum deposit technique. The thickness uniformity is better than 3%.

For transmission measurements the normalization, which is important in obtaining accurate results, was determined from fast cycling of the transmission sample into and out of the beam. This agreed within 0.8% with the normalization according to the total running time. Two neutron filters, 0.114 mm In and 0.254 mm Ag, were placed in the beam in order to evaluate backgrounds at 1.457 and 5.19 eV respectively. We determined the neutron background near the 1 eV region to be less than 1% of the full open count. A shape analysis for the 16.30 eV resonance in ^{107}Ag (taking an open run without the Ag filter) was performed to determine the effective time resolution of the system, since the Ag resonance parameters are accurately known[8] and the instrumental resolution of the experiment dominates in that energy region. It is found that for transmission measurements σ_t = 3.42 $\pm$ 0.10 μs, implying σ_E = 4.69 meV at 1.056 eV. The running time for each transmission sample condition was about 3000 minutes.

In capture measurements the saturation count at the resonance peak for each individual run is separately extracted from a least-squares shape-fit analysis. Therefore no relative normalization between runs is needed. The background correction for a well-isolated resonance as in the present case can be made by extrapolation from both sides of the resonance. In order to deduce the time resolution and the relative neutron flux versus energy a capture measurement with a 0.203 mm W sample, having the same size and positioned at the same place as the Pu target, was carried out at room temperature. A shape fit to the 7.65 eV resonance in ^{183}W and the 4.16 eV resonance in ^{182}W showed that for capture measurements σ_t = 3.00 $\pm$ 0.16 μs, where the level parameters were adopted from the recommended values of reference 9. To check internal consistency, the experiments were done for two separate series of runs, cycling through metallic and oxide samples, each for 3 temperatures at 294, 77.2 and 4.066°K. The useful running time for each individual run amounted to ~4000 minutes. The deduced sample effective temperatures are consistent within statistical fluctuations.

III. Methods of Analysis

III.A Transmission Measurement

Since the 1.056 eV resonance in ^{240}Pu is well isolated, we fit the measured transmission, T ($= T_p e^{-n\sigma}$), applying the single level formula,

$$\sigma = \sigma_0[\psi(x,s)+2kR'\chi(x,s)], \qquad (2)$$

where T_p = the transmission base line due to all potential cross sections other than the resonance in study,

$$\sigma_o(b) = \frac{2.604\times10^6}{E_o(eV)}\frac{\Gamma_n}{\Gamma},$$

$$x = 2(E-E_0)/\Gamma,$$

$$s = \Delta/\Gamma,$$

$$\Gamma = \Gamma_n+\Gamma_\gamma,$$

Δ = Doppler width = $18.565\ [E_0(eV)T'/A]^{1/2}$ meV,

and T' = effective temperature, as defined in the weak binding limit of Lamb model.

Here ψ and χ are the well-known Doppler line-shape functions for the resonance and interference cross sections. The resonance E_0 value is taken as 1.056 eV from the recommended value in ref. 9. We assume 9.5 fm for the potential scattering amplitude R' by referring to the known R' values[9] of nearby isotopes (9.6 fm for ^{242}Pu, 9.4 fm for ^{238}U, 9.65 fm for ^{232}Th). The R' value is not sensitive to the fit in the 1 eV low energy region.

The calculation also numerically convolutes resolution in transmission. The resolution function is taken as a Gaussian form with its width determined from a fit to the 16.30 eV resonance in ^{107}Ag. A least-squares shape-fit procedure is employed, which can fit Γ_n and Γ_γ together, or Γ_n and T' together, or any one of them separately.

III.B Capture Measurement

Considering finite sample thickness and gamma-ray self-absorption in target, the count rate for a first-order interaction leading to a detectable capture gamma ray at neutron energy E over a constant time interval is

$$N^{(1)} = Mn\sigma_\gamma\{1-\exp[-(p+b)]\}/(p+b). \qquad (3)$$

Here n = sample thickness of ^{240}Pu in target,

b = $n\sigma$,

p = $\Sigma_i(m_i p_i')/\cos 45°$,

where (1) 45° is the angle between the detector viewing direction and the target normal direction, (2) i runs through all isotopes contained in target, and (3) m_i and p_i' represent the i th sample thickness and its total γ-ray absorption coefficient.

The capture cross section $\sigma_\gamma = \sigma_0\psi\Gamma_\gamma/\Gamma$, and the total cross section $\sigma = \sigma_0[\psi+2kR'\chi]+\sigma_p$, where σ_p denotes the effective potential scattering cross section due to all isotopes in target. The factor M in equation (3) expresses the saturation count in case all neutrons were captured and no gamma-ray attenuation occurred in target. It depends on neutron flux and absolute efficiency of the detector, and varies smoothly with E. In our least-squares shape-fit procedure the M value at resonance peak is treated as a free parameter fitted together with other quantities.

Our target (either metal or oxide) is so thick that the observed neutron transmission at the 1 eV resonance peak is about 12%. Such a high neutron interaction probability gives a good chance that any scattered neutron is captured in the target. Each time a neutron is scattered, it loses part of its kinetic energy to the recoiling nucleus, $\Delta E = 2E(1-\cos\theta)/A$ where A is the target mass number and θ is the neutron scattered angle. In the present case $2E/A\sim 9$ meV, being several times less than the resonance intrinsic width. It is likely that the scattered neutron still has an energy well within the resonance region, but interacts with a quite different cross section from that prior to the scattering. This makes the multiple scattering correction complicated. The correction is, however, necessary in order to obtain an unbiased result. A code has been written for this purpose, which performs numerical integration over all scattering angles by considering the sample geometry, and takes account of the effect of cross-section change after scattering. In general the correction depends on the ratio of Γ_n/Γ, varies with incident neutron energy, and is more pronounced if it is on the high energy side of the resonance. We found that the correction in the present study varies from 1% through 6%.

The width of the time resolution function was obtained from a fit to W data in higher energy region. With the saturation count M and the analyzer channel number at resonance peak being two basic free parameters, a least-squares shape-fit

analysis is employed to extract the best value for any one of the Γ_n, Γ_γ, T' and Δt parameters, or for Γ_n and Γ_γ together.

IV. Results and Discussion

The formulas described in section III are based on the Lamb's theory for weak binding. If the fine structure in resonance line shape due to medium binding effect occurs prominently, one can identify it either by inspection of the data, or by obtaining a poor shape fit using the simple weak-binding formalism. We found that in all cases of the fit the χ^2 value per degree of freedom is near unity. This indicates that no fine structure can be detected within the sensitivity of our measurements.

We assume the correctness of the Lamb's theory for weak binding to describe metallic ^{240}Pu at room temperature. A plot of equation (1) shows that T' is not sensitive to θ_D at large T. While θ_D of ^{240}Pu metal is unknown, it will not introduce a large error, if we choose T'=300°K for ^{240}Pu metal at T=294°K (this implies θ_D=188°K). The capture measurement for a thick target is only sensitive to the product of neutron width and capture width. We find that a fit to the transmission data of ^{240}Pu oxide with the present sample thickness is particularly sensitive to the neutron width. But the T' of ^{240}Pu oxide at room temperature is an unknown parameter, and must be supplied from other data. An iteration procedure using least-squares shape-fit was made to obtain a set of results consistent among the three independent measurements at room temperature. Thus, we (1) fit the transmission data of ^{240}Pu oxide for Γ_n and Γ_γ simultaneously, (2) fit the capture data of ^{240}Pu metal for Γ_γ alone, and (3) fit the capture data of ^{240}Pu oxide for T' alone. The results and their statistical uncertainties are Γ_n = 2.32 ± 0.01 meV, Γ_γ = 32.4 ± 0.2 meV and T' of ^{240}Pu oxide at room temperature = 275 ± 8°K. Shown in Figs. 1, 2 and 3 are the final fits of the iteration process, where the statistical fluctuations of the data are represented by the error bars. We note that the T' value, 275 ± 8°K, of ^{240}Pu oxide at T = 294°K is less than T. This cannot be explained by the Lamb's theory for weak binding, and may be due to a transfer of the recoil momentum to the crystal lattice.

With these fine-tuned Γ_n and Γ_γ values we find T' by fitting all other capture data at liquid N_2 and He temperatures. The results averaged over 2 measuring cycles are given in Table I, where the quoted uncertainties reflect the statistical fluctuations. We subsequently obtain θ_D and its uncertainty from T' and T using equation (1), and these are also listed in Table I. θ_D may vary with T and depends on the target compound. Within statistical uncertainties all measured θ_D are consistently to be 175°K except the case of metallic ^{240}Pu at liquid N_2 temperature, where the θ_D value is a little higher. We are unaware of any other θ_D measurement for ^{240}Pu.

Table I

T' and θ_D for ^{240}Pu metal and $^{240}PuO_2$ at 3 measured temperatures

	T'=294°	T=77.2°		T=4.066°	
	T'	T'	θ_D	T'	θ_D
^{240}Pu Metal	300	110±12	237±52	60±12	160±32
$^{240}PuO_2$	275±8	95±7	170±39	71±7	189±19

By considering systematic uncertainties including those due to transmission data normalization, sample uniformity and the assumed value of R', the level parameters and their total uncertainties for the 1.056 eV resonance are Γ_n = 2.32 ± 0.06 meV and Γ_γ = 32.4 ± 1.0 meV. Compared to previously recommended values[9] the present results of neutron and capture widths are 0.9% and 4.5% higher respectively. The

previous values are mainly due to the transmission measurements by Ramakrishna and Navalkar,[10] giving Γ_n = 2.18 meV and Γ_γ = 28.82 meV. However, the present experiments have a higher neutron flux, better resolution and purer targets, and yield consistent results between independent capture and transmission measurements.

The recommended value[9] of thermal capture cross section of ^{240}Pu is 289.5 ± 1.4 b, mostly contributed from the resonance at 1.056 eV. Applying the present Γ_n and Γ_γ values, this resonance contributes 281.74 b. All other positive levels contribute only 1.02 b, calculated using the level parameters listed in reference 9 up to 600 eV and assuming a picket-fence model above it. Thus bound levels must contribute ∿6.74 b to thermal capture. Assuming that there is only one effective bound level to make this contribution, the ratio of its Γ_n°(meV) to $E_0(eV)^2$ is ∿0.053. While a_{coh} = 3.5 ± 0.1 fm,[9] to separately deduce the Γ_n° and E_0 values of the bound level one has to know the R' value at thermal energy which is not yet available.

The dilute resonance capture integral for the level at 1.056 eV is 8019.8 b from the present level parameters, and is 7931.5 b using previously recommended values. The difference, 88.3 b, is within 960 b, the uncertainty of the experimental value.[9]

Acknowledgement

Research has been performed under contract DE-AC02-76CH00016 with the U.S. Department of Energy. We thank the Research Materials Group at Oak Ridge for preparing the samples.

References

1. H. Bethe and G. Placzek, Phys. Rev. 51, 462 (1937).
2. W. E. Lamb, Phys. Rev. 55, 190 (1939).
3. H. H. Landon, Phys. Rev. 94, 1215 (1954).
4. H. E. Jackson and J. E. Lynn, Phys. Rev. 127, 461 (1962).
5. D. Bowman and R. A. Schrack, Phys. Rev. C17, 654 (1978).
6. R. E. Chrien and M. Reich, Nucl. Instrum. Methods, 53, 93 (1967).
7. R. L. Gill, M. L. Stelts, R. E. Chrien, V. Manzella, H. I. Liou and S. Shostak, 10th Intern. Conf. on Electromagnetic Isotope Separators and Techniques related to their applications, Zinal, Switzerland, September 1-6, 1980.
8. H. I. Liou, R. E. Chrien and R. Moreh, Proc. Conf. Nuclear Cross Sections and Technology, Knoxville, Tennessee, Oct. 22-26, 1979, P. 80, NBS Special Publication 594, National Bureau of Standards (1979).
9. S. F. Mughabghab and D. I. Garber, 'Neutron Cross Sections,' Vol. I, 'Resonance Parameters,' BNL-325, 3rd ed., Brookhaven National Laboratory (1973).
10. D. V. S. Ramakrishna and M. P. Navalkar, Proceeding of Second IAEA Conf. on Nuclear Data for Reactors, Helsinki, Finland, 15-19 June 1970, P. 553.

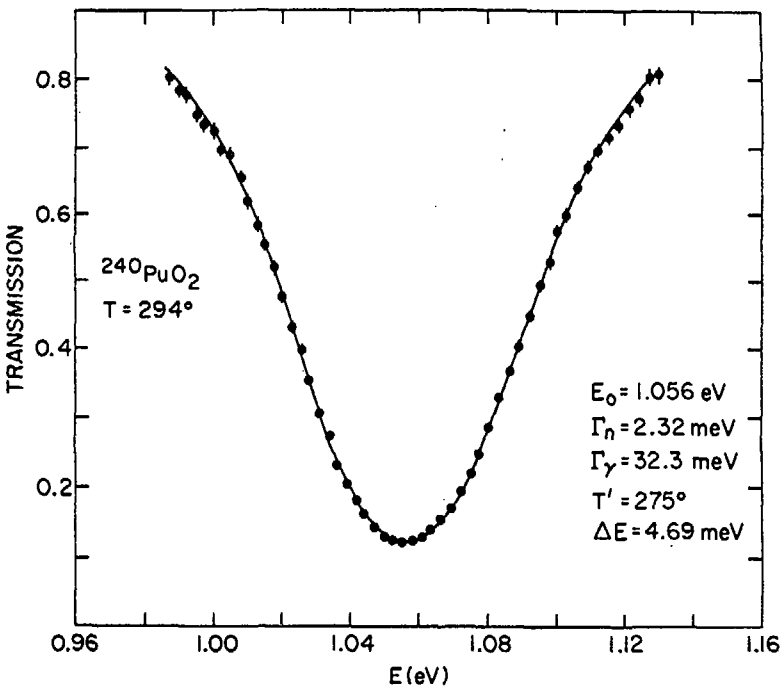

Fig. 1 An illustration of the final fit to ^{240}Pu oxide transmission data, collected at room temperature, for Γ_n and Γ_γ values of the 1.056 eV resonance. T'=275°K is chosen to be consistent with the capture data fit. The results are Γ_n=2.32±0.01 meV, Γ_γ=32.3±0.2 meV and χ^2/degree =1.156. The statistical uncertainties of the data are shown as the error bars or about the same size of the points plotted.

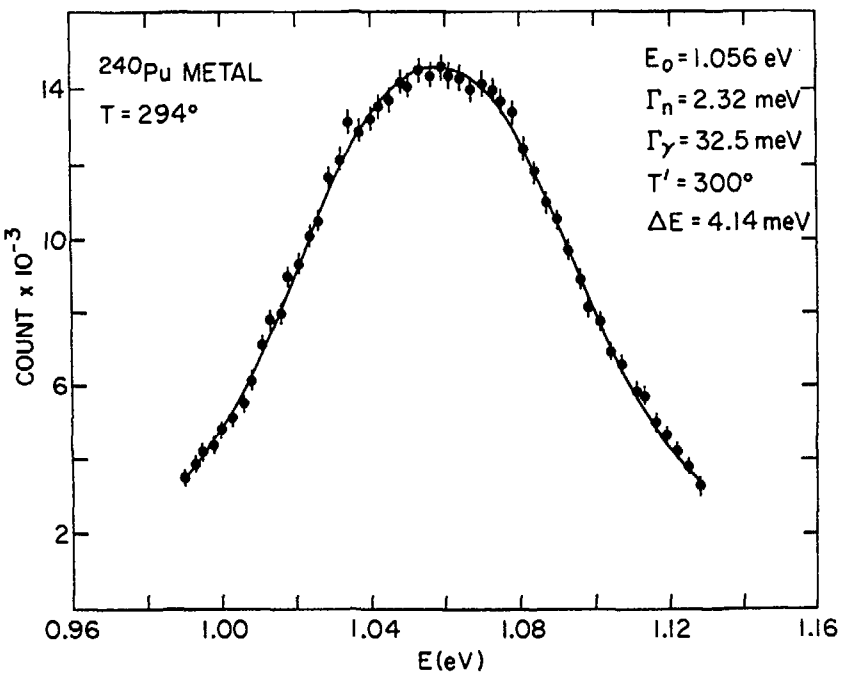

Fig. 2 This illustrates an example of the fit to ^{240}Pu metal capture data, measured at room temperature, for Γ_γ value of the 1.056 eV resonance. T' is assumed as 300°K, and Γ_n=2.32 meV is adopted from the result of the transmission data fit. We obtain χ^2/degree=0.632, and Γ_γ= 32.5±0.5 meV which agrees well with the transmission data.

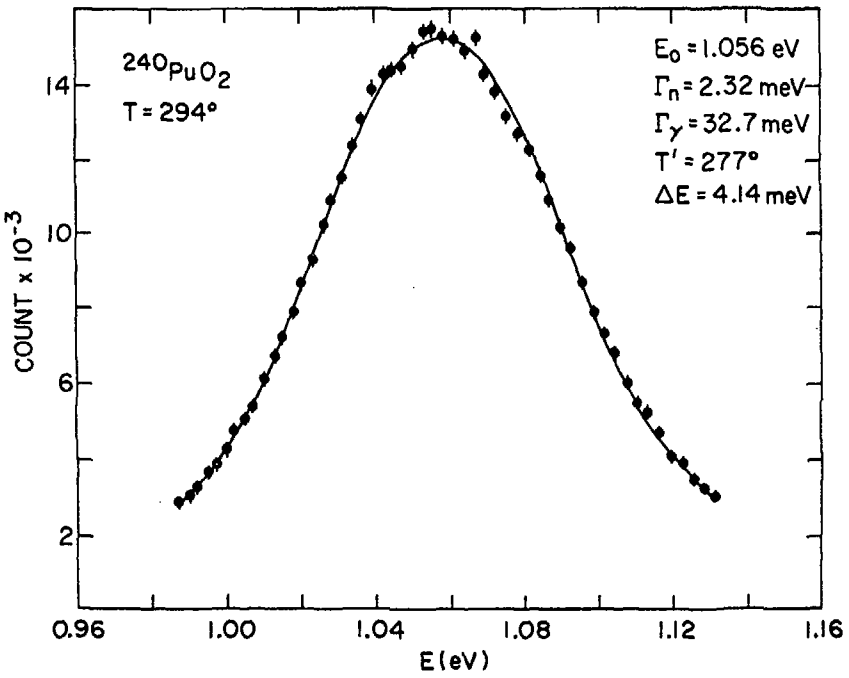

Fig. 3 An example of the shape fit, for the effective temperature T', to ^{240}Pu oxide capture data measured at room temperature. Γ_n =2.32 meV and Γ_γ=32.7 meV are assumed. The results are T'=277±9°K and χ^2/degree=1.442.

82-00917